Technical Report

TR-07-05

2nd Annual Workshop Proceedings of the Integrated Project "Fundamental Processes of Radionuclide Migration" – 6th EC FP IP FUNMIG

Edited by
Gunnar Buckau, Bernhard Kienzler
FZK-INE

Lara Duro, Vanessa Montoya
Enviros Spain

June 2007

Svensk Kärnbränslehantering AB
Swedish Nuclear Fuel
and Waste Management Co
Box 5864
SE-102 40 Stockholm Sweden
Tel 08-459 84 00
+46 8 459 84 00
Fax 08-661 57 19
+46 8 661 57 19

2nd Annual Workshop Proceedings of the Integrated Project "Fundamental Processes of Radionuclide Migration" – 6th EC FP IP FUNMIG

Edited by
Gunnar Buckau, Bernhard Kienzler
FZK-INE

Lara Duro, Vanessa Montoya
Enviros Spain

June 2007

FOREWORD

These are the proceedings of the 2nd Annual Workshop of the Euratom FP6 Integrated Project FUNMIG (fundamental processes of radionuclide migration). The Workshop was hosted by SKB (Svensk Kärnbränslehantering AB), and held in Stockholm 21 - 23 November 2006. The project started January 2005 and has a duration of four years. It has 51 Contractors and presently 27 Associated Groups. Annual workshops bring together, Contractors, Associated Groups and external interested groups. The first Annual Workshop was hosted by CEA, and held 28 November - 1 December 2005 in Saclay (France). The proceedings of that workshop are published as CEA-R-6122 report. The present proceedings will be followed by another two proceedings from the forthcoming annual workshops to be held in Edinburgh 26 - 29 November 2007 (hosted by NIREX/NDA), and at the end of 2008 in Karlsruhe (hosted by FZK-INE). The proceedings serve several purposes. The key purpose is to document and make available to a broad scientific community the outcome of the FUNMIG project. For this purpose, a considerable part of the project activity reporting is done through the proceedings, together with the outcome of topical sessions, a large number of scientific-technical contributions and one additional contribution on a specific area of project activities.

Information about the project can be found under www.funmig.com

TABLE OF CONTENTS

THE PROJECT

The EURATOM 6th EC Framework Program Integrated Project FUNdamental processes of radionuclide MIGration (FUNMIG) started in January 2005 and extends over 4 years. The main objective of the project is to deepen in the fundamental understanding of radionuclide migration processes in the geosphere, its application to the nuclear waste disposal Safety Case, training of next generation and communication of the results. The project tackles one of the main challenges for a sustainable European energy mix, namely scientific and social credibility of geologic HLRW disposal. To this aim, the project set up a consortium of 51 Contractors and presently 27 Associated Groups. The consortium includes key European Research Institutes, Universities, National Waste Management Agencies and SMEs. The participation and strong financial commitment of Waste Management Agencies ensures the proper technology transfer and application feedback. Active technology transfer and training is ensured, also by involvement of the additional associated groups interested in the subjects under study. The project is structured into six Research and Technological Development Components (RTDCs) and one Component on Training, Knowledge Management and Dissemination of Knowledge (C7). The six RTDCs cover basic processes common to all the disposal concepts under consideration in Europe, through to studies of host-rock type specific processes and application of the results to the disposal Safety Case. RTDC1 focuses on the study of well defined processes, such as ionic speciation, ionic exchange and surface complexation, organic complexation and solid solution and formation of secondary phases. RTDC2 focuses on the study of less-well defined processes, such as formation and migration of colloids, redox reactions at surfaces and biogeochemical processes. RTDC's 3 to 5 are devoted to specific host-rock types presently under consideration in Europe, namely clay host-rock (RTDC3), crystalline host-rock (RTDC4) and the overburden of salt formations (RTDC5). RTDC6 focuses on integration of scientific results for their application in the disposal Safety Case. Component 7 organizes management and dissemination of knowledge, and both project internal and external training. The present proceedings document the outcome of the 2nd Annual Project Workshop and. gives and overview of the outcome of the 2nd project year. The corresponding proceedings of the 1st Annual Project Workshop are published as CEA-R-6122 report.

THE SECOND ANNUAL WORKSHOP

The 2nd Annual Project Workshop was held in Stockholm 21-23 November 2006. The Workshop was hosted by SKB. 120 people attended the workshop, representing Contractors, Associated Groups, the European Commission, the Commissions external

expert and project external organizations. The workshop was organized in three days of oral presentations around the project, a poster session, a topical session and additional talks.

Objectives

This Workshop combined various types of activities and meetings with the following objectives:

- Inform about the scientific progress
- Inform about the administrative status
- Inform/agree upon forthcoming reporting
- Discuss various topics of interest (for example, various aspects of Integration..)
- Inform about and discuss training
- Agree upon the forthcoming work program

Emphasis was on scientific-technical topics with administrative issues kept to the minimum necessary.

RTDC sessions

Individual RTDC meetings were held in parallel during the annual workshop. The respective RTDC leaders gave plenary overviews of the work conducted so far within their respective RTDC's. In addition, the the summary overviews, scientific highlights were presented. These were:

RTDC1:

- Influence of inorganic carbon of Ni(II) and Co(II) sorption on Na-illite and Opalinus clay, by M.H. Bradbury & B. Baeyens (PSI, Switzerland)

- Adsorption of humics to iron oxides and its effects on ion adsorption, by W. van Riemsdijk (Wageningen University, The Netherlands)

RTDC2:

A summary of the following presentations was given by T. Arnold (FZD, Germany)

- -Sorption of Uranium onto granite and altered material from Äspö HRL, Jürgen Römer, Bernhard Kienzler, Dieter Schild, Institut für Nukleare Entsorgung (INE-FZK, Germany)

- Sorption and reduction of uranyl by Fe(II) minerals, by Simona Regenspurg, Maria E. Malmström, Industrial Ecology, Royal Institute of Technology (KTH, Sweden)
- Mobility of uranium during the reductive dissolution of iron oxides by sulfide, V. Alexandratos, T. Behrends, P. Van Cappellen, Faculty of Geosciences, Department of Earth Sciences – Geochemistry, Utrecht University (The Netherlands)
- U(VI/IV) adsorption mechanism on biotite surfaces and clarification of the influence of redox reactions on the U(VI) adsorption by Thuro Arnold, Nils Baumann, Robin Steudtner, Institute of Radiochemistry, (FZD, Germany)

RTDC3

- Interlayer hydration H_2O 'paradigm' (mono-porosity model) by Gilles Montavon (ARMINES, France)
- Porosity / mineral distribution characterisation (mm-cm scale) by J.C. Parneix (ERM, France)
- GIS system for COx 'transport pertinent' data sets, by C. Lerouge (BRGM, France)

Component 7 (management and dissemination of knowledge) was also presented. The outcome of the first two years training activities was given. Key events were two training courses. The first training course ("Fundamentals of Radionuclide Migration") was held in Barcelona, November 2005. The second training course ("The use of scientific results in site characterization") was held also in Barcelona in November 2006. A seminar entitled "The Use of Scientific Data in PA" was held the day before to the 2nd Annual Workshop. Other activities and issues related to Component 7 were also communicated.

Topical session

A topical session was held around subjects associated with performance assessment/the Safety Case, especially relevant for geologic disposal in crystalline rock. Tiziana Missana (CIEMAT) organized the topical session. The topics were:

- Role of biogeochemical processes on radionuclide migration.
- Characterization of geochemical conditions in crystalline rock/ Process identification and verification by real system analysis.
- Fluid flow system characterization in crystalline rock (Effects of the heterogeneity

and up-scaling)

Presentations within these topics were:

(A) Role of biogeochemical processes on radionuclide migration.

- K. Pedersen: Effects of microorganisms upon radionuclide migration - General aspects and results and conclusions from laboratory experiments and in situ investigations at Äspö hard rock laboratory.
- H. Moll: Interactions of microbes found at Äspö underground lab with actinides such as curium, uranium and plutonium.

(B) Characterization of geochemical conditions in crystalline rock/ Process identification and verification by real system analysis.

- M. Laaksoharju: Results from the groundwater hydrogeochemical investigation program in Sweden
- K.H Hellmut: Geochemical fluxes in the geosphere: quantitative understanding by identification and verification of processes

(C) Fluid flow system characterization in crystalline rock (Effects of the heterogeneity and up-scaling)

- J. Carrera: Effect of heterogeneities in transport & up- scaling
- P. Sardini: Diffusion process within crystalline matrices: from petrography to solute residence time distribution.

Additional presentations

Additional presentations were given on topics of general interest, especially the context of the present project within the Euratom FP7 program on geologic disposal. The additional presentations serve different purposes: i) they give opportunity to incorporate issues of interest for the project but not directly dealt with within the project, ii) the invited lecturers provide complementary views to the project, iii) they are useful ways of identifying opportunities of collaboration with other groups and iv) they give opportunity to other running initiatives to interact with the project in a more pro-active manner.

The presentations given in the 2nd annual workshop were selected so as to contextualize the project within the Euratom programme

- European OBservatory for Long-term Governance on RAdioactive Waste Management, OBRA Co-ordination Action running from October 2006, by M.

Martell (Enviros, Spain)

- Integrated Project PAMINA, running from October 2006, by J. Mönig (GRS, Germany)
- Integrated Project NF-PRO, running from 2004, will finish end of 2007, by N. Maes (SCK-CEN, Belgium)
- Treatment of influences of the near field on the geosphere in the Safety Case, by J.L. Cormenzana (ENRESA, Spain)
- Recent developments of the Euratom (Fission) Programme - Priority research area 'Management of Radioactive waste - Disposal of HLW & LLW' Towards FP7, by Michel Raynal (European Commission).

Structure of the proceedings

The proceedings are divided into the following sections:

- RTDC activity overviews,, with summaries of the Research, Technology and Development Components
- Topical Session, documenting some of the presentations given during the topical session
- Individual Scientific and Technical Contributions, containing reviewed scientific and technical manuscripts
- Additional contribution, presenting the work conducted at the FEBEX site within FUNMIG

Scientific-technical contributions submitted by Contractors were subject to an external review process. Two independent reviewers (Budhi Sagar, SWRI, and Mel Gascoyne, Geoprojects Inc.) reviewed the manuscripts and sent their comments to the authors for their consideration.

RTD COMPONENT ACTIVITY OVERVIEWS

RTD COMPONENT 1

Pascal Reiller
CEA, Centre d'Etude Nucléaire de Saclay
DEN/DANS/DPC/SECR
Laboratoire de Spéciation des Radionucléides et des Molécules
Bâtiment 391, pc 33
F-91191 Gif-sur-Yvette CEDEX, France

Michael Bradbury
Paul Scherrer Institut
Laboratory for Waste Management
CH-5232 Villigen PSI, Switzerland
mike.bradbury@psi.ch

Introduction

The main objective of this component is to provide fundamental process knowledge and the required data for processes with comparably well established conceptual understanding. The overall impact of natural organic coatings is included. Processes studied are fundamental and applicable to all types of host rocks and the proper parameters are derived for the relevant migration systems. The outcome is the fundamental understanding and quantification of the processes studied. The models are developed at the research model level. Thereafter, the advances of the research are summarised.

Advances within workpackages

WP1.1: Ionic species/speciation, processes determining physico-chemical conditions and generation of missing thermodynamic data

The work is focused on the determination of missing key thermodynamic data. The work is not only focused on the acquisition of free energies (formation constants), but also on enthalpies and entropies in order to properly account for temperature dependencies.

CEA has studied the speciation of U(VI) in acidic sulphate solutions in the temperature range 10-80°C. The objective is to determine the thermodynamic parameters related to the formation of the sulphate complexes $UO_2(SO_4)_i^{2-2i}$ (i = 1-3), and confirm the stability of the third complex $UO_2(SO_4)_3^{4-}$

Experimental work has mainly been carried out by time-resolved laser-induced fluorescence spectroscopy (TRLIFS), and also by electrospray ionisation – mass spectrometry (ESI-MS), to identify the stoichiometries, perform sensitivity analysis of the measurements, and derive thermodynamic data. The interpretation of the fluorescence measurements at 20°C is in good agreement with the formation constants for i = 1 and 2 from the literature, and particularly with the values selected by the NEA-TDB.

The determination of thermodynamic parameters namely $\Delta_r G°$ from ln K°, $\Delta H_r°$ from the Van't Hoff equation, $\Delta_r S°$ and $\Delta_r C_p°$ where also obtained.

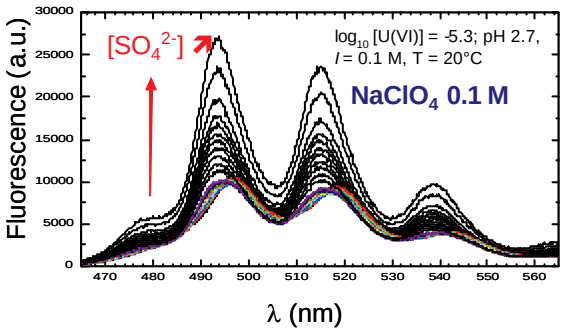

Figure 1: *Titration of U(VI) by SO_4^{2-} in $NaClO_4$ 0.1 M at T = 20°C. The apparent blue shift is in fact relative to UO_2OH^+ complex which actually dominates the fluorescence spectrum but not the speciation (CEA).*

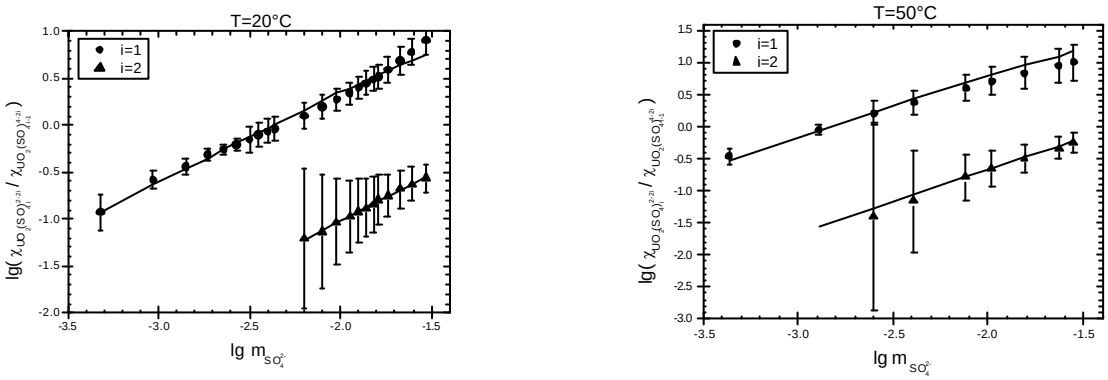

Figure 2: *Variation of the proportions of sulphato-complexes obtained from de-convolution of the TRLIFS spectra vs. the logarithm of the molality of SO_4^{2-} (CEA).*

The measurements at high sulphate concentrations indicate that the complex $UO_2(SO_4)_3^{4-}$ forms, and indeed dominates the speciation. Its formation constant has been determined. Extrapolation to zero ionic strength with the SIT formula provides a value which agrees fairly well with the selection by the NEA based on a single study. It should be noted that this extrapolated value is dependent on the estimated SIT parameters. The effect of the temperature on complexation was measured based on de-convolution techniques and a new set of thermodynamic parameters is proposed. A paper on this particular topic is being written for publication.

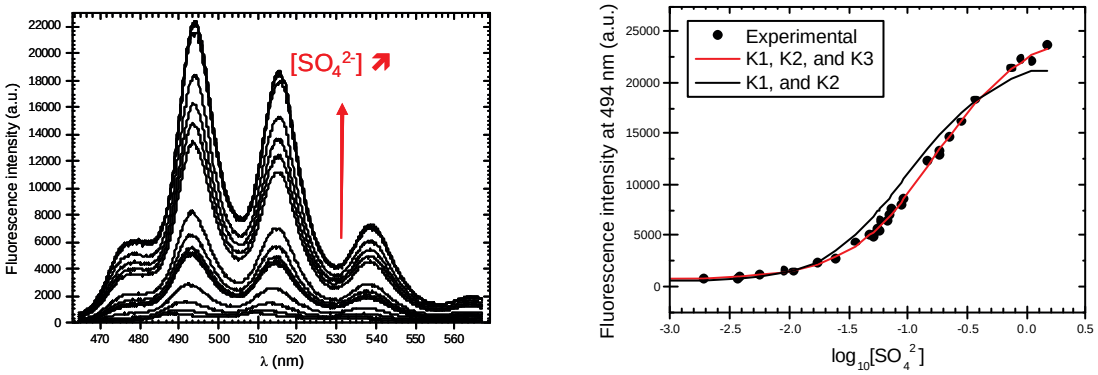

Figure 3: *Complexometric titration of U(VI) by SO_4^{2-} and treatment of the data (CEA).*

For the Ln(III)-sulphate, as previously mentioned, results obtained both by TRLIFS and ESI-MS techniques are in good agreement. For the U(VI)-sulphate, first results obtained are more complex to interpret and further experiments are in progress to confirm the observed trends.

In the framework of the geochemistry of radionuclides as a function of temperature, despite several efforts, we have not been able to design an electrochemical systems based on µcavity or carbon paste electrodes allowing measurement at temperatures above 60°C. Results were only obtained with a classical Hg electrode on the Ce(III)/Ce(IV) system (as mention in the implementation plan) between 5 and 50°C and was accepted in J. Electroanal. Chem. "Relative stabilities of Ce(IV) and Ce(III) limiting carbonate complexes at 5 to 50°C, an electrochemical study". Consequently, we will not be able to fulfil the rest of this task on that particular topic and M1.1.1 "Design of the electrochemical system" will not be fulfilled. Therefore, as first identified at the kick-off meeting in Barcelona as potential subject of common interest with Chalmers University (CTH), we have moved towards the study of the silicate-lanthanide(III) system, as presented at the last RTDC-1 meeting in Gothenburg (Sweden) in May 2006, and in agreement with the RTDC leaders. This aspect has been added to the 3rd implementation plan.

In the framework of a collaboration between CEA and CTH on the speciation of trivalent lanthanides or actinides (M^{3+}) with silicate, experimental work has been carried out by TRLFS, ESI-MS and solvent extraction to specifically determine the stability of the $M(OSi(OH)_3)^{2+}$ complexes. Spectrometric measurements have shown that, in addition to the formation of a monosilicate complex, numerous oligomeric silicate species form even at low Si concentrations. Experiments are on going to investigate the effect on the speciation of the metal ions.

The work performed so far within RTDC1 from CTH has mainly been focused on the complexation of thorium with phosphate. Stability constants have been obtained for this system at pH 8, and also at pH 7 and 9. The results will shortly be presented in the paper "Studies on the Complexation Behaviour of Thorium(IV).2. Phosphate Complexation". The investigations of Th-silicate complexes have proven to be difficult, and the results so far are somewhat uncertain. More experimental work is needed to ensure meaningful interpretations.

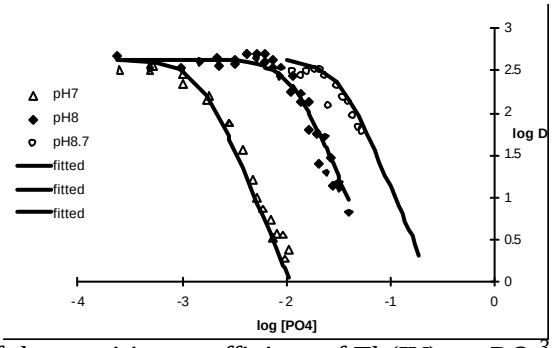

Figure 4: *Evolution of the partition coefficient of Th(IV) vs. PO_4^{3-} (CTH).*

WP1.2: Ion exchange and surface complexation

The work is focussed on the assessment of thermodynamic sorption models using surface complexation and ionic exchange models. Assessment is done on the laboratory systems up to real systems. Verification of the species involved is done by spectroscopic studies.

CEA (L3MR) has focused their works on the surface activity coefficients of sorbed species on illite du Puy. Results from batch experiments of caesium sorption onto potassic illite du Puy, with varying potassium and caesium concentrations in solution, and pH, have shown that sorbed species exhibit ideal thermodynamic behaviour: the sorption at trace caesium concentrations is constant, which means that the ratios between the activity coefficient of sorbed Cs^+ and sorbed K^+, and between sorbed Cs^+ and sorbed H^+ are also constants. The sorption isotherms of Cs^+ on illite du Puy comfirm the previous conclusion. The study of monovalent/trivalent cation exchange (i.e. americium/potassium/proton) is on going.

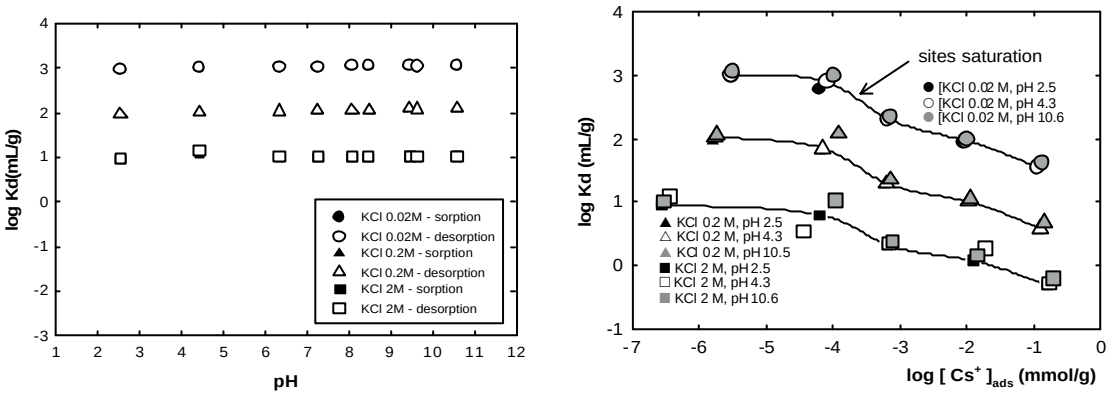

Figure 5: *Sorption of Cs on illite at various ionic strength: a. pH isotherm ; b. [Cs] isotherms at different pHs (CEA).*

A first version of the data base concerning montmorillonite, goethite, a-alumina and alkaline, alkaline-earths, actinides, was provided in August 2006. This is a selection of thermodynamic constants, obtained by CEA, consistent with the Ion-Exchangers Thermodynamic Theory (IXT2). Presently, a data base for illite (du Puy) is under construction. New experiments are planned in order to acquire data related to calcium and magnesium, completing the data base. These data are required for testing the

predictive capability of the sorption models in the case of illite and chloride-rich brines, simulating sea water and its dilutions.

The benchmarking of interface modelling SCM and IXT2 has begun. The first step is a chemical study of amorphous silica and gibbsite solubilities and surface equilibria. Gibbsite (synthesised in the laboratory) and amorphous silica (a Sigma-Aldrich product) were conditioned before solubility and solid-solution interface equilibria studies. Acid-base titrations have been performed with an automatic titrator (fast titration: 5 minutes between each added increment). Batch experiments have also been done in order to i) study the evolution of pH for longer contact times (1-30 days), ii) check the solubility of the minerals and iii) measure ζ potentials. Results show that the solubility equilibrium of SiO_2(am) is in good agreement with literature data (log K = -2.71), taking into account the formation of mono and polynuclear species in solution. For gibbsite, a solubility product of log K = -8.36 has been obtained from the experimental data. ζ potentials have been measured for long contact times (> 10 days) and are consistent with literature results. As expected, ζ is always negative for SiO_2(am) for 1<pH<11 and close to zero for 1 < pH < 3. For gibbsite, pH_{IEP} has been measured at 10.6 (literature value for pH_{IEP} is ~ 10 after 1 day equilibration). The acid-base titration of SiO_2(am) gave a $\log K_{a2}$ =-7.6 for silanol site, which is close to the literature results. The acquisition of surface acidity data for gibbsite is in progress.

CEA (LRSI) has undertaken several wet chemistry experiments and spectroscopic characterizations which have helped clarifying the uptake mechanism(s) of lanthanide by clay minerals. Firstly, wet chemistry experiments performed on the lanthanide-montmorillonite and lanthanide-hectorite systems have revealed comparable dependencies of the sorption on pH. Specifically, a strong increase in the amount of sorbed cations with pH at near-neutral pH conditions has been observed. Kinetic experiments of yttrium sorption on hectorite also revealed that this uptake results in an apparent short term increase of Mg, and a slowdown of Si release into the solution. These results suggest that Ln adsorb at the layer edges, and possibly associate with silica groups. Sorption experiments with cerium (III) and cerium (IV) also showed that the pH edge of cerium sorption is shifted to more acidic pH value as the oxidation state of cerium increases.

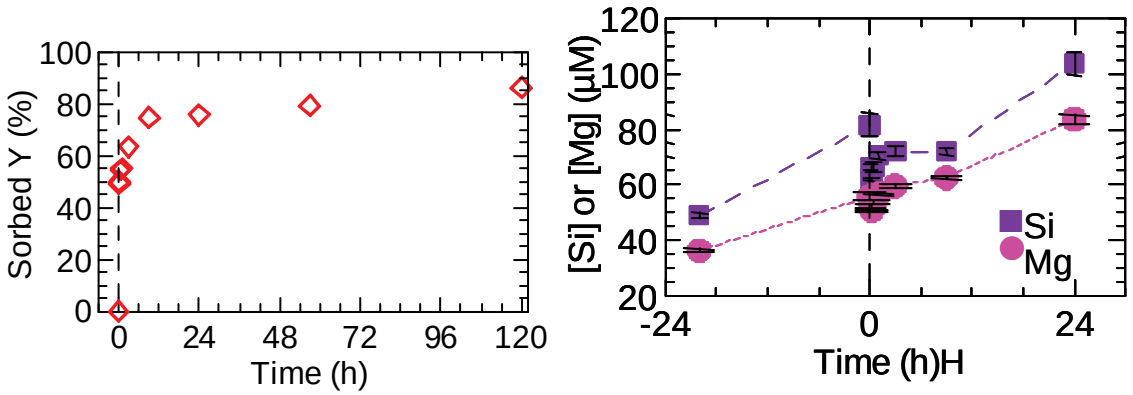

Figure 6: *Sorption kinetics of yttrium on hectorite; a. $[Y]_t$ = 50 µM, 1 g/L hectorite, 0.5 M NaCl, pH 7; b. Effect on $[Si]_{aq}$ and $[Mg]_{aq}$ (CEA).*

Time-resolved laser induced fluorescence (TRLIF) spectra of Eu sorbed on hectorite and montmorillonite revealed that the sorbed Eu is progressively dehydrated as pH increases. This progressive dehydration is attributed to the formation of Eu inner-sphere complexes at the surface of clay particles. The small number of water molecules remaining in the hydration sphere at basic pH may correspond either to the formation of silica-Ln-clay ternary surface complexes, or to the formation of new Eu-containing solids, presumably from Eu co-precipitating with species such as silica.

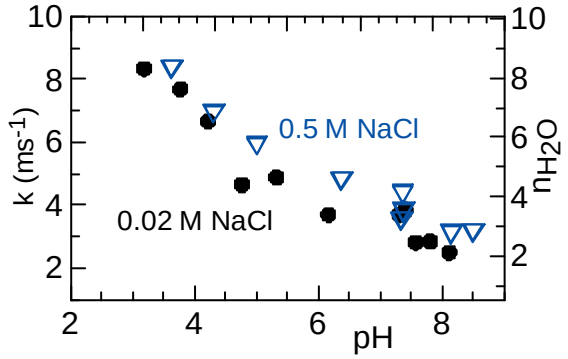

Figure 7: *Evolution of the reciprocal lifetime and number of water molecules in the hydration sphere of Eu sorbed on hectorite (CEA).*

Further insight into the molecular environment of sorbed Ln has been obtained by Y K-edge and Nd L3-edge Extended X-ray absorption fines structure (EXAFS) spectroscopy. Polarized EXAFS data collected on self-supported films of sorbate-reacted hectorite revealed that Nd and Y were both in anisotropic environments, demonstrating the structural association of the sorbate with the sorbent surface. Quantitative analysis of the EXAFS spectra revealed the presence of Mg/Si neighbouring cations at interatomic distances consistent with the formation of surface complexes at the edges of hectorite platelets. In the Y case, the sorption sites are probably located in structural continuity to the Mg octahedral sheet of the hectorite platelet. Thus, solution chemistry, TRLIFS and EXAFS results collectively point to Ln sorption on clay particles at near-neutral pH forming edge surface complexes.

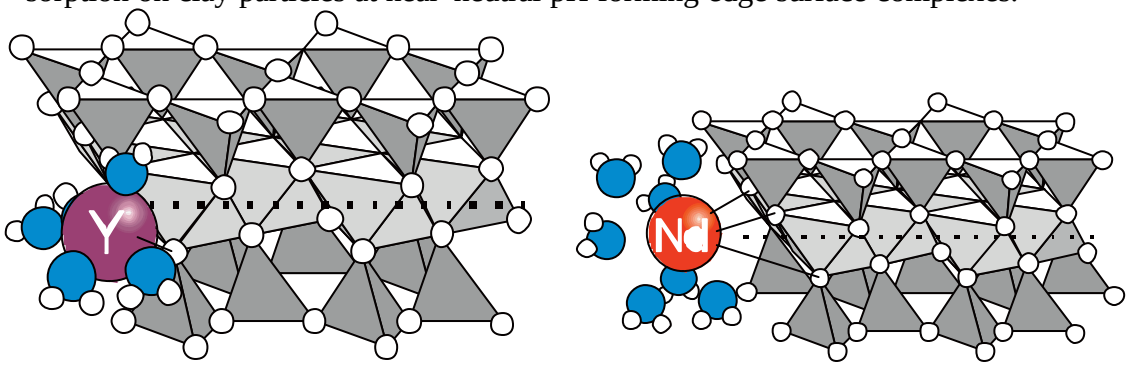

Figure 8: *Structural models proposed for Y and Nd sorption on hectorite (CEA).*

The aim of the work conducted by CIEMAT is to evaluate the Se and Pu sorption in clays. To interpret and quantify the interactions occurring at the clay/water interface by means of (quasi) thermodynamic models it is necessary to evaluate independently

the effects of the most important physico-chemical parameters such as pH, ionic strength and radionuclide concentration. Furthermore, with results from these tests the aim is to model the sorption behaviour of mixed clays knowing the sorption parameters of the main clay components. So far, CIEMAT has studied experimentally the sorption behaviour of Sr and Pu onto pure Na-illite, pure Na-smectite and illite/smectite mixtures.

The experimental work with Sr is finished whereas more experimental data on Pu sorption onto illite and illite/smectite sorption are needed to start the modelling. Two CIEMAT internal reports have been written which include the main experimental results for these two radionuclides: 1) A report on Pu sorption on smectite/illite. CIEMAT/DMA/2132/2/06 and 2) A report on Sr sorption on smectite/illite. CIEMAT/DMA/2132/3/06. Data obtained with Sr sorption on Na-illite and Na-smectite were modelled using the CHESS code and the main sorption parameters (for both ionic exchange and surface complexation included in the model) were obtained.

In order to test the Sr behaviour in the smectite/illite mixtures, sorption edges at 0.1 M $NaClO_4$ were carried out, using a mixture of 50/50 and 75/25 smectite-illite. Data on the mixtures are compared with those of pure clays. The final solid to liquid ratio is, in all the cases, 1 g/L. The experimental data obtained are shown in Figure 9a. Sorption data are hardly distinguishable in spite of the different characteristics of both clays. The proposed exercise was to try to reproduce the sorption in the mixtures using the sorption parameters previously obtained from the tests on pure Na-illite and Na-smectite. Figure 9b, shows the simulation obtained for pure illite, pure smectite and for 50/50 and 75/25 smectite/illite mixture. The simulations correspond very well to the experimental measurements and lie within the experimental error range. The model shows that the sorption due to ionic exchange is slightly higher when the montmorillonite content is increased. At pH values higher than 9, when surface complexation starts to make a significant contribution, the higher the illite content the higher the sorption. These differences were not be very distinct in the observed experimental measurements. The results showed that it was possible to model a system composed of a mixture of clays using the data extracted in the single mineral experiments.

Experiments with Pu on Na-smectite, and the two selected mixtures of Na-smectite and Na-Illite (75/25 and 50/50 smectite/illite) have not yet been completed since the study of Pu adsorption in the neutral alkaline regions involves some several difficulties. Concerning sorption in the acidic region, the following characteristics can be identified:

- A "plateau" is observed under very acidic conditions (pH < 3) where the sorption, which does not depend on the pH but does depend on the ionic strength, should be mainly ionic-exchange dominated;
- An intermediate region (pH 3-4) where the sorption tends to decrease slightly; this is not easy to explain, but possible effects due to a change in the Pu oxidation state, cannot be ruled out.
- A final region, in which sorption depends on the pH but not very significantly on the ionic strength, with a possible contribution due to surface complexation.

It is noteworthy that these different regions could be observed for the sorption on smectite and also in the smectite/illite mixtures. The qualitative behaviour is similar in all the cases, even if higher sorption is observed at higher smectite

contents, at least under acidic conditions. More data are needed before starting the modelling.

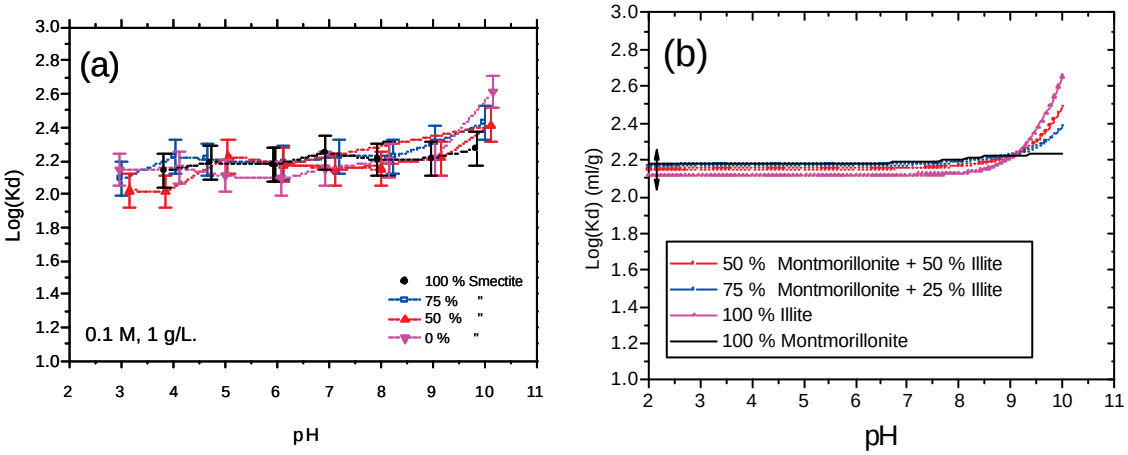

Figure 9: *Sr sorption edges on the illite/smectite. b) Modelling of data (CIEMAT)*

The sorption experiments on mineral slides from CTH have recently started after delays relating to the difficulties in obtaining suitable mineral slides for biofilm sorption experiments in RTDC-2. The preparation of circa 1 mm thick slices requires special methods. Since it is preferred to have the same material in both experiments, the sorption work on silicates and phosphates with and without a biofilm have been somewhat delayed.

The main efforts from PSI were focussed on the modelling of the Ni(II) sorption on Opalinus clay and of Co(II) sorption on illite and Opalinus clay in synthetic Opalinus clay porewater compositions. The 2 site protolysis non electrostatic surface complexation and cation exchange model was used to model (i) trace sorption of Ni as function of pH in order to obtain cation exchange selectivity coefficients and surface complexation constants for strong sites, and (ii) Ni sorption isotherms to derive in addition to the above the surface complexation constants on weak sites.

Dissolved inorganic carbon is ubiquitous in all natural groundwater and porewater systems and it is essential to be able to quantify the effects of aqueous carbonate speciation on sorption and include this in models for predicting radionuclide uptake in natural systems. To this end the effect of the presence of inorganic carbon was investigated. Under the assumption that Ni carbonato-complexes do not sorb, the model predictions and measurements agreed well with one another. From these investigations it is concluded that the carbonate concentrations present in the porewater of the Opalinus clay formation are insufficient to have a significant effect on Ni sorption.

As a next step the sorption of Ni on Opalinus clay from Mont Terri under realistic chemical conditions was investigated. The so-called bottom-up approach, *i.e.* trying to understand the simple system first, and build up gradually the knowledge to more complex systems, was tested. A Ni(II) isotherm on OPA was measured. The isotherm was calculated in a blind prediction using the 2SPNE SC/CE model developed for illite. In this approach, the 22 wt.% illite fraction was taken as the dominant sorbing phase. In a first step the presence of Fe(II) was neglected and a slight over-prediction at low Ni equilibrium concentrations was observed. However, if Fe(II) was included in the

modelling, the correspondence of the model prediction and measured data was improved.

Finally, a Co(II) sorption isotherm was also measured in support of the field diffusion experiments at Mont Terri. This isotherm was measured under the same chemical conditions as the laboratory diffusion data and the field measurements at the URL at Mont Terri. In the DI & DR experiments Co was used as a tracer. In a separate experiment the Co(II) sorption edge was determined on Na-illite and was modelled using the 2SPNE SC/CE model. Following the same procedure as given above, i.e. the bottom-up approach, a Co(II) isotherm was calculated for the Opalinus clay system. The predicted sorption data agreed well with the measured data.

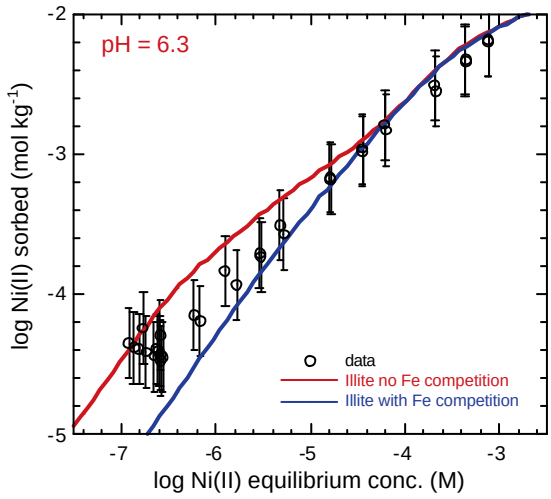

Figure 10: *Influence of iron competition on Ni(II) sorption on OPA (PSI)*

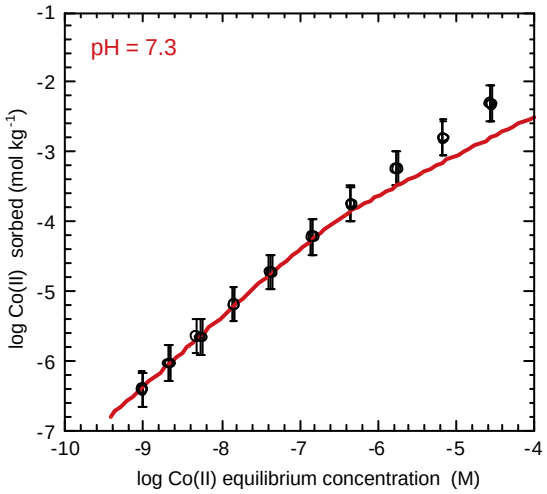

Figure 11: *Sorption of Co(II) on OPA, comparison between experiment and model (PSI).*

The objective of SCK-CEN works is to produce sorption datasets for the Boom Clay host rock determined under variable geochemical conditions in order to set up a Thermodynamic Sorption Model in support of the selection of radionuclide retention parameters for performance assessment for both non-disturbed and disturbed conditions. Sorption isotherms for both Am and Th onto Boom Clay under *in situ* pH and pCO_2 (pH~8.3 and anaerobic conditions with 0.4 % CO_2 atmosphere) conditions were measured in Real and Synthetic Boom Clay water for a S/L ratio of ~0.01 g/ml to determine the influence of the dissolved organic matter present in the Real BC water (~100 ppm C). Special emphasis was given to colloid formation; concentrations were determined for non-filtered (High-speed centrifugation only) and UF (30 kD) samples. The log K_D values for Am and Th are similar. The presence of dissolved OM in the clay water clearly decreases the K_D by one order of magnitude due to interaction with the NOM. Colloids are clearly present in the system because the K_D values differ by typically 1 order of magnitude between non-filtered (NF) and ultrafiltered (UF) samples. In the experiments with RBCW this is mainly attributed to the presence of NOM in the BC water which contains about 35% of NOM molecules > 30 kDa. However, a similar effect is observed for the experiments in Synthetic BC water which does not contain NOM but some organic matter is released from the BC in suspension

and these molecules are mainly > 100 kDa. New experiments are foreseen under varying pH and carbonate conditions.

UPC studied the interaction of Th(IV) with iron oxyhidroxides and oxides: magnetite and ferrihydrite, as an analogue for other tetravalent actinides. Kinetics experiments have been performed in order to determine the time needed to reach equilibrium. This process is dependent on pH in the case of magnetite and takes approximately 48h. A longer equilibrium time of up to 5 days is necessary in the case of ferrihydrite at pH 3. Sorption experiments have been conducted at pH 2 and 3 with different mass/volume ratios and initial Th concentration of 10^{-4} and 10^{-5} mol/L. Surface precipitation seems to occur at Th concentration above 8×10^{-5} mol/L at pH 2±0.4.

In the case of magnetite, taking into account the results obtained from the fits and geometric calculations based on crystal structural data from literature (d_{Fe-O}= 2.14Å, d_{Fe-Fe}= 2.97Å and d_{O-O}= 3.08Å; O-Fe-O angle= 92º), and the Th-O bond length from our EXAFS data analysis, it seems that Th(IV) is present in at least two different configurations: bidentate-corner arrangements both on the [FeO4] tetrahedra and the [FeO6] octahedra. In the case of ferrihydrite, the results obtained from the fits suggest that Th(IV) sorbs onto 2-line ferrihydrite by forming a bidentate corner-sharing surface complex. These distances match very well with the expected bond distances of this kind of configuration (3.53-3.60Å for a Fe-O-Th binding angle in the range ß= 104-107º).

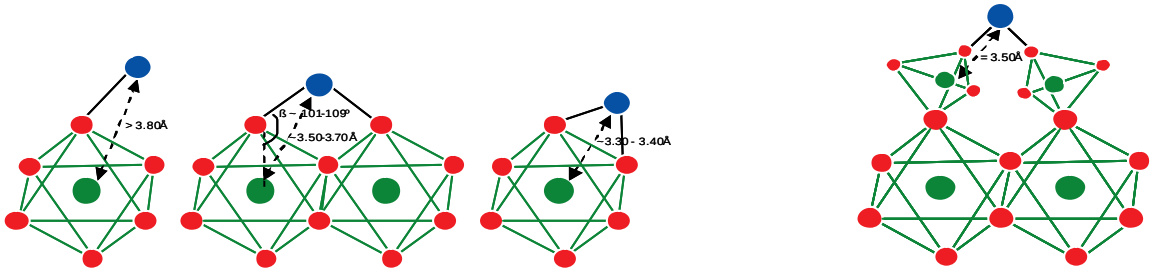

Figure 12: *Proposed structures for the bidentate site for Th(IV) on magnetite (UPC)*

KULEUVEN collected XANES and EXAFS data of selenite standard solutions and illite sorption sample suspensions in order to elucidate the molecular binding mechanism(s) of selenium surface complexes on illite clay. The aqueous selenite acid-base species, H_2SeO_3, $HSeO_3^-$ and SeO_3^{2-}, all had very distinct XANES and EXAFS patterns which reflected their molecular structure. All species were very well fitted with either one coordination shell (with SeO_3^{2-}) or two coordination shell (with $HSeO_3^-$ and H_2SeO_3) oxygen atoms and single-scattering fitting paths. The selenium sorption samples, at three different pH values (3.25, 4.34 and 5.90), all had XANES spectra which closely reflected the spectrum of $HSeO_3^-$, indicating they had a similar molecular structure with two oxygen atoms in the first coordination shell and one atom in the second coordination shell. The same observation is true for the EXAFS spectrum, which again closely resembled that of $HSeO_3^-$. However, in the Fourier-transformed RSFs new features different from the $HSeO_3^-$ standard were clearly observable and pointed to an inner-sphere sorption complex on the clay platelet edges. The new peak in the RSFs could be fitted by an aluminium atom located at 3.05 Å of the central Se absorber. Uncertainty concerning the exact molecular structure of the different sorption complexes, and the non-negligible presence of soluble selenite species in the collected

spectra however, prevented further interpretation of the spectra in terms of the precise binding mechanism (monodentate, bidentate mononuclear or bidentate binuclear).

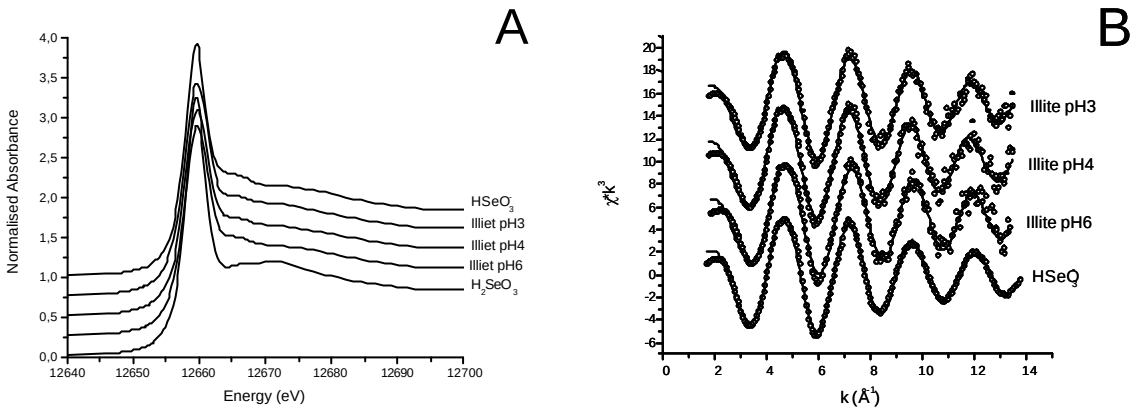

Figure 13: *XANES and Fourier-transformed EXAFS spectra of Se(IV) species, either free or sorbed on illite (KULEUVEN).*

For performing the study of Cm(III) sorption onto aluminium oxides/hydroxides, INE synthesized Gibbsite by precipitating aluminium hydroxide in a glove box under Ar atmosphere and subsequent dialysis at elevated temperature (70°C) for a time period of 4 months. The gibbsite was characterized using different experimental methods such as XPS, AFM, XRD, BET, SEM, TG and DTA. Additionally, zeta-potential measurements were performed as a function of pH and ionic strength as well as potentiometric titrations for the determination of surface acid-base properties and the concentration of surface sites. All of these characterizations revealed a well crystalline material with very small impurities on the surface and a relatively large surface area of about 50 m²/g. The pH dependent metal ion sorption was studied in batch sorption experiments at two different ionic strengths (0.1 M $NaClO_4$ and NaCl and 0.01 M NaCl) using Gadolinium as a model for the trivalent actinides. Gd concentrations were varied over 4 orders of magnitude between 1 ppb and 10 ppm at a constant gibbsite concentration of 2 g/L. All experiments were conducted in a glove box under Ar atmosphere. The phase separation was done by ultracentrifugation at 18.000 and 90.000 rpm and Gd concentrations in the supernatants were determined by ICP-MS. At Gd concentrations up to 100 ppm the pH edges are congruent, indicating the sorption being in the ideal sorption range. By further increasing the Gd concentration the pH edges shift to higher pH values, typical for the non-ideal sorption range. No significant influence of ionic strength was observed. First TRLFS experiments with Cm clearly show the presence of inner-sphere surface complexes. In the pH range 4 to 11.5 two different surface sorbed Cm species can be differentiated from the peak positions.

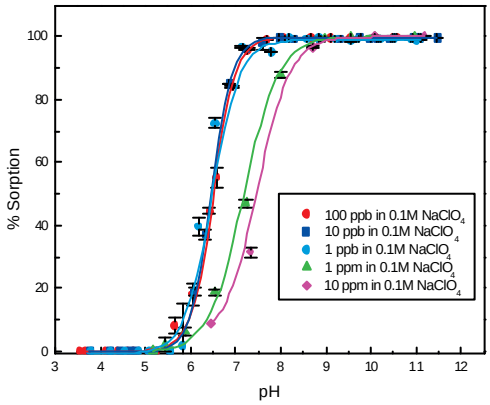

Figure 14: *Sorption edges of Gd on Gibbsite (INE)*

INE has developed a new version of a non-electrostatic adsorption model. Tests with the selenium – goethite systems showed that the model is capable of reproducing adsorption data in a similar way to electrostatic models. Adsorption models typically involve acid-base reactions of the surface functional groups. Common non-electrostatic models most frequently cannot describe mineral acid-base data. The proposed new non-electrostatic model was tested on two different sets of acid-base data (goethite and quartz). It was found that the non-electrostatic model cannot describe such data. Therefore, the adsorption model will not include an acid-base model of the surface. Presently a data set for uranyl adsorption on quartz is being modelled. First a reference electrostatic model is developed (a multi-site charge distribution model, including one surface site and the basic Stern model for the electrostatic part). The electrostatic model is based on spectroscopic information on the structure of the surface complexes. The model is being processed at present. Subsequently a non-electrostatic model will be designed. Both models will be compared with each other (i) in terms of the goodness of fit with respect to model calibration and (ii) in terms of predictions of both models under conditions that were not included in the model calibration. In particular two other sets of experimental batch adsorption data will be used for that purpose. Also it is planned to apply both models to published results of column experiments on this system and column experiments which are currently being started at INE with coarser quartz particles.

The contribution of University of Helsinki (HU) and Technical Research Centre of Finland (VTT) is focused on studying the sorption of Ni and Eu on selected rock types in the area of the planned repository in Finland. The main rock types in the area are mica gneiss, granodiorite and granite that is often porphyritic and poor in micaceous minerals.

The granodiorite and mica gneiss were characterized by optical microscopy for mineral contents of the samples. Thin section autoradiography of Ni-63, Cs-134 and Eu-152 was used to identify the minerals on which the radionuclides were mainly sorbed. Biotite was chosen as the mineral for the sorption experiments of Ni(II) and Eu(III). In addition to the biotite samples separated from granodiorite and mica gneiss, a

pegmatitic biotite from Luumäki in south-eastern Finland was studied. The biotite from Luumäki was a pure biotite and was used as a reference biotite in the experiments.

The elemental compositions of the biotite samples were determined after total dissolution by ICP-AES and ICP-MS methods. The surface areas were determined by the N_2 BET method. The cation exchange capacities (CEC) of the biotite samples were determined using the ammonium acetate method. The acidity constants of surface sites were determined by acid-base titrations of the biotite in $NaClO_4$ solutions. The titration results were fitted to a 1-pK surface complexation model by applying either the Diffuse Layer or the Constant Capacitance surface-charging model (using Fiteql 4.0 software). The sorption of nickel on biotite samples was determined in 0.05 M and 0.5 M $NaClO_4$ solutions buffered at pH 3 to 9.5. These results were modelled by applying the surface protonation model obtained from titrations, one surface complexation and one ion-exchange site for nickel ions. The sorption of europium on biotite was also studied in 0.05 M and 0.5 M $NaClO_4$ solutions buffered at pH 3 to 9.5. The biotite samples were separated from granodiorite and mica gneiss and biotite from Luumäki, Finland, as in the case of the nickel sorption studies. The results will be modelled by VTT using a surface complexation model.

Molecular-level modelling was applied to obtain atomic-level information about the biotite surface. This information will be up-scaled later to be used in the surface complexation modelling of biotite.

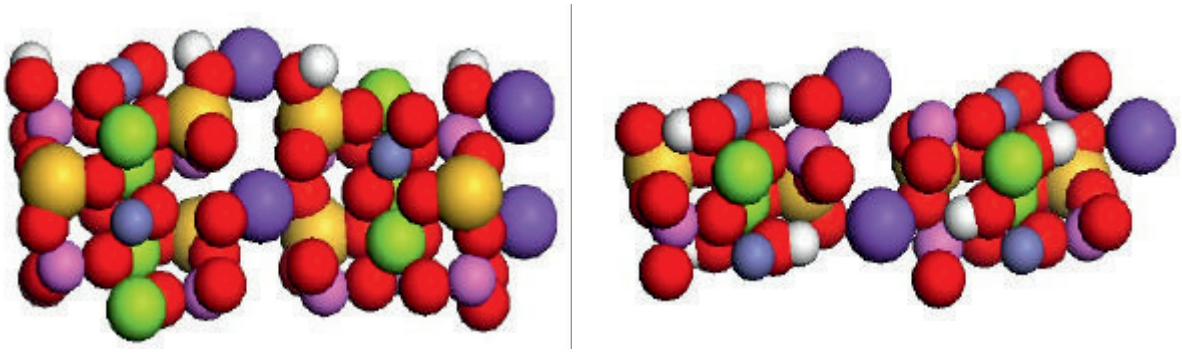

Figure 15: *Biotite surfaces; left (110) surface (side view) and right b. Biotite (111) surface (side view).*

WP1.3: Influence of organics on the retention of radionuclides by minerals

The work is focussed on the understanding of the influence of different organic matter/substances on the retention of radionuclides by mineral surfaces.

UNIMANCH, UNILOUGH and NIREX have collaborated on the interactions of Eu^{3+} ions, humic acid and quartz in ternary system experiments. The variations in the amount of humic acid and Eu^{3+} with time have been determined as a function of humic acid concentration. The desorption of both humic acid and europium have also been measured. A simple mathematical model has been developed that is able to predict the behaviour of both metal ion and humic acid. There is multi-component behaviour in the experiments, and the modelling suggests that for the sorption step at least, heterogeneity of the surface binding sites dominates. However, there is hysteresis in the desoprtion behaviour of the humic, which could be due to chemical and/or size fractionation on the

quartz surface. This work is more developed in the scientific contribution in this volume: *"Kinetic Studies Of The Quartz/Sand, Eu^{3+} And Humic Acid Ternary System: L.G. Abrahamsen, D.H. Farrelly, A. Pitois, P Ivanov, P. Warwick, N.D.M. Evans L. Knight and N.D. Bryan"*.

The same partners studied the interactions of Eu^{3+} ions, humic acid and iron oxides in ternary system experiments have been studied. The variations in the amount of humic acid and Eu^{3+} with time have been determined as a function of humic acid concentration. Two simple mathematical models have been developed to predict the behaviour of metal ions and humics in the experiments. The treatment of the binary interaction between humic acid and metal ion is common to both models: initial rapid uptake to an exchangeable fraction, followed by slower transfer to the non-exchangeable fraction. Both models assume that the interaction of the humic with the mineral surface is unaffected by the complexation of metal ions. The difference between the models is that the first (Model 1) assumes that the observed heterogeneity derives from multiple binding sites on the surface of the iron oxide, whilst the second assumes that it is the result of chemical or size heterogeneity of the humic itself. The behaviour of the magnetite system is best described by Model 1, but hematite follows Model 2 most closely, whilst goethite shows intermediate behaviour. This work is more developed in the scientific contribution in this volume: *"Initial Kinetic Studies Of Iron Oxide And Humic Acid Ternary Systems: D.H. Farrelly, L.G. Abrahamsen, A. Pitois, P Ivanov, B. Siu, N. Li, P. Warwick, N.D.M. Evans L. Knight and N.D. Bryan"*.

Finally the same partners collaborated in providing a procedure to assess the importance of chemical kinetics in the humic mediated transport of radionuclides in radiological performance assessment calculations. Based on previous work where it was shown that humic substances can bind metal ions in two fractions: the exchangeable, where it is available instantaneously for reaction with other sinks (such as mineral surfaces); and the non-exchangeable, from which it may only dissociate slowly. In the absence of metal ion/humic/mineral surface ternary complexes, if the dissociation rate is slow compared to the solution residence time in the groundwater column, then metal in the non-exchangeable will have a significantly higher mobility than that in the exchangeable. The critical factor is the ratio of the non-exchangeable first order dissociation rate constant and the residence time in the groundwater column, metal ion mobility increasing with decreasing rate constant. Sorption of humic/metal complexes at mineral surfaces may reduce mobility. In addition to direct retardation, sorption also increases the residence time of the non-exchangeable fraction, giving more time for dissociation and immobilisation. The magnitude of the effect depends upon the concentrations of the mineral surface humic binding sites and the humic in solution, along with the magnitudes of the equilibrium constant and the forward and backward rate constants. The non-exchangeable dissociation reaction and the sorption reaction may be classified in terms of two Damkohler numbers, which can be used to determine the importance of chemical kinetics during transport calculations. These numbers could be used to determine when full chemical kinetic calculations are required for a reliable prediction, and when equilibrium may be assumed, or when the reactions are sufficiently slow that they may be ignored completely. This work is more developed in the scientific contribution in this volume: *"A Procedure To Assess The Importance Of Chemical Kinetics In The Humic Mediated Transport Of Radionuclides In Radiological*

Performance Assessment Calculations: P. Ivanov, L.G. Abrahamsen, D.H. Farrelly, A. Pitois, P. Warwick, N.D.M. Evans, L. Knight and N.D. Bryan".

FZD studied the impact of humic acid (HA) on the sorption of Am(III) on clay minerals using kaolinite as a model mineral. The sorption experiments were carried out under ambient atmosphere ($pCO_2 = 10^{-3.5}$ atm) in a glove box, for an Am(III) concentration of 1×10^{-6} M and HA concentration of 10 mg/L in 0.01 M $NaClO_4$ solutions. The solid/liquid ratio was 4 g/L and the pH values were adjusted between pH 3 and 10. Kinetic experiments were performed to evaluate the time required to reach Am(III) sorption equilibrium (the same experimental conditions as in the sorption experiments, pH = 5). The sorption equilibrium was achieved very fast. 98% of Am(III) was adsorbed already after half an hour and the amount of adsorbed Am(III) did not change significantly within the time fame. In the absence of HA, Am(III) exhibits a very strong sorption onto kaolinite. It is almost independent of the pH value. The percentage of sorbed Am(III) amounts to 98% at pH 3 and to almost 100% at higher pH values. In the presence of HA there are small changes in the Am(III) sorption in comparison with the system without HA. At pH values < 5, HA enhances the sorption of Am(III) very slightly. Conversely, at pH values = 5.5, the presence of HA decreases the sorption of Am(III) in comparison to the system without HA due to the formation of dissolved americium-humate complexes. Generally, the trend in sorption behaviour of Am(III) in the presence of HA is consistent with the results reported in the literature for trivalent actinides. At low pH values the sorption was enhanced by the presence of HA, while at high pH values the presence of HA lowered the sorption. At pH > 8.5, HA has no influence on Am(III) sorption on kaolinite, which reaches almost 100%, as in the system without HA. Further batch experiments with varying experimental conditions will be performed. In addition, the Am(III) kaolinite surface complexes in the absence and presence of HA are studied by laser fluorescence spectroscopy.

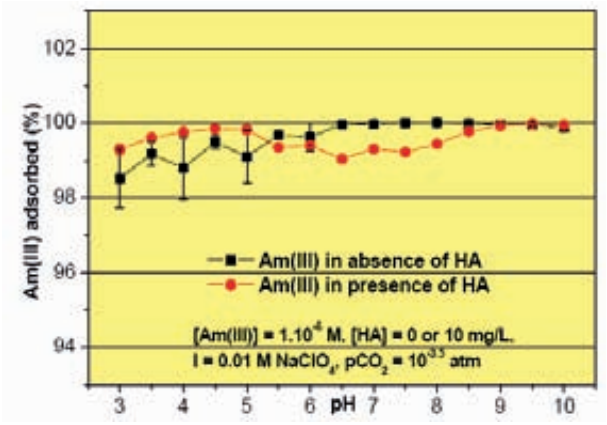

Figure 16: *Am(III) sorption onto kaolinite in absence and presence of HA (FZD)*

WU tackles the problem of non linear additivity interaction in ternary systems; metal-surface-HA. To model the adsorption of variable charge particles to charged surfaces, one has to be able to calculate the adsorption free energy involved. Expressions for the free energy change of variable charge particles were derived based on the equality of (electro)chemical potential of the particles in the bulk solution and adsorption phase. The expressions derived are called the "ADAPT model" (ADsorption and adAPTation), because they are based on the change of the average chemical state

(adaptation) of the particles upon adsorption. The LCD model (Ligand and Charge Distribution) has been recently proposed to describe the adsorption of humic substances to oxides, in which the CD-MUSIC model and the NICA model for ion binding to respectively oxides and humic substances are integrated. In this study, the LCD model is improved by applying the ADAPT model to calculate the equilibrium distribution of the humic substances. The improved LCD model is applied to calculate the adsorption of fulvic acid (Strichen) to goethite, in which it is assumed that the carboxylic type groups of fulvic acid can form inner sphere complexes with the surface sites. The calculation shows that the LCD model can describe sufficiently well the effects of pH, ionic strength and loading on the adsorption of fulvic acid. The model calculations indicate that the chemical complexation between fulvic acid and goethite is the main driving force for adsorption, while the electrostatic repulsion between the particles and the surface is the major limiting factor for further adsorption. This work is more developed in the scientific contribution in this volume: *"Improved ligand and charge distribution (LCD) model: L.P. Weng, W.H. Van Riemsdijk, T. Hiemstra"*.

INE's investigations focus in the first step on the effect of clay mineralogy, exchangeable cation composition (Na+, Ca^{2+}, Fe^{3+}) and temperature (25°C, 80°C) on the polymerisation of organic material. UV/VIS, µFTIR, XRD and STXM results demonstrate an increase of glucose+glycine polymerisation with temperature. The variation of exchangeable cation composition changed the degree of polymerisation in the order Fe^{3+}>>Ca^{2+}>Na^{+} and smaller clay size fractions (<0.15 µm) showed the highest aromatic content indicating a surface area catalysed polymerisation. Additionally, STXM images at nanoscopic resolution clearly show clay-OM association on edge sites and as coating in the glucose+glycine and catechol system. In the catechol system a formation of aromatic networks via C-O-C condensation could be observed, but a C=C (285.2eV) decrease indicates ring cleavage as a major process and dealkylation catalyzed by the clay surface. XRD analysis showed a small d001 increase of ~0.8 Å in the glucose+glycine system and peak broadening that can be explained by a size reduction of the coherent scattering domains (CSD). In the catechol and GoHy573 fulvic acid system the asymmetrical d001 peak and the shift in d003 indicates surprisingly the non-homogeneous distribution of organics in the clay interlayer. It turned out that the duration of polymerization experiments performed so far is clearly not sufficient to mimic the natural OM-clay system of the host rock formations (Opalinus Clay and Callovo-Oxfordian argillite). Further investigations, in cooperation with CEA, focused on the characterization of Callovo-Oxfordian extracted kerogen samples as well as aqueous extracts provided by the Associated Group (AG) UMR-CNRS. The extraction protocol was developed by J. Brevet during his PhD supported by Andra. Beside some inorganic impurities (pure carbonate and unknown minerals), relative uniform organic functionality has been found. The C(1s) spectra indicate a high aliphaticity of the kerogen and a considerable amount of carboxyl-type groups. Furthermore, the aromatic moieties seem to be condensed (poly-aromatic carbon like) and show no absorption in the energy region typical for phenol-type groups (286.6eV). Additional IR spectromicroscopy investigations at the U10B (NSLS) beam line with a 10µm spatial resolution on different regions of the kerogen confirm the C(1s) analysis and indicate high aliphaticity and C=O groups of carboxyl/ketone type. The mapping also indicates some heterogeneity concerning the distribution of ester/aldehyde type C=O in comparison to carboxyl/ketone C=O. Detailed analysis and interpretation of the

obtained results is underway. Overall, the data obtained so far clearly identifies oxygen-containing functional groups that might be available for radionuclide complexation.

WP1.4: Formation of solid solutions and secondary phases, including retardation of anions

The work is focussed on the thermodynamic definition of the standard state of solid solution and on experimental characterization of solid solution and secondary phases formation.

INE studied the structural incorporation of Np(V) into the host mineral calcite by co-precipitation in mixed flow reactors under steady-state conditions at room temperature. In this way reaction rates and partition coefficients can be determined under varying conditions. It was found that homogeneous partition coefficients for Np in calcite (0.5 – 11) are significantly higher than those reported for U(VI) (0.01-0.2). The local structural environment of incorporated Np(V) was characterized from the Np L3 EXAFS. The data suggest that the Np(V)-ions occupy calcium lattice sites. The two axial oxygen atoms of the linear neptunyl-ions substitute two carbonate groups in the first coordination sphere. Consequently, only four carbonates are observed to coordinate the neptunyl-ion. Np-O and Np-C interatomic distances (2.4Å and 3.3Å respectively) indicate slight structural relaxation of the carbonate groups from their ideal sites. A similar structural model is reported for U(VI) incorporated into calcite. This work is more developed in the scientific contribution in this volume: *"Np(V) co-precipitation with calcite: F. Heberling, M.A. Denecke, D. Bosbach"*.

The retention of Se(IV) on illite and synthetic montmorillonite was studied by ARMINES in the compacted state using capillaries for solid-to-liquid ratios of 9000 and 4600 g/L, respectively. The interaction was studied between pH 4 and 8 for Se concentrations varying between 5×10^{-3} and 10^{-6} M. The medium of investigation was 0.1 M NaCl and 0.05 M $NaClO_4$ for illite and montmorillonite, respectively. Effective diffusion coefficients of 1-2 – 10^{-10} m²/s were determined. To attain equilibrium, one month was shown to be necessary. At equilibrium, K_D values were obtained and compared with those measured in the dispersed state with the classical "batch method". No significant differences were observed. The data are reported in the deliverable PID 1.4.3. Se(-II)/pyrite system: pyrite was characterized (specific surface: 4.8 m²/g; number of site/nm²: 1.8). To allow the stability of both Se(-II) and pyrite, the experiments were carried out under a potential imposed in an specially designed electrochemical cell. The pH value and Se concentrations were chosen for the sorption studies so as to avoid precipitation or co-precipitation phenomena. Kinetic experiments showed that 1 day was necessary to reach equilibrium. The first K_D values have been obtained at pH 7 as a function of Se concentration.

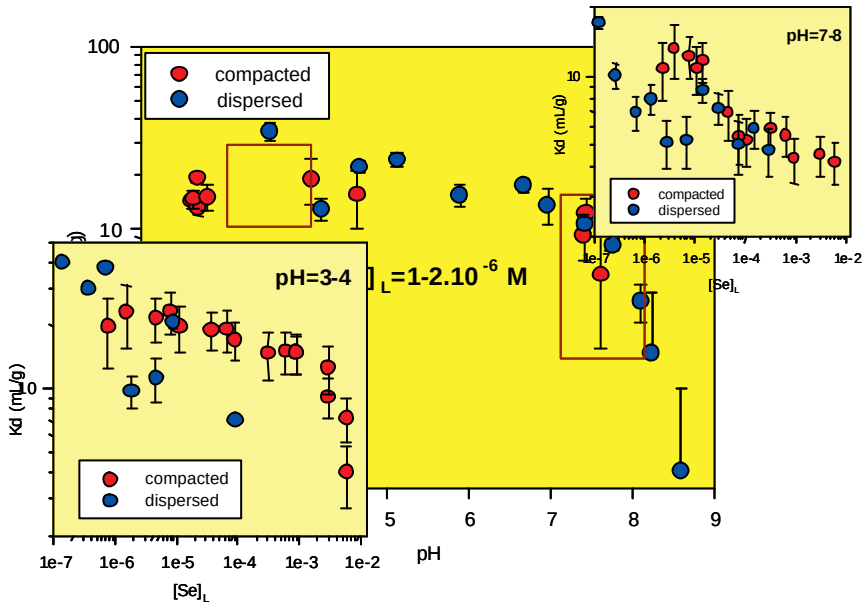

Figure 17: *Influence of compaction on the sorption of Se(IV) on montmorillonite (ARMINES).*

Perspectives

The activities of the partners and the new collaboration identified after the beginning of the project are progressing very well. A new activity between UNILOUGH in RTDC-1, and CEA and NRIRR in RTDC-2 on comparing actinide (IV)-humic complexation data has been identified.

The first RTDC meeting was hosted by CEA on June 3rd 2005 in Saclay (France). The second one was hosted by CTH on 30-31 May 2006 in Gothenburg (Sweden). The third RTDC-1 meeting will be hosted by UNILOUGH in June 2007 in Loughborough (United Kingdom).

RTD COMPONENT 2

Thorsten Schäfer
Institut für Nukleare Entsorgung (INE, Forschungszentrum Karlsruhe, P.O. Box 3640, 76021 Karlsruhe, Germany
schaefer@ine.fzk.de

Introduction

The overall objective of RTD Component 2 is to improve our knowledge on radionuclide retention processes which are currently not well understood in order to judge if they have to be considered for predictive analysis of the far field of geological repositories. The main topics dealt with in RTD Component 2 are the effect of the presence of inorganic/organic colloids, mineral redox processes and several aspects of microbiologically mediated processes on the transport of radionuclide. Knowledge gained in RTDC-2 will be transferred as direct input parameters for the host rock specific RTDC's 3-5. Scientific work in the nanometer resolution range with trace radionuclide concentrations expected to be found in far-field environments are a big analytical challenge and progress of scientific process understanding therefore relies *inter alia* on further development of analytical methods as well as on molecular modeling approaches. RTD Component 2 has been structured in 4 work packages and results obtained in the second project year are briefly summarized for each WP. Further, in detail information can be found in the **S**cientific & **T**echnical contributions and publications listed in chapter 4.

Advances within work packages

WP2.1: Formation, migraton and transport processes of inorganic colloids

In WP 2.1 the formation, migration and transport processes of inorganic colloids are investigated under near-natural conditions. Objective is a detailed process understanding and the determination of the fundamental thermodynamic parameters for the quantification of mineral surface interaction mechanisms and actinide sorption/desorption kinetics of inorganic colloids in relevant far-field systems. The studies in this work package include also the interaction of organic and inorganic colloids and the fate of radionuclide in this mixed systems.

FZK-INE continued to identify the geochemical conditions for the stability of montmorillonite colloids (derived from Febex bentonite) in granite ground waters. The experiments are carried out by varying pH, ionic strength and type of electrolyte. The dynamic light scattering technique (photon correlation spectroscopy) is used to measure the size evolution of the colloids with time. Agglomeration rates are higher in $MgCl_2$

and $CaCl_2$ than in NaCl solution. Relative agglomeration rates follow approximately the Schulze-Hardy rule. Increasing agglomeration rates at pH>8 are observed in experiments with $MgCl_2$ and $CaCl_2$ which are, however, caused by coprecipitation phenomena with carbonate phases. Bentonite colloid stability fields derived from the colloid agglomeration experiments predict low colloid stabilization in granite ground water taken from Äspö, Sweden, and relatively high colloid stability in Grimsel ground water (Switzerland) (*see S&T contribution Seher et al.*). Preliminary studies on the influence of low dissolved organic carbon concentrations (1mg/L DOC) typically found in granite formations show an increase of montmorrilonite colloid stability especially in the pH region below 8 where colloid platelet edge-face interaction is expected forcing colloid aggregation.

Partner TUM-RCM together with partner FZK-INE concentrated on the question whether actinides are prone to co-nucleate with Si and Al under normal conditions of temperature and pressure within a pH range of 4 – 9. Optimum conditions for the formation of HAS pseudocolloids of actinides are derived from a broad parameter screening experiment based on radiometric tracing of the actinides as they are distributed between three phases: solution (< 1.5 nm), colloids (1.5 – 450 nm) and precipitate (> 450 nm). Phase separation is performed by sequential filtrations. The chemical binding state of the actinides incorporated in the HAS colloids is analyzed by time-resolved laser fluorescence spectroscopy (TRLFS) , extended X-ray absorption fine structure spectroscopy (EXAFS) as well as by the ligand displacement method with EDTA. The results prove that all conditions enhancing actinide hydrolysis such as high pH, high concentration of actinide or co-nucleating elements (Si, Al), long reaction times, etc. also increase the actinide/HAS colloid binding affinity. Further investigations focused on the hydroxy-aluminosilicate colloids generation in the presence of humic acid at neutral pH, and how trivalent actinides are integrated into the process. For the experiment, ^{241}Am-tracer is introduced into colloid mother solutions where a competition takes place between two ligands, namely ^{14}C-labelled humic acid and silicic acid for the complexation of two trivalent metals Al and Am. The speciation of colloid-borne Cm(III) is made by TRLFS using direct (382 nm) and indirect (370 nm) excitation. The binding affinity of Am and Al for silicic and humic acid, leading to incorporation of the trivalent metals into the colloidal phase, is correlated with their different hydrolysis behaviour. The less hydrolyzing Am, as compared with Al, is favoured at the complexation with humic acid but discriminated at the conucleation with silicic acid. Under conditions promoting the hydrolysis of Am, e.g. at increased concentration of silicic acid above saturation, pH ≥ 7, and a humic acid concentration < 10 mg/L, synergic bond coupling of hydrolyzed-ionic Am species yields mixed, hybrid HAS-Am-humic colloids (see Fig. 1). Analysis of the mixed colloids by laser-induced breakdown detection (LIBD) reveals particles with an average size of a 10 nm hard sphere diameter, comparable to that of Am-HAS colloids, and remaining stable within

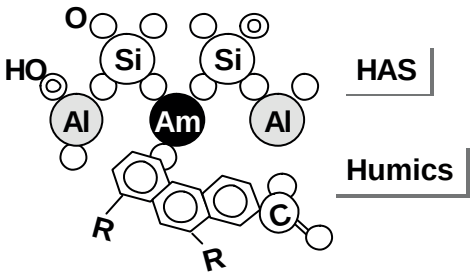

***Figure. 1**. Illustration of hybrid HAS-Am-humic*

two-months period of observation. The present study shows that the main natural aquatic colloids of HAS and humic acid bind actinides following different and complementary mechanisms enhancing the stability region of colloid-borne actinides (*see publication Kim et al.)*. Additional studies of TUM-RCM focused on the analyzes of the mechanisms regulating the binding affinity of humic colloids to metal ions of higher oxidation state (≥ 3), such as actinides, under conditions inherent to the natural aquatic system. ^{241}Am(III) or ^{234}Th(IV) were conditioned with ^{14}C-labelled humic acid colloids are separated from precipitate and solution by sequential filtration (450 nm and 1.5 nm). Formation of colloid-borne humic acid and actinide in the neutral pH range is ascertained radiometrically by determining the phase distribution of ^{14}C and Am(Th), separately. The binding affinity of Am and Th to humic acid, leading to their incorporation into the colloidal phase, can be correlated with their different tendencies to hydrolyze. These results show that humic colloids, contrary to HAS colloids, possess the maximum affinity for actinides under all conditions favouring the cationic actinide species *(S&T contribution Priemyshev et al.*).

Investigations into the formation of intrinsic colloids and pseudocolloids of uranium(IV) were performed by partner FZD. Coulometric titrations of strongly acidic U(IV) solutions in $HClO_4/NaClO_4$ medium were carried out in order to find the pH of first colloid formation. Quantification of traces of U(VI) by laser fluorescence spectroscopy proved that the tetravalent state of uranium had been maintained. LIBD was applied for the detection of traces of uranium colloids as the pH was increased. The pH values at the onset of colloid formation (see Fig. 2) were used for thermodynamic calculations aimed at determining the solubility products K_{sp}^0 of crystalline and amorphous uranium dioxide. The particle size of the colloids determined by means of LIBD was taken into account since it influences the solubility product. The results indicate the formation of crystalline UO_2(cr) at low pH~1 ($\log K_{sp}^0 = -59.6 \pm 1.0$) whereas the amorphous hydrous oxide $UO_2 \cdot xH_2O$(am) is formed at pH 2 to 3 ($\log K_{sp}^0 = -54.2 \pm 1.0$). Measurements by EXAFS, XRD and SEM corroborated the occurrence of these UO_2 phases. The obtained solubility products fit well in the known series of solubility products of the other tetravalent actinides and confirm the results of classical studies based on phase separation where the maintenance of uranium in the tetravalent state was ensured *(see Opel et al.)*.

Furthermore, the $UO_2 \cdot xH_2O$(am) colloids were investigated for their colloidal stability. The point of zero charge was found at pH - 6.9. Colloidal suspensions of 1 mMol/L $UO_2 \cdot xH_2O$(am) at a pH value of 2.5 proved to be stable over > 1.5 years if stored in an inert gas glove box and did not aggregate, which is in accordance with the relatively high zeta potential (= 30 mV).

The interaction of the forming $UO_2 \cdot xH_2O$(am) colloids with other colloid-forming species was tested. Therefore, coulometric titrations of U(IV) solutions in the presence of (a) dissolved Al(III) and (b) dissolved silicate were carried out. The presence of Al(III) does not significantly influence the formation of the $UO_2 \cdot xH_2O$(am) colloids, and the U(IV) does not significantly influence the behaviour of Al(III). Also silicate does not significantly influence the $UO_2 \cdot xH_2O$(am) colloid formation. However, the presence of U(IV) significantly influences the behaviour of the silicate. The nature of the interaction between the silicate and the U(IV) is not yet known (adsorption, possible formation of a coffinite precursor). Therefore, EXAFS experiments to elucidate the

local structure around the U(IV) atoms in the pseudocolloids have been performed end 2006.

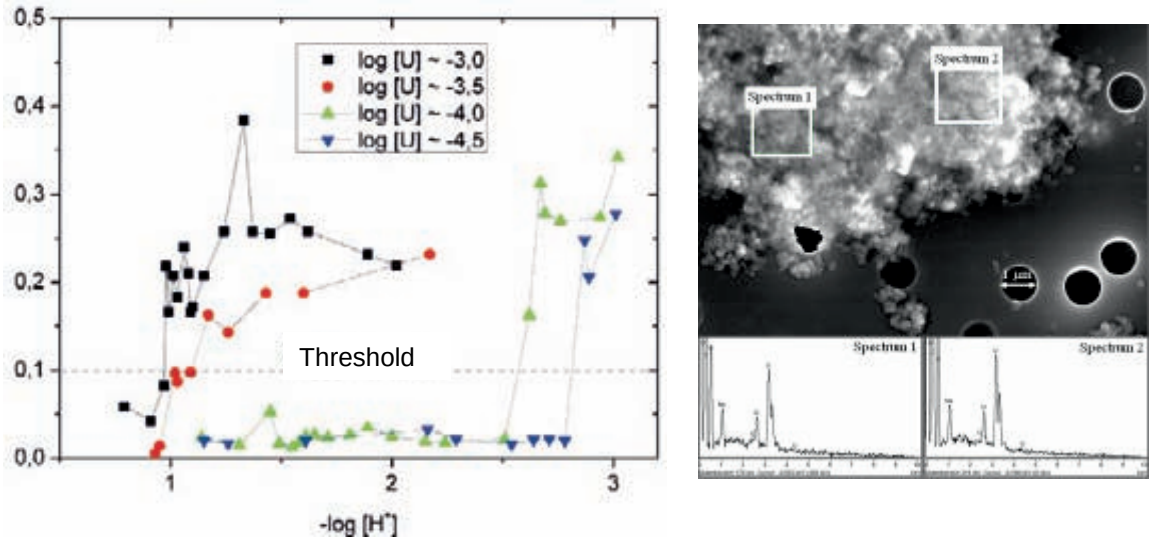

Figure 2. *(left) LIBD (laser pulse energy 1.5 mJ) derived breakdown (BP) probability as a function of pH. BD values over the threshold indicate an onset of colloid formation during the coulometric titration as a function of uranium concentration. (right) SEM image and EDX spectra of the $UO_2 \cdot xH_2O(am)$ produced by coulometric titration.*

WP2.2: Formation migration and transport processes of organic/humic colloids

In WP 2.2 the formation, migration and transport processes of organic/humic colloids are investigated. The main objective of this work is to provide process understanding and a fundamental thermodynamic basis for the interaction of humic colloids with radionuclides. This includes understanding of the complexation kinetic behavior. The work described here is aimed at obtaining a thermodynamically sound description of the metal ion humic matter interaction process and an evaluation of the interactions between organic colloids and radionuclides.

Spectroscopic investigations on the trivalent lanthanide and actinide humic substance (HS) complexation were carried out in close collaboration between the partners UPPC, FZK-INE, UNICYPRUS and CEA. Partner UPPC has continued the work on steady-state and time-resolved luminescence measurements of Ln(III) ions (Ln(III) = Eu(III), Tb(III)). The work focused on the investigation of intra- and intermolecular energy transfer processes in Ln(III)-HS complexes. The understanding of such has to be further developed in order to properly evaluate the experimental data obtained from time resolved laser fluorescence spectroscopy (TRLFS) measurements, e.g., to account for effects originating from quenching processes and for effects originating from the heterogeneous character of HS. With this respect, also “simple” model ligands (building blocks of HS), such as hydroxy-substituted benzoic acids, were investigated.

- Time-resolved fluorescence anisotropy experiments with humic substances (HS) in the absence and presence of Eu(III) were continued. The intrinsic HS (HS = Gohy573 HA, Aldrich HA and olive cake HS) fluorescence anisotropy changed upon Eu(III) complexation as well as upon changing the temperature. “Dead”

biomass by-products (e.g. olive cake) originating from plant tissues are ubiquitous and hence leached/extracted degradation products of this material could play a significant role on the migration of radiotoxic metals in the repository far-field. From the results it is concluded, that the metal complexation causes a "contraction" of the HS molecule *(see S&T contribution Eidner et al.)*.

- The sensitisation of luminescence in HS-Tb(III) and HS-Eu(III) complexes was further investigated. For HS-Tb(III) an activation energy of the energy back transfer from the Tb-ion to HS was calculated from temperature dependent luminescence measurements.
- From luminescence measurements at 5K the position of the $^5D_0$-$^7F_0$ transition has been determined for Eu(III) complexes with different model ligands and with a fulvic acid isolated from the Gorleben aquifer (GoHy573 FA). Further, the ultra low-temperature spectra were analysed with respect to the $^5D_0$-$^7F_1$ and $^5D_0$-$^7F_2$ transitions and the ligand field strength parameter N(ν) was determined. From the data the symmetry of the complexes formed with the different ligands was concluded.

FZK-INE investigated furthermore the reduction sequence of Pu starting with Pu(VI) in presence of hydroquinone (HQ) and fulvic acid (FA) as reducing compounds at various pH values between pH 1 and 7. The Pu species were monitored by UV-Vis spectroscopy and liquid-liquid extraction. The experiments showed that Pu(V) and (VI) are not stable in aqueous solutions containing hydroquinone or fulvic acid (FA) at pH 1 to 7. With 200 mg/L FA the reduction of Pu(VI) to Pu(V) is fast and complete after 30 minutes at pH 3. Compared to the reduction reaction at similar concentration of HQ, the FA reduction is slower. Pu(V) in same solutions is converted to Pu(IV), the most stable oxidation state in aqueous solutions containing FA at pH 3 - 7 (relevant for natural aquifers). Reduction of Pu(IV) to Pu(III) was found only at pH values < 5 for HQ and < 3 for FA. The reactions were also monitored by Eh measurements.

The present studies showed that a correlation between Eh values and thermodynamic calculations might be a capable tool for modelling redox reactions between Pu ions and hydroquinone or hydroquinone-like compounds like FA (see Fig. 3). It cannot be excluded that Pu(III) is more stable in solutions containing organic compounds with lower redox potential than the GoHy-573-FA batch used in the present studies *(see S&T contribution Marquardt & Seibert)*.

Partner UNICYPRUS studied humic acid (extracted degradation product of plant tissues; olive cake) interaction with a heavy metal ion e.g. Cu(II). Extraction and purification of the «olive cake» humic acid has been performed by alternating alkaline dissolution and acid precipitation. Characterization of the purified sample has been carried out by ICP-OES, FTIR, UV-Vis, TOF-MS, AFFFF. The interaction of the humic acid with Cu(II) ion has been studied by potentiometry using a Cu(II) ion selective electrode in aquatic solutions under normal atmospheric conditions at I = 0.1 M $NaClO_4$ and pH = 6 and the formation constant for the Cu(II) HA complex has been determined (5.3 ± 0.4). Furthermore, the structural characteristics and complex formation behaviour of «olive cake» humic acid with soil derived humic acids (Gorleben system) has been compared.

The studies on the solubility and stability of $UO_2(OH)_2$ and UO_2CO_3 solids as a function of the humic acid concentration in 0.1 M $NaClO_4$, in the pH range from 4 to 9, under normal atmospheric conditions and 4 and 6 under 100% CO_2 atmosphere, has been continued. Furthermore, the solid phases under investigation have been characterized by DRIFTS, XRD and solubility measurements. The experimental data have been evaluated and based on the solubility data (under atmospheric conditions) and the stability constant for the $UO_2OH(HA)$ has been determined *(see S&T contributions Kolokassidou)*.

The partner CEA has tackled several items during the second year that can be summarized as follows:

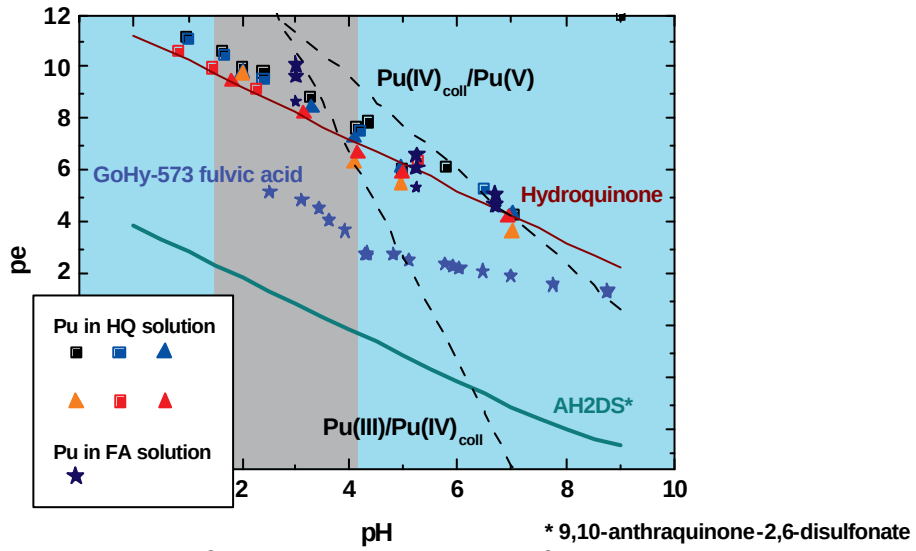

Figure. 3*. Eh measurements of hydroquinone (HQ) and fulvic acid (FA) solutions. The HQ and FA concentrations exceeded the total Pu concentration. Lines (solid, dashed) show thermodynamic calculations and the grey area symbolises the Pu(III)/Pu(IV) transition zone obtained from the experiment.*

- One of the techniques that have been used frequently to measure the free metal ion concentration of bivalent cations is the Donnan Membrane Technique (DMT). However, this method has limitations in terms of a relatively high detection limit (in relation to typical environmental concentrations) and a long equilibration time. CEA has therefore developed the Flux Donnan Membrane (FDM) technique, which is a dynamic modification of the standard DMT. It has been shown that experimental calibrations of metal ion transport in the FDM can be used to measure $[M]_{free}$ under conditions of either solution-controlled or membrane-controlled diffusive transport. The FDM was used to measure Co(II) and Mg(II) binding isotherms by a humic substance (HS) over a large range of free metal concentrations and pH *(see publications number 8-9)*. Application of the FDM method to the UO_2^{2+}-Mg-HS system worked at pH4, but clearly showed limitations at pH>5 due to the precipitation of U(VI) phases and electrostatic effects within the membrane. Therefore, application of this method for Th(IV) complexation studies is not promising and currently tests are underway to evaluate

the best alternative technique (i.e. dialysis, insolubilisation and the surface immobilized HS from NRIRR) to obtain the these data.

- The study of fractionation of NOM at the mineral surfaces was continued. During this year, the main objective was to characterize the Suwannee River Fulvic Acid (SRFA) and the Gorleben Humic Acid (GoHyHA) fractionation on α-Al_2O_3 using spectroscopic techniques (UV/VIS, C(1s)-NEXAFS) and mass spectrometric techniques *(see Claret et al.)*. For SRFA, a clear fractionation consisting of enrichment in aromatic functional groups on the alumina surface has been detected by both UV/Vis and NEXAFS spectroscopy, whereas for GoHyHA fractionation understanding is still pending. Mass spectrometry has been applied, but the salt content of our samples drastically reduced the organic signal and methods of salt removal are currently investigated.
- Characterisation of some real organic extracts from the Callovo-Oxfordian formation (as input for RTDC-3) and the complexation behaviour with lanthanides of these extracts were studied in collaboration with the Associated Group (AG) UMR-CNRS. The extraction protocol developed by J. Brevet during his PhD granted by Andra consists of an extraction with different polar compounds and acid alteration. The characterization was made by C1(s) NEXAFS spectroscopy. A comparison with previous obtained C(1s) NEXAFS on Opalinus and Callovo-Oxfordian isolated fulvic acid and humic acid (MHM FA and HA) using an alkaline extraction protocol suggests that the differences in extraction procedures lead clearly to differences in carbon functional groups distributions. Using acidic protocol, the ratio of carboxyl groups versus other carbon functionalities is probably higher than for OPA or MHM FA and HA. The complexation behaviour of organic extracts obtained after acid alteration toward europium (III) was studied by time resolved laser induced spectrofluorimetry *(see S&T contribution Brevet et al.)*. Again, the fluorescence spectrum and decay are strikingly different to the ones obtained on alkaline extraction products of the Callovo-Oxfordian argillite, and resemble a lower molecular weight organic fraction.

NRIRR in cooperation with FZK-INE and CEA has worked on the chemical immobilization of humic acids on silica gel and magnetite to facilitate investigations of the influence of humic substances (HS) on the migration of radionuclides. It is anticipated that these materials might serve as geochemical models of the humate-coated minerals that are likely to be present in the vicinity of the repositories. These solid phases have been characterized by BET surface area, C-content, HA-content, FTIR and acid-base titration. The complexation behavior of surface bound humic acid with Ag-110m, Sr-85, Am-241 and tetravalent radionuclides (Th, Pu) was investigated and the comparison with published literature data shows that these surface bound humic acids can be used for the determination of conditional stability constant ($\log_{10}$ ß) of nuclides with humic substances. Th(IV)-humate conditional interaction constants have been obtained by acquiring, at pHs 1-9, for SiO_2-HA non-linear regression binding isotherms of Th in 0.1 mol l^{-1} $NaClO_4$ solutions. The β_{ThHA} varies between $10^{7.58}$ at pH 1 to $10^{24.35}$ at pH 9. A satisfactory agreement with literature data sets have been resulted between pH 3-9. The pH dependence of the $\log_{10}$ ß can be described by the following equation: $\log_{10} ß_{Th} = 2.54\ pH - 0.22$ ($r^2 = 0.942$)

Furthermore, interaction of plutonium with HS has been investigated by a batch method use of the surface bound humic acid from perchlorate solutions at pH 1-6. By using these novel solid phases, complexing capacities and interaction constants are obtained. Pu(IV)-humate conditional stability constants have been evaluated by using non-linear regression of binding isotherms. The results have been interpreted in terms of complexes of 1:1 stoichiometry. *(see two S&T contributions by Szabó, and one S&T contribution by Guczi and Reiller, respectively)*

Partner SAS-IIC has developed and implemented a new method for relativistic quantum-chemical calculations of NMR spectra, using a new DKS2-RI approach developed by the SAS-IIC group recently. The approach treats spin-orbit relativistic effects variationally (two-component non-collinear unrestricted DFT approach). This new method allows one to calculate NMR chemical shifts on heavy nuclei. For calculation of ^{17}O and ^{13}C paramagnetic NMR (PNMR) shifts on ligand nuclei of a lanthanide complex with salicylic acid in water solution a perturbational approach developed recently was applied. These complexes served us as model compounds for simulation of more complicated lanthanide complexes with humic acids. The obtained data demonstrate that paramagnetic NMR spectra are very sensitive to the bonding details of the ligand. The calculations are in reasonable agreement with earlier experimental studies. The results of these calculations demonstrate that complexes with the single-bonded ligand are more stable. The analysis of the predicted NMR spectra and previous experimental data supports this finding. New experimental studies with the enriched ^{17}O and ^{13}C nuclei of carboxylate groups of the salicylic and humic acids are extremely desirable. SAS-IIC believes that the pilot studies form a firm basis for future joint theoretical/experimental investigations which would provide important structural information on the structure of humic/radionuclei complexes *(see S&T contribution Hrobárik et al. and publications 5-7).*

NRI-REZ research activities on sedimentary samples originating from the Ruprechtov site (Tertiary plastic clay with variable content of organic matter) continued based on results reached during the first year of FUNMIG project (details see PID2.2.7).

Additional information on organic matter content in different compartments of the Ruprechtov site were collected. The sampling focussed mainly on DOC concentration uncertainties in groundwater that were clarified (TOC - DOC relations). The great groundwater geochemical data set collected from various boreholes allows statistical treatment (HCA and PCA were applied - basic correlations have been identified). Furthermore, micro-petrographical characterisation of a reference sample with lower organic content (Tertiary clay, TC = 1.3 wt.%) was finalized. The study surprisingly revealed that an important part of organic matter was in immature state (recognizable remnants of plant tissues in low coalification stage, algae fragments, spores, etc.) and cannot explain the low DOC concentrations found in the groundwater. Groundwater organic matter was characterised by MALDI-TOF-MS (5 samples, both concentrated/evaporated and natural groundwater samples). The spectra of non-concentrated and concentrated samples are nearly identical (small differences can be caused by volatility of some sample compounds). Mass spectra indicate that rather lower molecular organic matter prevail in groundwater ("fulvic acids"). Fraction of HA with 1000 m/z is minimum. The most distinct spectrum has NA5 groundwater (see Fig. 4).

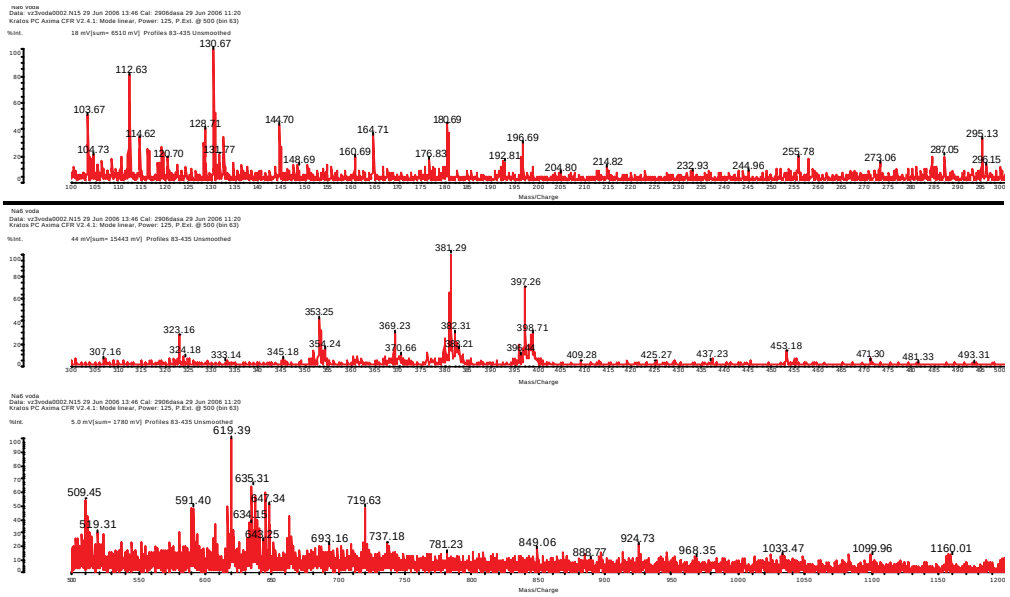

Figure. 4. *MALDI-TOF mass spectrum of groundwater NA5 (Ruprechtov site) indicating rather low molecular weight organic matter.*

Important part of work was focused on continuation of separation and characterisation of humic acid from a reference sample with higher content of organic matter (TOC = 4.1 wt.%). Mainly purification steps were highly improved due to tight association of sedimentary organic matter - clay (HA separated during the first stage of project has high content of inorganic components). Currently, 4.1 g of purified HA is available. IR spectra, organic analysis, acid-basic titrations and additional characteristics are underway. Alternative separation schemes applied (MIBK method, simple ultrasonic disaggregation method) for organic matter gave ambiguous results and therefore have to be improved in the upcoming year.

SCK·CEN and KULEUVEN are jointly working together on site specific questions related to the Boom clay formation. During the last year the work performed by KULEUVEN was mainly focused on the interaction of Se with "dissolved" natural organic matter (NOM). In Boom Clay, this dissolved NOM was obtained by a ~ 0.01 M $NaHCO_3$ extraction of the clay solid phase. Batch experiments were performed in which the interaction of Se(IV) and Se(VI) with dissolved Boom Clay and Gorleben humic substances was followed as a function of time. Particulate NOM and larger colloidal particles (> 25 nm) were first removed by centrifugation. The supernatant solutions were analyzed by a combination of ion chromatography, gel permeation chromatography and ultrafiltration to determine the Se solution speciation (Fig. 5). Experiments on SeO_4^{2-} Boom Clay NOM or Gorleben NOM interaction in synthetic Boom clay pore water (SBCW) background electrolyte (pH ~ 8.3) showed no changes in total Se solution concentration and Se speciation indicating negligible Se(VI) - NOM interaction in the three months' observation period. Upon contacting SeO_3^{2-} with the same HS-containing solution however, a decrease of ~ 95% in total Se solution concentration after centrifugation was noted and final Se solution concentrations of

4.4×10^{-8} M (Boom Clay NOM) and 1.3×10^{-7} M (Gorleben NOM) were measured after a six month observation time. Together with the decrease in total solution concentration, a change in the Se solution speciation was determined. After one month, the solution speciation in both systems was dominated by a colloidal Se species that was associated with NOM. The SeO_3^{2-} concentration decreased steadily to a final concentration of 1.9×10^{-8} M (Boom Clay NOM) and 1.5×10^{-8} M (Gorleben NOM). XANES-EXAFS measurements on these samples were collected at the DUBBLE BM26A beamline at the ESRF (Grenoble, FR) to elucidate the molecular nature of the different Se solution species, and more in particular of the species associated with NOM. Analysis of these data is currently being performed. Future experiments at KULEUVEN will investigate the interaction of Se(+IV) with purified Boom Clay humic acid, as well as the interaction with immobile NOM.

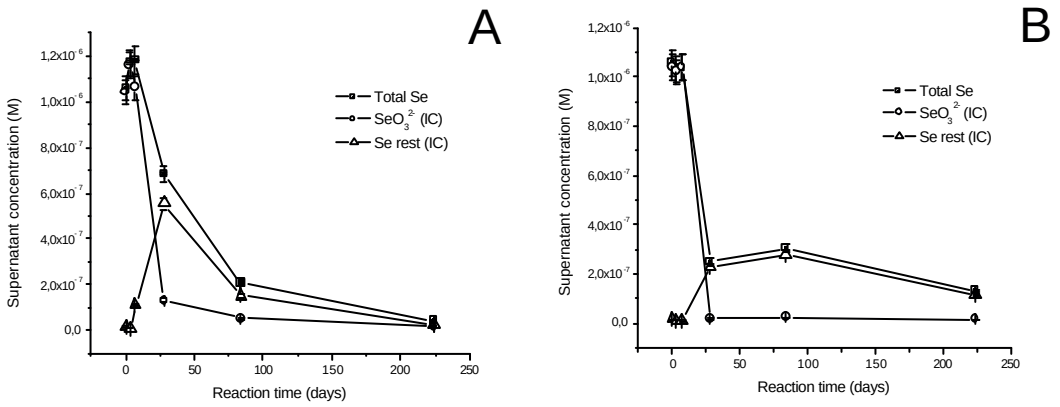

Figure 5. *Total Se concentration in solution and Se solution speciation in the supernatants after centrifugation as measured by IC, plotted as a function of equilibration time for systems initially containing $1\cdot10^{-6}$ M $^{75}SeO_3^{2-}$ and 128 ppm Boom Clay OM (figure A - left) or 160 ppm Gorleben OM (figure B - right). SeO_3^{2-} and SeO_4^{2-} concentrations are measured directly by a combination of IC and gamma counting, while the concentration of "Se rest" is calculated as the difference between total Se and the Se oxyanions. SeO_4^{2-} concentrations in all samples were below detection limit and are not shown on the figures.*

In order to provide SA/PA with sound data and conceptual models on the migration behaviour of tri-and tetravalent radionuclides in the Boom Clay, investigation on the speciation in the Boom Clay pore water, the interaction with possible complexing agents and its interaction with the solid phase are prerequisite. The idea of solubility/colloid enhancing factor of mobile NOM will be further elaborated., As complexation of Am and U with mobile NOM is relatively well studied, the colloidal aspect nevertheless still needs more attention with regards to their mobility. More important, there is a lack of data concerning the interaction with the solid phase (especially for U(IV)): sorption onto minerals (and the role of NOM), interaction with immobile NOM, role of redox controlling minerals (and the role of NOM) (linked to WP2.3).

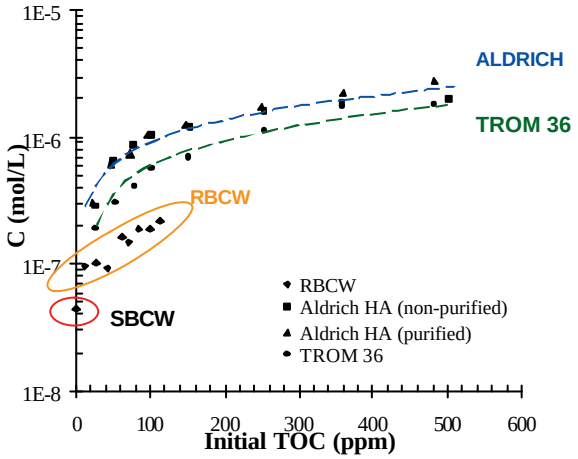

Figure 6. *Solubility of $Eu(OH)_3(cr)$ in Boom Clay waters at various concentrations of HA. The $Eu(OH)_3$ gradually changed to $Eu_2O(CO_3)_2$. The solubility determined in SBCW without NOM corresponds to 4.45e-08 mol/L and the solubility of $EU(OH)_3/Eu_2O(CO_3)_2$ is clearly increased through addition of NOM in the reference Boom Clay water (RBCW).*

The work of SCK·CEN acquiring site specific sorption data for Th (U) and Am (Eu) onto Boom Clay with the aim to establish a chemical sorption model based on the General Composite Surface Complexation Model approach is a close like to RTD component 1. SCK·CEN performed experimental work on the interaction of Th and Am with immobile NOM by means of adsorption experiments at high S/L ratio's in which attention was paid on the Am/Th partitioning towards the immobile NOM phase. These experiments were also used to prepare the sorption work within RTDC1. The SCK·CEN work on the interaction with immobile NOM will now concentrate on sorption experiments with isolated kerogen fraction (Kerogen isolated from Boom Clay by IFP). SCK·CEN conducted experiments on the solubility enhancing effect of mobile NOM on Eu. Previous investigations (EC project TRANCOM-II) showed the effect of dissolved NOM (Boom Clay NOM and Aldrich HA) onto the solubility of UO_2(am) and ThO_2 in real and synthetic Boom Clay pore waters (pH~8.3), For amorphous UO_2 the solubility (~10^{-8} mol/l, 30 kD ultrafiltration) was unaffected by NOM, but a strong colloid formation effect was observed increasing the total U in solution by 4 orders of magnitude. The nature of these colloids was mainly inorganic but an influence of NOM was noticed. A similar effect was observed for Th but here the colloids were mainly organic. Similar experiments were now conducted for Eu which has the advantage that more thermodynamic data is available which can help in the interpretation of the phenomena (see Fig. 6). Eu interacts with NOM by complex and colloid formation. The solubility (<30 kD) increases up to 1 order of magnitude due to complex formation, while the apparent solubility due to colloids formation increases up to 3 orders of magnitude. With respect to transport a more detailed characterisation of the size distribution of natural organic matter is needed to make estimations on colloid mobility. Contact with FZK-INE is established to perform flow-field flow fractionation (FFFF) analysis.

WP2.3: Radionuclide redox transformation on minerals

In WP 2.3 the impact of electron transfer processes at inorganic mineral surfaces on the retention of radionuclides is analyzed. The main systems investigated are Fe(II)-bearing minerals commonly found in granitic and in clay environments using advanced redox sensitive surfaces spectroscopy and microscopy. The investigations of KU, FZK-INE, FZD and KTH focus on redox processes in fractured rocks or mineral components thereof.

The study of partner KU on the structure of green rust sulfate is now complete. It has been proven that green rust incorporates both sulfate and either sodium or potassium (depending on solution conditions) in the hydrated interlayer (see Fig. 7). Evidence comes from chemical data, atomic force microscopy (AFM), X-ray diffraction (XRD) and transmission Mössbauer spectroscopy (TMS). Experiments to determine the thermodynamic properties of green rust sulfate are ongoing. Methods and experimental conditions have been tested and preliminary results have been obtained in the year 2006. Tests to determine the lower limit of aqueous ferrous iron concentration required for $GR_{Na,SO4}$ formation could show at an ionic strength of 10^{-2} M that Fe^{2+} and SO_4^{2-} concentrations as low as $2 \cdot 10^{-3}$ M are sufficient to form $GR_{Na,SO4}$.

KU has furthermore developed a method for investigating the interaction between green rust and redox sensitive elements and has defined mechanisms of reaction. Investigations of the interaction between green rust and chromate (Cr(VI)) can now be used as a base for studies of other compounds. Reaction rates were rapid and the end product was a Cr(III)-goethite (see Skovbjerg et al.) The interaction between green rust sodium sulfate ($GR_{Na,SO4}$) and oxidized selenium species is under investigation. Results so far indicate formation of metallic selenium or Se(-II) species, depending on initial concentrations.

Preliminary experiments on the uptake of lanthanides (as a model for trivalent actinides) by green rust indicate preferential incorporation of the heavier lanthanides. The interaction between Np(V) and $GR_{Na,SO4}$ has been investigated in collaboration with FZK-INE using several methods. Np(V) was reduced by green rust and removed from solution. During re-oxidation of the Np(IV)-GR solution, part of the Np(IV) re-oxidised to Np(V) and was released back to solution. The rest of the Np is likely to have been incorporated in the final iron(oxyhydr)oxide.

Furthermore, the attachment probability of GR colloids for typical fracture-filling materials was investigated. In-situ studies of green rust attachment to several mineral surfaces in solution under anaerobic conditions were performed. The results so far have shown that green rust sulfate attaches well to most fracture minerals. However, during oxidation, the green rust dissolves and reprecipitates as goethite, which offers the potential for adsorbed and incorporated components to be remobilized.

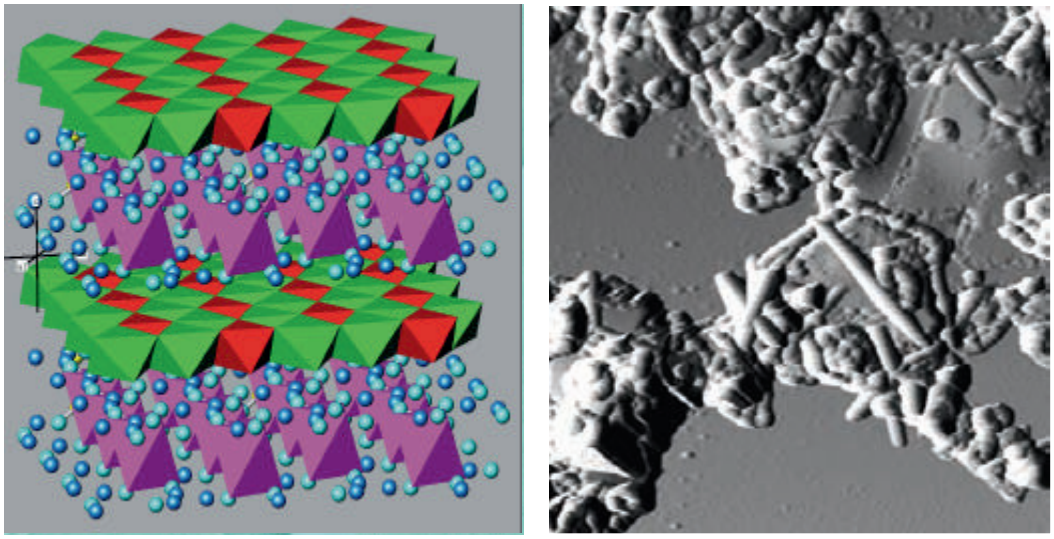

Figure7. *(left) Structural model of green rust sodium, sulphate ($GR_{Na,SO4}$) with P- 3 symmetry and a = 9.52 Å; c = 10.93 Å. (right) AFM image on reacted $GR_{Na,SO4}$ with SeO_4^{2-} showing comparable features (reaction rims) to the results obtained for chromate reduction (scale bar* 1µm).

FZK-INE performed batch sorption experiments with redox sensitive actinide elements such as Pu, Np and U as well as the fission product Tc are performed onto fracture filling material, which are obtained from Äspo Hard Rock Laboratory. Migration experiments using these elements showed a complex retention pattern along the flow path. For this reason a new SEM/EDX analysis technique was applied for identification retaining mineral phases. From previous investigations, it is known that Np(V) is retained by reduction to Np(IV) in the presence of Fe(II) minerals. The sorption coefficient for Pu is significantly higher compared to Np or U. Pu retention takes place on a multitude of minerals. Sorption of U is also strongly correlated with the occurrence of Fe oxide phases *(see S&T contribution Römer et al.)*. Post-mortem analysis on fracture surfaces of cores used in migration studies by microfocusing synchrotron based techniques have been performed and the data is currently under evaluation.

FZD has carried out investigations on the effect of sorptive reduction of actinides (U) surface species on a ferrous iron containing silicate biotite, typical for granitic host rocks. The experiments on biotite suspension (grain size 63 to 200 µm) were completed in 0.01 M NaClO4 media at various pH values (6.0 to 7.5) and different total uranium concentrations (1×10^{-5} M and 2×10^{-6} M) using a solid concentration of 12.5 g/L. All samples were in equilibrium with atmospheric CO_2. After 3 days contact time samples were centrifuged at 67500 g for 1 hour. To overcome Fe quenching effects and to improve the fluorescence intensity Kryo-TRLFS measurements were carried out at –120 °C. These Kryo-TRLFS investigations revealed a strong shift by approx. 10 to 15 nm for the first two peaks to lower wavelength. By comparison with published data this shift may indicate the presence of ternary uranium carbonate species ($((UO_2)_2(OH)_3CO_3^-$ and $UO_2(CO_3)_3^{4-}$). To find out if sorptive reduction of U(VI) has taken place the

respective samples were excited at 245 nm. This wavelength specifically excites U(IV) and triggers a charachteristic U(IV) fluorescence spectrum. No U(IV) could be detected and in conclusion it can be stated that the sorptive reduction seems to play an insignificant role in the immobilization behaviour of aqueous U(VI). However, the sensitivity of the method and in addition possible quenching effects caused by the presence of Fe impede a final statement to this topic. Work concerning the sensitivity and the quenching behavior in the presence of iron will be continued with internal funding.

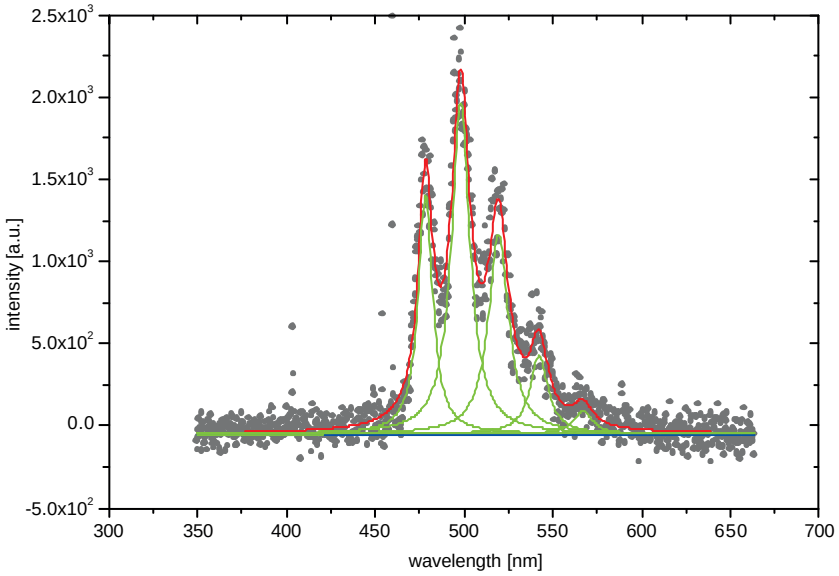

Figure 8. *Kryo-TRLFS spectra of a biotite suspension sample (pH 6.05, U_{Total} = 1×10^{-5} M) measured at -120°C.*

KTH studied the influence of mineral bond structural Fe(II) on the U(VI) reduction to describe the retention process of U by these minerals in terms of quantity and kinetics at natural conditions (especially in bicarbonate solutions). Experiments have been performed with Fe(II)-containing minerals frequently occurring in granite (magnetite, biotite, pyrite) and with similar Fe(II) free minerals (hematite, phlogopite, galena). After preparation of the natural minerals (particle size 20-50 or 50-90 µm) and characterization of the produced powders (by XRD, BET, XRF, SEM) batch and thin film flow-through reactor experiments were performed.

In batch experiments the minerals reacted with uranyl solution (0.8 – 800 µM) under near natural conditions (0.1M NaCl, 1mM bicarbonate, anoxic). U retention (adsorption+ reduction) was quantified by monitoring the aqueous concentration of uranium over time (1 month). Comparison of water chemistry results within the three mineral pairs indicated that reduction of U(VI) by Fe(II) in biotite and magnetite and by sulphide in galena may be possible. To obtain evidence of the formation of reduced, sorbed or precipitated U species and the adsorption of uranyl carbonate complexes, several spectroscopic techniques (EXAFS, XANES, XPS and FTIR spectroscopy) in cooperation with FZK-INE were applied. EXAFS showed the formation of U(VI)carbonate complexes on the surface of several mineral samples (hematite, magnetite, biotite, phlogopite). No direct evidence of U(IV) formation at the mineral

surface was found by XPS and XANES; FTIR-spectroscopy, on the other hand, gave indication of reduction of uranyl on galena. However, the formation of Fe(III) in biotite, observed by XPS, gave indirect proof of U reduction (Fig. 9). Possibly, U(VI) was reduced by magnetite, biotite, and galena during the experiments but later (mostly) re-oxidised during sample storage *(see S&T contribution Regenspurg et al.).* Further experiments in the frame of a NoE ACTINET project are planned.

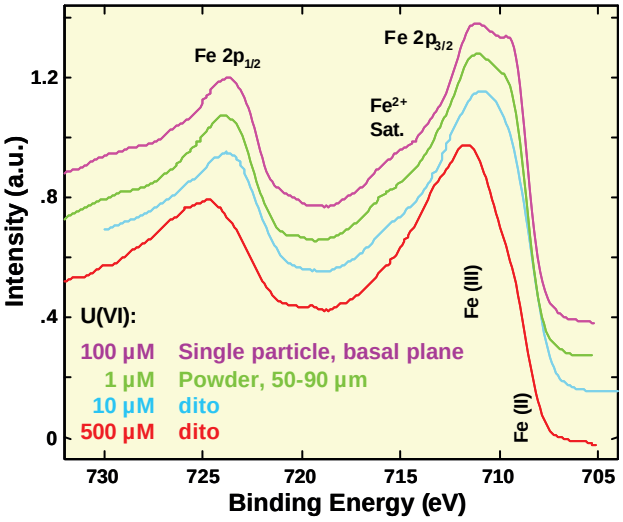

Figure.9. *XPS Fe 2p spectra of U(VI) sorption on biotite. Single particle basal plane showed low U sorption as identified by autoradiography and therefore no U reduction. Indirect evidence of U(VI) reduction by Fe(II) oxidation observed in the biotite powders with increasing U concentration. U(IV) was not observed by XPS, probably due to re-oxidation.*

Thin film flow-through reactor experiments with the minerals hematite and magnetite were performed to determine the kinetics of U removal by the minerals over several weeks as a function of solution chemistry. A solution (17 or 86 µM U(VI), 1 mM $NaHCO_3$, 0.1 M NaCl) was allowed to pass through the reactor with constant flow rate. Over 46 days, the outflow of the reactor was sampled and analyzed with respect to U content and pH. The pH value varied between 5 and 9. Not surprisingly, it was found that U retention is strongly pH dependent and that huge differences in sorption behaviour exist between the two minerals. However, no indication of U(VI) reduction by Fe(II) in the magnetite was observed, as the U retention on hematite was higher. In case of the higher concentrated U solution (86 µM), the observed strong U elimination from the aqueous solution was probably due to precipitation of U(VI) hydroxide.

KULEUVEN mainly worked on the interaction of Se(IV) with FeS_2. Cubic crystalline FeS_2 was ground with an agate ball-mill until the major part of FeS_2 particles was < 5 µm (N_2 (BET) area 4.34 m²/g). With this FeS_2, two types of batch experiments were performed in which the interaction with Se(IV) was followed as a function of time. In the first type, the FeS_2 was used with no further purification. SEM analysis showed that these FeS_2 crystals were covered with an amorphous crust. In a second type, FeS_2 was purified before use to eliminate the presence of Fe(III) phases at the FeS_2 surface which could have a profound impact on Se(IV) sorption.

Results from the first type of experiments showed that upon contacting several concentrations (ranging from ~ 10^{-8} – 10^{-5} M) of $^{75}SeO_3^{2-}$ with FeS_2, a decrease of ~90-95% in total Se solution concentration after centrifugation was noted after 1 day of equilibration. Hereafter, and up to 25 weeks of equilibration, Se solution concentrations remained more or less constant. Solution speciation studies (Ion Chromatography, Gel

Permeation Chromatography, Ultrafiltration at 30 kDa MWCO) showed that within methodological errors, all Se solution species were in the form of inorganic Se(IV) anions. The distribution coefficient in these systems also remained constant from 1 day to 25 weeks equilibration time and amounted to log $K_D \approx 3.0$-3.5.

Although thermodynamically in these systems (pH 8.7-8.9; -80 mV < E_h < -160 mV) a reduction (and subsequent precipitation) of Se(IV) to Se(0) is expected, the type 1 experiments seem to obey to an adsorption mechanism of Se(IV) onto Fe(III) phases probably present at the FeS_2 surface. XANES-EXAFS data to qualitatively describe the observed mechanisms were collected at the DUBBLE BM26A beamline at the ESRF (Grenoble, FR). Analysis of these data are currently underway *(see S&T contribution Bruggeman et al.)*. Future experiments performed by KULEUVEN will investigate the interaction of Se(IV) with purified (HCl-treated) FeS_2, as well as the interaction with $FeCO_3$.

SCK·CEN interest is on the interaction of U(VI) species with minerals present in the Boom Clay as pyrite and siderite. The work is directed towards the question, if this minerals are able to reduce U(VI), which phase will be formed, which solubility is obtained and what is the influence of NOM in these processes? The work in 2006 focussed on literature studies, preparation of the test protocols and making contacts for EXAFS measurements.

WP2.4: Impact of biogeochemical processes

In WP 2.4 the role and extent of microbiological mediated processes affecting radionuclide migration in the far-field of a repository will be investigated. The focus is on the identification of radionuclide interaction with detached microorganisms, retention through interaction with biofilm material, including microbiologically mediated reduction, and change in the geochemical environment generated by microbial metabolism, including the generation and influence of various chelating compounds.

CTH started the growth of biofilms on mineral slides of apatite, quartz and reference slides of glass. The biofilms grow in special reactors in which slices of material are mounted. Water is led through the reactor under in situ conditions in the Äspö Hard Rock laboratory (MICROBE site). After a few months of growth, the rock pieces can be carefully removed, placed in special sample holders and subjected to sorption experiments (see Fig. 10). The acquisition of suitable slides of apatite and quartz has been difficult and time-consuming. Apart from rock slide delays, CTH had technical problems with their inert glove box and in attaining correct spare parts. Due to these delays, the sorption experiments of Cs, Co, Am and Th onto biofilm have started end 2006, later than anticipated. Useful data on sorption/desorption is expected to be available for evaluation during the first half of 2007. The collaboration with the University of Gothenburg on the effect of complexing agents from microbial activity is on-going.

UNIUTRECH studies aims at unravelling the effect of iron mineral transformations on the mobility of radionuclides, in particular of uranium, in subsurface environments. Special attention is paid to iron mineral transformations induced by microbial mediated changes in redox regime. In 2006 the activities focussed on transformations of iron oxides caused by the transition from oxic to suboxic or anoxic conditions.

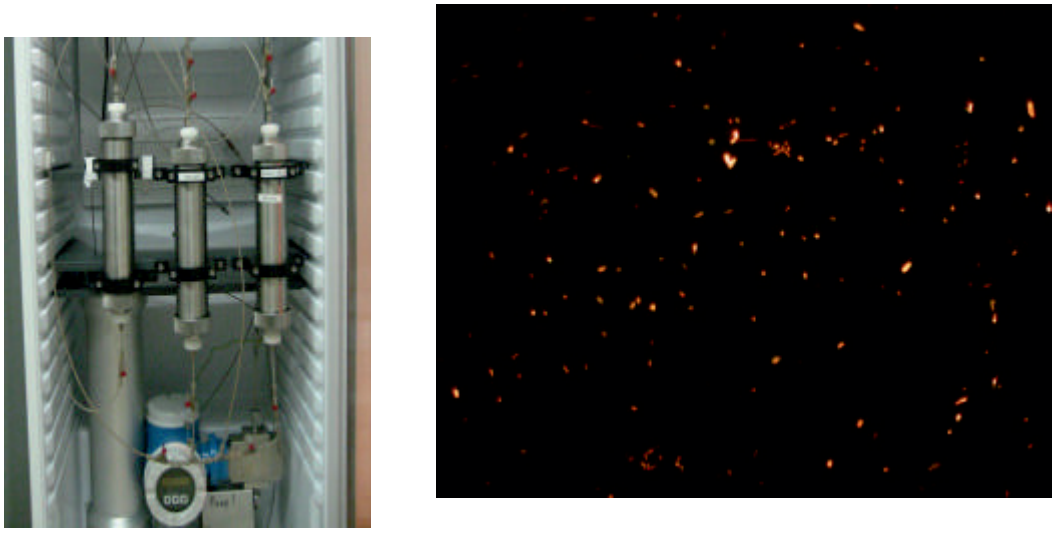

Figure10. *(left) Reactors at the MICROBE site (Äspö HRL) for biofilm generation on different mineral slides. (right) Fluorescence microscopy snapshot of biofilm produced.*

One research line has been devoted to potential pathways for uranium reduction accompanying microbial iron reduction. Three processes were studied in more detail: enzymatic reduction of U(VI), and the abiotic reduction of U(VI) by Fe(II) adsorbed onto iron oxide surfaces and by biogenic magnetite. A research highlight was the application of X-ray absorption spectroscopy (XAS) on samples obtained from laboratory experiments related to the three processes (ESRF experiments EC-120 and ME-1299). An important finding was that the immobilization of U(VI) caused by formation of biogenic magnetite or by Fe(II) production seems not to be related to reduction to U(IV) (see Fig. 11). This is in contrast to results reported from other studies. Resolving the ambiguities regarding the potential of structural bound Fe(II) to reduce U(VI) has been identified as an pivotal research goal and will be addressed in a recently started ACTINET project in cooperation with UNICYPRUS, KTH, FDR and coordinated by FZK-INE.

The second research line addressed the possibility of uranium mobilization when iron oxides with adsorbed U(VI) are reductively dissolved by S(II). The major achievement was the establishment of an experimental system suitable to investigate this process. First experimental results indicated that the hypothesized release of uranium upon S(II) addition to iron oxide suspensions takes place. This release can be explained by the competition between Fe(III) and U(VI) as oxidants for S(II) whereby reduction of Fe(III) seems to out compete U(VI) reduction. Furthermore, formation of soluble S(II) complexes and replacement of U(VI) from sorption sites due to Fe(II) production might contribute to the uranium mobilization. XAS analyses show that slow reduction of U(VI), presumably by FeS, can account for a re-immobilization of uranium as an U(IV) precipitate. Both projects demonstrate that equilibrium thermodynamics might lead to incorrect conclusions regarding the mobility of uranium under transient redox conditions.

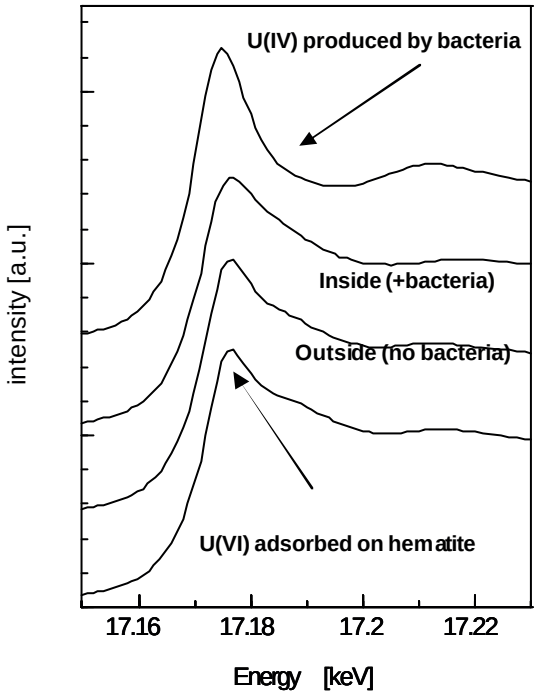

Figure 11. *XANES spectra of solids recovered inside (+ bacteria) and outside (no bacteria) of dialysis tube after reduction of nano-hematite. Also, spectra of U(IV) produced by microbial reduction of U(VI) acetate, and U(VI) adsorbed onto hematite are shown. Fitting analysis suggests that U(IV) was a minor component in samples. Main component is similar to U(VI) adsorbed on hematite surface. Reduction of U(VI) to U(IV) cannot be the sole explanation for increased immobilization of U.*

Miscellaneous

A second semi-annual meeting was hosted by FZK-INE in conjunction with the International Humic Substance Society (IHSS) conference in Karlsruhe on the 2. August 2006. Beside 24 participants from partner organisations two associated groups (OEKO and UMR-CNRS) were present and contributed with presentations. It has also to be mentioned that during the RTDC-2 individual meeting at the 2nd Annual meeting in Stockholm the associated groups MSU and CTU contributed with presentations.

The third semi-annual progress meeting will be held in conjunction with the MIGRATION'07 (August 2007) in Munich.

Publications in 2006

Publications

[1] Kim M.A. et al., Interaction of actinides(III) with aluminosilicate colloids, Colloids Surf. A: Physicochem. Eng. Aspects (2007, in press), doi:10.1016/j.colsurfa.2006.09.045.

[2] Breban, C., Provenance and characterization of aquatic actinide colloids: Interaction of aluminosilicate and humate colloids with actinides, Ph.D. thesis, Ruprecht-Karls-Universität, Heidelberg, Germany.

[3] Kim, J.I. et al., Aquatic Colloids: Provenance, characterization and significance to environmental monitoring, 6th International Symposium on Advanced Environmental Monitoring, June 27-30, 2006, Heidelberg, Germany.

[4] Opel, K., et al., Study of the solubility of amorphous and crystalline uranium dioxide by combined spectroscopic methods, Radiochim. Acta, in press.

[5] Komorovsky, L. et al. 2006, Resolution of identity Dirac-Kohn-Sham method using the large component only: Calculations of g-tensor and hyperfine tensor. Journal of Chemical Physics, 124(8).

[6] Malkin, E. et al. 2006, Scalar relativistic calculations of hyperfine coupling tensors using the Douglas-Kroll-Hess method with a finite-size nucleus model. Physical Chemistry Chemical Physics, 8(35): 4079-4085.

[7] Reviakine et al., R. 2006, Calculation of zero-field splitting parameters: Comparison of a two-component noncolinear spin-density-functional method and a one-component perturbational approach. Journal of Chemical Physics, 125(5).

[8] Marang, L. et al. 2006, Donnan membrane approach: From equilibrium to dynamic speciation. Environmental Science & Technology, 40(17): 5496-5501.

[9] Marang, L. et al. 2006, Kinetic approach of the Donnan membrane technique. Proceedings of the 13th IHSS Meeting, Schriftenreihe des Lehrstuhls für Wasserchemie und der DVGW-Forschungsstelle am Engler-Bunte-Institut der Universität Karlsruhe (TH), Vol. 45-1, p. 221-224, ISSN 1612-118x.

[10] Claret, F. et al. 2006, Fractionation of natural organic matter on alpha-alumina. Proceedings of the 13th IHSS Meeting, Schriftenreihe des Lehrstuhls für Wasserchemie und der DVGW-Forschungsstelle am Engler-Bunte-Institut der Universität Karlsruhe (TH), Vol. 45-2, p. 793-796, ISSN 1612-118x.

[11] Schäfer, T. and Claret, F. 2006, Organic Matter Clay association in natural and synthetic systems: what influences the organic matter preservation pathway?, Proceedings of the 13th IHSS Meeting, Schriftenreihe des Lehrstuhls für Wasserchemie und der DVGW-Forschungsstelle am Engler-Bunte-Institut der Universität Karlsruhe (TH), Vol. 45-2, p. 565-568, ISSN 1612-118x.

[12] Bruggeman, C. et al. (submitted), On the interaction of dissolved Boom Clay and Gorleben humic substances with Se(IV) and Se(VI), Applied Geochemistry.

[13] Skovbjerg, L.L. et al. 2006, The mechanisms of reduction of hexavalent chromium by green rust sodium sulphate: Formation of Cr-goethite. Geochimica Et Cosmochimica Acta, 70(14): 3582-3592.

[14] Szabó, G. et al. 2006, Radiochim. Acta, Investigation of complexation of thorium by humic acid using chemically immobilized humic acid on silica gel, 94: 553-557.

[15] Hrobárik, P., et al. 2006, Computational study of bonding trends in the metalloactinyl series EThM and MThM ' (E = N-, O, F+; M, M ' = Ir-, Pt, Au+). Chem. Phys. Lett. 431, 6-12.

[16] Hrobárik, P., et al., Density Functional Calculations of NMR Shielding Tensors for Paramagnetic Systems with Arbitrary Spin Multiplicity. Validation on 3d-Metallocenes", J. Chem. Phys. (in press).

S&T contributions to the Stockholm meeting

[1] Reiller et al.: Conditional stability parameters for the actinides(IV)-humic acid system: a search for consistency. (CEA, UNILOUGH and NRIRR)

[2] Szabó et al.: Determination of conditional stability constants for metals ions with humic acid using chemically immobilized humic acid on silica gel. (NRIRR, U-SAGA, FZK-INE, CEA and UK-HPA)

[3] Szabó et al.: Interaction of Th with humic acid over a wide pH region. (NRIRR, FZK-INE, CEA and UK-HPA).

[4] Römer et al.: Sorption of redox sensitive actinides onto granite and altered material from Äspö HRL. (FZK-INE)

[5] Claret et al.: Sorption induced fractionation of fulvic acids. (CEA and FZK-INE)

[6] Bruggeman and Maes: XANES-EXAFS analysis of Se(+IV)-FeS_2 systems (KULEUVEN)

[7] Priemyshev et al. Binding affinity of humic colloids to actinides – and what´s behind – (TUM-RCM)

[8] Kolokassidou et al. Physicochemical Properties and Complex formation Characteristics of Humic like Substances extracted from olive cake. (UNICYPRUS, FZK-INE and GSF).

[9] Brevet et al.: Complexation of Eu(III) by organic extracts from Callovo-Oxfordian argillites. (UMR-CNRS and CEA).

[10] Kolokassidou et al.: The effect of Humic Acid on the stability and solubility of $UO_2(OH)_2$ and UO_2CO_3 solid phases (UNICYPRUS and FZK-INE)

[11] Guczi et al.: Preliminary results for complexation of Pu with humic acid. (NRIRR, CEA, UK-HPA and FZK-INE).

[12] Eidner et al.: Effect of metal ion complexation on humic acid conformation. (UPPC and UNICYPRUS)

[13] Regenspurg et al.: Uranyl uptake on granitic minerals in presence of carbonate(KTH and FZK-INE)

[14] Marquardt & Seibert: The reduction of plutonium: comparison between hydroquinone and fulvic acid as reducing compound. (FZK-INE & ITU)

[15] Seher et al.: FEBEX bentonite colloid stability in ground water. (FZK-INE)

[16] Hrobarik et al.: Quantum chemical prediction of paramagnetic NMR spectra of lanthanide complexes with salicylic acid in water solution. (IIC-SAS, FZK-INE and UNI-Würzburg)

RTD COMPONENT 3

Scott Altmann
Andra Agence Nationale pour la gestion des Déchets Radioactifs.
1/7 rue Jean Monnet
F-92298 Chatenary Malabry CEDEX, France
Scott.altmann@andra.fr

Introduction

The primary objective of RTDC3 is to improve understanding of radionuclide *diffusion* and *retention by sorption* in clay mineral-rich geological formations under study as possible host rocks for deep geological disposal of high level nuclear waste. This understanding is needed in order to provide support for improved representation of these processes in performance assessment and to enhance safety case credibility (confidence building). The work is carried out in four complementary Work Packages (WP). WP1 deals with understanding basic phenomena affecting radionuclide transfer, mainly by studies using model clay minerals, while WP's 2 and 3 focus on understanding and modelling the combined effects of the key processes (in situ dissolved speciation, solid-solution partitioning, diffusion) determining radionuclide migration in four different geological formations, three of which benefiting from studies carried out in underground rock laboratories (URL):

- Boom Clay at Hades URL (B),
- Opalinus Clay at Mt Terri URL (CH),
- Callovo-Oxfordian argillite at Bure URL (F),
- Albitic Claystone Formation at Boda (HU).

WP4 focuses on developing methods / models for up-scaling transfer models and properties to the larger spatial (and longer time) scales pertinent for safety assessment of high level nuclear waste disposal concepts, with particular consideration of managing spatial heterogeneity.

Examples of key 'questions' being addressed by the research programs carried out within RTDC3 are:

- Can the differences in diffusion-driven transfer characteristics observed (at the macroscopic scale) in clay-rich compacted materials for non-sorbing anions (e.g. Cl^-), HTO and alkaline earth cations (e.g. Cs^+) be justified/explained in terms of 'mechanism-based' model(s)? Can models developed to explain data obtained at different space-time scales be made coherent?

- Are sorption values measured in batch tests on dispersed material compatible with those deduced from diffusion experiments on intact rock? In cases where apparent incompatibility is observed, is it possible to derive phenomenological models for 'scaling' between the two system states in a justified manner?
- Are models used for calculating radionuclide speciation in dispersed systems applicable for pore solutions in intact rock porosity? If not, what theoretical basis can be used for passing from one state to another in a thermodynamically rigorous fashion?
- Clay-rock formations display heterogeneity, at different spatial scales, regarding physical and chemical parameters which can potentially influence the transfer characteristics of radionuclides. Performance assessment models generally require relatively large mesh dimensions and long time steps in order to simulate radionuclide migration in the far field. Which are the best methods / models for carrying out this up-scaling in a consistent and justifiable manner?

The principal ambition of RTDC3 is to progress significantly along the road to answering these important questions. In order to do this, collaborative and complementary efforts involving teams from 24 different organizations (including research institutes, laboratories, SME, national radwaste management agencies and four Associated Groups) are underway or programmed within the FunMig IP. The remainder of this chapter is devoted to summarizing the principal activities accomplished during the first 12 months of the FunMig IP in this context.

Advances within work packages

WP3.1: Understanding key, basic processes affecting radionuclide transport in clay-rich porous media (small-scale, simplified model laboratory systems)

This work package is made up of complementary research efforts aimed at reaching a sound understanding of key phenomena determining radionuclide speciation and migration in highly compacted clay-rich porous materials. The overall objectives for WP 3.1 for the full FunMig project are:

- to improve our understanding of water and dissolved ion states in compacted clay pore water,
- to 'up-scale' these results to transport-retention processes modelling in simple-small-scale model porous systems,
- to verify the extended model by means of specifically measured diffusion data sets and
- to improve our understanding of the processes constraining clayrock porewater redox conditions.

Much of this work is being carried out by a consortium of contracting partners (AIED, BRGM, LGIT, LMM, LPEC, UJF), aided by two newly associated groups (*UniPoitiers, LAIEM*), with the objective of developing an innovative model of the physical-chemical behaviour of water and dissolved species in pore spaces of compacted clay minerals. During 2006 molecular dynamics (M.D.) calculations of water and ion distribution profiles in the vicinity of smectite clay basal surfaces were

performed successfully (Chapron et al., 2006). The preliminary results (cf. PID 3.1.2) show that water profiles are similar to those predicted in the literature for other clay minerals (e.g. talc, muscovite), but that the anion distribution is quite different from that expected based on classical macroscopic electrical diffuse layer models (Fig. 1). The H_2O data are being compared with the ^{2}H-NMR results obtained by SUBATECH-Faculté des Sciences de Nantes (*LAIEM*) on a model smectite mineral (prepared by LMPC). The results for anion distribution indicate the quasi absence of anion exclusion in the vicinity of the basal planes. If this result is confirmed in subsequent studies, the direct use of classical EDL models to estimate the effect of anion exclusion on pore solution composition in small sized pores may need to be adapted. Note that such a model has been developed by the associated group *CEREGE* (thesis and post-doc financed by Andra), in collaboration with BRGM and Andra, in conjunction with WP¨3.1 and 3.2 R&D activities (Leroy et al., 2006).

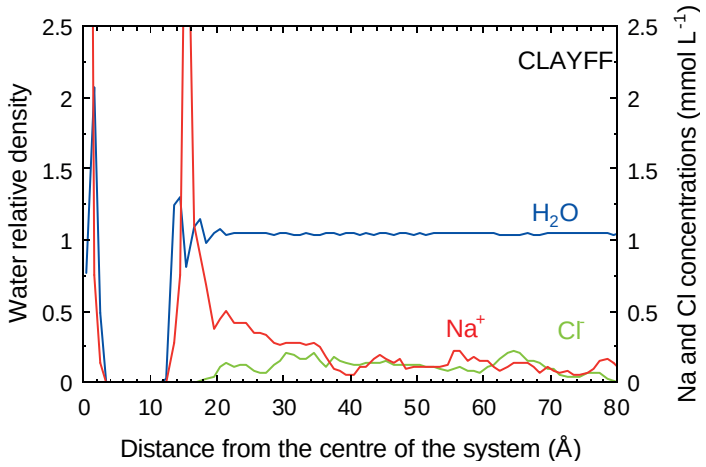

Figure. 1*. Water, Na and Cl profiles obtained using the CLAYFF force field parameters.*

The structural parameters of the hydration, hydrolysis and sorption of Sm (taken as a chemical analogue for actinides) in the interlayer space of the clay mineral (montmorillonite), as well as their dependence on chemical and physical factors which are important for radioactive waste management, are being investigated by **UJF** by means of neutron diffraction with isotopic substitution. The neutron diffraction experiment was carried out using the D4 diffractometer (Institute Laue-Langevin, Grenoble, France). The experimental results were measured on hydrated samples of Sm-montmorillonite prepared at pH > 8 and pH<7 in order to find out whether Sm is present as aqueous $Sm(OH)^o_3$, Sm^{3+}, or intermediate hydrolyzed species at pH>7, and how it is bonded to the clay surface. The data analysis is still in progress, but preliminary interpretation of the radial distribution functions describing the correlations between Sm atom and other neighbor atoms, obtained with D_2O and H_2O hydrated montmorillonite at different pH values suggests that the Sm – O distance is slightly shorter in the case of pH > 8, than for pH<. This might be interpreted as an indication of the fact that at least some of Sm is present as a hydrolyzed species. A molecular dynamics simulation of the system (cf. Fig. 2) was carried out with the use of computing facilities and software (Material Studio, DISCOVER) available at the Institute Laue-Langevin. The results are

being analyzed to obtain the structural and dynamic parameters of the clay interlayer. The structural data obtained by MD simulations will be compared with the results of neutron diffraction experiments. The dynamic data (diffusion coefficients, residence times, scattering functions) will then be used for the analysis of quasi-elastic neutron scattering (Fig. 3).

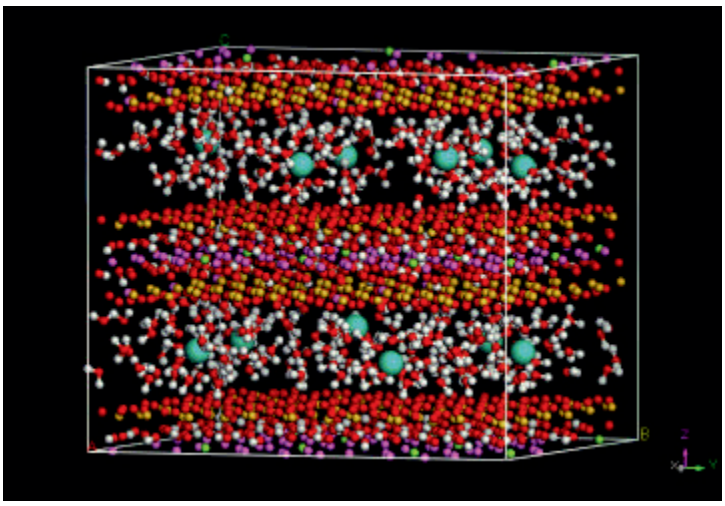

Figure. 2 *MD simulation box 31 Å x 36 Å x 31Å*

12 Sm^{3+}
336 H_2O
48 unit cells of montmorillonite
2940 atoms

Forcefield: ***CLAYFF***

Temperature: 298.00 K
Timestep: 1.00 fs
Duration: 1 ns

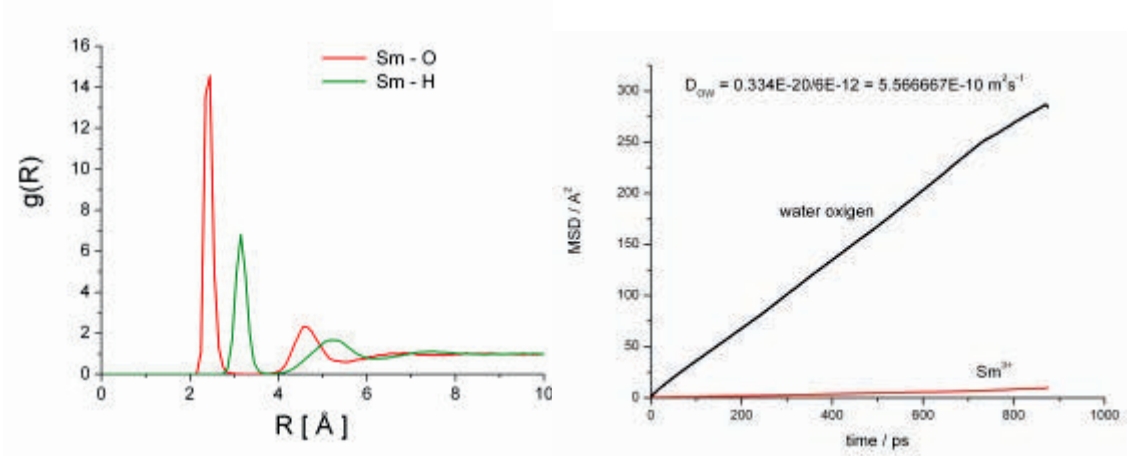

Figure. 3 *MD results: radial distribution functions (left) and mean-square displacements (right)*

At a more macroscopic scale, UJF and BRGM have continued investigation of the redox potential of iron sorbed on synthetic clay material. It was found that clay edge surfaces were able to supply electrons by oxidation of sorbed Fe(II) in absence of any other oxidant than water. This surprising effect was modelled considering H_2O as an electron acceptor with the production of surface-sorbed H_2. The resulting strong reducing capacity of smectite-Fe(II) was tested by reaction with Se(IV), which was found to be partly reduced to Se(0). Two papers have been submitted to GCA; the first in press (Gehin et al., 2006), the second under review (Charlet et al., 2006) (cf. also Charlet et al. 2006 – Proceedings ACS meeting) (PID3.1.15). The oxidation behaviour of argillite samples was also studied using microscopic (optical, SEM, TEM) and spectrometric (Mössbauer) techniques. The results described in 2005 were confirmed:

the most redox-reactive component in argillites is Fe(II) associated with naturally-present clay minerals (Lerouge et al., 2006; PID3.1.13). An oxidation scenario for the argillite rock is under construction (BRGM, *La Trobe*) based on these results, as well as on observations of newly precipitated mineral phases.

In 2006 ARMINES finished development of the initial versions of mono- and dual-porosity models for simulating radionuclide transfer in compacted clays (PID3.1.5), with both giving similar results for water and dissolved ion diffusion coefficients. Based on this, it was decided to retain only the mono-porosity version. A significant change in paradigm is proposed to describe diffusion accessible porosity in compacted bentonite - hydration water in the inter-layers is considered to be part of the solid phase, i.e. not as a constitutive part of overall porosity. This allows HTO retention to be explicitly accounted for by formulating exchange between HTO and water in the inter-layers. This means that only a single micro-porosity value is considered for anions, cations and neutral species. In the adaptation of the model to experimental data, a single value for the geometric factor fit constant (equal to 7) was used for all ions and neutral species, and for all densities between 0.2 and 1.8 $kg{\cdot}dm^{-3}$. Modeling of the simultaneous mass transfer of HTO, Cs, Br and Ni was carried out and the apparent diffusion coefficients obtained. In order to compare these values to corresponding effective diffusion coefficients available in the literature, the porosity hypothesis used for coverting between 'apparent' and 'effective' diffusion coefficients ($D_a \rightarrow D_e$) must be the same as that used in the literature (i.e. 'total porosity' for cations and HTO, 'macro-porosity' for anions). If this is done, the calculated apparent diffusion coefficients for HTO closely match measured values in the mentioned density range. Considering the large experimental data uncertainty, the agreement between anion diffusion data and calculations is acceptable (cf. Figure 4), while a slight underestimation for Cs is observed at lower bentonite densities.

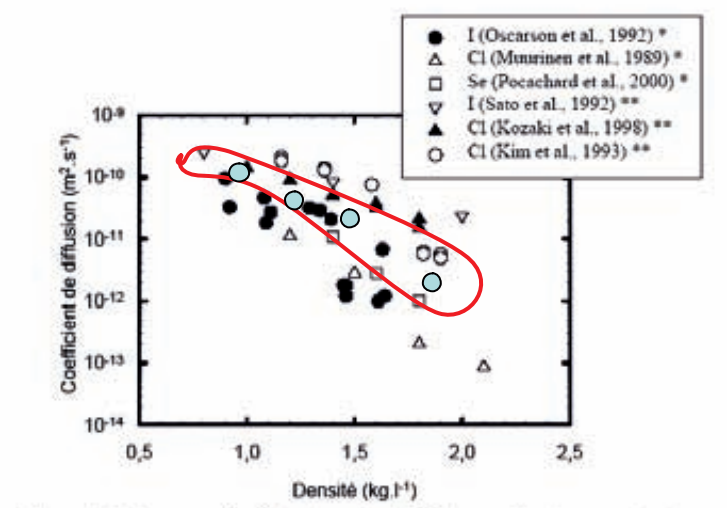

Figure. 4 *Comparison of calculated diffusion coefficients for anions (blue filled circles) with measured values reported in the literature, as a function of bentonite density..*

CIEMAT has been working on a preliminary conceptual model about the distribution of the different types of water (external and internal water) present in highly compacted clay-rich porous materials. The external water is related to the geochemical

porosity, which is the main water volume available for solute transport/chemical reactions of radionuclides, which depends on the porosity and the pore water solution chemistry. Different tests were performed with core samples from the Opalinus Clay and Callovo-Oxfordian formation, the same studied in WP3.2, in order to determine the dry and saturated state of the clay core samples, for example N_2 and water vapour isotherms and the Cl porosity/water loss porosity obtained from aqueous extracts and squeezing tests. A complete analysis will be performed by means of TG/DSC and FTIR techniques as a function of the water vapour adsorption. The calculated water volume accessible will be compared with the Cl porosity/water loss porosity obtained from aqueous extracts and squeezing tests (see following table).

Table: *Cl porosity data of samples from the Opalinus Clay (BDR) and Callovo-Oxfordian(EST) formations*

Sample	Cl inventory (mmol/kg)	Cl porosity	Cl porosity/water loss porosity (%)
EST 211 K-12	1.57	8.1	0.59
EST 212 K-1	4.33	7.6	0.41
EST 212 K-6	3.86	9.0	0.49
EST 212 K-13	1.65	11.2	0.83
BDR-0 m. 3.30-3.57	7.37	11.4	0.71

WP3.2: Radionuclide chemistry and transport in natural clay-rich host rocks at small scales

The overall objective of WP3.2 is to develop methods and models supporting mechanistically defendable representations of radionuclide migration in clayrock formations at the 'homogeneous' mineralogical scale (cm – dm). It is based on the interpretation and modelling of data obtained by studies carried out on small scale (~10^{-3} to 10^{-2} m) real clay-rock compact samples coming from the different formations. These 'facies scale' oriented studies constitute the core of the RTC3 research programme since it is at this scale that the realities of real rock samples (porewater composition uncertainties, complex mineralogical and organic matter composition, porespace structure…) impose their effects on, and must be taken into account in, the radionuclide migration model. It is also at this scale where the natural spatial heterogeneity of real rock samples must be explicitly dealt with in a scientifically coherent manner and where correct and justifiable means of quantifying and representing transport model parameter uncertainty are developed. The main activities carried out in 2006 are summarized below.

Porewater composition and clayrock- pore water conditions

A good understanding of the composition of clay-rock porewaters is essential for interpreting the radionuclide migration in clay formations. CIEMAT has characterized the main physical-chemical parameters of three different geological formation:

- *Boom Clay at Hades URL* (four different core samples were studied)
- *Opalinus Clay at Mont Terri (*two core samples were analysed from the borehole BDR-0, two more from the borehole BDR-2 will also be analyzed),

- *Callovo-Oxfordian argillite at Bure URL* (samples were analysed coming from boreholes EST211, EST212, PAC2001, PAC2002, PAC1001 and PAC1002. The core samples belong to the four lithostratigraphic series (C2c, C2b1, C2b2 and C2a).

The main physical properties analysed were dry density, water content, specific weight, total porosity and saturation degree. The mineralogical composition was analysed by XRD and SEM. The physico-chemical properties obtained were CEC, exchangeable cations and soluble. The total CEC of the samples ranges from 2.6 to 21 meq/100g. The pore water composition of the samples were analysed by aqueous extracts solutions and squeezing tests (cf. results shown in figure 5). The salinity of the porewaters analysed ranges from 0.20 to 0.08 M, the OPA samples having the more saline waters.

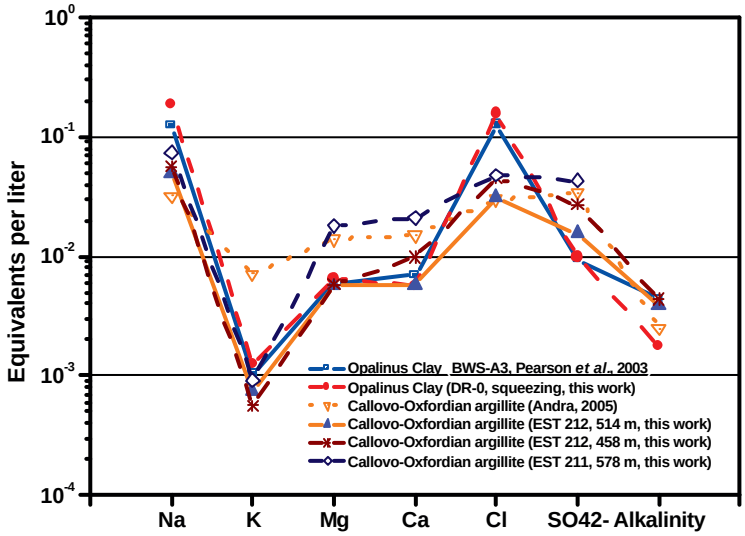

Figure. 5: *Schoeller diagram comparing the porewater composition of samples from Opalinus Clay and Callovo-Oxfordian formations.*

Understanding and modelling Rn diffusion-retention in heterogeneous clayrocks

An understanding of correlations, at relatively high spatial resolution, between (i) rock physical-chemical characteristics likely to influence radionuclide transport (pore dimensions and 'accessible' porosity, minerals in contact with pore solution…) and (ii) local-scale radioelement diffusion-retention behaviour, is needed in order to support radionuclide migration models, in particular for sorbing radionuclides. This information will also aid in developing models for correlating differences in macroscopic transport parameter values (e.g. Kd, De) observed on rock samples coming from different mineralogical facies, an important step toward defending up-scaling of sample scale measurements to the geological formation scale.

Much of this understanding will come from a program of coordinated and complementary studies being carried out by several partners (CEA, ERM, *Hydr'ASA*, ARMINES, Andra, PSI) on a selected, dm scale, rock sample from the Callovo-Oxfordian. The principal contributions are summarized in Figure 6, the green boxes showing operations being carried out on a single, cm-dm scale, volume of rock, with parameter value resolutions reaching in some cases to the near µm scale.

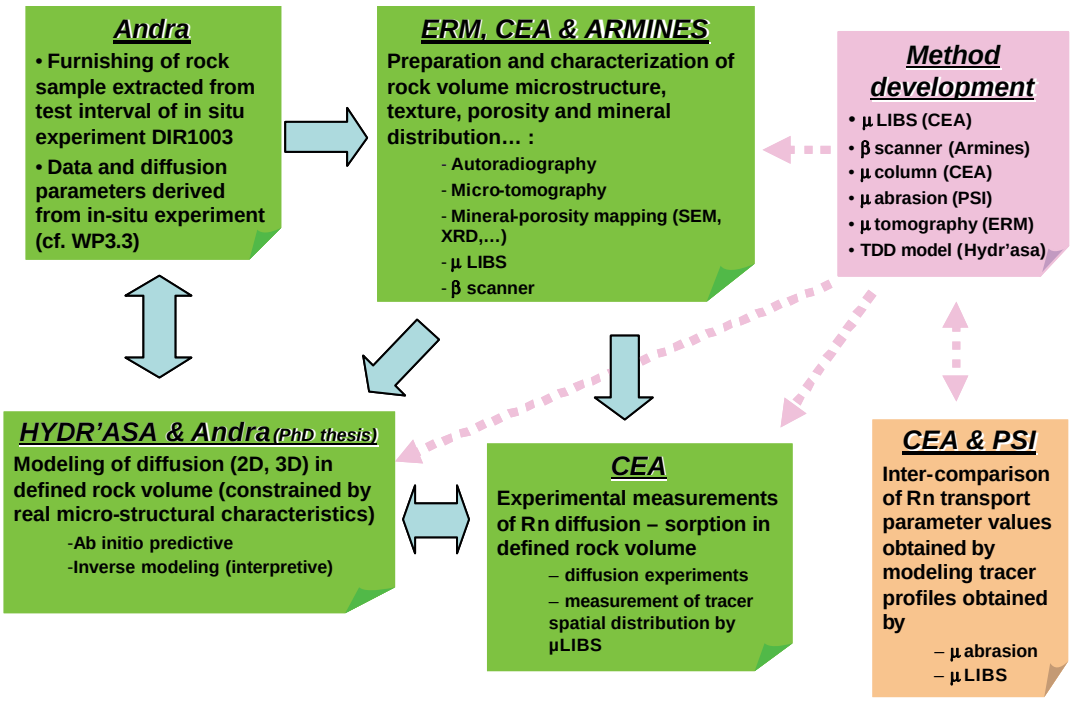

Figure. 6 *Schematic representation of coordinated and complementary studies being carried out on a selected, dm scale, rock sample from the Callovo-Oxfordian*

Analytical and modelling method development

Development of innovative methods for (i) characterizing parameters affecting, or representative of, radionuclide transport and (ii) modelling diffusion, in very small scale rock volumes (sub millimeter in the case of very strongly sorbing tracers) is a key aspect of WP3.2 (pink box in Figure 5). Much progress was made along these lines in 2006.

ARMINES continued development of a 2D beta imaging instrument employing a gaseous detector designed to permit rapid acquisition of quantitative, high spatial resolution images of the 2D distribution of isotopically labeled molecules which have been diffused into the surface layer of polished clayrock samples. The essential elements of the system are illustrated in the left-hand side of Figure 6. The main technical challenges are posed by the low energies of the electrons which are produced, which limit their escape depth (only the particles created in the last 5 μm of the sample can exit the rock) and make reduction of front end electronic noise important. Specific simulations were carried out to understand the path of point-source emitted ^{3}H electrons in the detector gas in order to understand effects on resolution (see example results on right hand side of Figure 7 for neon).

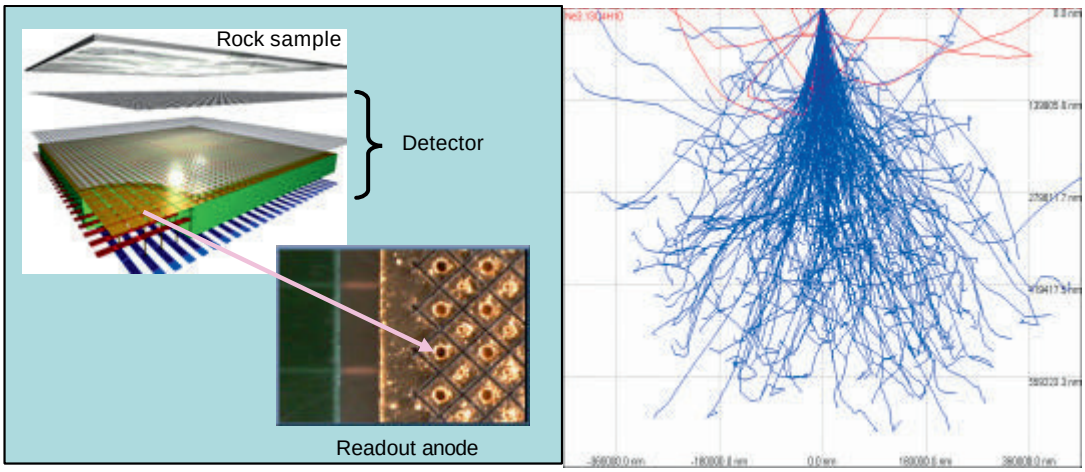

Figure. 7*. LHS: Schematic representation of beta detector under development by Armines; RHS: Simulations of* ^{3}H *electron paths in Neon (5 keV energy)*

The CEA used the LIBS microprobe it has developed to quantify Eu and Li (LHS Fig. 8) diffusion in Callovo-Oxfordian argillite and Sr diffusion in hardened CEM-I cement paste. The results show that this method can be used to determine the mean diffusion profiles for moderately to strongly sorbing tracer diffusion in complex solids, as well as providing information as to correlations between tracer localization and sample geochemical heterogeneity (RHS, Fig. 8). Preliminary results show that this innovative approach appears to be a powerful experimental tool to understand the mechanism of cation and anion diffusion in heterogeneous media, in spite of high geochemical background for several of them.

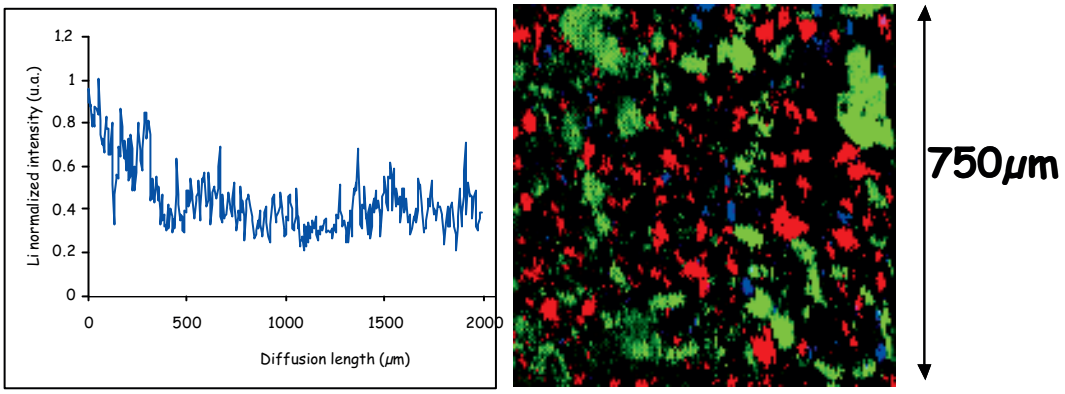

Figure. 7*. LHS: LIBS-measured diffusion profile for Li in argillite; RHS: Mineral phase distribution in same sample (5µm resolution)*

At a more macroscopic scale, the CEA has also made significant progress in 2006 in developing a column-based method for more rapid determination of radionuclide retention and diffusion parameters in clayrocks. Column design was completed and three configurations are currently being tested. The clayrock, prepared as thin plates 1 to 1.5 mm thick by 6 mm wide, are placed vertically in a 10mm ID column and equilibrated with the solution carrier phase. The number of plates and flow rate are varied depending on the sorption and diffusion characteristics of the test species. Tests are being carried out with tracers having well known transport and retention characteristics: Li, HTO, ^{36}Cl, Cs. The breakthrough curves for HTO, ^{36}Cl et Li for a

column with 5 rock slices are shown in Figure 8 a and b, and Figure 8c shows the initial results for Cs injection at trace levels in a column containing a single rock slice, for a flow rate of 1.2 mL/h. (PID3.2.4).

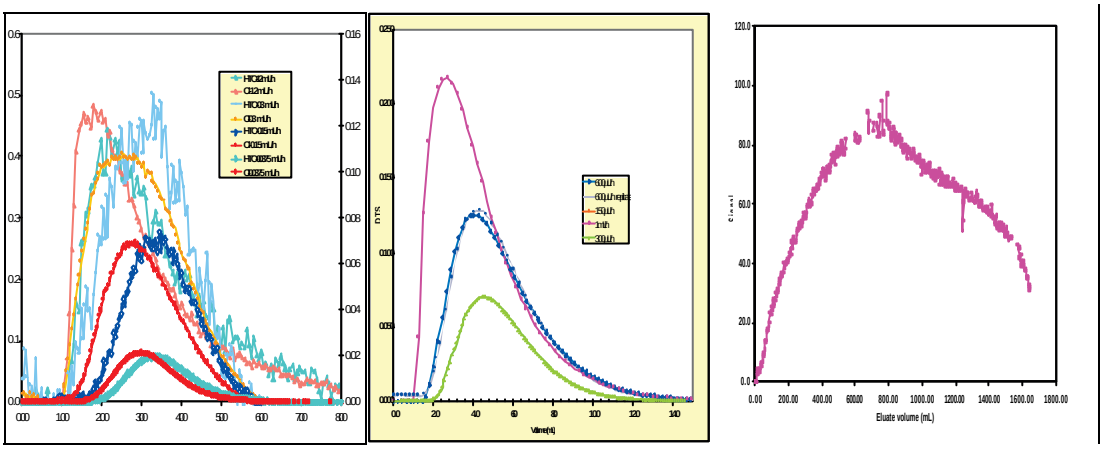

Figure. 8*. a) Break-through curves for HTO and Cl^- at different flow rates; (b) idem for Li^+; (c) preliminary break-through curve for Cs+ at 1.2* mL/h *flow rate*

ERM, in collaboration with *Hydr'asa*, is focusing on development of innovative ways for studying the role of mineral and textural spatial distribution on Rn transport. Development, calibration and validation of analytical methods was largely completed in 2005 and work in 2006 focused primarily on improvements to interpretation models for determining the relationship between the spatial distribution of mineral and micro-textural characteristics and solute diffusion in clayrocks. This work was carried out within the *Hydr'asa* research unit (associated group) thanks to an Andra-financed PhD thesis dedicated 100% to WP3.2 objectives (carried out by Jean Charles Robinet, an Andra-employee for a 3 year period). Much of the work carried out in 2006 focused on finalizing development and testing of a method for simulating diffusion in a numerical model of a real rock mineral-porosity structure. The method used, TDD for Time Domain Diffusion, is based on particle tracking (e.g. the solute mass is assimilated to a large number of particles), and simulates the particle motion by diffusion process in a 2D pixel grid by successive jumps between the centers of adjacent pixels. Each grid pixel is characterized by a porosity and an apparent diffusion coefficient. The TDD algorithm has been adapted to simulate in- and through-diffusion experiments (Robinet et al., 2006) and the inversion procedure (based on Gauss-Newton method) has been modified to interpret in-diffusion experiments. The TDD algorithm has also been adapted to a 3D voxel grid (Sardini et al., submitted and accepted). This model has been (and will be) used (i) to carry out ab initio direct simulations to predict the results of Rn diffusion experiments to be carried out on rock samples (by CEA and Armines) and (ii) to 'inverse model' diffusion experiment results in order to extract local diffusion parameter values.

Testing of the direct numerical simulation of in-diffusion experiments has been done using as constraint a mineral-porosity map of a COx argillite sample (sample EST205-07092) (Robinet et al., 2006). The mineral map was partitioned into 3 phases: the clay matrix, the minerals considered as non porous (quartz, carbonates…) and macro-pores (see figure 9, LHS). The diffusion coefficient and the porosity were fixed

for each phase. The results have shown (figure 9, RHS) that non-porous phases induced a macroscopic tortuosity of the clay matrix and create differences in diffusion transport depending on direction (relative to bedding).

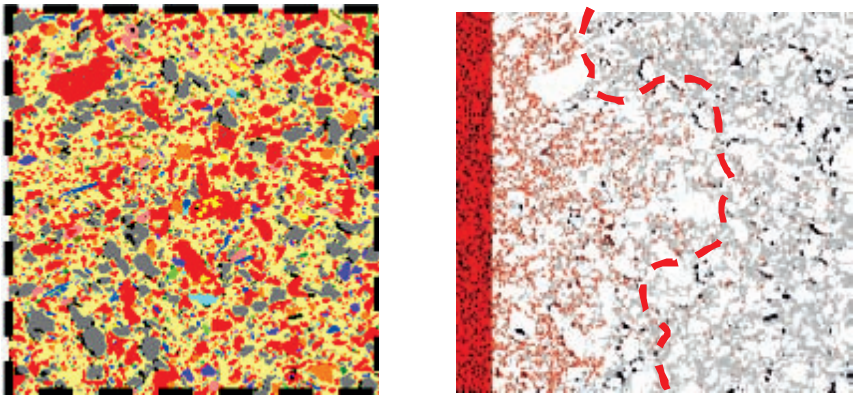

Figure. 9*. a) Mineral and porosity map of ~700µm by 700µm domain in argillite; (b) forward modeling predicted diffusion front in same system*

Integrated studies and modeling on Cox argillite sample

Much work effort in 2006 was devoted by ERM, CEA and Hydr'asa to studying a single 20 cm long, 6 cm diameter Callovo-Oxfordian argilite core sample[1] extracted from the test interval of one of the diffusion-retention experiments (DIR1003) being carried out by Andra in its Bure URL (cf. WP3.3). This turned out to be an extremely time consuming process because of the need to find solutions to unexpected difficulties arising from core heterogeneity and mechanical behavior. This required the core to be embedded in an epoxy resin for mechanical stability while it was cut (using a special wire saw), first into 3 parts (1, 2, 3), then each part into 3 sections (A, B, C) (cf. Figure 10). Parts A are devoted to diffusion experiments analysed by µLIBS (CEA), parts B to bulk analysis and petrographic description (ERM/Hydr'asa) and parts C to quantitative petrography (ERM/Hydr'asa). (PID3.2.9)

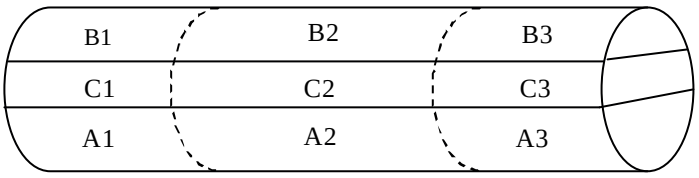

Figure. 10*. Sample localisation in the core DIR1003–EST 26059 (length 20 cm, Ø=6cm)*

ERM used a set of techniques to determine core petro-physical and mineralogical characteristics with resolutions ranging from centimeter to micrometer. Non-destructive X-ray radiography and tomography techniques were used at the core scale (samples C1, C2, C3) to visualize rock internal features at the centimeter to millimetre scale. The acquisitions were performed using a computer-controlled tomograph (Viscom X8050) at the University of Poitiers. The radiographs show elongated centimeter-sized

[1] EST 26059

heterogeneities related to dense phases and some fractures in the sedimentary plane (LHS, Fig. 11). The acquisition of a set of X-ray radiographs over a 360° rotation range were used for 3D volume reconstruction and visualization of denser phases (RHS, Fig. 11). These are mainly of tubular shape, and reflection and transmission optical microscopy and SEM observation showed that they are composed of pyrite (probably bioturbation worm tunnels). Since observed fractures and denser phases may influence solute diffusion, this macroscopic information represents the first step in sample selection for diffusion and micro-textural studies.

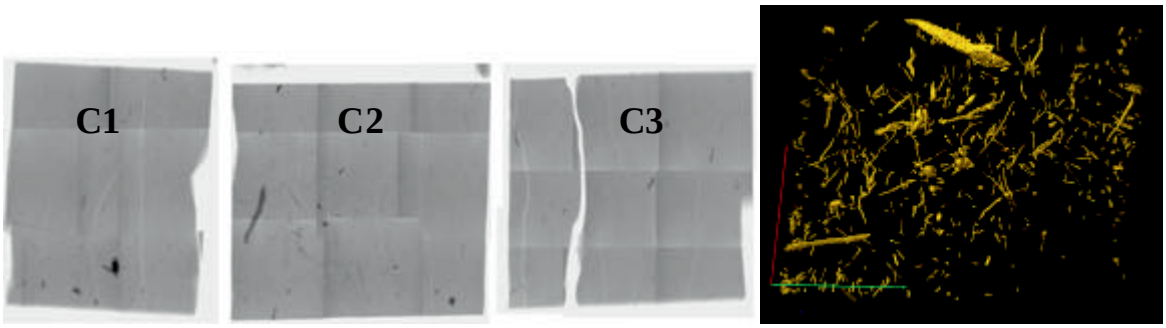

Figure. 11*. LHS: Mosaic of radiographs of parts C of the core, black mainly lengthened forms are due to the presence of pyrite. RHS: reconstruction of sample C2 analyzed by X-ray tomography, reconstruction of centimeter-scale pyrite structures.*

Classical bulk analysis (XRD, total carbonate, elemental analysis, CEC) was performed at centimeter intervals along the B samples. Mineral and porosity spatial distribution characterization were also performed after impregnation with a ^{14}C or ^{3}H doped MethylMethAcrylate (MMA) resin (polymerized by gamma irradiation). Porosity spatial distribution was determined using an autoradiographic method. Impregnations are in progress for B1, B3, C1, C2 and C3 (impregnation time ~ 2-3 mouths). This step will allow selecting of zones of interest for carrying out mineral and porosity maps by electron microprobe EPMA analysis. Based on these results, various zones will be selected for investigation at a sub 10^{-5} m scale resolution (micro-tomography using synchrotron radiation).

The rock volumes selected for carrying out the in-diffusion experiments will be analyzed both by the auto-radiographic + electron microprobe technique (ERM) and by the LIBS micro-probe (CEA) to furnish the mineral – porosity spatial distribution constraints for the numerical model to be used for performing direct simulations and inversion modeling (Hydra'asa). A similar approach will be carried out for samples studied by Armines using in-diffusion of a ß emitting tracer and detection of its spatial distribution in the porosity using the ß detector.

Kd's from batch and diffusion studies

A recurrent question faced by safety cases for disposal in clayrock formations is whether or not the Kd values measured in batch systems for moderately and strongly sorbing radionuclides (especially actinides) can be used to calculate migration retardation in intact rocks. This topic is addressed directly by experimental work being carried out by several RTDC3 partners (FZK-INE, PSI, CEA), and is the focus of an

inter-comparison organized by SCK-CEN of existing databases for the different clayrocks, supplemented by the results of specific experiments.

FZK-INE has designed and developed a sample cell - autoclave system for carrying out actinide diffusion experiments on clayrock samples at pressures representative of in-situ conditions (PID3.2.7). Activities in 2006 were devoted largely to studying Pu diffusion perpendicular to the bedding plane in an Opalinus clayrock sample (provided by Nagra from the Mont Terri URL). The variation of Pu-238 sorption as a function of pH sorption was measured using classical techniques on a ground sub-sample of the same core equilibrated with OPA porewater (under Argon atmosphere). As can be seen in Figure 12, starting from pH ~4.8, solution Pu-238 concentration decreased with increasing pH, reaching a sorption maximum at pH 7.2, then decreases for pH > 7. Strong Pu-238 sorption under the experimental conditions of the diffusion experiments is therefore expected.

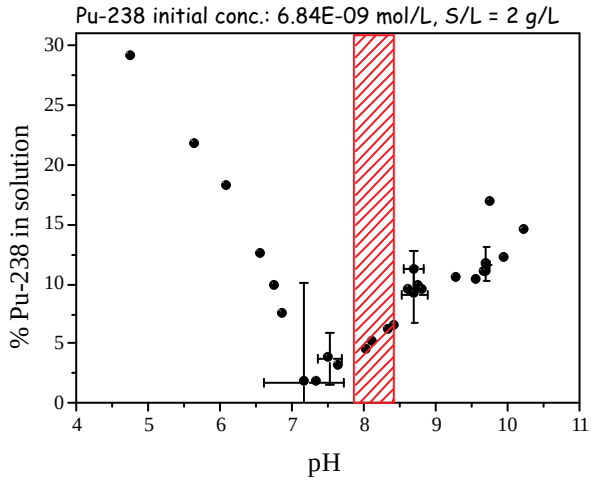

***Figure. 12**. Sorption experiments of Pu-238 on Opalinus Clay. The filled pattern indicates the pH region of the diffusion experiments*

Diffusion experiments were performed at two different initial pH values, pH 8.4 (initial Pu-238 concentration = 5.63E-09 mol/L) and pH 7.9 (Pu-238 initial concentration = 5.38 E-09 mol/L). The pH of the solution remained unchanged throughout the experiment. After completion of the diffusion experiments the clay stone cores were embedded in epoxy-resin before being cut perpendicular to the bedding in two pieces using a diamond saw in the glove box. One-half of the sample was used for autoradiography, the other for determination of the Pu-238 diffusion profile using the high-resolution abrasive peeling method (PSI, see below). A phosphor storage screen technology was selected for the autoradiography of the Pu-238 a-activity because of its higher sensitivity and the enhanced linear dynamic range relative to film-based detectors. Figure 13 shows two different diffusion profiles obtained by this method. The results of this initial demonstration and experimental development experiment shows that (i) about 40 % of Pu is sorbed on components of the experimental set-up, (ii) there is considerable impact of the samples natural alpha-emitting inventory, (iii) the mobile

Pu inventory is dominated by Pu(V), and there is no preferential transport pathway for Pu in the clay sample.

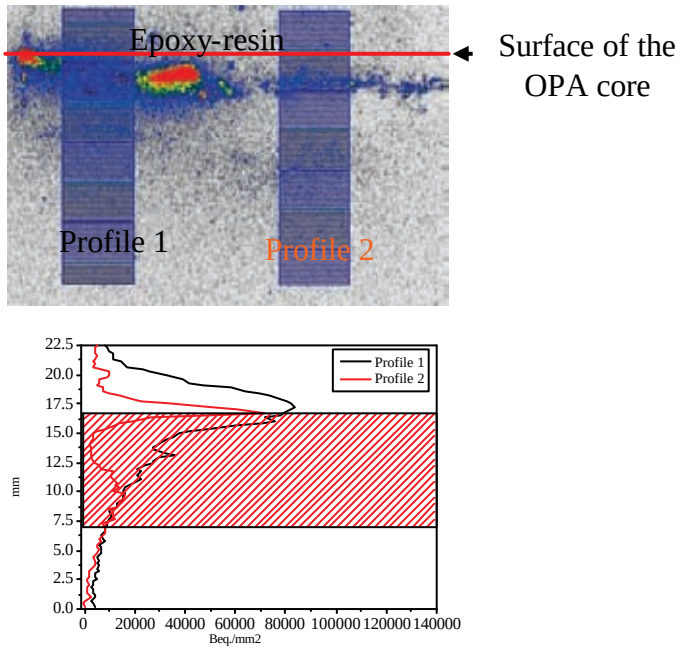

Figure. 13*. Diffusion profiles measured with autoradiography. The filled pattern indicates the clay sample. The dotted line indicates the background radiation from the Opalinus clay.*

The main goal of the PSI action in RTDC3 is to generate data directly applicable for linking sorption studies on dispersed systems with sorption and transport studies on intact (=compacted) systems for weakly and strongly sorbing radionuclides. In 2006, the sorption isotherm of Cs on intact rock samples was determined and in-diffusion studies of Cs at different total Cs concentrations were performed. Modeling of results (see LHS of Figure 14) is ongoing. It turns out that the through-diffusion data cannot be modeled when the isotherm measured on crushed rock is used. Using the isotherms measured on intact rock samples yields a slight improvement, but Cs-134 break-through in OPA is still faster than that predicted using the intact rock isotherm. A proper explanation cannot be given at the present time. One difference between the diffusion experiments and the sorption measurements on intact rock samples is the confining pressure. In the diffusion experiments, an external confining pressure between 4 and 14 MPa was applied. The sorption measurements were done without external confining pressure. Some additional measurements of sorption of Cs-134 on intact rock samples under different confining pressures are ongoing.

Much work was also carried out by PSI on strongly sorbing tracer diffusion in intact rock. In previous experiments under ambient conditions, oxidation of the pyrite present in OPA, and the resulting formation of $Fe(OH)_3$ in the system, were identified as major problems during diffusion experiments. Therefore, in-diffusion tests with $^{60}Co(II)$ and $^{152}Eu(III)$ were performed under anoxic conditions (N_2 glove-box, O_2<2ppm). In the case of $^{60}Co(II)$ improvements were observed. Much more mass was transferred from

the contacting solution into the rock: 60 % of the mass lost from solution was found within the rock mass, the remaining 40% was sorbed on the equipment (mainly filter). In the case of ^{152}Eu(III), no improvement was observed. Only 0.1% of the mass lost from solution was found in the rock, the remaining 99.9% was sorbed on the equipment. It was however still possible to quantify the diffusion profile of this tracer within the rock using the abrasive peeling technique (cf. RHS of Figure 14).

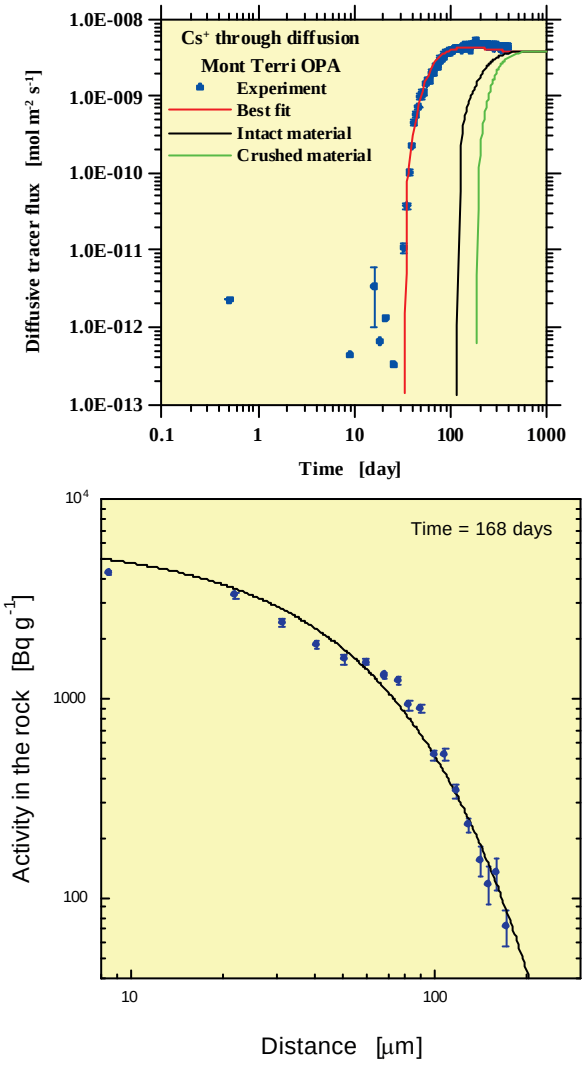

Figure. 14*. LHS: Predicted and measured break-through of ^{134}Cs(I) in OPA. The green line represents the prediction using the Cs-sorption isotherm measured on crushed OPA. The black line represents the prediction using a Cs-isotherm measured on intact OPA. The red line represents a best fit;*
RHS: Diffusion profile of ^{152}Eu(III) in Opalinus Clay from Mont Terri after 170 days in-diffusion. The diffusion distance is ca. 200 μm.

The results of these experiments with ^{60}Co(II) and ^{152}Eu(III) led **PSI** to the following conclusions:

- The abrasive peeling method is an excellent tool to measure shallow diffusion profiles of strongly sorbing tracers in shales.
- Sorption of tracers on the equipment causes difficulties in interpreting results and therefore in deriving diffusion and sorption parameters for the intact rock.
- In the case of $^{60}Co(II)$, indications of a dual porosity diffusion were observed.
- Alternative methods need to be developed to study strongly sorbing tracer diffusion in rock, in particular, ways of introducing tracer mass into the rock.

II-HAS continued and finished work on diffusion of anionic $^{99}TcO_4^-$ and $H^{14}CO_3^-$ species in Boda Claystone samples originated from ~1000 m depth. Measurements were performed on bore core discs (thickness: ca. 10 mm, diameter 47 mm). Break-through curves have been obtained by regularly measuring radioisotopes activities in the up-gradient and down-gradient compartments of the through-diffusion cell. Two samples were measured with slightly different mineral compositions (sample No. 1 without smectite, sample 2 with c.a.3 % smectite) at different pH values (pH= 8 and 12). The values obtained for the effective diffusion constants (D_e, $m^2\ s^{-1}$ x 10^{12}) are given in the following table. (PID3.2.8).

Tracer	$^{99}TcO_4^-$		$H^{14}CO_3^-$	
Sample	No. 1	No. 2	No. 1	No. 2
pH = 8	n.a.	1.16	0.39	1.57
pH = 12	n.a.	0.77	1.10	1.07

Similar measurements were also begun on samples having a different mineralogical composition obtained from a new borehole reaching a depth of ~ 570 m. Due to the shallower depth, the pressure –temperature conditions for diagenesis processes were more modest in comparison to the conditions characteristic at ~1000 m depth. The approximate mineral composition of the sample is: Phyllo-silicate (lllite-muscovite): 33%, Chlorite: 2%, Smectite: 2%, Analcime: 23%, Albite: 12%, Quartz: 11%, Calcite: 9%, Dolomite: 1%, Hematite: 7%. In these experiments, only one pH is set for the ground water (7.5 – 8.0). In addition, in order to obtain direct data on the self-diffusion of water, measurements with HTO were begun at the same time as measurements for $^{99}TcO_4$, and $H^{14}CO_3$. No detectable breakthrough had been observed after 2 months of observation. Details of these studies are given in Mell et al, 2006a, b. These results are Rock samples were provided to ERM for complex structure and mineral analysis and to CEA for sorption/diffusion studies.

CIEMAT has continued exploiting the previously developed large-scale diffusion methodology (cf. García-Gutiérrez, 2006; PID3.2.6) to (i) carry out additional experiments on both Opalinus (OPA) clay samples from the DR experiments in Mt-Terri and (ii) begin measurements on samples of the Callovo-Oxfordian (CO) clay from Bure. These new experiments are being carried out with HTO and ^{85}Sr in separate blocks; with selected strongly sorbing tracers (^{137}Cs, ^{60}Co and ^{152}Eu) being released in different regions of the same block. The blocks for the HTO experiments have been sampled (after 99 days for the OPA clay and 84 days for the CO), yielding 411 samples from Mont Terri block and 560 samples from Bure block. A regular sampling distribution was implemented in order to obtain the best representation of vertical and horizontal planes into the blocks. The analysis of the diffusion profiles is in progress. An example of the data obtained for HTO is shown in Figure 15.

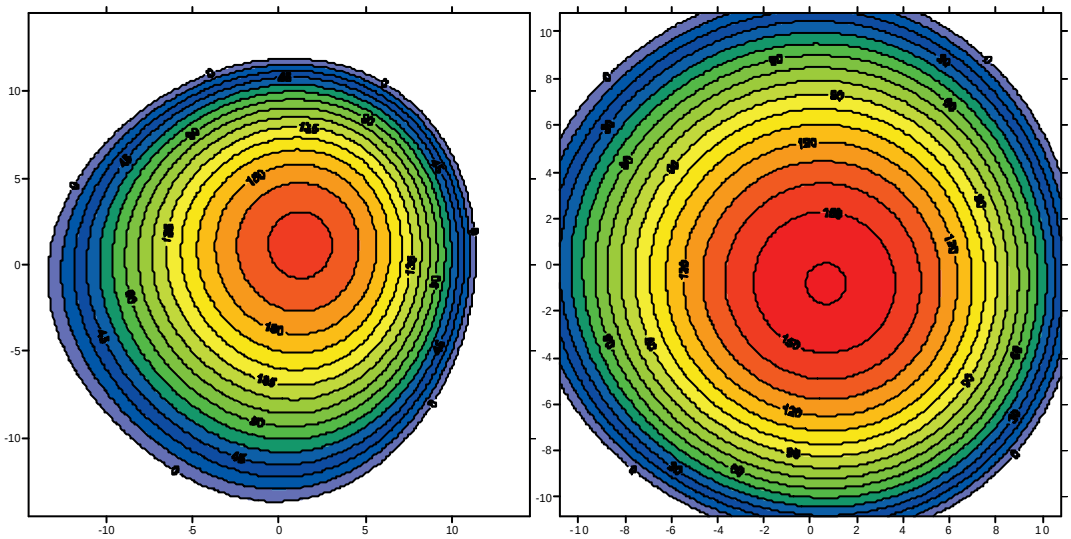

Figure. 15*. HTO concentration in the 10-12 cm horizontal plane LHS: Opalinus claystone after 99 days; RHS: Callovo-Oxfordien claystone after 84 days*

The blocks used for the ^{85}Sr experiments have also already been sampled (after 199 days for the OPA clay and 148 days for the CO clay), yielding 610 samples from the Mont Terri block and 420 samples from the Bure block. Analysis of the 3D tracer distribution is in progress. Sampling of the blocks with the strongly sorbing tracers is planned for the end of 2007.

UDC is using its fully 3D anisotropic model to calibrate transport-determining parameter values against available data.

CIEMAT has also carried out several diffusion experiments at laboratory scale with OPA and CO clays using the following tracers: HTO, ^{36}Cl, ^{233}U, ^{22}Na, ^{85}Sr, ^{75}Se, ^{137}Cs, ^{60}Co and ^{152}Eu. Different experimental methodologies are being used to determine the apparent and/or effective diffusion coefficients. A new methodology based on the RBS (Rutherford Backscattering Spectrometry) ion beam technique is being implemented for the determination of apparent diffusion coefficients of three elements presenting different sorption behavior into Mont Terri clayrock: I as non-sorbing element, Sr and Eu as low and strongly sorbing elements, respectively. It was possible to determine apparent diffusion coefficients for Eu, (1.50E-16 m^2/s) and an estimation of the lower apparent diffusion coefficient for Sr (> 4.00E-14 m^2/s). In addition, the lower apparent diffusion coefficient within the consolidated clay was estimated to be 10^{-17} m^2 /s using 2 nm size, negatively charged Au colloids. This information was used, combination with information on the solid pore structure (obtained by PMMA impregnation techniques carried out by the University of Helsinki, Finland) and with sorption values available in the literature, to calculate the effective diffusion coefficients. Further details on this work can be found in Alonso et al. 2006.

During 2006, SCK-CEN has pursued its efforts regarding the inter-laboratory collaboration on quantifying the relationship between Kd and R. The idea is to collaborate with other labs to perform batch sorption experiments together with migration tests on host rock clay materials. The sorption work is part of RTDC1 (WP1.2) and the migration work part of RTDC3 (WP3.2). The first action was to

acquire existing datasets and protocols from the partners joining this exercise. A small report compiling these data is in progress, and will be published under RTDC1. Experimentally, the sorption work (RTDC1) has been started (Cs and Am are done, Sr in preparation), the migration experiments are in preparation and will be initiated in 2007.

Organic colloids

Improving our understanding of the potential role played by the kerogen fraction of the organic matter present in the Callovo-Oxfordien argillites in influencing actinide speciation and mobility is one of the objectives of work carried out by ARMINES (in collaboration with the University of Poitiers and the G2R, Nancy). The motivation is based on several considerations: (i) it is known that kerogen is reactive in the presence of oxygen and it is hypothesized that it can interact strongly with metal ions and (ii) while kerogen is not mobilized in the presence of clay water, a fraction could be mobilized by the alkaline perturbation caused by concrete materials present in a radwaste repository. Two questions are under investigation in RTDC3.2: (i) does kerogen contribute to the total sorption capacities of unperturbed clayrock? and (ii) can organic matter mobilized from the kerogen fraction by an alkaline perturbation modify radionuclide speciation (formation of mobile 'colloidal' forms) and, if so, can these species diffuse in the compact rock? Preliminary experiments were performed in 2006 on 2 g of kerogen extracted by a HCl/HF treatment provided by G2R (Nancy). Some tests were made to quantify kerogen solubility in contact with a fresh cement-water solution. The parameters studied were the contact time, the solid-to-liquid ratio (1-10g/L) and the number of washing cycles. Five days were necessary to reach equilibrium. The results could be explained by considering the presence of two phases, one appearing to be completely soluble (~ 70 mg of C released per g of kerogen), a second, weakly soluble fraction controlled by a solubility product. First titration results show that the mobilized organic matter fraction had a proton buffering capacity of ~4.15 mmol/g (experiments realized from pH 4 to pH 10.5).

WP3.3 URL experiments for characterizing radionuclide chemistry and migration in clay-rich host rock formations at intermediate time and space scales

Datasets useful for validating, under in–situ conditions and at somewhat larger space (~dm - m) scales, the transport models developed in WP 3.2 will be furnished by experiments carried out in the Mont Terri URL and Bure URL. The Diffusion & Retention (DR) experiment being carried out by Nagra at Mont Terri is directly included in WP3.3 while the similar 'DIR' experiments carried out by Andra at Bure are not. However, the data generated by these latter experiments are being made available to Funmig as they are validated. The combined in situ databases and associated validated conceptual models will provide one of the key information bases for development of up-scaling and homogenization methods applicable to the intermediate (facies) scale, a key RTDC3 objective.

Nagra's DR experiment was initiated by the tracer injection in April 2006. Since then, evolution of the tracers has been closely monitored and samples taken at regular intervals. A joint Mont Terri/Funmig meeting was held at PSI in May 2006, where

further field, lab and modeling activities related to DR were agreed upon. In particular, it was decided to drill an additional borehole (in December 2006) for providing additional core samples for the experimental teams. A joint meeting between CEA, PSI and Nagra was held in October 2006 regarding collaboration related to diffusion work in general and to the DR experiment in particular.

Modeling work associated with the DR experiment involved mainly two activities. First, the work between the different modeling teams (UDC, GRS, CSIC, PSI) was coordinated by compiling input data for the calculations. Second, scoping calculations were performed with a 2D radial model using the code FLOTRAN, The results were compared with the in-house code radDiff, which in general showed good agreement. However, the effect of rock anisotropy on diffusion yielded ambiguous results. It appears that with the FLOTRAN code, the diffusive flux perpendicular to bedding is overestimated. This issue is presently being resolved. The simulations performed in 2006 are documented in a progress report (PID 3.3.1).

More specifically, UDC used a reactive transport code ($CORE^{2D}$) to carry out three-dimensional scoping calculations for the experiment, and compared the results with those obtained by CSIC (Soler, 2004). Code verification was done by comparing the results of simulations done using $CORE^{2D}V4$ and CORE3D, both of which gave the same results as those of CSIC. A 2D axi-symmetric model has been used in scoping calculations and predictive modeling, which consider both isotropic and anisotropic cases. Sensitivity analyses have been done on the following parameters: accessible porosity, diffusion coefficient, distribution coefficient. Relative sensitivities of computed concentrations in the borehole and in the clay formation have been calculated for various tracers (HTO, Na^+, Sr^{++}, I^-). These modeling efforts were used to select the final DR experimental configuration. A progress report (PID3.3.2) describes this work.

GRS is using data generated from in-situ diffusion experiments to test the relative advantages of two numerical codes of different complexity. In 2006 work was focused on the modeling of the DR-experiment. The modeling is done using the 3D transport program r^3t which accounts for anisotropic, element-specific diffusive transport, and retention by linear and non-linear sorption (by isotherms). A non-uniform grid model was built reproducing the DR-experiment geometry. Preliminary transport calculations have been performed for all the tracers injected in the DR-experiment. In Figure 16, the LHS shows the wire-frame model of the r^3t geometry and a cross section through the model, and the tracer plume propagating from the test interval. The different propagation distances parallel and perpendicular to the bedding due to the anisotropy in diffusion can clearly be seen. The RHS of figure 16 shows the predicted temporal evolution of the tracer concentration in the test interval for seven different tracers. The results of the program r^3t have been compared to the preliminary results created by the programs of four other modeling groups at the DR-experiment meeting (cf. PID3.3.3). Differences in the modeling results have been observed and there causes are under examination. Additional future work will be focused on comparison of the predictive modeling with the experimental results and an adjustment of the transport parameters to fit the experimental data.

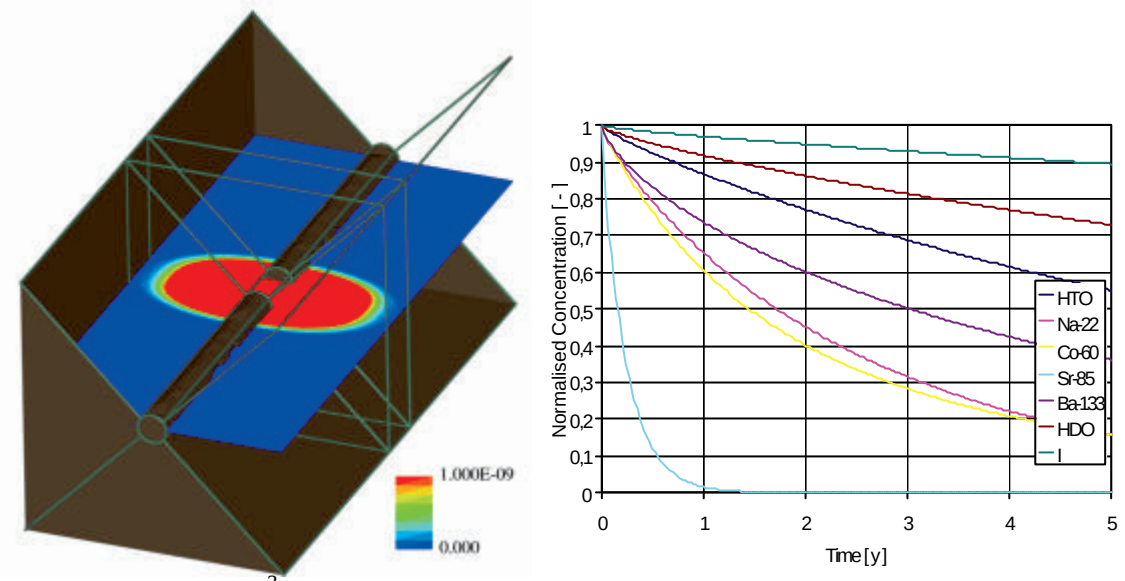

Figure 16: *LHS: r^3t model of the DR-experiment showing a tracer plume; RHS: Predicted temporal evolution of the tracer concentration in the test interval*

SCK-CEN and Niras/Ondraf, based on the results of internal discussions, came to the conclusion that, although technically feasible, carrying out a large scale in-situ migration experiment with sorbing tracers in its Hades URL would contribute little to up-scaling strategies. This is largely attributed to the likely presence of serious artifacts that would make the test difficult to interpret, especially with respect to up-scaling purposes.

WP3.4 Up-scaling to formation scale furnishing of tools useful for safety case studies

The overall objective of this WP is to produce data and methodologies useful for determining and justifying the use of transport parameter values (and associated uncertainty ranges) for host formation volumes sufficiently large to be useful for safety case studies (i.e. at the host formation scale and over long time frames). Two main types of research actions are programmed in order to advance along these lines:

- use of measurement, and interpretation by modelling, of the spatial distribution of natural tracer elements to obtain information on transport phenomena taking place under natural conditions at large space and long time scales.
- development of methods for analyzing and relating information available at all scales, for a given formation, concerning properties affecting directly or indirectly radionuclide transport,

In June-July 2006, UniBERNE carried out the second drilling and sampling program in the Opalinus Clay anticline at Mont Russelin needed to obtain samples for measurements of the spatial distribution of various natural tracers. Mineralogy analyses and bulk and grain density measurements have been conducted on the samples. Analysis of the stable isotope composition of pore water is in progress, as is the aqueous leaching of samples for Cl and Br analysis. Measurement of He is also underway. The available results were presented at the Goldschmidt 2006 conference (Koroleva et al, 2006) and numerical modeling is in progress. Information on tracers is available for chloride, stable water isotopes and helium. Anion data were obtained from aqueous leaching and

a small number of squeezing tests. The anion-accessible porosity was calculated from these data and corresponds to ca. 60% of water-loss porosity. The stable isotopic composition of water was obtained by the isotope-diffusive exchange method. The Cl^- distribution in pore water shows a regular and well-defined profile, with a conspicuous decrease towards the limestone aquifer in the hanging wall (LHS, Figure 17). The highest values, closely corresponding to the present seawater value, are found in the centre of anticline in the Liassic Claystones close to the contact with Opalinus Clay. Currently, data on both water isotopes and helium concentrations are available for six boreholes along the tunnel (the remaining samples are still in the laboratory). The spatial distributions of both d^2H and $d^{18}O$ are highest in the centre of the anticline and decrease towards the Dogger in the limb. Helium contents decrease from $4.19*10^{-4}$ ccSTP/gH_2O in the centre to lower values in the Dogger limestone (RHS, Figure 17). In contrast to Cl^- and the stable water isotopes, helium shows an anomaly related to a major fault zone close to the contact between Opalinus Clay and a tectonic slice of underlying Toarcian rock. (cf. PID3.4.1)

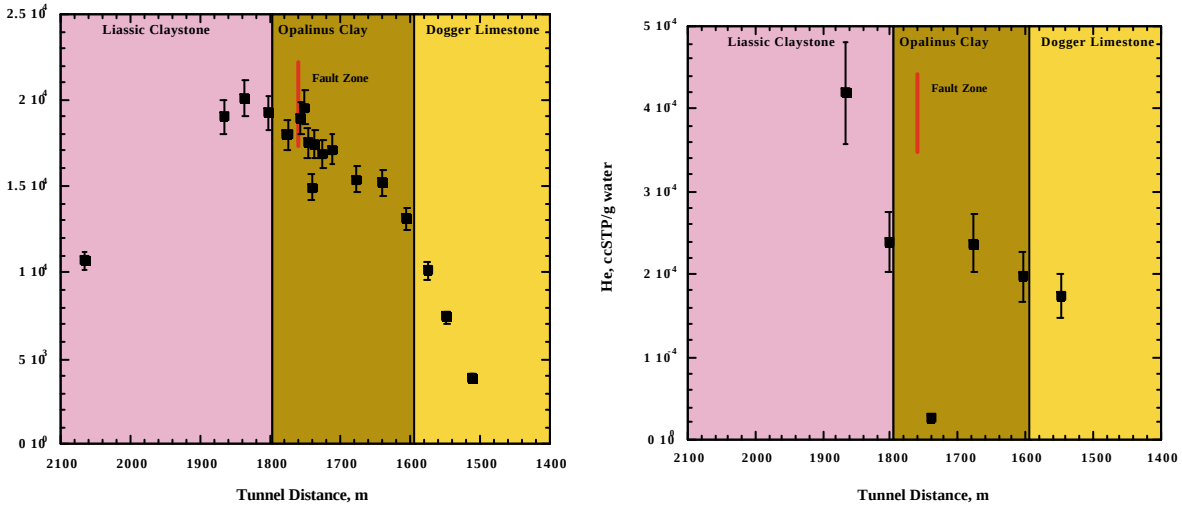

Figure 17. *Tracer profiles in pore waters sampled in a transect across the Opalinus Clay and adjacent formations: LHS: Chloride; RHS: ^4He.*

During 2006 GRS worked on modeling the profile of dissolved Helium content in the pore water at Mont Terri. The modeling was done using the r^{3}t transport program using different degrees of complexity regarding included model parameters. The results were compared to a simple analytical one-dimensional model already presented by Rübel et al. 2002. At first, a geometry for r^{3}t was created representing the situation at Mont Terri. The Helium concentration was modeled using a two-dimensional geometry, with the formation being divided into different facies, each having its own inclination angle relative to the tunnel. Three different cases have been examined and the resulting profiles are shown in figure 18. (1): homogenous transport parameters have been used; (2): variable porosity and isotropic diffusion has been used and (3): variable porosity and anisotropic diffusion has been used. A comparison of all four simulations for the Helium profile shows that the simplest one, the one-dimensional model fits best to the measured data. The simulation with variable porosity shows the largest deviation from the measured data, while the consideration of anisotropic diffusion smoothes out the effect of variable porosity. This is because the anisotropy (higher diffusion coefficient

parallel to the bedding than perpendicular to the bedding) leads to the fact that the surfaces of equal Helium concentration now are aligned more parallel to the bedding than before. Since the inclination angle is changing the most on the left side of the model this effect mainly affects the curve at this position and leads to an asymmetric movement of the left side of the curve. For the modeling of the Helium profile a higher model complexity neither led neither to a better adjustment of the modeled curve to the measured data, nor to better insight into the parameters of the formation.

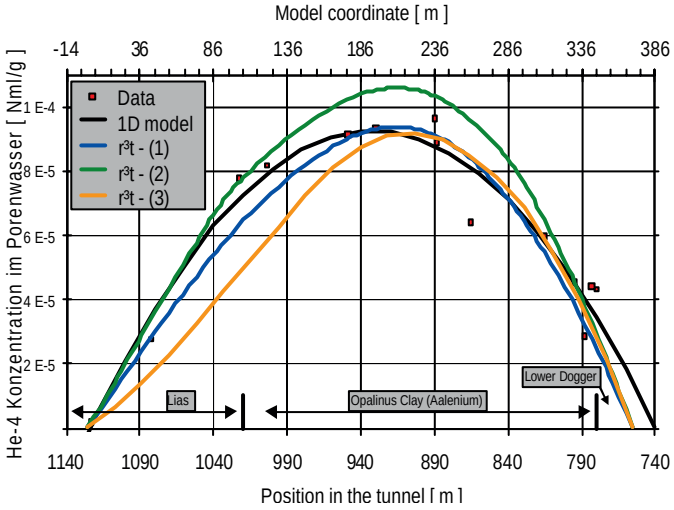

***Figure 18**: Modeled Helium concentration for a simple one-dimensional analytical model and three models with r^3t accounting for a different degree of complexity*

Several other actions in 2006 contributed to the 'up-scaling method development' aspect of WP3.4. The BRGM produced Version 1 of the geographical information systems of the COX formation (PID 3.4.2; Lerouge et al, 2006); a Version 2 was delivered at the end of 2006 (fixed bugs and errors on data).

SCK-CEN produced the "Report on considerations on up-scaling strategy in clay media" (PID 3.4.4).

Publications, Communications, PID in 2006

Publications & Communications

[1] Alonso U., T. Missana, M. García Gutiérrez, M. Siitari-Kauppi, L. Pentinnen. (2006) Radionuclide diffusion coefficients in consolidated clays determined by Rutherford Backscattering Spectrometry, Presented at the 4th Mediterranean Clay Meeting, (Ankara, Turkey-Sept. 2006) and submitted to the Applied Clay Science journal.

[2] Chapron, Y., Joubert, L., Tournassat, C. (2006) A new force fields for the investigation of clay minerals / water interfaces? CECAM workshop, Lyon, 29-31 May 2006, Modelling and simulation of clays.

[3] Charlet, L., Scheinost, A.C., Tournassat, C., Grenèche, J.M., Géhin, A., Fernández-Martínez, A., Coudert, S., Tisserand, D., Brendlé, J. (2006, submitted) Electron transfer at the mineral/water interface: Selenium reduction by ferrous iron sorbed on clay. *Geochimica et Cosmochimica Acta.*

[4] Charlet, L., Scheinost, AC., Grenèche, J.M., Tournassat, C., Géhin, A., Coudert, S., Brendlé-Miehé, J. (2006) Reactivity of ferrous iron in anoxic environments: electron transfers in Se(IV)-Fe(II)-mineral systems., in ACS National Meeting - 23rd - San Francisco - CA - 10-14/09/2006

[5] García-Gutiérrez M., J.L. Cormenzana, T. Missana, M. Mingarro and P.L. Martín (2006) "Large-scale laboratory diffusion experiments in clay rocks" presented in the MIGRATION'05 Conference and the results published in the journal *Physics and Chemistry of the Earth 31 (2006) 523-530*

[6] Géhin, A., Grenèche, J.-M., Tournassat, C., Brendlé, J., Rancourt, D.G., Charlet, L. (2006, in press) Reversible surface-sorption-induced electron-transfer oxidation of Fe(II) at reactive sites on a synthetic clay mineral. *Geochimica et Cosmochimica Acta.*

[7] Koroleva M., Mazurek M., Gautschi A., Bigler T., (2006) Natural tracer in a deep claystone formation (Opalinus clay of Mont Russelin, CH), Geochimica et Cosmochimica Acta, Volume 70, Issue 18, Supplement 1, August-September 2006, Page A331

[8] Lerouge, C., Gaucher, E., Beny, C., Tournassat, C., Blanc, P. (2006) Redox conditions in the callovian-oxfordian clayey formation., in Bridging Clay - Oléron - France - 04-07/06/2006

[9] Lerouge, C., Michel, P., Gaucher, E., Albrecht, A., Tournassat, C. (2006) A geological, Mineralogical and Geochemical Gis for the Andra URL: A tool for the water-rock interactions modelling at a regional scale., in Bridging Clay - Oléron - France - 04-07/06/2006

[10] Leroy P., Revil, A., Altmann, S., Tournassat, **C.** (2006, accepted) Modeling of the composition of the pore water of the Callovo-Oxfordian argillite. *Geochimica et Cosmochimica Acta*.

[11] Mell, P., Megyeri, J., Máthé, Z., Gsicsaic, J., Hámos, G., Lázár, K., (2006a) Sorption of Co, Sr and Cs onto argillaceous rock as studied by radiotracers, *Journal of Radioanalytical and Nuclear Chemistry*, **268**, 405 - 410.

[12] Mell, P., Megyeri, J., Riess, L., Máthé, Z., Hámos, G., Lázár, K., (2006b) Diffusion of Sr, Cs, Co and I in argillaceous rock as studied by radiotracers, *Journal of Radioanalytical and Nuclear Chemistry*, **268**, 411 - 417.

[13] Robinet, J.-C., Sardini, P., Sammartino, S., Prêt, D., Coelho, D., Management of mineralogical and textural spatial heterogeneities on solute species diffusion modelling in clayey rocks. Poster of the 43th annual meeting of the Clay Mineral Society. Bridging Clay, Oleron, France, June 3-7, 2006.

PID (months 13-24)

PID3.1.2	*REPORT OF RESULTS OF MOLECULAR DYNAMICS CALCULATIONS AND INCORPORATION OF THE EFFECT OF SURFACE ELECTROSTATICS ON ION DISTRIBUTIONS IN REACTIVE TRANSPORT MODEL.*	*BRGM*	*18*
PID3.1.5	*Report describing preliminary version (without osmotic equilibria) of the double-porosity model for simulating radionuclide transfer in compact clay materials*	*ARMINES*	*18*
PID3.1.13 (moved from WP3.2) ***Was PID3.2.13***	*Report on the redox reactivity of Fe bearing phases present in Callovian-Oxfordian rocks*	*BRGM*	*24*
PID3.1.15 (moved from WP3.2) ***Was PID3.2.3***	*Report on preliminary structural-based redox model for Fe-bearing phases in Callovo-Oxfordian based on use of Moessbauer to identify/characterize Fe-bearing phases and of oxidation potential tests on relevant pure material Fe phases.*	*UJF*	*18*
PID3.2.4	*Report on column-based experimental methodology and progress in development of the coupled laser-ablation / ICP-MS method for quantifying in-diffusion profiles of strongly sorbing radionuclides.*	*CEA*	*17*
PID3.2.6	*Report on designing and mounting of large scale test*	*CIEMAT*	*18*
PID3.2.7	*Report on experimental set-up, initial and boundary conditions for autoclave system*	*FZK-INE*	*18*
PID3.2.8	*Report and interpretation of TcO_4^- and HCO_3^- diffusion experiments on Boda claystone samples obtained from ~1000 m depth.*	*II-CRC-HAS*	*18*
PID3.2.9	*Report on sample preparation methodologies for carrying out 2D and 3D image analysis*	*ERM*	*18*
PID3.3.1	*PROGRESS REPORT ON MODELLING OF DR EXPERIMENT*	*NAGRA* *PSI*	*24*
PID3.3.2	*Report on numerical modelling of experiments including scoping calculations.*	*UDC*	*18*
PID3.3.3	*Progress report on modelling of an in situ diffusion data set using codes of different complexity*	*GRS*	*24*
PID3.4.1	*Report on natural tracer concentrations in the Opalinus clay anticline in the Mont Russelin tunnel*	*UNIBERN*	*18*
PID3.4.2	*Report on GIS of the Callovo-Oxfordian*	*BRGM*	*18*
PID3.4.4	*Report on considerations on up-scaling strategy in clay media*	*NIRAS, SCK•CEN*	*13*

R&T and poster contributions for Stockholm meeting

[1] Alonso U., Tiziana Missana, Alessandro Patelli, Miguel García-Gutiérrez, Marja Siitari-Kauppi, Laura Penttinen, Valentino Rigato "Determination of solutes diffusion coefficients in consolidated clays by Rutherford Backscattering Spectrometry: Methodology validation and preliminary results". *(paper, poster)*

[2] Bauer A., B. Fiehn, M. Klein, Ch. Marquart, Th. Schäfer, A. Görtzen, B. Kienzler Preliminary results on Pu-238 diffusion experiments *(paper and poster)*

[3] Fernández A.M., M.J. Turrero, A.M. Melón, D.M. Sánchez, M. Sánchez, R. Campos 'Results of the geochemical characterization of clayrocks from different locations: Opalinus Clay from Switzerland, Callovo-Oxfordian argillite from France and Boom Clay from Belgium' *(poster)*

[4] Lazar K., Megyeri J., Mathé Z. 'Influence of the mineral composition and the groundwater pH on the diffusion of $^{99}TcO_4^-$ and $H^{14}CO_3^-$ anions through borecore samples of Boda Claystone' *(paper, poster)*

[5] Lerouge, C., Gaucher, E.C., Beny, C., Tournassat, C., Blanc, P. 'Redox conditions in the callovian-oxfordian clayey formation' *(poster)*

[6] Lerouge, C., Michel, P., Gaucher, E.C., Tournassat, C. 'A geological, Mineralogical and Geochemical Gis for the Andra URL: A tool for the water-rock interactions modelling at a regional scale' *(poster + available Access database file on the FUNMIG website)*

[7] Robinet J-C., N. Diaz, F. Goutelard, J.C. Parneix, D. Menut, D. Prêt, P. Sardini, A. Mazurier 'From knowledge of microstructure to interpretation of modelling for diffusion of solutes in clay rocks.' *(paper)*

[8] Samper J., Qingchun Yang 'Scoping numerical calculation and predictive modelling of DR experiment' *(paper)*

[9] Sobolev O., Charlet L., Cuello G., Gehin A. 'Hydration and hydrolysis of Sm^{3+} in clay minerals. Neutron diffraction and molecular dynamics simulations – preliminary results' *(paper)*

[10] Tournassat, C., Chapron, Y. and Boulahya, F., 'Clay basal surfaces / solutes interactions : a molecular dynamics study' *(poster)*

RTD COMPONENT 4

Tizziana Missana
CIEMAT, Departamento de Medioambiente
Avenida Complutense, 22 – 28040 MADRID (SPAIN).
tiziana.missana@ciemat.es

Introduction

RTDC4 is structured in six work packages corresponding to the main investigations identified as necessary to address within the FUNMIG project: a) Characterisation of geochemical conditions in the crystalline rock including the geochemical gradients possibly induced by the bentonite buffer in the granite; b) Characterisation of the fluid flow system including fractures and the crystalline matrix itself; c) Investigation of the generation, stability and mobility of colloids through crystalline media; d) Experimental investigation of radionuclide transport mechanisms (advection, diffusion) and analysis of the effects of the presence of colloids on the radionuclide transport; e) Process identification and verification by the analysis of real systems; f) Up-scaling of processes and development of methodologies to facilitate the inclusion of processes in PA.

This paper is summarises the work carried out during the second year of the FUNMIG project, organised by work packages.

Advances within work packages

WP4.1: Characterisation of geochemical conditions in crystalline host rocks

One of the main objectives of this work-package is to study solute migration mechanisms in crystalline host-rock, influenced by the geochemical gradients, generated by the presence of the bentonite barrier. An important part of the work is carried out using data obtained *in-situ* from the FEBEX gallery (NAGRA's Grimsel Test Site, GTS, Switzerland) were the FEBEX experiment, reproducing at a real scale a high-level waste repository in granite, was installed more than 9 years ago. Another objective of this work-package is to evaluate the possible generation of bentonite colloids from the bentonite barrier in realistic conditions, for assessing their influence on radionuclide migration.

In order to carry out *in-situ* studies of the geochemical processes related to the solutes migration in crystalline rocks, and according to geological, hydro-geological and hydro-geochemical data, two investigation boreholes were drilled at the end of 2005 in the FEBEX gallery of the Grimsel Test Site (Perez- Estaún et al, 2005). More details on

the activities carried out at the FEBEX site, during the second year of the project, can be found in Missana *et al.* (2006a, this volume).

After the drilling of the new boreholes, a sampling campaign was performed in Sep 06 by CIEMAT. The sampling included the new boreholes and the old radial boreholes to continue the study of the water chemistry evolution in the FEBEX tunnel, summarised in Buil *et al.* (2006).

The blind model on the mass transfer from bentonite to granite was developed by ENVIROS and UPC-CSIC during the first year and it is being updated as far as new input data are available.

A preliminary analysis of water samples from the new boreholes to determine the presence of colloids was carried at CIEMAT. Photon correlation spectrometry (PCS) analyses were carried out for determining the concentration of colloids, in the different sampling intervals in respect to the Grimsel groundwater, and for measuring the size of the particles. The *"as-received"* samples presented a non negligible disturbance due to particle of large size, most probably resulted from the recent excavation. Therefore, further measurements were done on samples filtered by 0.45 μm membrane. The sample presenting the higher particle concentration (1 order of magnitude higher than that of Grimsel water) corresponded to the interval 2 of the FUN 1, in the region nearest to the bentonite surface. The size of these particles was around 110 nm with a poly-dispersivity relatively low (0.22). The nature, morphology and chemistry of these particles are being analysed. Colloid data obtained at CIEMAT will be compared with those obtained by FZK-INE (WP4.3) on the same samples.

Another task in WP 4.1 is to develop methods to establish the response of the bedrock to past redox perturbations caused by melt water intrusion. This type of information is of importance within PA analysis when glacial scenarios are considered. In particular, the precipitation of Fe and Mn oxy-hydroxides and the U mobilization are considered a consequence of oxidant intrusion in the system. Furthermore, as precipitation, dissolution and re-precipitation of Fe oxides depend very much on the geochemical conditions, in theory, the different Fe oxides formed can be used as indicators of the type of environment in which they formed. For this reason, HU investigated the Fe and Mn oxidized phases from olivine, as a function of the oxidation time and specific extraction procedures were applied to separate the oxidized phases. This work is carried out in collaboration with WP 4.5. More information on this activity can be found in www.helsinki.fi/radiokemia/funmig/.

Milestones M4.1.1 (Decision about the location of new boreholes in the FEBEX gallery and M4.1.2 (Start-up of drilling and instrumentation of new boreholes in the FEBEX gallery) were delivered on month 18.

WP4.2: Fluid flow system characterisation;

The main objective of this WP is to gain process understanding on fluid transport in crystalline rocks. As occurs within WP 4.1, the work is partly undertaken at a field scale, at the FEBEX gallery, but also at a laboratory scale with granite samples of different origin.

At the field scale, the main aim is to characterize the fracture network within the FEBEX gallery. To this scope, CSIC performed geophysical experiments, including

new borehole logging such as Natural Gamma and Borehole Ground Penetrating Radar (GPR) and Cross-hole Ultrasonic Tomography. The preliminary processing and integration of these different data sets indicated that the GPR record is adequate to provide images of the fractures, especially if they are fluid filled. The anomalies measured by the natural gamma can be correlated with the "diffractions" in the GPR and the fractures imaged by the borehole televiewer. More details on this work can be found in Carbonell *et al.*(2006, this volume).

The previous characterization of the fractures from borehole logging was fundamental for the decision on the type and length of the intervals of the new drilled boreholes FUN 1 and FUN 2 which had to be instrumented. As detailed in Missana *et al.*(2006a, this volume), FUN 1, which is parallel to the gallery and relatively near to the bentonite surface (20 cm), and therefore very interesting for a geochemical point of view, intersected several different regions worth to be analyzed. The *June* fracture corresponding to a small lamprophyre band; the nearly closed *July* fracture, the *August* fracture which lies approximately 22 cm near to the bentonite surface and the *September fault* region. FUN 2 lies approximately 60 cm far from the bentonite surface but the analysis of selected regions as the *December fault* region was considered useful for improving the hydro-geological model near the emplacement.

According to the previously mentioned analysis, the sampling intervals were selected and they were instrumented by AITEMIN, as detailed in Missana et al (2006a, this volume). For completing the geochemical evaluation, also the large FBX2 borehole, parallel to the gallery was re-instrumented.

AITEMIN and UPC carried out a preliminary hydraulic testing of the boreholes for the characterization of the flow around the gallery.

Apart from the global study of the fractures, *in-situ*, it was considered of interest to perform laboratory analysis of the extracted core samples using different techniques. The heterogeneity, anisotropy and porosity of these core samples are being investigated. No destructive analyses as tomography, ultrasonic methods etc., are carried out as a first step. "Destructive" analysis will be carried out in a second step. Most of the participants in WP 4.2 will be involved in this task, taking advantage of the different expertise and the available techniques in different organizations. Several samples from the FEBEX have been already distributed and a report with information of the sampling and the strategy for core selection is available (Montoto and Mateos, 2006a). OVIUNI started the analysis of these cores by ultrasonic "direct transmission method" of longitudinal waves (P waves). The zones selected for the study were: the contact with lamprophyre, *August* fracture, *September* fault zone in FUN05.001 and *December* fault zone in FUN05.002. Results showed that rock cores were anisotropic but with low anisotropy. As could be macroscopically observed, the direction of anisotropy is closely related to rock microstructures (particularly mineral lineations, fissures, cracks). The degree of heterogeneity of the rock matrix of the granite is low. In non-weathered granitic rocks the variations in the ultrasonic values seems basically related to fractographic features. These studies were also used for deciding the positions for the further cut of the samples for additional studies (Montoto and Mateos, 2006b).

As a support of diffusion studies, carried out in by CIEMAT WP 4.4 and WP 4.3, HU studied porosity and micro fracturing of different granite samples by ^{14}C-PMMA impregnation method. Visualization of the mineral specific porosity was performed with

film and digital autoradiography. More detailed analyses were done with field emission electron microscopy and energy dispersive X-Ray microanalysis (FESEM/EDAX). The porosity results were used to evaluate radionuclide diffusion coefficients obtained from previous experiments. The three types of granite analyzed come from Spain from U mine sites (El Berrocal and Los Ratones) and from Grimsel. The total porosity of Grimsel granite (0.75%) was significantly higher than the porosities of Spanish granites (0.30%). The feldspars porosities in Grimsel granite were twice to three times higher than the Spanish granites ones. By the other hand, no significant difference between the dark minerals porosities was observed. The main difference was found between the various quartz grains. The Spanish granites quartz crystals were basically nonporous when measured by the PMMA method whereas the quartz of Grimsel granite showed 0.50% intra granular porosity. These characteristics are in agreements with diffusion results obtained at a microscale by Rutherford backscattering spectrometry (RBS). The apparent diffusion coefficients calculated for uranium diffusion in Grimsel granite on different minerals were very similar ($2 \cdot 10^{-13} \pm 0.5$ m^2/s). On the other side, differences were found from one mineral to another ($9 \pm 1 \cdot 10^{-14}$ m^2/s in feldspars and $4.5 \pm 0.5 \cdot 10^{-14}$ m^2/s in quartz) on both Spanish granites, which furthermore presented always lower diffusion values than in the Grimsel granite. More details on this work can be found in Leskinen *et al.* (2006, this volume).

IIF, JGUM and FZK-INE worked in collaboration on radionuclides and colloid migration experiments and their modeling. In particular, the flow dynamics of a core from Äspö (Sweden), was investigated by JGUM with XCT (X-Ray Computed Tomography) and by IIF with PET (Positron Emission Tomography). The techniques allowed analysing, no-destructively, geometrical structure of pore space (porosity and fracture distribution) to model fluid and tracer transport on a micrometer scale. Transport simulations and modelling can be done with derived hydraulic parameters and functions; the results from the different techniques can be compared. Ideally, these transport parameters take into account inhomogeneities of the transport paths and anisotropy effects. The experimental results, obtained by these organizations, with conservative tracers yielded information about the impact of molecular diffusion with respect to the flow rate. It was clearly shown that under very low flow conditions the matrix diffusion processes may be relevant. On the other hand, studies of the colloid transport of humic acid, marked with ^{86}Y, indicated a strong retention of these colloids in the fracture. Figure 1 shows the colloid distribution in the Äspo core. More details on this work can be found in Grundig *et al.* (2006, this volume).

Finally, NILPRP worked on the implementation of the X-ray Dual Energy Tomography method and of a combined 3D tomography and X-ray fluorescence facility for the analysis of host rock structure and composition. More details on this work can be found in Tiseanu *et al.* (2006, this volume).

The Milestone M.4.2.1 (Hydraulic testing campaign) has been delivered on month 24.

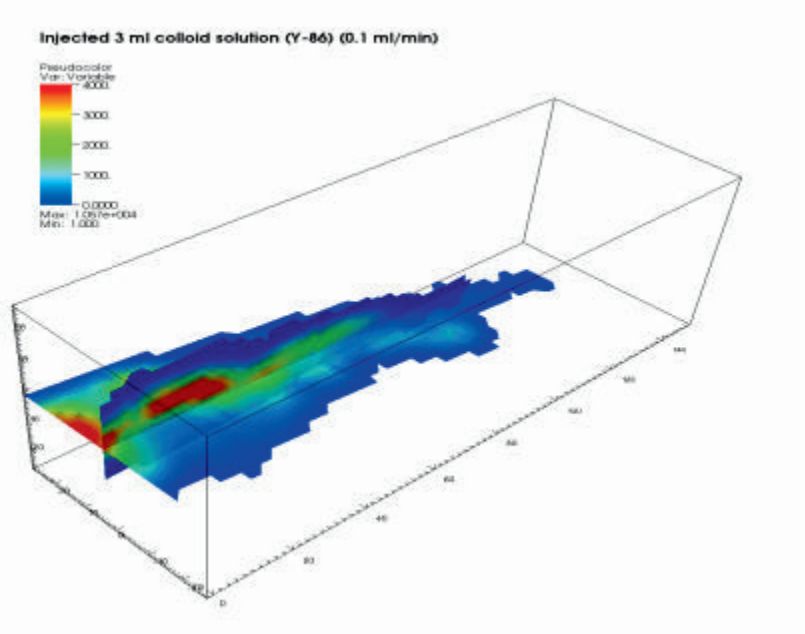

Figure 1: *Colloidal tracer distribution 86Y[Y-HA] in the horizontal and vertical midplane of the ÄSPÖ drill core*

WP4.3: Generation, quantification, characterisation, stability and mobility of groundwater colloid.

One of the mayor problems concerning this work package is the quantification and characterization of colloids originating from the bentonite engineered barrier. The stability and mobility of these colloids in the granite are evaluated by different methodologies. Special efforts are being done for determining the "source-term" of bentonite colloid in realistic conditions and for identifying their filtration mechanisms along their flow paths.

FZK-INE studied the stability of clay colloid (obtained by natural bentonites as MX-80 and FEBEX) as a function of pH (6-10) and ionic strength (10^{-3} – 1 M) in different electrolytes (NaCl, $CaCl_2$ and $MgCl_2$). In the NaCl system, colloid remained stable, within the observation time and in the pH region between 8 and 10, up to the ionic strength of 0.01 M. In the presence of bivalent cations, aggregation was observed in solution with ionic strengths as low as 2mM. In the acidic range, clay colloids were less stable. The study of the effects of organic matter on the colloids has been started.

There is a strong linkage of the studies described here to WP 1.2.

FZK-INE designed an experimental setup for colloid erosion experiments to study the release of colloids from a bentonite pellet and under the impact of different groundwater chemistries and flow velocities and also in condition of chemical equilibrium and stagnant flow.

Additional studies on the generation and stability of bentonite colloids from the compacted clays are being carried out at CIEMAT. The generation of bentonite colloids from compacted clay plugs, in contact with stagnant water was analysed as a function of (a) the density of the clay and (b) the groundwater chemistry. Results showed that the higher the clay dry density, the higher the quantity of colloids initially generated from

the plugs. Additionally it has been observed that the water chemistry controls the stability, size and concentration of the generated colloids. More details on these preliminary results can be found in Alonso *et al.* (2006, this volume). New test will be carried out using Na or Ca homoionised clays.

For identifying filtration mechanisms, FZK-INE studied the colloids interactions with granite surfaces by fluorescence microscopy using negatively charged fluorescent dyed polystyrene colloids. Preliminary results indicated that colloid attachment to the granite increased when pH decreased. However, attachment was observed also at higher pH when electrostatic repulsion between the colloid/rock should exist, possible due to enhanced surface roughness.

CIEMAT performed similar studies trying to identify the influence of different minerals on colloid attachment by μPIXE and similar conclusions were reached.

The methodology based on the application of the nuclear ion beam technique Rutherford backscattering spectrometry, already applied for estimating the bentonite colloid diffusion in granite, was applied by CIEMAT for studying colloid diffusion as function of the colloid size. Gold colloids were used in these tests as available in a wide range of monodisperse sizes. As expected, colloid diffusion was shown to be a size-dependent and size-limited process. The smallest colloids (2 nm) show the faster diffusion, while diffusion is hindered for largest ones (250 nm). Clogging effects that hindered the diffusion of colloids in the granite were observed at longer times.

To demonstrate that Au diffusion (and therefore colloid diffusion) took place in the granite, the RBS spectra were simulated with a proper equation assuming an Au concentration gradient in the granite and the temporal dependence of diffusion lengths was analyzed. Table 1 summarizes the main results obtained in this work for the colloids estimated in this study. D_a values are experimentally obtained, the others are calculated. As a consequence of these results, it was deduced that the smallest colloids are more easily filtered in the system. More details can be found in Alonso et al (submitted).

Table 1. *Evaluation of D_0, Dp, D_e, α and K_d for the gold colloids of different size. Da values are the ones experimentally determined from diffusion studies.*

Hydrodynamic Radius (m)	Da (m^2/s)	D_0 (m^2/s)	D_p (m^2/s)	De (m^2/s)	α	K_d (ml/g)
2.70E-09	7.0E-18	9.08E-11	5.83E-13	1.75E-16	25.0	9.37
1.00E-08	3.0E-18	2.45E-11	1.58E-13	4.73E-17	15.8	5.90
2.36E-08	2.5E-18	1.04E-11	6.68E-14	2.00E-17	8.01	3.00
4.75E-08	1.5E-18	5.16E-12	3.32E-14	9.95E-18	6.64	2.48
1.10E-07	ND	1.23E-12	1.43E-14	4.30E-18	ND	ND
			ε=0.0003			
ND = not determined			G=6.4E-03	Geometric factor		

This work has been carried out in close collaboration between CIEMAT and INFN-LNL within the frame of the EC - EURONS programme.

WP4.4: Radionuclide transport studies, including the effect of inorganic/organic colloids

The main objective of this WP is to obtain relevant transport parameters for develop conceptual and numerical migration models at a different scales. Matrix diffusion and advection are studied. Dynamic experiments are carried out with the elements of interests (Milestone M4.4.2) in the presence and absence of colloids, as to obtain additional inputs for the understanding of the colloid role in radionuclide transport in a fractured rock.

To support field investigations and their modelling, a large–scale laboratory experiment was proposed, simulating the *in-situ* FEBEX configuration. CIEMAT, in collaboration with UDC, designed a possible experimental configuration for carrying out the mock-up test. ENVIROS provided a report with the conceptual modelling of the experiment (Delos et al, 2006).

A large cylindrical granite block (40 cm diameter x 40 cm height) from the FEBEX gallery has been selected for migration studies. UNIOVI, analysed this large sample by ultrasonic methods for studying the anisotropy and heterogeneity. Results are available in Montoto and Mateos (2006c).

In order to simulate the migration of radionuclides at the bentonite/granite interface, a cylinder of FEBEX compacted bentonite has to be placed in the centre of the rock block. The whole block will be immersed in a bath with groundwater for maintaining the hydration. A net of small boreholes for water sampling is needed for monitoring the migration of the radionuclides that are previously emplaced within the bentonite. The net of boreholes was designed first, taking into account the technical constraints and afterwards, on the bases of this preliminary schematic, scoping calculations aided to decide the final configuration of the experiment. In particular: a) the size of the central compacted bentonite plug; b) the radionuclide injection method; c) the tracers to be used, d) sampling intervals. The Milestone M.4.4.1 (Decision on the optimisation, design and installation of mock-up experiment) has been delivered on month 18.

The tracers initially selected to perform scoping calculations were: HTO (conservative), ^{36}Cl (conservative, anionic exclusion) and ^{137}Cs (sorbing). The modelling included diffusion and anion exclusion. The input was used to analyse radionuclides diffusion in granite considering bentonite/granite interface. The concentration evolution (from 0 to 1-3 years) was calculated for each sampling point, for the three selected elements. Also the concentration changes in the marked profiles were calculated at the fixed time. Results showed that conservative tracer will move in one year between 8 and 10 cm. However, it seems difficult that Cs can be measured in granite, after this time. Sensitivity analyses were done for estimating the parameters uncertainties. Several sensitivity runs are preformed by changing one-at-a-time the following parameters: chloride accessible porosities in bentonite and in granite, Cs distribution coefficient in bentonite and in granite, effective diffusion coefficients of tritium, chloride and Cs in granite.

The porosity sensitivity analysis shows that chloride concentrations in borehole, bentonite and in granite are sensitive to changes in bentonite accessible porosities, while only chloride concentrations in granite are sensitive to changes in granite accessible porosities. After these evaluations, the mock-up experiment will be constructed as

designed. HTO, Cl and Cs will be injected even it seems that might have some problems in the Cs detection. More details on the experimental set-up and modelling can be found in Samper *et al.* (2006).

In this configuration, diffusion is expected to be the main migration mechanisms for solutes, therefore several diffusion tests, made with conventional techniques and ion beam techniques are ongoing. Several granite samples 4-6 mm thick and 68 mm of diameter has been obtained from the new FUNMIG boreholes for diffusion studies. The petrographic analysis of the samples used for diffusion experiments will be done by HU.

Column experiments allow studying radionuclide migration when advection is more relevant. Migration experiments in a granite fractured column from the Grimsel Test Site, using low water flow rates trying to approach realistic natural conditions, were carried out with bentonite colloids at CIEMAT. The objective was to quantify the filtration of colloids in the medium and to evidence the main factors affecting the retention, as well as possible experimental uncertainties, as a previous step to the analysis of radionuclide migration in presence of colloids. As already seen in preliminary tests, the breakthrough curves of bentonite colloids always presented an elution peak in a position very similar to that of conservative tracers but that their recovery critically depended on the colloid concentration and on the water flow rate.

Column experiments with europium or plutonium in the presence of bentonite colloids were also carried out at different flow rates and their recovery was analyzed. Both elements presented high adsorption onto the colloids (approx 80 % or higher) thus the migration of colloids should affect their migration. In fact, a peak of Eu or Pu in the same position than the conservative tracers was observed, clearly indicating that migration of these radionuclides is mostly colloid-driven. The recovery of Pu adsorbed onto the colloids was approximately the expected considering the filtration of bentonite colloid in the medium, whereas the recovery of Eu was always lower. The results seems to confirm that, along the flow path, part of Eu desorbs from the colloids and is retained on the fracture walls. More details of the work are presented in Missana *at al.* (2006b, this volume).

New columns with granite from the FUN 1 borehole were prepared to study colloid migration in the fracture as a function of the colloid size as a complement of the studies carried out in WP 4.3. In addition, special (half) columns to study the radionuclide retention at the fracture surface, in dynamic conditions were also designed as a support of the studies carried out in WP 4.6.

NRI-REZ activities focused on quantification of sorption and diffusion processes of PA relevant radionuclides considering the Czech deep geological repository concept.

WP4.5: Process identification and verification by real system analysis

The aim of the 4.5 work during the second year of the project was to a) perform analysis of real site processes in crystalline rock and b) to apply the approach developed to specified sites in view of site selection within the Swedish disposal program. HUT, HU, GEOPOINT and FZK-INE are working in collaboration.

The work forms part of a project which aims to (i) generate data and process

understanding for phenomena that cannot be obtained from laboratory studies, and (ii) to verify process up-scaling with respect to time, spatial scale and heterogeneity. It is based on the Swedish site investigation programme for a nuclear waste repository in crystalline rock. A database with background information has been established for the Forsmark site. A detailed analysis has identified plausible end-members as primary mixing components for the present groundwater. The portions of different groundwater contributors together with knowledge about the evolution history provide a good picture of the present hydrological situation. A large number of geochemical processes have been identified, including a detailed analysis of the origin of excessive U concentrations in some deep groundwater samples from Forsmark. Investigations of the palaeo aspects by using natural radioactive elements are under development. The results contribute to the safety assessment of nuclear waste disposal in the granitic rock investigated, with respect to the hydrological situation and relevant geochemical processes, both present ones and future site evolution with the onset of climatic changes.

The major processes and reactions that have been identified which affect the groundwater in Fennoscandia are: Climate, Flow/mixing, Reactions with the rock and microorganisms in the groundwater.

The geochemical process identification and verification by real system analysis has been one of the subjects of the Topical Sessions of the 2nd Annual FUNMIG meeting. More details on this subject can be found in Laaksoharju *et al.* (2006, this volume) and Hellmuth *et al.* (2006, this volume).

WP4.6: Up-scaling of processes

Different activities are ongoing in this WP, whose main aim is the up-scaling of different processes to facilitate their integration in PA models.

CIEMAT continued the studies on how the crystalline rock heterogeneity affects the RN retention, for a proper selection of K_d values to be used in predictive transport models. Experimental methodologies for the up-scaling of sorption parameter were tested. Dynamic experiments and the analysis of the retention zone at the fracture surface are combined. In particular, the nuclear ion beam technique μPIXE has been successfully used to determine the preferential areas of retention of different radionuclides. During this second year, mayor efforts were done to move from "qualitative" to "quantitative" analysis trying the deconvolution of the total spectrum in smaller selected areas. This is very promising since it can be useful for determining Kds in single minerals.

VTT analyzed different methods for the spatial up-scaling of the matrix diffusion. Since the field experience and modeling demonstrated that the preferential flow and transport paths may run over long distances, the up-scaling methods must consider long distance connections. Thus, fracture network modeling seems to be the only approach that is able to take into account the multi-scale structure of the fractured rock and directly determine the retention properties of the flow paths. However, this model is computationally very demanding. Conventional up-scaling methods are based on the continuum model but it was found that this approach is difficult to defend on the conceptual grounds. Other promising up-scaling methods have been developed based on the statistical description of the fracture network retention properties.

UPV is developing methodologies for the up-scaling of radionuclide transport both in porous media and fractured media also evaluating the advantages/disavantages of approaches.

Finally, CSIC and UPC are developing modeling methodologies for facilitating the transference of information to PA models.

CSIC started to develop a new object oriented structure for the organization and manipulation of chemical information that can be used in reactive transport codes. Entities representing a set of water types and batch experiments (Nodal Chemistry Class), and another entity that represent the thermo-kinetic models (Chemical System Class, which compute the chemical speciation) are considered. This entire structure is encapsulated in a class called Chemical Problem that offer general services to earth-science packages for solving reactive transport. The chemical system class is organized in species, phases, interphases and chemical reactions. The most important characteristics of oriented object concepts are used: (1) encapsulation, (2) inheritance and (3) polymorphism. These characteristics improve, simplify and make more flexible the design of future reactive transport programs.

UPC investigated, by analytical and numerical methods the interactions between chemical reactions and transport in heterogeneous media. This includes new concepts to quantify mixing of reactive components, effective transport coefficients as dispersion, retardation, velocities and homogeneous reactions. The results of multicomponent reactive transport under local equilibrium are included in Zavala *et al.* (2006).

Another new approach to reactive transport in homogeneous media based on mixing proportion has been developed (De Simoni et al., submitted). This formulation can be used in different reactive transport cases with computing advantages with respect to classical reactive transport formulations.

An additional line of research concerns the developing of a methodology to find the reactive transport homogeneous medium equivalent to a heterogeneous one, such as the double porosity model with mass transfer between low and high mobile zones. The equivalent medium allows obtaining expression for effective reaction rates. The amount of solute involved in a reaction can be decoupled in two terms, one corresponding to a homogeneous medium and another one including the reactions produced by the term of effective transfer. The decoupling enables to study the relative importance of the heterogeneity in the total of the reaction.

References

Alonso U., Missana T., García-Gutiérrez M. (2006), Experimental approach to study the bentonite colloid generation source term in different geochemical conditions, 2nd FUNMIG Annual Workshop Proceedings (Stockholm, Nov. 2006).

Alonso U., Missana T., Patelli A., Rigato V., Ravagnan J. (submitted) Colloid diffusion in crystalline rocks: experimental methodology to determine diffusion coefficients and evaluation of colloid-size dependence.

Buil B., Gómez P., Garralón A., Turrero M.J., Sánchez L. (2006), Hydrogeochemical characteristics and groundwater evolution at the GTS, Swtitzarland, CIEMAT/DMA/M2132/8/06, Ciemat Technical Report & PID 4.1.2.

Carbonell, R., Pérez-Estaún, A., Missana, T., Suso, J., Carretero, G., Bueno, J., Martínez, L., Buil, B., Garralón, A., Gómez, P., Hernán, P. Geology and Geophysics of new boreholes at the FEBEX site (2006), 2nd FUNMIG Annual Workshop Proceedings (Stockholm, Nov. 2006).

Delos A., Arcos D, Guimera J. (2006), Report on the conceptual modelling of the mock-up experiment in the FUNMIG project, ENVIROS Technical Report

De Simoni M., Sanchez Vila X., Carrera J., Saaltink M., (submitted) A mixing ratios-based formulation for multicomponent reactive transport problems, Water Resour. Res.

Grundig M. et al (2006), Studies of the spatial flow distribution and colloid transport in a crystalline rock core from Äspo with PET, 2nd FUNMIG Annual Workshop Proceedings (Stockholm, Nov. 2006).

Hellmut K.H., Read D., et al. (2006), Geochemical fluxes in the geosphere: quantitative understanding by identification and verification of processes, 2nd FUNMIG Annual Workshop Proceedings (Stockholm, Nov. 2006).

Laaksoharju M., Smellie J., Tullborg E.L., Molinero J., Gimeno M, Buckau G. (2006), Results from the groundwater hydrogeochemical investigation program in Sweden, 2nd FUNMIG Annual Workshop Proceedings (Stockholm, Nov. 2006).

Leskinen A., Penttinen L., Siitari-Kauppi M., Alonso U., García-Gutiérrez M., Missana T., Patelli A. (2006). Determination of granites mineral specific porosity by PMMA method and FESEM/EDAX, 2nd FUNMIG Annual Workshop Proceedings (Stockholm, Nov. 2006).

Missana T., Alonso U., García-Gutierrez M., Mingarro M. (2006b), Bentonite colloid filtration in a granite fracture, 2nd FUNMIG Annual Workshop Proceedings (Stockholm, Nov. 2006).

Missana T., Pérez-Estaún A., Carbonell R., Suso J., Carretero G., Bueno J., Martínez L., Buil B., Garralón A., Gómez P., Hernán P. (2006a). Overview of the activities carried out at the FEBEX site, 2nd FUNMIG Annual Workshop Proceedings (Stockholm, Nov. 2006).

Montoto M., Mateos F. (2006a) Sampling of rock-cores from boreholes FUN.05.001 and FUN.05.002, GTS, Switzerland, University of Oviedo, Technical Report.

Montoto M., Mateos F. (2006b)Profile of heterogeneity and anysotropy of selected cores from boreholes FUN.05.001 and FUN.05.002, GTS, Switzerland, University of Oviedo, Technical Report.

Montoto M., Mateos F. (2006c), Perfiles ultrasónico de la muestra RB0-1 (Grimsel), 07-06-06, University of Oviedo, Technical Report (In Spanish).

Pérez-Estaún, A. Carbonell, R. Martínez, L, Dentz, M. Suso, J. Carretero, G. Bueno, J. Buil, B. Garralón, A. Gómez, P, Arcos, D. Hernán, P. (2005), New boreholes to

investigate the bentonite/crystalline rock interface in the FEBEX tunnel (Grimsel, Switzerland), 1st Annual FUNMIG Workshop Proceedings (Saclay, France Dec. 2005).

Samper J. Yang Q., Yang C. García-Gutiérrez M. (2006), Decision on the optimisation, design and installation of mock-up experiment, CIEMAT/DMA/M2133/13/06, CIEMAT Technical report.

Tiseanu I. et al. (2006), Progress report on combined 3D tomography and X-ray fluorescence for crystalline rock analysis, 2nd FUNMIG Annual Workshop Proceedings (Stockholm, Nov. 2006).

Zavala V., Donado L.D. Dentz M., Sanchez-Vila X., Saaltink M., De Simoni M., Molins S., Carrera J., Guadagnini A, Ayora C., Multicomponent transport under equilibrium conditions, PID 4.6.1.

RTD COMPONENT 5

Ulrich Noseck
GRS mbH, Theodor-Heuss-Str., 4 D-38122 Braunschweig
Ulrich.Noseck@grs.de

Introduction

The investigations performed in RTDC5 are relevant for the overburden of a repository in rock salt. In a review meeting with the EC the question about the role of the overburden for the safety case in rock salt was raised. This point is shortly discussed in the beginning, before summarizing the progress in the distinct work packages.

In the past, emphasis in the GRS approach was put on the „brine intrusion scenario“ as the worst case. Brine inflow via the main anhydrite was assumed leading to radionuclide mobilisation and release on the same way into the overburden. In this scenario the overburden represents an important barrier for radionuclide transport. Currently, FEPs and scenarios are re-evaluated with emphasis on the „normal evolution scenario“ of a national project. This scenario is based on a complete confinement of the radioactive waste, due to reduction of voids within several 100 years and decrease of permeability of sealings and backfill down to values of undisturbed rock salt. In this case no transport of contaminants out of the salt dome can occur and transport through the overburden does not have to be regarded.

Nevertheless, investigations of processes in the overburden are of importance. In a Safety Case for a repository in rock salt it is needed to handle uncertainties, including alternative scenarios with brine intrusion and radionuclide release, which can not fully be excluded. The prerequisite for such a scenario is the formation of an interconnected system of cracks/fissures in the host rock, providing a pathway into the overburden. Processes which might contribute to that are generation of high pressure due to gas generation and temperature increase caused by heat production of the waste. Besides this other aspects as the misinterpretation of exploration results (e.g. the distance between anhydrite and rock salt is lower as expected) need to be taken into account. Furthermore recommendations of OECD/NEA and IAEA are to consider so-called what-if cases, i.e. which can strongly contribute to understanding of the whole system. Such what-if cases might be the failure of the shaft as main barrier or an exploration drilling, which again might lead to brine intrusion into and radionuclide release out of the repository.

In case of brine intrusion into the repository transport through the near field might occur relatively fast, because

- container life times are relatively short due to occurrence of corrosive brines,

- transport of radionuclides is driven by advective flow due to convergence of brine filled voids and, possibly, also by gas production and gas storage,
- there is no or only low sorption of radionuclides on salt rock or backfill

Therefore, in such cases radionuclide release from the salt formation can occur rather early and the overburden may represent one important barrier in the repository system, because dilution and retention processes decrease the potential radiation exposure and delay the arrival of contaminant peaks in the biosphere.

Key questions addressed are, which processes control the mobility of uranium and other trace elements in the natural system similar to the overburden of rock salt. Which properties and processes have impact on the generation of DOC in the natural system and how does DOC affect the mobility of uranium in the natural system?

Advances in workpackage programs

WP5.1: Determination and characterization of colloids und variation of geochemical conditions

FZK-INE performed analyses of colloid concentrations and size distributions and analyses of geochemical conditions in water from boreholes with sampling horizons in granite (RP1, NA8), which are regarded as wells in the infiltration area, in kaolin (NA7) and in clay / lignite sediments (NA6, NA12, NA13, NA10, RP2). Additionally a private well was sampled at a depth of about 7 m to obtain reference input data for the flow field ground water. The sampling depths in the investigated boreholes varied from -15 m to -37 m below ground level with about 1 m water column between sampling container and borehole bottom. Sampling and analyses have been performed with the method for geo-monitoring of groundwater (in-line with LIBD), which was described in detail in the overview report of last year.

One of the aims of the study is to verify that geochemical conditions (especially weakly reducing conditions) are maintained within the sampling container during transport and storage. A comparison of Eh and pH values (RP1, NA8, NA7, NA6) measured 14 days and 161 days after sampling show that with the exception of sample RP 2 no clear shift could be observed. This is taken as an indication that the sample cylinders are gas tight and original geochemical conditions are maintained.

Eh and pH values detected in the laboratory were additionally measured with an in-situ borehole probe at Ruprechtov site. In some cases, the data correspond closely with the laboratory determined data (RP1, NA8, NA7). In case of significant deviations (NA6, NA12, NA13) it is not clear, whether hydrochemical conditions in the flow field have changed (contact with oxygen) or sampling cylinders were leaking. The fact that all Eh values measured in-situ in March 2006 were positive even though they have been negative in some boreholes (e.g. NA7 and NA6) during an earlier measuring campaign (Mai 2003), suggests a change in geochemistry with time. This topic is under investigation and will be discussed in the first half of 2007.

Colloid concentrations vary between 170 and 740 µg/l whereby, however, a high fraction of the particles have sizes > 450 nm (Table 1). As such large particulates are supposed to settle under absence of mechanical forces as e.g. exerted by fast ground

water flow velocities, it is presently not clear, whether those colloids are stable for long time periods. The concentrations may, however be considered as upper limit values. A clear correlation of colloid concentration with element concentrations could not be observed.

A comprehensive compilation of colloid concentrations in different water samples as determined by LIBD was done and plotted versus the respective ionic strength. Increasing ionic strength usually destabilizes colloid dispersions which is reflected in the decreasing colloid concentrations in the respective groundwater.

In the Ruprechtov ground water samples the ionic strength varies between $2 \cdot 10^{-3}$ to $1.1 \cdot 10^{-2}$ mol/l with no significant influence on colloid population. The broad bandwidth of detected colloid concentrations in ground water of ionic strength < 100 mmol/l (Grimsel, Ruprechtov) suggests that different parameters besides ionic strength as e.g. pH and mechanical forces and ground water flow may control the actual colloid concentrations.

However, the studies suggest that an ionic strength of 100 mmol/l represents some kind of upper limit: colloids may persist in ground water with ionic strengths below this value for considerable time scales and variable colloid concentrations. At ionic strengths beyond 100 mmol/l natural aquatic colloid stability is effectively decreased.

A more detailed description of the results can be found in an S&T contribution in these proceedings and in the progress report on measurement of colloids and major geochemical parameters in natural ground water (PID5.1.2).

WP5.2: Geochemical behaviour of radionuclides in the natural host rock

After establishment of the different methods within the first project year, major task of the second year was the application of the methods mainly to uranium rich drill core sections from Ruprechtov site. The highest uranium concentrations are generally found in the lower part of the organic rich argillaceous layers near the interface to the underlying kaolin. The location of the investigated samples obtained from different boreholes is shown in Fig. 1.

After successful implementation of a µ-XRF method with very high spatial resolution FZK-INE performed a number of investigations on uranium rich samples from clay/lignite horizon (NA4, NA5). The small focus size can be reached by two different micro-focusing optics: the new planar compound refractive lenses (described in S&T contributions 2006) and Kirkpatrick mirrors.

By scanning the beam focus over the sample while registering fluorescence radiation elemental distributions are imaged. The use of different excitation energies, i.e. around the ionization energy for As(0) and As(V) allowed to distinguish between the elemental distribution in both redox states. By evaluation of results from numerous measurements correlations of U, As and Fe are determined. All uranium found in the hot spot regions is in the U(IV) state (µ-XANES, m-EXAFS). No correlation is observed between U and Fe. U is correlated with As(V) and there is no U which is not associated with As(V), since no U baseline is found in As(V)-U correlation. The strong correlation between As(0) and Fe confirms the occurrence of FeAsS layers on the pyrite nodules, postulated before. Details can be found in the S&T contribution.

The additional investigation of a thin section with app. 50 nm thickness from sample NA6 allowed the registration of transmission XRD patterns with a CCD camera behind the sample (s. Fig. 2). The comparison of diffraction patterns could not identify FeAsS or any other As sulphide, but correspond to FeS. The reason is probably that the amount of FeAsS on the surface of the pyrite nodule in the beam is much smaller than the FeS present.

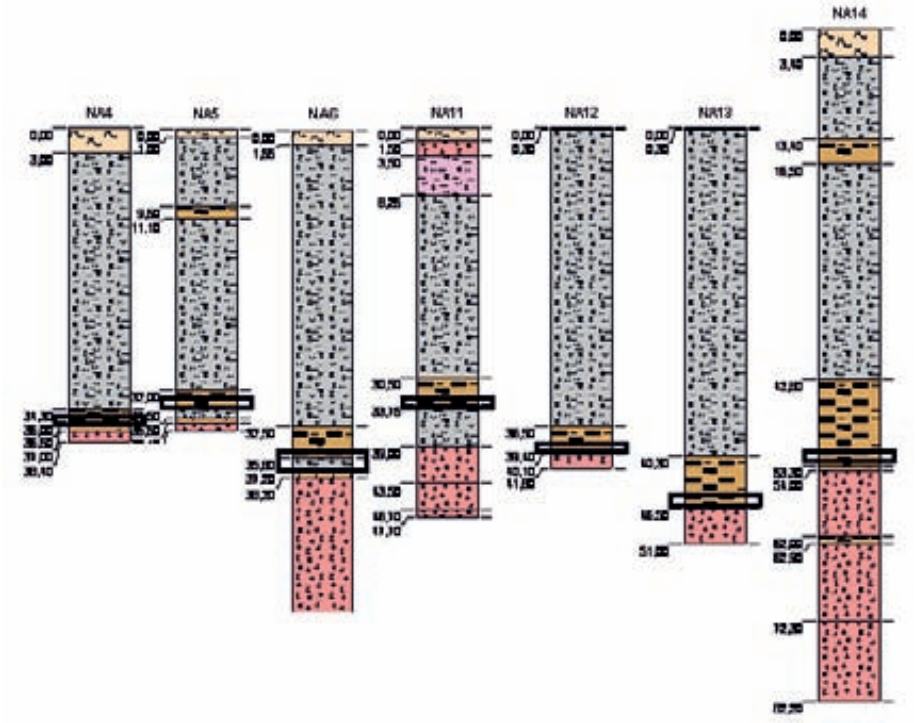

Figure. 1: *Profiles from drill cores with location of the investigated samples from clay lignite horizon*

µ-XANES spectra of the thin section show the presence of As(III) - which was never observed in analyses of the bulk samples - and no areas of As (0) alone. Apparently, the preparation of the thin sample changed the As valence in some regions of the sample. This underpins one advantage of the confocal method, i.e. experiments are conducted with almost no sample preparation, which might cause disturbances like oxidation of the sample.

By **NRI** an optimized sequential extraction (SE) scheme was applied to eight samples from six different boreholes. This scheme consists of five steps in order to quantify the following different uranium forms

- U bound on exchangeable sites
- U bound on carbonates
- U bound to Fe/Mn oxides
- U bound to organic matter / in reduced form
- U in residuum

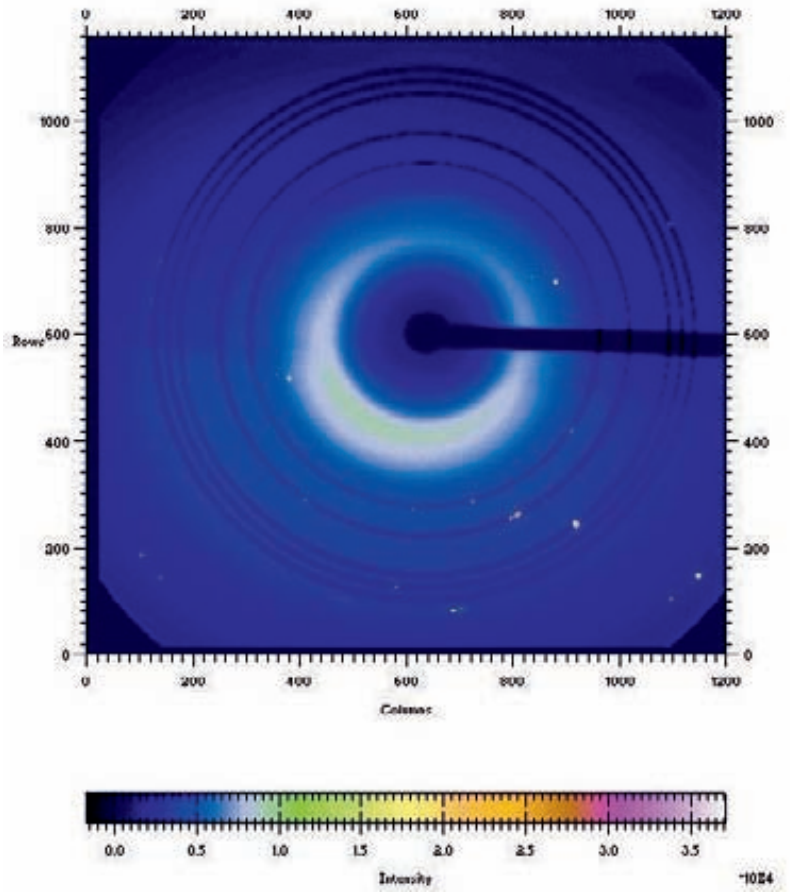

Figure. 2: *µ-XRD diffraction pattern collected at a 2 µm x 4 µm pixel having high As Ka fluorescence intensity and located on the rim of a Fe-nodule (pixel selected from µ-XRF Fe and As(0) distribution maps; E=18 keV; λ=0.6888 Å). Characteristic d-spacing pattern calculated for FeS_2 up to 27° is overlaid as dark circles.*

Samples of different composition were investigated: NA10 (kaolinized granite), NA11, NA12 (argillaceous clay) NA13, NA14 (high content of organic matter and uranium) and NA15 (kaolinized granite / argillaceous clay). Beside uranium the elements Na, K, S, Fe, As and P are analysed from each leachate. Most important results are that major amount of uranium of the highly uranium-enriched samples is found in the organic matter / reduced form phase. Cluster analyses of the SE results show a high correlation of U with As an P, whereas no direct dependence of U with Fe and S is found. These results are in good agreement with results from µ-XRF studies as well as with results from U(IV)/U(VI) separation (s. below). A more detailed description can be found in a separate S&T contribution.

CTU as associated group is involved in investigations of this work package by application of a method for determination of exchangeable uranium in the Ruprechtov samples. The exchangeable U is quantified by isotope exchange using not naturally occurring ^{233}U and synthetical seepage water from Ruprechtov site.

In few samples the oxidation of pyrite lead to acidic conditions, which increased the amount of exchangeable uranium and therefore, reflects a too high amount. However,

with exception of these samples the exchangeable U amount found within the ^{233}U experiment reached almost the same values as found in the sum of the first two steps of the sequential extraction, performed by NRI.

The method for separation of uranium (IV) and uranium (VI) has been further developed by UH for application to natural samples from uranium-rich tertiary clay horizon at Ruprechtov site, Czech Republic. It has been applied to four samples with different uranium content from different boreholes. The $^{234}U/^{238}U$ activity ratio in each phase was determined.

The data have been evaluated and interpreted by GRS and UH. The results confirms analyses from the first sample, that both forms U(IV) and U(VI) with significantly different $^{234}U/^{238}U$ ratios exist in the tertiary clay horizon and the major part is U(IV) (s. Fig. 3). The $^{234}U/^{238}U$ activity ratio of the U(IV) phase is below unity and varies between 0.45 and 0.91. This low values clearly shows the impact of a-recoil process and indicates the low mobility in this horizon. This result is consistent with those from sequential extractions of uranium rich samples, identifying most U in the phase "bound to organic / reduced form" and with the results from µ-XRF spectra, where crystalline uranium phases are found in U(IV) sate.

Nevertheless, a significant part of uranium is observed in the U(VI) state. The $^{234}U/^{238}U$ activity ratio above unity between 1.26 and 3.37 in this phase indicate that at least part of it was recently formed. Before final interpretation a partial oxidation of the drill cores after sampling need to be ruled out. Oxidation by the separation procedure can be excluded, since experiments with ^{232}U tracers do not show any oxidation of U(IV) to U(VI). Experiments focussing on the direct comparison of µ-XRF and µ-XAFS on the one hand and U(IV)/U(VI) separation on the other hand (planned within ACTINET) will contribute to answer this question. Further details can be found in the S&T contribution.

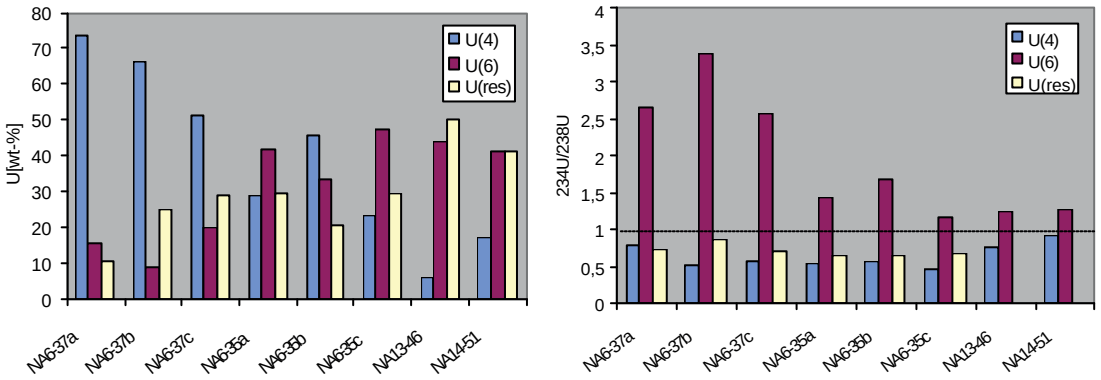

Figure. 3: *Fraction of uranium in U(IV), U(VI) and U(res) phase (left) and corresponding $^{234}U/^{238}U$ isotope ratios (right). The line has shows radioactive equilibrium.*

Further integration of results by all partners is on the way. In particular, it is intended to correlate the results from sequential extraction with results from U(IV)/U(VI) separation. Therefore, $^{234}U/^{238}U$ activity ratios in extracted solutions from

different steps will be determined and compared with the ratios measured in U(IV) and U(VI) phases.

WP5.3: Real System analyses

GRS and NRI performed additional sampling campaigns, with respect to analyses of ^{14}C and $d^{13}C$ in DOC and $d^{34}S$ in dissolved sulphates. These data are especially important to decide, if significant formation of DOC occurs in the clay/lignite horizon and whether microbial sulphate degradation plays a role.

Then all now available natural isotope data from groundwater wells at Ruprechtov site are evaluated by GRS with respect to the hydrogeological flow regime in the tertiary sediments close to the clay/lignite layers and the behaviour of carbon in the system. Differences in stable isotope data indicate two different infiltration areas in the outcropping granites in the western part as source for water in clay/lignite layers in the middle and north and another in the southern part as source for the clay lignite layers in the eastern part of the investigation area. It becomes more and more clear that water from NA8 (up to now considered as source) is infiltrating more locally and can not be regarded as main source for water in the clay/lignite horizon. Granite waters from wells NA10 (western part) and RP1 (south-western part) seem to be more adequate to be considered as source for the clay/lignite horizon. Differences in signatures in the northern part indicate very local connections probably via fault zones of the water system in the underlying granite and the tertiary sediments.

Concerning the carbon chemistry, especially the interrelation between SOC, DOC and DIC, first investigations for characterisation of DOC are performed by NRI. MALDI-TOF-MS measurements were carried out by Brno University on groundwater samples from four different wells in clay lignite horizon (NA4, NA5, NA6, and NA12) and one in the kaolin layer (NA9). The mass spectra indicate that rather low molecular organic matter with character of fulvic acids occur in all groundwaters.

Investigations of isotopes, in particular $d^{13}C$ and ^{14}C in DIC and DOC as well as $d^{34}S$ in dissolved sulphate, are evaluated. The increase of biogenic DIC with increasing DOC concentration and the increase of $d^{34}S$ in water from the clay/lignite layers compared to water from granite in the infiltration areas give rise for microbial reduction of SOC and generation of DIC and DOC in the clay lignite layers. The ^{14}C values in DOC do not show such a clear picture. But the current results are difficult to interpret due to contamination of DOC, which was identified in water from the western infiltration area.

All results are shortly summarized in an S&T contribution. A more detailed paper is in preparation.

RTD COMPONENT 6

Bernhard Schwyn
bernhard.schwyn@nagra.ch
Nagra, Hardstrasse 73, 5430 Wettingen, Switzerland

Introduction

Within the Integrated Project FUNMIG RDT Component 6 plays the role of the coordinator for linking the scientific work with the application of its results in Performance Assessment. The linking itself is in the custody of RTDCs 1 – 5. To play its role as coordinator an information exchange forum was furnished: On one hand all the Waste Management Organisations (WMOs) involved in FUNMIG participate in RTDC 6; on the other hand an Integration Monitoring Group (IMG) representing RTDCs 1 – 5 was established.

RTDC 6 is divided into three work packages (WPs):

- WP 6.1 deals with the boundary conditions to the near field and will consider the outcome of NF-PRO, a sister project within the sixth Framework Programme.
- WP 6.2 is the core task of RDTC 6. It monitors the scientific results of the project with respect to their application in PA and will give feedback to researchers.
- Within WP 6.3 Sorption data bases currently used by participating WMOs were compiled and a frame to compile sorption data acquired within FUNMIG will be established.

Advances in Work Package programs

WP6.1: Boundary conditions

The topic of FUNMIG is the investigation of radionuclide migration through potential host rocks for a repository. It is a prerequisite to have information on what radionuclides with which fluxes and in which concentrations may be released from the near-field of a repository into the surrounding rock. Such boundary conditions were documented for various European disposal concepts, namely from Spain, Switzerland, UK, France and Belgium, using the experience (recently carried out Performance Assessment exercises) from the corresponding WMOs. Analyses for the following concepts were compiled:

- "Spent Fuel/Carbon Steel Canister/Bentonite/Granite repository" by ENRESA (Spain)

- "Spent Fuel - HLW/Carbon Steel Canister/Bentonite/OpalinusClay" repository by Nagra (Switzerland)
- "ILW-LLW/Concrete/Granite" repository by Nirex (UK)
- Repository in Callovo Oxfordian Clay by ANDRA
    - B Waste/Concrete
    - Vitrified Waste/Steel Canister
    - Spent fuel/Steel canister/Swelling clay
- "Spent Fuel/Bentonite/Boom Clay" repository by ONDRAF/NIRAS and SCK/CEN

As an example a result from the Spanish analysis of a Spent fuel repository in granite is given in Figure 1. It shows the porewater concentration of nuclides in the excavation disturbed zone around the emplacement tunnel backfilled with bentonite.

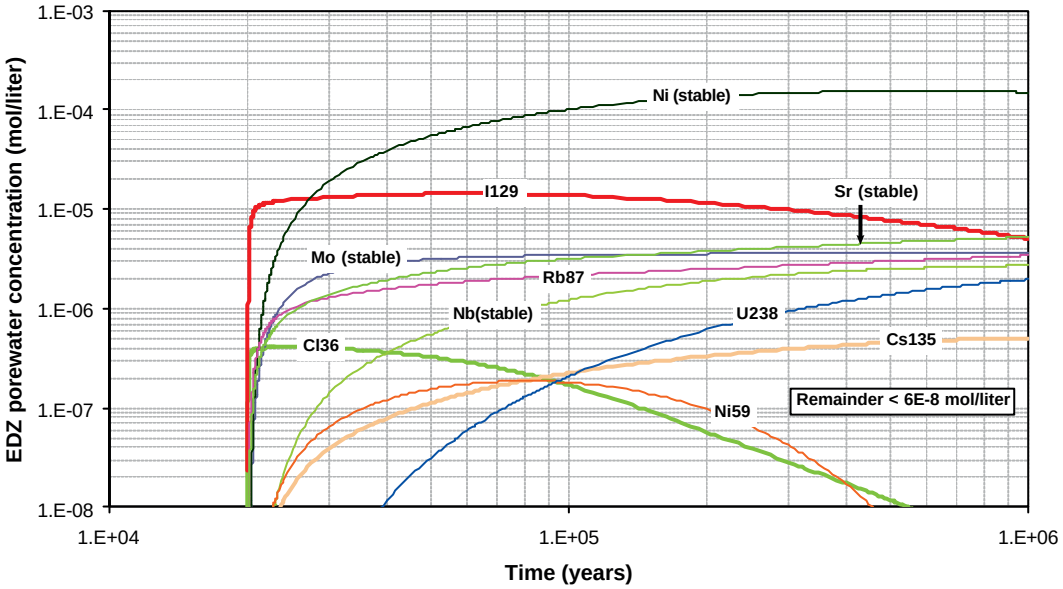

Figure. 1: *EDZ porewater concentrations (mol/liter) for a "Spent Fuel/Carbon Steel Canister/Bentonite/Granite repository"*

In general, radionuclide concentrations in water at the near field-far field interface are very small. For instance, Enresa calculations showed that ^{129}I is the only radionuclide with a concentration higher than 1ppm, and that only a few radionuclides reach concentrations higher than 1ppb. These results confirm the validity of the usual assumption that the radionuclides from the waste enter the far field groundwater in traces only.

WP6.2: Topics and processes dealt with in FUNMIG and their treatment in Performance Assessment for a geologic repository

In its role to coordinate the linking of scientific results to their application in Performance Assessment, RTD Component 6 in cowork with IMG developed a tool to evaluate FUNMIG results with respect to their use in PA:

The individual topics, processes and method developments within IP FUNMIG are listed and mapped on internationally accepted views for clay-rich and crystalline host rocks. FEPCAT (Mazurek et al. 2003) is a catalogue of Features, Events and Processes (FEPs) for argillaceous rocks. RETROCK (EU 2005) was a European project on the treatment of radionuclide migration in fractured rocks within safety assessment. A list of processes identified by the participants as safety relevant was used as a quasi FEP catalogue. Outside FUNMIG a FEP list for salt host rocks is under development and will be considered upon its completion. For this FEP mapping the structure of the project was adopted. Three Task Evaluation Tables (TETs) were prepared according to the three host rocks addressed, namely clay-rich rocks in RTDC 3, crystalline rocks in RTDC 4 and salt rocks in RTDC 5. The work of the two non host rock specific components RTDC 1 and RTDC 2 was included in each of the three host rock specific TETs. Figure 2 depicts the structure of the TETs (green boxes).

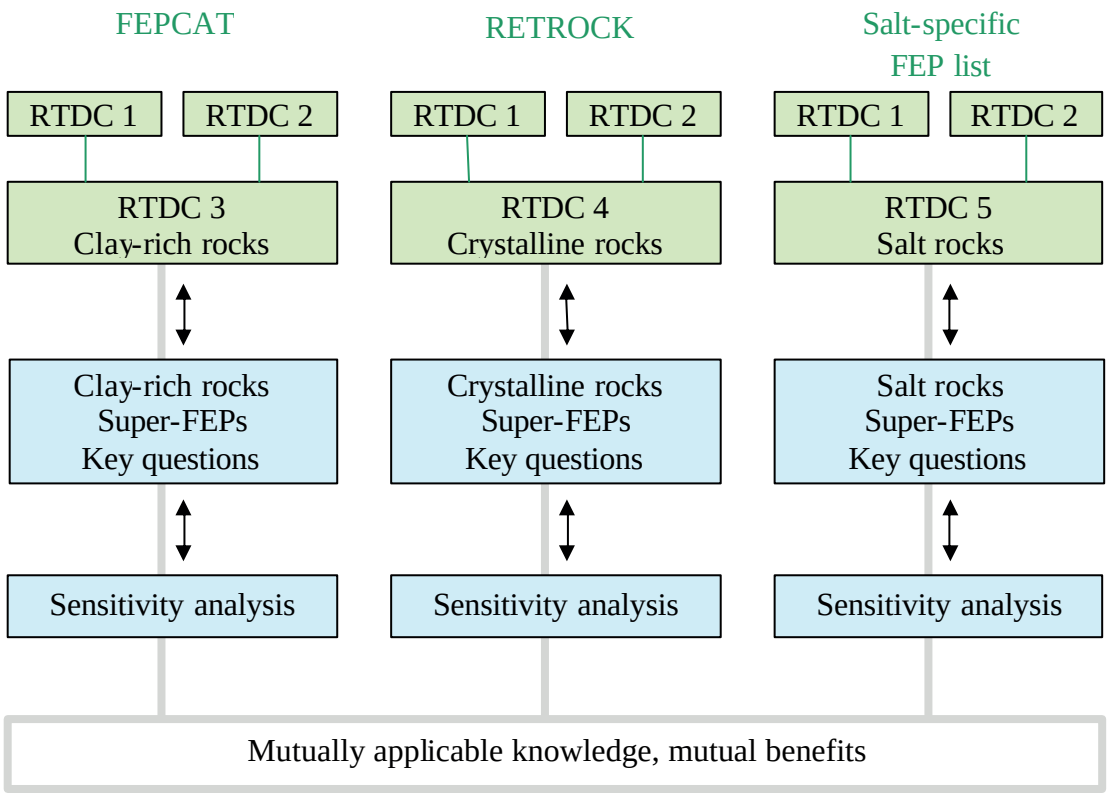

Figure 2. *Structure of task mapping and evaluation*

- RTDC 1: Well established processes (well defined)
- RTDC 2: Less established processes (ill defined)

Host rock specific, an overall picture will be synthesised starting from the individual tasks in the corresponding TETs. This may be done by lumping together individual FEPs (to which FUNMIG tasks were mapped) to "Super-FEPs" (see, e.g., Nagra 2002) and to compile a catalogue of key questions to be responded to within the FUNMIG project. This synthesis is carried out within the three host rock specific components RTDC 3, 4 and 5 in co-operation with the non host rock specific components 1 and 2. IMG – RTDC 6 play a coordinating role and bring the three syntheses under one roof. Inter alia, this will facilitate the formulation and carrying out of sensitivity analyses on one hand and the evaluation of mutual benefits and mutually applicable information among the three host rocks on the other hand (see Figure 2).

In a first step a list of tasks dealt with in FUNMIG was compiled. The rule applied to derive this list was to break down the FUNMIG work into thematically homogeneous tasks which are clearly assigned to one or several participants. Hence, the addressees of future feedback are explicitly defined. Tasks were sorted according to their affiliation to RTDCs and WPs. Table 1 gives an example of an entry in the task list. Such an entry consists of a title, an aim, a short description of the work, participants' names and other descriptions which may be task specific. In future, publications and other documentations will be referenced in the entries.

Table. 1: *Task 4.3.1 Generation of natural and bentonite colloids*

Aim	Generation of colloids under realistic conditions
Type of work:	**Lab work:** generation of colloids in low flow conditions from fracture fillings materials in a natural fracture. Characterization of the types of colloids to asses the effects of colloids in RN migration (ICP-MS, PCS, LIBD, ultrafiltration, ultracentrifugation). Generation of bentonite colloids from compacted bentonite in static conditions. Effects of the clay density in ionic strength oin the contact water. **In situ work:** Chemical analyses of groundwaters from new boreholes at different distances from the bentonite.
Indicators:	Presence of bentonite colloids in groundwater
Model	
Substrate:	Granite at Grimsel Test Site , Äspö
Participants:	CIEMAT, FZK-INE,
Publications / Documentation	*To be filled in*

Based on the task list, the three above mentioned Task Evaluation Tables were design: one for clay rich host rock, one for crystalline host rocks and one for salt host rocks. RTDC 1 and 2 are not host rock specific; their tasks were listed in all three TETs.

Table 2 lists the TET columns and specifies the responsibility to fill in columns, either the WMOs or the IMG representing RTDC 1 – 5.

Table. 2:*Task Evaluation Tables, columns and responsibilities*

Column in Task Evaluation Table	**Who?**
FUNMIG Task	RTDC 1-5 (IMG)
Investigated processes (translation into FEP terminology)	WMOs
Relevance for SA	WMOs
SA parameter	WMOs
Influence of investigated process on SA parameter uncertainty	WMOs
Relevance of SA parameter uncertainty	WMOs
Benefits of improvements ("added value" of investigation of process in FUNMIG)	WMOs
Prospects for achieving improvements within FUNMIG	RTDC 1-5 (IMG)

Currently the completion of the TETs in under way (version 1: Nagra, 2006). First conclusions may be drawn for clay rich host rocks. The translation into the FEPCAT terminology showed that virtually all tasks originating from RTDC 1, 2 and 3 could be mapped onto diffusion related FEPs, including transport and retardation mechanisms, and sorption related FEPs according to the broad FEPCAT definition which includes sorption, dissolution and precipitation of solids and solid solutions. In accordance with the experience of the involved WMOs it becomes apparent that Diffusion and Sorption (defined as retardation of RNs by chemical processes according to FEPCAT) can be designated as Super-FEPs (see Figure 2). The preliminary set of currently used Safety Assessment parameters affected by FUNMIG tasks consists of

- K_d Sorption value [m^3/kg],
- C_{sol} Maximum solubility [mol/m^3],
- D_e Effective diffusion coefficient [m^2/s] and
- ε Porosity [-].

The experience from Safety Assessment calculations by the involved WMOs shows that the affected parameters determine calculated doses to a large extent and that consequently the uncertainty bands of the affected parameters determine uncertainty bands of calculated doses. The current state of the evaluation does not allow conclusions about how the results from the individual tasks will improve “best guess” values and will decrease uncertainties of the affected parameters but it confirms the expectation that the FUNMIG results will narrow down uncertainties and will contribute to process understanding.

WP 6.3: Sorption data bases

Currently sorption is considered to be the most important chemical retention process for radionuclides in the geosphere and the FUNMIG results are expected to contribute to the current knowledge base. It is therefore important to make sorption databases available for safety assessors. In a first step the sorption databases currently used by the involved WMOs were compiled. The latter were asked about

- the type of sorption database used in their PA,
- the experiments from which sorption parameters were determined:
    - Type & conditions
    - Sample characterization
    - Data interpretation / model application,
- the availability of data and
- bibliographic records.

Distribution coefficients (K_d values) are widely used in PA. They are host rock or site specifically derived from experiments or taken from literature. Mechanistic models are increasingly used for the derivation. All safety relevant nuclides are considered including fission an activation products as well as actinides. The investigated solids include pure minerals, mixtures and natural rock samples; coatings are rarely considered. Within this first step not all sorption databases used in PA were made available, leaving the current compilation incomplete.

Subsequent work focuses now on the collection of sorption data to be measured and derived within FUNMIG. The structure of the database, which will be hosted parallel at the FZK/INE and FZD/IRC, is currently developed.

References

EU (2005): Treatment of radionuclide transport in geosphere within safety assessments (Retrock). Final Report. EUR 21230 EN. European Commission, Community Research, Brussels, 2005.

Mazurek, M., Pearson, F.J., Volkaert, G. & Bock, H. (2003): Features, events and processes evaluation catalogue for argillaceous media. OECD / NEA, Paris, 2003.

Nagra (2002): Project Opalinus Clay: FEP management for safety assessment: Demonstration of disposal feasibility for spent fuel, vitrified high-level waste and long-lived intermediate-level waste (Entsorgungsnachweis). Nagra Technischer Bericht NTB 02-23. Nagra, Wettingen, 2002.

Nagra (2006): Fundamental Processes of radionuclide migration: Topics and processes dealt with in the IP FUNMIG and their treatment in the Safety Case of geologic repositories for radioactive waste. Nagra Arbeitsbericht. Nagra, Wettingen, 2006.

TOPICAL SESSIONS

SUMMARY OF THE 1ST ANNUAL WORKSHOP TOPICAL SESSION ON 'DIFFUSION AND RETENTION IN COMPACTED CLAYEY MATERIALS'

Scott Altmann

Andra Agence Nationale pour la gestion des Déchets Radioactifs.
1/7 rue Jean Monnet
F-92298 Chatenary Malabry CEDEX, France

*Corresponding author: Scott.altmann@andra.fr

The main objective of this topical session was to provide an overview of the diversity of conceptual and experimental approaches which are being used to further our understanding of a key process for radwaste management: coupled 'diffusion – sorption' transport of radionuclides in compacted clay-rich materials (clayrock, bentonite…).

The introductory presentation by Eric Giffaut (Andra) entitled *'General conceptual framework for solute transport through compacted clays and frequent observations in diffusion studies*' provided a framework for the other talks. The commonly used means for characterizing steady state diffusion (e.g. through diffusion for determining De) and 'equilibrium' retention parameters (solid-solution partitioning in batch systems), as a function of key state parameters (aqueous phase composition, compaction density, sorbing element concentration….), on relatively small rock volumes / masses were mentioned. It was pointed out that, despite the significant existing databases of results from such measurements, various uncertainties remain which need to be reduced in order to increase confidence in safety cases. Cited examples included:

- Need for theoretically well-grounded representation (model) of the effect of ionic strength on anion diffusion (i.e. anion exclusion in negatively charged porous media).
- Need for demonstrating the transferability of sorption parameters (models) obtained by means of batch systems to calculating (modelling) the retardation effect during diffusion in compacted materials.
- Need for improving confidence in the use of physical-chemical 'analogy' arguments used for attributing diffusion and sorption parameter values to radionuclides for which direct measurements of parameter values are unavailable.

- Need for a more rigorous approach for 'up-scaling' from transport parameter databases obtained by measurements on a limited number of small volume samples to the safety case scale representation.

The utility of HTO as an indicator of sample integrity and maximum diffusion accessible porosity was illustrated, while mentioning that HTO diffusion is not representative of ionic species diffusion. Commonly observed characteristic transport behaviour of both anions (e.g. increasing De, w with ionic strength) and cations (e.g. increasing De for the alkaline earth elements in relation to their cation exchange intensity (Kd)) were shown. An improved understanding of the forces affecting cation dynamics at the molecular scale in charged clay media should help in explaining the latter phenomena. At a more macroscopic scale, particularly important for moderately to strongly sorbing radionuclides, the principal means of demonstrating / quantifying the links between Kd databases and coupled transport behaviour involves comparing Kd calculated by modelling observed diffusion profiles with the corresponding batch determined Kd. The importance for the safety case to be able to justify the models used to simulate the capacity of a host formation to limit radionuclide release by limiting diffusion flux (mainly anions) or sorbing radionuclide mass (mainly cations) is illustrated by the contrasting behaviour of ^{36}Cl and ^{135}Cs in Andra's PA reference calculations for migration into the host formation from spent fuel storage cells (cf. following figures).

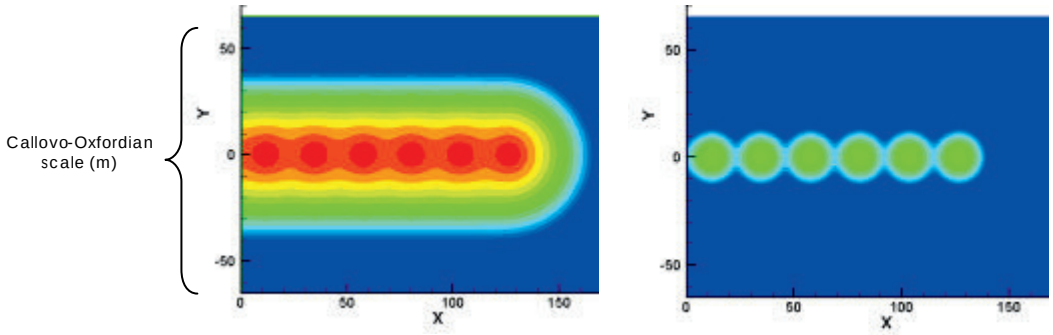

*Isoconcentrations at **20 000 years** for a non sorbing anionic tadionuclide, ^{36}Cl, in the 130 m thick Callovo-Oxfordien host formation (example for spent fuel cells)*

*Corresponding isoconcentrations at **200 000 years** for a sorbing cationic radionuclide, ^{135}Cs*

The most direct approach to determining the transport parameters needed for performance assessment models (e.g. apparent diffusion coefficient, retardation factor, accessible porosity) is to carry out direct measurements via migration experiments, and then to extract the parameter values by interpreting data with an appropriate model. This approach is the foundation for much of the program carried out by SCK.CEN for characterizing the Boom clay. The talk by Norbert Maes (SCK-CEN) entitled '*Experimental research on diffusion in natural clay samples. An overview of the Belgian experience*' illustrated how these type studies were carried out using different techniques applied to a variety of radionuclides in order both to understand migration mechanisms and to determine PA parameters representative of in situ conditions. A variety of small scale laboratory tests were used (through diffusion, impulse injection tests, percolation tests, electromigration) as well as large scale injection experiments in

the HADES URL, each with its own particular advantages and limitations. For example, application of hydraulic gradients or an electrical field significantly reduced the time necessary for measurements and, in certain cases, provides additional confirming information (e.g. effective permeability). The following figure shows an example of the diffusion profiles observed for various anionic and cation species during electro-migration from a planar source term situated in the middle of a plug of Boom clay.

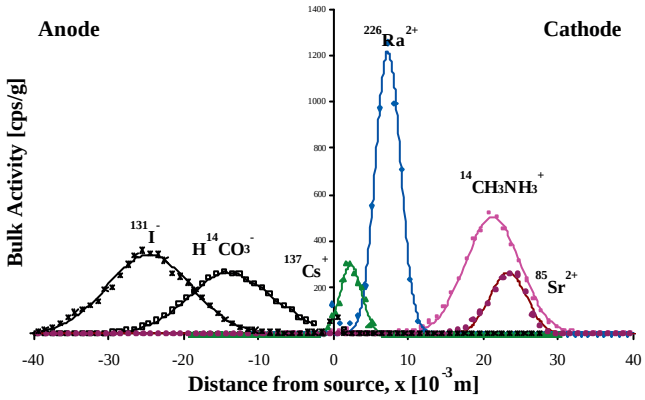

In certain cases (e.g. migration of Am complexes with Boom clay natural organic matter, SeO_3^{2-} migration), the experimental results showed complex behaviour indicating a need for additional research to consolidate the safety case. The excellent correspondence between (i) model predicted diffusion of HTO into the host formation (based on diffusion parameters initially determined on small scale samples) and (ii) data obtained during an ongoing very long time frame (~12 years) in situ migration test, shows that, for this simplest of tracers, parameter values measured on small samples can be upscaled to PA significant rock volumes. To conclude:

- Migration parameters for elements with a simple chemistry can be derived with a variety of techniques, thereby allowing the general transport parameters of the rock to be studied,
- For elements with a more complex chemistry, unambiguous interpretation is not possible based only on migration test results, complementary information is needed. These tests however give direct indications of the performance of the host rock.

It is well known that diffusion parameter values for anionic species measured on laboratory samples can vary significantly if the ionic strength of the porewater is changed. An example of the effects on De and accessible porosity for two Callovo-Oxfordien arglite samples is shown below.

The talk by Florence Goutelard (CEA) entitled *'Interpreting ionic strength effects on diffusion parameters'* gave an overview of the essential aspects of this important subject. Our current understanding of the origin of this effect is that it is due to the electrostatic repulsion of anionic solutes away from the negatively charged surfaces of the clay minerals in contact with the porewater. Electrical double layer theory tells us that the thickness of the pore solution layer influenced by the electrostatic field increases with diminishing solution ionic strength. This has the effect of reducing the porosity accessible for anion diffusion at lower ionic strengths, the so-called 'anion

exclusion', and accounts for the observed results (cf. figure above). No effect on the accessible porosity for cations or HTO is expected or observed. This conceptual model is coherent with observations of a clear correlation of the accessible porosity with the clay mineral content of samples coming from the different geological strata at the Bure URL site. It also indicates the necessity of having a good estimation of the in situ ionic strength of clayrock porewater. Several approaches were mentioned which should improve our understanding of this phenomena, and therefore strengthen the safety case, among which were a need for a better model of rock microstructure, comparative studies on different clayrocks and with different anions (polyvalents…).

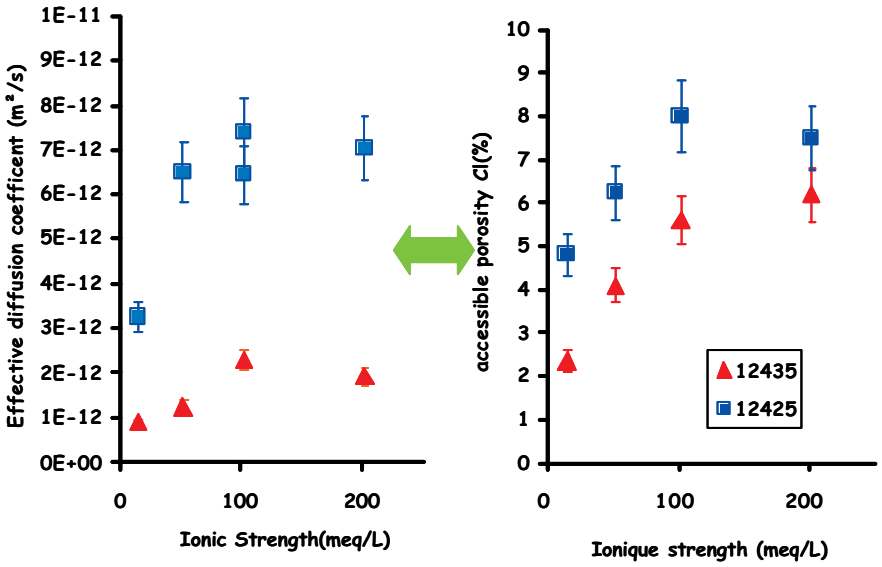

The title of the talk given by Mike Bradbury (PSI), *'Validity of distribution ratios measured in dispersed systems to intact rocks*', corresponds with one of the most frequently asked questions which must be addressed when making a safety case for the performance of clayrock and compacted bentonite systems. The reason this is so important is that the apparent diffusion coefficients (or equivalently, the retardation factor) used for modelling radionuclide migration in PA models are, in most cases calculated from separately determined parameters, the principal ones being the effective diffusion coefficient, De, and the distribution ratio, Rd. Rd values are taken from sorption databases obtained by measurements on crushed material in batch systems, mainly because of the prohibitively long experimental time frames needed for quantifying retardation factor in compacted materials for moderately to strongly sorbing radionuclides. In fact, in cases where comparisons of Rd values measured in batch systems with one determined by interpreting 'in-diffusion' data have been made, batch values were often found to be greater, sometimes significantly. In these cases, if the Da value used in PA was calculated form the batch Rd, the Da would be non conservative, which is a clearly unacceptable situation for the safety case. A strategy for progressing towards a better understanding of the real intensity of the effect of Rd on diffusion in

compacted rock was outlined. The approach for weakly sorbing species (e.g. Na^{+}, Sr^{++}) carried out on the Opalinus clay is shown in the following figure.

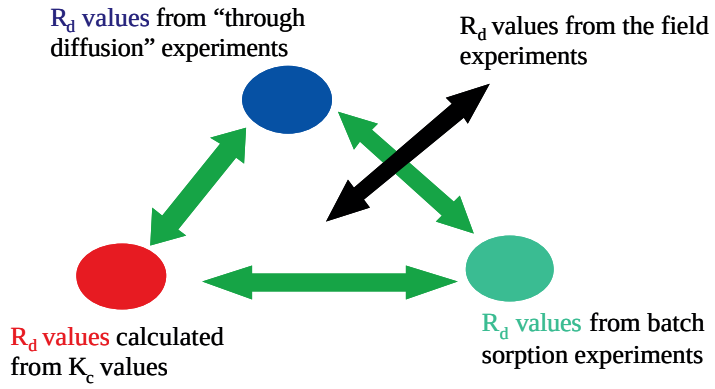

Several experimental aspects must be carefully controlled in order to insure that the Rd values extracted from the different approaches are truly comparable, particularly important being the solution chemistry and use of comparable rock samples. The preliminary conclusions of this approach are reassuring for weakly sorbing tracers with simple chemistries, i.e. the Rd value deduced from intact rock diffusion experiments is quite similar (within a factor of 2) to that measured in batch systems.

Arriving at the same level of comparison for strongly sorbing radionuclides (actinides…) is much more difficult, simply because they sorb so strongly and therefore migrate extremely slowly into compacted rock. Special techniques such as abrasive peeling have been developed to be able to quantify the in-diffusion profiles, which can be as shallow as 1 to 2 mm! Sorption on the surfaces of experimental systems is also a serious problem which must be taken into account when interpreting the results.

The importance of taking into consideration the coupled effects of different phenomena when modelling radionuclide transport in compacted clayey materials should be clear given what has been presented above, in particular the effect of charged clay surfaces on ion mobility (anion exclusion, cation sorption…). The talk be André Revil (CEREGE) entitled *'Use of coupled transport / triple layer model (TLM) for interpreting ion transport through compacted clays'* presented a model incorporating, in a single conceptual framework, the main coupled phenomena (see figure below) taking place when different potential gradients (fluid pressure, electrical, chemical) are applied to compacted clay materials (bentonite, argillite..).

"M"-form	Chimical potential	Electric potential	Fluid pressure	Temperature
Salt flux **J**d	**Fick's law**	**Electrophoresis**	**Convective diffusion**	**Soret effect**
Current density **J**	**Diffusion current**	**Ohm's law**	**Electrofiltration**	**Thermo-electricity**
Darcy velocity **u**	**Osmosis**	**Electro-osmosis**	**Darcy's law**	**Thermo-osmosis**
Heat flux **H**	**Dufour effect**	**Peltier effect**	**Convective flux**	**Fourier's law**

The model is capable of interpreting the data obtained by a variety of experimental systems exploring certain 'off diagonal' phenomena (in blue above), an example being

the variation in electrical potential difference between the two surfaces of a clayrock sample subjected to a change in hydraulic pressure (cf. figure below).

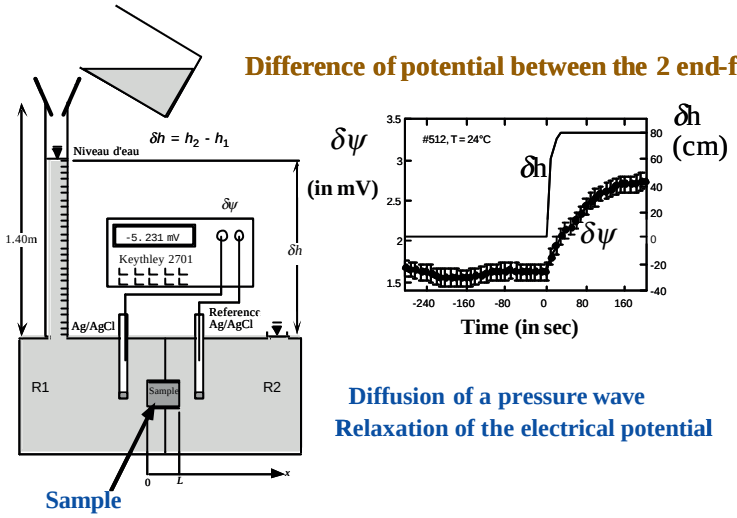

The combined measurement strategy and interpretive model offer a means of improving our theoretical understanding of the effects of such key parameters as material mineral and porewater composition, porosity and pore dimensions, etc. on the transport characteristics of ions of different sorption intensity and charge.

An enhanced understanding of the behaviour at the molecular scale is essential for understanding certain aspects of the transport of radionuclide species in compacted clays, in particular the observed correlation between the effective diffusion coefficient and Kd for alkaline earth cations. The presentation by Virginie Marry (LI2C) entitled '*Modelling transport in clays: microscopic simulations*' showed how molecular dynamics modelling can be used to study diffusion of ions such as Na^+ and Cs^+ at the nanometer scale within the interlayer spaces of model clay minerals. The model shows that Cs^+ tends to diffuse by 'hopping' from one charged site to another (cf. left hand figure below), while Na^+ diffuses in the middle of the pore space. The model also show that the H atoms of water molecules have preferential positions with respect to the clay surface (right hand figure).

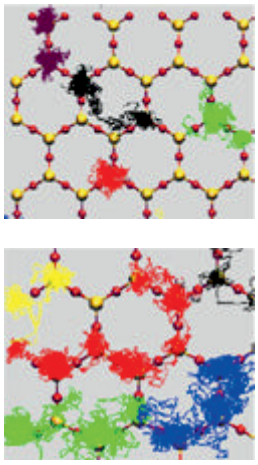

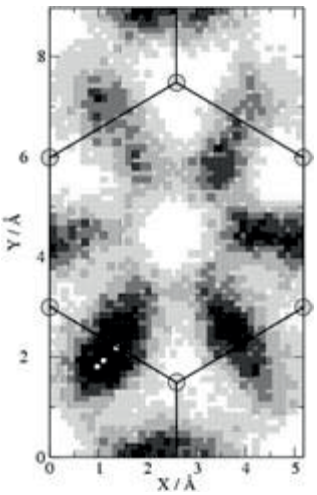

The diffusion coefficients calculated for a bihydrated interlayer space are two to three times lower than in bulk water, which corresponds to a constrictivity value range (0.3 to 0.5) similar to that obtained by I. Bourg by analysing macroscopic scale diffusion data on compacted bentonite (i.e. 0.3). Research is on-going in order to incorporate consideration of the tri-hydrated state and to understand the role of charged edge sites on access of ion to the interlayer spaces. These efforts we help in consolidating the conceptual model of how specificities in terms of ion behaviour at the microscopic scale affect their macroscopic diffusion transport, i.e. the up-scaling steps shown below.

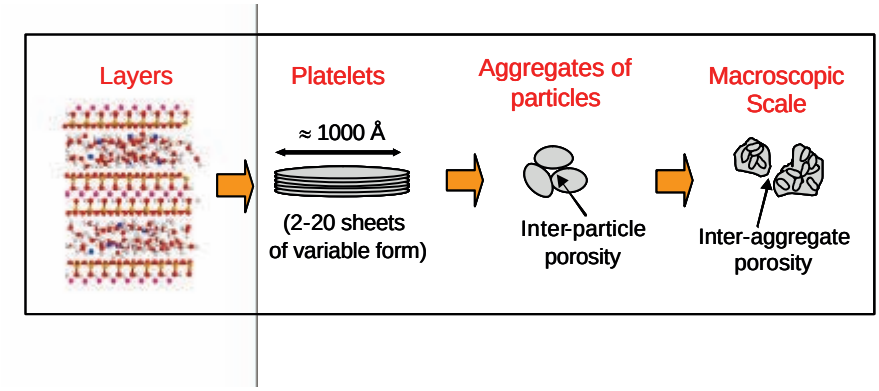

SUMMARY OF THE 2ND ANNUAL WORKSHOP TOPICAL SESSIONS

Tizziana Missana* and M.Jesús Turrero

CIEMAT, Departamento de Medioambiente,
Avenida Complutense 22 (MADRID) SPAIN

* Corresponding author; tiziana.missana@ciemat.es

Abstract

One of the main objectives of the Topical Sessions at the annual Meeting is to have *in-depth* presentations of topics and processes subject to IP- FUNMIG. The content of these presentations should help updating the important project deliverable "Key topics and treatment of processes in the Safety Case of Geological Disposal".

The Topics selected for the 2nd FUNMIG annual meeting were the following: **(1)** *Role of biogeochemical processes on radionuclide migration;* **(2)** *Characterization of geochemical conditions in crystalline rock/ Process identification and verification by real system analysis;* **(3)** *Fluid flow system characterization in crystalline rock: effects of the heterogeneity and up-scaling.*

The Topical Session included six very interesting talks: the full content of these presentations can be found in the intranet of the project (www.funmig.com).

In this paper, a short summary of the main outcome of the presentation will be given, focusing the attention on those aspects of particular interest for safety assessment.

Introduction

The Topical Session main objective is to treat selected topics and processes subject to IP-FUNMIG *in-depth* to extract useful information for the updating of the important deliverable "Key topics and treatment of processes in the Safety Case of Geological Disposal".

In the first FUNMIG Annual Meeting, the Topical Session was mostly devoted to the Component 6 of the project (RTDC6). Many waste management organizations described the base knowledge of the main processes influencing radionuclide migration and their implementation to performance assessment (PA) exercises. Additional topics were: (1) the *"NEA SORB project"* which treated the interpretation and prediction of sorption using thermodynamic sorption models and (b) *"Diffusion in clay"*.

This year, it was decided to focus the attention on processes and studies relevant for crystalline rocks. A detailed view of the treatment of radionuclide transport in geosphere within the safety assessment (SA), in different countries, was recently given after the RETROCK project (RETROCK, 2005), including indications on those issues that will deserve more attention, from the performance assessment (PA) point of view. This document can be considered as an initial communication bridge between PA and the scientific community interested on radionuclide migration in crystalline media.

Three Topics were selected for the 2nd FUNMIG annual meeting: all of them are of great interest for SA. The first topic was: *Role of biogeochemical processes on radionuclide migration*. Prof. K. Pedersen (Göteborg University) gave a talk on the effects of microorganisms upon radionuclide migration treating the general aspects and describing the most important results and conclusions from laboratory experiments and in-situ investigations carried out at Äspö hard rock underground laboratory (Sweden). Dr. H. Moll (FZR) presented the main results on the interactions of microbes found at Äspö laboratory with important actinides such as curium, uranium and plutonium (Moll, this volume).

The second Topic was: *Characterization of geochemical conditions in crystalline rock: process identification and verification by real system analysis.* Dr. M. Laaksoharju (GEOPOINT) detailed the results from the groundwater hydro-geochemical investigation program in Sweden (Laaksoharju et al, this volume) and Prof. K.H. Hellmut (STUK) gave an overview on the use of generic and site-specific information to gain a quantitative understanding on natural geochemical fluxes in the geosphere (Hellmut et al, this volume).

Finally, the third Topic was: *Fluid flow system characterization in crystalline rock: effects of the heterogeneity and up-scaling.* Prof. J. Carrera (UPC-CSIC) treated the effects of heterogeneities in transport modeling, describing different possibilities for the up-scaling. The possible implementation of coupled reactive transport was another issue treated. Dr. P. Sardini (HYDR'ASA Laboratory) analyzed the effects of heterogeneity in matrix diffusion phenomena, evidencing the importance of detailed petrography studies for the determination of the distribution of solute residence time in the rock matrix.

The Session resulted in an interesting, dynamic and constructive forum of discussion. The main questions rose and the outcome of the Topical Session are summarized below.

Role of biogeochemical processes on radionuclide migration

Microbes are present at all depths and in very different geochemical conditions. Microbial processes can influence radionuclide migration directly or indirectly and their effects can lead to either radionuclide mobilization or immobilization, depending on the type of process and the state of the microbes. Microbes can occur as planktonic cells floating in water or they can be attached to solid surfaces onto biofilms.

The microbial activity depends strongly on the type of microbe and the effects of this activity are different on different radionuclides, site-specific studies are thus

needed. Important processes directly affecting radionuclide partition between the solid and liquid phase are (Pedersen, 2005): (a) Bio-sorption, where radionuclides attach to the microbial cells surface through different possible ligands; (b) Bio-accumulation, where the elements are accumulated in the microbial cells; (c) Bio-mineralization, in which radionuclides precipitate with microbially-generated ligands (sulphide, carbonate, phosphate). Bio-transformations, in which the transformation of some radionuclides is catalyzed directly by microbes, metabolic redox reactions are very important for determining the radionuclide speciation in the environment. In general, microbial metabolism lowers the redox potential, and is also capable of directly reducing solute ions redox state affecting their solubility and geochemical behavior.

Organic surfaces and iron oxides are also very important in radionuclide retention: some microorganism is able to oxidize Fe(II) to Fe(III) resulting in biological iron oxides (BIOS) that where found everywhere at the Äspö hard rock laboratory and provides a strong retention capacity (Anderson and Pedersen, 2003). On the other hand, the formation of biofilms covering granite rock in fractures cannot be ignored as it may reduce the retention capability of the rock matrix (Anderson et al., 2006b).

The formation of some type of chelating compounds produced by microbes to increase the bioavailability of essential elements, can lead to the mobilization of heavy metals and radionuclides (Anderson et al., 2006).

Apart from having direct effect on radionuclides, microorganisms can modify the geochemical conditions of the environment and their evolution (redox, organics or ligand formation). Sometimes the effects of microbial activity are opposite. As an example, microbes may catalyze reactions that stabilize the redox potential in groundwater at a low and, therefore, beneficial level for a radioactive waste repository, but the production of sulphide is unfavorable for the copper canisters since it enhances their corrosion.

The understanding of geochemical conditions in a given site is possible only if the picture is complete and all the components are considered. Geochemical models may be wrong if not all the components are included: an effort is needed to include biogeochemical processes in these models.

The presence of microbial processes adds to the system a factor of “life” to chemistry, thermodynamics and transport which is sometimes complicated to predict and understand.

At moment, microbes are not included in performance assessment of nuclear waste repositories because of the knowledge of processes is considered average to poor. Conservative assumptions are generally made to overcome the problem (RETROCK, 2005).

However, examples showed that not all the microbiological processes are favorable to radionuclide retention. It is not totally clear that all the microbiological mediated effects can be “conservatively” excluded by the risk assessment.

Many efforts are being done to produce more knowledge, also at a mechanistic level, with the help of sophisticated techniques including, for example, Laser Induced Fluorescence Spectroscopy and X-ray Absorption Spectroscopy (Moll, this volume).

The role of biological mediated processes on radionuclide migration is being understood more and more and, in parallel, efforts to couple microbiology and chemistry are growing (Samper et al, 2003: Molinero et al, 2004).

It is important to highlight new advances in this field because they can be a fundamental support for the safety assessment. If microbial processes are overlooked it may result in models and SA not reflecting the true situation in future radioactive waste repositories. Furthermore, the optimal use of available knowledge on microbial processes can reduce conservatism in future safety assessments.

Characterization of geochemical conditions in crystalline rock. Process identification and verification by real system analysis

The characterization of the geochemical conditions in the geosphere has a direct influence on several processes important for radionuclide migration: adsorption, precipitation and dissolution, radionuclide speciation, redox, presence and stability of colloids.

Site-specific studies represent a direct support for performance assessment since, after screening and evaluation, geochemical data support site selection and SA. A site is adequate only if several criteria on basic parameters (Eh, pH, TOC, colloids presence, Mg-Ca, etc…) are met. The values obtained are used as input parameters for performance assessment calculations.

On the other hand, these studies represent an indirect but not less important support for PA. In fact, they are fundamental to understand phenomena that cannot be obtained from laboratory studies. The understanding of the hydro-geochemical condition of the past and present is the basis to predict future evolutions. Additionally, the thorough characterization of a site allows gaining capability and confidence for the extrapolation of data when the information is scarce or not available.

For a complete geochemical characterization, it is necessary to identify all water types, the possible (site-specific) processes and the related uncertainties affecting the water chemistry evolution. It is important to know water paths, residence times, flow/mixing region, redox condition, to determine the most relevant water/rock interactions and the possible effects of microorganisms or colloids. In certain environments (ej: Fennoscandian shield) the climate may have very important effects.

It is important remarking that to obtain the information needed for a complete description of the system the hydrogeochemistry should not be separated from geology and hydrogeological studies.

The analysis of natural geochemical fluxes and resulting elements concentration in the geosphere can be used as a complementary safety indicator, to be compared with calculated repository releases. The quantitative understanding of the observed site has a direct application to SA mainly because it improve the knowledge and give more confidence. The observation in nature of geochemical fluxes and their anomalies allows the development and evaluation of concepts (as chemical stability, radionuclide migration, changes in temporal and/or spatial scale), parameters, scenarios (effects of climate changes, paleo-evolution) and models.

The use of coupled transport models and their implementation in PA is desirable and, at the light of the last studies, it is already feasible. The coupling of processes with geochemistry is of paramount interest.

So far, in performance assessments the geochemical modelling of the water chemistry has not been directly coupled to radionuclide transport modelling. It has been used as a tool to provide the necessary background information to derive Kd values, defined specifically for each type of host rock (mineralogy and water chemistry).

In well characterized sites, models can be tested and advanced coupled reactive geochemical transport modeling approaches can be validated. The transferability of the information to a larger scale in space and time will be improved: one of the main limitations of PA models lies, in fact, on the impossibility of considering temporal variations. Mixing models can be used within PA and SA to evaluate changes of concentration of time.

Application of knowledge and the experiences from the natural sites to a repository site could result in decisive benefits for the regulatory evaluation of a safety case of a geological repository because it allows:

- To built confidence on the site
- To evaluate and reduce the existing uncertainties on concepts and estimated parameters;
- To make less conservative assumption on justifies and defendable bases;
- To increase confidence in extrapolations;
- To improve the transferability of the information;
- To evaluate the geochemical stability of a site with respect to given perturbations;
- To validate the radionuclide transport/retention concepts.
- To analyze different possible scenarios;
- To create multiple lines of argumentation for defending the selection of parameters to be used in PA.

Fluid-flow system characterization in crystalline rock: effects of the heterogeneity and up-scaling

In granite, the dominant transport mechanism is the advection in the rock fractures. The knowledge of the flow paths characteristics is a key topic for the SA in crystalline rocks. On the other hand, matrix diffusion is a physical process by which solutes are transferred from the flowing groundwater to the stagnant water in the pores of the rock matrix adjacent to the fractures: it is a very important retardation process.

Dimension, orientation and connectivity of the pore space determine the properties of the flow in the rock and radionuclide transport in a medium which is characterized by high heterogeneity.

Amongst the issues of interest related to the fluid flow characterization are the following:

- Treatment of the heterogeneity both in flow and matrix diffusion. It is recognized that the spatial heterogeneity is relevant to all retention processes.
- Treatment of the scale dependency of transport parameters, both from a conceptual and modeling point of view.
- Coupling of flow (physical properties of the rock) and geochemistry.
- Temporal variability. The limited treatment of time-dependence is considered a weakness of PA models.
- Analysis of the porous system structure by advanced high resolution techniques.

Different conceptual models exist for the description of the advective flow-paths in crystalline rocks: from continuum models that employs average properties of the medium to more complicated stochastic models. Different methods are used in different countries PA.

A challenge from a modeling point of view is trying to combine flow and transport modeling taking into account the possible effects of heterogeneities at different scales. Flow and transport modeling are continuously developing, but in PA, input parameters for transport are obtained separately from flow models.

For a modelling point of view, the interplay between transport parameters (D, k and ϕ) and chemical reactions is non-trivial but it is possible, as already shown. Reaction rates can also be successfully obtained from mixing ratios and disequilibrium within the medium can be often controlled by mixing.

The main difficulties come when the effects of space and time variability have to be included. Field data shows that some parameters are depending on the scale (hydraulic conductivity or dispersivity show variations with the spatial scale and the porosity seems to depend on the residence time), therefore the up-scaling problems arise.

Stochastic methods are useful to deal with variability but it is not possible, at moment include chemical reactions. Particle tracking, random walking, continuous time random walk methods do not represent mixing, therefore are inappropriate for reactive transport.

The multicontinuum method is a particular case of the continuous time random walk. It works quite well for conservative elements but it is still difficult to relate the geochemical properties of the medium with the residence time distributions obtained. Nevertheless, it seems to be a promising method for its application to multi-components reactive transport.

The theoretical bases of matrix diffusion are well established and the mathematical treatment is similar in different PA. The main open question is related to the depth of connected porosity in the natural rock. The main uncertainties are related to experimental diffusion data (laboratory measurements need long times and may include disturbances due to sample preparation).

The development of transport models that explicitly take into account the heterogeneity of the rock matrix is an issue of interest, also for the validation of up-scaling methods. Analysis of the porous system structure at a μm to mm scale with different techniques can be of help. Advances in imaging techniques could and should be coupled with pore-scale modelling to understand diffusion at the microscopic scale for a mechanistic approach to diffusion problem.

Matrix diffusion phenomena are characterized by residence time distribution (RTD), which is highly conditioned by rock petrography. At moment very little is known about the relationship between RTD and pore space geometry but efforts are being done. Recent studies (Sardini et al, 2006) showed that combining ^{14}C-PMMA impregnation of rock samples, SEM/FESEM analysis and modelling it is possible to provide the map of the connected porosity and the spatial distribution of mineral aggregates. A porous subset can be linked to a petrographic structure defined within the rock volume.

The modelling results indicated that a single diffusion coefficient in the heterogeneous medium does not represent well the reality at the microscale and that different diffusion coefficient may be associated to a porous subset. The measurement of diffusion coefficients at the microscale can be of interest.

The last reflexion comes from the discussion raised during the Session. The vision and treatment of heterogeneity is indeed an "interesting issue", but is also very interesting to observe how the perception of "heterogeneity" as a general concept is very different from a person to another (possibly depending on their discipline and sometime it seemed to become a controversial point.

The main question is: are the efforts to include heterogeneities in models worth? Indeed, the answer is "yes" because of any significant scientific advance will be of help for SA.

Nevertheless, it is important to remark that the mechanistic comprehension of the medium is fundamental for simplifying its description without losses of information.

Acknowledgements

All the speakers of the Topical Session are greatly acknowledged for their interesting talks.

References

Anderson C., Pedersen K. (2003): In situ growth of Gallionella biofilms and partitioning of lanthanides and actinides between biological material and ferric oxy-hydroxides. *Geobiology*, 1, 169-178.

Anderson C., Pedersen K., Jakobsson A.M. (2006b): Authoradiographi comparison of radionuclide adsorption between subsurface anaerobic biofilm and granitic host rocks. *Geomicrobiology Journal,* 23:15–29.

Hellmuth K.H., Read D., Black S., Buckby T., Oziabkin V., Marcos N., Markovaara-Koivisto M., Siitari-Kauppi M., Kelokaski M., Proust T., Vaganov P., Traber D., Tarvainen T., Backman B., Hatakka T., Savolainen H., Kaija J., Blomqvist R., Rasilainen K., Pitkänen P., Löfman J., Luukkunen A., Partamies S. (2007): Geochemical fluxes in the geosphere: quantitative understanding by identification and verification of processes, 2nd FUNMIG Annual Workshop proceedings (this volume).

Kalinowski B.E., Johnsson A., Arlinger J., Pedersen K, Odegaard-Jensen A., Edberg F. (2006): Microbial mobilisation of Uranium from Shale Mine Waste, *Geomicrobiology Journal*, 23:157–164.

Laaksoharju M. Smellie J. Tullborg E., Molinero J., Gimeno M., Buckau G. (2007): Results from the groundwater hydrogeochemical investigation programme in Sweden 2nd FUNMIG Annual Workshop proceedings (this volume).

Molinero, J., Samper, J., Zhang, G., Yang, C. (2004): Biogeochemical reactive transport model of the redox zone experiment of the Äspö hard rock laboratory in Sweden. Nuclear Technology, 148: 151–165.

H. Moll; M. Merroun, G. Geipel, Th. Stumpf, A. Rossberg, C. Hennig, S. Selenska-Pobell, G. Bernhard (2007) Interactions of microbes found at Äspö underground lab with actinides such as curium, plutonium and uranium. This volume

Pedersen K. (2005): Microorganisms and Their Influence on Radionuclide Migration in Igneous Rock *Environment Journal of Nuclear and Radiochemical Sciences*, Vol. 6, No.1, pp. 11-15.

RETROCK (2005): Treatment of radionuclide transport in geosphere within safety assessment EUR 21230.

Samper, J, Molinero, J., Yang, C., Zhang, G. (2003): Redox Zone II: Coupled modeling of groundwater flow, solute transport, chemical reactions and microbial processes in the Äspö Island. SBK Technical Report TR-03-16, 126 pp.

Sardini P., Siitari-Kauppi M., Beaufort D., Hellmuth K.H.(2006); On the connected porosity of mineral aggregates in crystalline rocks, *American Mineralogist*, 91; no. 7; p. 1069-1080.

RESULTS FROM THE GROUNDWATER HYDROGEOCHEMICAL INVESTIGATION PROGRAMME IN SWEDEN

Marcus Laaksoharju[1*], John Smellie[2], Eva-Lena Tullborg[3], Jorge Molinero[4], Maria Gimeno[5], Gunnar Buckau[6]

[1] Geopoint AB (SE)
[2] Conterra AB (SE)
[3] Terralogica AB (SE)
[4] University of Santiago de Compostela (ES)
[5] University of Zaragoza (ES)
[6] FZK-INE (DE)

* Corresponding author; marcus@geopoint.se

Abstract

This work forms part of the FUNMIG project which aims to: (i) generate data and process understanding for phenomena that cannot be obtained from laboratory studies, and (ii) to verify process up-scaling with respect to time, spatial scale and heterogeneity. It is based on the Swedish site investigation programmes for a nuclear waste repository in fractured crystalline rock. A database with background information has been established for the Forsmark site and a detailed analysis has identified plausible end-members as primary mixing components to explain the present groundwater chemistry. The portions of different groundwater contributors together with knowledge of the evolution history provide a good picture of the present hydrological situation. A large number of geochemical processes have been identified, including a detailed analysis of the origin of excessive U concentrations in some deep groundwater samples from Forsmark. Investigations of the palaeo aspects by using natural environmental isotopes are under development. The results contribute to the safety assessment of nuclear waste disposal in the granitic rock investigated by considering the hydrological situation and relevant geochemical processes, both at the present day and also to predict future site evolution with the onset of climatic changes.

Introduction

The work is associated with the Swedish site investigations for construction and operation of repositories for high-level long-lived radioactive waste. The present work is related to the Integrated Project Fundamental Processes of Radionuclide Migration

(IP-FUNMIG) where a number of Contractors contribute: Geopoint AB (SE), Svensk Kärnbränslehantering AB (SKB) (SE), Research Center Karlsruhe – Institut für Nukleare Entsorgung (FZK-INE) (DE) and Associated Groups: (Conterra AB (SE), Terralogica AB (SE), University of Santiago de Compostela (ES) and University of Zaragoza (ES). Siting studies for SKB's programme of deep geological disposal of nuclear fuel waste currently involves the investigation of two locations, Forsmark and Laxemar-Simpevarp, on the eastern coast of Sweden to determine their geological, hydrogeochemical and hydrogeological characteristics. Present work mainly includes data and results from the Forsmark Model version 1.2 (SKB R-05-17) which represents the second evaluation of the available groundwater analytical data collected up to June 2004. The data set includes water samples collected from the surface and sub-surface environment (e.g. soil pipes in the overburden, streams and lakes), and groundwater samples from drilled boreholes in the bedrock. The deepest fracture groundwater samples with sufficient analytical data reflected depths down to 1 km. Most of the waters sampled (66 %) lacked crucial analytical information that restricted the evaluation. Model version 1.2 focuses on geochemical and mixing processes affecting the groundwater composition in the uppermost part of the bedrock, down to repository levels (~ 400-600 m), and eventually extending to 1000 m depth.

Objectives

The overall objectives are to provide well-founded evidence in support of the safety case for nuclear waste disposal in fractured crystalline rock in Sweden, with respect to hydrological and geochemical processes. For this purpose, hydrological and geochemical data are gathered, scrutinised and integrated into a database. The database is used for interpretation of the relevant safety features existing in the far-field of a crystalline rock repository.

Results and discussion

Hydrological and hydrogeochemical studies

Four main groundwater types are found at the Forsmark site. In addition to the recent to young Na-HCO_3 type groundwater and older Na-Ca Cl(SO_4) type groundwater (with a Littorina Sea and glacial signature), there exist at greater depths (KFM03A; 645 m) an even older saline Na-Ca-Cl type groundwater with a small glacial component ($\delta^{18}O$ = -11.6 ‰ SMOW; δ D = -84.3 ‰ SMOW). At still greater depth (KFM03A: 990 m) the groundwater changes to a higher saline Ca-Na-Cl type characterised by an even greater glacial signature ($\delta^{18}O$ = -13.6‰ SMOW; δ D = -98.5‰ SMOW). Although only one deep sample exists, the A2 gently dipping deformation zone which traverses the Forsmark site appears to form the boundary between the Na-Ca-Cl and Ca-Na-Cl groundwater types (see Fig 1).

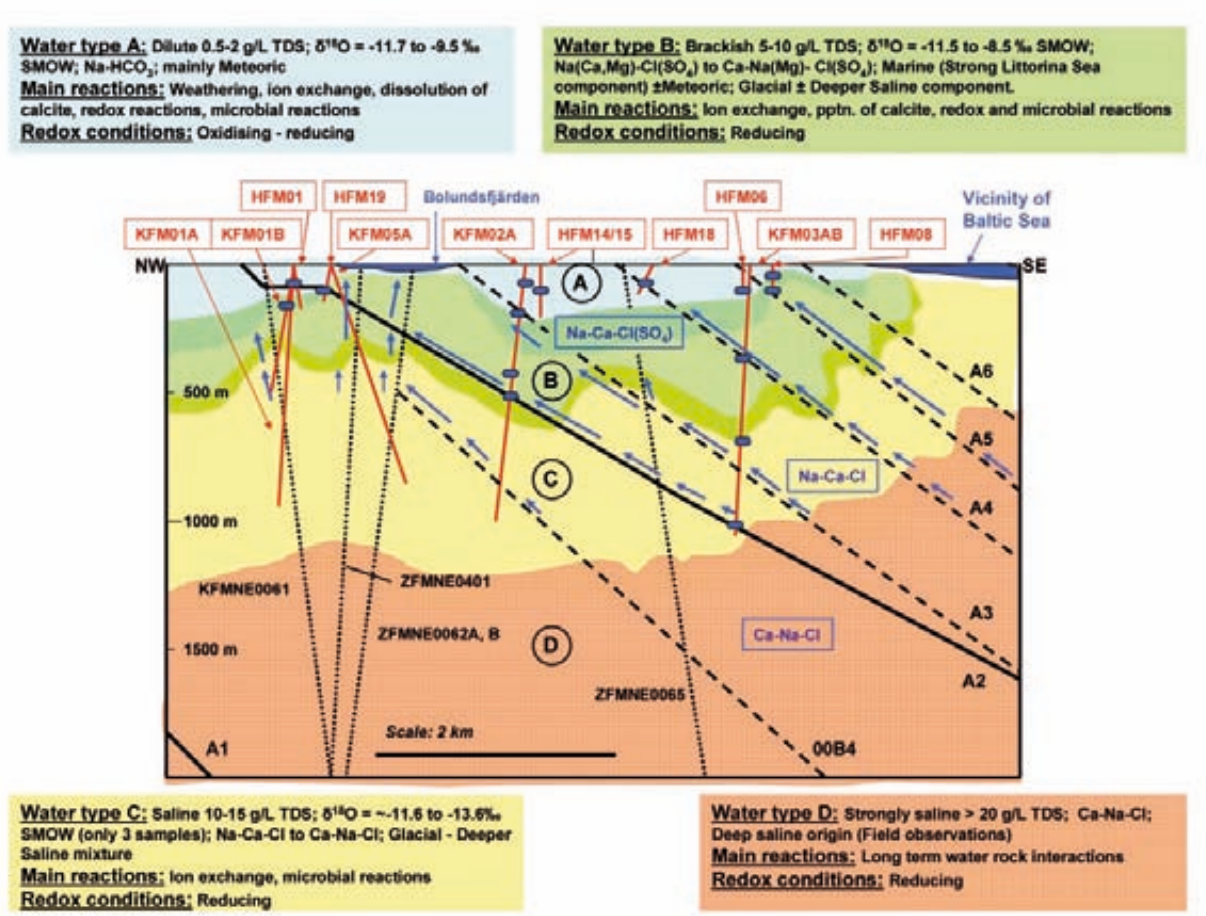

Figure 1: *Schematic 2-D groundwater model of Forsmark (SKB R-05-17), integrating the major structures, the major groundwater flow directions and the variation in groundwater chemistry (Types A-D) from the sampled boreholes (indicated in blue). The blue arrows are estimated groundwater flow directions and their respective lengths reflect relative groundwater flow velocities (short = low flow; longer = greater flow).*

The near-surface Na-HCO_3 groundwaters form a distinctive horizon at the centre of the site area which lenses out towards the SE Baltic coast where discharge of deeper groundwater probably occurs. From Bolundsfjärden to the NW a less marked horizon is indicated but data are few. In addition, the influence of the deformation zone A2 on the groundwater chemistry is not clear at this near-surface locality.

Bordering the shallow Na-HCO_3 groundwater, and extending from close to the surface (near the SE coast) to depths of around 500 m (along the gently dipping deformation zone A2), are the Littorina Sea type groundwaters. The possibility of an upward (discharging) movement of these Littorina Sea type groundwaters below Bolundsfjärden Lake is supported by the soil pipe groundwater sample SFM0023 collected close to the lake and showing increased Mg and SO_4. The Bolundsfjärden Lake discharge area may correspond to the intersection of steeply dipping deformation zones further connected to the gently dipping deformation A2 zone. On-going hydrogeological modelling should resolve better what is occurring at this location.

Most lines of evidence support that the sulphur system, microbiologically mediated, is the main redox controller in the deepest and most saline groundwater. On the other hand, Littorina-rich brackish groundwaters show variable and very high iron contents, in agreement with what has been observed in similar groundwaters elsewhere. The microbial analyses only found trace amounts of sulphate-reducing bacteria (SRB) in these samples, but very high numbers of iron-reducing bacteria (IRB). However, there is no correlation between Fe^{2+} concentration and the number of IRB in these groundwaters. Moreover, they show very low but detectable contents of dissolved S^{2-} and the $\delta^{34}S$ values are very homogeneous (around 25‰) and are clearly higher than in the present Baltic Sea, indicating that microbial sulphate reduction has operated. These observations could support the existence of an iron-sulphide precipitation process during the Littorina Sea phase of these groundwater but not intense enough to effectively limit Fe^{2+} solubility.

A modelling approach was used to simulate the obtained groundwater in the Forsmark area by introducing Littorina Sea water. These results indicate that re-equilibrium reaction processes are important in the control of some parameters such as pH (as well as Eh, and some minor-trace elements), moving the waters towards the adularia-albite boundary. However, the main compositional changes, and even the extent of reequilibration processes, are controlled by the degree of the mixing process.

Coupled transport modelling was used to model the measured water conservative elements, tritium contents and the water recharge into the granitic bedrock. The simulations indicate that Quaternary sediments may play a significant role since most of the infiltrated water could flow through the conductive layers in the sediment to discharge zones, mainly associated with lakes and the Baltic Sea coast line. Based on this hypothesis, the effective recharge into the granitic bedrock is estimated to be less than in other investigated sites such as Simpevarp and Laxemar, where the presence of Quaternary overburden is less important. The hydrogeologic behaviour of the Quaternary overburden in Forsmark provides a plausible explanation for the preservation of Littorina Sea signatures found in several groundwater samples, even at very shallow depths. Other (and complementary) explanations can be related to the flat topography, as well as including the fact that the Forsmark site has emerged over the sea level more recently than other investigated sites (e.g. Laxemar). The confidence level of the results is checked by the comparison between measurements and computed results. The model results are promising based on the comparison in terms of salinity and environmental isotope distribution.

The conclusion is that the complex groundwater evolution and patterns at Forsmark are a result of many factors such as: a) the present-day flat topography and proximity to the Baltic Sea, b) past changes in hydrogeology related to glaciation/deglaciation, land uplift and repeated marine/lake water regressions/transgressions, and c) organic or

inorganic alteration of the groundwater composition caused by microbial processes or water/rock interactions. The sampled groundwaters reflect to various degrees processes relating to modern or ancient water/rock interactions and mixing. The major processes and reactions that may affect the groundwater in Fennoscandia are (Laaksoharju et al., 2006):

- Climate
- Flow/mixing
- Reactions with the rock and microorganisms in the groundwater:
  - Introduction of CO_2 gas in the unsaturated zone
  - Dissolution and precipitation of calcite
  - Cation exchange
  - Incongruent dissolution of primary silicates with formation of clays
  - Oxygen consumption: organic carbon respiration, oxidation of iron minerals such as sulphides and biotite
  - Reduction of nitrate, oxidised iron and manganese and sulphate with anaerobic oxidation of organic compounds (DOC and CH4), with production of nitrogen gas, ferrous iron, manganese (II) and sulphide
  - Hydrogen oxidation with production of acetate and methane: organic fermentation or carbonate reduction

The modelling indicates also that the groundwater composition at repository depths is such that the representative samples from KFM02A:509-516m and KFM03A:448-453m can meet the SKB chemical suitability criteria for Eh, pH, TDS, DOC and Ca+Mg.

In this evaluation the groundwater flow model has been updated, the salinity distribution, mixing processes and the major reactions altering the groundwater have been modelled down to a depth of 1000m, and an updated Hydrogeochemical Site Descriptive Model version 1.2 has been produced. More groundwater and isotopic data, together with microbial information, colloids and gases, provided additional site descriptive information. Finally, the introduction of coupled modelling provided further possibilities to address independently the various processes in question.

Analysis of the origin of excessive U concentrations in Forsmark KFM groundwater samples

Data from the Forsmark deep groundwater samples (SKB R-06-69) show that numerous groundwater samples have uranium concentrations that are much in excess of what is expected in granitic bedrock. These data are examined further with the objective of explaining these excessive uranium concentrations. A total of eight KFM boreholes have been sampled at different depths. Sampling sometimes consisted of pumping for several days, weeks or even several months and normally several samples were collected. A key problem is the presence of high drilling-water contents which originate from shallower bedrock levels and now constitute a significant component in the open borehole waters and along intersecting single fractures and fracture zones. Even after

extended pumping or waiting for several years the drilling water still has not been adequately removed.

The high uranium concentrations: a) are found especially at shallow to intermediate depths down to 650 m in groundwaters of brackish composition (~ 5000-6000 mg/L Cl), b) are commonly but not always associated with the presence of drilling water, and c) show a weak correlation with the iron content. Mineralogical information and thermodynamic calculations indicate the presence of uranium minerals (i.e. pitchblende and/or other amorphous oxides) in the fracture fillings which could be the source for uranium. Alternatively the uranium can be associated with iron-bearing minerals in the accessible pore space.

It is suggested that at shallow depths the uranium either has not been deposited in the available pore space or it has been washed out by relatively oxidising water. At depths below approximately 700 m, it seems that the uranium minerals are stable in the presence of drilling water. This uranium issue requires, however, further study and modelling before conclusive conclusions can be drawn, but it may include drilling and sampling artefacts.

Relevance of the above results for PA

The results described in the previous sections can be directly or indirectly implemented in performance assessment (PA) evaluation. For example, the ingress of glacial melt water deep into the bedrock is indicated by the cold climate $d^{18}O$ signatures measured in the deeper groundwater types as described and illustrated in Figure 1. At their source these waters are assumed to be dilute and highly oxidising, but they are expected to quickly become reducing at depth when they come increasingly in contact with the buffering effect of the upper bedrock. This is an important scenario issue when considering the long-term safety and performance of a repository system. The mixing models used within the SKB hydrogeochemistry and hydrogeological programme can be used in performance assessment (PA) and safety assessment (SA) by the following:

- Provide understanding of water movement and timescales for calculating the dose and validation of hydrogeological models.
- Water types can indicate the presence of hazardous species (e.g. HS, CH_4, U and high Cl) in areas with little or no sampling.
- Mixing models can be used within PA and SA to indicate changes of concentrations with time.
- Confirmation and calibration of processes of importance for PA and SA.
- Site understanding builds confidence in the site.

The collected values and the process understanding can be used for: 1) input parameter values in calculating long-term repository safety, and 2) to understand the

present undisturbed hydrogeochemical conditions and how these conditions will change in the future. Parameter values for safety analysis include pH, Eh, S, SO_4, HCO_3, HPO_4 and TDS (mainly cations), together with colloids, fulvic and humic acids, other organics, bacteria and nitrogen. These values will be used to characterise the groundwater environment at, above and below repository depths. When the hydrogeochemical environment is characterised, this knowledge, together with an understanding of the past and present groundwater evolution, should provide the basis for predicting future changes.

Summary and Conclusions

The hydrological and geochemical characterisation of the selected sites in Sweden is progressing well. The origin of present groundwater and a series of key geochemical processes have been identified. This includes formation of secondary uranium silicate minerals that can be correlated with past climatic events. The results are not only directly relevant for the performance assessment with respect to the present hydrological and geochemical situation, but also in view of prediction in association with future site evolution.

Acknowledgement

The study has been financially supported by SKB and FUNMIG. Ignasi Puigdomenech, SKB is acknowledged for his support and helpful suggestions.

References

Laaksoharju M, Smellie J, Tullborg E-L, Gimeno M, Molinero J, Gurban I, Hallbeck L (2006): Hydrogeochemical evaluation and modelling performed within the site investigation programme. Submitted to Applied Geochemistry.

SKB R-05-17: Hydrogeochemical evaluation. Preliminary site description, Forsmak area – Version 1.2, Report SKB R-05-17, Svensk Kärnbränslehantering AB, March 2005.

SKB R-06-69: Hydrogeochemical evaluation of the Forsmark site, modelling stage 2.1 - issue report SKB R-06-69. In preparation.

INTERACTIONS OF MICROBES FOUND AT ÄSPÖ UNDERGROUND LAB WITH ACTINIDES SUCH AS CURIUM, PLUTONIUM AND URANIUM

H. Moll [1*]; M. Merroun [1], G. Geipel [1], Th. Stumpf [2], A. Rossberg [1], C. Hennig [1], S. Selenska-Pobell [1], G. Bernhard [1]

[1] Forschungszentrum Dresden-Rossendorf e.V., Institut für Radiochemie, P.O. Box 510119, 01314 Dresden, Germany.
[2] Forschungszentrum Karlsruhe, Institut für Nukleare Entsorgung, P.O. Box 3640, 76021 Karlsruhe, Germany.

* Corresponding author; h.moll@fzd.de

Abstract

Sulfate-reducing bacteria (SRB) frequently occur in the deep granitic rock aquifers at the Äspö Hard Rock Laboratory (Äspö HRL), Sweden. The new SRB strain *Desulfovibrio äspöensis* could be isolated. Results describing the basic interaction mechanisms of uranium, curium, and plutonium with cells of *D. äspöensis* DSM 10631^T will be presented. The interaction experiments with the actinides showed that the cells are able to remove all three actinides from the surrounding solution. The amount of removed actinide and the interaction mechanism varied among the different actinides.

The main U(VI) removal occurred after the first 24 h. The contact time, pH and $[U(VI)]_{initial}$ influence the U removal efficiency. The presence of uranium caused a damaging of the cell membranes. TEM revealed an accumulation of U inside the bacterial cell. *D. äspöensis* are able to form U(IV). A complex interaction mechanism takes place consisting of biosorption, bioreduction and bioaccumulation.

In the case of ^{242}Pu, solvent extractions, UV-vis- and XANES spectroscopy were used to determine the speciation of the Pu oxidation states. In the first step, the Pu(VI) and Pu(IV)-polymers are bound to the biomass. Solvent extractions showed that 97 % of the initially present Pu(VI) is reduced to Pu(V) due to the activity of the cells within the first 24 h. Most of the formed Pu(V) dissolves from the cell envelope back to the aqueous solution due to the weak complexing properties of this plutonium oxidation state.

In the case of curium at a much lower metal concentration of $3x10^{-7}$ M, a pure biosorption of Cm(III) on the cell envelope forming an inner-sphere surface complex most likely with organic phosphate groups was detected.

To summarize, the strength of the interaction of *D. äspöensis* with the selected actinides at pH 5 and actinide concentrations = 10 mg/L ([Cm] 0.07 mg/L) follows the pattern: Cm > U > Pu >> Np.

Introduction

The influence of microorganisms on migration processes of actinides has to be taken into account for the risk assessment of potential high level nuclear waste disposal sites. Therefore it is necessary to characterize the actinide-bacteria species formed and to elucidate the reaction mechanisms involved. Microbial activities can cause either dissolution and mobilization or immobilization of actinides by direct or indirect microbial actions in deep nuclear repositories and its environment, e.g., at the Äspö HRL. The Äspö (HRL) was established in Sweden in a granite rock formation for *in-situ* experiments with radionuclides. The aims of this facility are to examine which methods are most suitable for research in the bedrock, to develop and to demonstrate methods for deciding in what way a deep repository can be planned and constructed in accordance with the local characteristics of the bedrock, to increase scientific understanding of a deep repository's safety margins and to develop and demonstrate the technique that will be used during the disposal of spent nuclear fuel. Investigations of the microbial diversity at the Äspö site were published by Pedersen et al. [1-3]. The total number of microorganisms measured at Äspö range from $1x10^3$ to $5x10^6$ cells ml^{-1}, whereas the number of sulfate-reducing bacteria (SRB) was between 10^1 to $2x10^4$ cells ml^{-1}. The analysis of the bacterial populations of SRB in the Äspö aquifer is very important. In addition to their ability to reduce many metals and actinides/radionuclides, they posses also a corrosive potential for the used copper canisters due to their sulfide production.

Objectives

Our project is focused on the recovered SRB strain *D. äspöensis* which is indigenous at the Äspö site [4]. The aim of the presented work is to explore interaction processes of *D. äspöensis* with the actinides uranium, curium, and plutonium. It is unknown in which way *D. äspöensis* cells are interacting with the selected actinides. To summarize, the main goals of this study are: (i) interaction of uranium, curium, and plutonium with *D. äspöensis* cells, (ii) quantification of actinides bonded on the microbes in dependence of the experimental parameters, and (iii) spectroscopic characterization of the formed actinide complexes/compounds. The obtained results should help to improve the scientific basis for the performance assessment and safety of nuclear waste repositories concerning the influence of microorganisms on actinide migration.

Results and conclusions

Cultivation and characterization of the biomass

The cells of *D. äspöensis* were successfully cultivated under anerobic conditions in liquid and on solid medium. Under the given experimental conditions, the cells reached the stationary phase of the growth curve after 8 to 9 days after inoculation at 22 °C. The purity of the cultures was verified using light microscopy and by applying the

molecular microbiological method Amplified Ribosomal DNA Restriction Enzyme Analysis (ARDREA) as described in [5] (see Fig. 1).

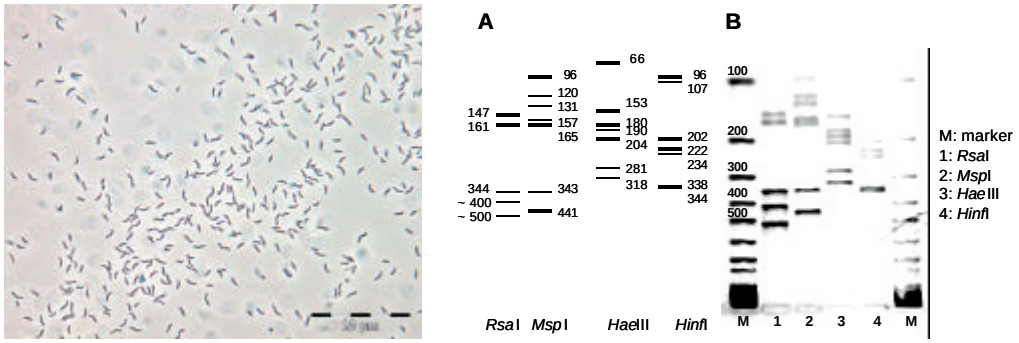

Figure 1: *Left: Visualization of D. äspöensis DSMZ 10631^T bacteria by light microscopy; Right: Identification of D. äspöensis based on 16S-ARDREA. A) Schema of the endonuclease-specific ARDREA profiles of D. äspöensis drawn on the basis of the sequence analysis of the 16S rRNA gene. B) Experimentally derived 16S ARDREA patterns of D. äspöensis.*

Figure 1 (right hand side) summarizes the results of the molecular analysis. The predicted pattern for each endonuclease is drawn in A and the experimentally determined pattern is presented in B. Both are in agreement and show the purity of the used bacterial cultures. To study the interaction of *D. äspöensis* with the selected actinides the cells were grown to the mid-exponential phase (4 days). The biomass was collected by centrifugation and washed three times with 0.9% NaCl. The collected biomass was 1.0 ± 0.2 $g_{dry\ weight}$/L.

Interaction of D. äspöensis with U(VI)

In this project, we could demonstrate for the first time the removal of U(VI) from solution due to the activity of the cells of *D. äspöensis* [6]. Three parameters are influencing the removal efficiency of U(VI): a) the interaction time, b) the pH, and c) the initial uranium concentration, $[U]_{initial}$, present in the test solutions. The amount of U bound to the biomass increased with increasing pH from 3 to 6. However, at pH 8 a strong decrease of the amount of accumulated uranium was observed. The cells of *D. äspöensis* removed 55% of the U(VI), 10.1 mg/$g_{dry\ weight}$, from an aqueous solution of 14.6 mg/l U(VI), supplemented with 10 mM lactate, after 72 h of incubation at pH 5. Within this investigation the first direct spectroscopic proof for a reduction of U(VI) to U(IV) most likely by an enzymatic reaction due to the activity of the cells was obtained [6]. The toxicity of U(VI) towards *D. äspöensis* could by proved using microbiological methods. As a consequence, the membrane system gets damaged and uranium can penetrate inside the bacterial cells (see Fig. 2).

The EDX spectrum derived from the U deposits indicated that they are composed of oxygen (O), phosphorus (P) and uranium (U). The high copper (Cu) peak is from the EM grid used to support the specimen. The lead (Pb) peak originated from the lead citrate solution which was used in order to improve the visualization of the uranium-treated cell thin sections.

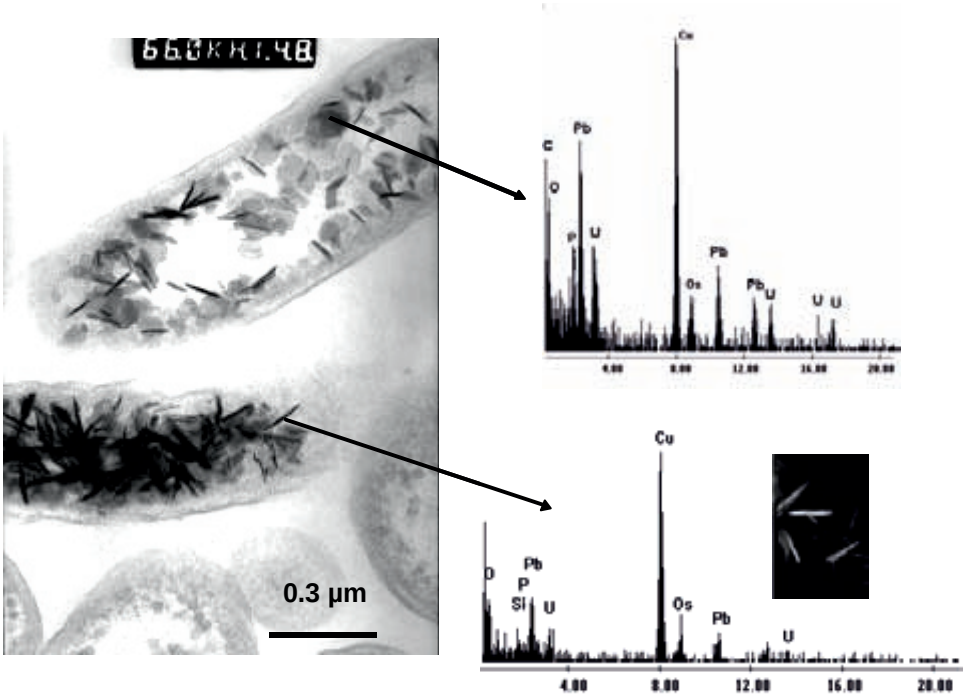

Figure 2: *TEM and EDX analysis of the cellular localization of uranium accumulated by the cells of D. äspöensis.*

The results are indicating a complex interaction mechanism consisting of biosorption, bioreduction, and bioaccumulation.

Interaction of D. äspöensis with Pu

The ^{242}Pu was provided as a mixture of ca. 46 % Pu(VI) and ca. 34 % Pu(IV)-polymer. Interactions between bacteria and plutonium in mixed oxidation states were not yet intensively investigated.

In this study, accumulation experiments were performed in order to obtain information about the amount of Pu bound by the bacteria in dependence on the contact time and the initial plutonium concentration [7]. We used solvent extractions, UV-vis spectroscopy and X-ray absorption near edge structure (XANES) spectroscopy to determine the speciation of Pu oxidation states. Extended X-ray absorption fine structure (EXAFS) spectroscopy was used to study the coordination of the Pu bound by the bacteria. Based on our results and taking into consideration the findings of Panak et al. [8], we developed a model describing the interaction of Pu(VI) and Pu(IV)-polymers with *D. äspöensis* (see Fig. 3).

In the first step, the Pu(VI) and Pu(IV)-polymers are bound to the biomass. Solvent extractions showed that 97 % of the initially present Pu(VI) is reduced to Pu(V) due to the activity of the cells within the first 24 h of contact time. Most of the formed Pu(V) dissolves from the cell envelope back to the aqueous solution due to the weak complexing properties of this plutonium oxidation state. Indications were found for a penetration of Pu species inside the bacterial cells.

The results are indicating again a complex interaction mechanism consisting of biosorption, bioreduction, and bioaccumulation.

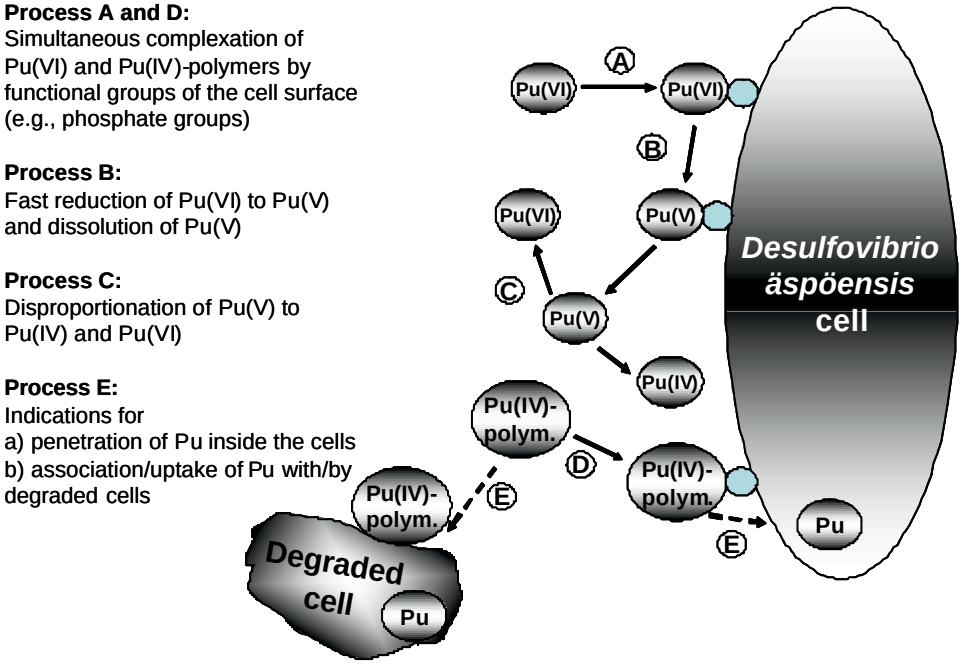

Figure 3. *Illustration of the different processes describing the interaction of Pu with Desulfovibrio äspöensis based on the schema developed by Panak and Nitsche in [8].*

Interaction of D. äspöensis with Cm

For Cm(III) at a trace concentration level of $3x10^{-7}$ M, we interpret the pH dependence of the fluorescence emission spectra with a pure biosorption forming an inner-sphere surface complex of Cm(III) onto the *D. äspöensis* cell envelope [5]. To our knowledge, there are no spectrophotometric data available for interactions of Cm(III) with bacteria and especially with sulfate-reducers of the Desulfovibrio genus. The Cm(III)-*D. äspöensis*-surface complex is characterized by its emission spectrum (see Fig. 4) and its fluorescence lifetime (162 ± 5 µs).

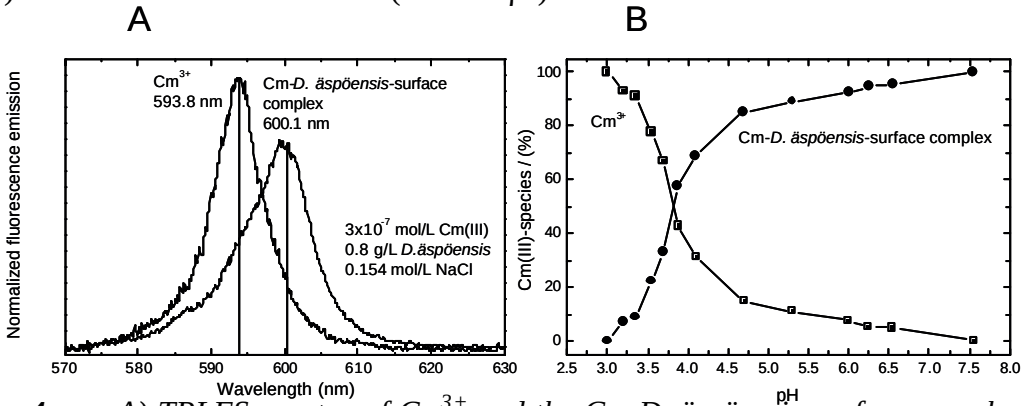

Figure 4: *A) TRLFS spectra of Cm^{3+} and the Cm-D. äspöensis-surface complex as derived by peak deconvolution; the spectra are scaled to the same peak area. B) Experimental species distribution of the Cm(III)-D. äspöensis system as a function of pH.*

From other investigations of biological systems and from a spectroscopic study of the complexation of Cm(III) with adenosine 5'-triphosphate [9], we conclude that mainly organic phosphate groups of the cell surface are involved in the bonding of Cm(III) to *D. äspöensis*. A reversible biosorption reaction was observed. Under the given experimental conditions, 84% of the Cm, 0.078 mg/$g_{dry\ weight}$, is bound to the bacteria at pH 5 after 72 h of incubation. No evidence was found for an incorporation of Cm(III) into the bacterial cells at this low initial actinide concentration.

Summary

Our study demonstrates that the interactions of uranium, plutonium and possibly neptunium (results not shown here) with *D. äspöensis* cause changes of the oxidation state of the actinides which have an impact on their migration behavior. Assuming attached cells of *D. äspöensis* to the granitic rock of the Äspö HRL, released Cm(III) in the aquifer gets immobilized due to a biosorption on the bacterial cells in the neutral pH range. In the case of the other actinides, the interaction mechanism is more complex and consists of sub-processes.

The results of this study improve the knowledge on direct interactions of bacteria of the species *Desulfovibrio äspöensis* with actinides. Important results were obtained about the cultivation and characterization of the biomass, their potential to remove the selected actinides from the surrounding solution and about the different interaction mechanisms dependent on the nature of the actinide element. Taking all results together they contribute to a more realistic description of the influence of microbial actions on the migration behaviour of actinides in the environment and are helpful for an improved risk assessment for instance for potential underground nuclear waste repositories.

Acknowledgement

This work was supported by the BMWi (no. 02E9491). The authors are indebted for the use of the Cm-248 to the U.S. Department of Energy, Office of Basic Energy Sciences, through the transplutonium element production facilities at Oak Ridge National Laboratory which was made available as part of a collaboration between FZD and the Lawrence Berkeley National Laboratory (LBNL). Thanks are given to M. del Mar Abad Ortega, C. Hidalgo Sanchez and M.T. González-Munoz for their support and help during the TEM/EDX measurements at the University of Granada (Spain). The XAS measurements were performed at BM20 (ROBL) at the ESRF in Grenoble (France). Thanks are given to T. Reich, C. Hennig, H. Funke, M. Walter for their support during the XAS beam time and their help in evaluating the data. The authors would like to thank K. Pedersen and his group at the Göteborg University, Department of Cell and Molecular Biology (Sweden) for the fruitful discussions and helpful comments concerning the cultivation of *D. äspöensis*.

References

[1] Pedersen, K.; Arlinger, J.; Ekendahl, S.; Hallbeck, L. (1996) 16S rRNA gene diversity of attached and unattached bacteria in boreholes along the access tunnel to the Äspö hard rock laboratory, Sweden, *FEMS Microbiol. Ecol.*, **19**, 249-262.

[2] Kotelnikova, S.; Pedersen, K. (1998) Distribution and activity of methanogens and homoacetogens in deep granitic aquifers at Äspö Hard Rock Loboratory, Sweden, *FEMS Microbiol. Ecol.*, **26**, 121-134.

[3] Pedersen, K. (1999) Subterranean microorganisms and radioactive waste disposal in Sweden, *Engineer. Geol.*, **52**, 163-176.

[4] Motamedi, M.; Pedersen, K. (1998) *Desulfovibrio aespoeensis* sp. Nov., a mesophilic sulphate-reducing bacterium from deep groundwater at Äspö hard rock laboratory, Sweden, *Int. Syst. Bacteriol.*, **48**, 311-315.

[5] Moll, H. ; Stumpf, Th.; Merroun, M.; Rossberg, A.; Selenska-Pobell, S.; Bernhard, G. (2004) Time-resolved laser fluorescence spectroscopy study on the interaction of Cm(III) with *Desulfovibrio äspöensis* DSM 10631^T, *Environ. Sci. Technol.*, **38**, 1455-1459.

[6] Moll, H.; Merroun, M.; Stumpf, Th., Rossberg, A.; Geipel, G. ; Selenska-Pobell, S. ; Bernhard, G. (2005) Interaction of Actinides with the predominant indigenous bacteria in Äspö Aquifer – Interactions of selected actinides U(VI), Cm(III), Np(V) and Pu(VI) with D. äspöensis. Final Report, BMWA Project No. 02E9491, Wissenschaftlich-Technische Berichte FZR-422.

[7] Moll, H.; Merroun, M.L.; Hennig, C.; Rossberg, A.; Selenska-Pobell, S. and Bernhard, G. (2006) The interaction of *Desulfovibrio äspöensis* DSM 10631^T with plutonium, *Radiochim. Acta*, **94**, 815-824.

[8] Panak, P. J.; Nitsche, H. (2001) Interaction of aerobic soil bacteria with plutonium(VI), *Radiochim. Acta*, **89**, 499-504.

[9] Moll, H.; Geipel, G.; Bernhard, G. (2005) Complexation of curium(III) by adenosine 5'-triphosphate (ATP): A time-resolved laser-induced fluorescence spectroscopy study, *Inorg. Chim. Acta*, **358**, 2275-2282.

GEOCHEMICAL FLUXES IN THE GEOSPHERE: QUANTITATIVE UNDERSTANDING BY IDENTIFICATION AND VERIFICATION OF PROCESSES

K-H. Hellmuth [1]*, D. Read[2], S. Black[2], T. Buckby[2] S. / V. Oziabkin[3], N. Marcos[4], M. Markovaara-Koivisto[4], M. Siitari-Kauppi[5], M. Kelokaski[5], T. Proust[6] P. Vaganov[3], D. Traber[7], T. Tarvainen[8], B. Backman[8], T. Hatakka[8], H. Savolainen[8], J. Kaija[8], R. Blomqvist[8], K. Rasilainen[9], P. Pitkänen[9], J. Löfman[9], A. Luukkunen[9], S. Partamies[9]

[1](STUK), Radiation and Nuclear Safety Authority, P.O.B. 14, FIN-00881 Helsinki
[2]University, Reading
[3]University, St. Petersburg
[4]Technical University, Helsinki
[5]University, Helsinki
[6]University, Poitiers
[7]University, Bern
8Geological Survey of Finland
9VTT, Espoo

*Corresponding author: karl-heinz.hellmuth@stuk.fi

Abstract

An overview is given over the use of generic and site-specific information on natural geochemical fluxes and resulting concentrations in various compartments in the geosphere and surface environment for the evaluation of the possible role of a geological nuclear waste repository as a component participating in natural geochemical cycles. Use is made of information from geochemical prospecting, geochemical mapping, weathering and river catchment studies as well as case studies at natural anomalies. Following the more globally orientated prestudy an overview is given over the compilation of a generic and site-specific geochemical flux and concentration data base of selected elements in Finland for use as complementary safety indicators to be compared with calculated repository releases. In the data base site-specific data is given for the Palmottu natural analogue site (U mineralization) and four repository investigation sites. Specific geological, hydrogeological, geochemical, topographical and climatic features of the glaciated terrain in Finland are the main reason that geochemical fluxes are mostly limited to the surface environment and influences mediated by groundwater transport from the depth are difficult to identify.

The methodology of the use of natural safety indicators has some potential for improvement. The importance of the geochemistry of the groundwater-rock system and the elements, in particular, in the site-specific data on U fluxes became evident. A deeper understanding of the driving forces, transport mechanisms and parameters and relevant spatial and time scales behind natural geochemical cycles in different

geological settings is needed to enable a validating evaluation of the suitability of concepts of chemical stability and radionuclide migration, scenarios such as glacial cycles and models of coupled chemical transport and could allow confidence building into the repository safety case by evaluating uncertainties and conservativeness using complementary modelling and multiple lines of reasoning. Observations in nature comprising groundwater-mineral interactions and U mobilization and fixation could be confirmed by reactive coupled chemical transport modelling. The relevant time scales behind the transport processes could be defined by dating and preliminary conclusions were achieved concerning glacial meltwater intrusion as the triggering mechanism. The transferability of this geo-information to a larger regional scale and in the time scale was confirmed. Some additional dating and analytical data on the Palmottu water-rock system and comparable sites is still necessary. Pretests for the application of advanced concepts and modelling tools at the repository site Olkiluoto were initiated in order to improve the regulator's capability to evaluate a safety case focussing on geochemical stability and radionuclide migration issues.

Funding: 1999-2003: STUK; 2004: KYT program; 2005: no KYT funding, (STUK); 2006: KYT; no STUK decision

Introduction and objectives

The starting point for the approach presented here to evaluate the safety of nuclear disposal in a geological repository is the basic idea that any material deposited in the geosphere will be participating to a various extend in geochemical cycles of the elements in a local, regional and global context. Generic and site-specific observations in nature are used in a qualitative way to get an overview of the dominating processes, their driving forces and the resulting consequences in the biosphere. Such knowledge can be used as additional, confidence building information in the decision making process creating multiple lines of reasoning or argumentation. Quantitative data bases of natural fluxes and concentrations in natural compartments can be used as a yardstick, so-called complementary safety indicators, to compare and evaluate calculated fluxes and concentrations from a waste repository. Thorough knowledge and understanding of natural geochemical cycles in different geological settings enables a validating evaluation of the suitability of repository sites and concepts.

Site-specific investigation of geochemical fluxes was started with the goal to gain a quantitative understanding of (i) the involved transport processes, (ii) the range of the relevant parameters, (iii) the relevant spatial and temporal scales, (iv) the influences of changes of external conditions (climate changes), (v) the chemical stability in the geosphere (redox buffering) and (vi) to test and validate advanced coupled reactive geochemical transport modeling approaches. The initial work focussed on the behaviour of uranium, the most suitable natural tracer. The topics (i-iii) are closely related to a parallel, methodologically somehow similar project on physical rock properties and diffusive transport mechanisms presented at this workshop. Topics (v-vi) are closely related to a previous project on natural redox-buffering minerals (e.g. olivine) and their interaction with oxidizing agents and redox-sensitive elements.

Application of the gained tools, knowledge and experiences to a repository site could result in decisive benefits for the regulatory evaluation of a safety case of a geological repository:

(i) evaluation and reducing uncertainties, (ii) evaluation of conservativeness, (iii) getting confidence in extrapolations, (iv) evaluation of the transferability of geo-information, (v) evaluation of the geochemical stability, (vi) evaluation and validation of radionuclide transport concepts, (vii) evaluation of scenarios and (viii) creating multiple lines of argumentation.

Natural geochemical fluxes and anomalies: generic overview and case studies

Qualitative information on natural geochemical fluxes and concentrations in relation to the geological setting, climate conditions and topography has been derived from the data and experiences reported in the geochemical ore prospecting literature worldwide and geochemical mapping programmes in Europe (IAEA, 2005). Also results from investigations on weathering rates and on erosional fluxes in river catchments have been used. By that a first overview was gained concerning the orders of magnitudes and the dominating processes leading to dispersion and enrichment of elements, putting the repository in a wider context, and also some certainty that nothing was overlooked. A large number of geochemical exploration case studies is reported from northern Scandinavia; all these cases are outcrops or suboutcrops below glacial overburden of anomalies and no deep-sited ores are represented. While in the high-relief areas anomalies are often visible in the surface layers, are the dispersion fans in the peneplane setting of Finland generally limited to the rock-till interface and the lower horizons of the till. Half of the cases were till anomalies with glacigenic mechanical dispersion as the dominating mechanism. Next important were secondary enrichments in mineralic and organic stream sediments, peat and humus. Compared to glacigenic mechanical transport chemical migration in till is a locally much more limited phenomenon resulting usually in minor downslope migration mediated by groundwater flow at the rock-till interface or diffusion. Due to the short time period since the last glaciation weathering has usually affected only the till surface and a redox front is generally visible in till which forms a migration barrier for some elements. The peculiarities of glaciated terrain have pronounced influence on geochemical fluxes of elements: the low hydraulic conductivity of till, the predominance of unweathered crushed rock material, the mostly unweathered bedrock, and the abundant presence of secondary sinks such as peat and sediments.

Active geochemical cycles lead to groundwater-mediated transport of significant amounts of elements to the surface environment (IAEA, 2005). In Europe thousands of thermal and mineral springs are known since long times. A review of those lead to the conclusion that the flow in the presented systems is topography driven; an additional head can result from the lowered water densities due to elevated temperatures or addition of gases. Typical altitude differences between recharge and discharge area amount to some hundreds of meters, while the flow systems typically extend to depths of a few kilometres. The existence of a well-developed fracture system to great depth is a prerequisite; this is typically fulfilled in regions with an active tectonic history. Maps from central Europe give ample evidence how systematic the occurrence of mineral/thermal water springs is in relation to the geology. Typical rates of discharge are in the range of a few l/s, with typical trace elements from deep circulation systems

in crystalline rocks such as As, B, Cs, Sr, Rb, Ba, F; the concentrations of toxic elements often exceed drinking water limits. A single spring can transport hundreds to thousands of kilograms of toxic components to the surface within a year.

Groundwater conditions in Finland are characterized by the basic distinctive features of an old basement overlain by thin overburden of young glacial and postglacial deposits (IAEA, 2005). Due to low hydraulical gradients in a peneplane (low relief) setting, generally low regional groundwater flow rates and constriction of groundwater movement to local hydraulic hights and near-surface zones prevail even in the case that conductive fracture systems are available; natural mineral or thermal water discharges do not occur in Finland. Deep groundwaters in bedrock are practically stagnant and characterized by increased salinity due to preserved waters of high age and the effects of long-lasting water-rock interaction.

Data base of generic and site-specific natural geochemical concentrations and fluxes in Finland for use as complementary safety indicators

A comprehensive data base comprising the elemental concentrations of As (selected as an additional indicator for deep groundwater discharge), Cu (major repository construction material), K, (Ra), Rb, Th and U (natural radioactive elements) in various compartments in Finland such as glacial till, stream sediment, lake sediment, stream water and groundwater from dug and drilled wells has been compiled (IAEA, 2005). The geochemical information produces a coherent picture of the regional differences in metal contents and enrichments in Finland identifying not only large scale geological/lithological units, but even small intrusions and tectonic features such as fracture and shear zones favouring geochemical dispersion, leading to anomalies which may even continue as secondary migration caused by postglacial weathering. Comparison of areal elemental distributions in different materials does not give direct information on natural geochemical fluxes, but allows some conclusions about the sources and dominating transport processes. On the larger scale glacial till and often the groundwater in drilled wells represents fairly well the composition of the underlying bedrock. The correlations between concentrations in different compartments from till to sediments and different water bodies are strong only for relatively mobile elements such as U. Thus the correlations could be indicators of fluxes from the geo- to the biosphere, but also for fixation in sinks. A drawback of the data base is the lack of rock geochemistry data (although the C-horizon of the soil reflects fairly well the rock composition) and the lack of data on mobile fractions (such analyses were started recently). The key to the successful application of concentration data and derivation of realistic geochemical fluxes is to thoroughly understand the exchange processes between bedrock and overburden.

Geochemical fluxes in Finland were derived from investigations on geologically and hydrogeologically well-defined small catchments monitored, where groundwater is discharging in springs (IAEA, 2005). For comparison estimations of heavy metal erosion rates for forest soils based on base metal weathering rates and heavy metal concentrations in till were used. In addition, natural fluxes of Cu and U from Finnish headwater streams from numerous basins were determined. Comparisons are necessary in these kind of estimations in order to reduce uncertainties caused by assumptions.

Groundwater chemistry and the observed large and rapid variations of the chemistry lead to the conclusion that groundwaters flow mostly in the Quaternary and the most fractured uppermost layers of bedrock in these catchments and represent shallow flow systems characterized by short contact times with the geological substrate. Influences of fluxes which might bring substances from greater depth cannot be distinguished in these catchments.

Site specific data from the Palmottu uranium mineralization gave estimations of U mass transport based on analyses of U concentrations in all relevant materials and calculations of groundwater flow rates based on hydraulic testing (IAEA, 2005). The uranium mass balance estimation for the Palmottu mineralization (about 1000-1500 t of U) showed that the U flux from the upper, oxidizing zone is much higher (160 g/a) than that from the lower, reducing zone (0.002 g/a), but in the same order as the U flux caused by surficial bedrock erosion and chemical weathering (70 g/a). Natural uranium fluxes are very limited under reducing conditions, but also under oxidizing conditions mineralization processes and organic complexation limit or delay transport of U. Considering long-term perspectives, there are indications that during past glaciations melt waters may have intruded deeper into the flow system at Palmottu, but reducing conditions were largely maintained by the redox buffering capacity of the rock. There is considerable scope for refining these preliminary U mass balance calculations.

Site-specific data from the four repository investigation sites in Finland were based on calculations using groundwater flow data and groundwater composition data for defined areas at certain depths (IAEA, 2005). The calculated fluxes reflect groundwater movement and chemistry. Although a general decrease of U fluxes is calculated to greater depth, the pattern of the U concentrations indicates that the whole flow system must be understood before relevant conclusions are possible. In particular, neglecting water-rock interaction makes the value of such estimations doubtful.

Summarizing the results, it becomes evident that the geochemistry of the groundwater-rock system and the chemical properties of the element are very prominent factors determining natural geochemical fluxes; the redox conditions are most prominent for U. It becomes also clear that U is the most suitable element that is reasonable to examine between the source area and possible discharge area within this type of study. Due to given conditions in glaciated terrain in Finland elemental fluxes are mostly restricted locally and to the upper horizons of the overburden and contributions of transport by deep groundwater are hardly detectable.

Quantitative understanding of observed site-specific uranium mobilization and fixation

The value of information on geochemical fluxes and concentrations for use in safety evaluations could be increased by a better understanding of the mechanisms of element mobilization and immobilization within geological time scales and natural spatial scales and a quantification of the migration processes by application of adequate modelling tools. Uranium was identified as the most suitable element. An additional benefit would be gained from information on the effects of glacial scenarios on U migration. The objectives were to: (i) constrain time frames for uranium mobilisation and fixation, (ii) determine whether uranophane precipitation is an ongoing process with

successive generations of crystal formation possible linked to episodic climatic events, and (iii) establish the relative contribution of secondary uranophane and residual uraninite to high uranium concentrations in shallow groundwaters. Further information was also needed to decipher the relationship between rock microstructure and the position of uranium phases. This is a key issue in understanding the role of the rock matrix and the fracture network in water-rock interactions. In addition, calculations were performed to investigate the controls on uranophane formation as a function of depth.

A more detailed characterization of the occurrence of primary and secondary U phases at the Palmottu site was conducted. In order to gain information from greater depths, samples from a second site nearby were dated. In the regional context it became evident that the results from the two Finnish sites are fully consistent with previous dating results reported from Sweden, reflecting the same glacial events over a period of about 100,000 years (Read et al. 2005). This information, giving realistic scenarios and boundary conditions, forms a necessary basis for constructing a credible model of U release and fixation over such long time scales and can be verified by observations of other U anomalies in nature. The results show that the trigger for U mobilization is the intrusion of oxidizing, glacial melt-water. It was postulated that uranophane near the surface could be very recent. This has now been confirmed (average age ≤ 2000 years). The objective to determine whether uranophane precipitation is an ongoing process or only a process linked to discrete climatic events (i.e. oxidation by glacial melt waters), is partly answered in the discovery of recent, post-glacial uranophane in the near surface zone. Relatively continuous dissolution and precipitation of uranophane is an ongoing process especially near the surface. At greater depths, however, the situation is less clear.There appear to be compositional and textural differences between secondary uranium silicates precipitated in large, open fractures and those bound in micro-fissures at the granular scale. The latter aspect deserves further investigation.

As a first step a pilot modelling study as a link between the CRP on natural geochemical fluxes and relevant developments in repository performance assessment was initiated, which was based on existing knowledge of the hydrogeology and geochemistry of the Palmottu site (Oziabkin et al. 2005). A dual porosity model to represent fractures and matrix coupled to chemical reactions is used. It is also possible to change rates of mineral precipitation-dissolution in response to physical constraints (variations in flow direction and rates). The time frame considered was 10 000 years, roughly the period since Palmottu emerged from the sea. According to the model calculations, around 44% of the uranium released by dissolution of the main ore mineral (uraninite) re-precipitates within the model domain as uranophane with 56% 'lost' as outflow. The proportion fixed by ion exchange or co-precipitation with fracture minerals was predicted to be negligible. The modelling exercise giving promising results demonstrated the potential usefulness of a reactive chemical transport model in a safety assessment framework. It accurately represented our understanding of radionuclide migration processes, employed fundamental thermodynamic, kinetic and site data at a mechanistic level and could be verified directly against observations from the field. Such models also provide new insights in terms of evaluating alternative scenarios of system evolution. If the behaviour of U at the Palmottu site could be simulated satisfactorily, then the modelling approach might be applied with greater

confidence to the Olkiluoto repository system. Preliminary work to apply reactive chemical transport modelling tools to selected relevant groundwater conducting structures at Olkiluoto was initiated.

A novel approach to describing the influences of changing external conditions on the Palmottu system has been further developed after completion of the pilot modelling study to cover a wider range of scenarios. These results describing the evolution of the modelled system under different initial conditions and its response to temporary or continuous changes of boundary conditions are detailed. Migration of U derived from uraninite through microfissures has been demonstrated by autoradiography of the fractured rock. Uranium is subsequently precipitated as uranophane from solution, often in open fractures. The results of this study indicate that uranium has migrated on the order of centimetres from its source before precipitating. No evidence has been found of replacement *in situ.*

Development and evaluation of: concepts (chemical stability; RN migration), scenarios (paleo-evolution; glacial cycles), models (coupled reactive chemical transport)

The use of natural safety indicators, by focussing on the behaviour of geochemical systems,

provides a firm basis for extrapolation. Comparison of model output with natural concentration ranges is an obvious means of assessing parametric uncertainty. It provides a check on the realistic bounds of the simulations. However, conceptual uncertainty is at least as important and is perhaps, the main area where such indicators offer potential for enhancing performance assessment exercises. No amount of statistical sampling will compensate if the parameters being sampled do not reflect the processes actually occurring.

The most complete and relevant data set for deriving a natural safety indicator methodology in Finland, and for verifying a safety case model is the Palmottu study (IAEA, 2005). The site experienced continental ice margin conditions and, thus a unique feature of the Palmottu exercise is that the influence of palaeoclimatic changes on groundwater geochemistry formed a central part of the investigation throughout. This, in turn, has lead to improved knowledge regarding the impact of glaciation and related phenomena (e.g. permafrost) on the hydrogeochemistry of deep fracture-controlled systems. With respect of land uplift, Palmottu provides an indication of the likely future evolution of Olkiluoto over the next few thousand years. At the very least, observations on natural systems provide a check on the realism of scenarios derived by elicitation or other methods. At best, they constitute the basis of a viable alternative to current approaches, though as noted below the methodology requires further work. In many respects, the geological history of the Palmottu deposit resembles the postulated evolution of the repository proposed for spent U fuel at Olkiluoto. These include the inventory, host rock and geographical setting; the deposit is limited in size and contains uranium mainly in the form of UO_2.

A common feature of all PA modelling carried out to date is the hierarchical sequencing of computer programs whereby detailed process-specific models are progressively simplified until one reaches a stylised representation of the entire

'disposal system' (IAEA, 2005; Read et al, 2002). Only at the last stage are parameters sampled and thus, the often-substantial uncertainties associated with the more fundamental aspects of modelling tend to be hidden. This provides much of the rationale for natural indicators, *i.e.* a more transparent safety case. Criticism of PA calculations is at least partly justified, therefore, as in actuality the models do not describe 'the system' but are merely simplistic calculations of groundwater-mediated radionuclide transport. It is possible that, in future, the additional layer of 'PA modelling' could be excluded from safety assessments in favour of an explicit treatment of geochemical transport. This would provide a means for direct comparison of output with natural fluxes and related indicators. If required, conversion of nuclide concentration profiles to dose or risk values could be performed easily by post-processing. In the short term, however, it is likely that both approaches will be applied in tandem.

The most recent assessment exercise undertaken by Posiva, TILA-99, adopts an entirely deterministic treatment. The main concern is not that the approach is deterministic, but that the tools take no account of interactions between geochemical and hydrological processes. Further, they fundamentally misrepresent the known geochemical behaviour of the uranium series elements. The calculations are biased towards dispersion and dilution of activity in the far field making it indistinguishable from its surroundings, an assumption not supported by observations from natural anomalies. Consequently, if there were to be an accumulation of activity as, for example at Palmottu, sinking a well into groundwater above the repository would give higher doses than those calculated.

A major advantage of the natural indicator approach is that it directs attention towards geochemical systems and processes rather than to more abstract concepts. The main activities required are: i) provision of thermodynamic/kinetic data, ii) compilation of concentration, flux and mass accumulation measurements for model verification, iii) model enhancement to incorporate advances in simulating fracture dominated transport and radioelement-matrix interactions. Although the geochemical behaviour of uranium is relatively well known, our ability to predict the fate of trace fission products and transuranics is in its infancy.

Conclusions

Considerable efforts have been undertaken to develop tools and support for repository safety case evaluation and decision making from the regulatory point of view. Understanding and quantitative description of natural geochemical mobilization and immobilization processes (geochemical cycles) provides versatile and powerful aid to gain confidence in performance assessment calculations. The evaluation of the relevance and adequate quantification of processes is facilitated by information from natural systems increasing mechanistic process understanding and predictive capability, understanding parameter ranges, spatial and time scales, as well as validating concepts and models of chemical stability and radionuclide transport. In addition to providing complementary safety indicators, the methodology creates multiple lines of reasoning building confidence in performance assessment calculations and creates a basis for chemotoxical and radiological risk comparison. Necessary scoping application of the

methodology to the repository site Olkiluoto is still at a preliminary stage and waiting for continuation of funding.

References

IAEA, 2005, Natural Activity Concentrations and Fluxes as Indicators for the Safety Assessment of Radioactive Waste Disposal, IAEA TECDOC Series No. 1464 (and literature cited therein)

Oziabkin V., Oziabkin S., 2005. Numerical modelling of coupled reactive chemical transport at the Palmottu natural analogue site: eastern flow system. Helsinki University of Techno-logy, Geoenvironmental Technology C, Working Report 1, TKK-GT-C-1, Espoo 2005.

Read, D., Hellmuth, K-H., Kaija, K., Ahonen, L., 2002. Natural Uranium Fluxes and Their Use in Repository Safety Assessment. In: Merkel, B.J., Planer-Friedrich, B., Wolkersdorfer, C., Uranium in the aquatic environment, Springer, Berlin, 2002, p.115-126.

Read D., Siitari-Kauppi M., Kelokaski M., Black S., Buckby T., Marcos N., Kaija J., Hellmuth K-H., 2004. Natural geochemical fluxes in Finland as indicators of nuclear repository safety. Helsinki University of Technology, Laboratory of Rock Engineering, Research Report TKK-KAL-A-34, Espoo 2004.

Read D., Black S., Buckby T., Proust D., Marcos N., Siitari-Kauppi M., 2005. Secondary uranium mineralization in southern Fennoscandia. Helsinki University of Technology, Geoenvironmental Technology, Research Report 2, TKK-GT-A-2, Espoo 2005.

INDIVIDUAL SCIENTIFIC AND TECHNICAL CONTRIBUTIONS

EVALUATION OF ISOTOPE DATA FROM RUPRECHTOV SITE

U. Noseck[1*], T. Brasser[1], A. Laciok[2], M. Hercik[2], V. Havlová[2], G. Buckau[3], K. Rozanski[4] and M. Dulinski[4]

[1] Gesellschaft für Anlagen- und Reaktorsicherheit, Theodor-Heuss- Str. 4, 38122 Braunschweig, Germany
[2] Nuclear Research Institute Rež plc, Waste and Environmental Management Department, Husinec- Rež, PSC 250 68, Czech Republic
[3] Forschungszentrum Karlsruhe, Institut für Nukleare Entsorgung, P.O. Box 3640, 76021 Karlsruhe, Germany
[4] AGH – University of Science and Technology, Faculty of Physics and Applied Computer Science, al Mickiewicza 30, 30-059 Krakow, Poland

* Corresponding author: ulrich.noseck@grs.de

Abstract

All available natural isotope data from groundwater wells at Ruprechtov site are evaluated with respect to the hydrogeological flow regime in the tertiary sediments close to the clay/lignite layers and the behaviour of carbon in the system. Differences in stable isotope data indicate two different infiltration areas in the outcropping granites in the south-western part as source for water in clay/lignite layers in the middle and north and another in the southern part as source for the clay lignite layers in the eastern part of the investigation area. Differences in signatures in the northern part indicate very local connections probably via fault zones of the water system in the underlying granite and the tertiary sediments.

Based on the conceptual model for the hydrogeological flow regime, data for $d^{13}C$ and ^{14}C in DIC and DOC as well as $d^{34}S$ in dissolved sulphate are evaluated. The increase of biogenic DIC with increasing DOC concentration and the increase of $d^{34}S$ in water from the clay/lignite layers compared to water from granite in the infiltration areas give rise for microbial reduction of SOC and generation of DIC and DOC in the clay lignite layers. A more detailed paper about the results presented here is in preparation [4].

Introduction

Ruprechtov site in Czech Republic is studied as an analogue for the behaviour of natural radionuclides in the overburden of salt domes because its geological conditions are similar to sedimentary sequences covering potential salt host rocks. The investigation area is a tertiary basin bordered in the west and south by outcropping granite. Main features of the investigation area are the crystalline

basement covered by kaolin layers with varying thickness (few up to several tens of metres). The basin is mainly filled with tertiary argillized pyroclastic sediments. The interface between kaolin and pyroclastic sediments is characterized by a strong morphology. The horizon of major interest is the so-called clay/lignite layer at the interface of kaolin and pyroclastic sediments, with high content of sedimentary organic carbon (SOC), zones of uranium enrichment and partly aquiferous horizons [3]. An important instrument to understand the hydrogeological flow regime and the interrelation of sedimentary organic carbon with dissolved inorganic (DIC) and dissolved organic carbon (DOC) is the investigation of natural isotopes in groundwater. The work presented here shows results from the evaluation of natural isotope data sampled in groundwater wells at Ruprechtov site. It mainly focuses on aspects of the carbon chemistry at Ruprechtov site.

Objectives

Based on the evaluation of stable isotope data a conceptual model for the current hydrogeological situation at Ruprechtov site was proposed in [3]. Major objective of the work in FUNMIG is the evaluation and understanding of processes connected with changes in carbon chemistry, i.e. the development of DIC and DOC contents including changes in their ^{13}C and ^{14}C isotope signatures during water flow through the system.

Experimental

Natural isotope analyses of distinct groundwaters have been performed to characterise the hydrogeological flow regime at the site and especially the evolution of DOC and DIC during transport through the clay/lignite formation in more detail. $^{2}H/^{1}H$ and $^{18}O/^{16}O$ – isotope ratios have been analysed at near surface waters to identify typical local infiltration waters. Additionally ^{3}H, ^{14}C concentrations as well as $^{13}C/^{12}C$ and $^{34}S/^{32}S$-isotope ratios have been determined in the deeper groundwaters from several wells. The isotope ratios of $^{2}H/^{1}H$, $^{18}O/^{16}O$, $^{13}C/^{12}C$ and $^{34}S/^{32}S$ are given as per mille deviation $\delta^{2}H$, $\delta^{18}O$, $\delta^{13}C$, or $\delta^{34}S$. A detailed description of the experimental procedure can be found in [3]

Results and discussion

Altogether 18 wells from recent drilling campaigns are available to sample and characterize undisturbed groundwater from aquiferous horizons. The position of boreholes is shown in Fig. 1. The blue font characterises water from either outcropping granite (NA8, NA10, RP1) or underlying granite (NA14, HR4).

Hydrogeological situation

Laboratory experiments at selected drill cores and on-site (pumping tests) measurements of hydraulic conductivities show that only distinct aquiferous horizons exist with kf-values of 10^{-5} to 10^{-8} m/s and thicknesses of about 1-2 meter

only, mainly close to the clay/lignite layers [3]. They do not represent a continuous aquifer but areas with increased water flow. Compared with this, the pyroclastic sediments and the underlying kaolin are low permeable with typical kf-values of 10^{-10} to 10^{-11} m/s. Additionally, fracture zones and areas with very low thickness of the underlying kaolin might represent hydraulic connections between clay/lignite layers and granite.

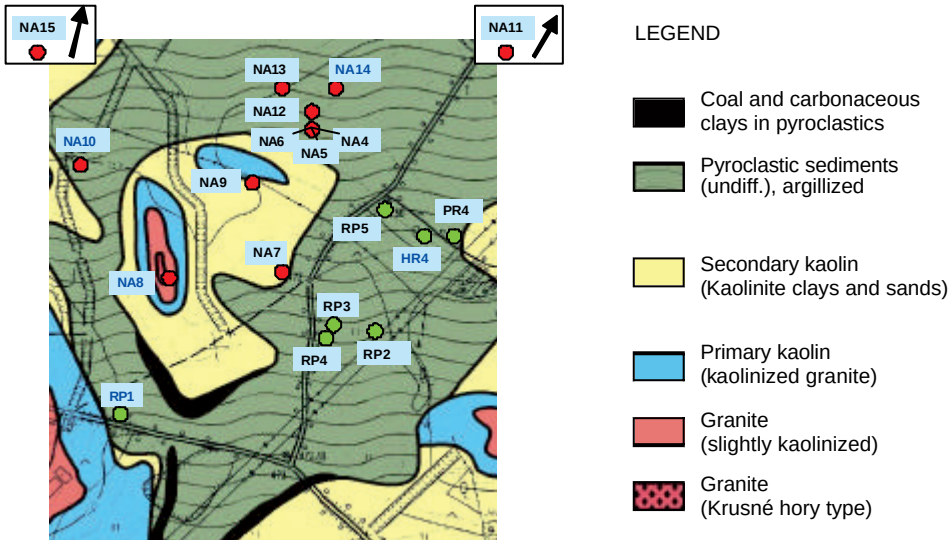

Figure. 1: *Detailed view of location of boreholes at Ruprechtov site correlated to geologic map. Boreholes in granite in blue font*

All isotope data including concentrations of DIC, DOC and dissolved sulphate are listed in Tab. 1. The results of the stable isotope analyses are shown in Fig. 2. From the figure on the left it is apparent that stable isotope composition varies in a rather broad range with $d^{18}O$ values from -9.8 to -8.8 ‰. In general the isotope signatures follow the world meteoric water line (WMWL). The data range of recent local infiltration waters is marked by the bold grey line.

Measurements of water levels confirm a hydraulic gradient from south west to north east [3]. Therefore, infiltration is expected in the outcropping granite areas in the western and southern part of the investigation area. Water with typical signature of local infiltration are found in granite well NA10, assumed to be representative for infiltration area in the western part. On the other hand isotopically light water is found in granite well RP1 in the south and in the boreholes in clay/lignite layers in the south-eastern part, indicating a second infiltration area in the South with major flow direction to north east. The wells in the kaolin and clay lignite layers in the middle and north show similar values as NA10, indicating that their water originates from the western infiltration area. However, some wells NA6, NA13, NA14 and HR4 occupy intermediate positions in the $d^{18}O$ - $d^{2}H$ diagram. An explanation is that they represent mixing waters of isotopically light and heavy waters. This might be the case for water from HR4 and NA14, which originates from the underlying granite and shows $d^{18}O$-values of approx -9.3. Similar isotope values in NA6 and NA13 might be caused by hydraulic pathways to underlying granite consisting of small fracture networks, which are only very locally connected.

Behaviour of carbon in the system

Carbon isotopes are measured in order to identify water ages, and/or to characterise water mixing processes as well as reactions within the carbon cycle. The ages of the waters calculated with ^{14}C values of DIC are in a range of 1,000 to more than 20,000 years. These ages are unexpectedly high. They are calculated without taking into account changes by chemical reactions of carbon compounds, i.e. it is necessary to look at the behaviour of carbon in more detail.

The most important reactions influencing ^{14}C and $d^{13}C$ ratios in dissolved inorganic carbon (DIC) are

Dissolution of sedimentary inorganic carbon (SIC) leads to a decrease in ^{14}C and increase in $d^{13}C$, because sedimentary inorganic carbon from the Tertiary does not contain any ^{14}C and $d^{13}C$-values are around 0 ‰.

Microbial degradation of sedimentary organic carbon (SOC). $d^{13}C$ of DOC is expected to be around -25 to -27 ‰. ^{14}C is 0 pmc in the tertiary organic material from the clay/lignite layers and expected to be around 50 to 60 ‰ in infiltration areas under forest prior to nuclear atmospheric testing (s. below).

Input of endogenic CO_2 from exhalations leads also to a decrease in ^{14}C and increase in $d^{13}C$ of infiltration waters. Typical $d^{13}C$-values determined in the Ohre rift area are -2.7 ‰ [5]. ^{14}C values are as a matter of course 0 pmc.

Another important observation is the low DOC concentration in groundwater from Ruprechtov site with values in the range of approx. 1 - 10 mg C/l with only slightly elevated values in water from the clay/lignite layers compared to granite. The concentrations are much lower than those observed in the overburden from Gorleben site where concentrations up to 200 mg C/l occur, although Ruprechtov clay/lignite layers contain up to 50 % SOC. In Gorleben aquifers conversion of sedimentary organic matter occurs by microbial reduction with release of DOC [1]. This process can also be expected at Ruprechtov site, since the prerequisites for sulphate reduction in the clay/lignite layer are fulfilled: (1) SO_4 is available in distinct amounts in all boreholes. Concentrations vary between 0.1 and 2 mmol/l (cf. Tab. 1). (2) Existence of sulphate reducing bacteria in the clay/lignite layer has exemplary been shown in sediments from borehole NA4 [3] Carbon and sulphate concentrations and isotope data are evaluated to understand the processes at Ruprechtov site. In the following only selected results are shown. A detailed description can be found in [4]

Table 1: *Depth of filter horizons, lithological units, natural isotope data and concentrations of DIC, DOC and dissolved sulphate in boreholes from Ruprechtov site*

Well No.	Filtered horizon [m]	Lithology	$d^{18}O$ [‰]	$d^{2}H$ [‰]	Tritium [TU]	^{14}C		$d^{13}C$		$d^{34}S$ SO_4^{2-} (‰)	DIC [mg/l]	DOC [mg/l]	SO_4^{2-} [mg/l]
						DIC [pMC]	DOC [pmc]	DIC [‰]	DOC [‰]				
NA-4	34.5 - 36.5	clay/lignite, U	-9.78	-68.0	0.0	3.2	39.96	-11.0	-26.6	24.63	74.2	4.22	19.8
NA-5	19.3 - 21.3	U	-8.98	-61.9	0.0	5.3		-10.9	-25		90.8		31.5
NA-6	33.4 - 37.4	clay/lignite, U	-9.27	-64.6	0.6	13.1		-12.4	-26.8	23.5	60	3.27	49.5
NA-7/1	15.5 - 19.5	kaolin	-8.96	-61.5	0.2					20.4	61.7	3.88	28.2
NA-7/2	10.5 - 11	clay/lignite, U	-9.00	-61.1	0.0	39.4		-16.1	-27.3		60.8		12.3
NA-8	8.5 - 24	granite	-9.22	-62.9	1.1	71.9	64.6	-21.9	-27.8	-8.5	14.5	3.01	59.1
NA-9	4.4 - 10	kaolin	-8.95	-60.8	0.0	72.1		-20.5	-27.1		37.1		11.8
NA-10	19.5 - 27.5	granite	-8.89	-61.5	1.6	54.6	193.67	-16.2	-26.4	0.2	33.8	1.99	40.8
NA-11	33.2 - 39	clay/lignite, U	-9.00	-65.5	1.5	7.8		-9.6			82.4		178.6
NA-12	36.5 - 39.3	clay/lignite, U	-8.87	-61.9	0.3	26.5	70.0	-16.0	-25.6	20.11	67	3.69	22.9
NA-13	42.2 - 48	clay/lignite, U	-9.24	-65.9	1.5		44.33		-27.2		68.8	2.32	22.9
NA-14	67.6 - 77.6	granite	-9.33	-64.9	0.6	9.8		-12.8		16.43	69.1		30.8
NA-15	28.8 - 31.6	granite	-9.88	-70.9	0.2	11.8		-13.7			39.4		40.1
RP-1	5 - 18	granite	-9.52	-66.9	0.2	21.0		-16.8		3.48	33.4	1.36	19.8
RP-2	25 - 43	clay/lignite, U	-9.81	-69.0	1.1	16.8		-13.2	-26.6		52.4	1.83	55.0
RP-3	25 - 48	clay/lignite, U (28 m)	-9.60	-68.2	1.0	13.3		-15.3	-26.6		59.7		24.6
RP-5	30 - 58	clay/lignite, U	-9.75	-68.4	0.0	6.4		-11.7			58.1		14.8
HR-4	46.5 - 95	granite	-9.31	-64.3	1.2	29.9		-14.5	-26.2				

The isotopic analysis of DIC at Ruprechtov site shows general trends. The $d^{13}C$ values decrease with increasing content of DIC. Additionally, ^{14}C-values decrease with increasing $d^{13}C$ [3]

Fig. 4 shows the correlation of DIC vs DOC. On the left only the biogenic DIC is plotted, assuming that the ^{13}C content of the source water is of inorganic origin with -27 ‰ and additional DIC is of organic origin. It is obvious that data for NA8 are different from the other infiltration waters with an extremely low DIC/DOC ratio. It is an additional indication that this water acts only to a low extent as source for water in the clay/lignite layers. Despite a spread of data they follow a line, with increase of biogenic DIC from infiltration waters NA10 and RP1 to waters from the clay/lignite layer. These data sugggest that formation of DOC takes place in the clay/lignite horizon.

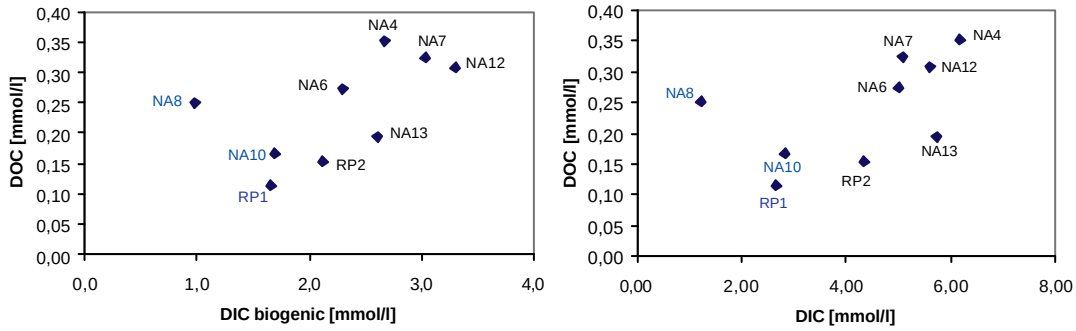

***Figure 4**: DIC and biogenic DIC vs DOC in selected boreholes*

If microbial activities are involved, these should be detectable, since microbial sulphate reduction is accompanied by isotope fractionation. The lighter isotope ^{32}S is preferentially metabolized by the microbes and therefore residual sulphate molecules in solution become enriched in the isotope ^{34}S. Therefore, DOC generation by sulphate reduction in the clay/lignite layers should be detectable by increased $d^{34}S$ values water from these layers.

The results of $d^{34}S$ analyses in water samples from the infiltration area as well as from clay/lignite layer are shown in Fig. 5. For the wells with infiltration water in the south and west of the area NA10 and RP1, the $d^{34}S$-values are low and vary between 0.2 and 3.48 ‰. Once more the water from infiltration area around NA8 is different with an even lower value of -8.45 ‰.

In contrast waters from the clay-lignite layer show increased $d^{34}S$-values in the range of 16.43 to 24.63 ‰. The significant enrichment of $d^{34}S$ in these boreholes is a clear indication that sulphate reduction occurs in the clay/lignite layers.

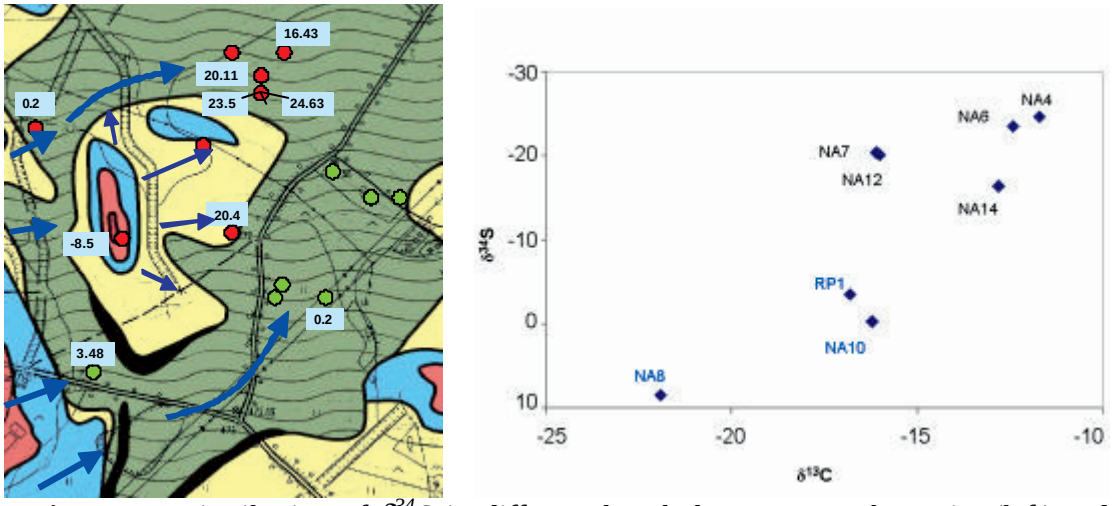

Figure. 5*: Distribution of $\delta^{34}S$ in different boreholes at Ruprechtov site (left) and $\delta^{34}S$ vs $\delta^{13}C$ (right)*

Conclusions

Isotope data from Ruprechtov site are evaluated with respect to the hydrogeological flow regime and behaviour of carbon in the system. The results so far show a rather complex hydrogeological situation with infiltration areas in the outcropping granites in the western and southern part, water flow in zones of only few metres thickness, which do not represent a continuous aquifer, but distinct areas with increased water flow. There is strong indication for very local connections of the flow systems in the underlying granite and in the tertiary sediments in the northern part, where kaolin thickness is low and fault zones are expected.

The complex hydrogeological situation hampers the interpretation of the carbon isotope data. Nevertheless, a general picture can be drawn. NA10 and RP1 are considered as water from infiltration areas in the western and southern part, respectively. There is strong indication that microbial reduction of sulphate contributes to the formation of DOC and biogenic DIC in the clay/lignite layers given by differences between water from infiltration area and water from clay/lignite layers especially by increase of $d^{34}S$ in dissolved sulphate and increase of biogenic DIC with increasing DOC.

Acknowledgements

This work has been / is financed by the European Commission, the German Federal Minstry of Economics and Technology (BMWi) under contract no. 02 E 9551 and no. 02 E 9995 and by the Czech Radioactive Waste Repository Authority (RAWRA) under contract no. 1999/31/NACH.

References

[1] Buckau, G.; Artinger, R.; Geyer, S.; Wolf, M.; Fritz, P.; Kim, J.I. (2000a) Groundwater in-situ generation of aquatic humic and fulvic acids and the mineralization of sedimentary organic carbon, Appl. Geochem., 15, 819-832.

[2] Buckau, G.; Artinger, R.; Geyer, S.; Wolf, M.; Fritz, P.; Kim, J.I. (2000b) ^{14}C dating of Gorleben groundwater, Appl. Geochem., 15, 583-597.

[3] Noseck, U.; Brasser, Th. (2006) Radionuclide transport and retention in natural rock formations - Ruprechtov site, Gesellschaft für Anlagen- und Reaktorsicherheit (GRS) mbH, GRS-218, Braunschweig, May 2006.

[4] Noseck, U.; Rozanski, K.; Dulinski, M.; Laciok , A.; Brasser. Th.; Hercik, M.; Buckau, G.; Hauser, W. (2007) Characterisation of hydrogeology and carbon chemistry by use of natural isotopes – Ruprechtov site, Czech Republic, Appl. Geochem. (under preparation).

[5] Weise, S.M.; Bräuer, K.; Kämpf, H.; Strauch, G.; Koch, U. (2001) Transport of mantle volatiles through the crust traced by seismically released fluids: A natural experiment in the earthquake swarm area Vogtland/NW Bohemia, Central Europe, Tectonophysics, 336, 137-150.

CONDITIONAL STABILITY PARAMETERS FOR THE ACTINIDES(IV)-HUMIC ACID SYSTEM: A SEARCH FOR CONSISTENCY

P. Reiller[1], N.D. Evans[2], and G. Szabó[3]

[1] Commissariat à l'Energie Atomique, CE Saclay, DEN/DANS/DPC/SECR, Laboratoire de Spéciation des Radionucléides et des Molécules, Bâtiment 391, p.c. 33, F-91191 Gif-sur-Yvette CEDEX, France
[2] Department of Chemistry, Loughborough University, Loughborough, Leics, LE11 3TU, United Kingdom
[3] "Frédéric Joliot-Curie" National Research Institute for Radiobiology and Radiohygiene, PO Box 101, Budapest, H-1775, Hungary

*Corresponding author: pascal.reiller@cea.fr

Abstract

The coherence of tetravalent actinide complexation by humic substances is reviewed. In a first attempt, the values of independent data from literature on Th, U, and Pu are collected, selected, and compiled. The data obtained follow the "classical" trend of increasing conditional formation "constant" with pH, led by the increase in the extensive hydrolysis of the tetravalent actinides. Even though a fair agreement is evident, the experimental uncertainties do not permit a full analogy between the tetravalent actinides to be ascertained. In a second attempt, the experiments from which the original data are available were reinterpreted using only one hydrolysis constant set for U(IV), considering that all actinides have analogous behaviour. Hence, the obtained evolution of conditional formation "constants" is fully coherent. This exercise demonstrates the treatment of data through analogy in the case of tetravalent actinides, and would permit to limit the number of necessary, but difficult, experiment with redox sensitive elements like U, Np, or Pu.

Introduction

Tetravalent actinides are often associated with natural organic matter and with humic substances (HS) in particular [11; 22]. Moreover, actinides in the +V and +VI redox state, are often reduced to +IV) by HS [10, 17], except uranium(VI) [4] where the transformation is mediated by bacteria [7]. It is often possible to compare the aqueous chemistry of the different tetravalent actinides through analogy [25]. For instance, the similarity in the migration behaviour of Pu(IV) and Th(IV) has been confirmed [1]. Complementary to data obtained in the late seventies [12;

16], more data were recently obtained on Th(IV) [13; 14; 20; 23, 24 U(IV) [3; 27], and Pu(IV) [8]. Nevertheless, there still maybe a problem with treatment by analogy due to the low numbers of data available. The inherent difficulties of working with tetravalent actinides in general, and with redox sensitive actinides in particular, often prevent the obtaining of reliable data. Hence, with due justifications, if the majority of the data could be more "simply" obtained with Th(IV), and extrapolated with a reasonable level of confidence, to the more "difficult" elements U(IV), Np(IV) and Pu(IV), this would help in reducing a lot of potential and real problems.

Objectives

The aims of this work are to compare the different data available on the tetravalent actinides, and to draw out some general complexing properties in order to increase confidence in complexation parameters estimated by analogy for redox sensitive actinides in their +IV redox state. Only the complexing properties of HS will be considered here, since their reducing properties have not been totally clarified.

Treatment of data

In this demonstration exercise, we will use the simplest model possible. Humic sites will be considered as homogeneous with no acid-base properties. Stability parameters will be conditional and related to pH. The formation of a metal-HS complex MHS can be written with the related constant:

$$Ac + HS \rightleftarrows AcHS \qquad ß(Ac) = \frac{[AcHs]}{[Ac]_{total}[HS]} \qquad (1),$$

where $[Ac]_{total}$ is the total concentration of Ac(IV) in solution, HS is the concentration of humic sites determined either by titration or $Ca(OAc)_2$ and $Ba(OH)_2$. This formation constant should be expressed *vs.* the free Ac^{4+} concentration as:

$$Ac^{4+} + HS \rightleftarrows AcHS \qquad ß(Ac^{4+}) = \frac{[AcHS]}{[Ac^{4+}]_f [HS]} \qquad (2),$$

where $[Ac^{4+}]_f$ is the concentration of free Ac^{4+} cation. Tetravalent actinides are strongly hydrolysed. The activity coefficients of ions and hydrolysis constants will be corrected using the Davies equation.

The side reaction coefficient expressing the reciprocal of the proportion of Ac^{4+} *vs.* $[H^+]$ is expressed as:

$$[Ac]_{total} = [Ac^{4+}] \left(1 + \sum_{n=1}^{4} \frac{{}^{*}\beta_n}{[H^+]^n}\right) = [Ac^{4+}] \cdot a_{Ac(IV)} \qquad (3).$$

Hence one can express the transformation of log ß(Ac) to log $ß(Ac^{4+})$ through:

$$\log ß(Ac^{4+}) \sim \log ß(Ac) + \log a \quad (4).$$

The acid-base as well as the metal complexation properties of HS have been shown to vary with ionic strength. The metal complexation properties for trivalent actinides seem to be more influenced when $I \leq 0.3$ mol/L, than for higher ionic strengths [5; 26]. The same behaviour could be expected for tetravalent actinides. No quantification of the influence of ionic strength on the behaviour of HS will be used in this exercise.

Compilation of data

Up to now, there is not a lot of data on the quantification of actinide(IV) complexation by humic substances in the literature [8, 12; 16; 13; 20; 21; 23; 24, 27, 28].

Li *et al.* [12] have proposed a log ß(U(IV)) = 6.98 at pH 6 for the strong sites on humic acids (HA), which was apparently not corrected for U(IV) hydrolysis. As the control of the uranium (IV) chemistry is not reported, the study should only be considered with care. Moreover, the total concentration of uranium (IV) in solution was between 0.1 and 10 mg/L for a total HA concentration of 20 mg/L. The lower uranium (IV) concentration is 133 times higher than total inorganic solubility of UO_2 under this pH, *i.e.* 3.2×10^{-9} mol_U/kg_w, using the data in Guillaumont *et al.* [9]. Using the results of a preceding calculation exercise [21], the solubility of amorphous ThO_2(am) would be enhanced at pH 6 by a factor of *circa* 60 in the presence of HA. As a comparison, the solubility enhancement observed for UO_2 in the presence of HA was a factor of *circa* 2 [27]. For lower uranium concentrations, the results could thus be used for comparison, but with great care.

The study of Zuyi and Huanxin is not reliable as it suffers from a mass balance problem (Table 1 in Zuyi & Huanxin [28]), and the results from Murphy *et al.* [13] are only traceable in the PhD document that was not available, but could perhaps, be used in the future.

Nash and Choppin determined complexation constants for Th(IV) at different pH values with different humic and fulvic acid samples, *i.e.* a lacustrine (Lake Bradford, Tallahassee, Fl., USA), a soil (Joliet, Il., USA), and a commercial (Aldrich Chemical Co.) sample [15; 16]. They used a solvent extraction technique in an acetate medium and the Schubert method.

Reiller *et al.* [20,21] determined conditional formation constants between pH 6.5 and 8 using the Schubert method in competition between HA and SiO_2. Total Th(IV) concentration was always lower than 10^{-10} mol/L so neither precipitation nor colloid formation was anticipated. The determination of the constants was either from pH isotherms, or from HA isotherms.

Szabó *et al.* worked in a wider range of pH using silica grafted HA [8; 23, 24]. The isotherms were constructed by varying the ratio of Th(IV) or Pu(IV) to the number of available sites. The grafting has been shown to modify neither the acid base nor the complexation properties of HA [6]. Sorption of Th(IV)/Pu(IV) onto

tube walls was taken into account and the total concentration was always under the solubility limit.

Recently, Warwick *et al.* [27] published conditional stability constants obtained from UO_2 solubility enhancement by HA from Aldrich, and from Boom Clay (Belgium). The stability of U(IV) was "fixed" by adding $Na_2S_2O_4$, which was also used to hinder the oxidation of Np(IV) [19]. In this work, the inevitable sorption of HA to UO_2 was not taken into account. There are calculation problems in Warwick *et al.* [27] for $[OH^-]$ and for the extrapolation to 0.2 mol/L of the hydrolysis constants for U(IV). Henceforth in this study, all constants have been re-determined from the experimental data. The results are reinterpreted related to the solubility of UO_2(am,hyd) recommended in Neck and Kim [18] for the sake of consistency.

The data are represented together on Fig. 1. For Th(IV), all the data were corrected for hydrolysis using the data in Baes & Mesmer [2]. For Pu(IV) and U(IV) the hydrolysis constants from Guillaumont *et al.* [9] and Neck & Kim [18] were used respectively. The classic increase in the metal-humic "formation constants" has been obtained throughout the pH range. The uncertainties are either calculated from the mean of different determinations, when raw data are available (*i.e.* $t_{0.05} \times s$), or estimated as ± 1.5 when the data are not available. The log ß(Ac^{4+}) values cannot be rigorously assumed as equal, with the exception of some values, *e.g.* pH ˜ 4, 7 and 7.5. Nevertheless, the values are in reasonable agreement.

Reinterpretation of data

The only data that can be reinterpreted with a reasonable level of confidence are the ones that are documented in the original articles or PhD theses, or directly obtained from the authors. It means that only the data for Aldrich HA [15; 16], and the data from Reiller *et al.* [20,21] Warwick *et al.* [27], and [8; 23, 24] can be used for these calculations. For the other data, estimation can be proposed assuming that:

$$\log ß(Ac^{4+}) = \log ß(Th^{4+}) + \log \frac{\alpha_{Ac(IV)}}{\alpha_{Th(IV)}} \quad (5).$$

As in a previous exercise [21], these conditional constants are only estimates and should be used, with caution, as guidelines for further studies.

All the data on Th(IV) [15; 16; 20; 21, 23, 24] U(IV) [27], and Pu(IV) [8] were treated with the hydrolysis of U(IV) [18]. The correlation hypothesised in Fig. 1, is evident in Fig. 2, after data treatment. It can be seen that the data are now more coherent with each other for the three different tetravalent actinides. A linear relationship has been obtained using linear regression, using only the $\log {}^{HA}ß$ from which the raw data are available:

$$\log {}^{HA}ß(Ac^{4+}) = (3.0 \pm 0.1)\ pH + (1.9 \pm 0.6) \quad (6);$$

the others are estimated using Eq. (5).

Using this kind of correlation, a $\log {}^{HA}ß$ value can be given with a 95% uncertainty of *circa* ± 2.0.

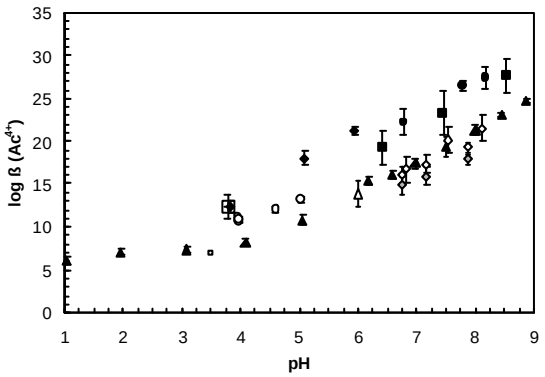

Figure 1. *Compilation of data for the actinide (IV)-humic acid system: for thorium (IV), ○ (Nash & Choppin, [16]), △ (Li et al [12]), □ (Murphy et al., [13], ◇ (Reiller et al., [20], ▲ (Szabó et al., [23,24], referring to hydrolysis in Baes & Mesmer [2] ⋄ [20] referring to hydrolysis in (Neck & Kim,[18]; ◆ Pu-SiO_2 grafted HA [8]); for uranium (IV), ● and ■ (U) (Warwick et al., [27]) referring to U(IV) hydrolysis [18]*

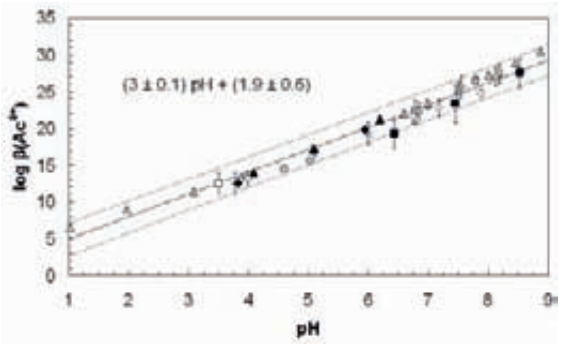

Figure 2. *Comparison of the log ß(Ac^{4+}) values obtained for different actinides corrected for U(IV) hydrolysis (Neck & Kim, [18]: ■ U-Aldrich HA, and □ U-Boom Clay HA (Warwick et al., [27]); ◇ Th-SiO_2-Aldrich HA, Schubert, and ⋄ Th-SiO_2-Aldrich HA, pH isotherm (Reiller et al., [20]; ▲ Th-SiO_2 grafted HA (Szabó et al [23], and △ (Szabó et al., [24]; ◆ Pu-SiO_2 grafted HA [8]; ○ Th-Aldrich HA, ○ Lake Bradford HA, and ● IHA (Nash & Choppin, [16]); □ Th-HA (Murphy et al., [13]); × U-HA (Li et al., [12])*

Conclusions

The treatment of the humic complexation of tetravalent actinides through analogy has been shown to be useful in estimating humic complexation constants. Indeed it permits visualisation of the good correlation of the experimental data found when consistent hydrolysis constants sets are used. A first estimation of the available tetravalent actinide concentration in the presence of HA can be obtained through this treatment. Nevertheless, for accurate determination, direct experiments are still needed due to the underlying uncertainties in the correlation process.

A common view paper will be proposed by the authors, possibly including other contributors from FUNMIG, with a deeper insight into these problems and interpretation of independent data.

References

[1] Artinger, R.; Buckau, G.; Zeh, P.; Geraedts, K.; Vancluysen, J.; Maes, A.; Kim, J. I. (2003). Humic colloid mediated transport of tetravalent actinides and technetium, *Radiochimica Acta*, 91(12), 743-750.

[2] Baes, C. F.; Mesmer, R. E. (1976). *The hydrolysis of cations*. Wiley Interscience Publication.

[3] Cachoir, C.; Lemmens, K.; Van Den Berghe, S.; Van Iseghem, P. (2003). UO_2 dissolution in Boom Clay conditions, *Journal of Nuclear Materials*, 321(1), 49-59.

[4] Czerwinski, K. R.; Buckau, G.; Scherbaum, F.; Kim, J. I. (1994). Complexation of the uranyl ion with aquatic humic acid, *Radiochimica Acta*, 65 111-119.

[5] Czerwinski, K. R.; Kim, J. I.; Rhee, D. S.; Buckau, G. (1996). Complexation of trivalent actinides ions (Am^{3+}, Cm^{3+}) with humic acids: the effect of ionic strength, *Radiochimica Acta*, 72 179-187.

[6] Czerwinski, K. R.; Cerefice, G. S.; Buckau, G.; Kim, J. I.; Milcent, M. C.; Barbot, C.; Pieri, J. (2000). Interaction of europium with humic acid covalently bound to silica beads, *Radiochimica Acta*, 88(7), 417-424.

[7] Gu, B. H.; Yan, H.; Zhou, P.; Watson, D. B.; Park, M.; Istok, J. (2005). Natural humics impact uranium bioreduction and oxidation, *Environmental Science and Technology*, 39(14), 5268-5275.

[8] Guczi, J.; Reiller, P.; Bulman, R. A.; Geckeis, H.; Szabó, G. (2007). Preliminary results for complexation of Pu with humic acid. In *2nd Annual Workshop proceeding of integrated project FUNMIG "Fundamental processes of Radionuclide Migration"*, submitted. SKB.

[9] Guillaumont, R.; Fanghänel, T.; Fuger, J.; Grenthe, I.; Neck, V.; Palmer, D. A.; Rand, M. (2003). *Update on the chemical thermodynamics of uranium, neptunium, plutonium, americium and technetium*. North-Holland.

[10] Kim, J. I.; Delakowitz, B.; Zeh, P. D.; Koltz, D.; Lazik, D. (1994). A column experiment for the study of colloidal radionuclide migration in Gorleben aquifer systems, *Radiochimica Acta*, 66/67 165-171.

[11] Kim, J. I.; Rhee, D. S.; Buckau, G.; Morgenstern, A. (1997). Americium(III)-humate interaction in natural groundwater: Influence of purification on complexation properties, *Radiochimica Acta*, 79(3), 173-181.

[12] Li, W. C.; Victor, D. M.; Chakrabarti, C. L. (1980). Effect of pH and uranium concentration on interaction of uranium(VI) and uranium(IV) with organic ligands in aqueous solutions, *Analytical Chemistry*, 52 520-523.

[13] Murphy, R. J.; Lenhart, J. J.; Honeyman, B. D. (1999). The sorption of thorium (IV) and uranium (VI) to hematite in the presence of natural organic matter, *Colloids and Surfaces A-Physicochemical and Engineering Aspects*, 157 47-62.

[14] Murphy, R. J. (2000). Thorium (IV) binding to organic and inorganic ligands: marine colloidal organic matter, marine polysaccharides and hematite, Colorado School of Mines.

[15] Nash, K. L. (1979). The interaction of thorium with humic and fulvic acids, Florida State University.

[16] Nash, K. L.; Choppin, G. R. (1980). Interaction of humic and fulvic acids with Th(IV), *Journal of Inorganic and Nuclear Chemistry*, 42 1045-1050.

[17] Nash, K. L.; Fried, S.; Friedman, A. M.; Sullivan, J. C. (1981). Redox behavior, complexing, and adsorption of hexavalent actinides by humic acid and selected clays. Stiring marine disposal of high-level radioactive waste, *Environmental Science and Technology*, 15 834-837.

[18] Neck, V.; Kim, J. I. (2001). Solubility and hydrolysis of tetravalent actinides, *Radiochimica Acta*, 89(1), 1-16.

[19] Rai, D.; Rao, L. F.; Moore, D. A. (1998). The influence of isosaccharinic acid on the solubility of Np(IV) hydrous oxide, *Radiochimica Acta*, 83(1), 9-13.

[20] Reiller, P.; Moulin, V.; Casanova, F.; Dautel, C. (2003). On the study of Th(IV)-humic acid interactions by competition sorption studies with silica and determination of global interaction constants, *Radiochimica Acta*, 91(9), 513-524.

[21] Reiller, P. (2005). Prognosticating the humic complexation for redox sensitive actinides through analogy, using the charge neutralisation model., *Radiochimica Acta*, 93(1), 43-55.

[22] Santschi, P. H.; Murray, J. W.; Baskaran, M.; Benitez-Nelson, C. R.; Guo, L. D.; Hung, C. C.; Lamborg, C.; Moran, S. B.; Passow, U.; Roy-Barman, M. (2006). Thorium speciation in seawater, *Marine Chemistry*, 100(3-4), 250-268.

[23] Szabó, G.; Guczi, J.; Reiller, P.; Geckeis, H.; Bulman, R. A. (2006). Investigation of complexation of thorium by humic acid using chemically immobilised humic acid on silica gel, *Radiochimica Acta*, 94(9-11), 553-557.

[24] Szabó, G.; Guczi, J.; Geckeis, H.; Reiller, P.; Bulman, R. A. (2007). Interaction of Th with humic acid over wide pH region. In *2nd Annual Workshop proceeding of integrated project FUNMIG "Fundamental processes of Radionuclide Migration"*, submited. SKB.

[25] Vitorge, P.; Capdevila, H. (2003). Thermodynamic data for modelling actinide speciation in environmental waters, *Radiochimica Acta*, 91 623-361.

[26] Wall, N. A.; Borkowski, M.; Chen, J. F.; Choppin, G. R. (2002). Complexation of americium with humic, fulvic and citric acids at high ionic strength, *Radiochimica Acta*, 90(9-11), 563-568.

[27] Warwick, P.; Evans, N.; Hall, A.; Walker, G.; Steigleder, E. (2005). Stability constants of U(VI) and U(IV)-humic acid complexes, *Journal of Radioanalytical and Nuclear Chemistry*, 266(2), 179-190.

[28] Zuyi, T.; Huanxin, G. (1994). Use of the ion exchange method for the determination of stability constants of thorium with humic and fulvic acids, *Radiochimica Acta*, 65(2), 121-123.

DETERMINATION OF CONDITIONAL STABILITY CONSTANTS FOR METALS IONS WITH HUMIC ACID USING CHEMICALLY IMMOBILISED HUMIC ACID ON SILICA GEL

G. Szabó[1*], J. Guczi[1], T. Miyajima[2], H. Geckeis[3], P. Reiller[4] and R. A. Bulman[5]

[1]National Research Institute for Radiobiology and Radiohygiene, PO Box 101, Budapest, H-1775, Hungary,
[2]Department of Chemistry, Faculty of Science and Engineering, Saga University, 1-Honjo, Saga 840-8502, Japan;
[3]Forschungszentrum Karlsruhe, Institut für Nukleare Entsorgungstechnik, 76021 Karlsruhe, Germany,
[4]Commissariat á l'Énergie Atomique, CE Saclay, Nuclear Energy Division/DPC/SERC, Laboratoire de Spéciation des Radionucléides et des Molécules. F-91191 Gif-sue-Yvette CEDEX, France;
[5]Radiation Protection Division, Health Protection Agency, Chilton, Didcot, United Kingdom, OX11 ORQ.

*Corresponding author; szabogy@hp.osski.hu

Abstract

Limitations on aqueous solution chemistries of humic acid, and also hydrolysis of some cationic species, restrict measurement of conditional stability constants of 4f- and 5f-series elements as humate complexes. Reported log ß values are determined by using non-linear regression binding isotherms, of Am(III) and Th(IV), and also Ag(I) and Sr(II), bound by a humic acid composite.

Introduction

Whereas complexation of toxic metal ions by humic substances is now recognised, the nature of the complexation remains poorly understood. The wide distribution of humic acids in the environment ranges from aqueous solutions and colloids in soil solutions and groundwaters to the surfaces of particles. This account will report more investigations of the interaction of a silica gel - humic acid composite (SiO_2-HA) with metal ions as diverse as Ag(I), Sr(II), Am(III) and Th(IV) by titration, at pH 6, of suspended SiO_2-HA in 0.1 M ionic solutions. These nuclides are selected (i) because their presence in the low and medium level radioactive waste from Hungarian pressurized water reactor at Paks [1], (ii) chemical analogue for tetravalent actinides. The stability constants for the

complexes formed through complexation by humic acid (HA) have been evaluated by using non-linear regression of binding isotherms. The results have been interpreted in terms of complexes of 1:1 stoichiometry.

Objectives

The aim of this work is to prove that the complexing behaviour of surface bound humic acid with radionuclides is similar to that of soluble humic acid. The interaction of surface bound humic acid with ^{110m}Ag(I), ^{85}Sr(II), ^{241}Am(III) and Th(IV) have been investigated.

Experimental

Material and methods

SiO_2-HA was prepared by chemical immobilisation of humic acid on silica gel and characterised as reported by Szabó *et al.* [2]. ^{241}Am was determined by liquid scintillation counting and ^{110m}Ag and ^{85}Sr by gamma-spectrometry. Th(IV) was determined by ICP-MS. The binding of Ag(I) was investigated in 0.1 M $NaNO_3$ at pH 6 by the titration method. The proton exchange capacity of SiO_2-HA was determined by potentiometric titration. The binding of Th(IV), Sr(II) and Am(III), on carrier Eu(III) [1], by SiO_2-HA was examined at pH 6 in 0.1 M $NaClO_4$.

Calculation of maximal binding capacity (B_{max}) and conditional interaction constants (β) of metals ions from binding isotherm

The conditional interaction constant (β) is relative to the following equilibrium:

$$M^{z+} + HA \leftrightarrow MHA \qquad \text{(Eq. 1)}$$

$$\text{with } \beta = \frac{[MHA]}{[M^{z+}]_f \; [HA]_f} \qquad \text{(Eq. 2)}$$

where: M^{z+} is the metal cations; HA is the humic acid; [MHA] is the concentration of the metal humate complex; $[M^{z+}]_f$ is the concentration of the non-complexed metal ion; $[HA]_f$ is the concentration of the free available binding site of humic acid. The assumption is made that HA is the central group and that complexation can be described in terms of a Langmuir-type adsorption equation. The free ligand concentration can be calculated in Eq. 2 by introducing B_{max}. A subsequent combination of Eqs. 2 and 3 provides Eq. 4, which on re-arrangement gives Eq. 5.

$$[HA]_f = [B_{max}] - [MHA] \qquad \text{(Eq. 3)}$$

where: B_{max} is maximal complexing capacity of humic acid.

$$\beta = \frac{[MHA]}{[M^{z+}]_f\ ([B_{max}]- [MHA])} \qquad \text{(Eq. 4)}$$

$$[MHA] = \frac{\beta\ [M^{z+}]_f\ B_{max}}{1 + \beta\ [M^{z+}]_f} \qquad \text{(Eq. 5)}$$

After plotting the bound metal [MHA] versus $[M^{z+}]_f$ and using the binding isotherms, the maximal binding capacity and the conditional interaction constants (β) of metal ion humate complexes were determinable.

Th^{4+} is readily hydrolysed and it is not expected that only Th^{4+} ions exist in solution at pH 6. From the $Th(IV)_{total}$ the $[Th^{4+}]$ can be calculated by using the stability constants of the hydroxo complexes $Th(OH)^{3+}$, $Th(OH)_2{}^{2+}$, $Th(OH)_3{}^{+}$ and $Th(OH)_4$ (3,4):

$$[Th(IV)]_{total}=[Th^{4+}] + [Th(OH)^{3+}] + [Th(OH)_2{}^{2+}] + [Th(OH)_3{}^{+}] + [Th(OH)_4] \qquad \text{(Eq. 8)}$$

$$[Th(IV)]_{total} = [Th^{4+}]\ \alpha_{Th} \qquad \text{(Eq. 9)}$$

where α is the Ringböm coefficient [5] concerning inorganic complexation:

$$\alpha = 1 + \sum_i \frac{{}^{*}\beta_i}{[H^+]^i}$$

If we assume that the hydrolysed species is not involved in the interaction with humic acid and measure the total Th(IV) concentration in the liquid phase, it becomes possible to calculate the conditional interaction constants ($\log \beta$) of ThHA using the following equation:

$$\log \beta_{total} + \log \alpha_{Th} = \log \beta_{ThHA} \qquad \text{(Eq. 10)}$$

Results and discussion

The characteristics of SiO_2-HA are reported in Table 1. The conditional stability constants ($\log \beta$), at pH 6, of humate complexes of Ag(I) , Sr(II) , Am(III) and Th(IV) are reported in Table 2.

Table 1. *Characteristics of SiO2-HA*

Substrate content (mg g^{-1})	19.9 ± 1.2
Proton exchange capacity (μeq g^{-1} solid matter)	67.3
Surface area (BET)[a] (m^2 g^{-1})	74 ± 8

[a]BET (Brunauer-Emmett-Teller) surface area of parent silica gel is 100 m^2 g^{-1}.

Typical binding isotherms, solid phase concentration versus liquid phase concentration in equilibrium, of Ag(I) and Sr(II) [see Figure 1.] and Am(III) and Th(IV) [see Figure 2.] on SiO_2-HA at pH 6 values in 0.1 M $NaClO_4$ are presented. By using the non-linear regression on the binding isotherms (Eq. 5), the conditional interaction constants (β) and maximal binding capacity (B_{max}) of metals with humic acid can be calculated (see Table 2). The interaction constant (log ß) increases with increasing oxidation state with the exception of Ag^+, a state which is likely to arise from the additional complexation by N- and S- containing moieties in HA [6].

Table 2. *Log β of humate complexes of Ag(I) , Sr(II) , Am(III) and Th(IV).*

	Ag^+	Sr^{2+}	Am^{3+}	Th^{4+}
B_{max} (μmol g^{-1})	13.1 ± 3.5	42.8 ± 13.1	16.7 ± 2.3	1.6 ± 0.4
Log β (l mol^{-1})	4.43 ± 0.11	3.37 ± 0.08	6.44 ± 0.36	12.81 ± 0.27

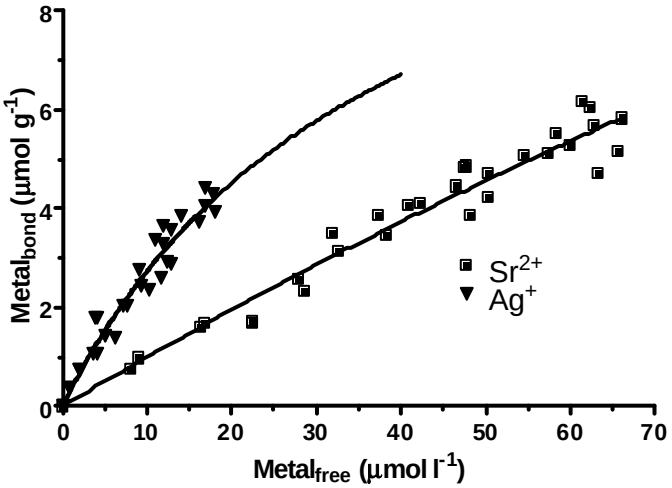

Figure 1*. Binding isotherm of SiO2-HA for Ag(I) and Sr(II) at pH 6.*

Modelling

The present work contributes to providing the scientific basis required for trustworthy application of geochemical modeling to radionuclide migration under the influence of humic substances.

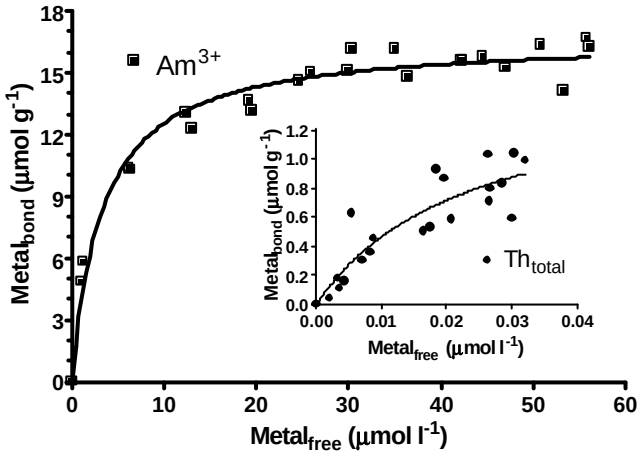

Figure 2. *Binding isotherm of SiO2-HA for Am(III) and Th(IV) at pH 6.*

Table 3. *Summary of reported Conditional Interaction Constants, Log β, for humic acid complexes of Ag(I), Sr(II), Am(III) and Th(IV).*

Species	pH	μ	Method	Log β	Literature
Ag(I)	6.5	0.1	ISE	3.95-4.51	6
Ag(I)	6.0	0.1	sorption	4.43±0.11	this work
Sr(II)	5.0	0.1	UF	3.51±0.27	7
Sr(II)	5.0	0.1	IEX	3.54±0.2	8
Sr(II)	6.0	0.1	sorption	3.37 ± 0.08	this work
Am(III)	6.0	0.1	UV-spect.	6.27±0.04	9
Am(III)	6.0	0.1	UF	6.53±0.30	9
Am(III)	6.0	0.1	sorption	6.44 ± 0.36	this work
Th(IV)	3.99	0.1	SE	11.1	10
Th(IV)	6.0	0.1	IEX	10.14±0.03	11
Th(IV)	6.75	0.1	IEX	16.2±1.0	12
Th(IV)	6.0	0.1	sorption	12.81 ± 0.27	this work

ISE: ion selective electrode, **UF:** ultrafiltration, **SE:** solvent extraction,
IEX: ion exchange, **UV-spect:** UV-spectroscopy

Conclusions

Evaluation of the sorption isotherms of metal ions by SiO_2-HA at pH 6 readily affords the conditional stability constants of the humic acid - metal ion complexes. SiO_2-HA is likely to be of value for modelling the role of humates in interacting with various metal ions species in soil solutions and groundwaters. Experiments show the silica carrier does not significantly contribute to binding [13, 14]. Therefore, HA is responsible for the metal ion binding sites and the pH dependence of binding processes. A comparison has been made (Table 3) of stability constants of Ag(I), Sr(II), Am(III) and Th(IV) with humic acid reported by others and determined here for this novel humic substance. There is a relatively

good agreement with all the literature data. It appears that the present method is a useful technique to determine stability constants for different elements. Also evident is the similarity of complexing characteristics of surface bound humic acid and soluble humic acid.

Acknowledgements

This work was partly supported by European Commission, EC Contract No. FP6-516514 (FUNMIG).

References

[1] Kanyár, B.: Az atomeromu hatósági környezeti sugárvédelmi ellenorzo redszerének 1988-as eredményeirol. Izotóptechnika Diagnosztika, 32/4, 198-210 (1989)

[2] Szabó, Gy., Guczi J., Koblinger-Bokori E., Bulman R. A.: An examination of the sorption characteristics of ^{241}Am(III) and Eu(III) bound by humic substances chemically immobilized on silica gel. Radiochim. Acta, 82, 355 (1998).

[3] Neck, V., Kim, J. I.: Solubility and hydrolysis of tetravalent actinides. Radiochim. Acta, 89, 1 (2001).

[4] Reiller, P.: Prognosticating the humic complexation for redox sensitive actinides through analogy, using the charge neutralisation model. Radiochim. Acta, 93, 43 (2005).

[5] Ringböm A., Complexation in Analytical Chemistry, Interscience, New York, 1963.

[6] Sikora, F.J., Stevenson, F J.: Silver complexation by humic substances: Conditional stability constants and nature of reactive sites. Geoderma, 42, 353 (1988).

[7] Rajec, P., Zemberyová, M., Sasköiová, G., Viacky, V.: Strontium and calcium complexation by humic acid. J. Radioanal. Nucl. Chem. 246(3), 623 (2000).

[8] Samadfam, M., Niitsu, Y., Sato, S., Ohashi, H.: Complexation thermodynamics of Sr(II) and humic acid. Radiochim. Acta, 73, 211 (1996).

[9] Kim, J. L., Buckau, G., Bryant, E., Klenze, R.: Complexation of americium(III) with humic acid. Radiochim. Acta, 48, 135 (1989).

[10] Nash, K. L., Choppin, G.R.: Interaction of humic acid and fulvic acid with Th(IV). J. Inorg. Nucl. Chem., 42, 1045 (1980).

[11] Zuyi, T., Huanxin, G.: Use of ion exchange method for the determination of stability constants of thorium with humic and fulvic acids. Radiochim. Acta, 65, 121 (1994).

[12] Reiller, P., Moulin, V., Casanova, F., Dautel, C.: On the study of Th(IV)-humic acid interactions by competition sorption studies with silica and determination of global interaction constants. Radiochim. Acta, **91**, 513 (2003).

[13] Guczi, J. Angelova, A., Bulman, R.A., Szabó, Gy.: Investigation of the interactions of $^{110m}Ag^{+}$ and $^{125}I^{-}$ with humic acid chemically immobilized on silica gel. Reactive Polymers, **17**, 61-68 (1992).

[14] Bulman, R.A., Szabó, Gy., Clayton, R.F., Clayton, C.R.: Investigation of the uptake of transuranic radionuclides by humic and fulvic acids chemically immobilized on silica gel and their competitive release by complexing agents. Waste Management, 17/4, 191-199 (1997).

KINETIC STUDIES OF THE QUARTZ/SAND, EU^{3+} AND HUMIC ACID TERNARY SYSTEM

L.G. Abrahamsen[1], D.H. Farrelly[1], A. Pitois[1], P Ivanov[1], P. Warwick[2], N.D.M. Evans[2]
L. Knight[3] and N.D. Bryan[1,*]

[1] Centre for Radiochemistry Research, School of Chemistry, The University of Manchester, Oxford Road, Manchester, M13 9PL, U.K.
[2] Department of Chemistry, University of Loughborough, Loughborough, U.K.
[3] U.K. Nirex, Harwell, Oxfordshire, U.K.

* Corresponding author: Nick.Bryan@manchester.ac.uk

Abstract

The interactions of Eu^{3+} ions, humic acid and quartz in ternary system experiments have been studied. The variations in the amount of humic acid and Eu^{3+} with time have been determined as a function of humic acid concentration. The desorption of both humic acid and europium have also been measured. A simple mathematical model has been developed that is able to predict the behaviour of both metal ion and humic acid. There is multi-component behaviour in the experiments, and the modelling suggests that for the sorption step at least, heterogeneity of the surface binding sites dominates. However, there is hysteresis in the desoprtion behaviour of the humic, which could be due to chemical and/or size fractionation on the quartz surface.

Introduction

Humic substances and mineral surfaces bind most cationic radionuclides very strongly. Therefore, under certain conditions, humic substances can increase the solution phase concentration of radionuclides by direct competition with mineral surfaces. Such behaviour could increase mobility. However, at other times, the formation of surface ternary complexes (metal bound to humic bound to surface) can increase the sorbed radionuclide fraction, decreasing mobility.

Objectives

The aim is to develop and test a mathematical model that can predict the reaction kinetics of the ternary system, which could be used in the calculation of radionuclide migration, for example in the post-closure radiological performance assessment (RPA) of radioactive waste repositories.

Experimental

The batch experiments (polysulphone tubes) contained quartz sand and humic acid solutions (0 – 500 ppm; pH = 6.0 ±0.1, adjusted with HCl/NaOH; I = 0.1, $NaClO_4$). The solid:solution ratio was 1 g: 2 ml. In addition, some experiments contained Eu: ^{152}Eu radiotracer (0.13 kBq ml^{-1}) and stable Eu to give total metal concentrations in the range $7.91x10^{-10}$ – $1x10^{-5}$ mol dm^{-3}. For some experiments, humic and Eu^{3+} were equilibrated prior to contact with the solid, whilst in others the metal and solid were equilibrated prior to the addition of the humic. At regular intervals, the tubes were allowed to settle for five minutes before aliquots were removed and filtered using Millex Millipore syringe driven filter units (PVDF, 0.1µm pore size, 33mm diameter). Humic substance concentrations were determined spectrophotometrically and Eu concentrations with a semi-conductor HPGe gamma-ray spectrometer. In some experiments, after a period of time, the solution and solid phases were separated, and either the solid or solution phase exchanged for a 'clean' sample. This technique allowed desorption behaviour to be studied.

Results

A selection of the experimental results from these systems are presented in the figures (1 – 4): not all data can be reported here due to the constraints of space. Some of the results (Figures 1,4) are presented as C/C_o versus contact time, where C is the concentration of humic acid or Eu in solution at any given time, and C_o is the total concentration in the system. Figure 1 shows that the initial rapid stage of adsorption of humic onto quartz sand occurs within minutes of contact. The fraction of Eu removed from solution (as either direct binary or ternary complex) decreases with increasing [HA]. For the 20, 50 and 100 ppm systems, a rapid initial fall in [Eu] over the first 24 hours is followed by a slower decrease. In the absence of humic, the system achieves equilibrium within minutes. The kinetic behaviour of the Eu^{3+} matches that of the humic, and is due to the formation of ternary complexes (Abrahamsen et al 2005), i.e., the slow sorption of Eu^{3+}/humic complexes. There are at least two first order processes involved in the adsorption of humic to sand: fast (several hours) and slow (days/weeks).

Modelling

Certain binary components of the system have been studied before, and there are existing, tested mathematical models, in particular the separate binary interactions of metal ion with the humic and mineral surface have already been addressed. However, the interactions of humic and metal-humic complexes with mineral surfaces are less well understood, and so two different approaches have been tested. Therefore, certain of the model processes and equations are common to all of the calculations, whilst others are specific to the two approaches, called Models 1 and 2. The humic sorption data in Figure 1 show two clear classes of behaviour (fast and slow), and there is clearly more than one chemical reaction. Therefore, both model approaches have used two equations. The heterogeneity

could be the result of heterogeneous humic binding sites on the surface, or due to the heterogeneity of the humic material in solution, or of course, both. Van de Weerd et al (1999)[2] have modelled humic uptake to iron oxide phases with a model that contains a single surface site and multiple (3 – 6) humic fractions. However, the surface is different here, and so the two distinct approaches have been tested: Model 1 assumes a single humic species in solution and two surface sites, and Model 2 has one surface site and two humic fractions in solution.

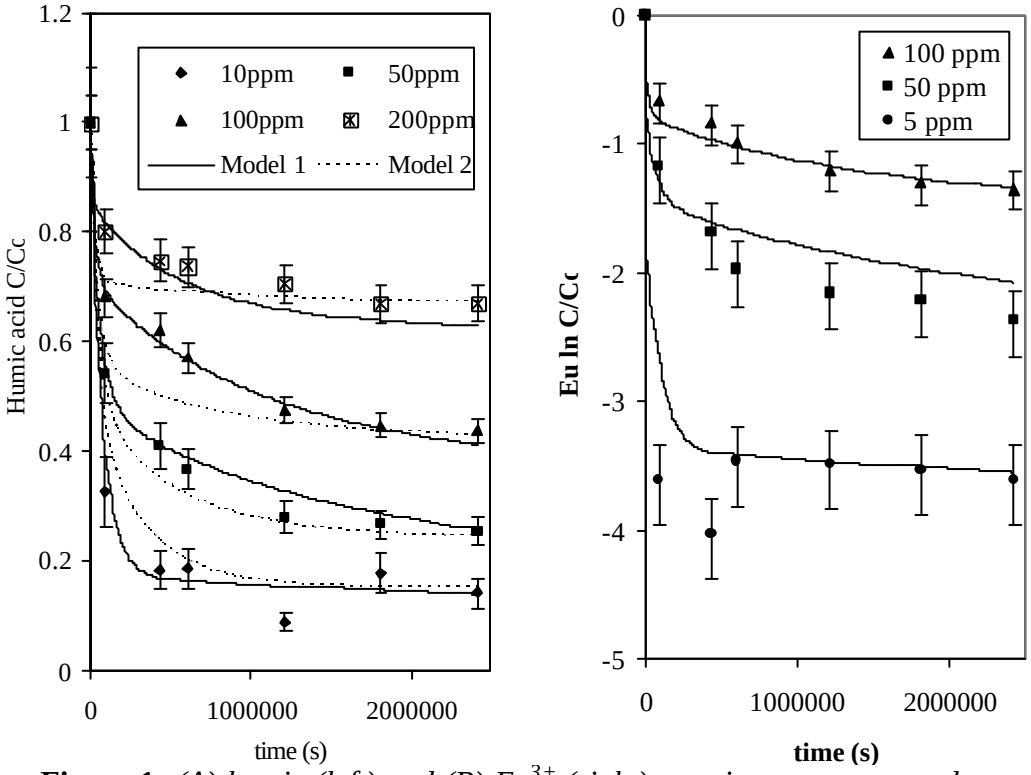

Figure 1: *(A) humic (left) and (B) Eu^{3+} (right) sorption to quartz sand, experiment and model fits: left, Models 1 and 2; right, Model 1 only.*

Processes and equations included in all calculations:

The interaction of Eu^{3+} with the humic is described using two components, with initial uptake to an exchangeable fraction, Eu_{exch}, which is assumed to be instantaneous,

$$Eu^{3+}_{(aq)} + HA_{exch} \leftrightarrow Eu_{exch} \qquad K_{exch} = \frac{[Eu_{exch}]}{[Eu^{3+}_{(aq)}].[HA_{exch}]} \quad (1),$$

where HA_{exch} is the humic exchangeable binding site, and K_{exch} $(1(\pm 0.5)x10^3$ dm^3 $mol^{-1})$ an equilibrium constant for the process. Subsequent transfer to and from the non-exchangeable fraction, $Eu_{non\text{-}exch}$, is a first-order kinetic (slow) process.

$$Eu_{exch} \underset{\leftarrow}{\rightarrow} Eu_{non-exch} \qquad \frac{d[Eu_{non-exch}]}{dt} = k_f[Eu_{exch}] - k_b[Eu_{non-exch}] \quad (2)$$

where k_f $(1.1x10^{-8}$ $s^{-1})$ and k_b $(1x10^{-7}$ $s^{-1})$ are the forward and backward rate constants, respectively. The results were found to be insensitive to these values, and they have been taken from previous work [1]

The interaction of Eu^{3+} with the quartz surface is described with a single reaction,

$$Eu^{3+}_{(aq)} + S_M \underset{\leftarrow}{\rightarrow} Eu_S \qquad \frac{d[Eu_S]}{dt} = k_{MSf}[Eu^{3+}_{(aq)}].[S_M] - k_{MSb}[Eu_S] \quad (3)$$

where S_M is a metal binding site on the quartz sand surface, Eu_S is Eu sorbed to the surface and k_{MSf} ($1(+1/-0.3)x10^{-3}$) and k_{MSb} ($1(+1/-0.5)x10^{-6}$) are the forward and backward rate constants, respectively.

Processes and equations used in Model 1 only:

$$HA_{free} + S_{HA1} \underset{\leftarrow}{\rightarrow} HA_{S1} \qquad \frac{d[HA_{S1}]}{dt} = k_{HAS1f}[HA_{free}].[S_{HA1}] - k_{HAS1b}[HA_{S1}] \quad (4)$$

$$HA_{free} + S_{HA2} \underset{\leftarrow}{\rightarrow} HA_{S2} \qquad \frac{d[HA_{S2}]}{dt} = k_{HAS2f}[HA_{free}].[S_{HA2}] - k_{HAS2b}[HA_{S2}] \quad (5)$$

where: S_{HA1} and S_{HA2} are surface binding sites, type 1 and 2, respectively ($[S_{HA1}]$=28(+10/-5) ppm; $[S_{HA2}]$ =89(±15) ppm); HA_{S1} and HA_{S2} are humic bound to surface sites, type 1 and 2, respectively; and k_{HAS1f} ($3(\pm2)x10^{-6}$ $ppm^{-1}s^{-1}$), k_{HAS1b} ($3(\pm2)x10^{-5}$ s^{-1}), k_{HAS2f} ($1(+2/-0.5)x10^{-8}$ $ppm^{-1}s^{-1}$) and k_{HAS2b} ($5(\pm4)x10^{-7}$ s^{-1}) are rate constants.

Processes and equations used in Model 2 only:

$$HA1_{free} + S_{HA} \underset{\leftarrow}{\rightarrow} HA1_S \qquad \frac{d[HA1_S]}{dt} = k_{HA1Sf}[HA1_{free}].[S_{HA}] - k_{HA1Sb}[HA1_S] \quad (6)$$

where $HA1_{free}$ and $HA1_S$ are humic species (fraction 1; 65(±5)%) that are in the solution phase and sorbed, respectively; S_{HA} is the surface binding site ($[S_{HA}]$=70(±5) ppm); and k_{HA1Sf} ($3(\pm2)x10^{-7}$ $ppm^{-1}s^{-1}$) and k_{HAS1b} ($5(\pm3)x10^{-6}$ s^{-1}) are the forward and backward rate constants. The equations for fraction 2 are (k_{HA2Sf} =$5(+5/-2)x10^{-8}$ $ppm^{-1}s^{-1}$; k_{HAS2b}=$1(+8/-0.8)x10^{-8}$ s^{-1}),

$$HA2_{free} + S_{HA} \underset{\leftarrow}{\rightarrow} HA2_S \qquad \frac{d[HA2_S]}{dt} = k_{HA2Sf}[HA2_{free}].[S_{HA}] - k_{HA2Sb}[HA2_S] \quad (7)$$

Discussion

Figure 1A shows the fit obtained to the humic sorption using the two models. Although both models are able to simulate the general behaviour, Model 1 is better on balance. However, the fit from Model 2 is sufficiently close that it cannot be eliminated with these data alone. Hence, a number of other experiments were used to test the models further: Figure 2 shows an example. In this experiment, the solution was separated from the solid after 20 days, and a new sample of sand introduced. The fit for Model 1 is clearly superior. In all of these more advanced tests, although Model 2 could be made to fit the data for a single system, by a suitable choice of parameters: it could not fit the data for more than one experiment simultaneously with a single parameter set, whereas Model 1 is able to fit all behaviour for a single sand sample with one set of parameters, even though it has the same number of adjustable parameters as Model 2. Therefore, Model 1 is the best

description of kinetic behaviour for these systems. Even though different samples of sand required slightly different parameters for the best fit, the variation is small, considering that the samples have different origins. Calculations have also been performed to simulate the behaviour of Eu^{3+}. All of these calculations assume that humic/metal complexes will sorb to the mineral surface in the same way as unbound humic, i.e., equations (4) and (5) with the same parameters are used to describe ternary complex formation.

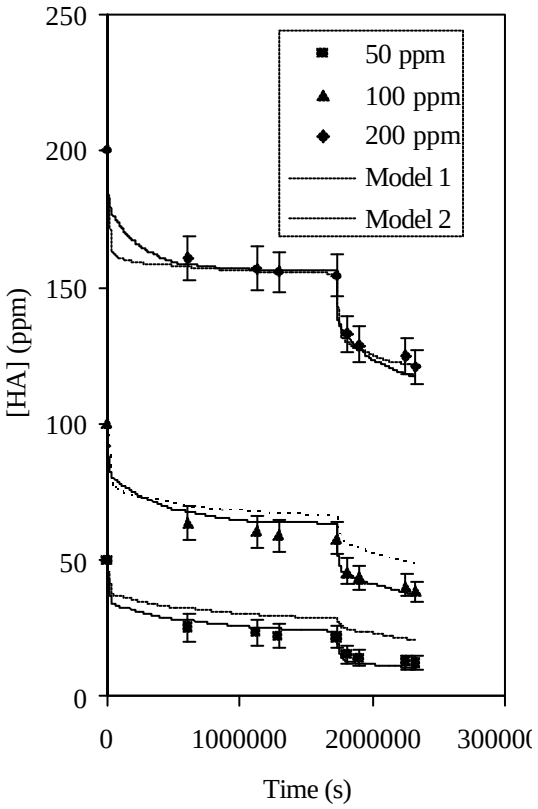

Figure 2: *uptake of humic acid onto sequential sand samples (with model fits).*

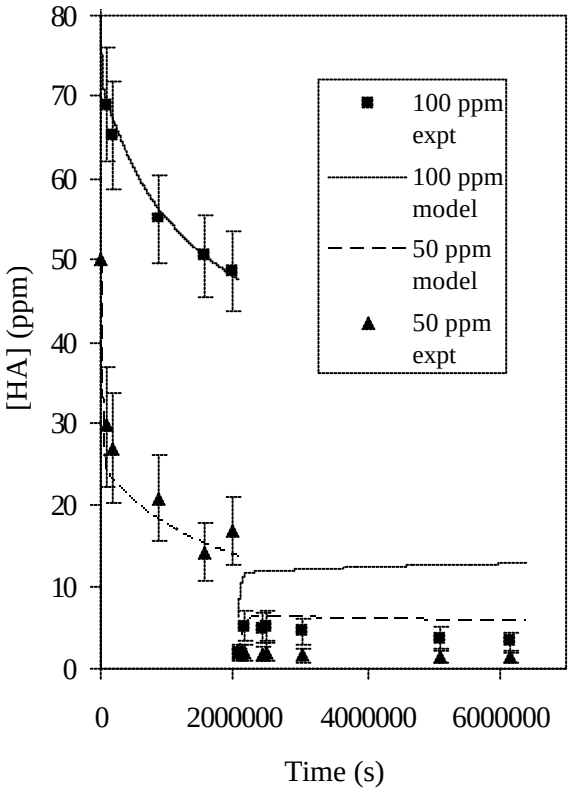

Figure 3: *sorption and desorption behaviour of humic acid on quartz sand (with model fit; Model 1 only).*

Figure 1B shows the fit to the uptake of Eu^{3+} in the ternary experiments as a function of humic concentration: the fit is reasonable, particularly given the complexity of the system. Figure 4A shows the variation in [Eu] with time, as a function of total [HA], for systems where Eu was pre-equilibrated with the solid phase for 24 hours prior to the addition of humic. Eu desorption increases with [HA]. After the addition of humic, [Eu] increases over several days up to a maximum. Following this, there is a subsequent decrease. This behaviour can be attributed to two simultaneous reactions. The humic in solution and the surface compete for Eu, and so there is an initial increase in [Eu]. However, the sorption of humic begins to return Eu to the surface, via ternary complexes, but this process is in part slow. In a separate experiment, this procedure was repeated, but using a 'pure quartz' sample, rather than sand: the results are shown in Figure 4B. The same mathematical equations and rate constants were able to simulate the behaviour in

this experiment. The only change that was required was in the surface site specific concentrations ([S1]=70(±5); [S2]=117(±30)), which is not surprising, given that the two solids are from different samples. For all of the Eu data, it is not possible to simulate the results without including ternary complexes. For the data in Figures 1 – 4 the fits (with Model 1) are quite good, especially given that the model is very simple. However, the fit is not perfect: for example, although it captures the general behaviour in Figure 4A, the model fit is not exact, especially for the 10 ppm system.

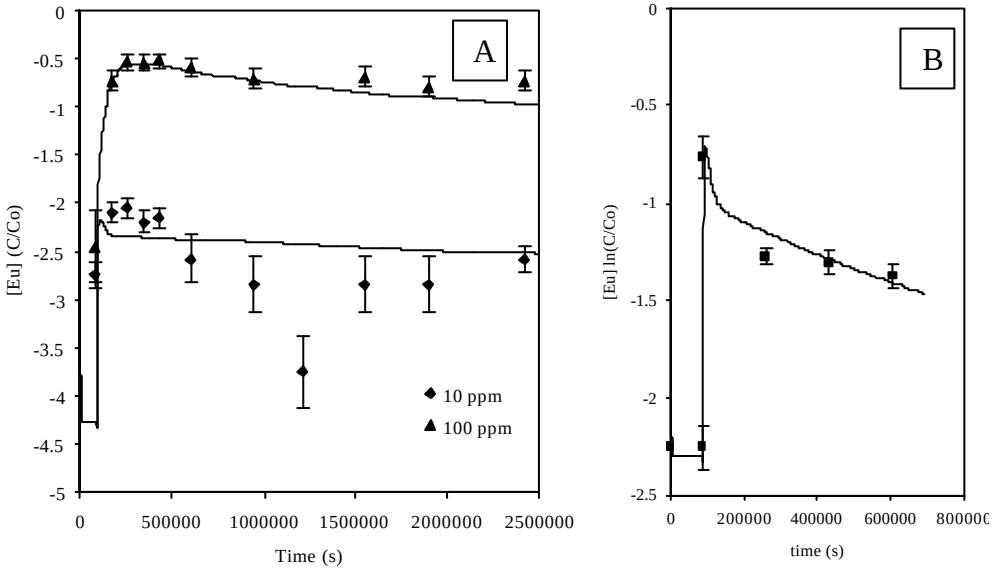

Figure 4*: desorption of sorbed Eu3+ from A – quartz sand, B pure quartz;*

Quartz is often considered to be a simple surface, and indeed we have found that these experiments have been largely predictable. However, even for this surface some complex behaviour has been observed. For example, Figure 3 shows the results of an experiment where humic acid was allowed to sorb to a sample of quartz sand, and after 24 days, the solution containing the humic was replaced with clean, humic free electrolyte (pH = 6, I = 0.1), and the desorption of the humic measured. The figure also shows the fits obtained with the model (Model 1). Although the fit to the sorption step is good, the fit is less good for the desorption: the model has overestimated the amount of humic re-entering the solution, which is evidence of hysteresis. The modelling has suggested that the majority of the heterogeneity during the uptake phase is due to surface binding site variability. However, these desorption results suggest that intrinsic heterogeneity in the humic itself may also be important.

Conclusions

A model has been developed to predict the kinetic behaviour of Eu^{3+} and humic in quartz ternary systems. It performs reasonably well, although there are certain aspects that need improvement, in particular, the desorption behaviour of the humic.

References

[1] Bryan, N.D.; Barlow, J.; Warwick, P.; Stephens, S.; Higgo, J.J.W.; Griffin, D. (2005) *J. Envion. Monit.* **7**, 196 – 202.

[2] Van de Weerd, H.; Van Riemsdijk, W.H.; Leijnse, A. (1999) *Environmental Science and Technology*, **33**, 1675-1681.

A PROCEDURE TO ASSESS THE IMPORTANCE OF CHEMICAL KINETICS IN THE HUMIC MEDIATED TRANSPORT OF RADIONUCLIDES IN RADIOLOGICAL PERFORMANCE ASSESSMENT CALCULATIONS

P. Ivanov[1], L.G. Abrahamsen[1], D.H. Farrelly[1], A. Pitois[1], P. Warwick[2], N.D.M. Evans[2] L. Knight[3] and N.D. Bryan[1,*]

[1] Centre for Radiochemistry Research, School of Chemistry, The University of Manchester, Oxford Road, Manchester, M13 9PL, U.K.
[2] Department of Chemistry, University of Loughborough, Loughborough, U.K.
[3] U.K. Nirex, Harwell, Oxfordshire, U.K.

* Corresponding author: Nick.Bryan@manchester.ac.uk

Abstract

Previous work has shown that humic substances can bind metal ions in two modes: the exchangeable, where it is available instantaneously for reaction with other sinks (such as mineral surfaces); and the non-exchangeable, from which it may only dissociate slowly. In the absence of metal ion/humic/mineral surface ternary complexes, if the dissociation rate is slow compared to the residence time of the humic in the groundwater column, then metal in the non-exchangeable will have a significantly higher mobility than that in the exchangeable. The critical factor is the ratio of the non-exchangeable first order dissociation rate constant and the residence time in the groundwater column, metal ion mobility increasing with decreasing rate constant.

Sorption of humic/metal complexes at mineral surfaces may reduce mobility. In addition to direct retardation, sorption also increases the residence time of the non-exchangeable fraction, giving more time for dissociation and immobilisation. The magnitude of the effect depends upon the concentrations of the mineral surface humic binding sites and the humic in solution, along with the magnitudes of the equilibrium constant and the forward and backward rate constants.

The non-exchangeable dissociation reaction and the sorption reaction may be classified in terms of two Damkohler numbers, which can be used to determine the importance of chemical kinetics during transport calculations. These numbers could be used to determine when full chemical kinetic calculations are required for a reliable prediction, and when equilibrium may be assumed, or when the reactions are sufficiently slow that they may be ignored completely.

Introduction

Over the last decade, chemical models of metal ion interactions with humic substances and of humic substances with mineral surfaces have been developed. Recently [2], a model has been reported that can describe the behaviour of metal ions, humic substances and humic-metal ion complexes in the presence of mineral surfaces. There are two components to this ternary system: (i) the interaction of metal ions with humic substances, and (ii) the interaction of humic substances and humic-metal ion complexes with mineral surfaces.

(i) Metal ion – humic interactions

Previous studies have shown that humic substances bind metal ions in two different modes. Initial uptake is to an 'exchangeable' fraction, where the metal ion is bound strongly, but may be removed instantaneously if a stronger competing sink is encountered. Over time, metal transfers to the 'non-exchangeable' fraction, where it is not more strongly bound, but it may not dissociate instantaneously, rather its release is kinetically controlled. While it is effectively 'trapped' within the non-exchangeable fraction, the metal ion takes on the characteristics of its host humic. The initial uptake to the humic exchangeable site is described as an equilibrium process,

$$M^{n+}_{(aq)} + HA_{exch} \leftrightarrow HA - M_{exch} \qquad K_{exch} = \frac{[HA - M_{exch}]}{[M^{n+}_{(aq)}][HA_{exch}]} \quad (1)$$

whilst the transfer between the exchangeable and non-exchangeable fractions is described with a rate equation,

$$HA - M_{exch} \underset{\leftarrow}{\overset{\rightarrow}{}} HA - M_{non-exch}$$

$$\frac{d[HA - M_{non-exch}]}{dt} = k_f[HA - M_{exch}] - k_b[HA - M_{non-exch}] \quad (2)$$

where HA_{exch} is the humic exchangeable binding site, HA-M_{exch} and HA-$M_{non\text{-}exch}$ are metal ions bound to the humic in the exchangeable and non-exchangeable modes, respectively, K_{exch} is an equilibrium constant, and k_f and k_b are first order rate constants. There will be a range of rate constants that vary between instantaneous and very slow.

(ii) Humic – mineral surface interactions

Again, kinetic effects are important. For some surfaces, the heterogeneity is surface based, with more than one mineral surface binding site, whilst for others it is the chemical heterogeneity of the humic molecules that dominates [2]. Therefore, if we are to have a generalised equation to describe the interaction of humic substances with mineral surfaces, then we need to account for the possibility of multiple mineral surface binding sites and humic fractions. Although different surfaces have different numbers of humic fractions and binding sites, the same chemical equation may be used to describe the interaction of a particular humic

fraction/molecule, HA_i, with a given surface binding site, $S_{HA,j}$, to give a sorbed humic molecule, $HA_{S,i,j}$.

$$HA_{free,i} + S_{HA,j} \underset{\leftarrow}{\overset{\rightarrow}{}} HA_{S,i,j} \qquad \frac{d[HA_{S,i,j}]}{dt} = \left\{k_{HASf,i.j}[HA_{free,i}].[S_{HA,j}]\right\} - \left\{k_{HASb,i,j}[HA_{S,i,j}]\right\} \quad (3)$$

where $k_{HASf,i,j}$ and $k_{HASb,i,j}$ are the sorption and desorption rate constants, and $HA_{free,i}$, represents molecules of fraction i in the solution phase, and $HA_{S,i,j}$ molecules of fraction i bound to a binding site of type j. Any metal ion bound to a humic molecule that sorbs to a mineral surface will itself be immobilised as a ternary complex. If $(HA\text{-}M_{exch})_{free,i}$ and $(HA\text{-}M_{non\text{-}exch})_{free,i}$ are metal ions bound to a humic molecule in the solution phase of fraction i, exchangeably and non-exchangeably, respectively, and $(HA\text{-}M_{exch})_{S,i,j}$ and $(HA\text{-}M_{non\text{-}exch})_{S,i,j}$ are those complexes immobilised on the mineral surface at surface binding site type j, then the same types of equation may be used to describe sorption:

$$\frac{d[(HA-M_{exch})_{S,i,j}]}{dt} = \left\{k_{HASf,i.j}[(HA-M_{exch})_{free,i}].[S_{HA,j}]\right\} - \left\{k_{HASb,i,j}[(HA-M_{exch})_{S,i,j}]\right\}$$

$$\frac{d[(HA-M_{non-exch})_{S,i,j}]}{dt} = \left\{k_{HASf,i.j}[(HA-M_{non-exch})_{free,i}].[S_{HA,j}]\right\} - \left\{k_{HASb,i,j}[(HA-M_{non-exch})_{S,i,j}]\right\}$$

Objectives

Humic interactions could affect the transport behaviour of radionuclides, and there are implications for the post-closure radiological performance assessment (RPA) of nuclear waste repositories. However, calculations that include kinetics are computationally expensive. Therefore, it is important to identify exactly when it is necessary to include them explicitly in transport calculations. The aim of this work is to develop rules that predict when, and in what manner, humic chemical kinetics should be considered in field scale transport calculations in support of R.P.A. This report is a short description of this work. Full details are being published elsewhere [1].

Modelling

Modelling 1: No Humic Sorption

At first, we will examine the effect of the non-exchangeable kinetic reaction (2). In the case where there is no sorption of humic-metal complex, i.e., $k_{HAS,f,i,j} \rightarrow 0$. In this case, the only processes that retards the migration of radionuclides is removal to the mineral surface. The dissociation of metal ion from the non-exchangeable mode and its immobilisation on a mineral surface may be rationalised using a Damkohler number, which is given by,

$$D_M = \frac{L}{V} k_b$$

where, L is the length of the column, k_b is the dissociation rate constant (eqn 2), and V is the linear flow rate. Systems with the same D_M always give the same the

final distribution, regardless of L, provided that the relative dispersivity is constant [1]. Only the desorption rate constant need be considered, because during transport the rate of transfer into the non-exchangeable is negligible [1]. It is possible to reduce any series of kinetic reactions, regardless of origin or chemistry, to just three classes:

1. Those reactions that are sufficiently fast to be treated as equilibria (high k);
2. Those that are sufficiently slow that they effectively do not take place (low k);
3. Those that are only accurately described with rate equations (intermediate k).

Therefore, we have the possibility of using the limiting behaviours if k is sufficiently large or small. We may use D_M to judge when it is necessary to consider chemical kinetics explicitly. As D_M decreases, the non-exchangeably bound metal tends towards the behaviour of the host humic, and for low D_M, the probability that a non-exchangeably bound metal ion will dissociate from its host humic molecule before that molecule traverses the column is virtually zero. Therefore, the reaction that connects the exchangeable and non-exchangeable modes (eqn 2) may be removed from the calculation, and the two fractions are treated as independent species: the great advantage of this 'decoupled' approach is that it is inherently conservative. At high D_M, the kinetic equation (2) could be replaced with an equilibrium. However, this approximation is not conservative, the size of the error decreasing as D_M increases. The consequences for a real R.P.A. exercise would depend upon the circumstances. At intermediate D_M, the kinetic equation must be used, although this will be computationally expensive. Ideally, we would like a set of rules to determine when to use the approximations, and when a chemical rate equation must be used, but, that depends upon the acceptable error, which is a function of D_M and distance from the source term [1]. The equilibrium approximation is particularly problematic, since it is not conservative. Fortunately, systems with the same D_M behave in the same way, and the likely error at any distance may be determined as a function of D_M. Therefore, in each case study, acceptable upper and lower limits for D_M, MAX2 and MIN2, respectively (Figure 1) could be calculated to act as thresholds. If D_M is less than MIN2, then the decoupled approximation may be used, and the non-exchangeable assumes the properties of of a conservative tracer, if there is no humic sorption. If D_M is greater than MAX2, then provided that we do not require a conservative approximation, we may replace the chemical rate equation (eqn 2) with an equilibrium constant. If D_M is between the values, then neither approximation will be valid, and the full rate equation (eqn 2) must be used.

Modelling: 2 With Humic Sorption

In the environment, mineral surfaces will be in equilibrium with the ambient concentration of humic substance. We may use equations of type (3) for each fraction and site to calculate the vacant site concentrations ($[S_{HA,j}]$), and then

combine $k_{HASf,i,j}$ and $[S_{HA,j}]$ to give a pseudo first order forward rate constant, $k'_{HASf,i,j}$, and hence define a Damkohler number for the humic sorption reaction, D_{HUM},

$$k'_{HASf,i,j} = k_{HASf,i,j}\,[S_{HA,j}],$$

$$D_{HUM} = \frac{k'_{HASf,i,j}}{V} L$$

As D_{HUM} approaches zero, the behaviour of a metal/humic complex tends towards a conservative tracer, whilst as D_{HUM} tends to 8, the extent of sorption will tend towards equilibrium behaviour, in which case the concentration of sorbed humic/metal complex, e.g. $(HA\text{-}M_{non\text{-}exch})_{S,i,j}$, at any point and time is given by,

$$[(HA\text{-}M_{non\text{-}exch})_{S,i,j}] = K'_{HAS,i,j}\,[(HA\text{-}M_{non\text{-}exch})_{free,i,j}]; \quad \{K'_{HAS,i,j} = k'_{HASf,i,j}/k_{HASb,i,j}\}$$

A kinetic calculation may be avoided by assuming that the humic/metal complex either: does not sorb at all, and so transports with the velocity of the groundwater (low D_{HUM}), which will be conservative; or that the interaction may be described with an equilibrium constant, $K'_{HAS,i,j}$ (high D_{HUM}), which will not be conservative. At intermediate D_{HUM}, only a full kinetic description will provide a reliable prediction. In the same manner as for D_M, thresholds may be defined to determine when the approximations could be used (MAX1 and MIN1; Figure 1).

In the case where sorption of humic-metal complexes to the mineral surface is significant, there are two processes that may lead to the immobilisation of non-exchangeably bound metal ion: dissociation from the non-exchangeable mode, followed by direct reaction with the mineral surface; alternatively, sorption of the host humic (formation of a ternary complex) will also lead to retardation. Sorption of humic/metal complex will cause direct retardation. However, sorption will also increase the residence time of the complex in the water column, allowing more time for removal of metal from the non-exchangeable mode. If D_{HUM} is small, then this effect will not be significant, and the original equation for D_M will still be valid,

$$D_M = \left.\frac{k_b}{V} L\right|_{D_{HUM}\to 0}$$

In the case of significant sorption (large D_{HUM}), this equation must be adapted to take account of the increased residence time, and the effective metal ion Damkohler number, $D_M^{effective}$, is given by,

$$D_M^{effective} = \left.\frac{k_b}{V} L(1+K'_{HAS,i,j})\right|_{D_{HUM}\to\infty}$$

For intermediate D_{HUM}, these two equations provide a range of Damkohler numbers, the most representative value lying somewhere in between. To assess the importance of humic kinetics one should first calculate D_{HUM}. If it is small, then D_M may be used to determine whether non-exchangeable kinetics are significant, whilst if it is large, $D_M^{effective}$ should be used. If D_{HUM} has an intermediate value, then D_M will provide an indication of the maximum possible effect of non-exchangeable kinetics, and $D_M^{effective}$ the minimum. Figure 1 illustrates the procedure: there are 9 possible options, 5 conservative and 4 non-conservative. 4 avoid all kinetics, 4 include 1 kinetic equation, and only 1 requires a kinetic description of both

interactions. The exact calculation with a kinetic description of both processes always gives the correct solution, but requires longer calculation times.

Conclusions

Damkohler numbers allow the importance of kinetics, and the validity of approximations to be determined. Unfortunately, the most convenient approximation, equilibrium, is not conservative. Currently, the only way to make a conservative prediction is either to make the calculation including kinetics, or to assume that the non-exchangeably bound metal transports as a conservative tracer. More experimental work is required to improve the understanding of ternary complex formation. When that understanding has improved, there are a set of rules to determine the implications for R.P.A.

References

[1] Bryan, N.D.; Jones D.L.M., Keepax, R.E.; Farrelly, D.H.; Abrahamsen, L.G.; Pitois, A.; Ivanov, P.; Warwick, P. and Evans, N. The Role of Humic Non-Exchangeable Binding in the Promotion of Metal Ion Transport in the Environment, (2007) *Journal of Environmental Monitoring* (in press).

[2] Farrelly, D.H.; Abrahamsen, L.G.; Pitois, A.; Ivanov, P.; Siu, B.; Li, N.; Warwick, P.; Evans, N.D.M.; Knight, L. and Bryan, N.D. Initial Kinetic Studies of Iron Oxide and Humic Acid Ternary systems, 2006 (this volume).

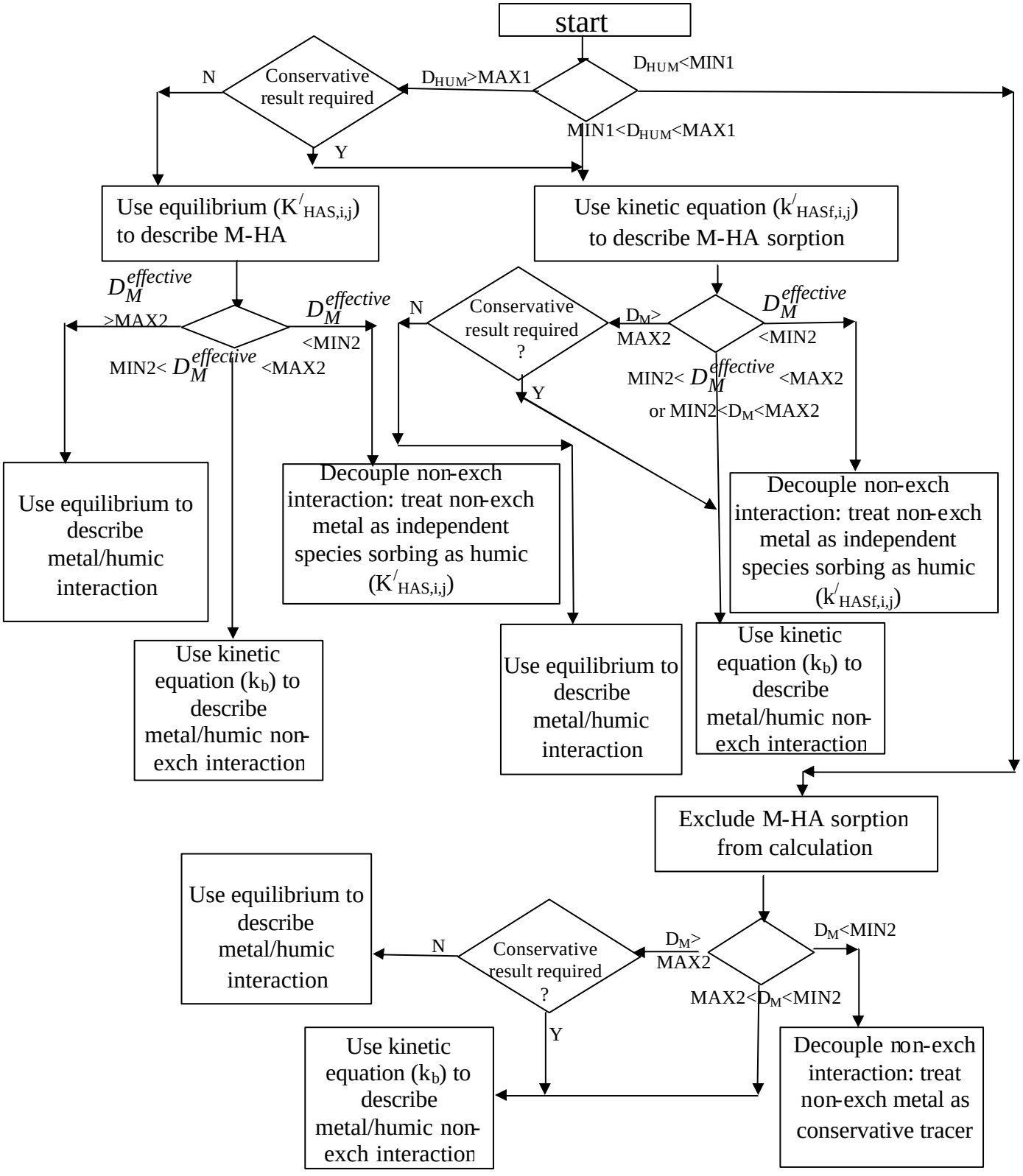

***Figure 1**: Procedure for assessing the importance of humic kinetics*

INITIAL KINETIC STUDIES OF IRON OXIDE AND HUMIC ACID TERNARY SYSTEMS

D.H. Farrelly[1], L.G. Abrahamsen[1], A. Pitois[1], P Ivanov[1], B. Siu[1], N. Li[1], P. Warwick[2], N.D.M. Evans[2] L. Knight[3] and N.D. Bryan[1,*]

[1] Centre for Radiochemistry Research, School of Chemistry, The University of Manchester, Oxford Road, Manchester, M13 9PL, U.K.
[2] Department of Chemistry, University of Loughborough, Loughborough, U.K.
[3] U.K. Nirex, Harwell, Oxfordshire, U.K.

* Corresponding author; Nick.Bryan@manchester.ac.uk

Abstract

The interactions of Eu^{3+} ions, humic acid and iron oxides in ternary system experiments have been studied. The variations in the amount of humic acid and Eu^{3+} with time have been determined as a function of humic acid concentration. Two simple mathematical models have been developed to predict the behaviour of metal ions and humics in the experiments. The treatment of the binary interaction between humic acid and metal ion is common to both models: initial rapid uptake to an exchangeable fraction, followed by slower transfer to the non-exchangeable fraction. Both models assume that the interaction of the humic with the mineral surface is unaffected by the complexation of metal ions. The difference between the models is that the first (Model 1) assumes that the observed heterogeneity derives from multiple binding sites on the surface of the iron oxide, whilst the second assumes that it is the result of chemical or size heterogeneity of the humic itself. The behaviour of the magnetite system is best described by Model 1, but hematite follows Model 2 most closely, whilst goethite shows intermediate behaviour.

Introduction

Iron oxide phases are ubiquitous in the environment as naturally occurring phases. They are also important products of corrosion processes. This, combined with the fact that they bind metal ions strongly (including most radionuclides), means that they could affect pollutant mobility in the environment.

Objectives

A kinetic study of the notionally simpler ternary system of quartz has already been reported (Abrahamsen et al 2006). That methodology has now been applied to

some iron oxide surfaces: goethite; hematite and magnetite. The partition of radionculides between solid and solution phase in these systems with time is very hard to predict, and adequate descriptions that may be used in the calculation of radionuclide migration in the post-closure Radiological Performance Assessment (RPA) of radioactive waste repositories do not exist. Therefore, the aim of this work is to develop a kinetic model of these systems.

Experimental

The experimental techniques used in this study have been described elsewhere in this volume for the quartz ternary system (Abrahamsen et al 2006). The only significant difference is that lower solid:solution ratios (0.1 – 10 g dm^{-3}) were used here, since these surfaces are more strongly sorbing.

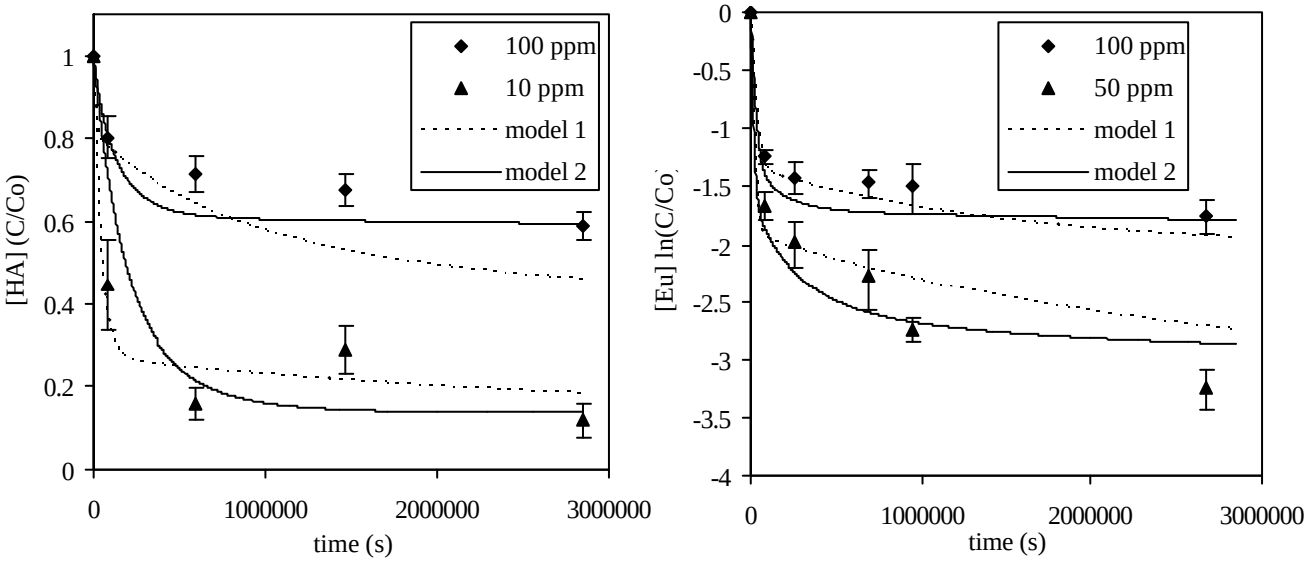

***Figure 1**: (A) humic (left) and (B) Eu^{3+} (right) sorption to goethite, experiment and model fits. Parameters: $K_{exch}=1(\pm0.5)x10^{3}$; $k_{Msf}=9(\pm2)x10^{-3}$; $k_{Msb}=1(\pm0.5)x10^{-5}$. Model 1: [S1]=20(±10); [S2]=50(±15); $k_{HAS1f}=3(\pm2)x10^{-7}$; $k_{HAS1b}=6(\pm3)x10^{-7}$; $k_{HAS2f}=1(+2/-0.5)x10^{-8}$; $k_{HAS2b}=1(+3/-0.5)x10^{-7}$. Model 2: [S]=50(±10); HA1=70(±10)%; $k_{HA1Sf}=1(+1/-0.5)x10^{-7}$; $k_{HA1Sb}=1(+1/-0.5)x10^{-6}$; $k_{HA2Sf}=6(\pm3)x10^{-9}$; $k_{HA2Sb}=1(+5/-0.5)x10^{-8}$.*

Results

A large number of experiments have been performed using the three solid phases. Due to space restrictions, a small selection is presented here (Figures 1 – 3). Some of the results (Figure 1) are presented as C/C_o versus contact time, where C is the concentration of humic acid or Eu in solution at any given time, and C_o is the total concentration in the system.

Modelling and Discussion

The experimental results have been simulated with a simple mathematical model, which was developed to simulate the quartz sand ternary system. The model has been described elsewhere (Abrahamsen et al 2006): the chemical and mathematical equations are shown in Table 1. A single kinetic equation (3; Table 1) has been used to simulate the interaction of the metal ion with the surfaces: this is essentially a kinetic surface complexation approach. The two equations used to define the metal humate interaction (1, 2; Table 1) are those that have been used to model metal-humate interactions in transport calculations previously [2]. Note, the model does not include any parameters to account for the electrostatic contribution to binding for any of the interactions. Clearly, if such procedures were included, then that would/could give a more realistic physicochemical description of the interactions. However, the aim of this work is to develop models that could be applied in calculations of migration in RPA, and to be useful, the model must be as simple as possible. Therefore, at least initially, the model has been developed using the minimum number of parameters, and ignoring the electrostatic contributions to the interactions. Previous work has shown that it is possible to simulate the transport of metal ions in column experiments without including electrostatic contributions [2]. For the systems were the models were able to reproduce the experimental data, the parameter values and estimates of the associated uncertainties are given with each of the figures (1-3), except for equation 2 (Table 1). The results were found to be insensitive to the values of k_f (1.1×10^{-8}) and k_b (1×10^{-7}), and they have been taken from previous work [2].

Table 1: *Model equations: HA_{exch} – humic exchangeable binding site, Eu_{exch} and $Eu_{non\text{-}exch}$ – humic bound exchangeable and non-exchangeable Eu, S_M – surface metal binding, Eu_S - Eu sorbed to the surface. Units: K_{exch} dm^3mol^{-1}; k_f, k_b, k_{MSb}, k_{HAS1b}, k_{HAS2b}, k_{HA1Sb} and k_{HA2Sb} s^{-1}; k_{MSf}=$dm^3mol^{-1}s^{-1}$; k_{HAS1f}, k_{HAS2f}, k_{HA1Sf} and k_{HA2Sf} $ppm^{-1}s^{-1}$.*

#	All Calculations	
1	$Eu^{3+}_{(aq)} + HA_{exch} \leftrightarrow Eu_{exch}$	$K_{exch} = \frac{[Eu_{exch}]}{[Eu^{3+}_{(aq)}].[HA_{exch}]}$
2	$Eu_{exch} \underset{\leftarrow}{\rightarrow} Eu_{non-exch}$	$\frac{d[Eu_{non-exch}]}{dt} = k_f[Eu_{exch}] - k_b[Eu_{non-exch}]$
3	$Eu^{3+}_{(aq)} + S_M \underset{\leftarrow}{\rightarrow} Eu_S$	$\frac{d[Eu_S]}{dt} = k_{MSf}[Eu^{3+}_{(aq)}].[S_M] - k_{MSb}[Eu_S]$
Model 1		**Model 2**
4A	$HA_{free} + S_{HA1} \underset{\leftarrow}{\rightarrow} HA_{S1}$	$\frac{d[HA_{S1}]}{dt} = k_{HAS1f}[HA_{free}].[S_{HA1}] - k_{HAS1b}[HA_{S1}]$
4B	$HA1_{free} + S_{HA} \underset{\leftarrow}{\rightarrow} HA1_S$	$\frac{d[HA1_S]}{dt} = k_{HA1Sf}[HA1_{free}].[S_{HA}] - k_{HA1Sb}[HA1_S]$
5A	$HA_{free} + S_{HA2} \underset{\leftarrow}{\rightarrow} HA_{S2}$	$\frac{d[HA_{S2}]}{dt} = k_{HAS2f}[HA_{free}].[S_{HA2}] - k_{HAS2b}[HA_{S2}]$
5B	$HA2_{free} + S_{HA} \underset{\leftarrow}{\rightarrow} HA2_S$	$\frac{d[HA2_S]}{dt} = k_{HA2Sf}[HA2_{free}].[S_{HA}] - k_{HA2Sb}[HA2_S]$

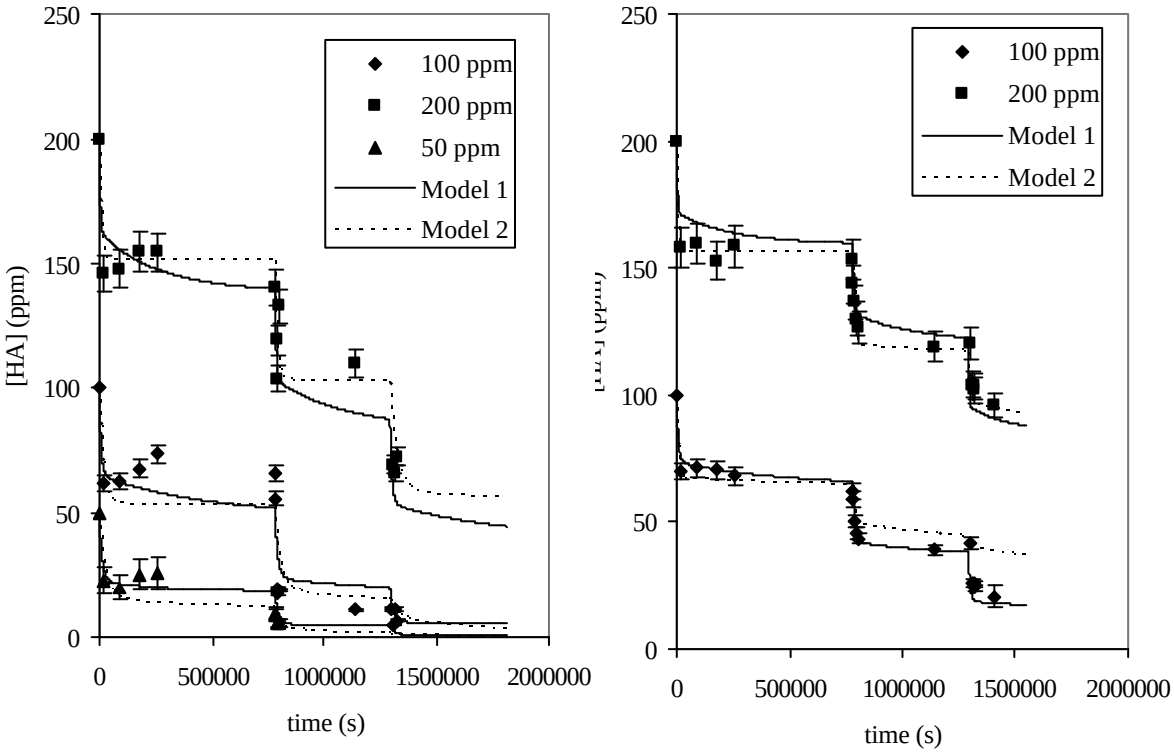

Figure 2: *Removal of humic from solution by sequential samples of solid, experiment and model fits. A (left) Goethite { Model 1: [S1]=40(±10); [S2]=30(±10); k_{HAS1f}=1.4(+2/-0.5)x10^{-6}; k_{HAS1b}=1.5(±1)x10^{-5}; k_{HAS2f}=2(+2/-1)x10^{-8}; k_{HAS2b}=6(±4)x10^{-7}. Model 2: [S]=50(±5); HA1=80(±10)%; k_{HA1Sf}=1(+3/-0.5)x10^{-6}; k_{HA1Sb}=3(±2)x10^{-6}; k_{HA2Sf}=2(+2/-1)x10^{-8}; k_{HA2Sb}=6(±4)x10^{-7}}; B (right) Magnetite { Model 1: [S1]=30(±2); [S2]=15(±3); k_{HAS1f}=1.4(+1/-0.5)x10^{-6}; k_{HAS1b}=1.5(+1/-0.5)x10^{-5}; k_{HAS2f}=2(±1)x10^{-8}; k_{HAS2b}=6(+20/-4)x10^{-7}. Model 2: [S]=50; HA1=50%; k_{HA1Sf}=3x10^{-6}; k_{HA1Sb}=2.7x10^{-5}; k_{HA2Sf}=1x10^{-8}; k_{HA2Sb}=7.5x10^{-7}}.*

The part of the ternary system that is least well understood is the reaction of humic substances and humic/metal complexes with surfaces. The experimental data from this work and previous studies (e.g.[3]) have shown that there is multi-component behaviour, i.e. more then one chemical reaction takes place. There are two possible explanations for this behaviour: it could be that there is more than one binding site on the surface, or there could be more than one type of humic molecule in solution; or of course, it could be both. Therefore, two approaches have been tested, Models 1 and 2, which have surface and humic heterogeneity, respectively. Therefore, for each system, two sets of calculations have been performed: Model 1, using equations 1, 2, 3, 4A, 5A; Model 2, using equations 1, 2, 3, 4B, 5B. In both cases, ternary complexes were included using the same equations as for the sorption of 'free' humic, i.e., in equations 4A/B and 5A/B, metal humic complex, M-HA, replaces free humic (HA_{free}, $HA1_{free}$ or $HA2_{free}$, etc.).

A number of 'standard' ternary uptake experiments have been modelled for all of the samples. Examples of the results (for goethite) are shown in Figure 1. For these experiments, it is not possible to be sure which of the models is the best

description of the behaviour: for the Eu data Model 1 gives a better fit for the 100 ppm system, but Model 2 is slightly better for the humic data. Similar results have been obtained for the other surfaces. Other work (Abrahamsen et al 2006) has shown that for the quartz system, it is not always possible to determine the most appropriate approach with these types of experiment alone. Therefore, a series of more complex experiments have been modelled for each surface.

Figures 2 and 3A show the results for a set of experiments where humic acid was sorbed to a sample of each solid phase, and at regular intervals, the solution phase was isolated from the solid, and a fresh solid sample added. The results vary between the systems: for the magnetite system, Model 1 provides the best fit, and for hematite, Model 2 is clearly better, whilst for goethite, neither approach is clearly superior, and both fail to match the experimental data exactly.

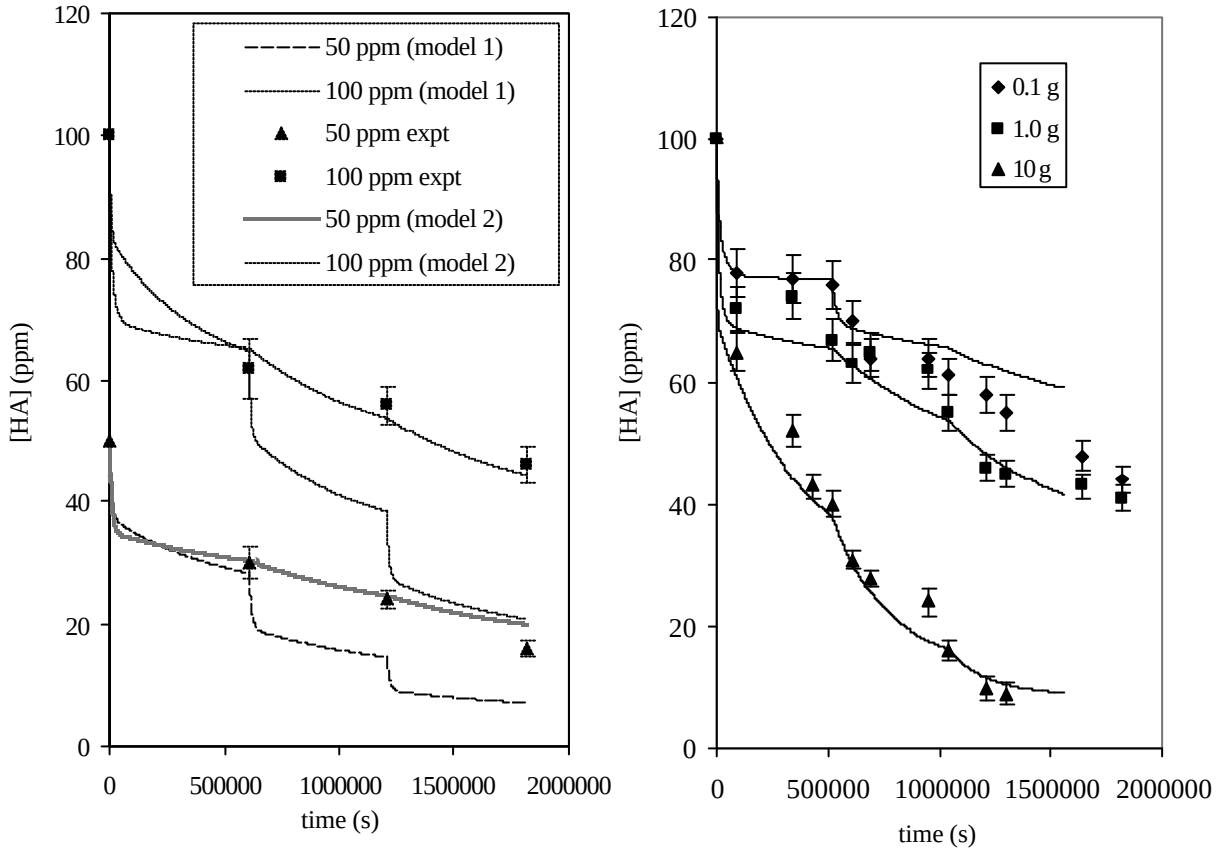

Figure 3: *Humic uptake onto hematite { Model 1: [S1]=22; [S2]=40; k_{HAS1f}=1.4x10^{-6}; k_{HAS1b}=4x10^{-5}; k_{HAS2f}=2x10^{-8}; k_{HAS2b}=6x10^{-7}. Model 2: HA1=30(±5)%; k_{HA1Sf}=3(+7/-2)x10^{-6}; k_{HA1Sb}=3(±2)x10^{-8}; k_{HA2Sf}=1(+0.1/-1)x10^{-8}; k_{HA2Sb}=7.5(+10/-2.5)x10^{-7}}. A (left, [S]=47(±5)) exposure to fresh (sequential) samples of solid; B (right) effect of increasing amount of hematite with time as a function of the mass of solid added with each step {[hem]=0.1g/l - [S_{HA}]=230 (±20); [hem]=1.0 - [S_{HA}]=47(±5); [hem]=10 - [S_{HA}]=20(±3)}.*

The position with these iron oxide systems is more complex than for the quartz system, which is relatively well behaved (Abrahamsen et al 2006). Figure 3A shows that Model 2 provided a reasonable fit to the hematite data for the experiment where the solid sample was replaced at regular intervals, and one might think that

Model 2 provides the best fit for this system. However, Figure 3B shows the results of a different experiment. Here, the amount of hematite in the system was increased incrementally during the experiment (at 0, 6 and 12 days, the amount of hematite in the system was increased by 0.1, 1.0 or 10 g l^{-1} each time). Model 2 fits are also shown in the figure. The fits to the data are good, and the same chemical rate constants and partition between the two humic fractions were used in each fit. However, the model is only able to produce these fits if the specific binding capacity varies with the concentration of hematite in the sample (values in figure caption).

It is useful to compare the behaviours of the various mineral surfaces, including the quartz sand results of Abrahamsen et al (2006). For the interactions of metal ions with mineral surfaces there is a single description that works for virtually all surfaces and ions (surface complexation). Similarly, for metal ions and humics there is one general description that fits all specifically binding cations, i.e., although the values of rate and equilibrium constants may vary, the same chemical and mathematical equations may be used. However, for the interaction of humics (and humic/metal complexes) with mineral surfaces, it seems that this is not the case. Quartz sand (Abrahamsen et al 2006) and magnetite seem to respond best to an approach with surface heterogeneity, whilst hematite responds best to a model that uses humic heterogeneity, whilst goethite seems to have intermediate behaviour. Although the same mathematical equations may be used to describe the two sets of surfaces, there are significant differences. For example, the quartz sand of Abrahamsen et al (2006) is a much weaker sorber than any of the iron oxides, and a much higher solid/solution ratio is required for the same order of magnitude of uptake.

Conclusions

Interim ternary system kinetic models have been developed for iron oxide surfaces. It has been found that sometimes, the experimental data are best described with an approach that includes binding site heterogeneity, whilst in others, the chemical heterogeneity of the humic dominates. However, although the current models are able to predict the general behaviour, they are not yet ready for use in predictions of radionuclide behaviour outside of the lab. Further experimental and modelling work is required to provide a reliable model that could be used in RPA calculations.

References

[1] Abrahamsen, L.G.; Farrelly, D.H.; Pitois A.; Ivanov P.; Warwick P.; Evans N.D.M.; Knight, L.; Bryan, N.D. (2006) *Kinetic Studies of the Quartz/Sand, Eu3+ and Humic Acid Ternary System*, This volume.

[2] Bryan, N.D.; Barlow, J.; Warwick, P.; Stephens, S.; Higgo, J.J.W.; Griffin, D. (2005) *J. Envion. Monit.* **7**, 196 – 202.

[3] Van de Weerd, H.; Van Riemsdijk, W.H.; Leijnse, A. (1999) *Environmental Science and Technology,* **33**, 1675-1681.

INFLUENCE OF THE MINERAL COMPOSITION AND THE GROUNDWATER pH ON THE DIFFUSION OF $^{99}TcO_4^-$ AND $H^{14}CO_3^-$ ANIONS THROUGH BORECORE SAMPLES OF BODA CLAYSTONE

K. Lázár[1]*, J. Megyeri[2] and Z. Máthé[2]

[1] Institute of Isotopes, Budapest, P.O.B. 77, H-1525, Hungary
[2] Mecsekérc Co., Esztergár L. 19., Pécs, H-7633, Hungary

* Corresponding author: lazar@iki.kfki.hu

Abstract

Diffusion rates of TcO_4^- and $H^{14}CO_3^-$ anions are compared in break-through experiments performed on bore core samples with different mineral compositions. Measurements were carried out using synthetic ground water of different pH-s (8 and 12).

Significant increase of the apparent diffusivities was observed in samples containing smectite constituent for both anions in experiments performed at pH = 8. Rock capacity factors were also different in dependence of the composition in experiments with $H^{14}CO_3^-$ at pH = 8. The presence of smectite is assumed to result in formation of microcracks, providing additional free volume for diffusion. In the diffusion of $H^{14}CO_3^-$ the isotope exchange between the carbonate forms, $CO_3^{2-}{}_{solution} \leftrightarrow CO_3^{2-}{}_{rock}$, plays probably also a role in the migration process.

Introduction

Anionic species migrate faster in clays than cationic species do, due to the less expressed sorption of the former ones. Thus, to predict the expected rate of spreading the radionuclides around a repositiory, study of anionic species is preferred in the first stage. Adopting this approach, diffusion of characteristic anionic species was studied in samples originated from one of the geological formations perspective for a repository, namely from Boda Claystone. A preliminary account was already given on break-through experiments performed with $^{99}TcO_4^-$ and $H^{14}CO_3^-$ species with ground water of pH= 8. Similar values were obtained for both the effective diffusivities of $H^{14}CO_3^-$ and $^{99}TcO_4^-$ (~ 10^{-12} m^2 s^{-1} [2]).

Objectives

The present report provides an account on the extension of the previous studies. Namely, the influence of mineral composition on the migration rate has been studied recently by comparing samples with different composition, and in addition, experiments were performed with ground water at two different basicities. pH = 8 was selected as characterising the unperturbed original state of the geological environment, and pH = 12 was chosen to model the conditions of an arising cement plume in the neighbourhood of a concrete barrier of a repository.

Experimental

Samples

Samples are originated from a drill driven at c.a. ~1000 depth (below the ground level). The formation, diagenesis and post diagenetic processes for the Boda Claystone are described in [1].

Table 1*.The main mineral components of the studied samples (in %)*

Sample	Quartz	Albite	Illite	Smectite	Kaolinite + chlorite	Hematite	Calcite
# 1	10	62	15	0	4	8	1
# 2	9	56	21	3	< 2	8	3

Ground water

The composition of the synthetic ground water is shown is Table 2. This composition corresponds to pH = 8. For the pH = 12 measurements NaOH was further added in appropriate amounts.

Table 2*. Main components in the ground water (mg / L):*

Na^+	K^+	Ca^{2+}	Mg^{2+}	Cl^-	SO_4^{2-}	CO_3^{2-}	HCO_3^-
323	< 5	10	< 10	18	37	21	729

Measurements

C.a. 8 mm thick discs were cut from the compact, dense borecores, and the break-through of radioisotopes was studied in two-compartment break-through cells, by recording the increase of the activity, i.e. the appearance of the radioisotope in the compartment, which was filled only with the inactive ground water at the start of the experiment. The break-through curves can be obtained by determining the increase of the activity in dependence of the elapsed time. The amount of $H^{14}CO_3^-$ used for spiking (3.7 MBq) is negligible in comparison to the original concentration of the HCO_3^- (1.2×10^{-2} mol/ L). This small amount practically does not result in any change in the concentration, thus, the experiment is performed at a negligible concentration gradient of HCO_3^-. Similar condsideration holds for the $^{99}TcO_4^-$, its concentration is 5×10^{-4} mol / L in the „active" compartment of the measuring cell.

Further, there is no pressure gradient during the measurement between the two compartments, either. Other details of the experimental conditions are described in [2.]. For illustration, the break-through data obtained for the $H^{14}CO_3^-$ anionic species at pH = 12 are shown in Fig. 1 (bottom). The top part of the figure shows the relative acivity in the „active" compartment.

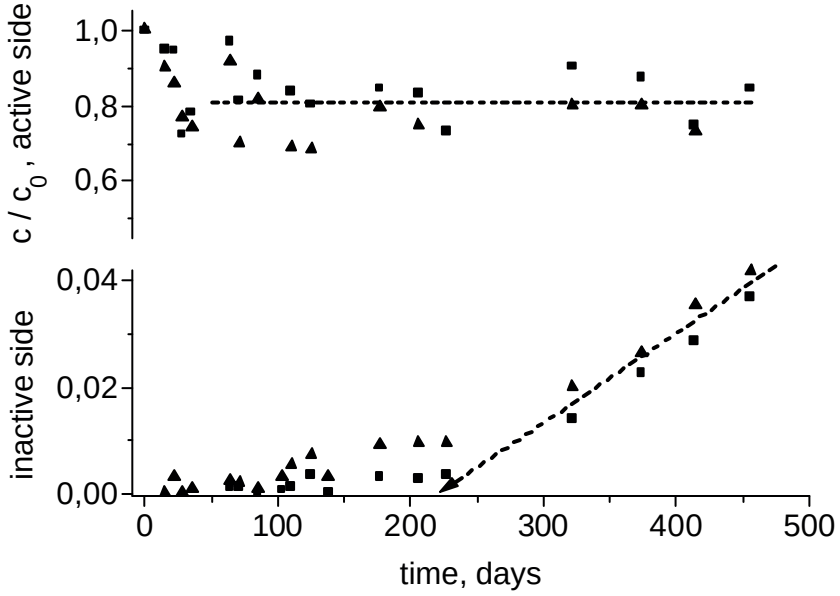

Figure 1. *The relative activities in the active compartment (t = 0, c_0 = 1; top part), and the break-through data (bottom part) recorded with $H^{14}CO_3^-$ on samples 1 (■), and 2 (▲) at pH = 12.*

Modelling

The results of the experiments are evaluated using the conventional approach described e.g. in [3]:

$$C(t) / C_0 = (A\, D_e)\, t / (VL) - (a\, A\, L) / 6V \quad , \qquad \text{(Eq. 1)}$$

where

C stands for the count rates, C (t) / C_0 is the relative activity change in the solution,
A: is the cross section of the sample disc,
D_e: is the effective diffusivity constant,
V': is the volume of the solution in the cell,
L: is the thickness of the bore core disc,
t: is the time elapsed,
α: is the so-called rock capacity factor.

The first part in Eq. 1 is the slope, the second is the intercept in the C_t/C_0 axis. Thus, D_e is calculated as:

$$D_e = C_t / C_0 \;\; x\,(VL) / A \;\; x\; 1 / \Delta t$$

The values of the effective diffusivities obtained with this approach the are shown in Table 3, and the α rock capacity factors in Table 4.

Table 3*.Values of the effective diffusion constants (D_e, $m^2 s^{-1}$ x 10^{12})*

Tracer	$^{99}TcO_4^-$		$H^{14}CO_3^-$	
Sample	# 1	# 2	# 1	# 2
pH = 8	n.a.	1.16	0.39	1.57
pH = 12	n.a.	0.77	1.10	1.07

Table 4*.α rock capacity factors in Eq. 1 estimated from plots of $H^{14}CO_3^-$ data*

Sample	# 1	# 2
pH = 8	0.08	0.51
pH = 12	1.15	0.96

Conclusions

Conclusions can be drawn by comparing the experimental results in dependences on the radioisotope, on the pH, and on the composition of samples as well.

First, it is worth comparing samples # 1 and # 2 when using $^{99}TcO_4^-$ tracer. On sample # 1 no break-through has taken place during ~ 500 days, whereas noticeable breakthrough is detected on sample # 2. As an apparent possibility the difference can probably be attributed to the presence or absence of the smectite component: sample # 1 does not contain smectite, whereas sample # 2 contains it in 3 %. Most probably swelling in the interlayers of smectite results in formation of additional pores or even cracks, providing larger pore volume available for diffusion.

In general, $^{99}TcO_4^-$ data indicate limited interactions between the rock and the tracer anion. The observed ~ 10^{-12} m^2 s^{-1} value for the effective diffusion constant can be interpreted as characteristic for non-interacting ions in aqueous solutions, since in a neutral rock with 0.5 – 2.3 % porosity similar data can be obtained using the self-diffusion constants of ions in electrolytes (~ 10^{-9} m^2 s^{-1}).

For the interpretation of data obtained from the measurements with $H^{14}CO_3^-$ three further conditions should be considered. First, in spite of the low amount of the applied $H^{14}CO_3^-$ tracer, the concentration of the HCO_3^- anion is large, the ground water is practically saturated with this anion, since the rock contains calcite in 1 to 3 per cent. Considering this condition, only limited interaction might be expected between the rock and the tracer anion. Secondly, the pH dependence of the equilibria between the different forms of the hydrocarbonate/carbonate ions should also be considered. In particular, the HCO_3^- <=> CO_3^{2-} equilibrium is shifted from the hydrocarbonate to carbonate form at pH 10.3 . The third point is that exchange of active $^{14}CO_3^{2-}$ may proceed from the aqueous solution to the solid phase, since the rock contains calcite.

The data obtained from the $H^{14}CO_3^-$ measurements can be iterpreted in correspondence with the mentioned three aspects. For instance, if we compare the D_e values calculated from pH = 8 data the difference between samples # 1 and # 2 is almost similar as in the case of $^{99}TcO_4^-$. Namely, the effective diffusion in sample # 2 is considerably larger than in sample #1, the difference can similarly be attributed to the presence of smectite in sample # 2 and absence in sample # 1. In a modest variation, D_e is measurable in sample # 1, in contrast with $^{99}TcO_4^-$, where D_e was not detectable. This variance can probably be attributed to the two orders of magnitude difference in the concentration, in favour of the HCO_3^- vs. $^{99}TcO_4^-$ ($\sim 10^{-2}$ vs. $5 . 10^{-4}$ mol L^{-1}, respectively).

In the case of pH = 12 samples, similar D_e values were obtained for samples # 1 and # 2. Most probably the change in pH from 8 to 12 resulted in the HCO_3^- => CO_3^{2-} conversion, and the latter form got into equilibrium with the solid carbonate of the rock via exchange. This may be reflected in a slight decrease of the D_e found in sample # 2 (from 1.6 to 1.1 x 10^{-12} m^2 s^{-1}). In correspondence, the enhanced interaction at pH = 12 with the rock is clearly reflected in the large values of rock capacity factors shown in Table 4.

The results of mesurements can be summarized in short as follows:

- The mineral composition influences the value of apparent diffusion, in particular the presence of smectite has a characteristic influence.
- The effect of the change of the pH of the ground water is also demonstrated. Namely, the HCO_3^- <=> CO_3^{2-} equilibrium is shifted to the right direction upon increasing the pH, and, at the pH = 12 case where the carbonate form is stabilized the distribution of $^{14}CO_3^{2-}$ between the liquid and solid phases can be suggested via isotope exchange.

References

[1] Árkay, P., Balogh, K., Demény, A., Fórizs, I., Nagy, G., Máthé, Z., (2000) Composition, diagenetic and post-diagenetic alterations of a possible radioactive waste repository site: the Boda Albitic Claystone Formation, southern Hungary, *Acta Geologica Hungarica*, 43, 351 - 360.

[2] Lázár, K., Megyeri, J., Máthé, Z., (2006) Diffusion of anionic species in borecore samples from Boda claystone formation, *2nd Annual Workshop Proceedings, FUNMIG IP, Stockholm,* this volume.

[3] Mell, P., Megyeri, J., Riess, L., Máthé, Z., Hámos, G., Lázár, K., (2006) Diffusion of Sr, Cs, Co and I in argillaceous rock as studied by radiotracers, *Journal of Radioanalytical and Nuclear Chemistry*, 268, 411 - 417.

IMPROVED LIGAND AND CHARGE DISTRIBUTION (LCD) MODEL

L.P.Weng[1], W.H. Van Riemsdijk[1] and T.Hiemstra[1]

[1]Department of Soil Quality, Wageningen University, P.O. Box 8005, 6700 EC, Wageningen, The Netherlands

* Corresponding author: liping.weng@wur.nl

Abstract

Humic substances present in nature interact strongly with mineral particles. This interaction influences the solubility of natural organic matter, as well as ion adsorption to mineral surfaces. To model the adsorption of variable charge particles to charged surfaces, one has to be able to calculate the adsorption free energy involved. In this work, expressions for the free energy change of variable charge particles are derived based on the equality of (electro)chemical potential of the particles in the bulk solution and adsorption phase. The expressions derived are named ADAPT model (ADsorption and adAPTation), because they are based on the change of the average chemical state (adaptation) of the particles upon adsorption. The LCD model (Ligand and Charge Distribution) has been recently proposed to describe the adsorption of humic substances to oxides, in which the CD-MUSIC model and the NICA model for ion binding to respectively oxides and humic substances are integrated. In this study, the LCD model is improved by applying the ADAPT model to calculate the equilibrium distribution of the humic substances. The improved LCD model is applied to calculate the adsorption of fulvic acid (Strichen) to goethite, in which it is assumed that the carboxylic type of groups of fulvic acid can form innersphere complexes with the surface sites. The calculation shows that the LCD model can describe sufficiently the effects of pH, ionic strength and loading on the adsorption of fulvic acid. The model calculations indicate that the chemical complexation between fulvic acid and goethite is the main driving force of the adsorption, while the electrostatic repulsion between the particles and the surface is the major limiting factor for further adsorption.

Introduction

Fulvic acids (FA) and humic acids (HA) are the most important reactive fractions of natural organic matter (NOM) in soils, sediments, groundwater and surface water. They play a vital role in the biogeochemical processes for many elements in the environment. In the first place, interactions between NOM and

many cations are significant. Secondly, FA and HA adsorb readily onto oxide minerals. Both processes are important in controlling the mobility of various cations and anions in the natural environment.

Modeling the adsorption of humic substances to charged surfaces is a very challenging subject. Many models developed treated humic substances in a similar way as small molecules, in which *a priori* assumptions are made with respect to a limited number of surface species of the adsorbed humic substances. By reducing the number of species in these models, the calculated speciation of the adsorbed particles is most probably chemically and physically not very realistic.

To further improve our understanding of the adsorption of humic substances to oxides, and to use existing knowledge of modeling ion binding to both oxides and humic substances, the concept of the LCD (Ligand and Charge Distribution) model has recently been proposed. In comparison to other models developed for the adsorption of humic substances, the great advantage of the LCD model is that it allows for the incorporation of details that are already present in both the CD-MUSIC and the NICA model. For a given humics-mineral oxide system, this means that many model parameters are already known. Only the characteristics of the interactions between the humic substances and the oxides have to be adapted.

For any model that deals with the adsorption of variable charge particles to charged surface, it is crucial to correctly formulate the equilibrium condition of the particle distribution between the solution phase and the adsorption phase. In the previous version of the LCD, the adsorption of the particles is calculated using the overall reaction formalism [2,3]. In this formalism, the concentration of fully dissociated humics molecules is required, which is however not correctly calculated in the previous LCD.

Objectives

In this work, expressions are derived theoretically for the free energy change of variable charge particles based on the ion adsorption model of Langmuir, Langmuir-Freundlich and NICA. The expressions for the contribution of the diffuse ions to the free energy change of the particles are also derived for the electrostatic Donnan model. Based on the equality of the (electro)chemical potential of the particles in difference phases, relationships are derived that can be used to calculate the equilibrium distribution of variable charge particles between the bulk solution phase and a charged surface phase [5]. For the convenience of the description, we name these types of relations the ADAPT model (ADsorption and adAPTation). To improve the LCD model, the ADAPT module is introduced into the model structure. This new module replaces the overall reaction formalism of the previous LCD and defines the equilibrium condition of the phase distribution of humic substances. The improved LCD model is applied to describe the adsorption of fulvic acid to goethite. The calculated results are compared with experimental data of Filius et al. and Weng et al. [1,4] on Strichen fulvic acid adsorption to goethite that show the effects of the pH, ionic strength and fulvic acid loading on the adsorption [6].

Experimental

The experimental data of fulvic acid adsorption and proton co-adsorption with fulvic acid to goethite have been published previously [1,4]. More detailed descriptions of the material and methods can be found in those papers..

Adsorption of FA to goethite was measured with batch experiments in the work of both Filius *et al.* [1] and Weng *et al.* [4]. In the first series, 75, 150, 300 mg/l FA was added to 5.0 g/l goethite suspension in 0.015M and 0.1M $NaNO_3$[1]. In the second series, 75, 150, 300 and 450 mg/l FA was added to 5.8 g/l goethite in a background electrolyte solution of 0.1M $NaNO_3$ [4]. Acid or base solution (0.100 M NaOH and HNO_3) was added to the suspensions to adjust the pH to the desired values in the range of 3-11. The solutions were prepared under a N_2 atmosphere and stored in air-tight bottles. Thus prepared suspensions were shaken at 20°C for 3 days, and then centrifuged at 18,000 *g* for 30 minutes. The concentration of dissolved carbon was measured with a TOC analyser. The final pH in the supernatant was measured using a pH meter.

The co-adsorption of protons upon adsorption of FA to goethite was measured with pH-stat FA titrations at pH 4.0, 5.5 and 7.0 in a background of 0.01M and 0.1M $NaNO_3$ [1,4] The experiments were designed in such a way that practically speaking all FA added was adsorbed. The proton co-adsorbed is calculated from the amount of acid-base added after each addition of FA to keep the pH constant.

Modelling

Free energy variable charge particles. The change of the free energy of particles due to ion binding (specifically and non-specifically) can be calculated from:

$$dF = -\sum N_i d\mu_i \qquad (1)$$

where dF (J/mol) is the change of the free energy per mol particles, N_i (mol/mol) is the (excess) amount of ion i bound per mol particles and $d\mu_i$ is the change of the chemical potential of ion *i*. Similarly, the change of the free energy of particles as a result of the release of ions can be calculated as:

$$dF = \sum (N_{\max} - N_i) d\mu_i \qquad (2)$$

where $N_{\max}$ (mol/mol) is the maximum amount of ion i that can be bound to one particle. The (electro)chemical potential (μ_p, J/mol) of particles can be written as:

$$\mu_p = \mu_p^0 + \Delta F + \mathrm{RT} \ln C_p \quad (3)$$

where $\mu^0{}_p$ (J/mol) is the standard chemical potential of the particles, which can be defined as the chemical potential of one mol particle at an arbitrarily chosen reference state (often the neutral charge state is used), ΔF (J/mol) is the change of free energy of the particles from the chosen reference state to the actual state, C_p (mol/l) is the total concentration of the particles in the phase of concern, R and T are

respectively the gas constant and absolute temperature. The change of the free energy of the particles (ΔF) can be calculated by taking the integral of Eq. 1 or 2. At equilibrium, the (electro)chemical potential (μ_p) of the particles in the solution phase and in the adsorption phase should be equal, which leads to:

$$C_{p,ads} = C_{p,sol} K_p = C_{p,sol} e^{\frac{\Delta F_{sol} - \Delta F_{ads}}{RT}} \qquad (4)$$

Subscripts 'sol' refers to the solution phase and 'ads' the adsorption phase to which the particles adsorb, K_p is the adsorption affinity of the particles.

Improved LCD model. The improved LCD framework consists of four modules: NICA-Donnan, NICA-LD, CD-MUSIC and ADAPT (see Figure 1). The NICA-Donnan part of the LCD model (I in Figure 1), makes use of the NICA-Donnan model, which, in combination with the chemical speciation of inorganic ions in solution, calculates the adsorption of ions to the FA particles in the solution phase. The NICA-LD (LD: Ligand Distribution) module in the LCD model (II in Figure 1) calculates the complexation of both small ions and the surface sites with the reactive ligands of the adsorbed particles. For this purpose, the NICA approach is used to calculate the average chemical state, or ligand distribution, of the fulvics adsorbed. We assume that the adsorbed FA is present in a layer at the surface of goethite, with the layer thickness (L) equal to the diameter of the FA particles, which is estimated as 1.2 nm. The carboxylic and phenolic type of groups of the adsorbed FA that are not involved in the complexation with the surface sites are located in the d-plane. We further assumed that innersphere complexes between the carboxylic groups of adsorbed FA and the singly coordinated surface sites on goethite can be formed. In the LCD model, the CD-MUSIC module (part III, Figure 1) is used to calculate the adsorption of small ions to the oxides and the charge balance and electrostatic potential at the oxide surface. The ADAPT module (Part IV, Fig. 1) in the LCD model calculates the equilibrium distribution of humic substances between the solution phase and an adsorption phase. The name ADAPT characterizes the concept that adsorption and adaptation are directly related, *i.e.* the driving force for the adsorption or phase distribution of the variable charge particles is the change of the free energy of the particles as a result of the shift in their average chemical state upon adsorption (adapt).

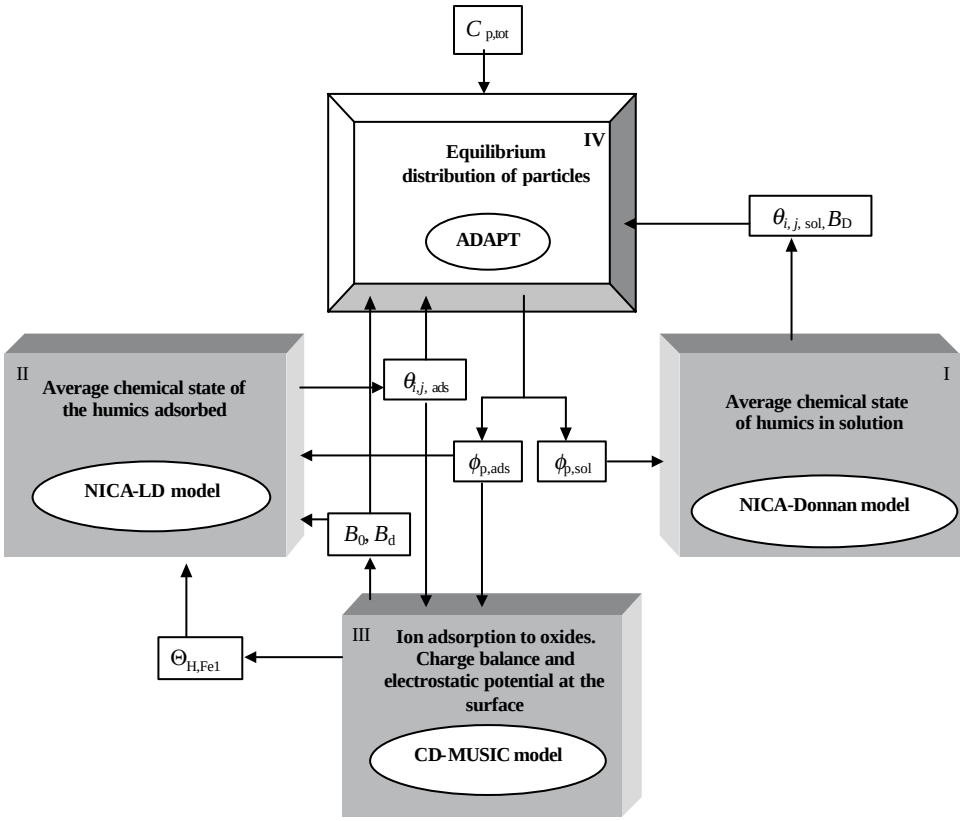

Figure 1. *Structure of the improved LCD model.*

Conclusions

The change of the free energy of the variable charge nano-particles upon adsorption can be calculated from the change of their average chemical state. The free energy change of variable charge nano-particles can be divided into a specific (ΔF_{sp}), and a non-specific part (ΔF_{nsp}). The mathematical expressions for the free energy of these two parts depend respectively on the ion-binding model and the electrostatic model chosen. In this paper, we have derived the expressions for the specific part of the free energy for the Langmuir, Langmuir-Freundlich and NICA model. Both the Langmuir-Freundlich and NICA model deal with ion binding to heterogeneous particles. In fact, the NICA equation can be considered as the most general equation for all the three ion-binding models considered since the Langmuir model and the Langmuir-Freundlich model are limiting cases. The expressions derived for the particle free energy change and corresponding particle adsorption affinity ($K_{p,sp}$) are:

$$\Delta F_{sp} = \mathrm{RT}\frac{N_{max}}{n_H p}\left\{\ln\left(1-\sum\theta_i\right)+\ln\left(\tilde{K}_H C_H\right)^{n_H p}\right\} \qquad (5)$$

$$K_{p,sp} = \left(\frac{1-\sum\theta_{i,sol}}{1-\sum\theta_{i,ads}}\right)^{\frac{N_{max}}{n_H p}}\left(\frac{C_{H,sol}}{C_{H,ads}}\right)^{N_{max}} \qquad (6)$$

where the parameter n_H is the non-ideality parameter for proton adsorption, p is the width of the affinity distribution, $\tilde{K}_H$ is the mean affinity constant for proton adsorption, C_H is the local concentration of proton, $1-\sum\theta_i$ is the fraction of the ligands in the dissociated form.

Expressions for the non-specific part of the free energy were derived for the Donnan model for a system that contains symmetric 1:1 electrolyte ions:

$$\Delta F_{nsp} = -C_{salt} V_{D,m} f (B_D + \frac{1}{B_D} - 2) \quad (7)$$

$$K_{p,nsp} = e^{\frac{C_{salt} V_{D,m} f}{RT}\left(B_{D,ads} + \frac{1}{B_{D,ads}} - B_{D,sol} - \frac{1}{B_{D,sol}}\right)} \quad (8)$$

where C_{salt} (mol/l) refers to the concentration of the electrolyte ions in the bulk solution, $V_{D,m}$ (l/mol) indicates the Donnan volume of one mol particle, and B_D is the Boltzmann factor for the Donnan phase, f is the activity coefficient for the monovalent salt ions.

The LCD model was improved by replacing the general reaction formalism with the ADAPT module. The advantage of this improved version of LCD compared to the old version is that the theoretical basis for the calculation of humics distribution is sound. The new version of the LCD model was applied to describe fulvic acid adsorption to goethite at different FA loadings, pH values and salt concentrations, and proton coadsorption with FA. The simulation shows that electrostatic interactions alone cannot explain the amount of FA adsorbed. However, by considering the formation of the innersphere complex between the carboxylic groups of adsorbed FA and the sites of the goethite surface, the model can simulate the effects of pH, salt concentration and the loading of FA on the adsorption of FA using only one adjustable parameter (Fig. 2). The crossing point of the two lines of two salt levels around pH 8-9 is the shifting point from a salt reduced adsorption at low pH to a salt enhanced adsorption at high pH. With the same set of model parameters, the proton coadsorption data can be simultaneously well described. The model simulation indicates that the formation of the chemical bond between the groups on FA and sites on goethite is the most important driving force for the adsorption of FA, whereas the electrostatic repulsion between the adsorbed FA particles is the most important factor that limits further adsorption. The mean-field assumption used in the model leads to a relatively small model artifact,

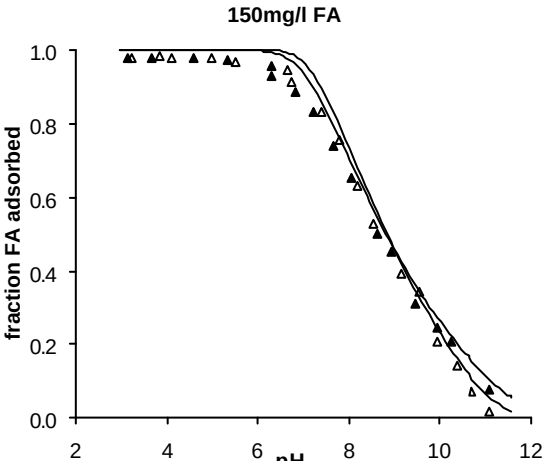

Figure 2. *Adsorption of FA to goethite calculated (lines) and measured (symbols). (filled symbols and thick lines: 0.1M $NaNO_3$, open symbols and thin lines: 0.015M $NaNO_3$*

which results in a somewhat overestimated electrostatic contribution to the adsorption energy.

The good agreement between the simulation and the data suggests that the LCD model structure is promising and leads to a better understanding of the behavior of humic substances at oxide surfaces.

References

[1] Filius, J.D.; Lumsdon, D.G.; Meeussen, J.C.L.; Hiemstra, T.; Van Riemsdijk, W.H. (2000) Adsorption of fulvic acid on goethite. *Geochimica Et Cosmochimica Acta*, 64(1): 51-60.

[2] Filius, J.D.; Meeussen, J.C.L.; Hiemstra, T.; Van Riemsdijk, W.H. (2001) Modeling the binding of benzenecarboxylates by goethite: The ligand and charge distribution model. *Journal of Colloid and Interface Science*, 244(1): 31-42.

[3] Filius, J.D.; Meeussen, J.C.L.; Lumsdon, D.G.; Hiemstra, T.; Van Riemsdijk, W.H. (2003) Modeling the binding of fulvic acid by goethite: the speciation of adsorbed FA molecules. *Geochim. Cosmochim. Acta.* 67(8): 1463-1474.

[4] Weng, L.P.; Koopal, L.K.; Hiemstra, T.; Meeussen, J.C.L.; Van Riemsdijk, W.H. (2005) Interactions of calcium and fulvic acid at the goethite-water interface. *Geochimica Et Cosmochimica Acta*, 69(2): 325-339.

[5] Weng, L.P.; Van Riemsdijk, W.H.; Hiemstra, T. (2006). Adsorption free energy of variable-charge nanoparticles to a charged surface in relation to the change of the average chemical state of the particles. *Langmuir*, 22: 389-397.

[6] Weng, L.P.; Van Riemsdijk, W.H.; Koopal, L.K.; Hiemstra, T. (2006). Ligand and Charge Distribution (LCD) model for the description of fulvic acid adsorption to goethite. *Journal of Colloid and Interface Science*, 302: 442-457.

URANIUM REDOX STATE AND $^{234}U/^{238}U$ RATIO ANALYSES IN URANIUM RICH SAMPLES FROM RUPRECHTOV SITE

J. Suksi[1]; U. Noseck[2*], J. Fachinger and S. Salminen[1]

[1] University of Helsinki, Laboratory of Radiochemistry, P.O. Box 55, FI-00014 Helsinki, Finland
[2] Gesellschaft für Anlagen- und Reaktorsicherheit, Theodor-Heuss- Str. 4, 38118 Braunschweig, Germany
[3] Forschungszentrum Jülich – Institut für Sicherheitsforschung und Reaktortechnik, 52425 Jülich, Germany

* Corresponding author: ulrich.noseck@grs.de

Abstract

A method for separation of uranium (IV) and uranium (VI) has been further developed for application to natural samples from uranium-rich tertiary clay horizon at Ruprechtov site, Czech Republic. It has been applied to four samples with different uranium content from different boreholes. The $^{234}U/^{238}U$ activity ratio in each phase was determined.

The results show, that both forms U(IV) and U(VI) exist in the tertiary clay horizon. The $^{234}U/^{238}U$ ratio significantly differs between the forms with values below unity between 0.45 and 0.91 in the U(IV) phase and values above unity between 1.26 and 3.37 in the U(VI) phase. On one hand it clearly shows the impact of a-recoil process on the U(IV) phase, indicating its low mobility in this horizon. On the other hand the finding of clear U(VI) phases and their high $^{234}U/^{238}U$ ratio indicate that at least part of the U(VI) phase was recently formed. Results are discussed with regard to uranium enrichment scenarios at the site.

Introduction

Analyses of enrichment processes of radionuclides under natural conditions can contribute to the understanding of the long-term behaviour of geological formations as part of the barrier system of a repository for radioactive waste. At Ruprechtov site, uranium occurs in concentrations up to 400 ppm in lignite-rich argillaceous sedimentary layers. Previous results showed that uranium accumulation occurred by a multi phase process. Secondary U(IV) phases uraninite and ningyoite as well as uranium bearing primary minerals monazite, xenotime and zircon were detected [4]. The secondary U(IV) minerals were shown to be at least partly accumulated by transport of U(VI) and subsequent reduction to U(IV) by oxidation

of As(0) in FeAsS surface layers on pyrite nodules to As(V) [1,2]. Application of the U(IV)/U(VI) separation method with analyses of the $^{234}U/^{238}U$-activity ratios can help to better understand the enrichment processes and give information about the stability of the respective phases.

Objectives

Major objective of the study is the further development of the method with respect to its application to the uranium-rich sedimentary samples from Ruprechtov site. After confirmation of its applicability the aim is to quantify U(IV) and U(VI) fractions in these sediments and receive further information about time scales and processes associated with the different phases.

Experimental

Uranium dissolution was performed by extracting the sample material with the mixture of 4 M HCl and 0.03 M HF in Ar-atmosphere. Solid to solution ratio was ~ 0.1. Uranium dissolution was intensified performing extraction in ultrasonic bath and at the same time mixing the solution with Ar-bubbling. Uranium could not be dissolved quantitatively. Dissolution yield varied between 50% and 90%. Insoluble U was thought to represent U(IV) minerals.

Oxidation states U(IV) and U(VI) were determined using a slightly modified method from the one presented in [3] U(IV) and U(VI) were separated from each others in anion exchange column regenerated with the extraction solution; U(IV) was collected in the first 20 ml and U(VI) was eluted with 20 ml of 0.1 M HCl. Separation is quantitative and no overlapping of U(IV) and U(VI) has been observed in the tracer experiments. Both fractions were purified from the daughters by another anion exchange step. Purified U was mounted on a plastic plate with "massless" CeF_3 precipitate for measurement. U concentration was determined using α-spectrometry. Alpha activities were measured by PIPS-detectors of 450 mm^2 area with a nominal resolution of 20 keV. A counting time varied between one and five days.

.

Results and discussion

The U(IV)/U(VI) separation was performed on four samples from three different boreholes in the so-called clay/lignite sand horizon, where uranium enrichment up to 500 ppm occurs in distinct layers of approx. 3 m thickness. Two samples were taken from borehole NA6, one from the major U-peak at 35 m and one from a second, smaller peak at 37 m. The other two samples were taken from the highest uranium peaks in borehole NA13 and NA14. The distance between each borehole is approx. 50 m.

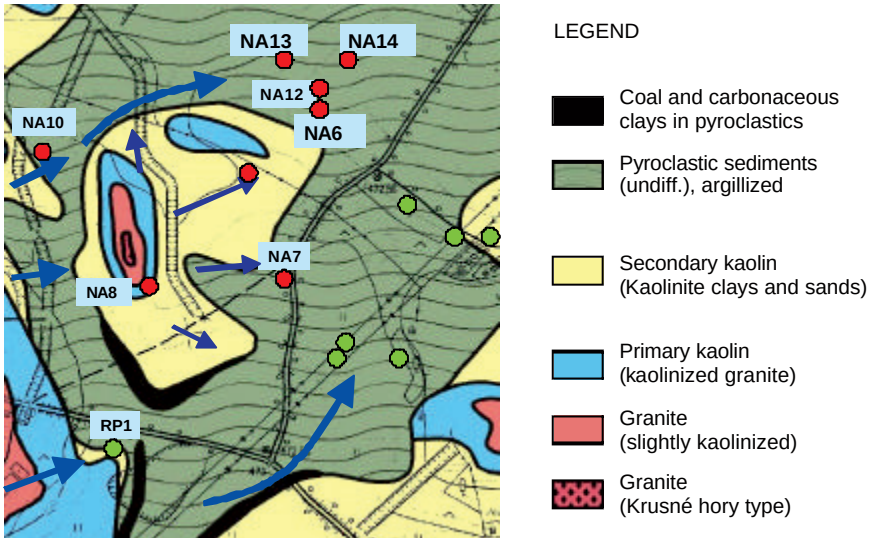

***Figure 1**: Location of the boreholes analysed for $^{234}U/^{238}U$ AR in groundwater and for U(IV)/U(VI) separation of immobile uranium phase (NA6, NA13, NA14)*

The results of all measurements are listed in Tab. 1. Total uranium content in the samples varies between 35 and 468 ppm with lowest uranium content in sample NA6, from 37 m depth (35 to 48 ppm). In the other samples uranium content is significantly higher with highest values of 468 ppm in NA6 from 35 m depth.

***Table. 1:** Amount of uranium and $^{234}U/^{238}U$-activity ratios in the different phases from uranium separation*

sample	U [ppm]	U(IV)		U(VI)		U(res, IV)		U(IV) total
		[%]	$^{234}U/^{238}U$	[%]	$^{234}U/^{238}U$	[%]	$^{234}U/^{238}U$	[%]
NA6 35a	356±7	28.7	0.54 ± 0.01	41.9	1.42 ± 0.02	29.5	0.65± 0.01	58.1
NA6 35b	468±9	45.9	0.56± 0.01	33.3	1.69 ± 0.03	20.7	0.64± 0.02	66.7
NA6 35c	369±8	23.3	0.47± 0.01	47.4	1.16± 0.02	29.3	0.67± 0.01	52.6
NA6 37a	37.3±2	73.7	0.79 ± 0.03	15.7	2.66± 0.07	10.6	0.73± 0.01	84.3
NA6 37b	47.5±1, 5	66.2	0.52± 0.01	9.0	3.37± 0.15	24.8	0.86± 0.02	91.0
NA6 37c	35.7±2	51.3	0.58± 0.01	19.8	2.56 ±0.08	28.9	0.71± 0.04	80.2
NA13 46	208±5	5.8	0.76± 0.07	43.9	1.23± 0.03	40.3		56.1
NA14 51	341±9	17.0	0.91± 0.04	41.5	1.27± 0.03	41.5		58.5

The first main observation is that immobile uranium consists of both U(IV) and U(VI). A second observation is that during the extraction procedure not all uranium is mobilized. The content of uranium in this residual phase is denoted as U(res).

The weight fraction of uranium in the different phases is graphically presented in Fig. 2 (left) and the corresponding $^{234}U/^{238}U$-activitiy ratios (denoted as AR) are shown in Fig. 2 (right). AR differs significantly in the U(IV) and U(VI) phases with ratios <1 in the U(IV) phase and ratios >1 in the U(VI) phase. The AR of the residual phase is very similar to that observed in the U(IV) phase. Taking into

account the higher stability of U(IV) phases we assume that residual uranium exists in oxidation state IV. Based on this assumption in all samples U(IV) represents the major uranium fraction with contents between 52 to max. 90 wt-%. The highest U(IV) fraction is found in sample NA6-37 which comprises the lowest total U content.

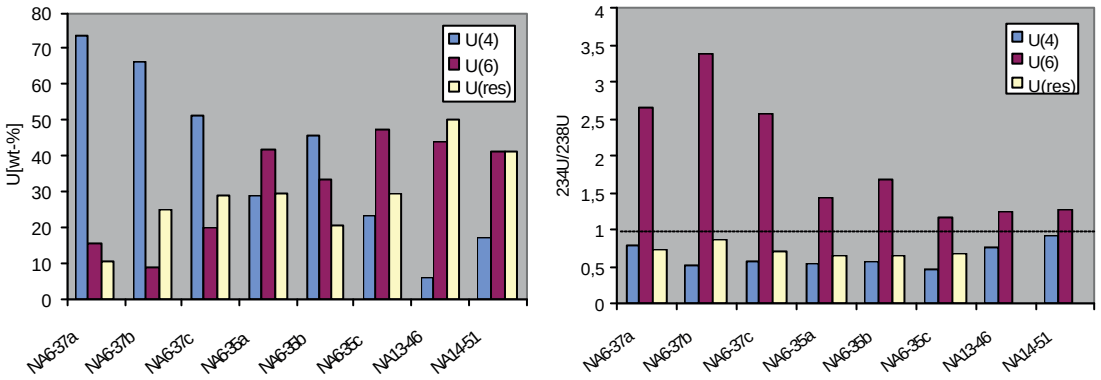

Figure. 2: *Fraction of uranium in U(IV), U(VI) and U(res) phase (left) and corresponding $^{234}U/^{238}U$ isotope ratios (right). The line has been drawn to show radioactive equilibrium.*

The $^{234}U/^{238}U$-activity ratios are strong indicators for the stability of the immobile uranium phases. Ratios significantly below unity are caused by the preferential release of ^{234}U. This is due to the a-recoil process and a correlated selective oxidation of the ^{234}U (e.g. [5]). In order to obtain low ratios of approx. 0.5 as observed in the U(IV) phase it must have been stable for sufficiently long time, i.e. no significant release of bulk U has occurred during at least the last several 100 kys. This is in agreement with the scenario assumed for the major uranium input into the clay/lignite horizon, which occurred during Tertiary, more than 10 Mio years ago [4]. This stability of the U(IV) phases is also supported by geochemical calculations based on groundwater conditions with low Eh values especially in NA6 in the clay-lignite horizon indicating stability of uraninite and ningyoite under the today conditions.

The $^{234}U/^{238}U$ activity ratio in the groundwater generally reflects the nature of water-rock interaction and is therefore sensitive to groundwater conditions (see [5]): in oxidising conditions both isotopes release in the groundwater in the ratio they occur in the rock and in anoxic conditions the release of ^{234}U is favoured. The low $^{234}U/^{238}U$ ratios in the U(IV) phase as observed in this study goes together with AR values >1 in porewater and groundwater from the clay/lignite horizon, which is shown in Fig. 3. This is expected because of the anoxic sediment conditions and preferred mobilisation of ^{234}U.

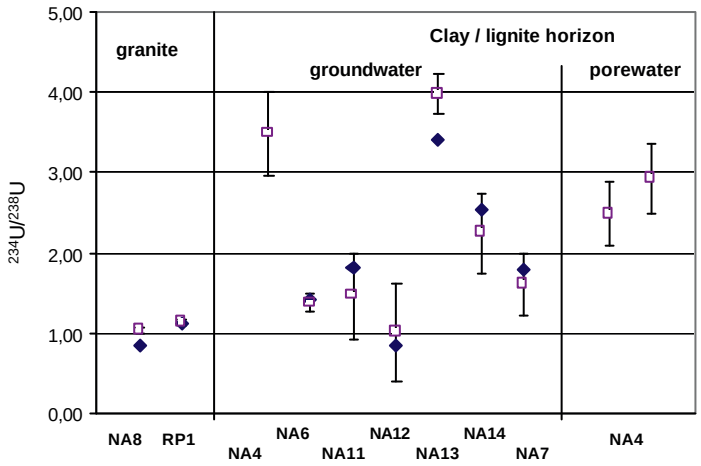

Figure. 3: *$^{234}U/^{238}U$ activity ratios in groundwater from outcropping granite boreholes with high water flow and groundwater /porewater from clay lignite horizon measured by a-spectrometry (open squares) and ICP-MS (filled)*

The variation of $^{234}U/^{238}U$ activity ratios in the groundwater of the different boreholes could be caused by differences in water flow conditions. In order to check this all available AR data of the different groundwaters are plotted versus the hydraulic conductivity of the corresponding water bearing horizons. At least for the clay/lignite horizon the hydraulic conductivity is considered as a suitable measure for water flow. Fig. 4 shows a clear trend, i.e. a decrease of $^{234}U/^{238}U$-activity ratio with increasing hydraulic conductivity.

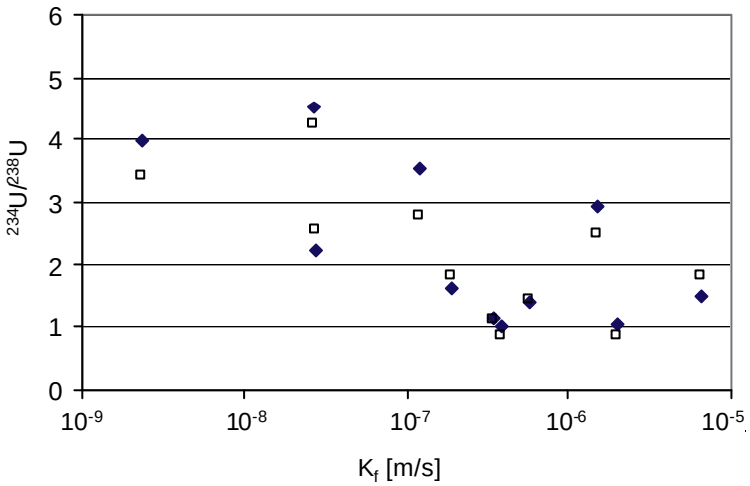

Figure. 4: *$^{234}U/^{238}U$ activity ratios in groundwater from granite and clay lignite horizon versus hydraulic conductivity*

For interpretation of activity ratios in the sedimentary U(VI) phase, we compare the data with the groundwater of corresponding horizons. The AR >1 indicates a recently formed (during the last several 100 ky) uranium phase. Therefore, it might be expected that this phase is more easily accessible and reflects a similar AR as the groundwater.

However, for the two samples from NA6 (35a and 35b) we recognize different values for the U(VI) phase. The value in the upper layer is about 1.2 to 1.7 and the value in the lower layer is in the range of 2.5 and 3.4. The value of the corresponding groundwater is about 1.4, i.e. similar to the value in the upper layer where also more U(VI) can be found. An explanation for different ARs in the U(VI) phase in the layers can be found in the spatially limited water flow in these horizons. The water transport mainly occurs on small fractures in the clay lignite or small sandy layers. For NA6 the water bearing layer overlaps with the area of the upper peak. The lower peak is approx. in 1 m distance of the water bearing layer. Therefore, the water exchange between pore water of the lower layer with smaller uranium peak is much slower than water exchange with the upper layer preventing U accumulation in the lower layer. As a result total U content in the lower layer remains smaller and the transfer process of ^{234}U from U(IV) phase to U(VI) phase is not as masked as in the upper layer, leading to observed ^{234}U enrichment in the U(VI) phase and in the porewater.

The AR in the U(VI) phases for NA13 and NA14 lies between 1.2 and 1.3. A comparison with groundwater is only possible for NA13, since NA14 water stems from the underlying granite horizon. The AR of groundwater from NA13 is 3.4 to 4, i.e. significantly higher than the value of the U(VI) phase in the sediment. This can be explained, if the major part of the U(VI) phase was not formed recently but over very long time scales. In this case one would expect to see much higher AR in the U(VI) phase, however. Another explanation for lower AR in the sedimentary phases than in the groundwater is that part of U(IV) is oxidised subsequently after sampling, either during U(IV)/U(VI) separation or during the time of sample storage. Partial oxidation of U(IV) with AR <1 after sampling would result in reduced AR for U(IV). Possible oxidation of U(IV) during the chemical separation procedure can be studied using U(IV) tracer in the procedure. In experiments with the ^{232}U(IV) tracer oxidation could not be observed.

The examination, whether oxidation occurred during sample storage is not done until now. It is planned to compare the results with those from a five step sequential extraction procedure and if possible to measure ARs of fractions from different steps. Furthermore it is planned to apply the method on samples, which have been stored under reducing conditions in a glove box directly after sample distribution.

Conclusions

The results from U(IV)/U(VI) separation identified the existence of both U(IV) and U(VI) phases in the uranium enriched clay/lignite horizon at Ruprechtov site. The major part of uranium is U(IV) and its fraction varies from 55 to 90 % in the investigated samples. This agrees well with results from SEM-EDX and µ-XANES and µ-EXAFS, which identified uraninite and phosphate (or sulphate) U(IV) minerals like ningyoite in hot spots found in the same horizon. The generally low $^{234}U/^{238}U$-activity ratios (<1) in the U(IV) fraction gives evidence that this phase is rather stable and immobile at Ruprechtov site because if water-sediment interaction had affected bulk U such activity ratios would not be possible.

The results for the U(VI) fraction are not so clear yet. At least part of U(VI) is recently formed. The AR in this fraction varies from 1.2 to 3.4 and is not in all cases similar to the fraction observed in groundwater. This can be explained, if part of U(VI) is formed more than several 100 ky ago. But a decrease of AR might also be caused by oxidation subsequent to sampling. A disturbance of the originally reducing conditions and therewith oxidation of U(IV) to U(VI) could occur either by the separation procedure or during storage of the sample material. However, oxidation of low $^{34}U/^{238}U$-activity ratio U(IV) fraction by the separation procedure can be excluded, since experiments with ^{232}U tracers do not show any oxidation of U(IV) to U(VI). Concerning possible oxidation during storage, further experiments are planned with sample material stored from the beginning in a glove box under reducing atmosphere. These experiments will focus on the direct comparison of µ-XRF and µ-XAFS on the one hand and U(IV)/U(VI) separation on the other hand on the same sample.

Acknowledgements

This work has been / is financed by the European Commission, the German Federal Minstry of Economics and Technology (BMWi) under contract no. 02 E 9551 and no. 02 E 9995.

References

[1] Denecke, M.A.; Janssens, K.; Proost, K.; Rothe, J.; Noseck, U. (2005) Confocal micro-XRF and micro-XAFS studies of uranium speciation in a tertiary sediment from a waste disposal natural analogue site, Env. Sci. Technol. 39, 2049-2058.

[2] Denecke, Havlova, (2006) Element correlations observed in Ruprechtov sediments from micro-focus fluorescence mapping and cluster analysis of sequential extraction results, Proceedings of the 2. Annual FUNMIG workshop, Stockholm, 21.-23. November 2006.

[3] Ervanne, H. and Suksi, J., (1996): Comparison of Ion-Exchange and Coprecipitation Methods in Determining Uranium Oxidation States in Solid Phases. Radiochemistry, Vol. 38, 324-327.

[4] Noseck, U.; Brasser, Th. (2006) Application of transport models on radionuclide migration in natural rock formations - Ruprechtov site, Gesellschaft für Anlagen- und Reaktorsicherheit (GRS) mbH, GRS-218, Braunschweig, March 2006.

[5] Suksi, J.; Rasilainen, K.; Pitkänen, P. (2006) Variations in the $^{234}U/^{238}U$ activity ratio in groundwater – A key to characterise flow system? *Physics and Chemistry of the earth*, Volume 31 (10-14), 556-571.

STUDIES OF THE SPATIAL WATER FLOW DISTRIBUTION AND COLLOID TRANSPORT IN A CRYSTALLINE ROCK CORE FROM ÄSPÖ WITH POSITRON EMISSION TOMOGRAPHY

M. Gründig[1*]; M. Richter[1]; J. Kulenkampff[1] and A. Seese[2]

[1] Institut für Interdisziplinäre Isotopenforschung, Permoserstr. 15, 04318 Leipzig, Germany
[2] Universität Leipzig, Klinik und Poliklinik für Nuklearmedizin, Stephanstr. 11, 04103 Leipzig, Germany

* Corresponding author: gruendig@iif-leipzig.de

Abstract

For the development of models of transport processes of contaminants in geological formations it is necessary to consider the influence of heterogeneous structures of the solid geological matrix. New investigation methods are required which enable to measure directly the spatial distribution of the flow parameters in representative samples.

In the present paper it is demonstrated that the positron emission tomography (PET) is a radiotracer method which allows to carry out such measurements with a sufficient spatial resolution. Spatially resolved data for modelling of the transport processes can be derived from the reconstructed images of the radiotracer concentration distributions.

The PET measurements are carried out in a granitic drill core with a longitudinal fracture from ÄSPÖ test site. Positron emitting radionuclides (^{86}Y, ^{18}F, ^{124}I) are used as radiotracers to describe transport processes of dissolved components and colloids in the crystalline matrix at various flow velocities. The reconstructed images of the spatial radiotracer concentration distributions in the fracture at different times are represented. Studies of organic colloid transport in the granitic fracture show that the transport velocity of the colloids is considerably lower than the velocity of the conservative tracer. On basis of the quantitative pixel values of the PET images the distribution functions of velocity and dispersivity are calculated. These PET results can be used in connection with tomographic X-ray structure measurements for validation of the modelling calculations. PET data are also the basis for the direct development, validation and parameter estimation of mesoscalic transport models which consider the influence of the real pore and fracture structures.

Introduction

The influence of heterogeneous structures of the solid geological matrix is increasingly considered for the modelling of geochemical transport processes. For these studies methods are required which enable to measure directly the spatial distribution of the mass flow. Appropriate investigations at potential host rock formations for final deposits for spent nuclear fuel are necessary to specify the occurring processes and to enhance the scientific fundamentals for the development of the prognostic models.

The positron emission tomography (PET) can determine spatially resolved transport distributions at samples and drill cores with real structures. The optimum use of information obtained by PET investigations of transport processes in geological layers demands a special evaluation system to determine spatially resolved model parameters. A combination of software modules of commercial PET cameras with components of other scientific image evaluation programs and special relations which consider the demands of process modelling are the basis of the geoscientific image evaluation system [1, 2].

Investigations in a granitic drill core from the hard rock laboratory Äspö demonstrate the information content of the PET method.

Objectives

In a granitic drill core from ÄSPÖ test site with a longitudinal fracture residence time measurements were done by FZK-INE using a $^{3}H_2O$ tracer. X-ray tomographic measurements of the pore structure were carried out at BAM Berlin. On basis of these data the transport modelling will be done by JGUM. The PET results of the spatially resolved radiotracer measurements of the solution transport in the fracture are used for the validation of the modelling suppositions.

Experimental

X-ray tomographic measurements of the pore structure were carried out at the Federal Institute for Material Research and Testing (BAM) Berlin.

Production of the tracer solution. The tracer [^{18}F]KF ($T_{1/2}$ = 110 min) was produced at the cyclotron of the Clinic and Polyclinic of Nuclear Medicine of the University of Leipzig. The tracer [^{124}I]KI ($T_{1/2}$ = 4.2 d) was produced at the cyclotron of the Clinic and Polyclinic of Nuclear Medicine of the University of Essen. The tracer nuclide ^{86}Y ($T_{1/2}$ = 14.7 h) was produced at the cyclotron of the Institute for Radiopharmacy, Research Centre Dresden - Rossendorf.

PET Measurement. The measurements were carried out at the commercial PET camera ECAT EXACT HR^{+}/CTI Siemens at the University of Leipzig.

A granitic drill core from Äspö test site (diameter 5 cm, length 15 cm) with a longitudinal fracture was enclosed in a plexiglass column. The core was flushed with CO_2 gas before the solution supply to avoid air inclusions in the fracture. A

constant water flow of 0.1 and 0.001 mL/min was realized using a double piston HPLC-pump (Waters 590). Between the pump and the core input a 6 way valve with a 5 ml dosing loop was installed for the tracer injection in form of a step-function. For solution transport studies 5 mL of the radiotracer solution (^{18}F[KF], 0.01 M KF, 300 MBq, 0.1 mL/min), (^{124}I[KI], 0.01 M KI, 150 MBq, 0.001 mL/min) were injected. For studies of the colloid transport humic acid (Aldrich) was marked with the PET nuclide ^{86}Y. 5 mL of the colloidal solution (40mg/L ^{86}Y[Y-HA], 100 MBq, 0.1 mL/min) were injected in form of a step function. The spatial tracer concentration distribution was measured with the PET camera in intervals of 15 min (solution transport) and 10 min (colloid transport) after the start of the tracer injection. A transmission measuring was carried out before the tracer measurement. With these data the radiation attenuation of the sample was corrected before the image reconstruction.

Results

The PET studies enable a quantitative analysis of the tracer concentration distribution, the calculation of the local distribution of the flow velocity and of the local dispersion parameters. The distributions of these parameters show the real influence of the solid state structure on the migration processes.

Studies of the colloid transport of ^{86}Y[Y-HA] in the granitic fracture show that the transport velocity of the colloids is considerably lower (Figure 3) than the velocity of the conservative tracer (Figure 1 and 2).

Investigations under very slow flow conditions (0.001 mL/min) indicate an additional effect. The slow decrease of the tracer concentration after the maximum value points to an influence of dead space or matrix diffusion processes (Figure 4).

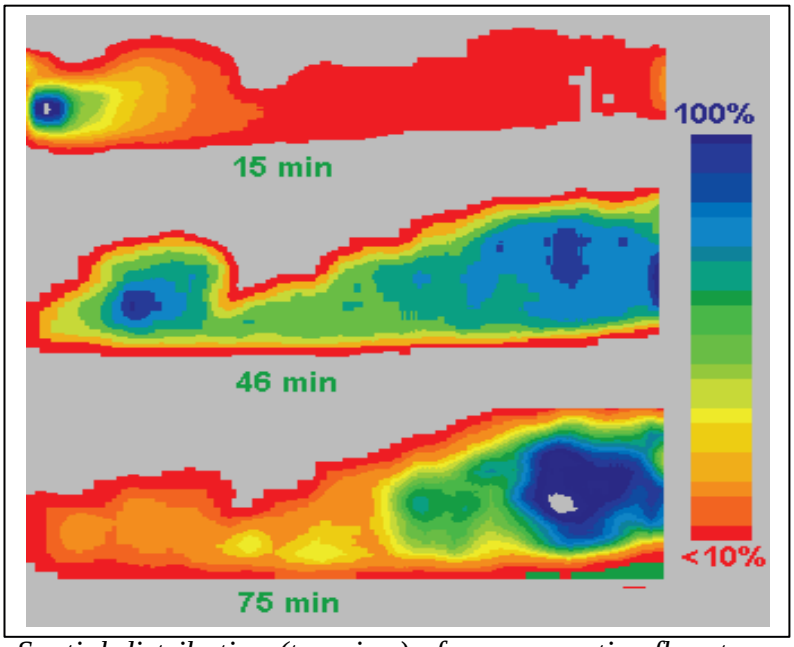

Figure 1*. Spatial distribution (top view) of a conservative flow tracer (^{18}F[KF]) in the fracture breadth of the Äspö drill core at different times (input solution flow: 0.1mL/min).*

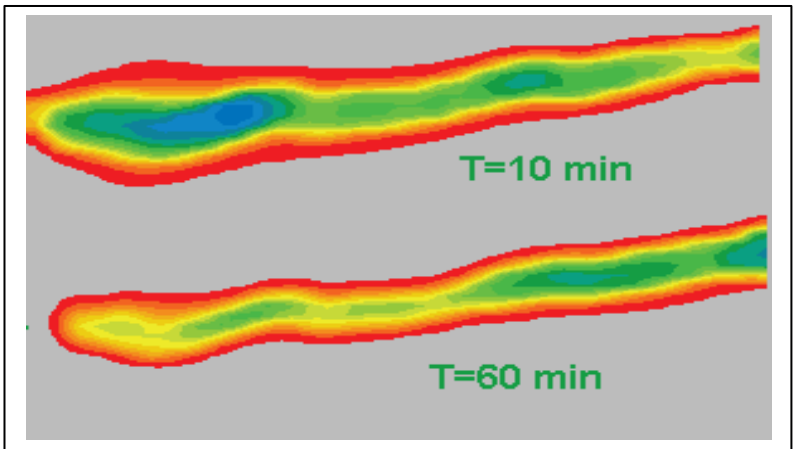

Figure 2. *Spatial distribution (side view) of a conservative flow tracer (^{18}F[KF]) in the fracture thickness of the Äspö drill core at different times (input solution flow: 0.1mL/min).*

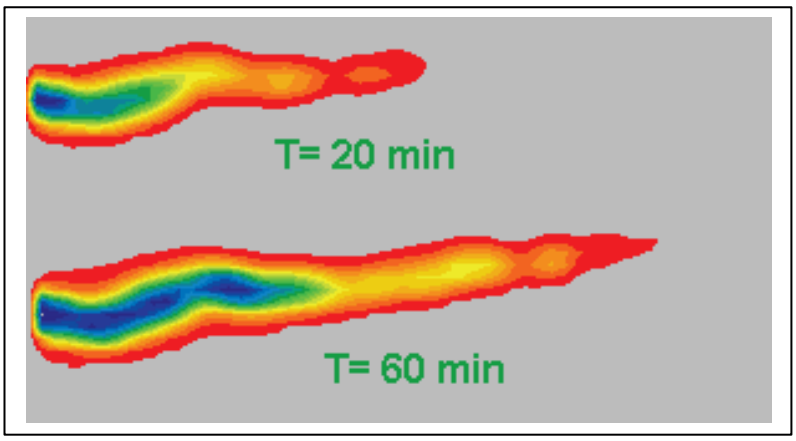

Figure 3*. Spatial distribution (side view) of a colloidal tracer (^{86}Y[Y-HA]) in the fracture thickness of the Äspö drill core at different times (input solution flow: 0.1mL/min). The breadth of the grey area is equivalent to the core length of 15 cm.*

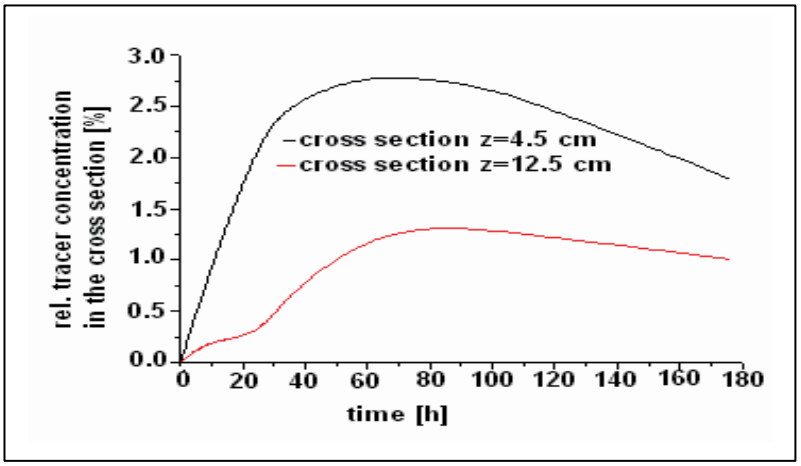

Figure 4*. Relative tracer concentration in two cross sections of the granitic fracture of the Äspö drill core, flow input: 0.001mL/min, tracer: ^{124}I[KI].*

The velocity and dispersion distributions were calculated on basis of the spatiotemporal tracer concentration distributions. A step tracer input function was used for the PET studies of the flow in the granitic fracture. The tracer concentration values in the area elements of two neighbouring cross sections of the core were determined at two times during the tracer transition and after saturation. The velocity and dispersion distribution can be estimated on basis of the one-dimensional dispersion model for each separate area element. Thus it is supposed that the transversal mixing effects are negligible owing to the short distance of the two cross sections compared with the longitudinal effects. The distributions (Figure 5 and 6) were calculated on basis of this modelling conception. The velocity distribution (Figure 5) can be used for the verification of modern modelling concepts for the transport in fractures which are filled with porous media of different structures. Different pore structures result in different velocity distributions [3].

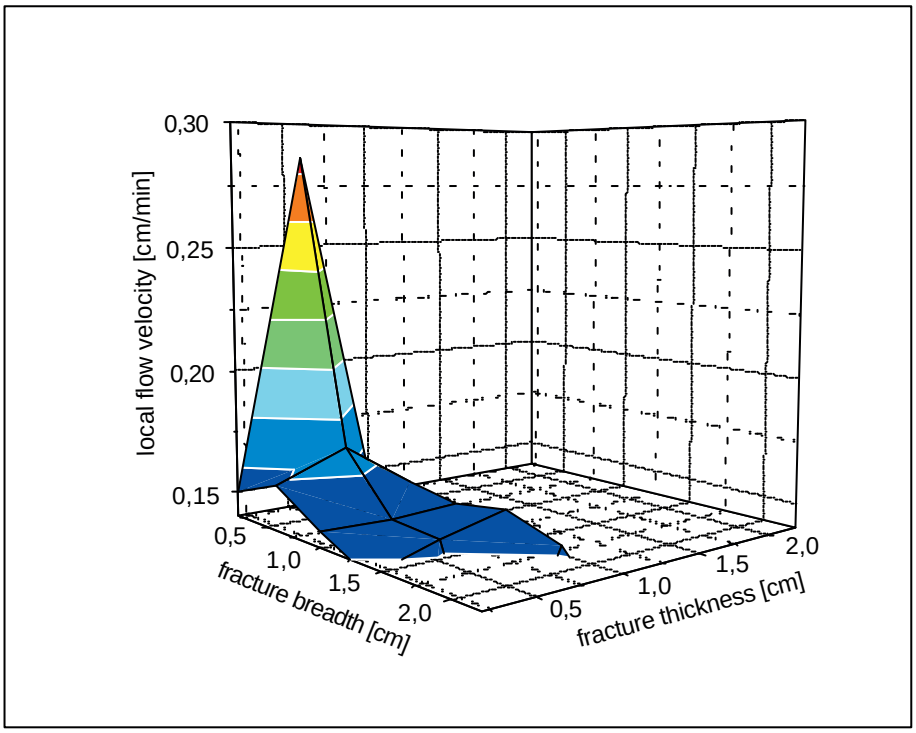

***Figure 5**. Local velocity distribution of colloids in the cross section of the fracture (distance 40 mm from the input section).*

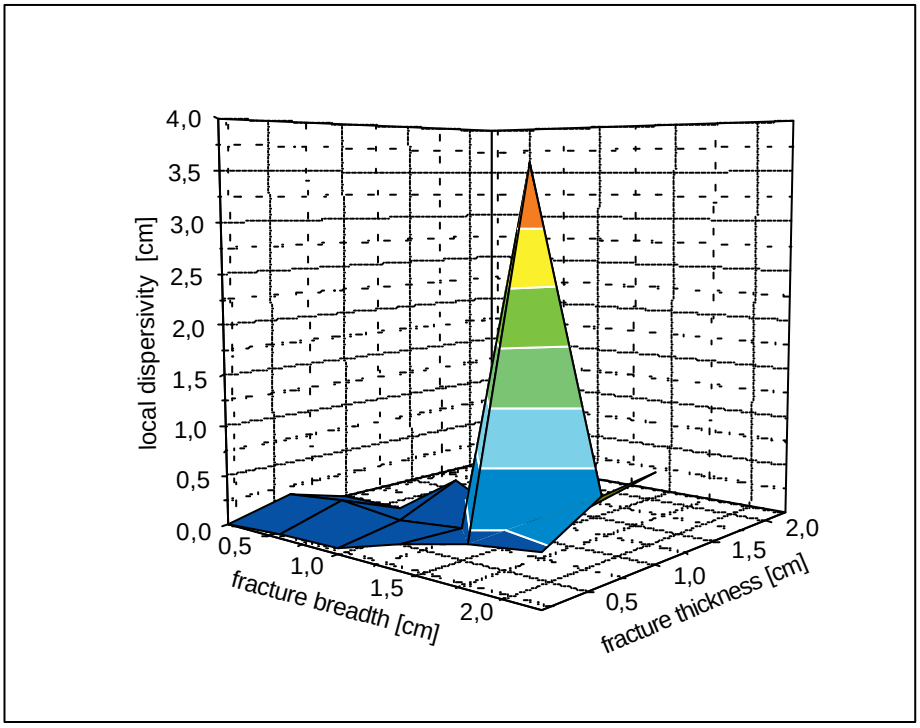

***Figure 6**. Distribution of the local dispersivity of colloid transport in the cross section of the fracture (distance 40 mm from the input section).*

Conclusions

The applicability of PET measurements for nondestructive investigations of the spatial distribution of transport processes in granitic drill cores is demonstrated. The method is suited for transport investigations of dissolved components and colloids. On basis of temporally resolved tracer experiments the data of the spatial distribution of velocity and dispersivity are calculated with a local resolution of 5 mm. These parameters show large variations in different regions of the fracture cross section. The values are the basis for the development, validation and parameter estimation of mesoscalic transport models which consider the influence of the real pore and fracture structures.

References

[1] Richter, M. (2002) Concepts for Modelling of Heterogeneous Flow Processes in Soil Columns on Basis of Tomographic Radiotracer Experiments in "Geochemical Processes – Concepts for Modelling of Reactive Transport in Soils and Groundwater" (Ed.: H. D. Schulz, G. Teutsch), Wiley-VCH, Weinheim, 20-38.

[2] Richter, M.; Gründig, M.; Zieger, K.; Seese, A.; Sabri, O. (2005) Positron Emission Tomography for Modelling of Geochemical Transport Processes in Clay, *Radiochimica Acta* 93, 1-9.

[3] Lunati, I.; Kinzelbach, W.; Sörensen, I. (2003) Effects of pore volume-transmissivity correlation on transport phenomena, *J. Cont. Hydr*. 67, 195-217.

RESULTS ON THE PU DIFFUSION IN THE OPALINUS CLAY

A. Bauer*, B. Fiehn, Ch. Marquardt, M. Klein, J. Römer, Th. Schäfer, A. Görtzen and B. Kienzler

Forschungszentrum Karlsruhe, Institut für Nukleare Entsorgung, PO Box 3640, D-76021 Karlsruhe

* Corresponding author: andreas.bauer@ine.fzk.de

Abstract

The Opalinus Clay (OPA) is a potential host rock for a repository for spent fuel, vitrified high-level waste and long-lived intermediate-level waste in Switzerland. Owing to its small hydraulic conductivity (10^{-14}-10^{-13} ms^{-1}), it is expected that transport of solutes will be dominated by diffusion. The diffusion is a very sensitive parameter in performance assessment (PA). The process is well understood for non-retarded solutes with simple chemistry, but little is known for retarded solutes. Therefore, the objective of this work is to understand the Pu-238 diffusion in clay mineral-rich geological formations in order to provide support for improved representation of these processes in performance assessment and to enhance safety case credibility.

We started our investigation with sorption experiments of Pu-238 on the Opalinus Clay (OPA) in the OPA porewater. According to the results of the batch sorption data, a strong Pu-238 sorption under the experimental conditions of the diffusion experiments is expected. The diffusion experiments were performed at two different initial pH values (pH 8.4, initial Pu-238 conc.: 5.63E-09 mol/L & pH 7.9, initial Pu-238 conc.: 5.38 E-09 mol/L). The continuously in-line measured Eh was found to be 440 mV for sample cell - autoclave system (**SCAS**) 1 and 392 mV for SCAS 2. In the OPA porewater Pu(V) is the dominant oxidation state in solution. The results of autoradiography indicate that that the Pu-238 diffusion within the OPA is inhomogeneous, without following an obvious preferential pathway.

Introduction

The objective of this work is to understand actinide diffusion in clay mineral-rich geological formations in order to provide support for improved representation of these processes in performance assessment and to enhance safety case credibility. The samples were collected in the Mont Terri underground

laboratory where the OPA is situated -200 to -300 m below the surface. Therefore a sample cell - autoclave system (**SCAS**) was developed for carrying out actinide diffusion experiments in clay stones under their natural, confining pressure. The pressure applied in our experiments was 30 bar to simulate the in-situ confining pressure of the natural system.

Experimental Set-up

The design of the INE diffusion cell /autoclave system (SCAS)

To counteract the swelling of clay in contact with groundwater and to simulate the confining stress within the geological formation, a specifically adapted experimental set-up was developed. The heart of the diffusion cell is a thin-walled stainless steel cell which holds the clay sample (∅ 20 mm, length 10 mm). All parts of the diffusion cell which are in contact with solution are coated with PEEK. The thickness of the wall of the stainless steel is 2/10 mm. After the positioning of the sample two PEEK distribution plates are placed on each side of the sample and the autoclave is sealed with screws. This cell is then placed in an autoclave. This autoclave has a volume of 300 ml and is filled with 250 ml of water. With help of a stainless steel pump we pressurized the autoclave with pressures between 0-100 kbars. Due to the construction of the cell, the confining pressure acts isotropically onto the clay sample. The tubing for tracers and sampling are constructed in such a way that they are kept under ambient pressure and tracer injection and sampling can be performed in closed circulation loops.

The solutions are circularly pumped from 100 mL PE storage containers in split cycles with a 2-channel peristaltic pump (IPC, Ismatec, Idex, USA). The Opalinus Clay samples were re-saturated by circulating these solutions in contact with the respective end of the sample for 5 weeks. This time was found to be sufficient to reach re-saturation [4] Subsequently, the solutions were replaced by fresh ones and the solution in the large container was spiked with the desired tracer.

Sample preparation and characterisation

The Opalinus (OPA) clay stone sample used for our experiments was provided by NAGRA from the Mont Terri underground research laboratory (URL). The bore core (BEZ A24/3) with a diameter of 100 mm was sliced into 2-cm-thick pieces using a diamond saw (no lubricating fluid was used). Each slice was cut in two parts. A 20mm diameter core was drilled out of the inner part of each slice to avoid the use of artificially oxidized clay rock material. All samples were drilled perpendicular to the bedding plane.

The residue of the core was ground in a glove box and the mineralogy of the samples was determined using X-ray diffraction. Quantitative analysis was performed using the Rietfeld method (TOPAS, Bruker AXS). The mineralogical composition is comparable to the one published in [1]. The porosity of the sample was measured by mercury porosimetry and was found to be 10 %. The total organic matter (TOC) in the starting material was measured to be 0.5-1.3 wt % using a LECO-125 C/S analyser.

After completion of the diffusion experiments the clay stone cores were pushed out of the diffusion cell and embedded in epoxy-resin (Struers, Fellbach, Germany) to avoid drying out of the sample. These samples were cut perpendicular to the bedding in two pieces using a diamond saw in the glove box (no lubricating fluid was used) after the epoxy-resin had hardened. The intersection was cleaned with Tesafilm (Beiersdorf, Hamburg) to remove remaining sawdust.

One half of the sample was used for autoradiography. Therefore, the phosphor storage screen technology was used (Cyclone, Storage Phosphor System, Packard Instrument Company, USA). The measurement period was between 1 h and 7 days. Radiation is stored in reusable phosphor screens of $BaFBrEu^{2+}$ crystals as defect energy. For reading out, the screens are scanned with a red laser and the emission of blue light stored in crystal defects is detected. The main advantages compared to film techniques are the higher sensitivity and the enhanced linear dynamic range. The lateral resolution is 600 dpi equal to about 40 µm. The a-activity of the Pu-238 in the diffusion sample was determined against a 500 ppm NIST standard of natural U-238.

In the other half of the sample, the diffusive Pu-238 profile in the rock was determined using the high-resolution abrasive peeling method [3]. Therefore, the sample was mounted on a sample holder and 46 grinding steps using a P220 abrasive paper and 32 grinding steps using a P80 abrasive paper were performed. The grinding paper was manufactured by Struers (Fellbach, Germany). The grinded samples were acidified (HNO_3, HF and HCl) and shaken for 24 hours.

Artificial Pore Water

The recipe for the artificial pore water used in the diffusion experiments is given in [4]

Activity measurements

The activity of the Pu-238 in solution was measured by liquid scintillation counting (LSC). 100 µl of the sample was acidified with 20 µl of 65 % HNO_3. Then 20 µl was placed in a 20-ml polyethylene (PE) counting vial and 10-ml scintillation cocktail was added (Ultima Gold XR, Canberra-Packard). The samples were vigorously shaken and placed in a liquid scintillation counter (Quantulus, WALLAC). The counting efficiency for each tracer was measured using artificial pore water with known amounts of activities. Background measurements were performed in a similar way using artificial pore water without radiotracers.

Sorption experiments

The Pu-238 sorption pH edge was measured at 20°C in the OPA porewater. All experiments were performed in a glove box under Argon atmosphere. The pH was adjusted by adding analytical grade KOH or HNO_3. The experiments were performed in 10 ml Polypropylene Copolymer centrifuge vials (Oakridge) with a solid/solution ratio of 2 g/L. At the end of the experiment the solid was separated from solution by centrifugation.

Starting from pH ~4.8 the Pu-238 concentration in solution is decreasing with increasing pH and reaches a sorption maximum at pH 7.2 (Fig. 1). Under alkaline conditions > 7 the Pu-238 concentration in solution is increasing again. According to the results of the batch sorption data a strong Pu-238 sorption under the experimental conditions of the diffusion experiments is expected.

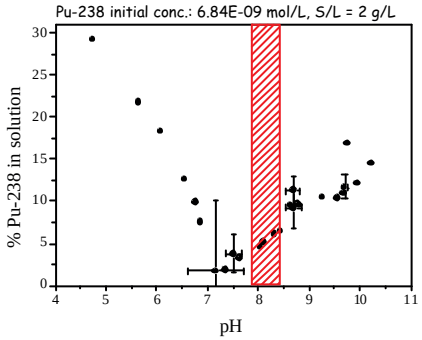

Figure. 1: *Sorption experiments of Pu-238 on Opalinus Clay. The filled pattern indicates the pH region of the diffusion experiments.*

Results on the Pu-238 diffusion in OPA

The diffusion experiments were performed at two different initial pH values. At pH 8.4 the initial Pu-238 concentration was 5.63E-09 mol/L in SCAS 1. In SACS 2 the initial pH was 7.9 and the initial Pu-238 concentration 5.38 E-09 mol/L. The pH of the OPA porewater remained unchanged throughout the experiment. The Pu-238 concentrations dropped in SCAS 1 by one order of magnitude to reach a plateau value of ~1.93E-10 mol/L after 400 hours. In the SACS 2 experiments the decrease in the Pu-238 solution concentration appeared faster. After 724 hours the maximum decrease in Pu-238 concentration was observed, followed by a "steady state" concentration of ~ 3E-10 mol/L. The continuously in-line measured Eh value using an IONODE SI30 gel redox-electrode was found to be 440 mV for SCAS1 and 392 mV for SCAS 2. Although glove-box operations were performed as careful as possible two times an intrusion of oxygen (~ 8000 ppm for 12-24 hours) into the glove box was monitored

On the blank concentration side of the experiments the first a-activity was measured after 30 days experimental duration. A selective Pu extraction indicated that the detected a-activity was not due to through-diffusion of Pu-238, but came from Th-228 released to the solution from the Opalinus clay sample.

At the end of the SACS 2 experiment the autoclave system and connected tubings were washed for two hours with 65 % HNO_3 to check sorption to the experimental set-up. This test showed that around 50-60 % of the initial Pu-238 concentration was sorbed on the container walls and tubings of the diffusion experiment.

Pu-238 oxidation states in solution

The Pu-238 oxidation states (Fig. 2) as a function of time in the Opalinus porewater were determined by BMBP-extraction [2]. Whereas in the stock solution

85 % Pu(VI) and 15 % Pu(IV) were observed the Pu oxidation state changed to predominantly Pu(V) (85%) after four days equilibration time in the OPA porewater. In the Opalinus porewater the pH was adjusted to pH 8.2. After two months the Pu-238 oxidation states changed to 10 % Pu(IV), 80 % of Pu(V) and 10 % of Pu(VI) in the OPA porewater. At the end of the experiment SACS 2 the Pu oxidation state in the solution was also determined. Like in the Opalinus porewater without contact to the Opalinus clay we found as the dominant oxidation state Pu(V) with 77 %, followed by Pu(IV) 17 % and 6% Pu(VI).

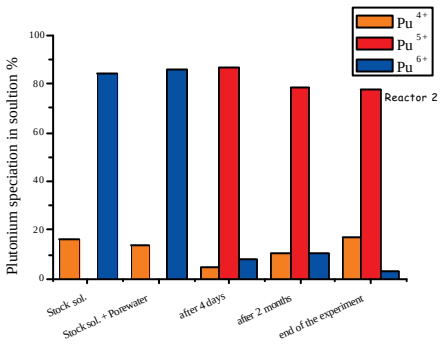

Figure. 2*: Pu-238 speciation in the OPA porewater and in the solution of SACS 2 determined by BMBP-extraction. The Pu-238 concentration of the stock solution was 2E-07 mol/L. In the OPA porewater the Pu-238 concentration was 4 E-09 mol/L and at the end of the experiment in Reactor 2 (after 93 days) 3.12E-010 mol/L.*

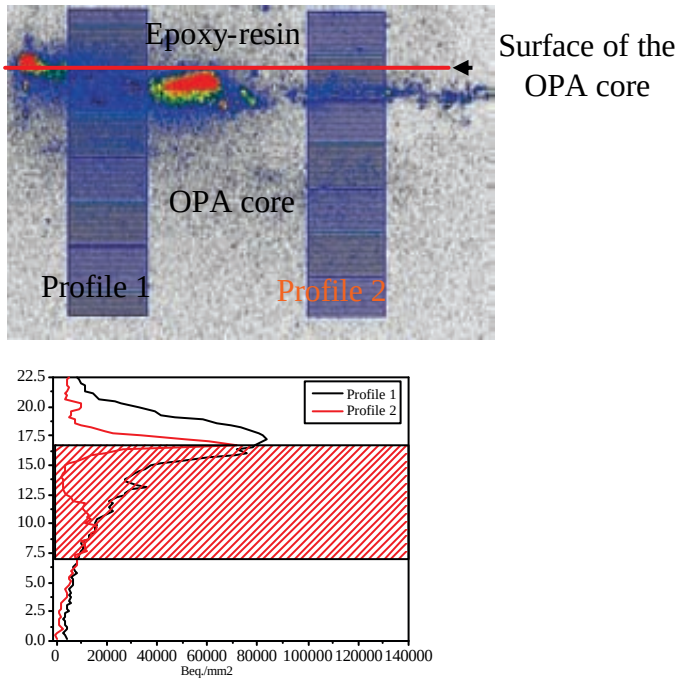

Figure. 3: *Two different diffusion profiles measured with autoradiography. The filled pattern indicates the clay sample. The dotted line indicates the background radiation from the Opalinus clay. Each horizontal bar represents a data point in the diffusion profile. The different colors represent different concentrations. Red indicates the highest and the grey color the lowest concentration.*

Autoradiography

Traces of saw dust contaminated the embedding medium (epoxy-resin), therefore the interface between embedding medium and the clay sample was difficult to determine (Figure 3). The figure also shows clearly that no preferential pathways for the migration of Pu-238 exist. It is evident that the Pu-238 diffusion within the Opalinus Clay is not homogenous. The Pu-238 is concentrated in Figure 3 in two distinct areas (red spots) and on the left side of the picture. SEM-EDAX analysis showed no specific elemental concentration or any specific mineral phase in this area. The measured profiles are subsequently different for the two sides of the sample. Whereas profile 1 shows the diffusion of the Pu-238 of ~ 5 mm at the end of the experiment (93 days) the diffusion in profile 2 is much more restricted (~ 1 mm). The background activity varied between 5000-10000 Beq./mm^2.

Conclusions

Trustworthy determination of the diffusion behavior of actinide ions in clay requires carefully designed experimental set-ups and development and application of a series of analytical techniques. Careful cross-checking is required in order to verify that the samples are not subject to undue disturbances, especially those resulting in preferential artificial transport pathways. Furthermore, delineation of natural activity inventory from the studied ions and identification of inventory lost in the equipment is a precondition for adequate interpretation of the experimental results. Trustworthy interpretation of transport experiments also requires batch sorption data and 3D distribution of along the diffusion samples. The present work shows that all these objectives have been demonstrated for an in-house built diffusion experiment system and development and application of the required associated analytical techniques. For this purpose Pu transport in an Opalinus clay core was studied. This initial demonstration and experimental development experiment shows that (i) about 40 % of Pu is sorbed on components of the experimental set-up, (ii) there is considerable impact of the samples natural alpha-emitting inventory, (iii) the mobile Pu inventory is dominated by Pu(V), and there is no preferential transport pathway for Pu in the clay sample.

These ongoing investigations will provide the necessary basis for credible description of sorbing radionuclide mobility in clay for the nuclear waste disposal safety case.

References

[1] NAGRA, 2002. Projekt Opalinuston; Synthese der geowissenschaftlichen Untersuchungsergebnisse, Wettingen.

[2] Nitsche, H., Roberts, K., Xi, R., Prussin, T., Becraft, K., Mahamid, I. A., Silber, H. B., Carpenter, S. A., and Gatti, R. C., 1994. Long Term Plutonium Solubility and Speciation Studies in a Synthetic Brine. *Radiochim. Acta* 66.

[3] Pearson, F. J., 1998. Opalinus Clay experimental water: A1 Type, Version 980318. In: TM-44-98-07, P. I r. (Ed.). Paul Scherrer Institut, Villigen PSI, Switzerland.

[4] Van Loon, L. R. and Eikenberg, J., 2005. A High Resolution Abrasive Method for Determining Diffusion Profiles of Sorbing Radionuclides in Dense Argillaceous Rocks. *Applied Radiation and Isotopes , ,* 11-21.

[5] Van Loon, L. R., Soler, J. M., and Bradbury, M. H., 2003. Diffusion of HTO, Cl-36(-) and I-125(-) in Opalinus Clay samples from Mont Terri - Effect of confining pressure. *J. Contam. Hydrol.* 61, 73-83.

INTERACTION OF Th WITH HUMIC ACID OVER A WIDE pH REGION

G. Szabó[1*], J. Guczi[1], H. Geckeis[2], P. Reiller[3] and R. A. Bulman[4]

[1]National Research Institute for Radiobiology and Radiohygiene, PO Box 101, Budapest, H-1775, Hungary;
[2]Forschungszentrum Karlsruhe, Institut für Nukleare Entsorgungstechnik, 76021 Karlsruhe, Germany,
[3]Commissariat á l'Énergie Atomique, CE Saclay, Nuclear Energy Division/DPC/SERC, Laboratoire de Spéciation des Radionucléides et des Molécules. F-91191 Gif-sue-Yvette CEDEX, France;
[4]Radiation Protection Division Division, Health Protection Agency, Chilton, Didcot, United Kingdom, OX11 ORQ.

*Corresponding author; szabogy@hp.osski.hu

Abstract

The influence of humic substances on the migration of tetravalent actinides in the far-field of nuclear waste repositories has been modeled by examining the uptake of Th(IV) by a silica/humic acid composite. It is anticipated that this material might serve as a geochemical model of the humate-coated minerals that are likely to be present in the vicinity of the repositories. The binding of Th(IV) by the immobilized humic acid was examined at pH 1-9 in 0.1 mol l^{-1} $NaClO_4$ by the batch method. Th(IV)-humate conditional stability constants have been evaluated from data obtained from these experiments by using non-linear regression of binding isotherms. The results have been interpreted in terms of complexes of 1:1 stoichiometry.

Introduction

Safety assessments of radioactive waste disposal in geologic formations have to draw upon *in vitro* studies as well as by environment-based investigations. As pointed out in the literature [1, 2], formation of complexes with humic substances might play an important role in the migration behaviour of radionuclides such as those of the transuranic series. Predictably, both sets of literature are extensive. Reports by Choppin and his co-workers [3, 4], Moulin and Ouzounian [5] Moulin and Moulin [6] and Zhang et al. [7] give accounts of the relevant literature for both research topics.

Satisfactory data on tetravalent and redox sensitive actinides are scarce due to experimental difficulties, namely, the low solubility of their oxide-hydroxide [8, 9] and their high affinity for vessel walls [10]. In order to study the interaction between humic acid, especially when adsorbed on to the surface of minerals, and dissolved redox sensitive radionuclides, it is advantageous to reduce the number of uncertain experimental parameters. This can be achieved by using chemical analogues (eg Th(IV)) of transuranic tetravalent actinides [11, 12]. In previous studies the composite material SiO_2-HA has been used to evaluate conditional stability constants for complexes formed by Am^{3+} and Eu^{3+} with humic acid [13]. Previous experiments have shown, that silica carrier does not contribute to metal binding [14]. Therefore, humic acid is responsible for the pH dependence of Th binding processes.

Objectives

Migration of species such as Pu(IV) in groundwaters away from nuclear waste repositories is likely to be mediated by complexation with humic acid in solution and also on the surfaces of minerals. Data to aid in such modelling scenarios have been obtained as conditional stability constants (β) of humate complexes of Th(IV), a species similar to Pu(IV), by using as a model substrate a silica-humic acid composite (SiO_2-HA) prepared by chemical immobilization of humic acid on silica gel.

Experimental

Materials and methods

The chemically bound humic acid on silica gel (SiO_2-HA) was prepared and characterized as described elsewhere [13]. Stock solutions of Th(IV) were prepared by dissolving thorium nitrate pentahydrate in 0.1 mol l^{-1} $NaClO_4$ at different pHs to obtain the concentrations 10^{-7} mol l^{-1}. The Th(IV) concentrations in solutions were determined by ICP-MS (HP-4500, Hewlet-Packard, USA).

Determination of binding isotherms of Th(IV) on SiO2-HA

Accurately weighed quantities of the gels, typically about 2 mg, were added to 20 ml of 0.1 mol l^{-1} $NaClO_4$ solutions (pH 1-9) containing different concentrations (10^{-8} - 10^{-7} mol l^{-1}) of Th(IV). The resulting suspensions were shaken at room temperature for 48 h. Total concentrations of Th(IV) in a clarified aliquot, which was collected by centrifugation, were measured by ICP-MS. After sorption, the Th(IV) sorption on to vial walls was determined. The vials were washed with distilled water and dried, then 10 ml aliquots of 2 mol l^{-1} $HClO_4$ were added and the vials shaken for 48 h. The Th(IV) concentration in the washing solutions was determined by ICP-MS. The amount of Th(IV) bound by SiO_2-HA was calculated as the difference between the initial Th(IV) concentration (10^{-8} -10^{-7} mol l^{-1}) and the sum of the amounts of Th(IV) remaining in solution and Th(IV) sorbed on to the vial walls. Isotherms were then plotted.

Calculation of conditional interaction constants (β) of Th_{total} from binding isotherm

The conditional interaction constant (β) is relative to the following equilibrium:

$$M^{z+} + HA \leftrightarrow MHA \qquad \text{(Eq. 1)}$$

$$\text{with } \beta = \frac{[MHA]}{[M^{z+}]_f \; [HA]_f} \qquad \text{(Eq. 2)}$$

where:

M^{z+}: the metal cations; HA: the humic acid; [MHA]: the concentration of the metal humate complex; $[M^{z+}]_f$: the concentration of the free thorium ion; $[HA]_f$: the concentration of the free humic acid.

The assumption is made that the macromolecule is the central group and the complexation can be described in terms of a Langmuir-type adsorption equation. The free ligand concentration can be calculated in Eq. 2 by introducing B_{max}

$$[HA]_f = [B_{max}] - [MHA] \qquad \text{(Eq. 3)}$$

where:

B_{max}: maximal complexing capacity of humic acid at the experimental condition

A combination of Eqs. 2 and 3 gives the relationship that could be used for calculation of conditional interaction constants:

$$\beta = \frac{[MHA]}{[M^{z+}]_f \; ([B_{max}]- [MHA])} \qquad \text{(Eq. 4)}$$

or after alteration

$$[MHA] = \frac{\beta \; [Mz+]f \; Bmax}{1 + \beta \; [M^{z+}]_f} \qquad \text{(Eq. 5)}$$

After plotting the bound Th(IV) [MHA] versus $(Th_{total})_{free}$ $[M^{z+}]_f$ and using the binding isotherms, the maximal binding capacity and the conditional interaction constants (β) of Th_{total} could be determined.

Calculation of conditional interaction constants (β) of ThHA

The reaction between Th^{4+} and HA can be written

$$Th^{4+} + HA \leftrightarrow ThHA \qquad \text{(Eq. 6)}$$

$$\text{with } \beta = \frac{[\text{ThHA}]}{[\text{Th}^{4+}]_f \, [\text{HA}]_f} \qquad \text{(Eq. 7)}$$

Th^{4+} is readily hydrolysed and it is not expected that only Th^{4+} ions exist in solution beyond pH 3. From the $Th(IV)_{total}$ the $[Th^{4+}]$ can be calculated by using the stability constants of the hydroxo complexes [8, 12]:

$$[Th(IV)]_{total} = [Th^{4+}] + [Th(OH)^{3+}] + [Th(OH)_2{}^{2+}] + [Th(OH)_3{}^{+}] + [Th(OH)_4] \qquad \text{(Eq. 8)}$$

$$[Th(IV)]_{total} = [Th^{4+}] \, \alpha_{Th} \qquad \text{(Eq. 9)}$$

where α is the Ringböm coefficient [15] concerning inorganic complexation:

$$\alpha = 1 + \sum_i \left[\frac{{}^{*}\beta_i}{[H^+]}\right]^i$$

If we assume that the hydrolysed species is not involved in the interaction with humic acid and measure the total Th(IV) concentration in the liquid phase, it becomes possible to calculate the conditional interaction constants (log β) of ThHA using the following equation:

$$\log \beta_{total} + \log \alpha_{Th} = \log \beta_{ThHA} \qquad \text{(Eq. 10)}$$

Results and Discussion

The main characteristics of SiO2-HA are reported in Table 1.

Table 1. *Characteristics of SiO2-HA*

Substrate content (mg g^{-1})	19.9 ± 1.2
Proton exchange capacity (μeq g^{-1} solid matter)	67.3
BET surface area [a] (m^2 g^{-1})	74 ± 8

[a] The surface area of the parent silica gel is 100 m^2 g^{-1}

Determination of conditional interaction constants (β) of Thtotal from binding isotherm

Typical binding isotherms (solid phase concentration vs. liquid phase concentration in equilibrium) of Th(IV) on SiO_2-HA at 1-6 pH values in 0.1 mol l^{-1} $NaClO_4$ are presented in Fig. 1. By using the nonlinear regression on the binding isotherms (Eq. 5), the conditional interaction constants (β) of Th_{total} with humic acid can be calculated (see Table 2 and Figure 2). From Table 2 and Figure 2, it is apparent that the conditional interaction constants appear insensitive to pH. It proves that this calculation is related to the Th_{total} and not to Th^{4+}.

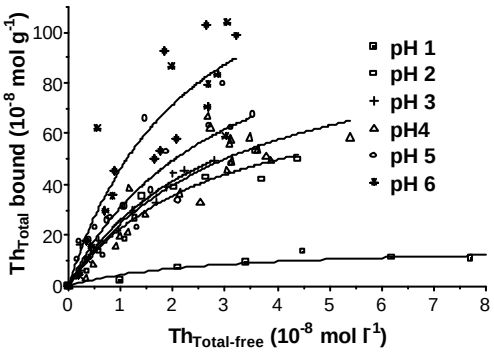

***Figure. 1**. Binding isotherm of SiO_2-HA for Th(IV) in 0.1 mol l^{-1} $NaClO_4$*

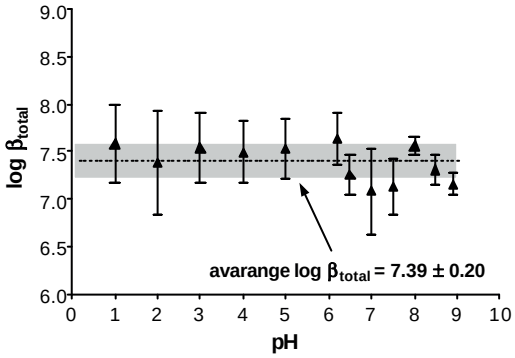

***Figure. 2.** dependence of the interaction constants log $ß_{Total}$ for Th humic complexes as a function of pH*

Calculation of the conditional interaction constants of ThHA (log β_{ThHA})

The log β values for Th_{total} with humic acid are presented in Table 2. From this table the conditional interaction constants of Th^{4+} with humic acid (β_{ThHA}) can be calculated by using Eq. 10 and hydrolysis constants from Neck and Kim [8]. Fig. 3 shows the pH dependency of log β_{ThHA}. The β_{ThHA} varies between $10^{7.58}$ at pH 1 to $10^{24.35}$ at pH 9. The regression line has the following equation:

$$\log \beta_{ThHA} = 2.21\ pH + 1.99 \text{ with } r^2 = 0.896.$$

The observation that the β value increases with pH is expected since this behaviour is observed on complexation of metal ions by humic substances (16, 17).

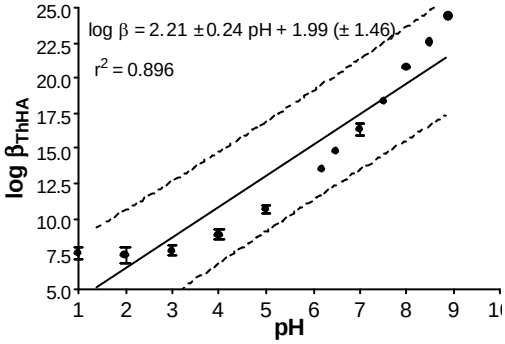

***Figure. 3**. Variation of the stability constants log β_{ThHA} for Th^{4+} humic complexes as a function of pH.*

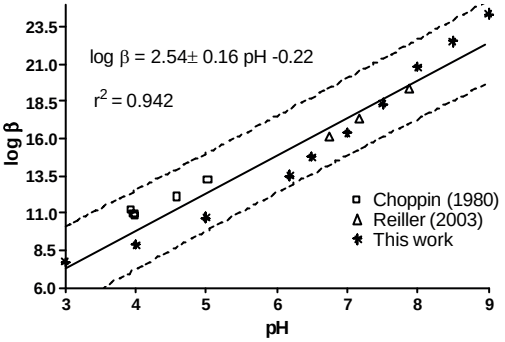

***Figure. 4.** Comparison of the log β_{ThHA} values obtained in this study with other reported values.*

***Table 2**. Conditional interaction constants (log β) of Th_{total}, side reaction coefficient (log α_{Th}) and log β_{ThHA}, as a function of pH in 0.1 mol l^{-1} $NaClO_4$, according to the hydrolysis constants from Neck and Kim [8]*

pH	Log β_{total} (l mol^{-1})	Log α_{Th}	Log β_{ThHA} (l mol^{-1})
1.02	7.58 ± 0.42	0.01	7.59 ± 0.42
1.98	7.38 ± 0.55	0.06	7.44 ± 0.55
3.09	7.54 ± 0.36	0.18	7.72 ± 0.36
4.07	7.49 ± 0.33	1.38	8.87 ± 0.33
5.07	7.53 ± 0.31	3.17	10.70 ± 0.31
6.192	7.64 ± 0.27	5.87	13.51 ± 0.27
6.57	7.25 ± 0.21	7.50	14.75 ± 0.21
7.03	7.08 ± 0.45	9.30	16.38 ± 0.45
7.54	7.13 ± 0.29	11.20	18.33 ± 0.29
8.06	7.56 ± 0.10	13.20	20.78 ± 0.10
8.53	7.31 ± 0.16	15.20	22.51 ± 0.16
8.92	7.16 ± 0.12	17.20	24.35 ± 0.12

It is interesting to compare our results with other values from the literature [17, 18] at the environmentally significant pH values, providing that the hydrolysis constants are the same. The log β_{ThHA} values, calculated from the procedure of Baes and Mesmer [19], are reported in Figure 4. It can be seen that there is a satisfactory agreement between the three independent data sets.

Modelling

The present work contributes to providing global interaction parameter of Th-humate that varies with pH. This parameter can be applied in the geochemical modelling of the migration of Th(IV) and Pu(IV) under the influence of humic substances. The authors have no doubt about using assumption that hydrolysed Th species is not involved in the interaction with humic acid, is an over simplification of the processes. However, deduction of complexation constants for individual Th(OH)x-HA without exact determination of species can give only fitting parameters not chemical reality.

Conclusions

The ready synthesis of SiO_2-HA has been established. The potential of such materials to complex cations such as Th^{4+} has been demonstrated. From an examination of the sorption isotherms of Th(IV) at different pHs it is apparent that conditional stability constants of Th^{4+} (log β_{ThHA}) can be easily calculated. This investigation indicates that humic acid materials such as SiO_2-HA are likely to be of value for modelling the role of humates in interacting with complexes of transuranic entities, such as Pu(IV) and Am(III), in groundwaters.

Acknowledgements

This work was partly supported by European Commission, EC Contract No. FP6-516514 (FUNMIG).

References

[1] Choppin, G.R., Allard, B.: Complexes of actinides with naturally occurring organic compounds. In: Handbook on the Physics and Chemistry of the Actinides (Freeman, A.J., Keller, C. Eds.) Amsterdam 1986, Chap 11.

[2] Kim, J.I.: Chemical behaviour of transuranic elements in natural aquatic system. In: Handbook on the Physics and Chemistry of the Actinides (Freeman, A.J., Keller, C. Eds.) Amsterdam 1986, Chap 8.

[3] Choppin, G. R.: Humics and radionuclide migration. Radiochim. Acta, 44/45, 23 (1988).

[4] Choppin, G. R.: The role of natural organics in radionuclide migration in natural aquifer system. Radiochim. Acta, 58/59, 113 (1992).

[5] Moulin, V., Ouzounian G.: Role of colloids and humic substances in the transport of radioelements through the geosphere. Appl. Geochem. Suppl., 1, 179 (1992).

[6] Moulin, V., Moulin, C.: Fate of actinides in the presence of humic substances under conditions relevant to nuclear waste disposal. Appl. Geochem., 10, 573 (1992).

[7] Zhang, Y. J., Bryan, N. D., Livens, F. R., Jones, M. N.: Selectivity in the complexation of actinides by humic substances. Environ. Pollut., 96, 361 (1997).

[8] Neck, V., Kim, J.I.: Solubility and hydrolysis of tetravalent actinides. Radiochim. Acta, 89, 1 (2001).

[9] Fanghanel, Th., Neck, V.: Aquatic chemistry and solubility phenomena of actinide oxides/hydroxides. Pure Appl. Chem., 74, 1895 (2002).

[10] Östhols, E.: Thorium sorption on amorphous silica. Geochim. Cosmochim. Acta, 59, 1249 (1995).

[11] Choppin, G.R.: Utility of oxidation state analogs in the study of plutonium behaviour. Radiochim. Acta, 85, 89 (1999).

[12] Reiller, P.: Prognosticating the humic complexation for redox sensitive actinides through analogy, using the charge neutralisation model. Radiochim. Acta, 93, 43 (2005).

[13] Szabó, Gy., Guczi J., Koblinger-Bokori E., Bulman R.A.: An examination of the sorption characteristics of 241Am(III) and Eu(III) bound by humic substances chemically immobilized on silica gel. Radiochim. Acta, 82, 355 (1998).

[14] Bulman, R.A., Szabó, Gy., Clayton, R.F., Clayton, C.R.: Investigation of the uptake of transuranic radionuclides by humic and fulvic acids chemically immobilized on silica gel and their competitive release by complexing agents. Waste Management, 17/4, 191-199 (1997).

[15] Ringböm A., Complexation in Analytical Chemistry, Interscience, New York, 1963.

[16] Hummel, W.: Binding Model for Humic Substances. In: Modelling in Aquatic Chemistry, Ed. Grenthe, I., Puigdomenech, I., NEA-OECD (1997).

[17] Reiller, P., Moulin, V., Casanova, F., Dautel, C.: On the study of Th(IV)-humic acid interactions by competition sorption studies with silica and determination of global interaction constants. Radiochim. Acta, 91, 513 (2003).

[18] Nash, K. L., Choppin, G. R.: Interaction of humic and fulvic acids with Th(IV). J. Inorg. Nucl. Chem. 42, 1045 (1980).

[19] Baes, C. F., Mesmer, R. E.: The hydrolysis of cations. Wiley Interscience Publication, New-York (1976).

SORPTION OF REDOX SENSITIVE ACTINIDES ONTO GRANITE AND ALTERED MATERIAL FROM ÄSPÖ HRL

J. Römer*, B. Kienzler and D. Schild

Institut für Nukleare Entsorgung, Forschungszentrum Karlsruhe GmbH
D-76021 Karlsruhe, GERMANY

* Corresponding author: roemer@ine.fzk.de

Abstract

Sorption experiments with redox sensitive actinide elements such as Pu, Np and U as well as the fission product Tc are performed onto fracture filling material, which are obtained from Äspo Hard Rock Laboratory. Migration experiments using these elements showed a complex retention pattern along the flow path. For this reason a new SEM/EDX analysis technique was applied for identification retaining mineral phases. From previous investigations, it is known that Np(V) is retained by reduction to Np(IV) in the presence of Fe(II) minerals. Sorption of U is also strongly correlated with the occurrence of Fe oxide phases. The retention mechanism onto Fe(II) phases is evaluated for Np but is not yet confirmed for U and Tc. These tracer concentrations were to low along the flow path. Additionally, the internal surface areas of the fracture play a dominating role for retaining the redox sensitive radionuclides.

Introduction

The Äspö Hard Rock Laboratory (HRL) was established in a granite rock formation in Sweden for in-situ testing of disposal techniques and for investigations concerning migration and retention of radionuclides [1]. Groundwater flow through fractures in granite host rocks may cause migration of radionuclides from the repository. Within the scope of a bilateral cooperation between Svensk Kärnbränslehantering AB (SKB) and Forschungszentrum Karlsruhe, Institut für Nukleare Entsorgung (FZK-INE), actinide migration experiments with Pu, Am, Np, U and Tc are conducted at the Äspö Hard Rock Laboratory [2].

To understand the findings of the migration experiments, series of laboratory experiments were performed. Batch experiments provide information on the sorption behavior of the different solids present in fractures from Äspö HRL [3]. The results of these experiments are reported, previously.

Objectives

The objectives of the FZK-INE investigations are focused on the quantification of the retention and the relevant mechanisms of various actinide elements onto individual natural fracture surfaces of a granite host. Furthermore, the in-situ actinide migration experiments at the Äspö HRL are directed to examine the applicability of data determined in laboratory to natural conditions and to verify the batch sorption studies. Migration experiments have been conducted with the actinides Am, Np, Pu U and Tc in drill cores having natural fractures. In order to get insight in the retention/sorption mechanisms, laboratory experiments were performed onto granite and altered granite.

Fig. 1 shows the measured breakthrough of HTO, ^{233}U and ^{99}Tc for an in-situ migration experiment as function of time. For both tracers, an initial breakthrough peak is observed which occurs at the same time as for inert HTO.

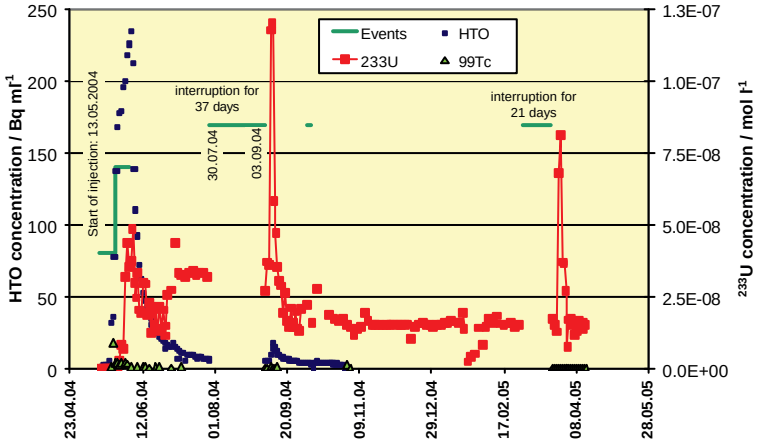

***Figure. 1**: Breakthrough of HTO, ^{233}U and ^{99}Tc tracers during the duration of the migration experiment with core #7.*

The present paper investigates the relevance of different mineral phases flanking a natural fracture and discusses the effect on radionuclide retention.

Experimental

After termination of the migration experiment, the core is cut perpendicular to the fracture and investigated with respect to element distributions [4, 5]. The abraded material from cutting is analysed by ICP-MS. Fig. 2 shows the ^{99}Tc and ^{233}U distributions along flow path as well as the distribution of natural uranium and thorium. In a distance of ~100 mm from point of injection, significant concentrations of natural U and the ^{233}U tracer are found. Also the ^{99}Tc concentration is increased in this region. In contrast to U, a decrease of the Th concentration (from ~8 ppm to ~4 ppm) is measured in this region. At the same location, matrix elements show also deviations from the average values: Mg concentration is decreased by a factor ~5, Ca is increased by about 2. Fe and K show also deviations from average values.

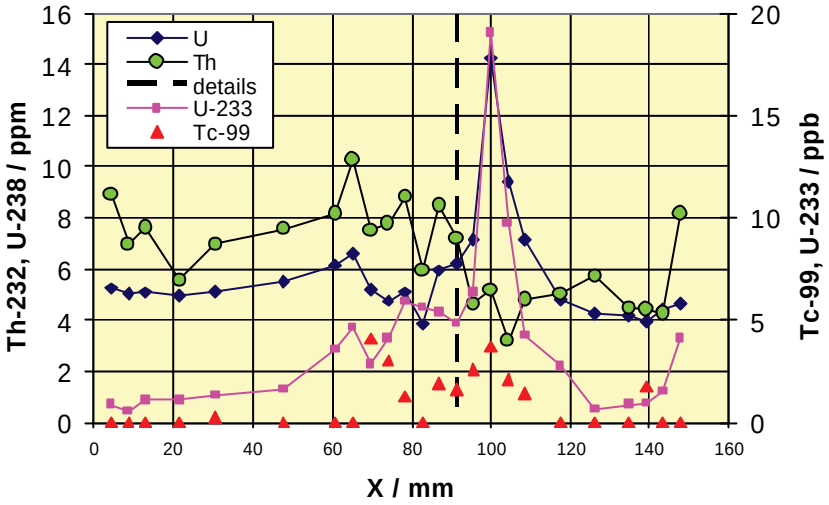

***Figure 2**: Concentrations of ^{99}Tc and ^{233}U tracers as well as of natural U and Th of the abraded material obtained by slice cutting of a core. (Dashed line: Part of the fracture for detailed analysis)*

From the migration experiments as well as from supporting batch experiments, information on the retention mechanism is obtained. For batch and migration experiments, the actinides are applied in following redox states: Am(III), Pu(IV), Np(V), U(VI) and Tc(VII). Determination of the redox state of retained Np is investigated by TTA extraction and by XPS. Both methods show Np(IV) retained onto the samples. Potential sites for the reduction processes might be pyrite and Fe(II) containing clay minerals which are detected in the Äspö granite. As described previously, by XPS Tc was found onto iron rich phases as well as onto $CaAl_2(SiO_4)_2$ minerals. Significant sorption is observed onto iron-free areas, also. XPS analyses show a clear shift of the Tc binding energy to a reduced redox state. Comparisons between Np and Am show for the different migration experiments that both actinides were retained at the same locations. For this reason, the flanking components of the flow path are determined by different methods such as visualization, α-autoradiography, SEM/EDX as well as element analysis and investigations of correlations between the detected elements.

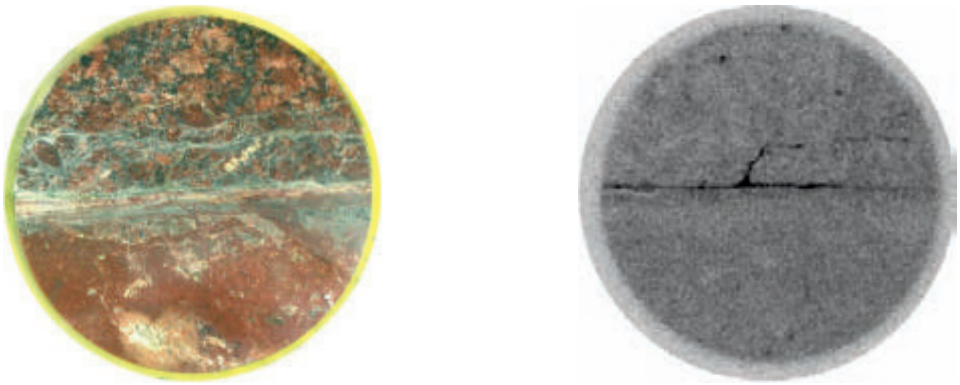

a.) Visual image of slice #21 b.) α-autoradiography of slice #21

***Figure. 3**: Investigations of the flow path in slice #21*

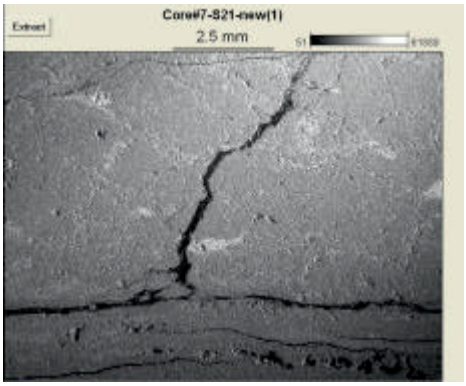

a.) SEM image of slice #21

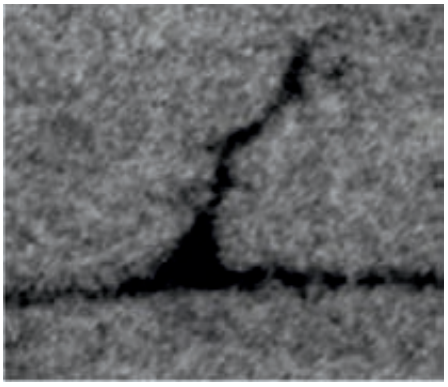

b.) Magnification of the α-auto-radiography at the same area of slice #21

Figure. 4*: Magnification of the flow path (region of highest α-activity) in slice #21*

The region with the highest α-activity is investigated in detail (see Fig. 4). Fig. 4a shows an electron back scattering image of a SEM which is sensitive to differences of the atomic number of the elements. White areas represent Ti containing phases. The element mapping (Fig. 5a) shows the distributions of the elements Ca (yellow), Si (green) and Fe (red) adjacent to the surfaces of the fracture in slice #21 shown in Fig. 4. In total Ca, Al, Si, K, Ca, Ti, Fe are analysed. By local correlation of the element compositions, some characteristic mineral compositions are deduced (Fig.5b).

Fig 5b shows characteristic constituents of mineral phases composed of Si-Al-Mg-K (red), Si-Al-Mg-Fe (violet) and pure Ca (blue). Both, the element distribution and the combination of elements show that iron is present at the same locations where the highest α-activity is observed. Also, pure Ca phases (presumably calcite) are found also in this region.

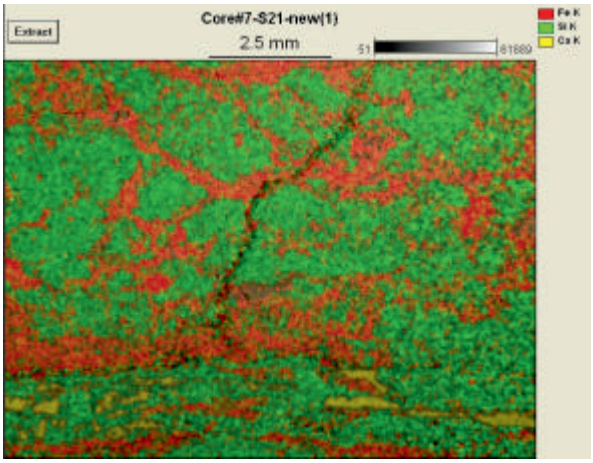

a.) Element compositions
Ca (yellow), Si (green) and Fe (red)

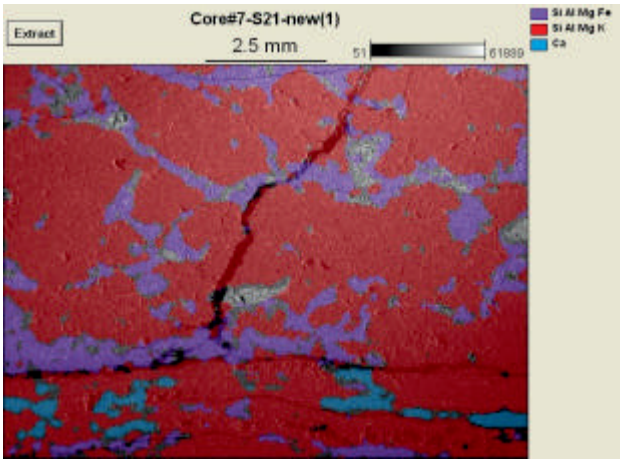

b.) Characteristic constituents of minerals
Si-Al-Mg-K (red), Si-Al-Mg-Fe (violet), pure Ca (blue)

Figure 5*: Detailed element analysis of the region of highest α-activity by superposition of SEM image and element distribution*

Unfortunately, the concentrations of Th, U and Tc are below detection limit of the EDX analysis. Retained α-activity and local geometry of the fracture are compared (see Fig. 6). For this comparison, the SEM image of the fracture is used (Fig.4a) and the α-autoradiography (Fig. 4b) is evaluated by pixel counting. Fig. 6a shows the correlation for the analysed grids showing open fracture areas between 0.1 and 0.4 (rel. units) and activities between (0.8 - 1.8)x10^5 units. Only at the bifurcation of the fracture, a significantly higher fracture area (0.8 rel. units) is observed which shows also a significantly higher radioactivity (5x10^5 units).

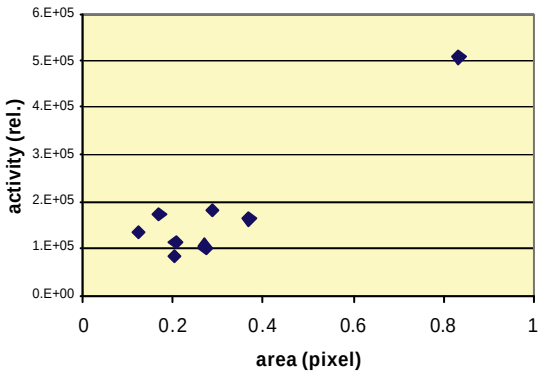

a.) Correlation between measured fracture area and α-activity of the same unit area

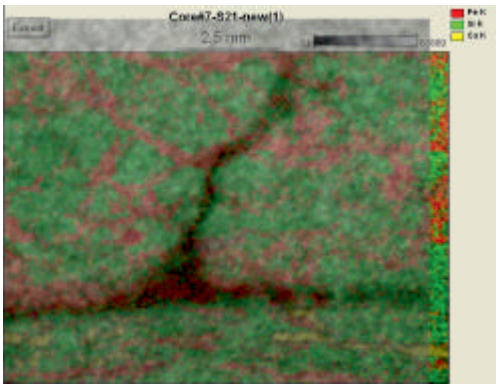

b.) Superposition of the α-autoradiogram and the element distribution

***Figure 6**: Comparison between retained α-activity and local geometry of the fracture*

Fig. 6b shows the superposition of two images: the α-activity and the element composition for the bifurcation of the fracture. Combination of information of Fig 2a and 6 indicates that at the bifurcation, the fracture surfaces are rich in Fe phases. It is obvious that the surface area at this region of the bifurcation is significantly higher than elsewhere in the fracture. Both, the surface area and the Fe concentration contribute to the retention of U and Tc.

Modelling

Modelling of the groundwater flow, the residence time of tracers in the different parts of the fracture and the correlated retention of actinides in fractures is investigated in cooperation with the Institut für Interdiziplinäre Isotopenforschung, Leipzig [6] and the University Mainz [7].

Conclusions

Granite and altered granite provide a multitude of minerals where retention of redox sensitive U and Tc takes place. In previous batch experiments, element compositions of the mineral phases retaining U, Np and Pu were determined. In the flow path of the migration experiment, main retention is observed on to phases

having similar element compositions. Fe containing phases are located directly on the inner surfaces of flow path. The reductive retention process onto Fe(II) phases is elucidated for Np. Reductive retention is not yet confirmed for U and Tc, as the concentrations of the tracers are below detection limit onto the natural mineral phases of the flow path. The internal surfaces areas of the fracture exposed to the tracer play also an important role for retention of these radionuclides.

References

[1] Bäckblom, G. The Äspö hard rock laboratory - a step towards the Swedish final repository for high-level radioactive waste. Tunnelling and Underground Space Technology 4, 463-467 (1991).

[2] Jansson, Mats, Erikson, Trygve E., CHEMLAB In-Situ Diffusion Experiments Using Radioactive Tracers, Radiochimica Acta 82, 153-156 (1998).

[3] Kienzler, Bernhard; Römer, Jürgen; Vejmelka, Peter; Jansson, Mats; Eriksen, Trygve E.; Spahiu, Kastriot; Actinide Migration in Granite Fractures: Comparison between In-Situ and Laboratory Results Scientific Basis of Nuclear Waste Management XXVI, MRS Conf. Boston, Dec. 2-5, 2002.

[4] Kienzler, B.; Vejmelka, P.; Römer, J.; Luckscheiter, B.; Kisely, T.; Soballa, E.; Walschburger, C.; Seither, A. Actinide migration experiment in the ÄSPÖ HRL in Sweden: analysis of retained uranium and technetium with core # 7. (Part V). Report FZKA-7196 (Februar 2006)

[5] Kienzler, B.; Vejmelka, P.; Römer, J.; Schild, D.; Jansson, M. Experiences with underground laboratory experiments. Internat.High Level Radioactive Waste Management Conf. (IHLWM), Las Vegas, Nev., April 30 - May 4, 2006

[6] Gründig M.; Richter M.; Kulenkampff J.; Seese A. Studies of the spatial water flow distribution and colloid transport in crystalline rock core from Äspö with positron emission tomography, 2nd Annual Workshop Proceedings Stockholm, 21st – 23th Nov. 2006

[7] Enzmann F. et al. Studies of Solution Transport in a Natural Granitic Fracture, 2nd Annual Workshop Proceedings Stockholm, 21st – 23th Nov. 2006

SORPTION INDUCED FRACTIONATION OF FULVIC ACIDS

F. Claret[1,*]; T. Schäfer[2] and P. Reiller[1]

[1] CEA/DEN/DANS/DPC/SECR/LSRM, Bâtiment 391, F-91191 Gif-sur-Yvette CEDEX.
2 FZK-INE, Karlsruhe, P.O. Box 3640 , D-76201 GERMANY

* Corresponding author; francis.claret@cea.fr

Abstract

The fractionation of humic substances is thought to be responsible of the failure of linear additive models in ternary systems consisting of metal-surface-humic substances. Hence, the fractionation of Suwannee River Fulvic Acid (SRFA) onto $\alpha-Al_2O_3$ at pH 6 is studied using spectroscopic techniques (UV/VIS, C(1s)-NEXAFS). Comparison of dissolved organic carbon (DOC) analysis with spectrophotometric measurements at 254 nm revealed a decrease in chromophoric compounds of surface associated SRFA. This latter is related to the decrease of aromatic and phenol type groups as seen by C1(s) NEXAFS and UV/Vis spectra deconvolution.

Introduction

Sorption to mineral surfaces and complexation by Natural Organic Matter (NOM) are two important processes influencing the cycling of potentially toxic trace metals in the environment [5, 12]. Both, the sorption of metal cations onto pure oxides/clay minerals and the binding of trace metals to NOM (e.g. humic and fulvic acids) have been extensively studied. However, the specific interactions between metal cations and mineral surface absorbed NOM are still matter of debate. Indeed, comparison of results obtained using simple linear additive model (LAM), which essentially describes the system as a physical mixture of independent sorbent phases, with direct measurement in the ternary system (metal-NOM-mineral surface) showed significant deviations [2, 15] Among hypotheses, the mineral surface induced fractionation of NOM is advanced [5]. Even thought results found in the literature might sometimes be contradicting, carbon functional group composition is clearly affected by mineral surfaces [10, 13, 16]. Therefore, a detailed process understanding of the organic matter - mineral surface interaction is needed.

Objectives

The main objective in the present study is to characterize the Suwannee River Fulvic Acid (SRFA) fractionation induced by $\alpha-Al_2O_3$ minerals using UV/VIS and C(1s) Near-Edge-X-Ray-Fine-Structure (NEXAFS) spectroscopy.

Experimental

SRFA is used as received from the International Humic Substance Society (IHSS) without any further purification steps. Carbonates are removed from $\alpha-Al_2O_3$ following the protocol described by Alliot *et al.* [1] to avoid any carbonate induced $\alpha-Al_2O_3$ surface property changes. In order to validate the success of this pre-treatment step the isoelectric point (pH_{IEP}) was determined at 9.5 in good agreement with published data [1]. For the sorption studies a pH ~ 6 was adjusted to i) favour first order mechanisms like ligand and anions exchange and ii) to give a good ratio between the adsorbed and dissolved SRFA concentration to be in the detection range of the analytical methods foreseen. The ionic strength was fixed to 0.1 M $NaClO_4$ and the pH is adjusted using freshly prepared NaOH and $HClO_4$. Due to its minimum adsorption in the UV/Vis range $NaClO_4$ was chosen. The electrode filling solution is modified with $NaClO_4$ 0.1M/ NaCl 10^{-2}M in order to prevent $KClO_4$ precipitation in the frit of the combined electrode.

Batch sorption experiments are conducted at room temperature using polycarbonate screwcap vials. The suspension was shaken continuously for 24 hours and the pH was checked frequently until a constant pH value was reached (usually 2 to 4 hours).The solid phase ($\alpha-Al_2O_3$ + sorbed organics) was separated from the dissolved organics *via* ultracentrifugation (246,960 g for 1 hour). SRFA concentration is then measured spectrophotometrically at 254 nm using a Shimadzu UV-3150 spectrophotometer and the dissolved organic concentration (DOC) in solution was determined with a Shimadzu 5000 TOC analyser. Sample are acidified and purged with argon in order to outgas inorganic carbon as CO_2.

C1(s) NEXAFS

Carbon K-edge NEXAFS spectra were measured at the Scanning Transmission X-ray Microscopy (STXM) beamline X1A1 (NSLS), operated by the State University of New York at Stony Brook. The principle of the method is described in detail elsewhere [8]. The absorption by different carbon structures follows the Lambert-Beer-Law, i.e. the absorption is directly proportional to the mass absorption coefficients of different carbon functionalities as a function of the x-ray wavelength. Images are recorded between 280 eV and 305 eV, using the image stack option [9]. Image alignment of the stack sequence is used for correcting small sample stage displacement during the energy scan. NEXAFS spectra are then extracted from the region of interest, setting the $I_o(E)$ in a region free of sample.

STXM sample preparation was performed by drying 1µl of SRFA solution on a Si_3N_4 window (100 nm thick). Energy calibration of the spherical grating monochromator was achieved by using the photon energy of the CO_2 gas adsorption

band at 290.74 eV [7]. For the comparison of different NEXAFS spectra, all spectra were baseline corrected and normalized to 1 at 295eV prior to peak fitting. The spectra were then de-convoluted following the procedure of Schäfer *et al.* (2003):

(i) an arctangent function for the ionization potential at 290.5 eV of aromatic/aliphatic carbon [6],
(ii) six Gaussian functions (284.4, 285.0, 286.6, 287.4, 288.6 and 289.4 with a FWHM of 0.4eV) for the five π^* transitions below the ionization energy. The 287.4 eV mixed Rydberg/valence state transition band was also fitted using a gaussian function. Additionally two second, higher transition (1s-2π^*) for aromatic carbon bonded to either hydrogen or carbon and for aromatic carbon bonded to oxygen approximately 4 eV above the energy of the 1s-π^* were implemented.[3], and
(iii) two broad Gaussian functions were used for the σ^*-transitions.

UV/Vis

UV/Vis spectra of SRFA show no specific features but a strong steady increase with decreasing wavelength. The functional groups containing the electrons that are promoted when a molecule absorbs light are referred to as chromophores. In NOM, the majority of the chromophores that absorbs in the UV region are aromatic groups with various degrees and types of substitution. By analogy to benzene, Korshin *et al.* [11] proposed a simplified deconvolution approach to allow a better understanding of the chromophoric group functionalities. It was proposed that the 200-400 nm region represents three bands that can be simulated by three Gaussian peaks.

(i) A very intense local excitation band (LE) centred at 180 nm linked to the transition $^1A_{1g} \rightarrow {}^1E_{2u}$
(ii) A benzenoid band (Bz) centred at 203 nm due to vibrational perturbations in the π-electron system and linked to the transition $^1A_{1g} \rightarrow {}^1B_{1u}$
(iii) An electron transfer band (ET), corresponding to the $^1A_{1g} \rightarrow {}^1B_{2u}$ transition in benzene, is centred at 253 nm with a low intensity due to strong quantum-mechanical prohibition. This band is strongly affected by the presence of ring associated polar functional groups.

Results

In Figure 1, the percentage of sorbed SRFA onto the alumina surface is plotted as a function of the ratio between the SRFA and $\alpha-Al_2O_3$ concentration R_{SRFA}. If R_{SRFA} is < 20, sorption values obtained by UV/Vis are bigger than those determined by DOC analysis. This phenomena was previously observed by Gu *et al.* [4] for Suwannee River NOM sorption on iron oxides and supports the idea of preferential sorption of chromophoric functional groups on $\alpha-Al_2O_3$ Indeed, in this case the measured absorbance in the supernatant will be lower and therefore the calculated sorbed concentration higher than the one calculated from DOC analysis. UV/Vis spectra where deconvoluted using a procedure published by Korshin *et al.*

[11]. The ratio $A_{0,Et}/A_{0,Bz,}$ where A is the relative band intensity, is plotted as a function of R_{SRFA} (cf. Figure 1). In the region of comparable UV/Vis and DOC analysis (R_{SRFA}>20) the $A_{0,Et}/A_{0,Bz}$ ratio is almost constant around 1, whereas for R_{SRFA} values <20 the band ratio is decreasing until 0.5. According to Korshin *et al.* [11] the decrease of the $A_{0,Et}/A_{0,Bz}$ ratio indicates the loss of aromatic functional groups substituted with hydroxyls, carboxyl, esters and carbonyls groups.

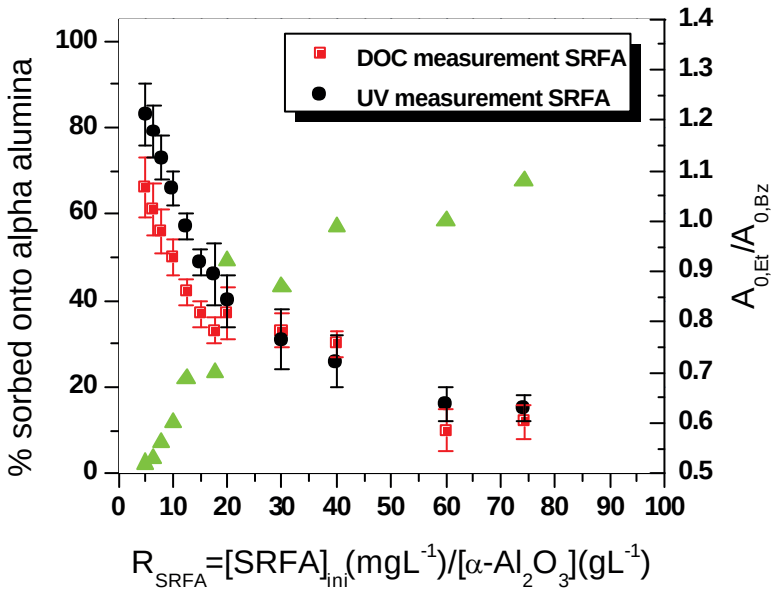

***Figure 1**: $R_{SRFA}=[SRFA]_{ini}$ $(mgL^{-1})/[\alpha–Al_2O_3](gL^{-1})$ dependent adsorption of SRFA on alumina in 0.1 M $NaClO_4$. Circles and squares represent UV/Vis measurement and DOC analysis, respectively. Triangles represent the evolution of the $A_{0,Et}$ and $A_{0,Bz}$ band ratio obtained after de-convolution of the UV/Vis spectra.*

C(1s) NEXAFS measurements made on the supernatant after sorption (cf. Figure 2) indicates a decrease in aromatic, phenolic and aliphatic groups content with decreasing R_{SRFA} (cf. Table 1) and an increase in carboxyl groups. These results corroborate the diminution of aromatic functionalities substituted by hydroxyls groups seen in the UV/Vis measurements.

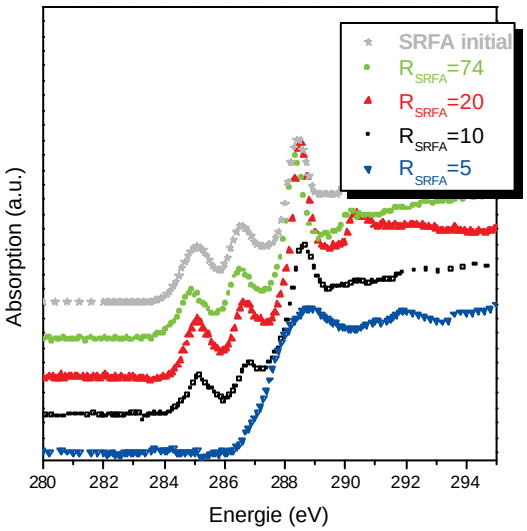

***Figure 2**: C(1s) NEXAFS spectra obtained on SRFA supernatant after sorption for different R_{SRFA}. From top to bottom are represented the initial SRFA, and spectra obtained for R_{SRFA} = 74, 20, 10 and 5, respectively.*

***Table 1**: Semi quantitative analysis of C(1s) NEXAFS from SRFA found in the supernantant after sorption on alumina.*

Functionnal group	R_{SRFA}=10	R_{SRFA}=20	R_{SRFA}=74	Initial
C aromatic	9%	12%	13%	15%
Phenol	10%	12%	12%	14%
C aliph. CH_2,CH_3	7%	12%	14%	14%
Carboxyl	45%	31%	27%	25%
COH	23%	25%	23%	23%
Carbonate	6%	9%	11%	9%

The spectra obtained for an initial ratio of 5 was not de-convoluted. Due to the low carbon content within this sample, the authors want to remeasure this sample to reconfirm the data obtained.

Conclusions

Combination of UV/Vis and NEXAFS spectroscopy on the non-sorbed fraction of SRFA indicates a fractionation at surface concentrations $R_{SRFA} < 20$ and a decrease in phenol-type functional groups. Moreover, NEXAFS indicates also a decrease in C=C double bonds and an increase in carboxyl functional groups. This might be an explanation to the deviation between LAM calculation and experiment. The next step will be to check the complexation properties of the non sorbed fraction using time resolved laser fluorescence spectroscopy.

References

[1] Alliot, C., Bion, L., Mercier, F., and Toulhoat, P. (2006). Effect of aqueous acetic, oxalic, and carbonic acids on the adsorption of europium(III) onto alpha-alumina: *Journal of Colloid and Interface Science*, 298 (2), 573-581.

[2] Christl, I., and Kretzschmar, R. (2001). Interaction of copper and fulvic acid at the hematite-water interface: *Geochimica Et Cosmochimica Acta*, 65 (20), 3435-3442.

[3] Francis, J. T., and Hitchcock, A. P. (1992). Inner-shell spectroscopy of p-benzoquinone, hydroquinone, and phenol: Distiguishing quinoid and benzenoid structures: *J. Phys. Chem.*, 96, 6598.

[4] Gu, B. H., Schmitt, J., Chen, Z. H., Liang, L. Y., and Mccarthy, J. F. (1994). Adsorption and Desorption of Natural Organic-Matter on Iron-Oxide - Mechanisms and Models: *Environmental Science & Technology*, 28 (1), 38-46.

[5] Heidmann, I., Christl, I., and Kretzschmar, R. (2005). Sorption of Cu and Pb to kaolinite-fulvic acid colloids: Assessment of sorbent interactions: *Geochimica et Cosmochimica Acta*, 69 (7), 1675-1686.

[6] Hitchcock, A. P., and Ishii, I. (1987). Carbon K-shell excitation spectra of linear and branched alkanes: *Journal of Electron Spectroscopy and Related Phenomena*, 42 (1), 11-26.

[7] Hitchcock, A. P., and Mancini, D. C. (1994). Bibliography of atomic and molecular inner-shell excitation studies: *J. Electron Spectrosc.*, 67, 1-132.

[8] Jacobsen, C., Williams, S., Anderson, E., Browne, M. T., Buckley, C. J., Kern, D., Kirz, J., Rivers, M., and Zhang, X. (1991). Diffraction-limited imaging in a scanning transmission x-ray microscope: *Optics Communications*, 86, 351-364.

[9] Jacobsen, C. J., Zimba, C., Flynn, G., and Wirick, S. (2000). Soft x-ray microscopy from sub-100nm regions: *Journal of Microscopy*, 197, 173-184.

[10] Kaiser, K. (2003). Sorption of natural organic matter fractions to goethite (alpha-FeOOH): effect of chemical composition as revealed by liquid-state C-13 NMR and wet-chemical analysis: *Organic Geochemistry*, 34 (11), 1569-1579.

[11] Korshin, G. V., Li, C. W., and Benjamin, M. M. (1997). Monitoring the properties of natural organic matter through UV spectroscopy: A consistent theory: *Water Research*, 31 (7), 1787-1795.

[12] Kretzschmar, R., and Schäfer, T. (2005). Metal retention and transport on colloidal particles in the environment: *Elements*, 1, 205-210.

[13] Reiller, P., Amekraz, B., and Moulin, C. (2006). Sorption of Aldrich humic acid onto hematite: Insights into fractionation phenomena by electrospray ionization with quadrupole time-of-flight mass spectrometry: *Environmental Science & Technology*, 40 (7), 2235-2241.

[14] Schafer, T., Hertkorn, N., Artinger, R., Claret, F., and Bauer, A. (2003). Functional group analysis of natural organic colloids and clay association kinetics using C(1s) spectromicroscopy: *Journal De Physique Iv*, 104, 409-412.

[15] Vermeer, A. W. P., McCulloch, J. K., Van Riemsdijk, W. H., and Koopal, L. K. (1999). Metal ion adsorption to complexes of humic acid and metal oxides: Deviations from the additivity rule: *Environmental Science & Technology*, 33 (21), 3892-3897.

[16] Wang, K. J., and Xing, B. S. (2005). Structural and sorption characteristics of adsorbed humic acid on clay minerals: *Journal of Environmental Quality*, 34 (1), 342-349.

XANES-EXAFS ANALYSIS OF Se(+IV)-FeS_2 SYSTEMS

C. Bruggeman and A. Maes*

Laboratory for Colloid Chemistry, Katholieke Universiteit Leuven, Kasteelpark Arenberg 23, B-3001 Leuven, Belgium

*Corresponding author: Andre.Maes@biw.kuleuven.be

Abstract

The reduction of Se(+IV) in the presence of FeS_2 and the subsequent formation of a Se precipitate was confirmed by analysis of the Se speciation on the solid phase by means of XANES-EXAFS analysis. Standard XAS spectra were collected from reduced Se solid phases such as amorphous and crystalline elemental selenium, and FeSe. It was shown that the XANES edge is indicative for the Se valence state, and that also the XANES region can be used to identify reduced Se solid phases. EXAFS spectra and RSFs could be fitted very well using maximum two coordination shells. When comparing the solid phase from an experiment in which FeS_2 was contacted with SeO_3^{2-}, with the standard XAS spectra, it was observed that the resulting spectrum corresponded to (amorphous) elemental selenium, providing more conclusive evidence that FeS_2 controls the redox speciation of Se in Boom Clay. A similar sample in which FeS was contacted with SeO_3^{2}, showed the formation of FeSe as end product.

Introduction

Only a very limited amount of information is available concerning the interaction between Se oxyanions and sulphidic mineral phases such as pyrite, troilite and mackinawite. However, it is a well-known fact that in sediments Se is closely correlated with pyrite (Elson and MacDonald, 1979), where it can substitute for sulphur and thus form FeSe, $FeSe_2$ or mixed FeS_xSe_y phases which control its solubility (Masscheleyn *et al.*, 1991). Also in the Boom clay sediment, it was already established that autogenic native Se is mainly correlated with (framboidal) pyrite minerals. Moreover, the *in situ* E_h of Boom Clay is considered to be mainly controlled by the presence of pyrite (Baeyens *et al.*, 1985).

Objectives

In the present study, the interaction between Se oxyanions and FeS_2 will be investigated with XANES-EXAFS measurements to elucidate the chemical structure of Se accumulated on the solid phase.

Experimental

Selenite XAS standard consisted of aqueous solutions containing ~ 100 mM $HSeO_3^-$ (> 98%). Selenium(0) XAS standards were prepared by chemical reduction of selenite solutions through the addition of Na-ascorbic acid. Selenide (-II) XAS standard was taken from commercial FeSe powder (Alfa Aesar). Standard Se samples were analysed in transmission mode.

Experimental XAS samples were prepared in a N_2-flused gloveblox from aqueous suspensions of 100 gL^{-1} FeS_2 or FeS whereto a total amount of 123 µmoles Na_2SeO_3 was added from a 1 M stock solution. The samples were then brought to a pH of 8.0 with 1 M HCl. Samples were allowed to equilibrate over three weeks before phase separation by centrifugation (Beckman J2-21 Centrifuge, rotor JA-17, 15000 rpm, 2hrs, cut-off ~25 nm). Supernatant solutions were carefully pipetted off and analysed for Se using ICP-OES, and pH. XAS samples were taken by transferring the pellet to 2 mL translucent disposable screw tread vial sealed by a cap equipped with an ethylene-propylene O-ring (Alltech Associates, Inc.). These samples were analysed in fluorescence mode.

XANES and EXAFS spectra were collected at the Se K-edge (12.658 keV) at the DUBBLE BM26A beamline at the European Synchrotron Radiation Facility (ESRF) located in Grenoble, France. Se standard samples were analyzed in transmission mode while FeS_2/FeS samples were analysed in fluorescence mode using a solid-state 9-element Ge detector. All samples were analyzed in "spinning mode" to avoid any redox-induced reactions by the beamline.

Results and Modelling

Oxidation levels of selenium are characterised by the specific value of the first inflection point of the XANES spectrum (Oger *et al.*, 2004). This is illustrated by the characteristic half-peak values of biselenite, amorphous and crystalline selenium metal and iron selenide standards given in table 1. For analysis however, all Se spectra were calibrated at the same energy value of 12658 eV. When the normalised XANES spectra are now compared, differences related to the molecular structure of Se can be used to identify the species. A very clear distinction between the different redox states of Se can be made by the difference in intensity of the so-called "white line", or absorption peak at the K-edge of the standards (figure 1). This white line decreases with a decrease in oxidation state. However, the intensity for crystalline and amorphous selenium metal is almost identical, and thus, can not be used to discriminate between the two. Therefore, it is also important to analyse the XANES region located directly behind the white line. Crystalline selenium

shows a less pronounced dip at 12664 eV, a less higher shoulder at 12668 eV, and an extra peak at 12673 eV compared to amorphous selenium.

Table 1: *Energy values of the first inflection point of XANES spectra from Se standards*

Se Standard	Energy of first inflection point (eV)
$HSeO_3^-$	12664
Se^0 amorphous	12660
Se^0 crystalline	12660
FeSe	12659

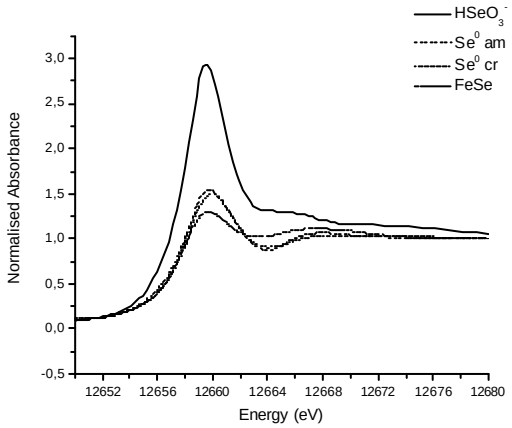

Figure 1: *Normalised XANES spectra of different Se standards ($HSeO_3^-$, solid; Se^0 amorphous, dash; Se^0 crystalline, dot; FeSe, dash-dot), all calibrated at 12658 eV*

Apart from the XANES spectra, also the EXAFS spectra can distinguish between these four selenium standards (figure 2). The Se K-edge spectra clearly show the difference in backscatterer distance form the central adsorbing Se atom between the Se(+IV) standard and the Se(0, -II) standards. This is also reflected in the position of the first coordination shell in the Radial Structure Function (RSF) graph. The differences between the other Se standards are less pronounced, but still markedly present. Firstly, the difference between selenium metal and FeSe can be made out from the larger FeSe signal in the low-energy k-range (< 5 $Å^{-1}$) of the EXAFS spectrum (figure 2 – left), and the lower FeSe Fourier transform peak in the RSF plot. Also, a slight phase difference can be discerned between Se^0 and FeSe in the EXAFS plot (figure 2 - right). These observations arise from the difference in the first coordination shell backscatterer atom in respectively FeSe, where Fe is the backscatter, and Se^0, where Se is the backscatter.

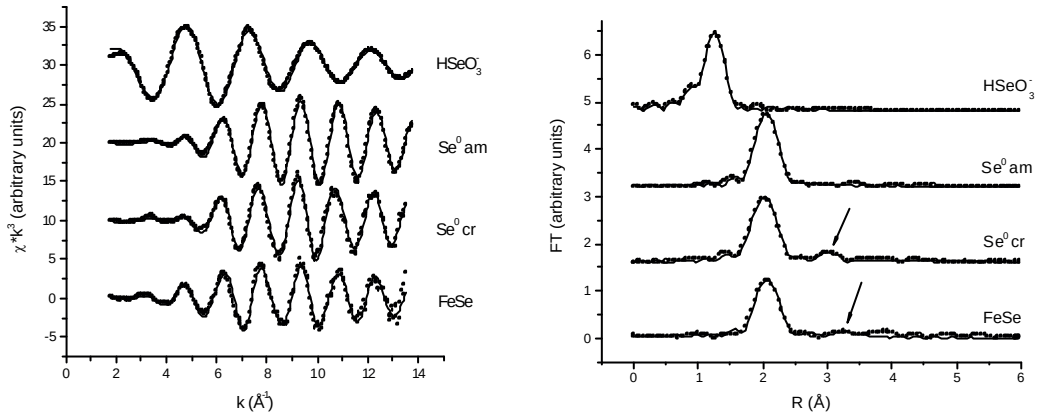

Figure 2*: Se K-edge EXAFS spectra (left) and Fourier-transformed Se K-edge EXAFS spectra (right) of different Se standards ($HSeO_3^-$; Se^0 amorphous; Se^0 crystalline ; FeSe). Open symbols denote experimental points, solid lines are theoretical fits.*

Secondly, amorphous Se metal and crystalline Se metal can be distinguished by the following features: amorphous Se^0 has a larger amplitude EXAFS signal and a larger first shell peak in the RSF. Also, crystalline Se^0 shows some additional features in the RSFs beyond the first coordination shell (arrows in figure 2 - right). These peaks are completely absent in the Fourier transform of amorphous Se^0, and are attributed to the more crystalline nature of the sample under study (Zhao *et al.*, 2004). Coordination numbers for amorphous and crystalline Se^0 are about 1.5, while the interatomic distance is slightly different with 2.35 Å as the best model fit for amorphous Se^0 and 2.37 Å for crystalline Se^0.

Now that the Se XAS standards are analysed, they can be compared with XANES and EXAFS spectra of FeS_2 and FeS samples contacted with SeO_3^{2-}. Three weeks reaction time was allowed for the samples, which would assure that reduction, if present, has already sufficiently taken place (Bruggeman *et al.*, 2005). Table 2 summarises the experimental parameters for the two samples that were analysed with XAS.

Table 2*: Experimental parameters for XAS samples*

Sample	Solid-to-liquid ratio	$[Se]_{ini}$ (M)	$[Se]_{out}$ (M)	$[Se]_{solid}$ (moles/g)	pH
1	100 gL^{-1} FeS_2	6.15×10^{-3}	9.0×10^{-4}	5.25×10^{-5}	8.21
2	100 gL^{-1} FeS	6.15×10^{-3}	$< 10^{-6}$	6.15×10^{-5}	7.89

In both cases, the sulphide minerals are responsible for removing the largest part (> 85% for FeS_2, > 99% for FeS) of Se from solution. After three weeks, the remaining Se supernatant concentration in presence of FeS was below the limit of detection for ICP-OES. Clearly, FeS is much more reactive than FeS_2 with respect to Se(+IV). This was also visually observed: already after one day, a red glimmer was present in the water and on the FeS surface, which is indicative for the presence of (amorphous) Se^0. In the FeS_2-containing sample, no such observation was noted.

The normalised XANES spectra (calibrated at 12658 eV) of the fluorescence samples, the K-edge EXAFS spectra and the Fourier-transformed EXAFS signal are shown in figures 3, 4 - left and 4 - right respectively

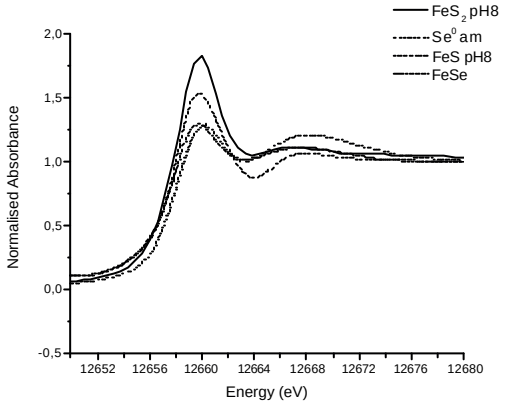

Figure 3: *Normalised XANES spectra of Se XAS samples containing FeS_2 (solid) and FeS (dot); Reference spectra of amorphous Se^0 (dash) and FeSe (dash-dot) are shown as well. All spectra were calibrated at 12658 eV*

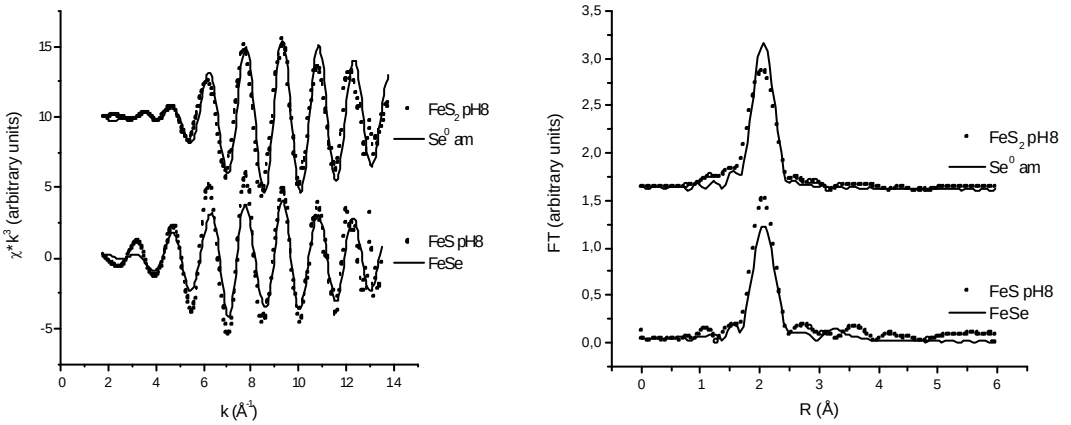

Figure 4: *Se K-edge EXAFS spectra (left) and Fourier transformed Se K-edge EXAFS spectra (right) of Se XAS samples containing FeS_2 and FeS (open symbols); Reference spectra of amorphous Se^0 and FeSe (solid lines) are shown as well.*

When comparing all the data from the FeS_2 and FeS samples with the reference Se standard spectra shown before, the Se species present on the FeS_2 solid phase was identified as amorphous Se^0, while the Se species present on the FeS phase was FeSe. For illustrative purposes, the respective spectra of these two compounds were added to figures 3 and 4. The Se species present on the FeS_2 surface shows the typical features of amorphous Se^0 metal: a white line intensity intermediate to Se(+IV) and Se(-II), a relatively pronounced dip and shoulder in the XANES region, an EXAFS spectrum with only very small signals in the low-energy range, and a Fourier transform spectrum with no peaks beyond the first coordination shell. The Se species present on the FeS surface shows the features of FeSe: a very low white line intensity, an EXAFS spectrum with pronounced signals in the low-energy range, and a Fourier transform spectrum with distinct features beyond the

first coordination shell. Thus, XANES and EXAFS give substantial evidence that reduction of Se(+IV) species occurs at the surface of sulphide minerals. However, in contrast with assumptions made by other authors who studied FeS as an analogue for FeS_2 (e.g. Yllera de Llano *et al.* (1996)), the interaction of Se(+IV) with both phases does not necessarily lead to the same Se end product.

Conclusions

Via analysis of data collected through XANES-EXAFS, it was shown that FeS_2 acts as a redox controlling phase for Se(+IV) resulting in the formation of elemental selenium on a relatively short-term timescale (3 weeks). Interestingly, similar experiments performed with FeS showed that FeSe was formed on the same timescale, indicating that the two sulphide minerals cannot be regarded as geochemically similar species.

These results thus give direct evidence for the reduction of Se(+IV) in sediments where the redox conditions are controlled by the presence of iron sulphide minerals, which in turn has dramatic effects on the mobility and availability of Se in performance assessment calculations.

References

[1] Baeyens, B., Maes, A., Cremers, A., Henrion, P.N. (1985). Insitu physicochemical characterisation of Boom Clay. *In:* Radioactive Waste Management and Environmental Restoration, Harwood Acad Publ Gmbh 6: 391-408.

[2] Bruggeman, C., Maes, A., Vancluysen, J., Vandemussele, P. (2005). Selenite reduction in Boom Clay: Effect of FeS_2, clay minerals and dissolved organic matter, *Environmental Pollution*, 137, 209-221

[3] Elson, C.M., MacDonald, A.S. (1979). Determination of selenium in pyrite by an ion exchange electrochemical atomic-absorption spectrometric method, *Analytica Chimica Acta*, 110, 153-156

[4] Masscheleyn, P.H., Delaune, R.D., Patrick, W.H. (1991). Biogeochemical behaviour of selenium in anoxic soils and sediments – an equilibration thermodynamics approach. *Journal of Environmental Science and Health – part A*, 26, 555-573

[5] Oger, P.M., Daniel, I., Cournoyer, B., Simionovici, A. (2004). In situ micro X-ray absorption near edge structure study of microbiologically reduced selenite (SeO_3^{2-}), *Spectrochimica Acta Part B*, 59, 1681-1686

[6] Yllera de Llano, A., Bidoglio, G., Avogadro, A., Gibson, P.S., Rivas Romero, P. (1996). Redox reactions and transport of selenium through fractured granite, *Journal of Contaminant Hydrology*, 21, 129-139

[7] Zhao, Y.H., Lu, K., Liu, T. (2004). EXAFS study of mechanical-milling-induced solid-state amorphization of Se, *Journal of Non-Crystalline Solids*, 333, 246-251

BINDING AFFINITY OF HUMIC COLLOIDS TO ACTINIDES – AND WHAT´S BEHIND –

A. Priemyshev[1], M.A. Kim[1,*] and J.I. Kim[2]

[1] Institut für Radiochemie, Technische Universität München, 85748 Garching, Germany
[2] Institut für Nukleare Entsorgung, Forschungszentrum Karlsruhe, 76021 Karlsruhe, Germany

*corresponding author: mak@rad.chemie.tu-muenchen.de

Abstract

This study analyzes the mechanisms regulating the binding affinity of humic colloids to metal ions of higher oxidation state (≥ 3), such as actinides, under conditions inherent to the natural aquatic system. For the experiment, ^{241}Am(III) or ^{234}Th(IV), are conditioned with ^{14}C-labelled humic acid. Colloids are separated from precipitate and solution by sequential filtration at 450 nm and 1.5 nm pore sizes. Formation of colloid-borne humic acid and actinide in the neutral pH range is ascertained radiometrically by determining the phase distribution of ^{14}C and Am(Th), separately, varying the pH, the concentration of reaction components, conditioning time as well as temperature in a broad screening experiment. Binding affinities of humic acid to actinides are appraised from the ratio between the fractions of colloid-borne ^{14}C and Am(Th) and further evaluated by ligand displacement with EDTA. The binding affinity of Am and Th to humic acid, leading to their incorporation into the colloidal phase, can be correlated with their different tendencies to hydrolyze. The Am^{3+} ion, less hydrolyzing than the Th^{4+} ion, is favoured at the complexation with humic acid. However, the original hydrolysis potential of the ion can be suppressed and its binding affinity to humic acid correspondingly enhanced, by changing values of thermodynamic as well as kinetic solubility parameters. For example, the EDTA-resistant colloid-borne fraction of likely hydrolyzed Th^{4+} ions becomes gradually enhanced at decreasing pH, increasing concentration of humic acid, prolonged conditioning time or raising temperature.

Introduction

Migration of actinides in the geosphere is mainly due to the irreversible association of actinides with natural aquatic colloids [1]. In our previous work, we have investigated aluminosilicate colloids interacting with trivalent actinides by time-resolved laser fluorescence spectroscopy of Cm [2-4]. The present work analyzes humic colloids for their binding mechanisms of actinides in general, e.g.

also non-fluorescing tetravalent actinides, and is based therefore exclusively on non-spectroscopic methods.

Objectives

The observed discrepancy between the much higher binding affinities of actinides or analogs within naturally occuring humic acid as compared with those achieved through complexation of actinides with purified humic acid in the laboratory [5], is an intriguing fact. To find out the underlying reason for such phenomenons, is the main objective of the present study.

Experimental

Two parameter screenings are performed. In the first experiment, actinides (An) are interacted with purified ^{14}C-labelled humic acid of PEC of 4.82 ± 0.05 meq/g [6,7], varying the following parameters of solubility: pH: 6.6 and 7.8 in 0.01 M MOPS buffer; oxidation state of An: ^{241}Am(III) and ^{234}Th(IV); concentration of reaction components: for Am(Eu) from $5x10^{-8}$ M to 10^{-5} M, for Th from $5x10^{-11}$ M to $5x10^{-4}$ M and for humic acid from 0.2 to 8.0 mg/L; conditioning time: 10 days and 33 days; conditioning temperature: 23 ºC, 50 ºC, 90 ºC. Each sample is submitted to sequential filtrations at 450 nm and 1.5 nm pore sizes. The activity in the solutions after each filtration is measured by liquid scintillation counting and related to the input activity. Activity fractions are determined in solution (< 1.5 nm), colloid (< 450 nm and > 1.5 nm) and precipitate (> 450 nm) phases. In the second experiment, desorption through addition of $5x10^{-3}$ M EDTA is performed on samples containing Th and humic acid under selected parameter conditions as described above. After the EDTA contact time of one day, the filtration processes are applied, and the activity in each of three phases is determined. The non-desorbed activity fraction is called the EDTA-resistant fraction and related to that of the sample without EDTA to obtain normalized EDTA-resistant Th fraction (of total humic-borne Th).

Result

Representative examples show the effect of the investigated solubility parameters such as actinide oxidation state, pH, concentration of reaction components, reaction time and temperature on the binding affinity of humic colloids to actinides. Fig.1 illustrates the different behaviours of Am(III) and Th(IV) in interaction with humic colloids at pH 6.6 and 23 ºC after 35 days reaction time as a function of the concentration of humic acid (HA) at a constant concentration of An = 10^{-5} M from the view of actinides (An-curves) as well as from the view of humic acid (^{14}C-curves). The curves reflect the neutralization of negatively charged humic acid colloids with an increasing amount of cationic species of An, followed by precipitation (x-axis: from right to left), or transition of precipitated An to the colloidal phase due to their binding with a gradually increasing amount of humic acid (x-axis: from left to right). The point of HA-neutralization (or precipitation), as

indicated by arrows in Fig. 1, informs us about the amount of HA that can possibly complex with the introduced amount of An-species with charge z:

$$z = [HA]_{mg/L} \times PEC_{meq/L} / [An]_{mM}$$

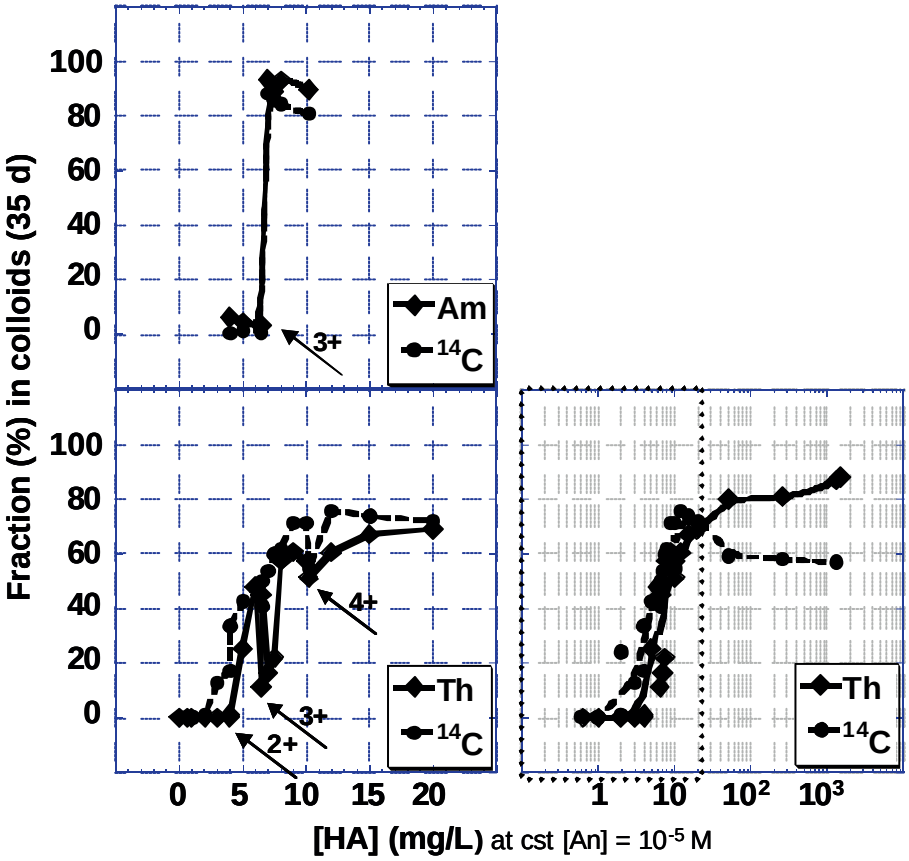

Figure.1: *Am(III) or Th(IV) in inter-action with [^{14}C]-humic colloids at pH 6.6: activity fraction (%) in colloids after 35 days con-ditioning time at 23 ºC as a function of the concentration of HA at constant concentration of Am(Eu) or Th (10^{-5} M).*

From the observed HA-neutralization points, we calculate that the An-species reacting with HA under given conditions ([An] =10^{-5} M, pH 6.6) are: for Am(III) only one species, namely Am^{3+} , and for Th(IV) three species with varying charge from 2+ to 3+ to 4+ as the amount of humic acid relative to that of Th is enhanced. Without HA under the same conditions, the prevalent species are Am^{3+} and $Th(OH)_4$ [8, 9]. Observed oscillations in the Th-curve indicate that, on increasing the HA-concentration, transition from one Th-species into another takes place. If all Th-species would occur simultaneously, the result would be a step-curve. For further interpretation of the results, we also compare the relative positions of ^{14}C- and An-curve. Complete curve overlapping is expected, when only one complexing cationic An-species is present, as almost the case of Am(Eu) at pH 6.6. If the ratio between the fractions of colloid-borne An and ^{14}C changes as a function of the [HA]/[An]-ratio, e.g. from < 1 to > 1, as it is obviously the case for Th, different An-species with gradually increased binding affinities to HA are

formed. The similar trend is followed by Th interacting with HA at pH 7.8 (Fig. 2). The HA neutralization curves are shifted to the left, indicating the prevalence of lower cationic charged An-species as compared with those at pH 6.6. The deviation between ^{14}C- and An-curves is more pronounced at the higher pH and insinuates correspondingly lower An/HA binding affinities. From the result, we may now correlate pH and relative concentrations of reacting components with An-species charges and in their turn with An/colloid binding affinities: " At lower pH and higher [HA]/[An] concentration ratio, the actinide is more ionized and its complexation with humic colloids is better".

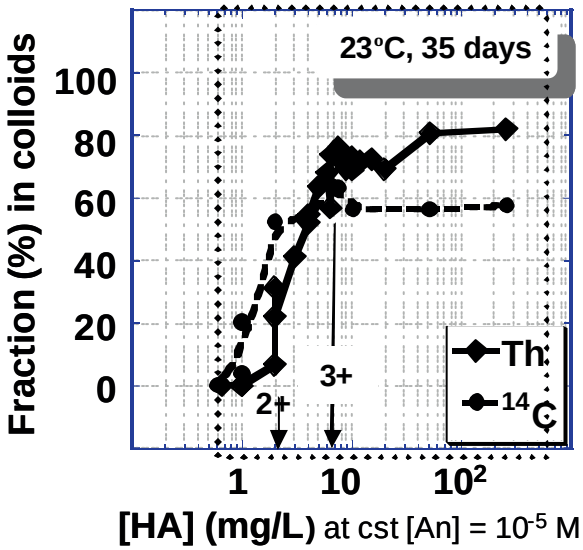

Figure 2: *Th(IV) in interaction with [^{14}C]-humic colloids at pH 7.8: activity fraction (%) in colloids after 35 days conditioning time at 23 ºC as a function of the concentration of HA at constant concentration of Th (10^{-5} M).*

The effect of conditioning time and temperature on the Th/ humic colloid interaction at pH 7.8 is illustrated by Fig. 3. The Th/HA affinity is here reflected by the normalized EDTA-resistant Th-fraction as a function of the concentration of Th at a constant concentration of HA = 6 mg/L. We observe increased EDTA-resistance of HA-borne Th at: (1) decreasing [HA]/[Th] (from right to left). The result corroborates our previous findings as expressed by Figs 1 and 2, anticipating an enhanced Th/colloid binding affinity from the relative positions of ^{14}C- and An; (2) increasing reaction time from 10 to 33 days. The presence of HA suppresses the hydrolysis of Th, but kinetics are involved; (3) increasing temperature from 23 ºC (10 and 33 days) to 50 ºC (4 days) to 90 ºC (4 days). Following the Arrhenius equation, relating reaction velocities (k) or times with reaction temperatures (T):

$$\ln(k_2/k_1) = E_a/ R (1/T_1-1/T_2)$$

where E_a is the activation energy (~ 80 kJ/mol), and R the gas constant (8.3 J K^{-1} mol^{-1}), we calculate the corresponding reaction times at 23 ºC: 10 and 33 days, 60 days, and 4.5 years. For the example of HA/Th interaction at 23 ºC and 33-35

days reaction time, we may now appreciate the increase of the EDTA-resistant Th-fraction (Fig. 3, see upper x-scale) of the total humic colloid-borne Th (Fig. 2) as the relative humic acid concentration is augmented.

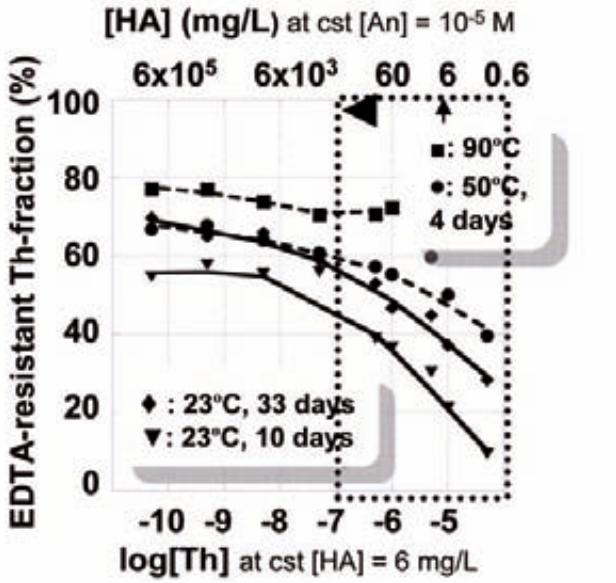

Fig.3: *Th(IV) in interaction with humic colloids at pH 7.8: EDTA-resistant Th-fraction (%) in colloids after several conditioning times and temperatures as a function of the concentration of Th (HA) at constant concentration of HA (6 mg/L) (Th (10^{-5} M)) (lower & upper x-axis).*

Conclusions

Behind the binding affinity of humic colloids to actinides stands the hydrolysis potential of actinides that may be influenced by underlying thermodynamic and kinetic parameters of solubility. Low pH, small amount of actinide versus high concentration of humic acid, long reaction time and/or increased temperature, shift the equilibrium between ionic and hydrolyzed actinide species in favour of the cationic species. Under the nature-relevant conditions, e.g. neutral pH, 1-100 mg/L humic acid and = 10^{-5} M Am or Th, Am^{3+} and Th^{4+} may be the prevalent An-species that undergo extremely strong chelate complexation (irreversible binding) with humic colloids.

References

[1] Kim, J.I. (2006) Significance of actinide chemistry for the long-term safety of waste disposal, *Nuclear Engineering and Technology*, 38, 459-482.

[2] Kim, M.A.; Panak, P.J.; Yun, J.I.; Kim, J.I.; Klenze, R.; Köhler, K. (2003) Interaction of actinides with aluminosilicate colloids in statu nascendi. Part I: generation and characterization of actinide(III)-pseudocolloids, *Colloids and Surfaces A: Physicochem. Eng. Aspects*, 216, 97-108.

[3] Panak, P.J.; Kim, M.A.; Yun, J.I.; Kim, J.I. (2003) Interaction of actinides with aluminosilicate colloids in statu nascendi. Part II: spectroscopic speciation of

colloid-borne actinides(III), *Colloids and Surfaces A: Physicochem. Eng. Aspects*, 227, 93-103.

[4] Kim, M.A.; Panak, P.J.; Yun, J.I.; Priemyshev, A.; Kim, J.I. (2005) Interaction of actinides(III) with aluminosilicate colloids in statu nascendi. Part III: Colloid formation from monosilanol and polysilanol, *Colloids and Surfaces A: Physicochem. Eng. Aspects*, 254, 137-145.

[5] Geckeis, H.; Rabung, Th.; Manh, T.N.; Kim, J.I.; Beck, H.P. (2002) Humic colloid-borne natural polyvalent metal ions: dissociation experiment, *Environ. Sci. Technol.*, 36, 2946-2952.

[6] Buckau, G. (2004) Humic substances in performance assessment of nuclear waste disposal: actinide and iodine migration in the far-field, *Second Technical Progress Report, Forschungszentrum Karlsruhe*, FZKA 6969, 113-124.

[7] Mansel, A. (2006) in preparation.

[8] Neck, V.; Fanghänel, Th.; Kim, J.I. (1998) Aquatische chemie und thermodynamische Modellierung von trivalenten Actiniden, *Wissenschaftliche berichte, Forschungszentrum Karlsruhe*, FZKA 6110.

[9] Neck, V.; Kim, J.I. (2001) Solubility and hydrolysis of tetravalent actinides, *Radiochim. Acta*, 89, 1-16.

COMPLEXATION OF EUROPIUM(III) BY ORGANIC EXTRACTS FROM CALLOVO-OXFORDIAN ARGILLITES

J. Brevet[1], P. Reiller[2,*], F. Claret[2], L. Grasset[1], B. Amekraz,[2] C. Moulin[2], and A. Amblès[1]

[1] Université de Poitiers, Synthèse et Réactivité des Substances Naturelles, CNRS UMR 6514, 40, avenue du Recteur Pineau, 86022 POITIERS CEDEX
[2] Commissariat à l'Energie Atomique, CE Saclay, CEA/DEN/DANS/DPC/SECR, Laboratoire de Spéciation des Radionucléides et des Molécules, Bâtiment 391, p.c. 33, F-91191 Gif-sur-Yvette CEDEX.

*Corresponding author: pascal.reiller@cea.fr

Abstract

The complexation behaviour of organic extracts obtained after acid alteration of Callovo-Oxfordian argillites toward europium (III) is studied in time resolved laser induced spectrofluorimetry. The presence of fluoride ions in one extract, originated from the dissolution of remaining silicates in HCl/HF, precludes the correct study. Nevertheless, the dialysis of the extract at 500 Da permits to obtain a clearer evolution of the complexation pattern. The fluorescence spectrum and decay are strikingly different the ones obtained on alkaline degradation products of the Callovo-Oxfordian argillite, and resemble more to a small organic molecule pattern.

Introduction

The influence of organic matter (OM) present in the Callovo-Oxfordian (COx) argillites on the speciation of radionuclides is important to determine. It has been shown that the organic extracts obtained after alkaline alteration can complex curium(III) with a fluorescence pattern in line with humic substances (HS) properties, *i.e.* same λ_{max} of emission and bi-exponential decay [1]. Nevertheless, alkaline alteration is known to imply hydrolysis reaction [2] and the complexation properties of the "intact" OM from the COx is to be determined. In order to obtain a basic "state of the art", the organic extracts obtained after an acid alteration of the COx can be used as a grand mean of the complexing properties.

Experimental

Core samples from the COx formation were collected between depths of 450-500 m in the EST 212 borehole drilled by ANDRA in the northeast of the Paris Basin (France) in the vicinity of the underground research laboratory of Bure. The mud used for the drilling was a common mixture of bentonite and polymers. No major chemical contamination was detected [3]. Samples were packed under N_2(g) and stored at 4°C. The outer portions of the cores were removed by hand in a glove box under N_2(g) to avoid artefacts due to oxidation or other type of contamination. In order to have a sufficient quantity of OM, all the core samples coming from the same litho-stratigraphic units (facies C2b2 from 455.80 m to 472.50 m depth) were mixed after crushing and sieving to a grain size of <500 µm in a glove box under N_2(g). The detailed extraction protocol is presented in figure 1.

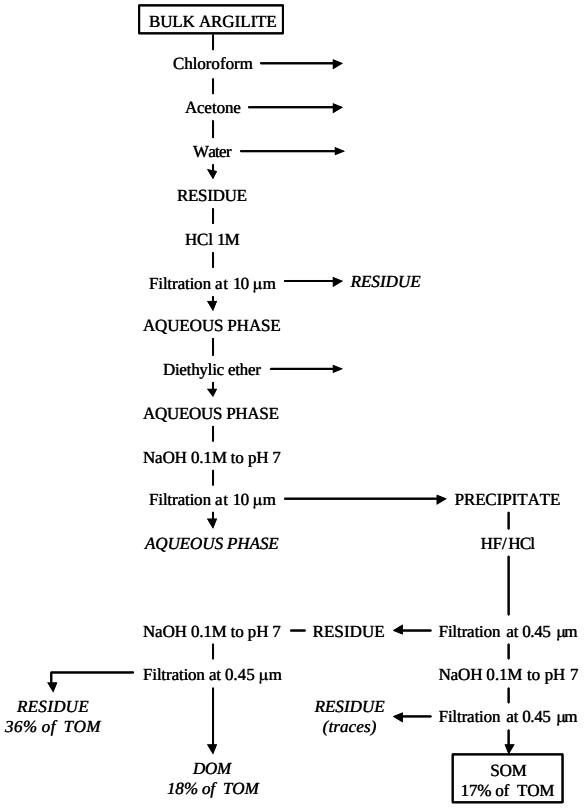

***Figure 1**: The detailed extraction protocol of the fractions*

The bitumen fractions were extracted with chloroform followed by acetone at 80°C, 100 atm using a technique of accelerated solvent extraction with a Dionex ASE 100 apparatus. An extraction with water was carried out under the same conditions. Under a N_2(g) stream, the solid residue was submitted to a HCl (1M) treatment, with stirring and stopped when no more carbonates reacted, followed by a filtration of the residual solid on 10 µm fritted glass. The aqueous phase was then shaken with diethyl ether, to extract remain bitumens, prior to neutralization at pH 7 using NaOH (0.1 M). The resulting precipitate (70.7% of the Total Organic Matter, TOM) was firstly filtrated (at 10 µm); treated with HF/HCl to remove remaining

silicates before filtration at 0.45 µm. The filtrate was then neutralised to pH 7 using NaOH (0.1 M) prior to a control filtration at 0.45 µm. The filtrate was named Soluble OM (17% of the TOM). Lyophilisation was performed with an Alpha 1-4 Bioblock Scientific freeze dryer with controlled LDC-1M at -50°C and 1.031 mbar. The percentages of TOM in the solid fractions were determined by DTA/GTA.

On figure 2 are plotted the Eu(III) fluorescence spectra, normalised to their maxima, obtained from 10^{-4} mol_{Eu}/L and pH 4 with increasing proportion of SOM (delay 10 µs, gate length 300 µs). The modification of these spectra reveals a complexation phenomenon by: i) the rise of the $^5D_0 \rightarrow {}^7F_0$ transition (578 nm, loss of symmetry), ii) the increase of the $^5D_0 \rightarrow {}^7F_2$ hypersensitive transition and an accompanying 0.9 nm blue shift, and iii) a 0.8 nm blue shift observed on $^5D_0 \rightarrow {}^7F_1$. The ratio $^7F_2/{}^7F_1$ is reported on figure 3. The evolution of this ratio only permits to evidence one complexation step.

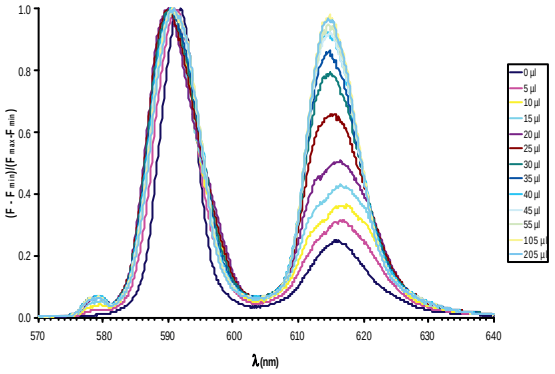

Figure 2: *Normalised europium (III) spectra 10^{-4} M at pH = 4 with increasing proportion of SOM.*

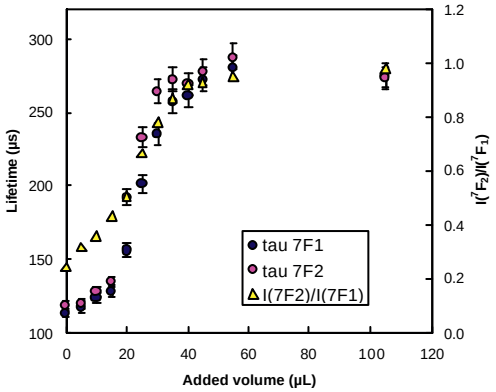

Figure 3*: Variation of fluorescence lifetime of a 1 ml [Eu] = 10^{-4} M solution vs. added volume of SOM.*

The lifetime evolutions determined for the different solution on figure 2, are also reported on figure 3. All the data can be satisfactorily fitted with a mono-exponential decay, but a bi-exponential decay implying Eu^{3+} and the final complex improves the fit. A standard deviation of 5% from 6 measurement on free Eu^{3+} at pH = 4 ($t_{^7F_1}$ = 114 ± 3 µs on and $t_{^7F_2}$ = 119 ± 4 µs) was applied to all the data. It appears that at the beginning and at the end of the complexation process, $t_{^7F_1}$ and $t_{^7F_2}$ cannot be distinguished. This is clearly not the case in between where the free and complexed Eu(III) coexist. The decays for these extracts are neither in agreement with the ones observed for Cm(III) after alkaline alteration of COx [1], nor with other lanthanides with HS [4], where the first component is faster than M^{3+}. The number of water molecules in the first hydration sphere of Eu(III) can be estimated [5]. The 8 to 9 water molecules in the hydration sphere of Eu(III) are gradually displaced through the complexation process, which leaves 3-4 water molecules at the end of the process.

Further analysis in electrospray ionization mass spectroscopy (ESI-MS) revealed the presence of inorganic salts, mainly NaF (loss of 42 in MS-MS Figure 4), coming from the HCl/HF attack of the original extracts (data not shown). The analysis in ionic chromatography of the aqueous solution used for complexation

studies is reported in table 1. The speciation of Eu(III) under the conditions of the experiments on figure 2 and 3 are presented on figure 5 referring to [6]. The coincidence with the $^7F_2/^7F_1$ ratio and the rise of EuF^{2+} complex led us to use a synthetic water of the composition in table 1.

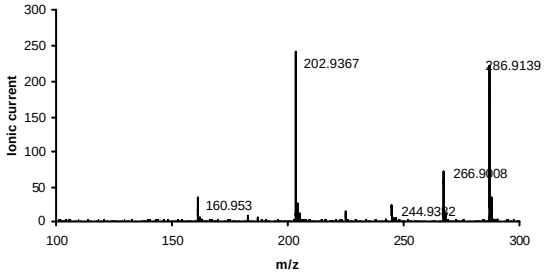

Figure 4: *MS-MS fragmentation of sharp peak at 286 m/z.*

Table 1: *Ionic composition of the SOM fraction & synthetic water*

Ion	SOM (mg/kg$_w$)	Synth (mg/L)
F^-	607.0	607.0
Cl^-	486.7	486.4
NO_3^-	43.0	42.1
HPO_4^{2-}	86.1	86.1
SO_4^{2-}	60.7	67.0

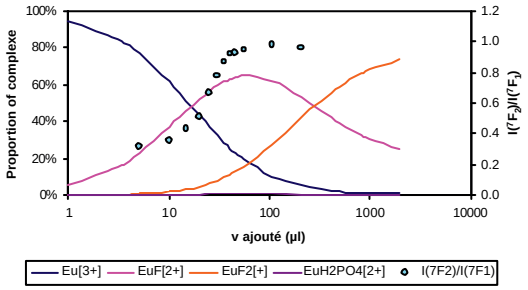

Figure 5: *Speciation of Eu(III) under the conditions of the experiment in figure 2 when adding solution of composition in table 1.*

The different spectra obtained at two different excitation wavelengths are compared on figure 6. From this comparison the two different solutions are only slightly different and can hardly be distinguished. Only the values of t determined on $^5D_0 \rightarrow {}^7F_2$ bands are different: t_{SOM} = 280 µs (3-4 H_2O) and t_{Synth} = 380 µs (2-3 H_2O) (Figure 7), suggesting either two different complexes or a dynamic quenching effect (of organic) on the same complex.

Further purification of SOM has been done using dialysis against pure water (500 Da, 24 h). The concentrate was used for Eu(III) complexation experiment. The evolution of the ratio $^7F_2/^7F_1$ is reported on figure 8a. The fluorescence spectrum obtained at the end of the process is reported on figure 8b. The evolutions are different than on figures 2, 3 and 6. One can note a stronger loss of symmetry ($^5D_0 \rightarrow {}^7F_0$, 578 nm), a 1.6 nm blue shift on $^5D_0 \rightarrow {}^7F_1$ accompanied by a shoulder at longer wavelength, and a small 0.5 nm shift on the $^5D_0 \rightarrow {}^7F_2$ band accompanied by a shoulder at shorter wavelength. These shoulders can either be the sign of another complex, or to the difference in the maximum number of water molecules in the hydration sphere [7] between Eu^{3+} and complexed Eu(III).

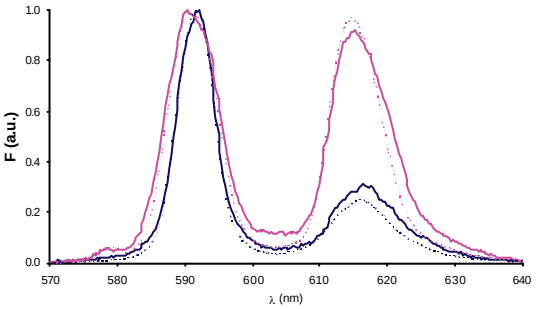

Figure 6: *Comparison of Eu(III) at pH = 4 at λ_{exc} = 395 nm (---) and λ_{exc} = 355 nm (–): blue spectra are free Eu(III) and magenta spectra are SOM (---) and synthetic water (–).*

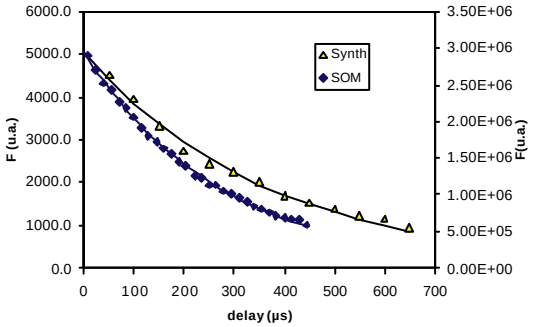

Figure 7: *Comparison of Eu(III) fluorescence decay in SOM and Synthetic water at pH = 4.*

As the fluorescence decays are mono-exponential on the three bands, only one complex is present. The fluorescence decay is also shorter when fitted on the three bands, *i.e.* t = 136 ± 7 µs (Figure 8c), leaving 7 water molecules in the hydration sphere of Eu(III). The final $^7F_2/^7F_1$ is higher than glycolic acid complex (1.25, t = 190 µs) and acetic acid complex (*viz.* 1, t = 120 µs) [8].

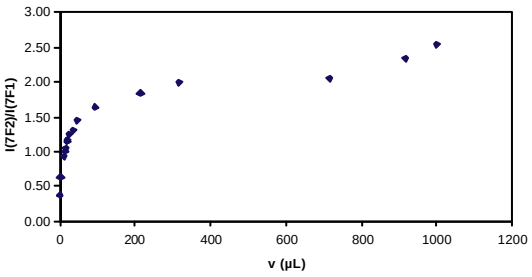

a.

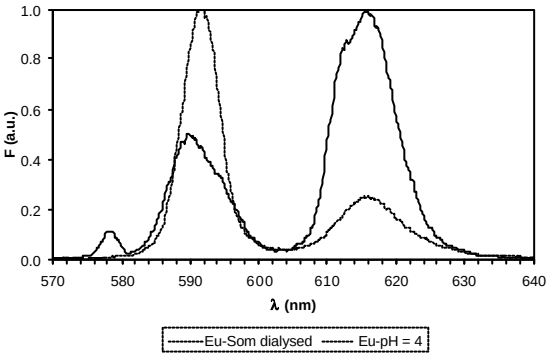

b.

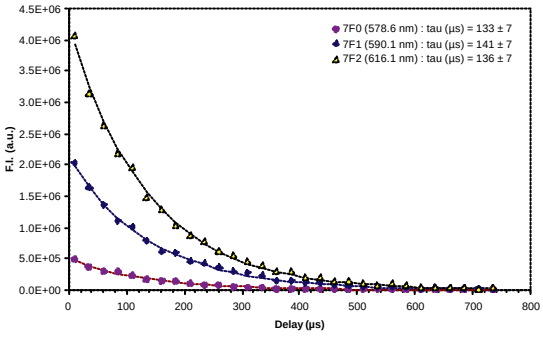

c.

Figure 8: *Europium (III) fluorescence evolution of $I(^7F_2)/I(^7F_1)$ ratio with increasing amount of dialysed SOM (a), spectrum (b) and decay (c) for Eu(III)-dialysed SOM at pH 4.*

Conclusions

The complexation of Eu(III) by acid extracted OM from COx was studied. The presence of F^- that remains in solution after the dissolution of minerals can be removed by dialysis, giving rise to more close insight on the complexation of organics. Even if significant organic loss can occur after dialysis, it can be postulated that the extracts obtained are different than the ones obtained after alkaline alteration of the COx [1]. Further studies are needed in order to better characterise the organic extracts and to obtain complexation constants.

Acknowledgement

Julien Brevet PhD grant was funded through an ANDRA grant, in the framework of a partnership between the University of Poitiers and BRGM.

References

[1] Claret, F.; Schafer, T.; Rabung, T.; Wolf, M.; Bauer, A.; Buckau, G. (2005). Differences in properties and Cm(III) complexation behavior of isolated humic and fulvic acid derived from Opalinus clay and Callovo-Oxfordian argillite, *Applied Geochemistry*, 20 (6), 1158-1168.

[2] Kumke, M. U.; Specht, C. H.; Brinkmann, T.; Frimmel, F. H. (2001). Alkaline hydrolysis of humic substances - spectroscopic and chromatographic investigations, *Chemosphere*, 45 (6-7), 1023-1031.

[3] Gaucher, E. C.; Altmann, S.; Blanc, P.; Bardot, F.; Jacquot, E.; Lassin, A.; Tournassat, C.; Braibant, G.; Crouzet, C.; Gautier, A.; Negrel, G. (2006). Modelling the porewater chemistry of the Callovian-Oxfordian formation at a regional scale., *Compte Rendu Geoscience* (in press doi:10.1016/j.crte.2006.06.002).

[4] Kumke, M. U.; Eidner, S.; Kruger, T. (2005). Fluorescence quenching and luminescence sensitization in complexes of Tb^{3+} and Eu^{3+} with humic substances, *Environmental Science and Technology*, 39 (24), 9528-9533.

[5] Kimura, T.; Choppin, G. R.; Kato, Y.; Yoshida, Z. (1996). Determination of the hydration number of Cm(III) in various aqueous solutions, *Radiochimica Acta*, 72 61-64.

[6] Hummel, W.; Berner, U.; Curti, E.; Pearson, F. J.; Thoenen, T. (2002). Nagra/PSI chemical thermodynamic data base 01/01. Rapport NAGRA NTB 02-06. Parkland, Florida.

[7] Tilkens, L.; Randall, K.; Sun, J.; Berry, M. T.; May, P. S.; Yamase, T. (2004). Spectroscopic evidence for equilibrium between eight- and nine-coordinate Eu^{3+}(aq) species in 0.1 M $EuCl_3$(aq), *Journal Of Physical Chemistry A*, 108 (32), 6624-6628.

[8] Plancque, G.; Maurice, Y.; Moulin, V.; Toulhoat, P.; Moulin, C. (2005). On the use of spectroscopic techniques for interaction studies, part I: Complexation between Europium and small organic Ligands, *Applied Spectroscopy*, 59 (4), 432-441.

THE EFFECT OF HUMIC ACID ON THE SOLID PHASE STABILY AND SOLUBILITY OF $UO_2(OH)_2$

K. Kolokassidou and I. Pashalidis*

Department of Chemistry, University of Cyprus, P.O. Box 20537, 1678 Lefkosia, Cyprus

* Corresponding author: pspasch@ucy.ac.cy

Abstract

The stability and solubility of the $UO_2(OH)_2$ solid has been studied as a function of the humic acid concentration in 0.1 M $NaClO_4$, in the pH range from 4 to 9 under atmospheric conditions. Furthermore the solid phases under investigation have been prepared by alkaline precipitation in the presence and absence of humic acid and characterized by TGA, ATR-FTIR, XRD and solubility measurements. According to the experimental data $UO_2(OH)_2$ is stable and remains the solubility limiting solid phase even in the presence of increased humic acid concentration in solution (up to 0.5 g/l). The $\log K_{sp}$ has been determined to amount 20.5 ± 0.3. Based on the solubility data the stability constant for the $UO_2OH(HA)$ species has been determined to be $\log \beta_{1101}$=15.3 ± 0.5 at pH 6.5.

Introduction

The hexavalent state is the most stable oxidation state of uranium under normal atmospheric conditions in natural aquatic systems. The chemical behaviour of uranium in such systems is governed by hydrolysis, complexation with naturally occuring ligands, colloid generation, geochemical interaction with mineral surfaces etc. In natural water systems where humic acid is present, the complexation with humic acid plays a significant role in the geochemical behaviour and migration of uranium and other actinide ions in the geosphere [1]. For the speciation and the thermodynamic characterisation of the formed U(VI) complexes with humic acid, several investigations based on various methods such as TRLFS, EXAFS, cation exchange, ultrafiltration, calorimetric and electrochemical measurements have been performed.

Although solubility measurements are often involved in the evaluation of the chemical behaviour of actinides in aqueous solution, e.g. in the determination of formation constants and the solubility product of the solubility limmiting solid

phase, there do not exist any solubility studies for the evaluation of the interaction of actinides with humic acids and the effect of humic acid on the stability of U(VI) solid phases. Considering a stable solubility limmiting solid phase, solubility studies are advantageous with respect to the determination of the free metal ion and the total metal concentration in solution and a wide pH range in which measurements can be carried out.

The the schoepite solid phases (e.g. schoepite and metascoepite) are important secondary U(VI) phases resulting from the hydrolysis of U(VI) in acidic to near neutral pH systems. The structures of these solids have been resolved by X-ray diffraction (XRD) into distinct polytypes. These layered phases are composed of two-dimensional sheets of U(VI)-polyhedra and associated oxygen and hydroxide anions with waters of hydration occupying the interlayer. The polytypes differ both in the degree of hydration and in the sheet topology. The equivalent formulas for schoepite, metaschoepite and dehydrated schoepite are UO_3 2.25 H_2O, UO_3 2.0 H_2O and UO_3 0.75 H_2O, respectively [2].

To ascertain the effect of humic acid complexation on the solid phase stability and the chemical behaviour of U(VI) in aqueous solutions, the solubility and stability of $UO_2(OH)_2$ solid has been studied as a function of the humic acid concentration in 0.1 M NaClO4, in the pH range from 4 to 9 and under normal atmospheric conditions. Furthermore the solid phases under investigation have been prepared in the presence and absence of humic acid and characterized by DRIFTS, XRD and solubility measurements

Experimental

U(VI) solutions were prepared by dissolution of $UO_2(NO_3)_2$ $6H_2O$ (Merck Co) in aqueous 0.1 M $NaClO_4$. $UO_2(OH)_2$ was prepared by alkaline precipitation of a U(VI) solution under normal atmospheric conditions at 25 ^oC. Preparation of the solids was performed also in the presence of 0.1 g L^{-1} humic acid. The yellow precipitates were separated from the solution washed with bidestilled water, dried and characterized by thermogravimetric analysis (TGA-50 Shimadzu), FTIR-ATR spectroscopy (IR Prestige-21 Shimadzu) and X ray diffraction (XRD 6000 Shimadzu). For solubilty studies $UO_2(OH)_2$ solid was conducted with pure 0.1 M $NaClO_4$ solutions or $NaClO_4$ solutions containing 0.1 g/L, 0.3 g/L and 0.5 g L^{-1} humic acid, respectively. Humic acid solutions were prepared from humic acid isolated from Gorleben groundwater (Gohy-573), purified and characterized as described elsewhere [3].

Solubility measurements were carried out in 0.1 M $NaClO_4$ under atmospheric conditions at 25 ^oC. pH was varied by addition of 0.1 M NaOH or 0.1 M $HClO_4$. Following equilibration time (from 2 weeks to six months), pH was measured by using a glass electrode (Hanna Instruments pH 211) and the analytical U(VI) concentration in solution was determined spectrophotometrically (UV 2401 PC Shimadzu) by means of arsenazo III according to a previously described method

[4]. The molar extinction coefficient for the U(VI)-Arsenazo(III) complex at 650 nm was estimated to be 65700 ± 1500 L $mol^{-1}cm^{-1}$.

Results and Discussion

In order to study the stability of $UO_2(OH)_2$ under normal atmospheric conditions in aqueous systems in the presence of increased humic acid concentration, well characterised $UO_2(OH)_2$ was contacted for several months with 0.1 M NaClO4 aqueous solutions containing defined amounts of humic acid (e.g. 0.1, 0.3 and 0.5 g L^{-1}). Moreover, the alkaline precipitation of the uranium(VI) solid phases was performed in the presence of humic acid (0.1 g L^{-1}) in solution. The resulting solid phases were characterised by TGA, ATR-FTIR and XRD and their solubility behaviour has been measured in the pH range between 4 and 7.

TGA Analysis

Thermograms of U(VI) solids prior and after equilibration with HA solutions or even U(VI) solids precipitated in the presence of HA, show similar mass losses with temperature, indicating on solids of similar composition. According to literature data these mass losses correspond to metaschoepite (UO_3 $2H_2O$)

ATR-FTIR Spectra

Fig.1 shows ATR-FTIR spectra of $UO_2(OH)_2$ solid phase in equilibrium with aquatic solutions of 0.1 M $NaClO_4$ containing various amounts of humic acid (0.1, 0.3 and 0.5 g L^{-1} HA). Fig.1 includes also the ATR-FTIR spectrum of the solid phase obtained by alkaline precipitaion of U(VI) in an aquatic solution of 0.1 M $NaClO_4$ containing 0.1 g L^{-1} of humic acid, under normal atmospheric conditions and the ATR-FTIR spectrum of well characterized $UO_2(OH)_2$ solid phase. Independent of the humic acid concentration and the way of solid phase preparation all spectra show similar features. The two intensive absorption bands at 3440 cm^{-1}, 1660 cm^{-1} in the FTIR spectrum correspond to O-H stretching and to H-O-H bending respectively and the weak absorption bands at 1100 cm^{-1} and 930 cm^{-1} to the symmetric and anti-symmetric stretching of the UO_2 moiety, respectively.

XRD Spectra

Fig.2 shows the XRD spectra of $UO_2(OH)_2$ solid phase in equilibrium with aquatic solutions of 0.1 M $NaClO_4$ containing various amounts of humic acid (0.1, 0.3 and 0.5 g L^{-1} HA). Fig.3 includes also the XRD spectrum of a well-characterized $UO_2(OH)_2$ solid phase. In agreement with the FTIR spectra, these spectra indicate also only on the presence of $UO_2(OH)_2$. In particular, the x-ray powder diffractogram is similar to the diffractogram of metaschoepite (UO_3 $2H_2O$). However, broadening of the peaks could be attributed to the impact of humic acid on the solid phase texture, particularly in the solutions of increased humic acid concentration (0.5 g L^{-1} HA).

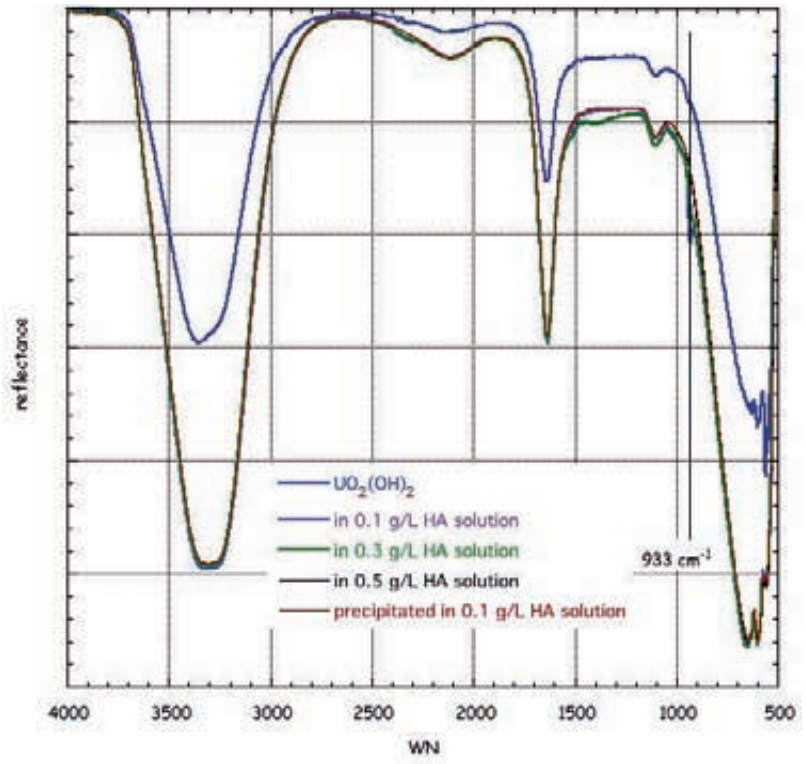

Figure 1. *ATR-FTIR spectra of $UO_2(OH)_2$ solid phase in equilibrium/precipitated with/in aquatic solutions of 0.1 M $NaClO_4$ containing various amounts of humic acid, under normal atmospheric conditions*

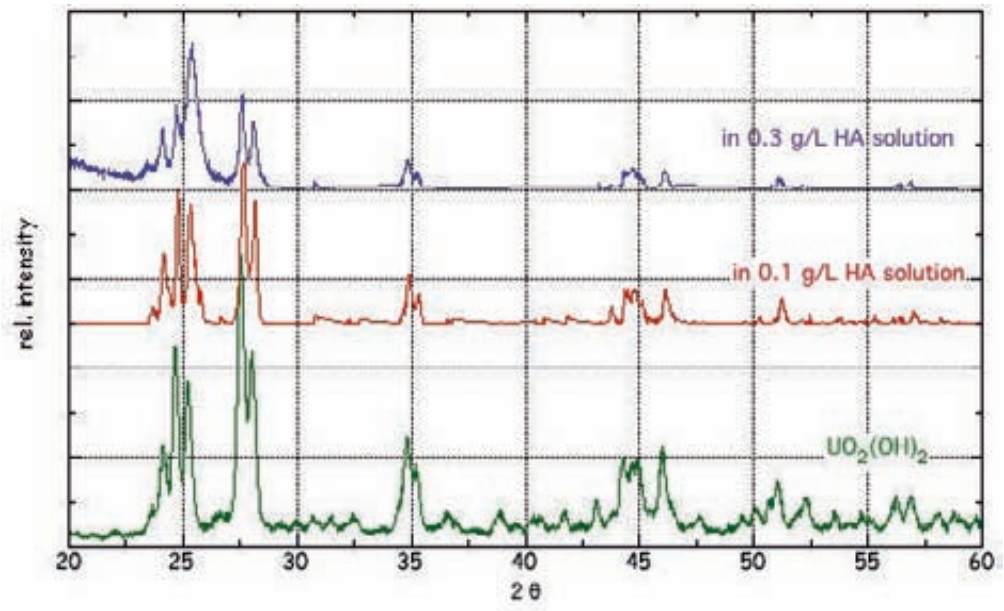

Figure 2 *XRD spectra of $UO_2(OH)_2$ solid phase in equilibrium/precipitated with/in aquatic solutions of 0.1 M $NaClO_4$ containing various amounts of humic acid, under normal atmospheric conditions*

Solubility Measurements

Solubility measurements were performed with $UO_2(OH)_2$ under normal atmospheric conditions as a function of pH in aquatic solutions of 0.1 M $NaClO_4$ containing 0.1 and 0.3 g L^{-1} HA of humic acid.

Fig. 5 shows the theoretical solubility curve (dotted line), which was calculated as the sum of the species concentration formed predominantly in solution in the absence of humic acid e.g. UO_2^{2+}, hydrolysis products and carbonate complexes [5]. This solubility curve is calculated based on literature data and validated by experimental solubility data obtained from this study. Using the literature data (formation constants) for the predominant species in the fitting equation, the solubility product for the solid phase was estimated to amount $\log K_{sp}$ = 20.5 ± 0.3. The circles correspond to experimental solubility data obtained from systems containing different amounts of humic acid. The pH was adjusted to cover pH values close to neutral pH (pH 7), however, after equilibrium the systems with humic acid were self-buffered around pH 6.5. The complexation of U(VI) by humic acid is obvious and leads to increased solubility of U(VI), which can expressed as:

$$[U(VI)]_{tot} = [UO_2^{2+}] + \sum \left(\beta_{1lm} \cdot [UO_2^{2+}]^1 \cdot [OH^-]^l \cdot [CO_3^{2-}]^l \cdot [HA]^m \right) \quad (1)$$

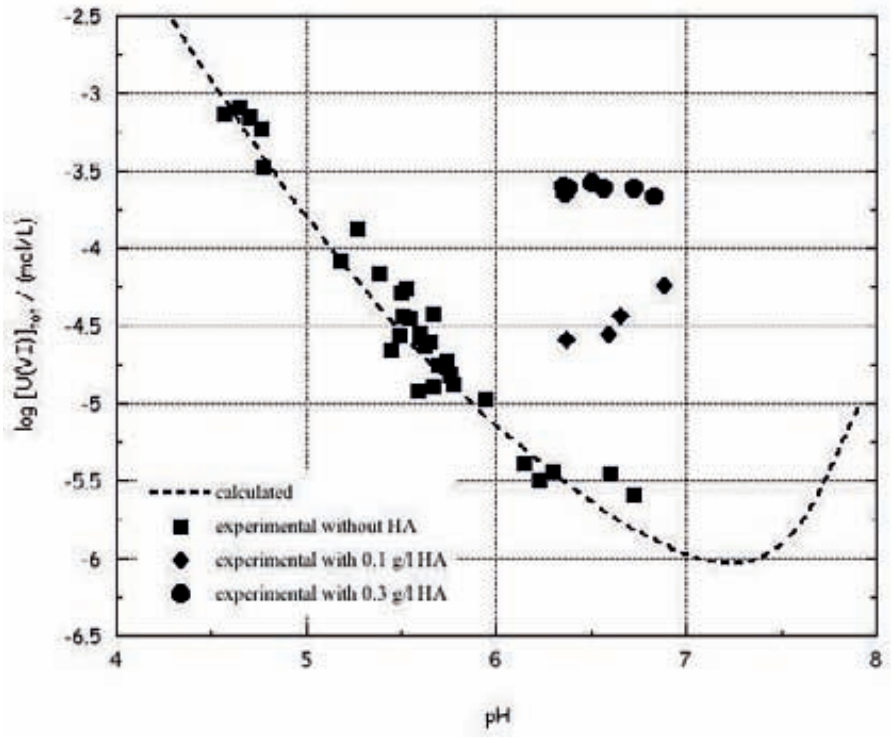

Figure6. *Solubility of $UO_2(OH)_2$ solid phase as a function of pH in aquatic solutions of 0.1 M $NaClO_4$ containing various amounts of humic acid, under normal atmospheric conditions*

According to the solubility measurements under the given conditions and in the pH range between 6 and 7, the U(VI) humate complexation determines the solubility and the contribution of the hydrolysis products and the carbonate

complexes can be neglected. Moreover, taking into account recent investigations under similar conditions that show $UO_2OH(HA)$ to be the predominant species in solution [6, 7], equation (1) can be simplified as follows:

$$[U(VI)]_{tot} = \beta_{1101} \cdot [UO_2^{2+}] \cdot [OH^-] \cdot [HA] \qquad (2)$$

Since $[UVI)]_{tot}$ is experimentally measured, $[OH^-]$ is evaluated from pH, $[UO_2^{2+}]$ is calculated from the solubility product of the solid phase and [HA], which corresponds to the effective humic acid concentration is estimated from literature data [7], the formation constant of the mixed hydroxo-humate complex of U(VI) can be evaluated from solubility data. The average value for the formation constant evaluated from solubility data obtain from this study is found to be: log $\log b_{1101}=15.3 \pm 0.5$ at pH 6.5.

References

[1] Kim J.I. (1993) Chemical Behaviour of Transuranic Elements in the Natural Environment, Mat. *Res. Soc. Symp. Proc*. 294, 3-17

[2] Sowder A.G., Clark S.B., Fjeld R.A. (1999) The Transformation of Uranyl Oxide Hydrates: The Effect of Dehydration on Synthetic Metaschoepite and Its Alteration to Bequerelite, Environ. Sci. Technol. 33, 3552-3557.

[3] Kim J.I., Buckau G., Li G.H., Duschner H., Psarros N. (1990) Characterization of Humic and Fulvic Acids from Gorleben Groundwater, *Fresenius J Anal Chem* 338(2), 245-252.

[4] Borak,J., Slovak,Z., Fischer, J. (1970) Verwendung mäßig dissoziierter komplexe bei spektralphotometrischen bestimmungen—II : Reaktionen von arsenazo iii mit uranyl und thorium(IV) *Talanta* 17(3), 215-229.

[5] NEA-TDB (2003) "Update on the Chemical Thermodynamics of Uranium, Neptunium, Plutonium, Americium and Technetium, Volume 5. Thermochemical database of the OECD-NEA (Organization for Economic Co-operation and Development - Nuclear Energy Agency).

[6] S. Sachs, V. Brendler, G. Geipel. Uranium(VI) Complexation by Humic Acid under Neutral pH Conditions Studied by Laser-induced Fluorescence Spectroscopy *Radiochim. Acta* (submitted)

[7] Buckau G. (2004) "Approach for Physico-Chemical Interpretation of An(III) and An(VI) Humate Complexation", Annex 3 in: "Humic Substances in Performance Assessment of Nuclear Waste Disposal: Actinide and Iodine Migration in the Far-Field (Second Technical Progress Report)", Ed. G. Buckau, Report FZKA 6969, Research Center Karlsruhe, ISSN 0947-8620

SORPTION OF CELLULOSE DEGRADATION PRODUCTS AND ASSOCIATED COMPONENTS TOCLAY MINERALS UNDER FAR FIELD CONDITIONS OF AN INTERMEDIATE TO LOW LEVEL NUCLEAR WASTE REPOSITORY

P. Warwick[1]; T, Lewis[1,*]; N. Evans[1]; N. Bryan[2]; and L. Knight[3]

[1] Loughborough University Department of Chemistry, Leics LE11 3TQ, UK
2 University of Manchester, Oxford Road, Manchester M13 9PL, UK
[3] UK NIREX, Curie Avenue, Harwell, Didcot, Oxfordshire, OX11 ORH, UK

*Corresponding author: t.m.lewis@lboro.ac.uk

Abstract

Herein is detailed the determination of the distribution ratios (R_d) of binary (ligand-solid) systems using a standard batch adsorption technique. Two complexing organic ligands of major concern to nuclear waste management agencies have been used; cellulose degradation products (CDP), and ISA (Isosaccharinic acid, the major component of CDP). These two ligands have been used with the solids montmorillonite, kaolinite and a-goethite.

Concentrations of CDP were determined using TOC (Total Organic Carbon) analysis over a concentration range of 1 mol L^{-1} to 1 x 10^{-4} mol L^{-1}. Concentrations of the organic ligand ISA were determined using radiometric analysis using both non-active ISA and radioactive ^{14}C labelled Ca-ISA and ^{14}C labelled Na-ISA over a concentration range of 1 mol L^{-1} to 1 x 10^{-6} mol L^{-1}.

Construction of sorption isotherms has provided the maximum sorption capacities of the solid surfaces for the organic ligand ISA, along with calculation of R_d values for ISA and CDP sorption.

The results suggest that sorption of ISA and CDP is minimal under near-neutral conditions over a wide ligand concentration range and that, therefore, retardation of these metal ligand complexes would be insignificant under far-field environmental conditions.

Introduction

Organic material present in the waste of an intermediate to low level waste underground repository can be degraded to products exhibiting complexing properties. One of the main components that will be subject to degradation processes is cellulose (in waste and cement additives) which has been found to

produce degradation products with strong complexing properties [1]. It is well understood that cellulose degradation products (CDP), including its main component ISA, are both strongly complexing and may effect the mobility of radionuclides from an engineered nuclear waste repository to the biosphere [2].

Several investigators have studied the effects of CDP and ISA on sorption of radionuclides onto cement and other solid surfaces under near-field conditions (reducing/ high pH) of a nuclear waste repository [3] [4], but little research has been carried out as to other effects under far-field conditions (near-neutral conditions).

To determine the possibility of radionuclide mobility reduction under far-field conditions the extent of sorption of ISA and CDP to clay mineral components which are likely to be present in the far field has been investigated. Work reported here examines the extent of ligand sorption to clay mineral components as a function of ligand concentration under far-field conditions.

Objectives

To perform experiments to measure distribution ratios of organic ligand-solid interactions using the batch experiment method.

Experimental

Materials

Unless otherwise stated, all chemicals were reagent grade. Water for all experiments was supplied from a Barnstead/Nanopure water system. The solids Kaolin ($\sim Al_2Si_2O_6(OH)_4$, Aldrich Chemical Company), Montmorillonite (K-10 Grade, Aldrich Chemical Company) and a-Goethite (Fe(OH)O, Fluka) were all used as supplied from their commercial manufacturers. Sodium perchlorate (0.1 mol dm^{-3}) was obtained from Fisher and used throughout to control the ionic strength.

Calcium isosaccharinate was synthesized as described by Whistler and BeMiller [5]. The sodium salt of ISA was obtained by contacting an aqueous suspension of Ca-ISA with Chelex-100 (BioRad) cation exchange resin in the Na-form, thereby exchanging Ca against Na. Active ^{14}C Na ISA was prepared using [D-glucose-1-^{14}C]Lactose supplied from Amersham Biosciences. This was used to radiolabel ISA by replacing the a-lactose monohydrate with active [D-glucose-1-^{14}C]Lactose and following the method as described by Whistler and BeMiller. An active Ca-ISA was also supplied curtsey of NIREX UK/SERCO which was originally supplied by Amersham Biosciences.

Cellulose degradation products were prepared by contacting 20 g of tissues (standard household paper tissues) with 200 g of Nirex (UK) Reference Vault Backfill (NRVB) in 0.5 dm^{-3} of deionised water. The reaction was carried out in a sealed temperature controlled 3-necked round bottomed glass flask set at 80 ºC with a continuous flow of nitrogen to maintain reducing conditions. The degradation mixture was left for 30 days after which the mixture was filtered and stored in a fridge at 2 ºC in Teflon ™ containers.

Where possible, solution pH for the batch experiments was maintained at near-neutral conditions with small additions of either HCl (aq) or NaOH (aq). Unless otherwise stated all experiments were prepared and conducted on the bench at ambient temperature. During equilibration periods samples were stored in a fridge at 2 ^{o}C on a rotary shaker set at 300 rpm.

Solutions

All organic ligand solution dilutions were typically made by weight from an ISA, 1 mol L^{-1} (w/v), stock solution. The CDP solution dilutions were made by weight from a standard stock prepared in the laboratory as described above and the molarities estimated by correlation with ISA spectra using HPLC.

Ligand Solid Binary Batch Experiments

ISA/sodium perchorate 0.1 mol dm^{-3} solutions (1.0 x 10^{-4}, 5.0 x 10^{-4}, 1.0 x 10^{-3}, 5.0 x 10^{-3}, 1.0 x 10^{-2}, 5.0 x 10^{-2}, 0.1, and 0.2 mol dm^{-3} metal salt; 20 cm^{3}) were contacted with 0.1 g of either montmorillonite, kaolin or goethite (solid:solution ratio 1:200). The pH of the solution was checked after 24 hrs contact with each solid and adjusted again to near-neutral pH. The samples were prepared in duplicate and mixed and equilibrated for 7 days. After equilibration, the pH was measured and radiometric measurements taken for the ^{14}C-ISA samples and TOC measurements for the CDP samples.

Control samples were prepared containing no solid which were used to draw calibration graphs for each ligand and to check for precipitation/biodegradation of the batch solution samples.

TOC (Total Organic Carbon) Analysis

Sodium perchlorate 0.1 mol dm^{-3} solution was used as a baseline for all analysis measurements. An average TOC value of 5 injections was used for all measurements. Using the TOC of each standard solution, calibration graphs were used for determining the amount of bound and solution phase organic ligand for all the binary experiments using a Shimadzu 5000 TOC.

Activity Measurements.

^{14}C labelled Ca-ISA was measured by liquid scintillation counting on a Canberra Packard TRI-Carb 2750TR/LL.

Distribution Ratios

Using measurements generated from the TOC analysis and radiometric measurements the amount of solute bound per mass of adsorbent was determined by:

$$\frac{x}{m} = \frac{C_0 - C}{m} V \qquad \textit{units of mol } g^{-1}$$

where x/m = *amount of solute bound, mol* g^{-1}
m = *mass of adsorbent in added to reaction container, g*
C_0 = *initial solute concentration (determined analytically) before exposure to adsorbent, mol* cm^{-3}
C = *solute concentration after exposure to adsorbent at equilibrium, cm* cm^{-3}, *and*
V = *volume of solute solution added to reaction container,* cm^3.

The amount of solute sorbed by each mineral (bound, mol g^{-1}) plotted as a function of the amount of solute remaining in the solution phase (free, mol cm^{-3}) provided an adsorption isotherm from which the distribution ratio R_d, was determined:

$$R_d = \frac{C_{bound}}{C_{free}} \qquad \text{units of } cm^3\ g^{-1}$$

Results

Tables 1 to 6 show the averaged distribution ratio's (R_d) for the ligand solid binary systems of ISA and Gluconic Acid and % sorption amounts for CDP. Figure 1 shows the sorption isotherms of ISA to (I) Montmorillonite, (II) Kaolinite, and (III) Goethite.

Discussion

ISA-Solid Binary Data from the sorption study was fitted to sorption isotherms as shown in Figure 1. An R_d for the linear range of each isotherm can be identified and are presented in Table 1. The maximum adsorption capacity of each solid for ISA was found to be approximately 1.0 x 10^{-5} mol g^{-1}, 4.0 x 10^{-6} mol g^{-1}, and 7.5 x 10^{-6} mol g^{-1} for montmorillonite, kaolinite and goethite respectively.

***Table 1**: ^{14}C-Ca ISA (1.0 x 10^{-6} to 1.0 mol L^{-1}) Sorption Study using Radiometric Analysis; Average Ligand-Solid Distribution Ratio's (R_d)*

Solid	R_d (mol g^{-1}/mol cm^{-3})	Linear R_d ISA Concentration Range/ mol L^{-1}
Montmorillonite	12.42	1.0e-06 - 1.0e-03
Kaolinite	3.28	1.0e-06 - 5.0e-04
Goethite	8.1	1.0e-06 - 1.0e-03

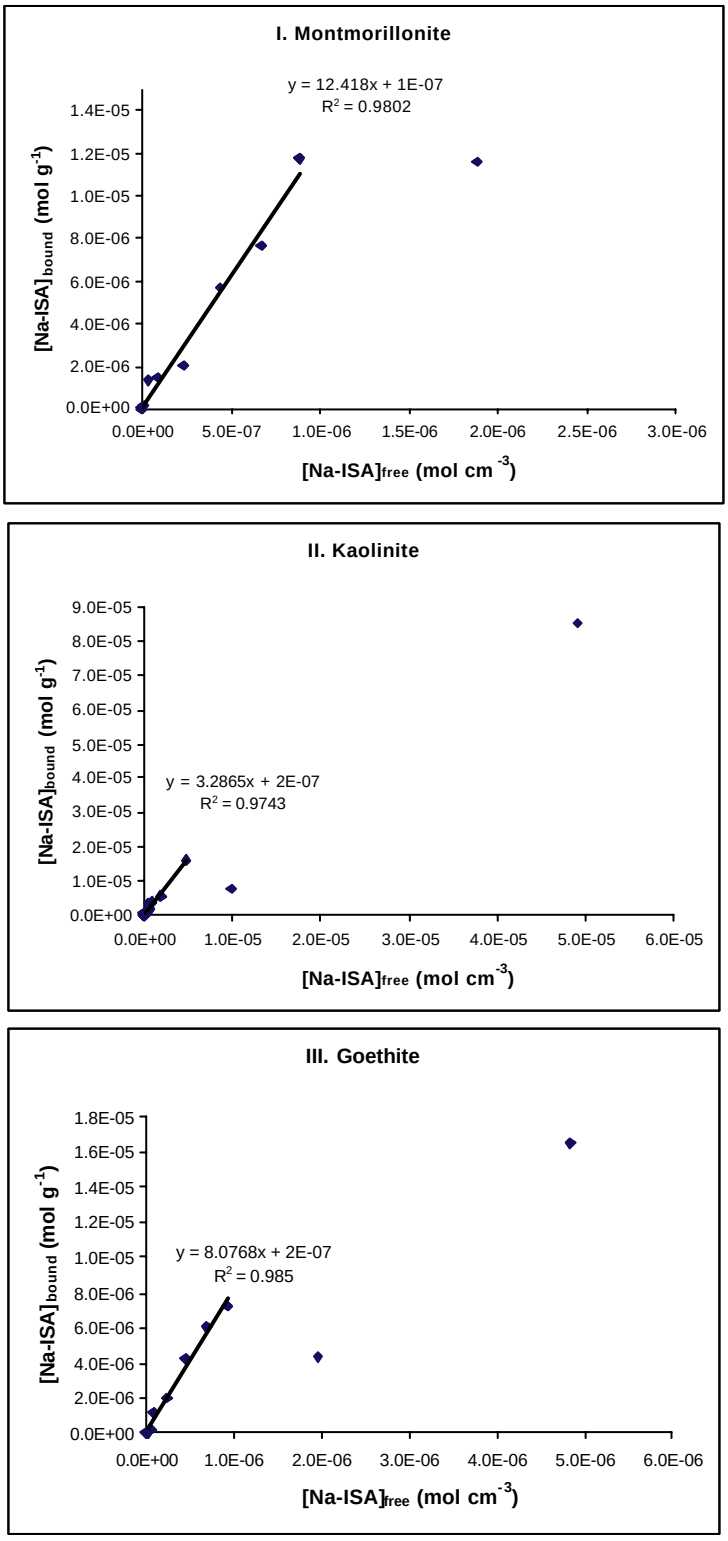

***Figure 1**: Sorption Isotherms of ISA to (I) Montmorillonite, (II) Kaolinite, and (III) Goethite*

CDP (Cellulose Degradation Products)-Solid Binary results are in agreement with the ISA results. The sorption never reached over 10% at near-

neutral and low pH for any of the solid materials and, as expected, sorption was slightly more at high pH. R_d values for CDP sorption are presented in Table 2.

Table 2 *Non active CDP (Concentration approx equivalent to 1.0 e-03 mol L-1 Na-ISA) Sorption Study using TOC Analysis; Average % Sorption*

Ligand-Solid Average *% Sorption*	**Montmorillonite**		**Kaolinite**		**Goethite**	
Initial pH	% Sorption	Final pH	% Sorption	Final pH	% Sorption	Final pH
11.50	12.16	12.03	1.78	13.12	4.97	13.12
8.00	24.30	7.13	28.08	7.20	2.35	7.20
7.00	9.23	4.64	3.08	5.90	< 1	6.89
4.50	< 1	4.01	< 1	4.48	< 1	5.11

Conclusions

From the sorption data of ISA and CDP it is clear that sorption of these organic complexes to the solid minerals montmorillonite, kaolinite and goethite at pH 6 was minimal. Because sorption was small, the impact of these organic ligands on metal sorption in a real environmental situation would be slight, when compared to the impact of other ligands present in a typical far-field environment, e.g. such as humics and fulvics (which would be present at much larger concentrations) and also, depending on the cation, carbonates. Based on the results of ligand sorption to mineral surface it can be concluded that mineral-ligand-metal ternary complexes are unlikely to be present in the environment and so metal sorption enhancement also unlikely.

References

[1] G. Fanger, K. Skagius, and M. Wiborgh. Project SAFE. Complexing agents in SFR. SKB Report R-01-01. January 2001.

[2] M. A. Glaus, L. R. van Loon, S. Achatz, A. Chodura, and K. Fischer: Degradation of cellulosic materials under the alkaline conditions of a cementitous repository for low and intermediate level radioactive waste. Part I: Identification of degradation products. Analytica Chimica Acta 398 (1999) 111-122.

[3] L. R. Van Loon and M. A. Glaus , 1998. Experimental and theoretical studies on alkaline degradation of cellulose and its impact on the sorption of radionuclides. PSI Bericht Nr 98-07 or Nagra TR 97-04.

[4] M. Bradbury and L. R. Van Loon, 1997. Cementitious Near-field Sorption Data Bases for Performance Assessment of a L/ILW Repository in a Palfris Host Rock. PSI Bericht Nr. 98-01, January 1998, ISSN 1019-0643; CEM-94: Update I, June 1997.

[5] R. L. Whistler, J. N. BeMiller, In: Methods in carbohydrate chemistry, vol. 2: Reactions of carbohydrates, Academic Press. Page 477ff (1963

MODELLING THE INFLUENCE OF HUMIC ACID ON THE SORPTION OF CADMIUM TO MONTMORILLONITE

N Evans[1*], M H Khan[1], P Warwick[1], T Lewis[1], N Bryan[2] and L Knight[3]

[1] Department of Chemistry, Loughborough University, Loughborough, Leics, UK
[2] Department of Chemistry, University of Manchester, Manchester, M13 9PL
[3] U.K. Nirex, Harwell, Oxfordshire, U.K.

* Corresponding author: n.d.m.evans@lboro.ac.uk

Abstract

Modelling is crucial to the assessment of heavy metal pollution in the environment, due to the number of possible systems to be investigated. The linear additive model has been used to predict the distribution of cadmium, a pollutant in its own right and a representative divalent cation, in a ternary system involving humic acid and montmorillonite, using the three binary interactions. Therefore, the interactions of cadmium with humic acid, humic acid with montmorillonite and cadmium with montmorillonite, as well as the ternary system were determined experimentally, to test the model.

The distribution of cadmium between aqueous and solid phases followed the model predictions very well. The difference between model and experimental data was well within an order of magnitude. The distribution of cadmium in the ternary system between solid and aqueous phase was correlated with the humic acid distribution. Sorption of cadmium was enhanced by a factor of 2.6 over the value that would be predicted if the cadmium distribution between aqueous and mineral phases simply followed the distribution of humic acid. This demonstrates that the surface had an effect on sorption even when apparently saturated with humic acid.

Introduction

Humic Acids (HA) sorbed onto geological surfaces and mobile in groundwaters, are important in the enhancement or retardation of the transport of radionuclides due to their substantial capacity to complex radionuclides, and to interact with mineral surfaces. Hence, the fate of radionuclides in the geosphere are strongly dependent on the extent of their sorption on solid phases. Sorption is a complex function of the properties of the solid surface, pH, concentration, speciation and competing ions. Clay minerals are important sorbents due to their high abundance, large negative surface area, and reactive surface hydroxyl groups.

There are too many possible ternary systems of metal, ligand and surface to determine experimentally, so modelling is crucial. Much binary data is available which can be used for predictive purposes, so the testing of ternary system models such as the linear additive model (LAM) is vital to establish reliable assessments of the migration of radionuclides through the geosphere. The LAM has been used to predict the distribution of Cd in a system involving HA and montmorillonite, using the 3 binary interactions, Fig 1. Therefore, the interactions of Cd with HA (Rd_1), HA with montmorillonite (Rd_2) and Cd with montmorillonite (Rd_3), as well as the ternary system were determined experimentally.

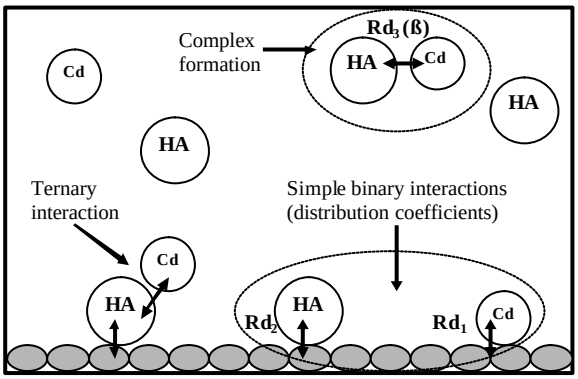

Figure. 1*. Schematic of Ternary System.*

Objectives

To test the predictive capability of the LAM on the ternary system of Cd, HA and Montmorillonite.

Experimental

Technical Grade Na salt of Montmorillonite (K-10) and HA characterised by King *et al.* (Aldrich) [1] were used. MES, [2-(N-morpholino) ethanesulphonic acid] and $Cd(NO_3)_2$ were obtained from Fisher. Whatman Cellulose Nitrate Membrane Filters (0.1 µm), syringe filter units (Minisart) and 5 ml syringes (BD Plastipak) were used. All water was 18 MO deionised from a Barnstead NANOpure system. pH was measured with a Model 720A meter in conjunction with an Orion Combination electrode. Aldrich Na humate (2.0 g) was purified by dissolution in 1 dm^3 of de-ionised water with approx. 4 cm^3 of 0.1 mol dm^{-3} NaOH solution, and sonicated using a Decon FS100 ultrasonic bath for 24 h to ensure complete dissolution. The HA was precipitated by acidifying to pH <1 with conc. HCl. The solid was filtered under vacuum, through a cellulose (0.45 µm) nitrate membrane. An HA stock solution was prepared in MES buffer solution (0.1 mol dm^{-3}) after sonication. The pH was adjusted to 6.0 using NaOH and HCl. A series of HA solutions (2 - 300 mg dm^{-3}) were prepared in MES from the stock solution. A $Cd(NO_3)_2$ stock solution in MES buffer was adjusted to pH 6.0. Cd solutions were prepared by appropriate dilution with MES buffer. A career free ^{109}Cd solution (Amersham, UK) was prepared by taking 50 µl from a stock solution (37 MBq /

1000 µl water) in 0.1 mol dm^{-3} MES buffer solution. Experiments were conducted in pre-washed polyethylene vials (20 cm^3). The optical density of HA was measured using a Cary 50 Series UV/Vis Spectrophotometer in a 1 cm^3 quartz cuvette. The ^{109}Cd activity was measured on a Packard Cobra II, Auto-Gamma Counter.

Schubert method

Cation exchanger, in Na form was placed in NALGENE vials (10 mg; BioRad AG50W X2; 100-200 mesh). An aliquot (15 cm^3) of HA solution was added, followed by MES buffer (pH = 6.0) and ^{109}Cd tracer solution (0.50 cm^3). The vials were equilibrated for 2 weeks at room temperature with intermittent shaking. A filtered (0.45 µm) sample of each supernatant was taken (1.0 cm^3) and placed in 15 cm^3 of Ecoscint cocktail. The activity was determined using liquid scintillation counting.

Cd-HA acid-montmorillonite

A 3 component set was prepared in duplicate from 0.1 g of montmorillonite suspended in 20 cm^3 HA solution of known concentrations (2.0 - 300.0 mg dm^{-3}) in 0.1 mol dm^{-3} MES buffer solution adjusted to pH 6.0. These sets were alternatively shaken and equilibrated in a water bath at 25°C for 7 days. Duplicate sets were spiked with 0.1 cm^3 tracer (^{109}Cd) and equilibrated further for 7 days after thorough mixing using a Fisons Whirlimixer. A reference set (non-spiked) was also equilibrated in the same way. pH and γ activity were measured for duplicate samples, whereas only pH and absorbance was measured for the non-spiked set.

Modelling and Discussion

The LAM assumes the distribution of metal between solution and mineral phases in a ternary system can be calculated using distribution ratios measured from binary systems. The three binary interactions and Rd values are:

(i) Cd and montmorillonite, i.e.: $Rd_1 = \frac{[Cd]_{montmorillonite}}{[Cd]_{solution}}$

(ii) fraction of Cd-HA complex sorbed to montmorillonite:

$Rd_2 = \frac{[CdHA]_{montmorillonite}}{[CdHA]_{total}}$

It should be noted that the ratio of the concentrations of CdHA sorbed to montmorillonite and in the aqueous phase is not easily measured, so the following assumption is made, i.e. that the complexed and uncomplexed HA behave in the same way: $Rd_2 = \frac{[CdHA]_{montmorillonite}}{[CdHA]_{total}} = \frac{[HA]_{montmorillonite}}{[HA]_{total}}$

(iii) Cd complexed to HA in solution, i.e. the stability constant for the CdHA complex formed: $Rd_3 = ß = \frac{[CdHA]}{[Cd][HA]}$

The model assumes that the montmorillonite exerts an effect on Cd sorption even when the surface is saturated with HA i.e.:

$$Cd_{sorbed} = Cd_{montmorillonite} + CdHA_{montmorillonite}$$

Where Cd_{sorbed}, $Cd_{montmorillonite}$ and $CdHA_{montmorillonite}$ are the concentrations of total Cd sorbed, Cd sorbed to montmorillonite and CdHA complex sorbed to montmorillonite. The assumption can be indirectly tested experimentally by investigating the following relationship: $\frac{[Cd]_{sorbed}}{[Cd]_{solution}} a \frac{[HA]_{sorbed}}{[HA]_{solution}} = c \frac{[HA]_{sorbed}}{[HA]_{solution}}$

Hence, a graph of $[Cd]_{sorbed}/[Cd]_{solution}$ against $[HA]_{sorbed}/[HA]_{solution}$ is plotted, and if the gradient (c) is equal to 1, then the LAM is not applicable, since $[Cd]_{sorbed}$ and $[Cd]_{solution}$ are determined only by $[HA]_{sorbed}$ and $[HA]_{solution}$. However, if c is greater than 1, then the surface is contributing to $[Cd]_{sorbed}$, and the LAM can be used to determine the distribution of Cd between solution and mineral phases. The version of the LAM used in this study ($Rd_{(M+HA+S)}$) is given by:

$$R_{(M+HA+S)} = \frac{\text{Total Cd on solid}}{\text{Total Cd in solution}}$$

Therefore: $R_{(M+HA+S)} = \frac{[Cd]_{montmorillonite} + [CdHA]_{montmorillonite}}{[Cd]_{solution} + [CdHA]_{solution}}$

Given the definition of Rd_2 above, as the fraction of Cd-HA complex sorbed on the surface, then $[CdHA]_{montmorillonite}$ is given by: $[CdHA]_{montmorillonite} = Rd_2[CdHA]_{total}$, and $[CdHA]_{solution}$ by: $[CdHA]_{solution} = (1-Rd_2)[CdHA]_{total}$. Using the definition of Rd_3 above, $[CdHA]_{montmorillonite} = Rd_2Rd_3[Cd]_{solution}[HA]$, and $[CdHA]_{solution} = (1-Rd_2)Rd_3[Cd]_{solution}[HA]$

Substituting gives: $R_{(M+HA+S)} = \frac{Rd_1[Cd]_{solution} + Rd_2Rd_3[Cd]_{solution}[HA]}{[Cd]_{solution} + (1-Rd_2)Rd_3[Cd]_{solution}[HA]}$

And cancelling $[Cd]_{solution}$ gives: $R_{(M+HA+S)} = \frac{Rd_1 + Rd_2Rd_3[HA]}{1 + (1-Rd_2)Rd_3[HA]}$, (Samadfam *et al.)[2]*

The standard Schubert method was applied to the measurement of the Cd-HA stability constant, by placing ^{109}Cd tracer in contact with a cation exchange resin (Na form), in the presence and absence of varying concentrations of HA. Appropriate D and D_0 values, i.e. the distribution coefficients ($[Cd]_{resin}/[Cd]_{solution}$), in the presence and absence of HA, were derived from supernatant activity measurements. ß values were calculated using the classical Schubert relationship.

Binary System – Cd and Montmorillonite (Rd_1)

Rd_1 for the interaction of Cd with montmorillonite was determined to be 73 ± 5 (dimensionless) at pH 6. The isotherm is shown in Fig. 2. In the absence of HA the sorption of Cd is strong, with only *ca.* 1.5% of the Cd remaining in solution.

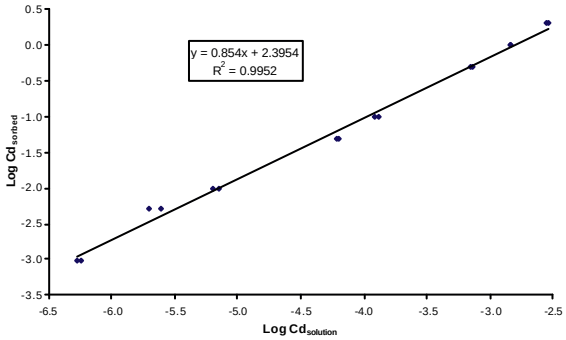

Figure. 2 *Isotherm for Cd Montmorillonite*

Binary System – HA and Montmorillonite (Rd_2)

The isotherm is shown in Fig. 3. Below the point of zero charge (pH = 6.5) the montmorillonite surface is +ve, and that of HA is -ve as shown by Wanner *et al.* [3]. This makes adsorption possible by electrostatic interactions.

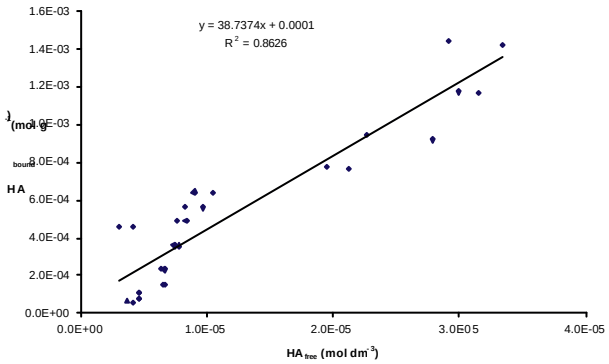

Figure. 3 *Isotherm for HA and Montmorillonite in Ternary System*

Binary System – Cd and HA (Rd_3)

The stability constant for the interaction between Cd and AHA was determined to be ß = 1.7 x 10^4. Fig. 4 shows the classical Schubert plot with a slope of 0.92 giving a strong indication of a 1:1 correspondence between the Cd^{2+} ions and the carboxylate groups on the HA.

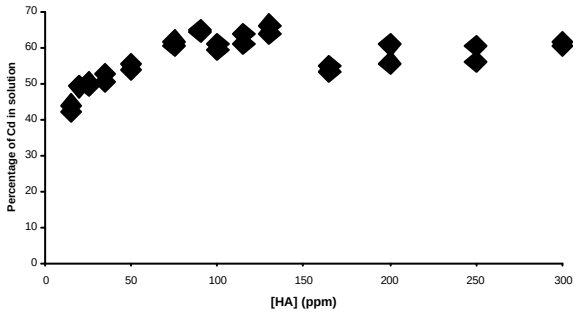

Figure. 4 *Schubert plot for Cd-HA Binary System*

Ternary System – Cd, HA and Montmorillonite

Fig. 6 shows the percentage of Cd sorbed in the ternary system at [HA] from 15 to 300 ppm. The presence of HA has mobilised between 40 and 60% of the Cd, with higher degrees of mobilisation at higher HA concentrations. However, above 75 ppm HA a plateau is reached, when increasing HA concentrations have no effect on Cd mobilisation, for reasons that are as yet, unclear. This suggests that the montmorillonite is having an influence on the sorption of Cd, even though it may be completely coated with HA. Fig. 7 shows the ratio of bound to free Cd as a function of the ratio of bound to free HA. Were the Cd distribution to follow the HA distribution slope would be equal to 1. In fact, the gradient is 2.6 indicating that the surface is causing a higher level of Cd sorption than can be accounted for by just measuring the HA acid sorption.

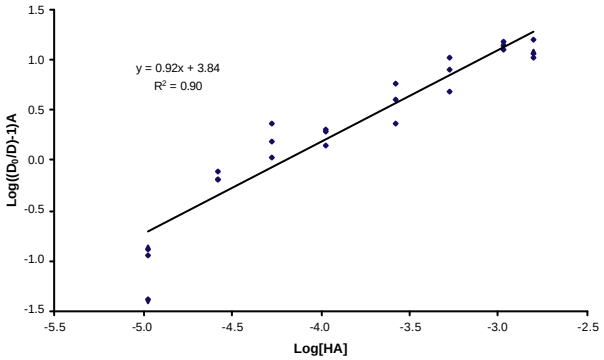

Figure. 5. *Percentage Cd Sorbed in Ternary System*

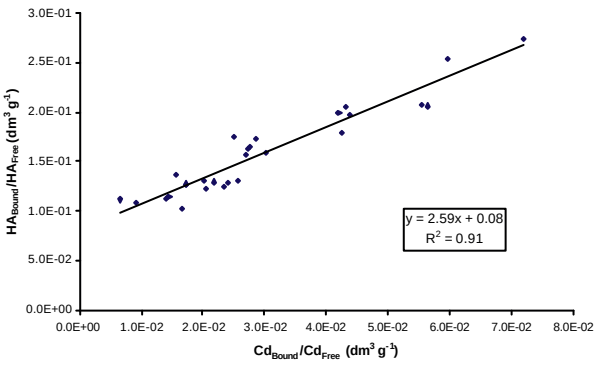

Figure. 6. *Enhancement Factor of Cd Sorption in Ternary System.*

Conclusions

The LAM allows a plot of predicted [Cd] against measured [Cd] shows that the net result is that the model predicts very well the concentration of Cd in solution, Fig. 8.

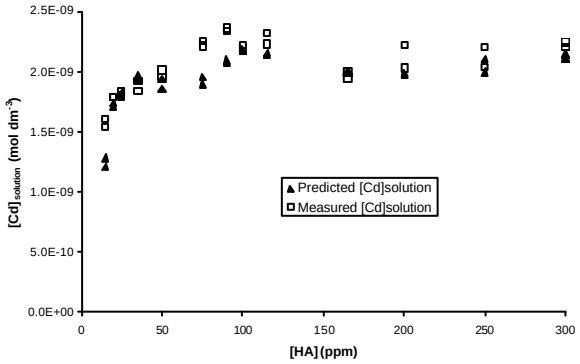

Figure. 7. *Calculated and Measured [Cd] in Ternary System*

References

[1] King, S.J.; Warwick, P.; Hall, A.; Bryan, N.D.; (2001) The Dissociation Kinetics of Dissolved Metal-Humate Complexes, *Phys. Chem. Chem. Phys.* **3**, 2080-2085.

[2] Samadfam, M.; Jintoku, T.; Sato, S.; Ohashi, H.; Mitsugashira, T.; Hara, M.; Suzuki, Y.; (2000) Effects of Humic Acid on the Sorption of Am(III) and Cm(III) on Kaolinite, *Radiochim. Acta,* **88**, 717-721.

[3] Wanner, H.; Albinsson, Y.; Kaml, O.; Wieland, E.; Wersin. P.; Charlet, L., (1994) The Acid/Base Chemistry of Montmorillonite, *Radiochim. Acta,* **66/67**, 733-738.

Np(V) CO-PRECIPITATION WITH CALCITE

F. Heberling[1], M.A. Denecke[1] and D. Bosbach[1*]

[1)] Institute for Nuclear Waste Disposal, Forschungszentrum Karlsruhe, PO Box 3640, 76021 Karlsruhe, Germany

*Corresponding author: Dirk.Bosbach@ine.fzk.de

Abstract

The migration behaviour of the actinyl ions $U(VI)O_2^{2+}$, $Np(V)O_2^{+}$ and $Pu(V,VI)O_2^{(+,2+)}$ in the geosphere is to a large extend controlled by sorption reactions (inner- and outer-sphere adsorption, ion-exchange, co-precipitation/structural incorporation) with minerals. We study the structural incorporation of Np(V) into the host mineral calcite by co-precipitation in mixed flow reactors under steady-state conditions at room temperature. In this way reaction rates and partition coefficients can be determined under varying conditions. We found that homogeneous partition coefficients for Np in calcite (0.5 – 11) are significantly higher than those reported for U(VI) (0.01-0.2 [1]). The local structural environment of incorporated Np(V) is characterized from the Np L3 EXAFS. Our data suggest that the Np(V)-ions occupy calcium lattice sites. The two axial oxygen atoms of the linear neptunyl-ions substitute two carbonate groups in the first coordination sphere. Consequently, only four carbonates are observed to coordinate the neptunyl-ion. Np-O and Np-C interatomic distances (2,4Å, 3,3Å, respectively) indicate slight structural relaxation of the carbonate groups from their ideal sites. A similar structural model is reported for U(VI) incorporated into calcite [2].

Introduction

The disposal of high-level nuclear waste in deep geological formations poses major scientific and social challenges to be met in the next decades. One of the key issues is the long-term safety of a waste repository over extended periods of time, up to 10^6 years. Demonstrating the repository safety over geological time spans requires a sound understanding of the migration behaviour of radionuclides in the geosphere. Np(IV) is expected to be retained efficiently in any compartment of the multibarrier system. The key uncertainty is associated with the expected unretarded mobility of Np(V) and the other actinyl ions that may form under oxidizing conditions at the EDZ and close to the interface to the biosphere.

The environmental behaviour of the actinyl ions $U(VI)O_2^{2+}$, $Np(V)O_2^{+}$ and $Pu(V,VI)O_2^{(+,2+)}$ is to a large extent controlled by sorption reactions (inner- and outer-sphere adsorption, ion-exchange, co-precipitation/structural incorporation)

with minerals. Structural incorporation is not yet commonly considered in the safety analysis for repository systems, although these phenomena are quite common and extensively studied in natural systems. The main reason for this discrepancy is the lack of thermodynamic and kinetic data needed for the quantitative description of these processes. Here we study the structural incorporation of Np(V) into the host mineral calcite by co-precipitation. The aim of this work is to investigate if neptunyl-ions can be incorporated onto stable lattice sites in the calcite crystal lattice and to quantify the uptake by the homogeneous Henderson-Kracek partition coefficient. The structural environment of neptunyl in calcite is characterized by EXAFS Spectroscopy in order to identify the substitution mechanism. The results will provide basic information for modeling the neptunyl-calcite aqueous-solution solid-solution system.

Experimental

Four neptunium containing calcite samples are synthesized in a mixed-flow-reactor under varying conditions, two at a pH of about 10.3, one at pH 12.8, and one at pH 8.2 to check if the aqueous speciation has an influence on the incorporation. At the chosen solution compositions the pure NpO_2^+-ion dominates the aqueous speciation at pH 8.2, at pH 10.3 the neptunyl monocarbonato complex dominates, and at pH 12.8 the neptunyl dihydroxo complex. SI(calcite) of the input solutions is chosen to be between 1 and 1.3 in order to avoid homogeneous nucleation ($SI = \log_{10}(IAP/K_{sp})$, with the Ion Activity Product, IAP, and the Solubility Product, K_{sp}). All the experiments are conducted with a Np concentration of 1µmol/L and a background electrolyte concentration of 0.01M NaCl. The input solution is undersaturated with respect to all known solid neptunium phases. As seed crystals we use ~150mg Merck suprapur calcium carbonate with a diameter of 11-15µm (sieved). The reactive surface in the reactor is ~0.2m^2 (measured by BET). The stock solutions are prepared with MilliQ water and Merck p.a. chemicals. Three stock solutions, the first containing NaCl and Na_2CO_3 (+ $NaHCO_3$ or NaOH, to adjust the pH), the second NaCl and NpO_2^+ (taken from a 0.073 mol/L pH 3 perchloric acid stock solution) and the third NaCl and $CaCl_2$, are pumped continuously into the reactor (see Figure 1). Calcium and neptunium concentrations are sampled before and after the reactor and analyzed by ICP-MS. The calcite suspension in the reactor is stirred by a magnetic stirring bar ((1) in Figure 1). In the reactor steady-state conditions are attained and the neptunium containing calcite grows homogeneously onto the seed crystals. From the concentrations, the mole balance Δc ($= c_{in} - c_{out}$) and the flowrate the reaction rate R (equation(1)) and the homogeneous partition coefficient D (equation (2)) can be calculated.

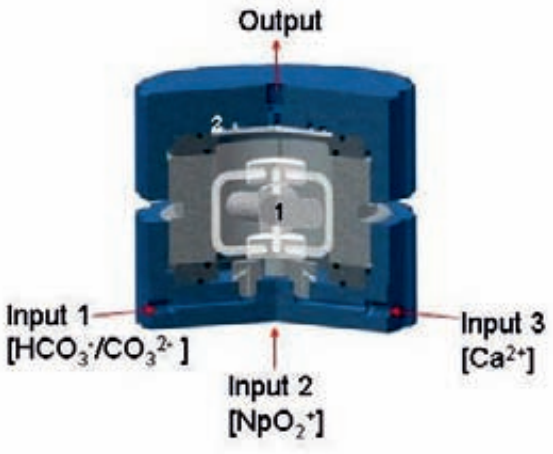

***Figure 1**: The mixed-flow-reactor used for the co-precipitation experiment. The suspension in the reactor is stirred by a magnetic stirring bar (1). A filter (2) before the output tube keeps the seed crystals in the reactor*

$$R = \frac{flowrate \cdot \Delta c}{surface} \qquad (1)$$

$$D = \frac{X_{Np} / X_{Ca}}{[NpO_2^+]/[Ca^{2+}]} \qquad (2)$$

with X_a being the molfraction of a in the precipitated solid phase and $[a]$ being the concentration of a in the steady-state solution.

The four samples are examined by EXAFS measurement at the Np L3 edge (17.608keV). The measurements are performed at the INE-Beamline at ANKA in fluorescence-mode. As monochromator crystals we use Ge(422). The energy calibration is done by parallel measurement of a Zr-foil, defining the first inflection point as 17.998keV. We record seven to ten spectra for each sample from about 150eV beneath the absorption edge up to 700eV-1100eV above the edge and analyze the resulting averaged spectra using backscattering amplitude and phase shift functions calculated with Feff 8 [3] and the FEFFIT 2.54 software. Background removal is done with WinXAS 3.1 [4].

***Table 1:** Results of the mixed-flow-reactor experiments.*

Experiment	pH_{input}	SI_{input}(calcite)	R [$\cdot 10^{-8}$ mol/($m^2 \cdot s$)]	D
1	10.3	1.0	1.0	2
2	10.3	1.1	1.1	0.5
3	12.8	1.3	3.2	8
4	8.2	1.3	3.5	11

Results and discussion

Results from the mixed-flow-reactor experiments are summarized in Table 1. The partition coefficients D range from 0.5 to 11. They are therefore significantly higher than those reported for the structurally equivalent uranyl (0.01-0.2 [1]). The experimental conditions at which the calcite precipitates are close to equilibrium. No homogeneous nucleation takes place. The precipitation rates at which we conduct our experiments of 1.0 -$3.5 \cdot 10^{-8}$ mol/(m^2*s) are very low (see summary in [1] for comparison). Therefore the measured partition coefficients should be well applicable for further modeling of the aqueous solution – solid solution system. The different aqueous neptunium speciation at the differing pH values chosen for the synthesis of the four samples has no observable influence on the incorporation. We do find an indication that reaction rate and partition coefficient correlate; samples 3 and 4 with the largest D precipitated at the highest rate.

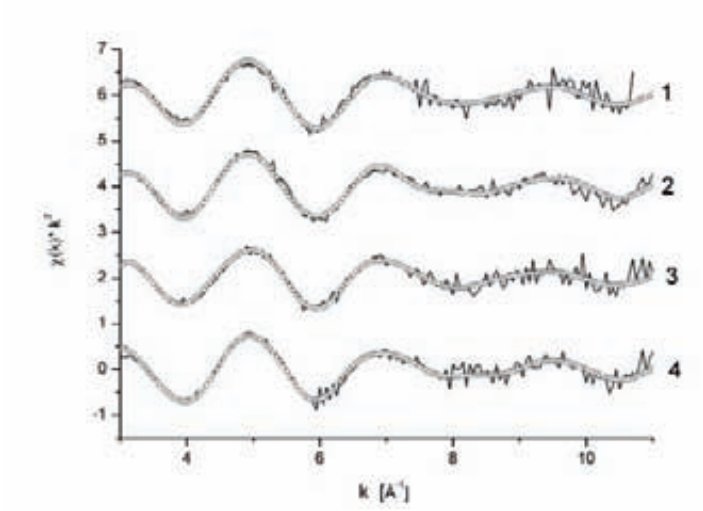

***Figure.2**: EXAFS spectra of the samples 1 to 4 and the corresponding fits in K-space. (Spectra and fits are shifted along the y-axis for clarity.)*

***Table 2**: Results of the EXAFS fits. Coordination numbers N, interatomic distances r and Debye-Waller Factors s^2 (uncertainties in parenthesis) for the neptunium environment in the calcite samples 1 to 4. ([1)]: held constant during the fit = means the parameter is correlated to the one listed)*

1	N	r [Å]	s^2 [Å^2]	2	N	r [Å]	s^2 [Å^2]
1st shell O-yl	2[1)]	1.843 (0.006)	0.0018 (0.0008)	1st shell O-yl	2[1)]	1.855 (0.008)	0.002[1)]
2nd shell O-carb1	4.08 (1.05)	2.402 (0.011)	0.0093 (0.0039)	2nd shell O-carb1	3.61 (1.41)	2.414 (0.015)	0.0065 (0.0044)
3rd shell C-carb	= $N_{O\text{-}carb1}$	3.257 (0.168)	0.0395 (0.0370)	3rd shell C-carb	= $N_{O\text{-}carb1}$	3.344 (0.114)	= $s^2_{O\text{-}carb1}$

3	N	r [Å]	s^2 [Å^2]	4	N	r [Å]	s^2 [Å^2]
1st shell O-yl	2[1)]	1.857 (0.008)	0.0029 (0.0019)	1st shell O-yl	2[1)]	1.855 (0.010)	0.0017 (0.0013)
2nd shell O-carb1	4.88 (1.15)	2.399 (0.011)	0.0125 (0.0048)	2nd shell O-carb1	4.3[1)]	2.413 (0.017)	0.0073 (0.0022)
3rd shell O-carb2	4[1)]	3.411 (0.015)	0.0132 (0.0028)	3rd shell C-carb	4[1)]	3.380 (0.127)	0.0140 (0.0246)
				4th shell O-carb2	4[1)]	3.527 (0.084)	0.0102 (0.0138)
				5th shell Ca	6[1)]	4.003 (0.071)	0.0245 (0.0103)

Np L3 k-weighted EXAFS for all four samples and their corresponding fit curves are displayed in Figure 2. The model spectra fit the data very well. The structural parameters obtained from the EXAFS fits are summarized in Table 2. The relative shift in ionisation energy ($\Delta e0$) and the amplitude reduction factor (S_0^2) are held constant at their initial first and second shell fit values (6.1, 5.6, 9.2, and 9.8 and 0.92, 0.87, 0.89, and 0.87 for the samples 1, 2, 3, and 4, respectively) and than repeating the fit. All samples show within the uncertainties the same result, i.e. the same nearest neighbour ordering of atoms surrounding Np. The degeneracy of the scattering paths corresponding to the carbonate ions in the first coordination sphere around the central neptunyl-ion (i.e. coordination number for O-carb1, C-carb, and O-carb2) is about four. Therefore we conclude that the neptunyl-ions occupy calcium sites in the calcite lattice with the oxygens of the linear neptunyl molecule substituting two carbonate-ions in the first coordination sphere. Consequently the neptunyl is coordinated by four carbonates only. The interatomic distances indicate structural relaxation of the remaining four carbonate groups from their ideal sites (r(O-carb1) = 2.39Å to 2.41Å instead of 2.35Å [5], r(C-Carb) = 3.26Å -3.41Å instead of 3.20Å [5], and r(O-carb2) = 3.52Å instead of 3.44Å [5]). This relaxation causing structural strain indicates a positive enthalpy of mixing. Therefore a complete solid solution series of mixing at room temperature cannot be expected. The small Debye-Waller Factors (s^2) are evidence for the high order in this structure. A picture of the suggested near-ordered structure for neptunyl incorporated into the calcite host at a calcium site is shown in Figure 3. A similar structural model was reported for U(VI) incorporated into natural calcite [2].

This structure leaves a charge excess of +3 in the calcite lattice (loss of two carbonate molecules and replacement of divalent calcium with single charged neptunyl cation). There is not yet evidence how this charge is balanced. Possible charge balancing mechanisms would be substitution of Ca^{2+} by Na^+ or vacant Ca^{2+} sites. The critical scattering path to obtain information about coupled substitution mechanisms would be the calcium shell surrounding the incorporated neptunyl. Fits to this shell are only possible for the spectrum of sample 4. The best fit result is however achieved with a model using six Ca^{2+} ions near 4Å. This distance is to within the uncertainty of the EXAFS analysis equal to the calcium-calcium distance in the calcite lattice (4.03Å [5]). The next distant calcium coordination sphere (4.97Å [5]) where the charge could also be balanced is too far away to be measured in the room temperature EXAFS data.

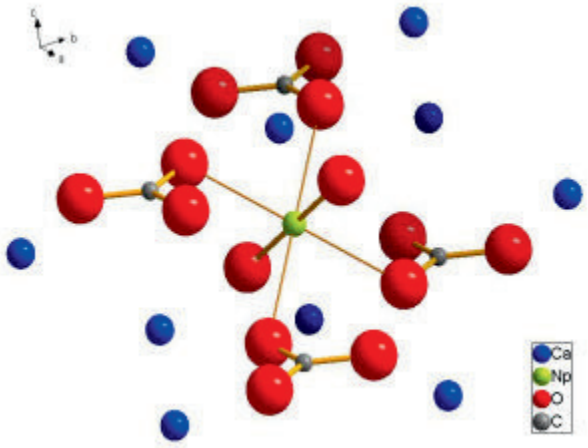

***Figure. 3**: Structural model of neptunyl incorporated into the calcite host.*

Conclusions

In this study neptunium(V) doped calcite is synthesized at low precipitation rates at conditions close to equilibrium. No homogeneous nucleation takes place during the co-precipitation experiments and the solid-solution precipitates homogeneously under steady state conditions. The measured partition coefficients D range from 0.5 to 11. These are one to two orders of magnitude higher than those reported for uranyl [1]. We observe that the aqueous speciation of neptunyl has no major influence on the incorporation. Neptunyl is found to occupy a calcium lattice site in the calcite host. The two oxygen atoms of the linear neptunyl molecule substitute two carbonate groups in the first coordination sphere, consequently only four carbonates coordinate the neptunyl-ion.

References

[1] Curti, E. (1997) Coprecipitation of radionuclides: basic concepts, literature review and first applications, *PSI-Bericht*, **97**.

[2] Kelly, S.D.; Newville, M.G.; Cheng, L.; Kemner, K.M.; Sutton, S.R.; Fenter, P.; Sturchio, N.C.; Spötl, C. (2003) Uranyl Incorporation in Natural Calcite, *Environmental Science and Technology* **37**, 1284-1287.

[3] Rehr, J.J.; Mustre de Leon, J.; Zabinsky, S.I.; Albers, R.C. (1991) Theoretical X-ray absorption fine structure standards, *Journal of the American Chemical Society* **113**, 5135

[4] Ressler, T. (1997) WinXAS: A new software package not only for analysis of energy dispersive XAS data, *Journal of Physics*, **IV 7 (C2)**, 267-270.

[5] Warchtow, R. (1989) Datensammlung nach der Learnt-Profile Methode für Calcit und Vergleich mit der Background peak background Methode (PBP), *Zeitschrift für Kristallographie* **186**, 300-302.

GEOLOGY AND GEOPHYSICS OF NEW BOREHOLES AT THE FEBEX SITE

R. Carbonell[1], A. Pérez-Estaún[1], T. Missana[2], J. Suso[3], G. Carretero[3], J. Bueno[3], L. Martínez[3], B. Buil[2], A. Garralón[2], P. Gómez[2]* and P. Hernán[5]

1 Instituto Jaume Almera, CSIC, Spain
[2] CIEMAT, Spain
[3] AITEMIN, Spain
[4] Universidad Politécnica Cataluña, Spain
[5] ENRESA, Spain

* Corresponding author; rcarbo@ija.csic.es

Abstract

Geophysical data has been acquired to characterized the fracture network of the surrounding volume within the FEBEX gallery. The geophysic data include new borehole logging such as Natural Gamma and Borehole Ground Penetrating radar and cross hole ultrasonic tomography. The preliminary processing and integration of these different data sets indicates that the GPR record can provide images of the fractures, specially if they are fluid filled. The GPR is specially sensitive to the water content as it directly affects the electrical conductivity and the dielectric permittivity Therefore it is adequate for mapping water conductive fractures of the crystalline rock. The correlation of the anomalies measured by the natural gamma can be correlated with the "diffractions" in the GPR and the fractures imaged by the borehole televiewer. The cross hole ultrasonic tomography data is under processing and no interpretations have been attempted yet.

Introduction

The FEBEX gallery was excavated in the Aar Granite, a heterogeneous granite containing from very leucocratic facies to granodiorites. The geology of the gallery shows the existence of various sets of fractures with different attributes: geometry, kinematics, fracture infilling, etc. The study of previous structural data, new observations on the FEBEX gallery and borehole televiewer data acquired in the new boreholes, have allowed to identify four sets of fractures (Figures 1, and 2).

The first group of fractures has a typical distribution and characteristics of en echelon tension fractures and were formed in late magmatic stages, according with the paragenesis of the minerals that filled the craks. The main strike is around 300 (280-300). These fractures are deformed and displaced by the other group of faults.

The second group corresponds to the lamprophyre dikes, of mantelic origin, with an orientation oblique to the tunnel, and slightly oblique to the first group of fractures (strike, 310-330). They were formed during an extension event well evidenced by their irregular margins and flame structures into the granite. The margins of these dikes show several reactivations as strike slip faults.

The third group corresponds to very few faults located at the end of the gallery, subvertical and normal to the tunnel (blue in figure 1). Their kinematics character is unknown since there are not possibilities of direct observations.

Longitudinally to the tunnel there are bands with small fractures, at small angles, and cataclastic zones that form brittle shear zones, with small-accumulated displacement (main strike: 60, Fig. 1). These fracture zones are well visualized in a tomographic study (big scale) developed and published in 1999.

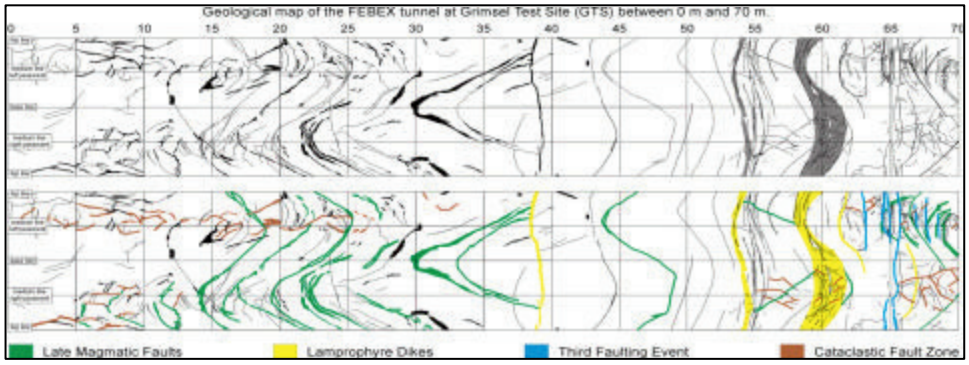

Figure. 1.- *Map sowing fracture systems in the FEBEX gallery*

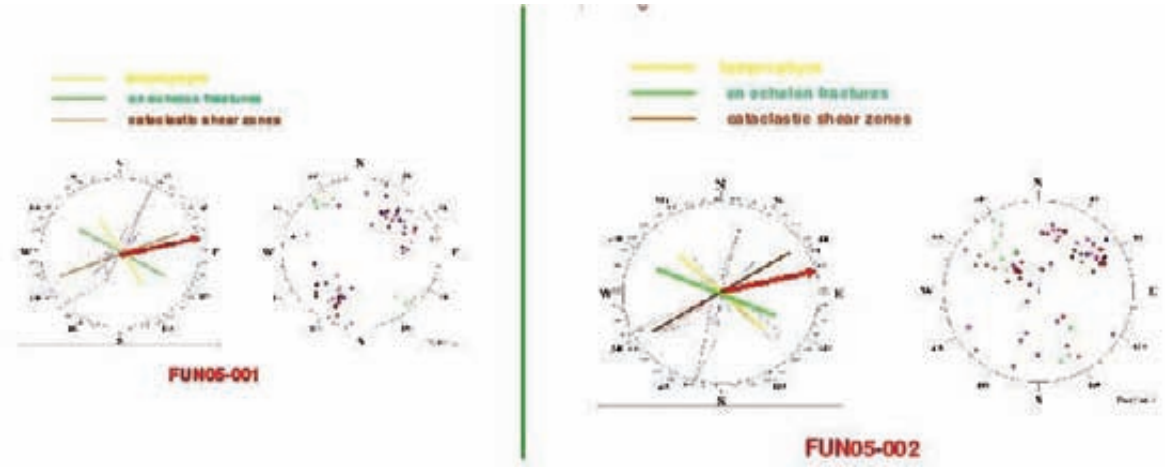

Figure. 2 *(a) Stereographic projection of the discontinuities found in FUN005-01 from borehole televiewer data. Colour lines in the stereographic plot are main directions of the different set of fractures. Red arrow: direction of FEBEX gallery. (b) Stereographic projection of the discontinuities found in FBX95-002 from borehole televiewer data. Colour lines in the stereographic plot are main directions of the different set of fractures. Red arrow: direction of FEBEX gallery.*

New Geophysics data acquired with the FUNMIG project

The geophysical characterization of the fracture network included the acquisition of new data sets in the FBX92-02 and also in the newly drilled FUN005-001 and FUN005-002. The data acquired included: Natural Gamma, Borehole Televiewer Imaging, Borehole Ground-Penetration Radar and Cross-hole ultrasonic tomography.

The geophysic experiments carried out in the newly drilled boreholes include natural gamma, borehole televiewer images, ground-penetrating radar imaging and ultrasonic monitor crosshole tomography. Logging, natural gamma and the televiewer images were also acquired in the FEBEX 02 from 40 m to 130 m. Note that all the boreholes are horizontal and the tools need to be pushed along the borehole which generated an additional difficulty. Natural gamma measured along boreholes FUN005-01, FUN005-002 and FBX95-002 allow correlating the position of the lamprophyre dikes as well as some major fractures at the end of the FEBEX gallery (Fig. 3).

The structural study of boreholes FUN005-01 and FUN005-002 has identified the existing fractures and those of major interest for migration studies. Fractures June (8.59-8.62 m; Fig. 4), August (14.75-14.85 m) and September (17.53-17.86 m), from FUN005-001, are minor faults and shear zones that will be studied in more detail and will be used to take samples for water chemical control and rock analyses. The Lamprophyre reactivated contact (8.98 m; Fig. 4) and the December shear zone (16.66-17.40 m) are two zones from FUN005-02 that will be used for the same purposes. The correlation of fractures among the existing boreholes allows presenting a 3D distribution in the volume of rock closed to the FEBEX wall (at the end of the gallery) that needs to be validated with the geophysical experiments.

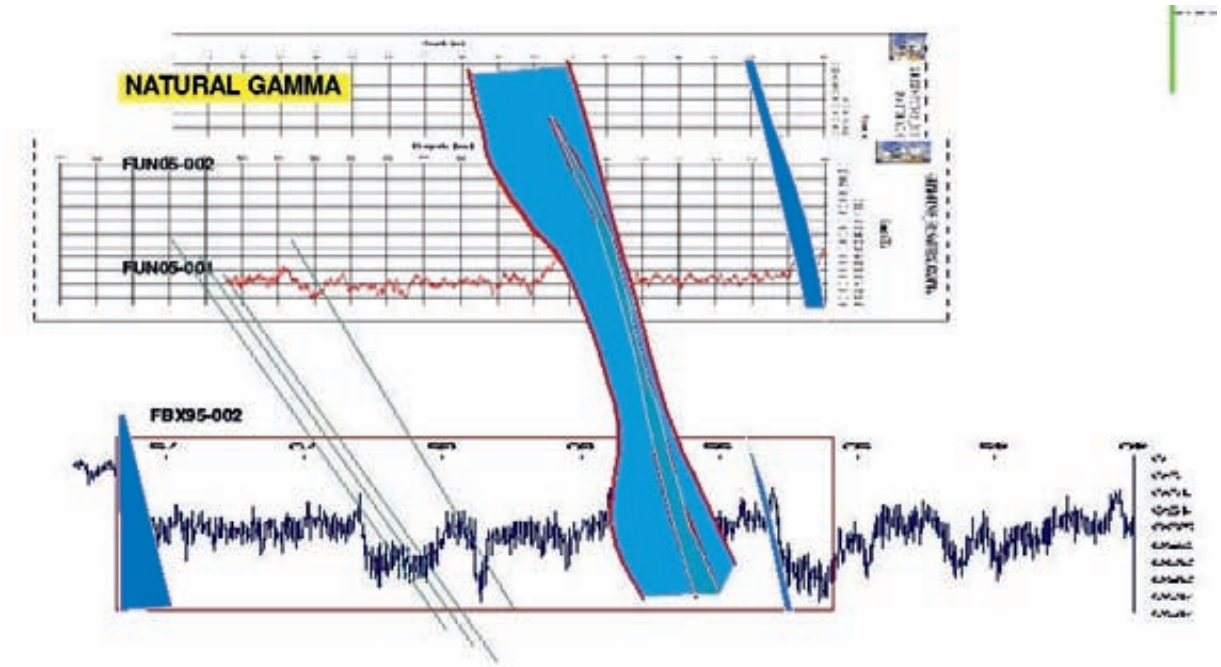

***Figure. 3**: Gamma natural measured in FUN05-01, FUN05-02 and FBX95-002. Correlation of different structures. In blue: lamprophyres. In green: fracture traces.*

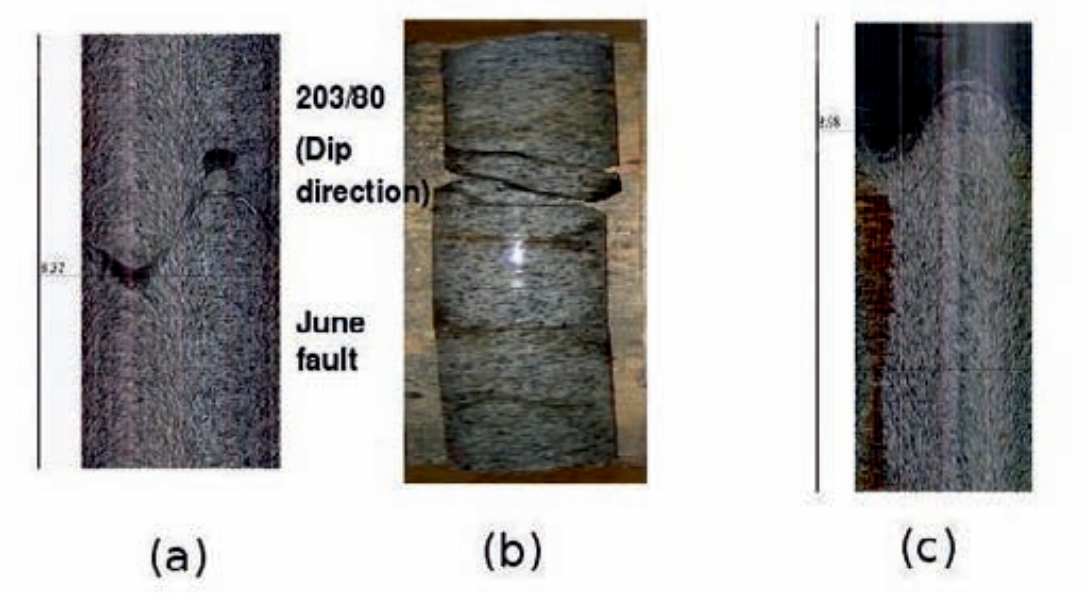

Figure. 4. *(a) Image from BTW and core. (b) June fault at 8.59 m in FUN05-01. (c) Lamprophyre-granite contact in FUN05-02. Dip direction and dip: 227/65. Image from BTW.*

Two geophysical experiments to characterize the volume of rocks in the surroundings of the FEBEX tunnel by using high-resolution tools (GPR and cross-hole ultrasonic tomography) have been acquired. The main objective is to image possible faults, and/or volumes of rocks which feature different physical properties than the granitoid itself. Fault zones in granitic rocks have different physical properties than the surrounding host rock. The presence of fractures, adjacent geochemically altered material and fluids (water) gave rise to lower seismic velocities in the fault zones than in the fresh unfractured granite located between them. Therefore, a carefully designed seismic tomography experiment should be able to map velocity differences within the granitic massif in 3-D.

The data acquisition experiments consist on acquiring geophysical data using borehole FBX-2 and the recently drilled boreholes to image the volume of rock in between the boreholes and the main tunnel. Two experiments were developed:

Tomographic GPR experiments (Fig. 5, 6) using the three boreholes: a) Transmission mode GPR: Emission at A and receiving at B, C and the tunnel; b) Transmission mode GPR: Emission at B and receiving at A and C; c) Reflection mode in A; and d) Reflection mode in B.

CHUM cross-hole ultrasonic tomographic measurements. Very high resolution experiment using ultrasonics as the source energy. Only one receptor and one emisor are used, and they are displaced every 10 cm along the boreholes FUN005-01, FUN005-02, FUN005-03, FUN005-04, and FUN005-05.

Borehole Radar Experiment

Ground-penetrating radar (GPR) is mostly controlled by the electrical conductivity and the dielectric permittivity of the soil and rock. In particular, the penetration of radar waves is limited by the conductivity of the material surrounding the borehole. Radar acquisition system consists of a transmitter and a receiver connected through an optical cable to a control unit. This unit is used for both, signal generation and data recording. In this case, as the radar probe is inserted in the boreholes it should be able to detect and map geological targets away from the surface. Under favourable conditions such as this one, surveys in crystalline rocks, the radial detection range of the borehole radar equipment may be greater than 100 m.

The downhole radar tool can be operated in reflection and transmission modes. Reflection mode implies that the same tool emit the source signal and records its echoes. Transmission mode consists in using two antennas, one as a source and a second one as a receiver. Using this mode we can acquire crosshole radar tomography data.

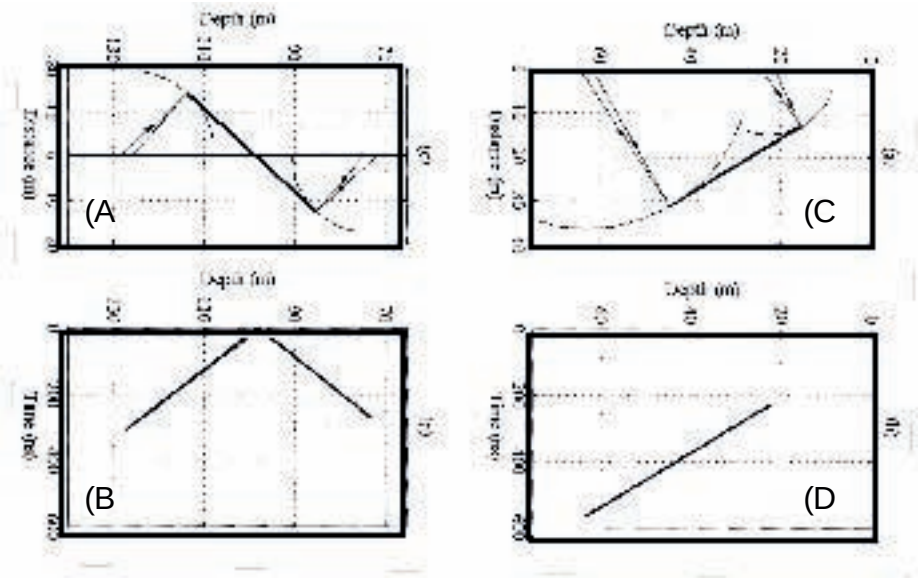

Figure 5*. Key to the interpretation of borehole GPR images. Sketches illustrating the relationship between planar fractures and their images on borehole radar data: (A) A dipping planar structure that intersects the borehole and its corresponding GPR image (B). (C) a fracture that does not intersect the borehole. (D) the radar image of fracture sketched in C. Note that as there is axias simetry, any planar structure (fracture) that had the same dip, distance and length relative to the borehole axis would result in the same reflection pattern.*

The reflection mode data acquisition in a single hole simulates a single channel normal incidence seismic reflection acquisition. The antennas used were dipole omni-directional antennas. They radiate pulse signals and receive reflections from all directions (i.e. azimuths spanning 360 °). This introduces some difficulties in the interpretation of the records, as it is not possible to determine the azimuth of a

reflector using the data from a single borehole. What can be determined is the distance to the reflector and we can estimate its minimum length (Fig. 5 and 6). It the reflector is a planar feature, we can determine the angle between the reflector and the borehole axis. The data are being processed at this moment.

The geophysical data acquired using the different methodologies was correlated in order to provide a key to the interpretation of the GPR images. Therefore the borehole televiewer images revela the fractures and dikes as sinusoidal features. These features coincide with anomalous reading in the Gamma logs they indicate the presence of fractures. Then the location of these features is identified as events in the GPR images.

The borehole televiewer and the Gamma logs play the role of validating our interpretaions (Fig. 6).

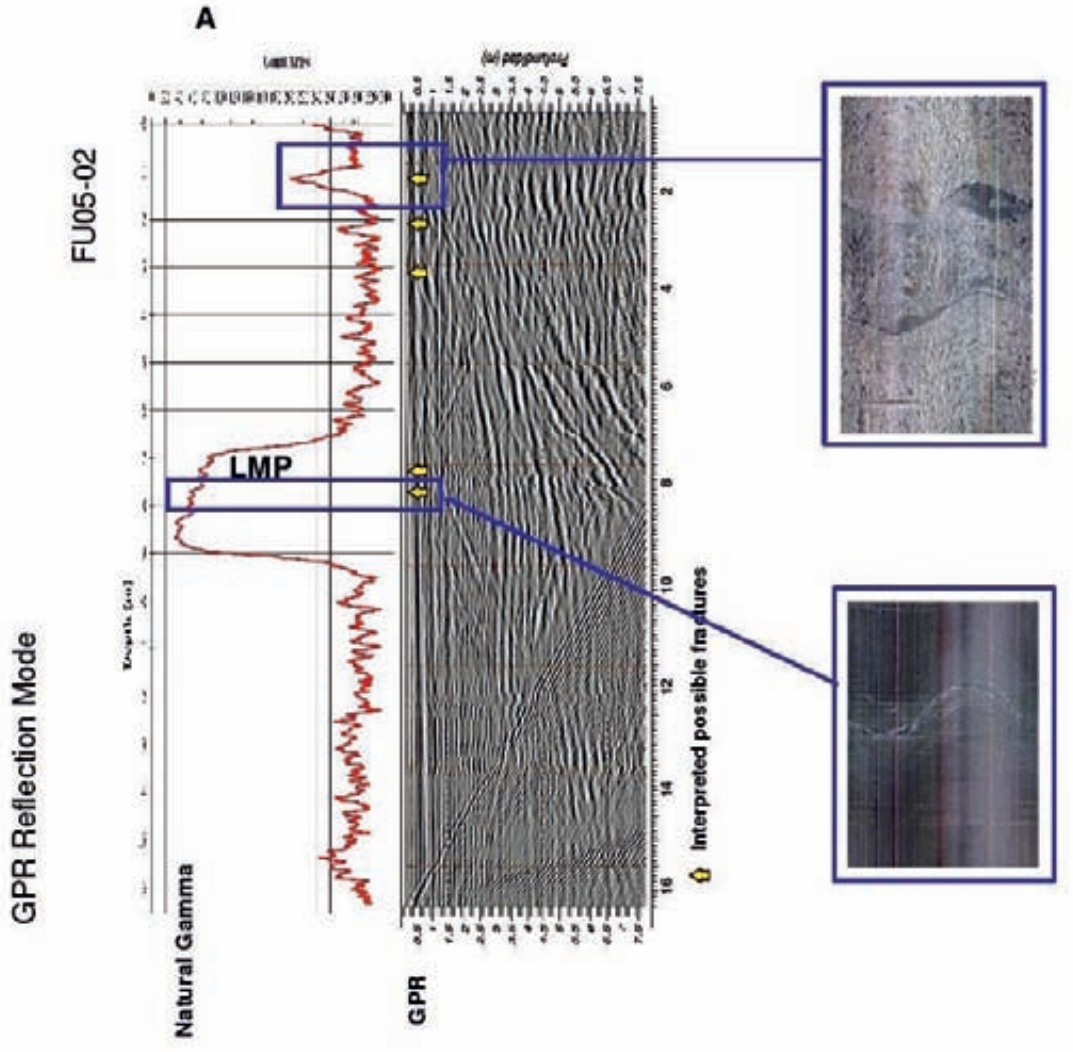

Figure 6*. Correlation between the natural gamma, GPR section and the borehole televiewer images.The GPR is specially sensitive to the water content as it directly affects the electrical conductivity and the dielectric permittivity. Therefore it is adecuate for mapping water conductive fractures of the crystalline rock. The correlation of the anomalies measured by the natural gamma can be correlated with*

the "diffractions" in the GPR and the fractures imaged by the borehole televiewer. A illustrates the correlation between the data for borehole FU05-02 and B for the borehole FU05-1. Note that the large lamprophyre structure reveals a very distinctive signature. This is marked by LMP.

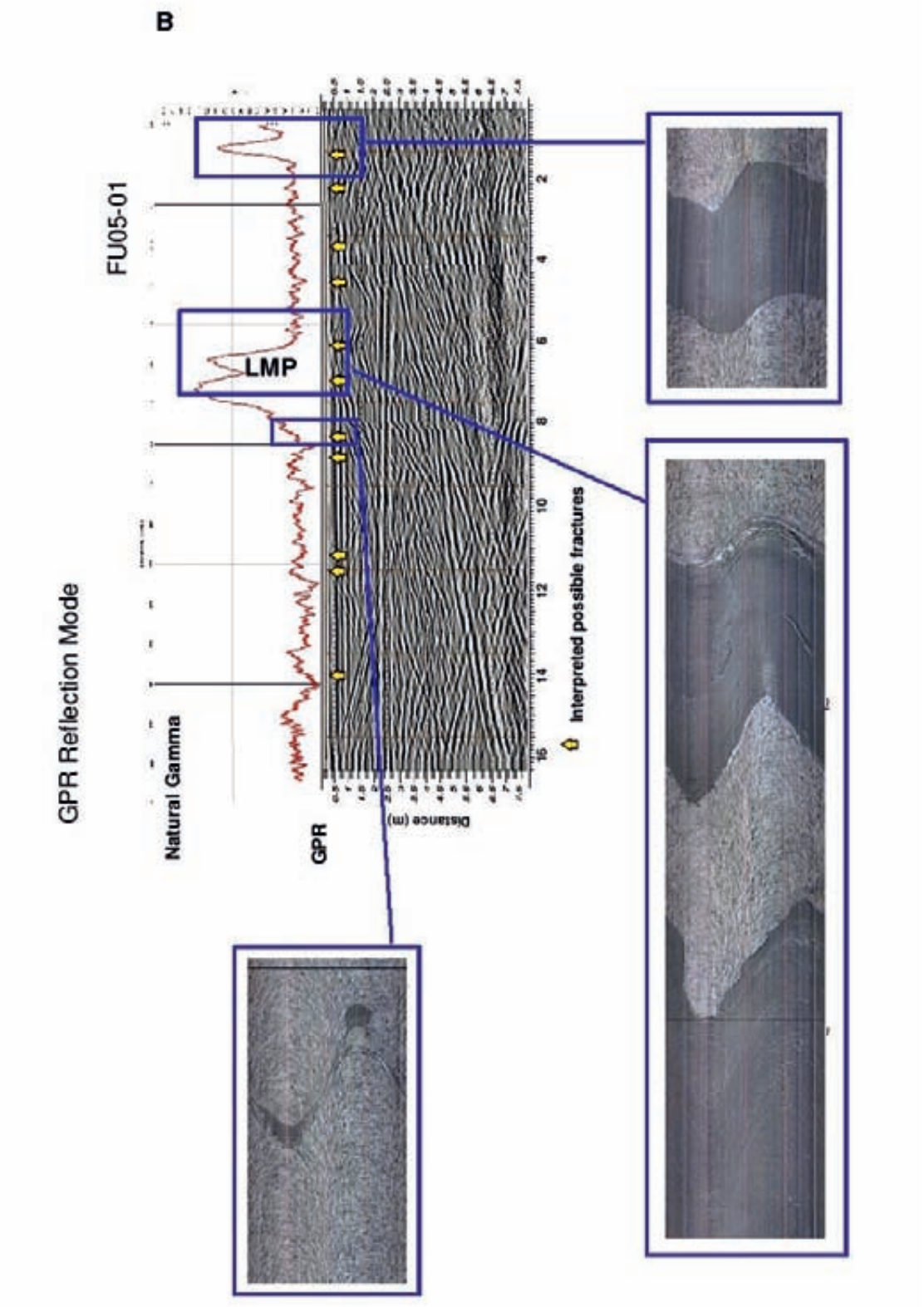

The GPR images are specially sensitive to the fluid content. Dry fractures a less visible than fluid filed cracks. Therefore, the features, events which are sub-parallel to the borehole axis (Figure 7) are suggesting of fractures with some fluid content which are located under the FEBEX Galery.

Conclusions

The correlation of the anomalies measured by the natural gamma can be correlated with the "diffractions" in the GPR and the fractures imaged by the borehole televiewer. Gamma anomalies correlate with fractures in th the borehole images. This correlation was was used as the main interpretation tool for the GPR data. The geophysical data acquired in this experiment provided evidence for the suggestion of a fracture beneath the FEBEX Gallery and sub-parallel to its axis. The cross hole ultrasonic tomography data is under processing and no interpretations have been attempted yet.

ELEMENTAL CORRELATIONS OBSERVED IN RUPRECHTOV TERTIARY SEDIMENT: MICRO-FOCUS FLUORESCENCE MAPPING AND SEQUENTIAL EXTRACTION

M. A. Denecke[1]* and Václava Havlová[2]

1 Forschungszentrum Karlsruhe, Institut für Nukleare Entsorgung, P.O. Box 3640, D-76021 Karlsruhe, Germany.
2Nuclear Research Institute Rež plc, Waste and Environmental Management Department, Husinec- Rež, PSC 250 68, Czech Republic

*Corresponding author: melissa.denecke@ine.fzk.de

Abstract

Sequential extraction (SE) is used for determination of U and other elements in a U-rich sediment from the Natural Analogue Site Ruprechtov. In Tertiary clayey samples U is found to be bound onto organic matter and/or be present in reduced form. In granitic samples carbonates/alumosilicates play a more important role in the U distribution.

Extended element analyses (Na, K, S, Fe, As, P) of SE leachates were completed. Cluster analyses of these results are used for identifying possible correlations between elements and for comparing these to previous correlations derived from μ-XRF and μ-XAFS investigations. According to the SE cluster analysis P, As and P can be assigned into one group. Fe and S are separated from U, i.e. we find no direct dependence of U on Fe and S. K and Na are mainly associated with residual minerals. Agreement with micro-scale measurements is observed: U in the sediment is associated with As and is present as phosphate in reduced U(IV) form.

Introduction

The Natural Analogue Study at the Ruprechtov site aims at understanding behaviour of natural radioelements in plastic clay formations. This system is chosen as an analogue for sedimentary overburden of radioactive waste repository host rocks (salt, granite, clay). The most similar proposed repository systems studied are Gorleben (Germany) and Mol (Belgium).

Objectives

The main objective of the Ruprechtov analogue site study is to find and describe the main mobilisation/immobilisation processes for performance assessment (PA)-relevant elements, namely uranium, thorium and radium. The system consisting of U – argillized clay – organic matter – granite – groundwater is studied both in-situ and in the laboratory in both a macro- and microscale. The investigations include drilling, field tests, geochemical and hydrogeological modelling, as well as monitoring, sampling, both in situ and laboratory characterisation of sediment and groundwater. One of the aims was to study uranium association with other sediment constituents. Modern material surface analyses methods were used: micro x-ray fluorescence (μ-XRF) and micro x-ray absorption fine structure (μ-XAFS) on core sections of Tertiary clay samples images were in this case compared with the results of sequential extraction (SE) of the same material type.

μ-XRF / μ-XAFS is performed in order to assess mechanisms leading to immobilization of the U during diagenesis [2]. SE is a widely used tool for speciation of selected elements (in this study, U) bound onto different fractions of sediment (see, e.g.,[6, 7,8]).

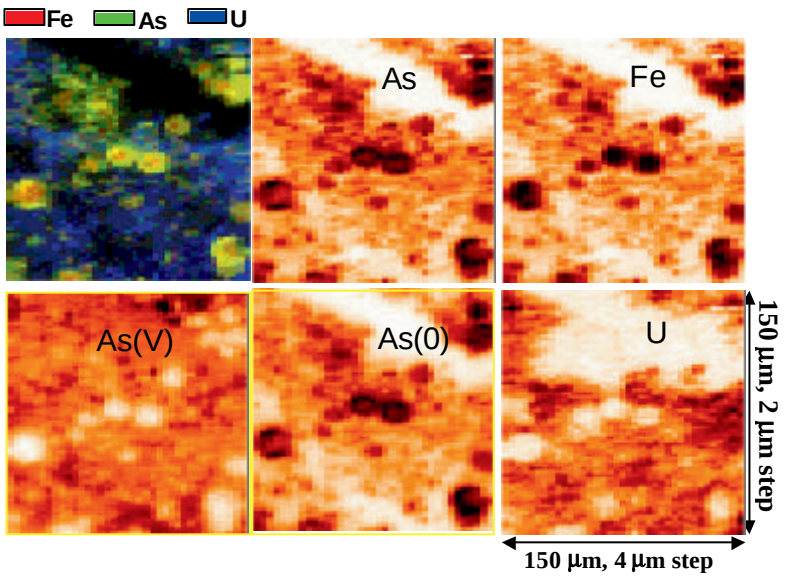

***Figure.1**: μ-XRF distribution maps for a 150*150 μm2 area of a thin section of a sample from NA5. The distribution of the total As, Fe and U measured with Eexcite = 18 keV and its corresponding Red-Blue-Green (Fe, As, and U, respectively) image , as well as the arsenic chemical state distributions for As(V) and As(0) are shown. As(0) is obtained from the As Kα fluorescence recorded using Eexcite =11.861 keV; As(V) distribution is the difference between As Kα fluorescence recorded using Eexcite = 11.870 keV and Eexcite 11.861 keV, i.e. map at 11.87 keV minus the As(0) map*

Results and discussion

μ-XRF and μ-XAFS results show uranium to be present as a tetravalent phosphate/sulfate in the regions studied and that U(IV) is associated with As(V) [6]. Arsenic is present in the sediment as either As(V) or As(0);we did not find any evidence for As(III). The As(0) is observed to be intimately associated with the surface of Fe(II) nodules and likely arsenopyrite.

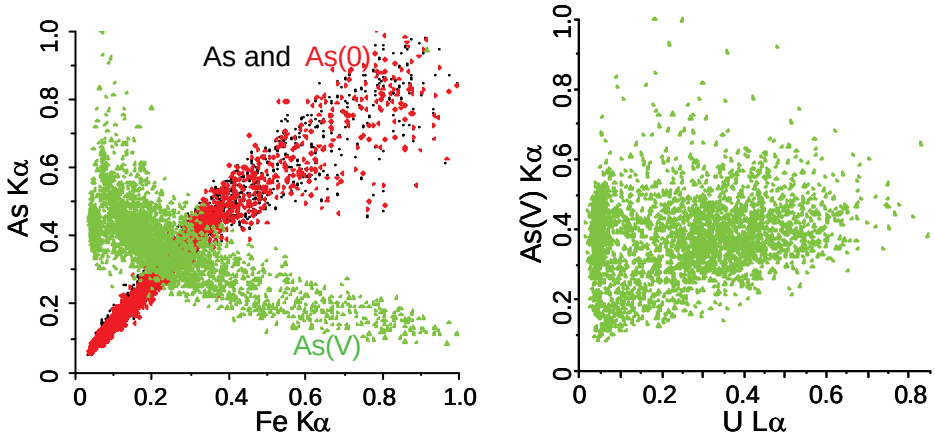

Figure 2: *Correlation plots between Fe and As(0) [◆], As(V) [▲], and total As [ ] (left) and between U and As(V) (right).*

Numerous correlation functions between As and U are determined from measured fluorescence intensities of elemental distribution maps recorded for samples NA4 and NA5. An example of distribution maps measured for a 150*150 μm^2 area of a thin section of a sample from borehole NA5 is shown in Fig. 1.

In this case it is possible to selectively differentiate between As(0) and As(V) in the maps by tuning the incoming incident photon energy (E_{excite}) to the corresponding ionisation energy. The correlation between U and As(V) and between As (total As, As(0) and As(V)) and Fe is shown in Fig. 2. We observe a correlation between As(V) and U. The linear correlation between As(0) and Fe shows that these are in the same phase, which is another indication of arsenopyrite presence in the sample. The difference between the correlation between As(0) and Fe and between the total As and Fe is hardly different, indicating that As(V) is a minority species.

The sequential extraction (SE) scheme is applied to Ruprechtov samples of different origin (6 boreholes, different depths, different rock types – kaolinized granite/Tertiary argillized clay). Samples are leached using different extractants in order to quantify various forms of U present in the sediment. The SE scheme consists of: following steps:

1. U bound on exchangeable sites (leaching with $MgCl_2$)
2. U bound on carbonates (leaching with ammonium acetate with acetic acid)
3. U bound to Fe/Mn oxides (leaching with hydroxylaminehydrochloride in acetic acid)

4. U bound onto organic matter/in reduced form (using H_2O_2 and HNO_3)
5. U in residuum (using boiling with HNO_3)

SE results of the uranium associated with the various fractions, expressed as percent of total U content are shown on Figure 3.

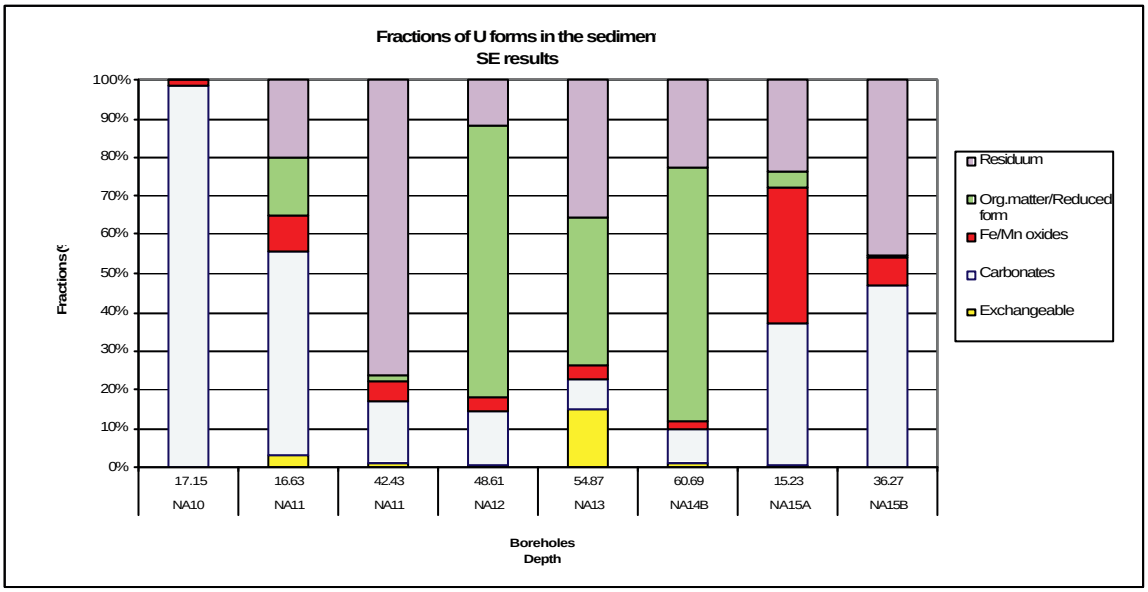

Figure. 3: *Fractions (in %) of U in the sediment samples (SE results). NA10&NA15A kaolinized granite, the rest of the samples – argillized Tertiary clay.*

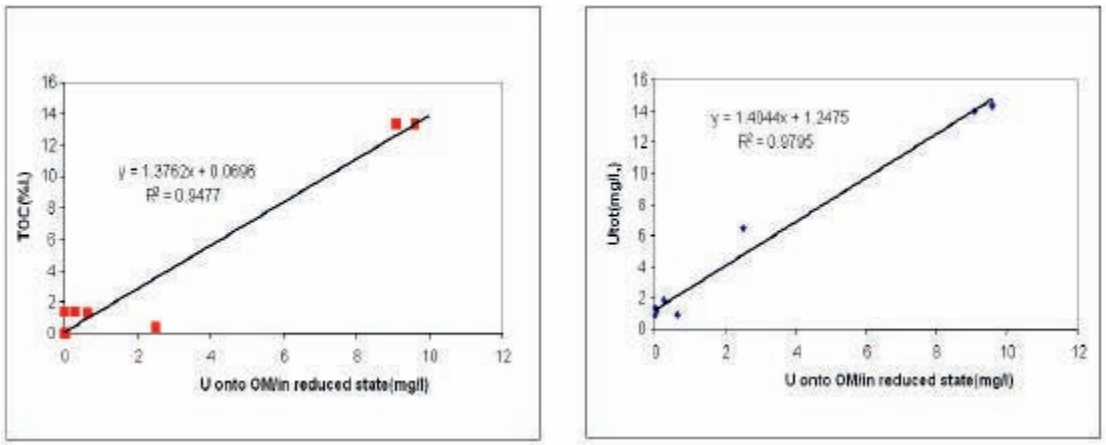

Figure. 4: *Dependency of the U fraction bound onto organic matter(OM)/in reduced form in mg/l on TOC in percent (left) and on Utot in mg/l (right). Lines depict linear dependency results, both yielding a slope of around 1.4.*

In Tertiary clay samples (all samples except NA10 and NA15B) we find U bound onto organic matter and/or in reduced form to be proportional to the total U content (Utot) and on total organic carbon content (TOC). In other words, observed increases in Utot and TOC are associated with increasing content of U bound to organic matter and/or in reduced form (see Fig. 4). In granitic samples (NA10,

NA15B) we find that carbonates/alumosilicates play a more important role in U binding.

Extended element analyses (Na, K, S, Fe, As, P) of SE leachates are completed for two samples in order to define phases dissolving in each extraction step. Therefore, cluster analyses are then used to process the data in order to identify possible interrelations between elements and further prove dissolution/leaching in the sediment. Clustering is one of the most commonly used methods of multivariate data analysis in statistical data processing. The routine produces a dendrogram showing how data points can be clustered [1, 4]. According to that, PAST, paleobiological statistical software package [5] was used for the analyses of trace element content (U, P, As, Na, K, S, Fe) in each SE leachate sample (see Fig. 5). P, As and U can be assigned into one group. This is in agreement with observations derived from the µ-XRF and µ-XAFS measurements. Fe and S are not interrelated with U, i.e. there is no direct evidence of U dependence on Fe and S. The major elements K and Na are mainly bound in residual minerals (SE step 5). As K is also leached in SE step 2 (signed as carbonates, although there is low occurrence of those minerals on the site), we can assume that alumosilicates and/or carbonate complexes are more responsible for U distribution than carbonate minerals themselves.

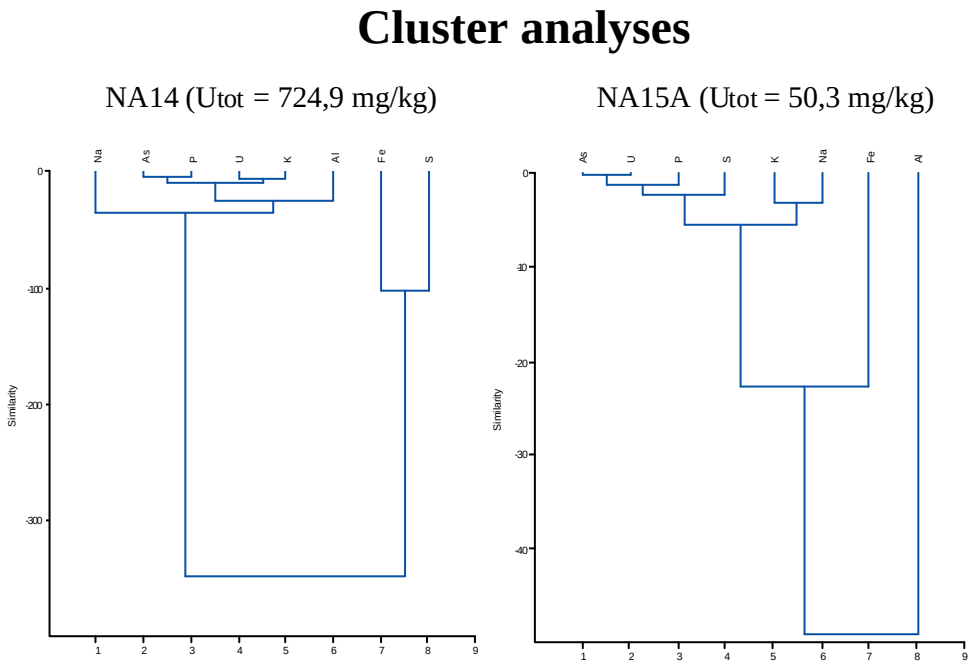

Figure. 5: *Cluster analyses (PAST) for trace element content in each sequential extraction leachate for 2 Tertiary clay samples from the Ruprechtov site. NA14 - Tertiary clay, rich in organic matter, high U content, NA11 - Tertiary clay, low organic matter and U content.*

Conclusions

Both micro-focus fluorescence mapping and sequential extraction of Ruprechtov clay samples showed that U accumulation in the sediment is associated with As. Analysis of μ-XAFS reveals the presence of U-phosphate phases in the sediment, corroborated by the cluster analysis showing a correlation between U and P. Cluster analysis further shows that there was no direct interrelation between U and Fe and S. This is in agreement with the observation in the elemental distributions for Fe and U by μ-XRF/μ-XAFS. U is observed to be located in sample areas void of Fe. In this comparative study the application of independent methods, i.e. SE and μ-XRF/μ-XAFS, yields complementary results. This is important as we find similar elemental correlation results using the x-ray based methods as in SE. This indicates that SE results are not erroneously fraught with artefacts caused by speciation changes during the extraction processes.

References

[1] Davis, J.C. 1986. Statistics and Data Analysis in Geology. John Wiley & Sons, New York.

[2] Denecke, M.A., Janssens, K., Proost, K., Rothe, J., Noseck, U. (2005) *Environ. Sci. Technol.* 39(7), 2049-2058.

[3] Denecke, M.A., Somogyi, A., Janssens, K., Simon, R., Dardenne, K., Noseck, U. (2006) *Microscopy Microanal.* (invited contribution; accepted)

[4] Harper, D.A.T. (ed.). 1999. Numerical Palaeobiology. John Wiley & Sons, New York

[5] Hammer Ø., Harper D.A.T., Ryan P.D. (2001): PAST: PALEONTOLOGICAL STATISTICS SOFTWARE PACKAGE FOR EDUCATION AND DATA ANALYSIS. Copyright: Palaeontological Association, 2001.

[6] Havlová V., Laciok A. (2006): Geochemical study of uranium mobility in Tertiary argillaceous system at Ruprechtov site, Czech Republic. *Czech Journal of Physics*, Vol. 56, Suppl. D. (in press).

[7] Percival J. B. (1990): Clay mineralogy, geochemistry and partitioning of uranium within the alternative halo of Cigar Lake uranium deposit, Saskatchewan, Canada. Carleton University, Ottawa, PhD thesis.

[8] Tessier A., Campbell P.G.C. and Bosson M.(1979): Sequential extraction procedure for the speciation of particulate trace metals**.** *Anal. Chemistry* 51 844-851.

DETERMINATION OF GRANITES MINERAL SPECIFIC POROSITIES BY PMMA METHOD AND FESEM/EDAX

A. Leskinen[1]; L. Penttinen[1]; M. Siitari-Kauppi[1*]; U. Alonso[2]; M. Garcia-Gutierrez[2]; T. Missana[2] and A. Patelli[3]

[1] Laboratory of Radiochemistry, University of Helsinki, P.O. Box 55, FIN-00014 University of Helsinki, Finland
[2] Ciemat, Avda. Complutense 22 - 28040 Madrid, Spain
[3] CIVEN, Via delle Industrie 9, 30175 Venezia-Marghera, Italy Institution

*Corresponding author; marja.siitari-kauppi@helsinki.fi

Abstract

Over extended periods, long-lived radionuclides (RN) or activation products within geologic disposal sites may be released from the fuel and migrate to the geo/biosphere. In the bedrock, contaminants will be transported along fractures by advection and retarded by sorption on mineral surfaces and by molecular diffusion into stagnant pore water in the matrix along a connected system of pores and micro-fissures.

The total porosity of the Grimsel granite (0.75%) was significantly higher than the porosities of the El Berrocal and Los Ratones granites (0.3%). The porosities of the Grimsel granite feldspars were two to three times higher than the porosities of the El Berrocal and Los Ratones granites' feldspars. However, there was no significant difference between the porosities of the dark minerals. A clear difference was found between the various quartz grains. Quartz crystals were nonporous in the El Berrocal and Los Ratones granites when measured by the PMMA method, but the quartz crystals in the Grimsel granite showed 0.5% intra granular porosity. The apparent diffusion coefficients calculated for uranium diffusion within Grimsel granite on different minerals were very similar ($2 \cdot 10^{-13} \pm 0.5$ m^2/s), but differences within both Spanish granites were found from one mineral to another ($9 \pm 1 \cdot 10^{-14}$ m^2/s in feldspars and $4.5 \pm 0.5 \cdot 10^{-14}$ m^2/s in quartz) - always presenting lower diffusion values than in the Grimsel granite.

Introduction

The determination of transport parameters, such as RN diffusion coefficients, within the geological barrier of a radioactive waste repository (HLWR) is required for performance assessment (PA) calculations. The physical properties of

the granite matrix pores are at the heart of a proper understanding and representation of radionuclide migration.

In the frame of geological disposal of nuclear fuel long lived radionuclides or activation products may be released from the fuel to the geo/biosphere. In bedrock, contaminants will be transported along fractures by advection and retarded by sorption on mineral surfaces and by molecular diffusion into stagnant pore water in the matrix along a connected system of pores and micro fissures. Since chemical interactions of groundwater and transported components with inner mineral surfaces play a major role as retardation process, the effectiveness of the rock matrix as natural barrier is decisively influenced by size, shape and spatial arrangement of the effective rock porosity network. A reliable picture of the pore space structure in rock minerals phases can be achieved by using different complementary methods for characterisation.

The ^{14}C-PMMA method makes it possible to study the spatial distribution of the pore space and the heterogeneities of rock matrices on submicrometric to centimetric scales. Subsequent autoradiography and digital image analysis enable features limited in size by the range of ^{14}C beta radiation to be measured. The structures of various minerals were studied in more detail by using FESEM/EDAX which allows the determination of minerals according to their elemental composition. The ^{14}C-PMMA [5,6] method makes it possible to study the spatial distribution of the pore space and the heterogeneities of rock matrices on submicrometric to centimetric scales. Subsequent autoradiography and digital image analysis enable features limited in size by the range of ^{14}C beta radiation to be measured. The structures of various minerals were studied in more detail by using FESEM/EDS which allows the determination of minerals according to their elemental composition.

Objectives

The porosity of three granites; Grimsel granite (Switzerland), Ratones granite (Spain), El Berrocal granite (Spain) was studied by ^{14}C-PMMA method. followed by FESEM/EDAX analyses. The determination was focused on the mineral specific porosities because the uranium migration was investigated for the same sample types by two novel techniques; Rutherford backscattering spectrometry (RBS) and proton induced X-ray emission (μPIXE) [1,2]. Objective of this work was to study the effect of the mineral microstructure; porosity and micro fissures, to the uranium diffusion results.

Experimental

Samples

In this study, three different granites coming from different locations, namely Grimsel granite (Switzerland) [3], El Berrocal granite (Spain) [4] and Los Ratones granite (a former U mine, Spain) were selected. The mineralogical composition of the Grimsel granite includes K-feldspar (~ 30-35 vol %), plagioclase

(~ 28-32 vol %), quartz (~ 33-37 vol %) and dark minerals (~ 3-7 vol %). The mineral composition of the El Berrocal granite includes quartz (~ 40 vol %), K-feldspar (~ 20 vol %), plagioclase (~ 30 vol %) and dark minerals (~ 10 vol %). The dark minerals include muscovite, chlorite and biotite. The El Berrocal granite is a heterogranular, medium- to coarse-grained granite; the rock is rather weathered and the plagioclase shows strong alteration. From the mineralogical point of view the Los Ratones granite is like the El Berrocal granite.

The ^{14}C-PMMA method

The (1x3x3) cm^3 sized rock samples were dried in an oven (100±5) ºC for two weeks. The samples were impregnated with ^{14}C-MMA tracer (518 kBq/mL) in initial vacuum for 22 days. Then the samples were irradiated by a ^{60}Co source to polymerize the monomer (total dose 72 kGy). After the polymerization, the samples were sawn into pieces, and the sawn surfaces were polished for autoradiography. The exposure times on films varied from 4 to 27 days. The qualitative and quantitative interpretations were based on the digital image analysis of the films. The 2D autoradiographs were digitized with a table scanner (CanoScan 9900F, Canon, optical resolution 2400 dpi) and analyzed by Matlab 7.0 using the Image Processing Toolbox (The MathWorks, 3 Apple Hill drive Natick MA 01760-2098, USA). The Mankeli Program (Version 2, 2005) measured the intensities of the film from the scanned 8-bit images, converted the intensities to optical densities and used the information to calculate porosities. The preconditions for applying this method are: (i) a known bcal bulk rock density; (ii) the presence of only two phases - mineral and PMMA; and (iii) the homogeneous distribution of pores and minerals are below the limit of the lateral resolution of autoradiography.

FESEM/EDAX

The scanning electron microscopy and energy dispersive X-ray analyses were performed on the PMMA impregnated rock samples to study the pore apertures of porous regions in greater detail. In addition, the micro fissure apertures were determined. The FESEM/EDAX analyses were done to determine the corresponding minerals. The analyses of the polished rock sections (polished with 0.25 µm diamond paste) were performed using a Hitachi FE-SEM S-4800 field emission scanning electron microscope and the elemental composition of the minerals was analyzed quantitatively using a INCA350 EDS system with a UTW Si(Li) detector operated in the backscattered electron mode (BSE). The operating conditions in the course of measurements were 20 kV acceleration voltages and a 20 µA beam current with a spot diameter of approximately 0.5 µm. The samples were carbon-coated. Magnifications of up to 1000 times were used to reveal apertures down to a size of 500 nm. The contrast between the pore space and the solid rock was enhanced by the PMMA impregnant inside the pores and the micro-fissures of the granite samples.

Diffusion experiments

The nuclear ion beam technique Rutherford Backscattering Spectrometry (RBS), which is widely applied to determine diffusion profiles in thin film science, is being examined as a suitable technique to determine RN diffusion coefficients within granite (FUNMIG project in WP.4.4). The RBS is a surface technique that allows measuring concentration profiles in areas of 1 mm^2 and analyses can be performed on single minerals. The solute concentration profiles versus distance, measured in the samples with the ion microprobe, allow evaluation of the apparent diffusion coefficients. The granite samples were cut into millimeter-sized slices with an average area of 1 cm^2 and polished. Because the RBS is more sensitive to heavy elements, in the first attempts, uranium was selected as the diffusant. Uranium solutions were prepared by dissolving $UO_2(NO_3)_2 \cdot 6H_2O$ (MERCK) in a low-mineralized water (Na-HCO_3 type, pH 8.3 and conductivity 282 μS/cm) to a final uranium concentration of $5.71 \cdot 10^{-3}$ M and a final pH value of around 5. After their immersion in the uranium solutions, granite samples were analyzed by RBS. The RBS measurements were performed in different minerals for the three selected granites. It is interesting that different behavior was observed amongst the obtained values.

Results

Examples of the autoradiographs of the El Berrocal and Grimsel granites are shown in Figures 1 and 2. Different shades of gray on the autoradiographs correspond to different porosities; the darker the shade, the higher the porosity.

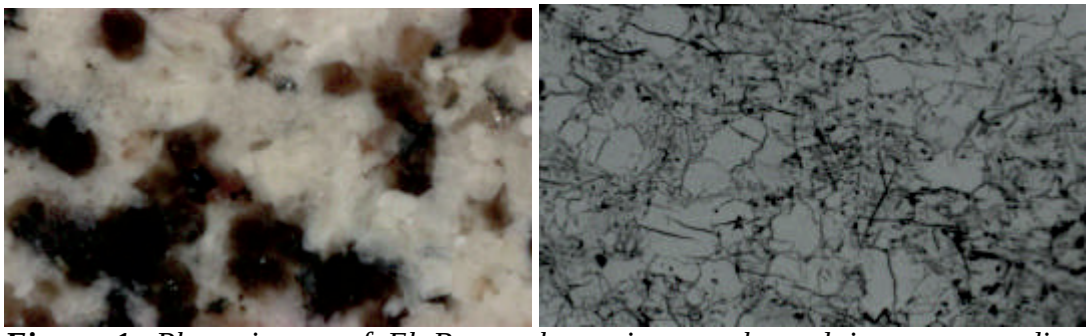

Figure 1. *Photo image of El Berrocal granite sample and its corresponding autoradiograph. Width of sample is 2.5 cm. MMA has not intruded into quartz grains indicating nonporous phases in the rock.*

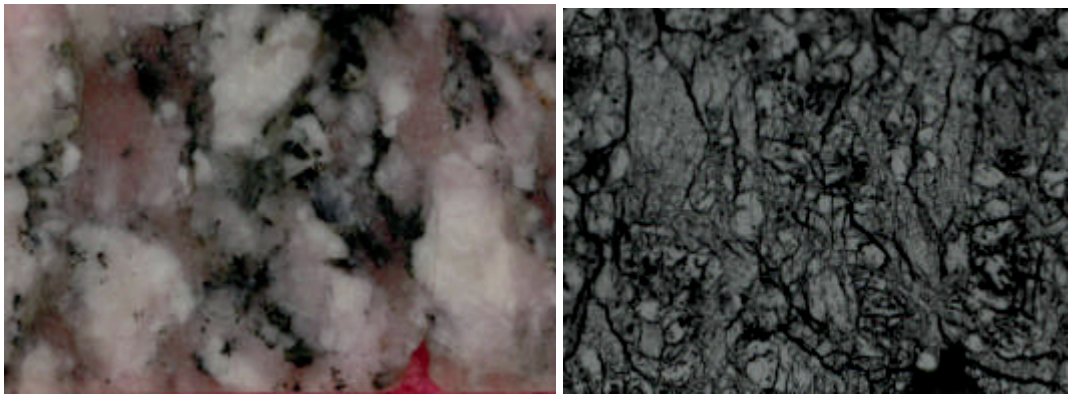

Figure 2. *Photo image of Grimsel granite sample and its corresponding autoradiograph. Width of sample is 2 cm. Porosity of quartz grains was determined to be 0.5 %.*

The mineral-specific porosities are listed in Table I. The total porosity of the Grimsel granite (0.75 %) was significantly higher than the porosities of the El Berrocal and Los Ratones granites (0.3 %). The porosities of the Grimsel granites' feldspars were two to three times higher than the porosities of the El Berrocal and Los Ratones granites' feldspars. However, there was no significant difference between the porosities of the dark minerals. The clear difference in the porosity and the pore structure was found between the various quartz grains. The quartz crystals of the El Berrocal and Los Ratones granites were nonporous when measured with the PMMA method, but the quartz of Grimsel granite showed 0.5 % intra-granular porosity. Figure 3a shows the BSE image of the Grimsel granite quartz crystals. Clear intra-granular pore network is found; apertures being 1 µm and below. Figure 3b shows the BSE image of the El Berrocal granites' K-feldspar and quartz grain boundary opening, which has an aperture of about 10 µm. The grain boundary porosity is significant. However, the K-feldspar showed high intra-granular porosity; both pores and micro-fissures were found indicating well-defined connective migration routes for RN on the tens of micrometers scale.

Table I. *Total PMMA porosities of studied samples and mineral specific porosities; quartz, feldspars and dark minerals. The error is evaluated to be 10%.*

sample	*total PMMA porosity*	*quartz*	*feldspar*	*dark minerals*	*notes*
Grimsel granodiorite	**0.75%**	**0.5%**	**0.5%**	**>1.4%**	**all mineral grains porous**
Los Ratones granite	**0.3%**	**no PMMA porosity**	**0.3%**	**>1.1%**	**grain boundary + in feldspars intra-granular**
El Berrocal granite	**0.3%**	**no PMMA porosity**	**0.3%**	**>0.8%**	**grain boundary+ in feldspars intra-granular**

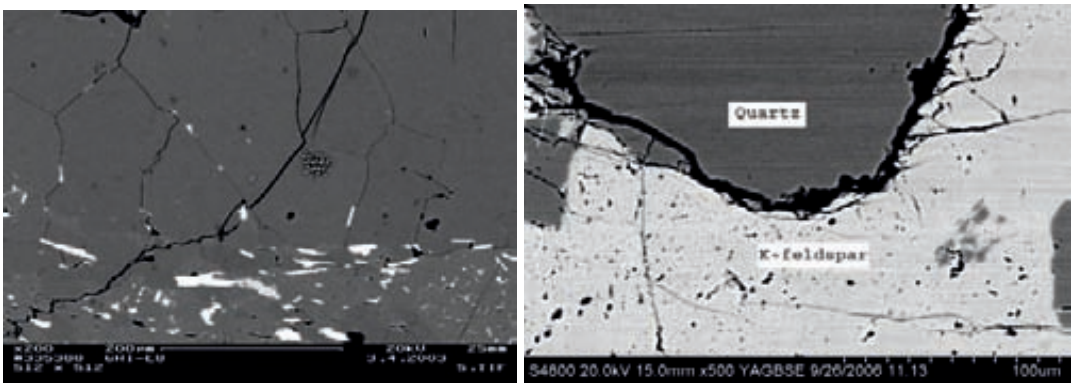

Figure 3. a) *Backscattered electron image of Grimsel granite quartz grains. The aperture of the fissure is about 10 µm. The intra-granular micro fissure network has openings of 1 µm and below. 200-fold magnification.* ***b)*** *Backscattered electron image of El Berrocal granites' feldspar and quartz grains. Open grain boundary between a quartz and a feldspar grain is seen. The aperture of the fissure is about 10 µm. Intra-granular micro-fissures are found in feldspar grain as well as in clear pores. 500-fold magnification.*

The apparent diffusion coefficients calculated for uranium diffusion in the Grimsel granite on different minerals were very similar ($2 \cdot 10^{-13} \pm 0.5$ m^2/s), because all minerals were porous. However, differences in the El Berrocal and Los Ratones granites were found from one mineral to another: $9 \pm 1 \cdot 10^{-14}$ m^2/s in feldspars and $4.5 \pm 0.5 \cdot 10^{-14}$ m^2/s in quartz. The El Berrocal and Los Ratones granites presented always lower diffusion values than the Grimsel granite, due to their lower porosity values in the mineral grains.

It has to be noted that the differences among the obtained diffusion coefficients are small from a PA point of view. The fact that the technique allows the observation of such differences confirms the sensitivity of the technique for the determination of diffusion coefficients of high-sorbing RN within granite, which cannot be achieved by conventional diffusion experiments. Nonetheless, the possibility of relating the solute diffusion coefficients to the medium porosities can be of great interest for understanding the treatment of the heterogeneities and up-scaling information from laboratory to PA.

Conclusions

The total porosity of the Grimsel granite (0.75%) was significantly higher than the porosities of the El Berrocal and Los Ratones granites (0.3%). The porosities of the Grimsel granite feldspars were twice to three times higher than the porosities of the El Berrocal and Los Ratones granites' feldspars. However, there was no significant difference between the porosities of the dark minerals. A clear difference was found between the various quartz grains. The quartz crystals of the El Berrocal and Los Ratones granites were nonporous when measured with the PMMA method, but the quartz of the Grimsel granite showed 0.5% intra-granular porosity. The apparent diffusion coefficients calculated for the uranium diffusion in the Grimsel granite on different minerals were very similar ($2 \cdot 10^{-13} \pm 0.5$ m^2/s).

Differences in the El Berrocal and Los Ratones granites were found from one mineral to another ($9 \pm 1 \cdot 10^{-14}$ m^2/s in feldspars and $4.5 \pm 0.5 \cdot 10^{-14}$ m^2/s in quartz), always presenting lower diffusion values than in the Grimsel granite.

References

[1] Alonso, U.; Missana, T.; Patelli, A.; Ravagnan, J.; Rigato, V. (2003a) RBS and μPIXE analysis of uranium diffusion from bentonite to the rock matrix in a deep geological waste repository *Nucl. Instr. and Meth.in Physics Research B* 207 195-204

[2] Alonso, U.; Missana, T.; Patelli, A.; Rigato, V.; Rivas, P. (2003b) Study of the contaminant transport into granite microfractures using nuclear ion beam techniques *J. Contam. Hydrol.* 61 95-105

[3] Bossart, P.;and Mazurek, M. (1991) Structural Geology and Water-flow paths in the migration-shear-zone Nagra Technical Report NTB 91-12

[4] Fernandez-Merayo, N.; Siitari-Kauppi, M.; Montoto, M.; Hellmuth, K-H. (1996) Characterization of rock matrix structure using microscopy ^{14}C-PMMA method for the study of retardation mechanisms in granite *Radiochimica Acta* 74, 211 (1996).

[5] Hellmuth, K.H.; Siitari-Kauppi, M.; Lindberg, A. (1993) Study of Porosity and Migration Pathways in Crystalline Rock by Impregnation with ^{14}C-polymethylmethacrylate. *Journal of Contaminant Hydrology*, 13: 403-418.

[6] Hellmuth, K.H., Lukkarinen, S. and Siitari-Kauppi, M. (1994) Rock Matrix Studies with Carbon 14-Polymethylmethacrylate (PMMA); Method Development and Applications. *Isotopenpraxis Environ. Health Stud.*, 30: 47-60.

EXPERIMENTAL APPROACH TO STUDY THE BENTONITE COLLOID GENERATION SOURCE TERM IN DIFFERENT GEOCHEMICAL CONDITIONS

U. Alonso, T. Missana, and M. García-Gutiérrez

CIEMAT, Dpto. Medio Ambiente Avda. Complutense 22, Madrid, Spain

* Corresponding author; ursula.alonso@ciemat.es

Abstract

To guarantee the long-term safety of a high-level waste repository, all mechanisms that could affect the radionuclide (RN) migration rate must be well defined and quantified. The particular interest of this work lies on the possible contribution of bentonite colloids, generated at the compacted bentonite barrier, to RN transport. The main parameters necessary to assess the colloid-mediated RN transport are the source term and the stability behavior in the medium geochemical conditions. In the present work, two experimental set-ups were designed, with the aim of quantifying the bentonite colloid generation rates, at laboratory scale and under "realistic" conditions, by static hydration (no flow) of the compacted bentonite, in a confined system.

Preliminary results showed that bentonite particles were generated with an average size in the colloid range, equivalent to that of bentonite colloids prepared in the laboratory. At the same time, the experimental set-up allowed performing stability studies which indicated that the colloids generated in the lower strength waters remained stable over months. The possible mechanisms responsible of colloid generation are discussed according to the obtained preliminar results in different experimental conditions.

Introduction

In order to assess the relevance of colloids on the RN migration, the determination of their nature and amount in a given environment [1] are critical. In particular, it is necessary to establish the conditions in which the compacted bentonite barrier generates colloids, to quantify the bentonite colloid "source term" and to evaluate the extent of colloids stability.

There are several mechanisms that can lead to colloid generation [1,2]. The bentonite colloid generation will be primarily related to the hydration of the clay. Due to the entrance of water, effects of physical gradients (e.g. erosion) can promote

bentonite colloid generation. The kinetics of the colloid generation will be related to the particle /surface interactions, as well as to the medium hydrodynamic conditions. In presence of a water flow, bigger particles have thinner bonding layers, so that just dragging or shearing forces may be sufficient for particle detachment.

If a local hydraulic gradient does not exist, the driving force for their mobilisation would be diffusion, to overpass the bond energy barrier [3]. The static of the release processes is related to the energy interaction between the particle and the pore surface, on which the particle is adhered. Thus, release of colloidal particles can be result of changes in the solution chemistry. A favorable chemical environment (p.e continuous incoming of low ionic strength waters) promotes the peptisation (defloculation mechanism) and dispersion of the clay gel, that can occur spontaneously [4] It is known that changes in the solution ionic strength and pH affect the electrostatic interactions between colloids and the grain surfaces. Indeed, numerous studies demonstrated that dispersion and releases of colloid particles are favored at high pH and low ionic strength [5]

Objective

The aim of the present work is to design an experimental set-up to quantify the bentonite colloid generation rates under static conditions (no flow) at different chemical environment, in terms of bentonite compaction and environment ionic strength, and to analyze the preliminary results obtained. The experiments were designed to study the colloid formation in a confined system, with very small density loss of the bulk bentonite during hydration.

Experimental set-up

Materials

The bentonite selected in this work, FEBEX bentonite [6] comes from the Cortijo de Archidona (Spain) deposit. This clay has a very high smectite content (93±2%), with quartz (2±1%), plagioclase (3±1%), cristobalite (2±1%), potassic feldspar, calcite and trydimite as accessory minerals. The electrolytes selected for studying colloid generation are: deionised water, NaCl at different ionic strengths (10^{-3} M and 10^{-2} M) and Grimsel water, coming from the Grimsel Test site [7] In Table 1 the chemical information of all selected electrolytes are gathered.

Cells design.

In Figure 1 the two experimental set-ups designed with the aim of quantifying the bentonite colloid generation rates are presented: (Figure 1, Left) Radial cells and (Figure 1, Right) Planar cell. Compacted bentonite at different compaction densities (1.2, 1.4 and 1.6 g/cm^3) was used in these tests.

The Radial cell represents the “repository- geometry”. In this case, the compacted bentonite (about 100 g, depending on the density) is introduced in open

cylindrical stainless steel porous filter. The up and down surfaces of the cylinder are closed by two methacrylate grids and the whole cell is adequately tightened. The porous stainless steel cylinder has 50 mm length and a thickness of 2.54 mm, with a porous size of 100 μm. Colloid generation is expected to take place at the external surface of the porous cylinder. The bentonite hydration is facilitated by immersing the confined cells in 2 litres of NaCl at different ionic strength.

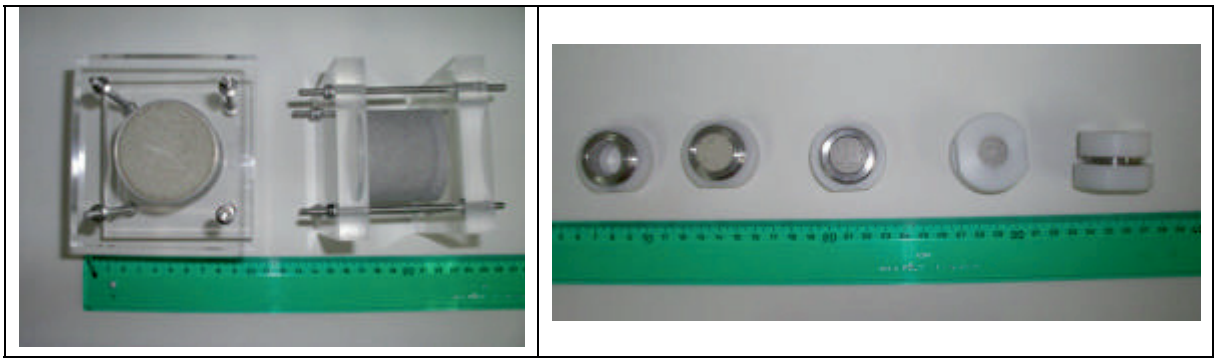

Figure 1. *(Left) Pictures of the Radial cells designed for bentonite colloids generation experiments under static conditions. (Right) Pictures of the Planar cell designed for bentonite colloids generation experiments under static conditions.*

The Planar cell configuration is presented in Figure 1 (Right): it consists on introducing compacted bentonite (about 4 g, depending on the clay density) in a stainless steel cylinder with an external thread. The bentonite tablet is sandwiched between two sintered stainless-steel filters (20 mm diameter, 3 mm thick and 100 μm porous size). The cell is closed by two open Delrin grids, allowing the colloid generation at both filter surfaces. Because of being of smaller than the Radial cell, the Planar cell is immersed in 200 ml of different aqueous solutions. The electrolytes were selected accounting for its ionic strength, from the most favorable conditions (deionised water, i.e the lowest ionic strength) to Grimsel groundwater (ionic strength 10^{-3} M) and NaCl 10^{-2} M. These studies were performed at room temperature in a globe box, under N_2 atmosphere.

Table 1 summarizes the experimental conditions of all the cells installed, indicating the configuration (Radial or Planar), the bentonite density and the selected solution (indicating the volume, the pH and the initial and present -after 170 days- conductivity). It has to be mentioned that, because of having lower bentonite mass (4 g compared to about 100 g in the Radial cells), it is expected faster hydration. Moreover, because of having higher water volume (200 ml compared to 2 liters) it is expected later detection of colloid. The Planar cells have simpler geometry, more feasible for changing the experimental conditions.

Bentonite colloid analysis.

The bentonite colloid generation is analyzed by periodical sampling about 2 ml of the aqueous phase. Several techniques can be used depending on the parameters that we would like to determine [8,9]. In particular, in this study the

Photon Correlation Spectrometry (PCS), technique is selected for evaluating the colloid size distribution. Moreover, after adequate calibration [10] it is also applied to evaluate the colloid concentration. In order to perform stability studies, the evolution of the colloid hydrodynamic was followed by PCS measurements [11] The PCS measurements were performed with a laser power of 1 Watt and with the photomultiplier set at 90º in respect to the incident light. The detection limit is about 0.4 ppm. The PCS measurements previously performed on the obtained bentonite colloids previously prepared in the laboratory, indicated that the mean size of these colloids is 248 ± 2 nm.

Table 1. *Experimental conditions of the cells installed.*

Cell	Compacted density (g/cm^3)	Electrolyte	pH	Initial conductivity σ (μS/cm)	Present conductivity σ (μS/cm)
Planar 1.2D	1.2	200 ml of deionised water	6.34	38.2	134.3
Planar 1.4 D	1.4	200 ml of deionised water	"	"	123.2
Planar 1.6 D	1.4	200 ml of deionised water	"	"	125.8
Planar 1.2G	1.2	200 ml of Grimsel water	9.41	104	217
Planar 1.4G	1.4	200 ml of Grimsel water	"	"	221
Planar 1.6 G	1.6	200 ml of Grimsel water	"	"	195.7
Planar 1.2 M2	1.2	200 ml of NaCl 10^{-2} M	5.07	1262	1314
Planar 1.4 M2	1.4	200 ml of NaCl 10^{-2} M	"	"	1308
Planar 1.6 M2	1.6	200 ml of NaCl 10^{-2} M	"	"	1318
Radial N12M3	1.2	2 L NaCl 10^{-3} M	5.07	132.2	602
Radial N14M3	1.4	2 L NaCl 10^{-3} M	"	132.2	529
Radial N12M2	1.2	2 L NaCl 10^{-2} M	"	1262	1824
Radial N14M2	1.4	2 L NaCl 10^{-2} M	"	1262	1725

Results and discussion

So far, no significant colloid concentration was detected in the Radial cells because of having higher mass content (100 g compared to 4 g), what enlarged the hydration period.

However, the hydration of the Planar cells was complete at about one week. The first colloid detection, by PCS measurements performed on the solution was obtained after 20 days of cells immersion. In Figure 2A and 2B, and 2C the colloid generation rates measured so far for the Planar cells (Figure 1 (Right)) in different electrolytes: (A) Deionised water, (B) Grimsel water ad (C) NaCl 10^{-2} M, at the different compacted densities (1.2 1.4 and 1.6 g/cm^3), are presented.

Steady state conditions have not been yet achieved, and it can be appreciated that in all the Planar cells, the colloid concentration increases with time in all the electrolytes, for the three studied densities (1.2 1.4 and 1.6 g/cm^3), even when in some cases tends to a saturation. The higher colloid concentration is observed for the samples of higher initial density.

Comparatively, the colloid generation rates are hundred times higher in the deionised water, which represents the chemically most-favorable conditions case

(*12*). The average diameters measured for the colloids generated from all densities in the Planar cells immersed in deionised or Grimsel water were about 300 nm, similar to that of the laboratory prepared bentonite colloids (250 nm), as can be seen in Figure 2D. Only in case of the NaCl 10^{-2} M the colloids generated has higher diameter (600 nm), as can be seen in Figure 2D.

Another interesting feature of the experimental set-up, it is that it allows performing stability evaluation at the same time. Indeed, the stability evaluation is an experimental study on the coagulation kinetics of the colloids. In Figure 2D the mean hydrodynamic diameter measured by PCS for the bentonite colloids generated in all the electrolytes, at different compaction densities, and as a function of time, is presented. Considering that the mean average diameter in any of the cases changed with time, it can be concluded that, after months the colloids generated remain stable.

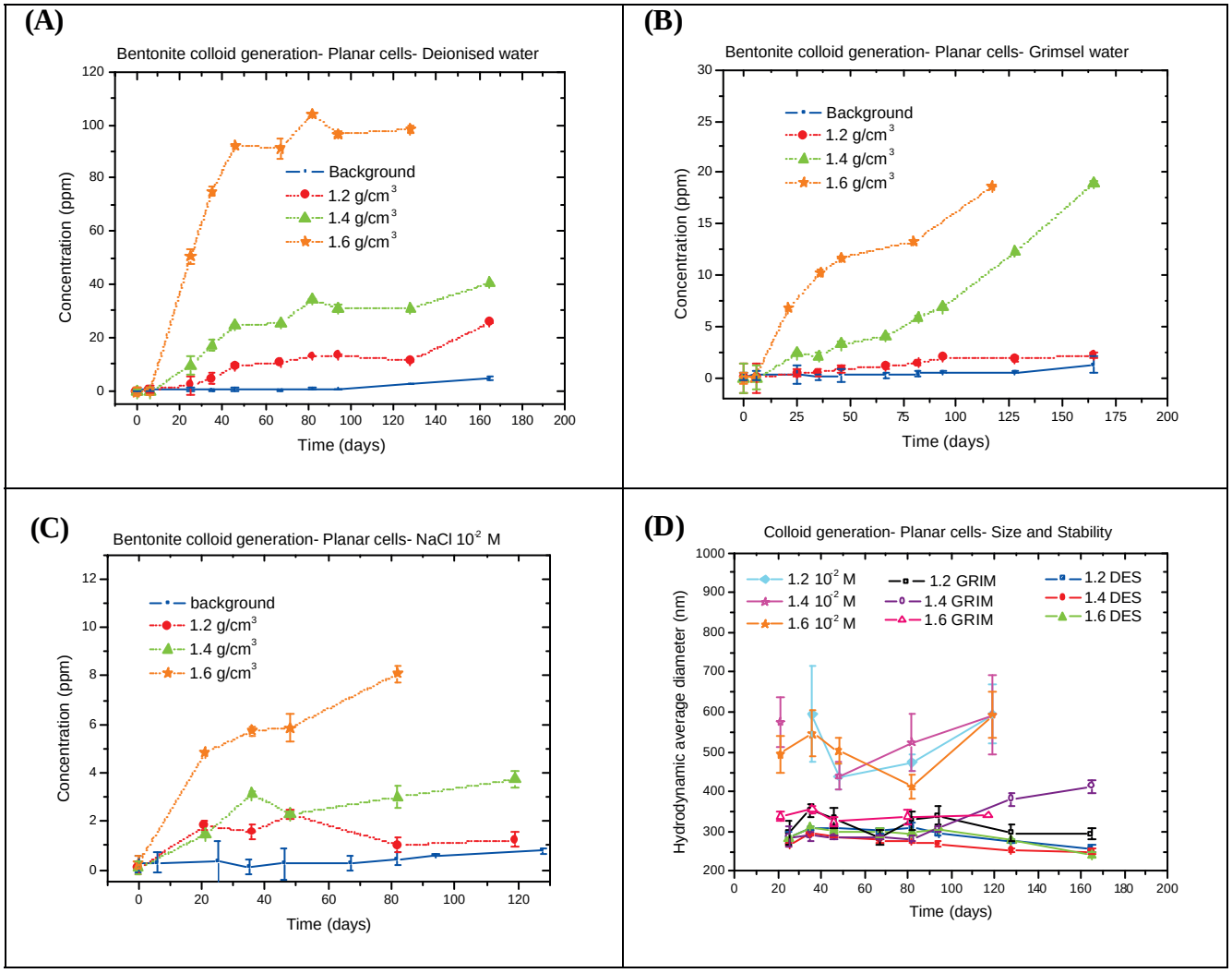

Figure 2. *Concentration of bentonite colloid generated from the Planar cells as function of time and at different compaction densities, inmersed in (A) deionised water, (B) Grimsel water (C) NaCl 10^{-2} M. (D) Mean hydrodynamic diameter measured by PCS for the colloids generated in at different compacted densities and as a function of time, for each water type.*

Because of working in static conditions (no-flow), the contribution to the bentonite colloid generation attributed to diffusion is first considered. According to the equation presented in [13] for the expected lost of mass that may escape, in our experimental conditions, considering a colloidal particle of 300 nm ($D = 1.63 \cdot 10^{-18}$ m^2/s) and the properties of our filter (described in the experimental section), after a time of 80 days only about 0.08 ppm of the detected colloids could be attributed to a diffusion mechanism.

The experimental configuration, in which the bentonite at a certain density is emplaced in a sort of "confined chamber" with pore apertures that allow the water pass, would promote that the clay extruded into the slots. However, it has to be noted that, despite the filter porous sizes were 100 μm, the particles generated were always in the colloid size range (Figure 1D).

The electrolyte used in the experiment is, as expected, a critical parameter for the colloids stability, but less critical for the initial generation rates. This suggests that changes in the internal pore water ionic strength, caused by the hydration are playing an important role. In addition, the effects of the interchangeable cations, could also be of importance since, the adsorption of cationic surfactant on a charged surface leads to significant modification of the charge distribution in the electrical double layer, and, thus, in the interaction of particles with each other. All this mechanisms, possible responsible of colloid generation will be analyzed in the future, accounting for more experimental conditions (e.g. [Ca] and [Na]- homoionised bentonite).

Application to PA

The quantification of the bentonite colloid generation source term and the evaluation of their stability in a given environment, are fundamental parameters for the PA evaluation of the bentonite colloid-mediated RN transport.

Conclusions

Two new experimental cells were designed with the aim of quantifying the bentonite colloid generation rates under static conditions which allowed studying the colloid formation from the compacted bentonite in a confined system. Moreover, the experimental set up allowed performing stability evaluation at the same time. The parameter analyzed so far were: (a) initial density of the clay and (b) contact solution

Results showed that the initial generation rate is mostly controlled by the density of the compacted clay and the solution chemistry and that the characteristics of colloids and their stability are mainly chemistry-controlled. Colloid generated in favorable conditions presents the lower size (around 250 nm), while at higher ionic strengths colloids are bigger (500 nm). For the evaluation of generation mechanisms, it is necessary to study the effects of additional parameters, as for example the nature of the clay exchange complex.

Acknowledgments

This work was partially supported by the EU within the FUNMIG (Fundamental Processes of Radionuclide Migration) project and in the framework of the CIEMAT-ENRESA association.

References

[1] J. N. Ryan and M. Elimelech, *Colloids Surfaces A:* 107, 1 (1996).

[2] R. Pusch. SKB Technical Report TR 99-31, 1999.

[3] N. Kallay, E. Barouch, and E. Matijevic, *Advances in colloid and Interface Science* 27, 1 (1987).

[4] S. Yariv and H. Cross, "Geochemistry of colloid systems," p. 450. Springer-Verlag, Berlin, 1979.

[5] T. K. Sen and K. C. Khilar, *Adv. in Colloid. Interf. Sci.* 119, 71 (2006).

[6] F. Huertas, J. L. Fuentes-Cantillana, F. Jullien, P. Rivas, J. Linares, P. Fariña, M. Ghoreychi, N. Jockwer, W. Kickmayer, M. A. Martinez, J. Samper, E. Alonso, and F. J. Elorza, 2000.

[7] M. H. Bradbury, Ed. NAGRA, 1989.

[8] J. F. McCarthy and C. Degueldre, *in* "Environmental Particles" (J. B. a. H. P. v. Leeuwen., ed.), Vol. 2. Lewis Publishers, Boca Ratton, FL:, 1993.

[9] J. Buffle and G. G. Leppard, *Environmental Science and Technology* 29, 2176 (1995).

[10] A. Ledin, S. Karlsson, A. Düker, and B. Allard, *Anal. Chim. Acta* 281, 421 (1993).

[11] H. Holthoff, S. U. Egelhaaf, M. Borkovec, P. Shurtenberger, and H. Sticher, *Langmuir* 12, 5541 (1996).

[12] J. N. Ryan and P. M. Gschwend, *Journal of Colloid and Interface Science* 164, 21 (1994).

[13] P. Grindrod, M. Peletier, and H. Takase, *Engineering geology*. 54, 159 (1999).

SCOPING NUMERICAL CALCULATION FOR THE DESIGN OF THE IN SITU DIFFUSION AND RETENTION (DR) EXPERIMENT

J. Samper and Q. Yang

Escuela de Caminos, Universidade da Coruña, Campus de Elviña, 15192 Coruña, Spain,

*Corresponding author: jsamper@udc.es,

Abstract

Safety assessment of nuclear waste disposal in a deep geological repository requires understanding and quantifying radionuclide transport through the hosting geological formation. Radionuclide diffusion is the main transport mechanism in clay formations. Thus, understanding diffusion and determining diffusion parameters under real conditions is necessary for the performance assessment of a deep geological repository. Scoping numerical calculations for the DR experiment have been performed with CORE^{2D}. Diffusion of neutral (HTO), anionic (I) and sorbing cationic tracers with different distribution coefficients (^{22}Na and ^{85}Sr) has been simulated taking into account anisotropic diffusion. Numerical simulations have been compared with those obtained by CSIC (Barcelona). Then, a series of sensitivity runs have been performed by changing one-at-a-time the following parameters: porosity, effective diffusion coefficients (parallel and perpendicular to bedding) and distribution coefficient. Sensitivities of computed concentrations to model parameters reveal that concentrations of HTO and iodide are most sensitive to accessible porosity while concentrations of sodium and strontium are most sensitive to the distribution coefficient. Concentrations of all tracers in the in injection interval and in the host rock are sensitive to effective diffusion coefficients.

Introduction

Three-dimensional scoping calculations for the DR experiment have been performed using a reactive transport code CORE^{2D} [1]. The concept for the DR experiment is similar to previous in situ diffusion experiments such as DI-A [2,3; 4; 5](see Fig. 1). However, the concept has been optimized for determining diffusion anisotropy in situ. DR injection intervals will be shorter than those of previous diffusion experiments. Since DR will last longer, transport distances will be larger than the length of the injection interval and it is expected that the tracer plume will reflect the effect of anisotropy. Tracer plumes are expected to be ellipsoidal in shape due to the faster diffusion along bedding planes.

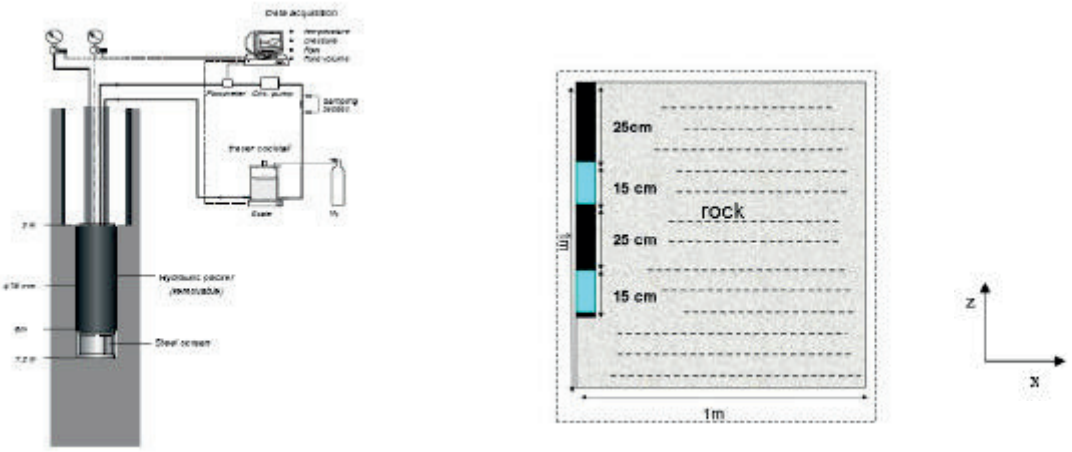

Figure 1. *Schematic design of the injection borehole and its equipment for the DI-A experiment (left) and schematic diagram showing the modified design for DR (right).*

Our scoping calculations assume that the injection borehole will be drilled perpendicular to bedding. Also, two different injection intervals have been taken into account. Tracers are not allowed to diffuse directly downwards from the bottom of the lower interval because there is a metal plate at the bottom. Tracer concentrations in the injection system will be monitored with time. At the end of the experiment, the rock around the injection intervals will be overcored and tracer distribution profiles will be measured. The time evolution of tracer concentrations in the injection system and tracer profiles in the rock should provide a unique set of effective diffusion coefficients and accessible porosities for conservative tracers and sorption parameters for sorbing tracers.

Objectives

The main objective of this contribution is the numerical scoping calculation of the DR in situ diffusion experiment, an experiment which aims at obtaining in situ estimates of diffusion anisotropy for the Opalinus Clay. Scoping calculations will be useful for the optimum design of the DR experiment.

Experimental conditions

The DR experiment will be performed using neutral (HTO), anionic (I^-) and cationic (Na^+ and Sr^{2+}) tracers. HTO and I are conservative tracers although I^- is an anion and therefore its diffusion is affected by anion exclusion. Strontium is weakly sorbed in Opalinus clay. Accessible porosity, ϕ_α, coincides with total porosity for HTO and cations while it is only a fraction of total porosity for anions. In simulations, anion exclusion is modelled by assigning an accessible porosity smaller than total porosity. Model parameters are listed in Table 1. Model predictions were

performed for both isotropic and anisotropic diffusion. In the latter case, effective diffusion coefficient perpendicular to bedding is 4 times smaller than diffusion parallel to bedding.

Table 1. *Parameters used in the model*

Tracer	Accesible porosity ϕ_α	Capacity factor α	K_d ($cm^3\ g^{-1}$)	D_e ($m^2\ s^{-1}$)
HTO	0.15	0.15	0.00	$4.0 \cdot 10^{-11}$
Na^+	0.15	0.62	0.2086	$5.7 \cdot 10^{-11}$
Sr^{2+}	0.15	3.13	1.3229	$4.0 \cdot 10^{-11}$
I^-	0.08	0.08	0.00	$1.3 \cdot 10^{-11}$

Scoping calculations of the DR experiment

The configuration of tracer diffusion plumes shows symmetry with respect to the borehole axis. A domain of 1m × 1m has been taken into consideration for the numerical model. The length of the borehole interval where tracers are injected is 1.5 dm. Borehole radius is 0.28 dm. The model domain is discretized into triangular finite elements using COSMOS/M®. Elements are smaller near the borehole and increase their size far away from the borehole. The mesh of the model has 3636 nodes and 7000 elements. The numerical mode considers 3 material zones: (1) the packed-off section of the borehole where tracers are injected; (2) the packer between the two injection intervals and (3) the Opalinus Clay. The model domain is a 2D vertical section aligned with the borehole axis (see Fig. 1). The left-hand-side boundary of the domain corresponds to the borehole axis. Symmetry around the borehole axis is assumed in the simulations. All outer domain boundaries are no-flux boundaries. Calculations have been performed for isotropic and anisotropic conditions. The results in Figure 2 indicate that the transport distance perpendicular to bedding is larger than that along the bedding for the isotropic case. When a 1:4 anisotropy ratio is considered the transport distance along the bedding is slightly larger than that perpendicular to bedding. Tracer depletion in the injection interval for isotropic conditions is larger than that of the anisotropic case (Figure 3). The tracer added in the upper interval does not reach the lower interval.

Figure 4 illustrates that the transport distance of sodium is smaller than that of HTO. The depletion of strontium in the injection interval is larger than that of HTO. Depletion of sodium and strontium is larger than that of HTO (Figure 5). The depletion of iodide is smaller than that of HTO (Figure 6). Iodide does not appear at measurable concentrations at the upper interval.

A series of sensitive runs have been performed by one-at-a-time changing porosity for HTO and iodide, effective diffusion coefficient for all tracers and distribution coefficient for sodium and strontium. The results of sensitive runs are evaluated by means of normalized sensitivities which are summarized in Table 1. Here we report only the results of the sensitivity of HTO concentrations to changes

in clay porosity and sodium concentrations to changes in efective diffusion coefficients (see Tables 2 and 3).

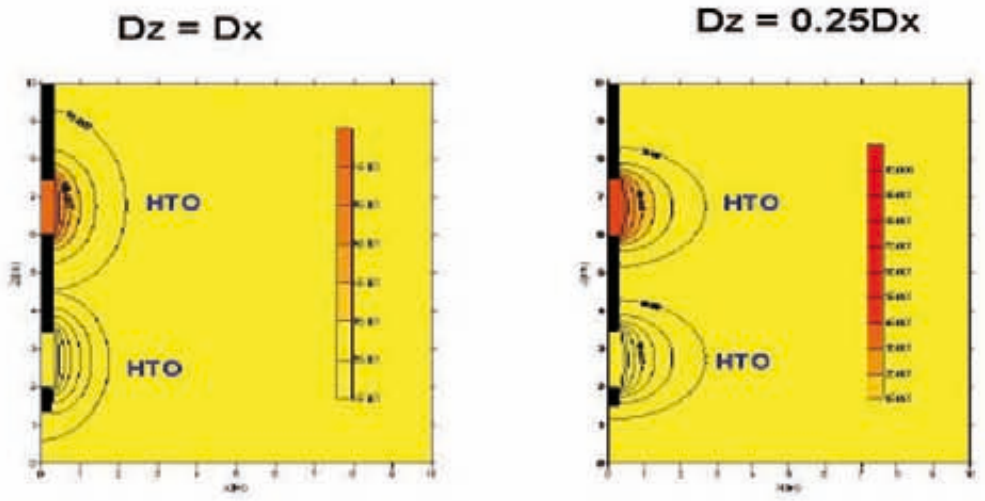

Figure 2 *HTO concentration in the rock after 5 years for isotropic (left) and anisotropic conditions (right).*

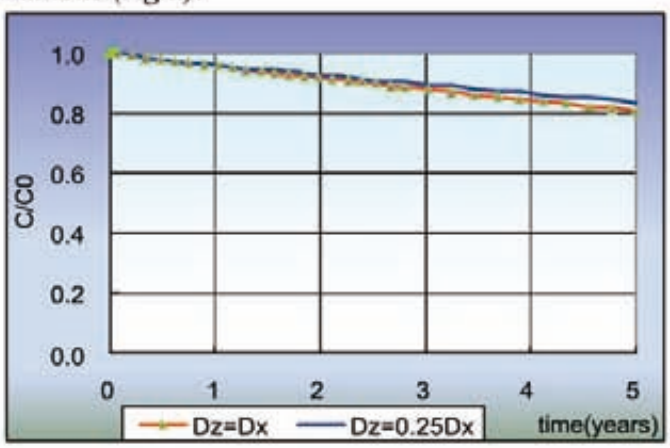

Figure 3. *HTO concentration in the injection interval for the isotropic and anisotropic cases.*

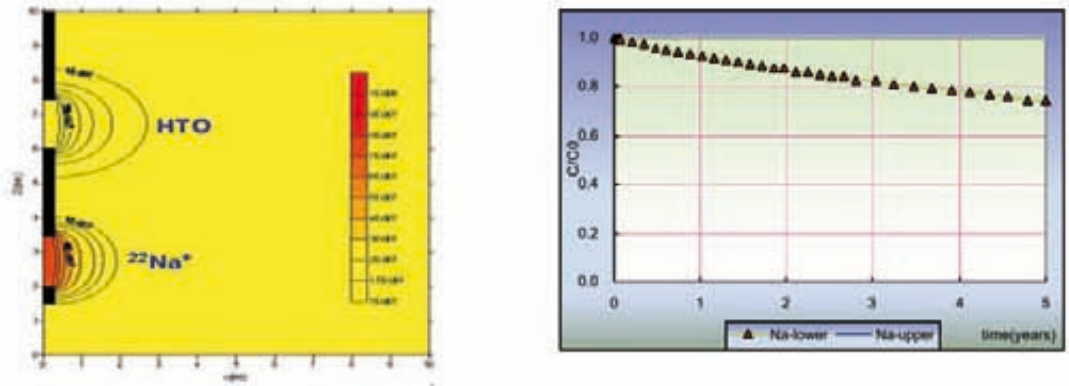

Figure 4. *Predictions of Na^+ injected in the lower interval and HTO (upper interval) after 5 years (left) and dilution curves of Na^+ at the lower and upper intervals (right) for the anisotropic case.*

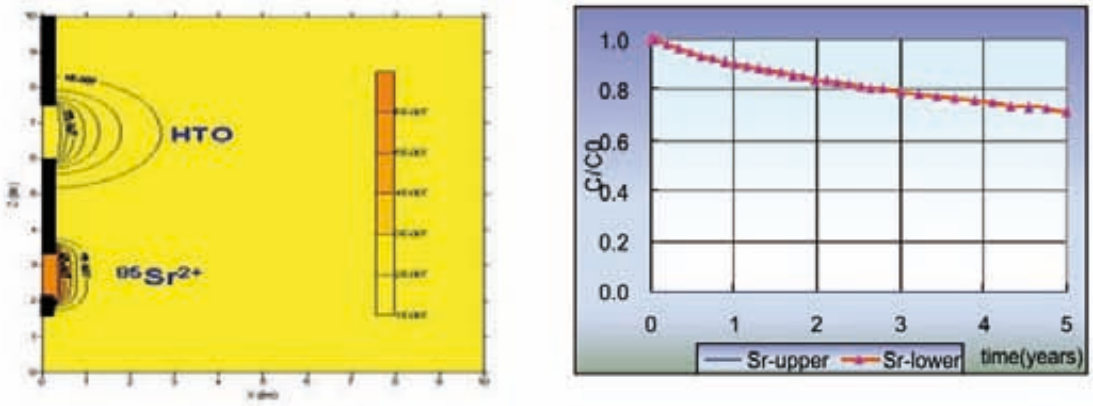

Figure 5. *Predictions of Sr^{2+} injected in the lower interval and HTO (upper interval) after 5 years (left) and dilution curves of Sr^{2+} at the lower and upper intervals (right) for the anisotropic case.*

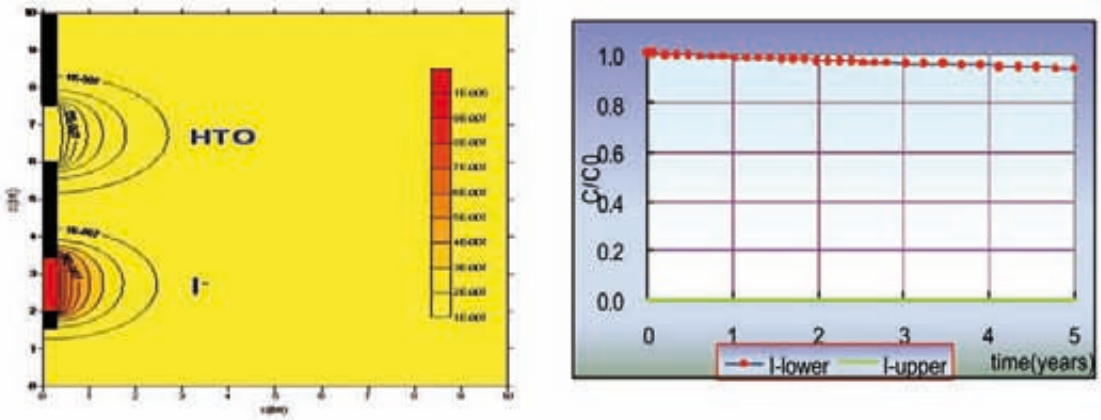

Figure 6. *Predictions of I injected in the lower interval and HTO (upper interval) after 5 years (left) and dilution curves of I at the lower and upper intervals (right) for the anisotropic case.*

Table 2. *Sensitivities of HTO to changes in porosity*

Parameter		Output					
		In the borehole		In the host rock(x<0.05m)		In the host rock(x>0.05m)	
Total porosity	Relative change (%)	Relative change (%)	Relative Sensitivity	Relative change (%)	Relative Sensitivity	Relative change (%)	Relative Sensitivity
0.1	-33.3	-15.6	0.472	-63.2	1.92	-99.1	3.00
0.2	33.3	-16.9	-0.051	-65.9	-2.01	-99.8	-3.02

Note: Relative changes of parameters (CP) are defined as $\frac{P_c - P_b}{P_b} \times 100$, and relative change of concentrations (AS) as $\frac{C_c - C_b}{C_b} \times 100$, where P_c and P_b are the parameter used in the sensitivity run and the calibrated base run, and C_c and C_b are the concentration of HTO in the sensitivity run and the calibrated base run, respectively. Relative sensitivity is defined as $\frac{AS}{CP}$.

Table 3. *Sensitivities of sodium concentrations to changes in effective diffusion coefficient.*

Parameter		Output					
Effective diffusion	Relative change (%)	In the borehole		In the host rock(<0.04m)		In the host rock(x>0.04m)	
		Relative change (%)	Relative Sensitivity	Relative change (%)	Relative Sensitivity	Relative change (%)	Relative Sensitivity
0.5De	-50	-16.38	0.3275	-72.09	1.458	-99.99	1.99
2De	100	-40.37	-0.4037	-74.79	-0.748	-99.62	-0.99

Performance assessment contribution

Our scoping calculations of the DR experiment aim at contributing to the optimum design of the experiment. The results of this experiment will provide additional insight into the role of diffusion anisotropy and sorption parameters for radionuclides in clays. Sensitivity analysis is performed to see which parameters are more sensitive in different locations for different tracers, which will be useful to the optimum design of the DR experiment.

Conclusions

The results of the scoping calculations of the DR experiment indicate that HTO concentrations are sensitive to the effective diffusion coefficient and porosity. The larger the porosity the larger the sensitivity. For iodide, the larger the accessible porosity the smaller the sensitivity. Computed concentrations of sodium and strontium are most sensitive to the distribution coefficient. The larger the distribution coefficient the larger the sensitivity. Computed concentrations of all tracers are sensitive to the effective diffusion coefficient. One common feature is that the larger the effective diffusion coefficient, the smaller the concentration near the borehole and the larger the concentration computed at the tails of the profile. Each tracer has different transport distance sensitivities. For HTO, concentrations are sensitive up to a distance of 6 dm while for sodium are sensitive up to 4 dm, for strontium is less than 2 dm and for iodide is about 5 dm. Results of our simulations have been useful for the optimum design of DR experiment, including definition of: 1) Length of testing intervals, 2) Separation between them; 3) borehole radius, and 4) volume of injection system. They will also be useful for defining the appropriate duration of the experiment and for the design of the final overcoring.

References

[1] Samper J., C.B. Yang, L. Montenegro, 2003. Users Manual of CORE2D version 4: A Code for groundwater flow and Reactive solute transport, Technical Report, UDC, 83 pp.

[2] Van Loon, L. R., Soler, J., Müller, W., Bradbury, H., 2004a. Anisotropic diffusion in layered argillaceous rocks: A case study with Opalinus Clay. Environ. Sci. Technol. 38: 5721-5728.

[3] Van Loon L. R., Wersin P., Soler J. M., Eikenberg J., Gimmi Th., Hernán P., Dewonck S., Savoye S. 2004b In-Situ Diffusion of HTO, 22Na+, Cs+ and I- in Opalinus Clay at the Mont Terri Underground Rock Laboratory. Radiochimica Acta 92, 757-763.

[4] Wersin, P., Van Loon, L. R., Soler, J., Yllera, A., Eikenberg, J., Gimmi, T., Hernan, P., Boisson, J.-Y, 2004. Long-term Diffusion Experiment at Mont Terri: First Results from Field and Laboratory Data. Appl. Clay Sci. 26: 123-135.

[5] Yllera, A., Hernández, A., Mingarro, M., Quejido, A., Sedano, L.A., Soler, J.M., Samper, J., Molinero, J., Barcala, J.M., Martín, P.L., Fernández, M., Wersin, P., Rivas, P., Hernán, P., 2004. DI-B experiment: planning, design and performance of an in situ diffusion experiment in the Opalinus Clay formation. Applied Clay Science 26: 181-196.

BENTONITE COLLOID FILTRATION IN A GRANITE FRACTURE

T. Missana*, U. Alonso, M. García-Gutiérrez and M. Mingarro.

CIEMAT, Departamento de Medioambiente
Avenida Complutense, 22 -28040 MADRID (Spain)

*Corresponding author: tiziana.missana@ciemat.es

Abstract

In the performance assessment of a high level waste repository, to establish the conditions in which the presence of colloids can favour contaminant migration is a critical task. The filtration of colloids in the medium will hinder the migration of those radionuclides adsorbed on the colloids, therefore this is a very important point to be analysed.

Migration experiments in a granite fractured column, using low water flow rates trying to approach realistic natural conditions, were carried out with bentonite colloids. The objective was to quantify the filtration of colloids in the medium and to evidence the main factors affecting the retention, as well as possible experimental uncertainties, as a previous step to the analysis of radionuclide migration in presence of colloids.

Results showed the breakthrough curves of bentonite colloids always presented an elution peak in a position very similar to that of conservative tracers but that their recovery critically depended on the colloid concentration and on the water flow rate.

Column experiments with Eu or Pu in the presence of bentonite colloids were also carried out at different flow rates and their recovery was analysed. Both elements presented high adsorption onto the colloids (>80 %) thus the migration of colloids should affect their migration. In fact, a peak of Eu or Pu in the same position than the conservative tracers was observed, clearly indicating that migration of these radionuclides is mostly colloid-driven. The recovery of Pu adsorbed onto the colloids was approximately the expected considering the filtration of bentonite colloid in the medium, whereas the recovery of Eu was always lower. This probably indicates that, along the flow path, part of Eu desorbs from the colloids and is retained on the fracture walls.

Introduction

In the frame of performance assessment of a deep geological repository (DGR), it is a very important issue to determine the type and the concentration of the colloidal species present in a certain environment because, provided they are

stable and mobile, they can be relevant for the migration of radionuclides (RN) towards the geosphere. At present, it is recognised that the data available for advanced modelling of RN-colloid interaction in a DGR is scarce (RETROCK). In addition, the modelling of filtration in fractured rock presents difficulties and uncertainties mainly due to the lack of experimental data obtained in realistic conditions.

Recent studies performed at the NAGRA's Grimsel Test Site (CRR project, [8] demonstrated that, in crystalline fractured rocks, colloids can be specially relevant in the migration of tri- and tetravalent radionuclides [2].Compacted bentonite is considered as an adequate engineered barrier in most of the DGR designs since the clay limits the income of water to the waste and delays the possible radionuclide transport to the geosphere. In addition, it presents high retention capability for most radionuclides. Therefore, the generation of bentonite colloids at the near field / far field interface, i.e. in the regions in which bentonite comes in contact with the groundwater, could be of importance in the migration of contaminants, above all for strongly sorbing radionuclides. In order to play a possible role in the migration of radionuclides, it is assumed that colloids must exist in a no-negligible concentration, be mobile, stable and to be able to adsorb radionuclides in irreversible form (MILLER et al., 1994)

Previous studies showed that, in low mineralized waters, bentonite colloids may fulfil several of the above-mentioned conditions and, for this reason, it is very important to analyse their effects on radionuclide migration in depth. Previous laboratory experiments of generation of bentonite colloids showed that the hydration and the loss of density of the bentonite backfill is a necessary condition for the colloids to be formed [6].

The stability of bentonite colloids was already investigated in laboratory as a function of the main geochemical parameters: pH and ionic strength. It was shown that bentonite colloids are very stable in low ionic strength ($=1\cdot10^{-3}$ M) and alkaline water. [6]

Previous transport studies at the GTS [2,3,9] demonstrated that the bentonite colloid migration was not retarded with respect to the water flow. In these experiments, the colloid recovery was high, but depended on not-identified filtration processes (size exclusion, rock/colloids interactions and diffusion in the rock matrix) taking place along the flow path. Thus, the understanding and quantification of filtration processes was recognised extremely important to adequately describe the migration of colloid-bond radionuclides. The importance of kinetic phenomena related to radionuclide sorption both onto the rock and colloids and sorption irreversibility was also pointed out [2]

The main limitation of the colloid migration tests carried out *in-situ* at the GTS, was the very high flow rate used for the experiments so that, for a better explanation of radionuclide behaviour in presence of bentonite colloids, it was deemed necessary to perform more experimental studies at laboratory scale. Since the colloid-mediated radionuclide transport is affected by a large number of processes, laboratory experiments are very useful to acquire deeper knowledge on the underlying mechanisms.

Objectives

The aim of the present work is trying to improve the knowledge on the colloid mechanisms affecting the radionuclide migration in a DGR and provide useful data for the performance assessment of radioactive waste repositories in crystalline rocks. Particular attention will be paid to the colloids and radionuclides recovery, during the transport experiment, as the indication of the degree of colloid filtration in the medium. The effect of the bentonite colloids on the migration of Eu and Pu is analysed.

More details on the experimental part and results can be found in a more extended document [5]

Experimental

The water used in all the experiments was the groundwater from the Grimsel Test Site (GTS, Switzerland). The main characteristics of the Grimsel water are: Eh = - 200 ± 50 mV, pH = 9.5 ± 0.2 and very low ionic strength. The bentonite used in these experiments (FEBEX bentonite) comes from the Cortijo de Archidona deposit (Almeria, Spain).

The preparation of bentonite colloids is detailed elsewhere[7]. Photon Correlation Spectroscopy (PCS) by means of a 4700 Malvern apparatus equipped with a Spectra Physics 4W argon laser (λ=514 nm) is used for determining the colloid concentration in column experiments. Since the events detected in the photomultiplier, counts, are dependent on the number of colloid in the suspension, calibration curves (counts vs. bentonite colloid concentration) can be generated to determine the concentration of bentonite particles a given sample. In addition, suspensions of different colloid concentration were chemically analysed in order to find the relation between the clay concentration and the presence of significant elements like Al, Fe, Mg, Zn, Ti, which could be used as indicators of presence of clay particles in the water. Calibration curves (element concentration vs. bentonite colloid concentration) can be plotted and, in general, a good linear correlation is found [5]

Column transport experiments were carried out using a large core from the Grimsel Test Site (GTS), with a longitudinal fracture (Fig. 1). The experiments with this fractured core were always performed using natural Grimsel groundwater and under anoxic conditions (N_2 atmosphere, O_2< 1ppm).The Grimsel water is introduced at the top of the column with a HLPC pump. The water is periodically collected with a fraction collector in previously weighted polyethylene tubes.

In a second step, experiments were carried out also with bentonite colloids traced with Eu and Pu. The main characteristics of the bentonite colloids (size and charge) did not change significantly after the addition of trace concentration of the tri and tetravalent elements.

***Figure 1**: Image of the fractured core sample used for column experiments*

Results

Different column tests using bentonite colloid suspensions at different concentrations (from 12 to 160 ppm) were carried out. Another parameter that has been varied in the experiments was the water flow rate (from 3 to 11 mL/h approximately). The elution curves were obtained determining the colloid concentration by PCS or by chemical analysis of important clay elements, as explained in the experimental section. Generally, after approximately 40 ml of eluted volume, the colloid concentration was lower than the resolution of both techniques.

Figure 2 shows an example of different bentonite colloid breakthrough curves obtained using different flow rate or colloid concentration, compared to the HTO breakthrough curve. The column presents a natural fracture and the migration of the conservative tracer shows a main peak and a secondary one (much less evident) which has been attributed to a secondary flow path within the column. Here, the main result to be remarked is that the bentonite colloids breakthrough curves always showed an elution peak in a position very similar to that of HTO (also the secondary peak), indicating that bentonite colloids are not retarded with respect to the water flow. However, whereas the recovery of conservative tracers was always very high (90 % at the end of the experiment, or approximately a 68% after 40 ml of eluted volume) the colloid recovery was strongly dependent on the initial colloid concentration and also on the water flow rate.

Figure 3 (left) shows the dependence of the recovery of bentonite colloids as a function on the initial colloid concentration. It can be seen that the recovery is maximum for the lowest concentration used (12 ppm), but it decreases very rapidly increasing the initial colloid concentration. However, if the colloid concentration is fixed, flow rate dependence can be evidenced, as shown in Figure 3 (right). The percentage of recovery obtained in different column tests using colloid suspensions of 26 ± 2 ppm, varying clearly increase when the flow rate increases. The size of the eluted colloids did not vary significantly with respect to the initial one, in general, a small increase in size is observed.

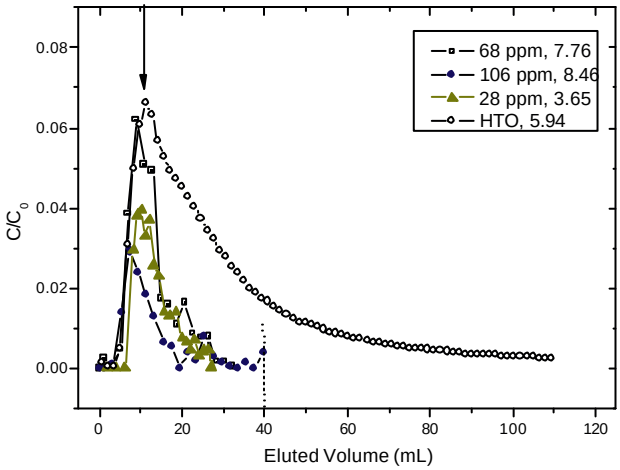

Figure 2: *Breakthrough curve of bentonite colloids obtained by PCS. The HTO "reference" curve is presented for comparison.*

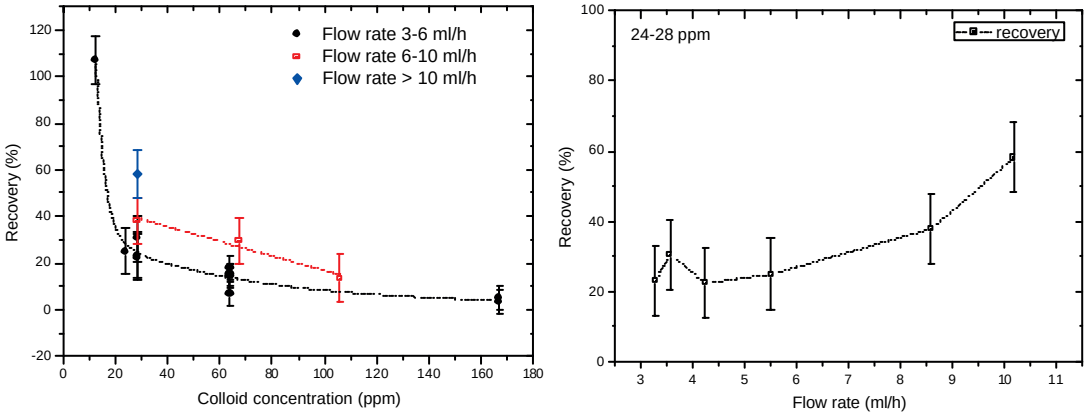

Figure 3*: Recovery of colloids in the column as a function of left) colloid concentration and right) Flow rate.*

The main conclusion drawn from these experiments is that the mobile fraction behaves as the conservative tracer but, depending on the initial experimental condition, a significant fraction could be immobilised in the column.

Different breakthrough curves of Eu and Pu in the presence of bentonite colloids (26 ppm) were obtained at different flow rates (from 6 to 8 ml/h), [5] Pu is, initially, in the oxidation state 4+ . In the conditions of the Grimsel water this was the most stable oxidation state calculated. All the curves presented a tracer peak in a position very similar to that of HTO (11 ml), and therefore it can be concluded that part of the injected tracers were able to move without retardation undoubtedly due to the presence of bentonite colloids. The Eu recovery however did not present a clear relation with the water flow rate and, interestingly, the Eu recovery was always relatively small, being always lower than 7 % of the injected activity Figure4 (left). As previously shown, for a colloid suspension of approximately 26 ppm the colloids recovery, for water flow rates from 5 to 10 ml/h, varies from a 25 % to a 58 % approximately. Taking into account that more than 80 % of Eu is initially colloid-bound, the recovery of Eu should be higher than a 20 %. The reason why less Eu than the expected is recovered might due to the fact that Eu desorbs from the colloids and adsorbs on fracture walls.

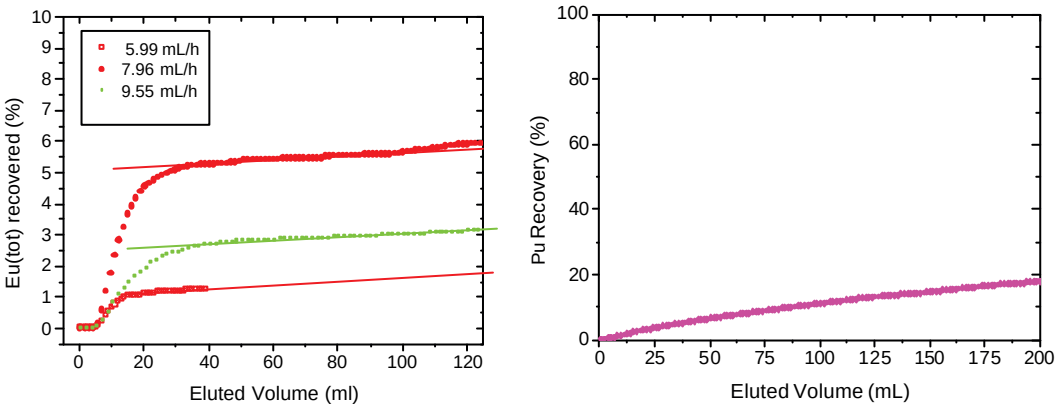

***Figure 4**: Recovery of tracers column: left) Europium ; right) Plutonium .*

In the case of the Pu experiment, recovery expected for bentonite colloid for this flow rate (4 mL/h) is around the 25 %. Considering that an 88 % of the injected Pu is adsorbed onto colloids, the activity of Pu recovered should be approximately a 22 % of the injected one, value in good agreement with the value observed.

Conclusions for PA

Flow and concentration of bentonite colloids have been shown to be important factors to take into account for determining the possible filtration of colloids in the medium and therefore to assess the possible relevance on the colloid-borne radionuclide migration. In particular, in Grimsel groundwater conditions, the Pu migration is affected by the presence of colloids. In the case of Eu, the relevance of colloids seems to be more limited, even if the only mobile Eu fraction is colloid driven, possibly due to the reversibility of the sorption process. This last point has to be investigated in depth.

References

[1] Alonso U., T. M., H. G., García-Gutiérrez M., Turrero M. J., A. M., Schafer T., Patelli A., and Rigato V. (2006) Role of inorganic colloids generated in high-level deep geological repository in the migration of radionuclides: open questions. *J. of Iberian Geology* 32(1), 79-95.

[2] Geckeis H., Schafer T., Hauser W., Rabung T., Missana T., Degueldre C., Möri A., Eikenberg J., Fierz T., and Alexander W. R. (2004) Results of the CRR experiment at the GTS, Switzerland. Impact of reaction kinetics and speciation on radionuclide migration. *Radiochim. Acta* 92, 1-10.

[3] Hauser W., Geckeis H., Kim J. I., and Fiertz T. (2002) A mobile laser induced breakdown detection system and its application for the in-situ monitoring of colloid migration. *Colloids and Surface A* 203, 37.

[4] Miller W., Alexander W. R., Chapman N., McKinley J., and Smellie J. (1994) *Natural analogue studies in the geological disposal of radioactive waste.* Elsevier.

[5] Missana T., Alonso U., Garcia-Gutierrez M., and Mingarro M. (2006) Role of colloids on the migration of europium and plutonium in a granite fracture: laboratory experimental results and related uncertainties. *Journal of Colloid and Interface Science (submitted)*.

[6] Missana T., Alonso U., and Turrero M. J. (2002) Generation and stability of bentonite colloids at the bentonite/granite interface of a deep geological radioactive waste repository. *J. Cont. Hydr.* 61, 17-31.

[7] Missana T., García-Gutiérrez M., Turrero M. J., Alonso U., and Mingarro M. (2003) The role of colloids in the radionuclide transport in a deep geological repository: participation of CIEMAT in the CRR project. *ENRESA TECHNICAL REPORT* 05/03.

[8] Mori A., Alexander W. R., Geckeis H., Hauser W., Schafer T., Eikenberg J., Fierz T., Degueldre C., and Missana T. (2003) The colloid and radionuclide retardation experiment at the Grimsel Test Site: influence of bentonite colloids on radionuclide migration in a fractured rock. *Colloids and Surfaces a-Physicochemical and Engineering Aspects* 217(1-3), 33-47.

[9] Möri A., Alexander W. R., Geckeis H., Hauser W., Schäfer T., Eikenberg J., Fierz T., Degueldre C., and Missana T. (2003) The colloid and radionuclide retardation experiment at the Grimsel Test Site: influence of bentonite colloids on radionuclide migration in fractured rock. *Colloids Surface A* 217, 33-47.

PRELIMINARY RESULTS FOR COMPLEXATION OF Pu WITH HUMIC ACID

J. Guczi[1*], P. Reiller[2], R. A. Bulman[3], H. Geckeis[4] and G. Szabó[1],

[1]National Research Institute for Radiobiology and Radiohygiene, PO Box 101, Budapest, H-1775, Hungary;
[2]Commissariat á l'Énergie Atomique, CE Saclay, Nuclear Energy Division/DPC/SERC, Laboratoire de Spéciation des Radionucléides et des Molécules. F-91191 Gif-sue-Yvette CEDEX, France;
[3]Radiation Protection Division, Health Protection Agency, Chilton, Didcot, United Kingdom, OX11 ORQ.
[4]Forschungszentrum Karlsruhe, Institut für Nukleare Entsorgungstechnik, 76021 Karlsruhe, Germany,

*Corresponding author; guczi@hp.osski.hu

Abstract

Interaction of plutonium with humic substances has been investigated by a batch method use of the surface bound humic acid from perchlorate solutions at pH 4-6. By using these novel solid phases, complexing capacities and interaction constants are obtained. The complexing behavior of plutonium is analyzed. Pu(IV)-humate conditional stability constants have been evaluated from data obtained from these experiments by using non-linear regression of binding isotherms. The results have been interpreted in terms of complexes of 1:1 stoichiometry.

Introduction

Extensive research over the years has established that humic substances play an important role in the geochemical cycling of metal ions and radionuclides. By the chemical nature of humic acids it was anticipatable that they would influence the speciation of plutonium in the environment [1-3]. Although several investigations have confirmed the suppositions, the chemistry of the interactions of plutonium with humic substances needs to be understood in fine detail especially with the humic matter sorbed on solid phases so that humate-mediated movement of this transuranic element through the environment can be predicted [3-6]. Satisfactory data on tetravalent and redox sensitive actinides such as plutonium are scarce due to experimental difficulties, namely, the low solubility of their oxide-hydroxide [7, 8] and their high affinity for vessel walls [9]. The main objectives of this work are to provide equilibrium complexation data for plutonium humic

interaction by laboratory experiments on designed controlled systems because scientifically proved data for Pu-humate complexes are rare in the literature.

Objectives

Unfortunately, quantitative data for Pu(IV) complexation with humic acid are very scarce and are mostly simulated by Th(IV) behavior. It is highly expected to provide proved data for Pu(IV), so the main objectives of this work are to provide equilibrium complexation data for plutonium(IV) humic interaction by laboratory experiments on designed controlled systems. Data to aid such a requirement have been obtained as conditional stability constants (β) of humate complexes of Pu(IV) by using as a model substrate a silica-humic acid composite (SiO_2-HA) prepared by chemical immobilization of humic acid on silica gel.

Experimental

Materials and Methods

The composite material SiO_2-HA was prepared and characterized as described elsewhere [10]. ^{239}Pu was determined by liquid scintillation counting in a Packard Tri-Carb 2550 liquid scintillation counter (U.S.A). The proton exchange capacity of the immobilized HA was determined by potentiometric titration (see Table 1). The Pu(IV)-nitrate was adjusted from ^{239}Pu-nitrate (in 4 M HNO_3) stock solution (Czech Institute of Metrology, Prague) by diluting with 1:1 0.1 M $NaNO_2$ solution. After one week the resulting solution was adjusted to pH 4, 5 and 6 and passed through a membrane of porosity 25 nm (Millipore Ltd.) to minimize the presence of colloidal transuranic species. ^{239}Pu activity was determined by LSC. The oxidation states of plutonium in the stock solution, in the clarified aliquot after sorption experiment and in the washing solution were determined by TTA extraction method and NdF_3 coprecipitation method [11, 12]. Plutonium was found to be predominantly (= 92 %) as Pu(IV).

Determination of maximal complexing capacity (B_{max}) and conditional interaction constants (β) for Pu_{total} of the prepared solid phase

The complexing capacity (B_{max}) of SiO_2-HA was determined for Pu(IV). Accurately weighed quantities of the gels, typically about 2 mg, were added to 20 ml of 0.1 mol l^{-1} $NaClO_4$ solutions (pH 4-6) containing different concentrations (10^{-8} mol l^{-1}) of Pu(IV). The resulting suspensions were shaken at room temperature for 48 h.

Total concentrations of Pu(IV) in a clarified aliquot, which was collected by centrifugation, were measured by LSC. After sorption, the Pu(IV) sorption on to vial walls was investigated. The vials were washed with distilled water and dried, then 20 ml aliquots of 2 mol l^{-1} HNO_3 were added and the vials shaken for 48 h. The Pu(IV) concentration in the washing solutions was determined by LSC. The amount of Pu(IV) bound by SiO_2-HA was calculated as the difference between the initial

Pu(IV) concentration and the sum of the amounts of Pu(IV) remaining in solution and Pu(IV) sorbed on to the vial walls. Isotherms were then plotted.

Calculation of maximal binding capacity (B_{max}) and conditional interaction constants (β) of Pu_{total} from binding isotherm

The conditional interaction constant (β) is relative to the following equilibrium:

$$M^{z+} + HA \leftrightarrow MHA \qquad \text{(Eq. 1)}$$

$$\text{with } \beta = \frac{[MHA]}{[M^{z+}]_f \; [HA]_f} \qquad \text{(Eq. 2)}$$

where:

M^{z+}: the metal cations
HA: the humic acid
[MHA]: the concentration of the metal humate complex
$[M^{z+}]_f$: the concentration of the free thorium ion
$[HA]_f$: the concentration of the free humic acid

The assumption is made that the macromolecule is the central group and the complexation can be described in terms of a Langmuir-type adsorption equation. The free ligand concentration can be calculated in Eq. 2 by introducing B_{max}

$$[HA]_f = [B_{max}] - [MHA] \qquad \text{(Eq. 3)}$$

where:

B_{max}: maximal complexing capacity of humic acid

A combination of Eqs. 2 and 3 gives the relationship that could be used for calculation of conditional interaction constants:

$$\beta = \frac{[MHA]}{[M^{z+}]_f \; ([B_{max}] - [MHA])} \qquad \text{(Eq. 4)}$$

or after alteration

$$[MHA] = \frac{\beta \; [M^{z+}]_f \; B_{max}}{1 + \beta \; [M^{z+}]_f} \qquad \text{(Eq. 5)}$$

After plotting the bound Pu(IV) [MHA] versus (Putotal)free [Mz+]f and using the binding isotherms, the maximal binding capacity and the conditional interaction constants (β) of Putotal could be determined.

Calculation of conditional interaction constants (β) of PuHA

The reaction between Pu^{4+} and HA can be written

$$Pu^{4+} + HA \leftrightarrow PuHA \qquad \text{(Eq. 6)}$$

$$\text{with } \beta = \frac{[\text{PuHA}]}{[Pu^{4+}]_f \; [HA]_f} \qquad \text{(Eq. 7)}$$

Pu^{4+} is readily hydrolysed and it is not expected that only Pu^{4+} ions exist in solution at pH 4-6. From the $Pu(IV)_{total}$ the $[Pu^{4+}]$ can be calculated by using the stability constants of the hydroxo complexes $Pu(OH)^{3+}$, $Pu(OH)_2{}^{2+}$, $Pu(OH)_3{}^{+}$ and $Pu(OH)_4$ [13, 14]:

$$[Pu(IV)]_{total} = [Pu^{4+}] + [Pu(OH)^{3+}] + [Pu(OH)_2{}^{2+}] + [Pu(OH)_3{}^{+}] + [Pu(OH)_4]_{aq} \qquad \text{(Eq. 8)}$$

$$[Pu(IV)]_{total} = [Pu^{4+}]\, \alpha_{Pu} \qquad \text{(Eq. 9)}$$

where α is the Ringböm coefficient (15) concerning inorganic complexation:

$$\alpha = 1 + \sum_i \frac{{}^{*}\beta_i}{[H^+]^i}$$

If we assume that the hydrolysed species is not involved in the interaction with humic acid and measure the total Pu(IV) concentration in the liquid phase, it becomes possible to calculate the conditional interaction constants ($\log \beta$) of PuHA using the following equation:

$$\log \beta_{total} + \log \alpha_{Pu} = \log \beta_{PuHA} \qquad \text{(Eq. 10)}$$

Results and Discussion

The main characteristics of SiO_2-HA are reported in Table 1.

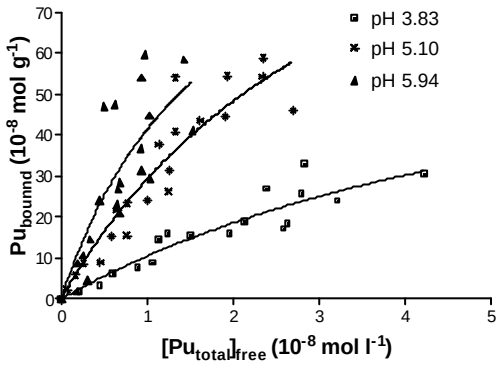

Figure. 1*. Binding isotherms of SiO_2-HA for Pu(IV) in 0.1 mol l^{-1} $NaClO_4$.*

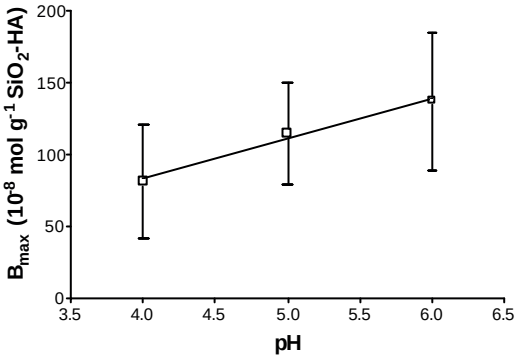

Figure. 2*. Variation of the maximal binding capacity (B_{max}) of SiO_2-HA for Pu(IV).*

Table 1*. Characteristics of SiO_2-HA*

Substrate content (mg g^{-1})	19.9 ± 1.2
Proton exchange capacity (μeq g^{-1} solid matter)	67.3
BET surface area [a] (m^2 g^{-1})	74 ± 8

[a] The surface area of the parent silica gel is 100 m^2 g^{-1}

Determination of maximal binding capacity (B_{max}) of SiO_2-HA and conditional interaction constants (β) of Pu_{total} from binding isotherm

Typical binding isotherms (solid phase concentration vs. liquid phase concentration in equilibrium) of Pu(IV) on SiO_2-HA at different pH values in 0.1 mol l^{-1} $NaClO_4$ are presented in Fig. 1. As seen from Table 2 and Figure 2, the complexing capacity of SiO_2-HA increases with increasing pH. This increase with pH is likely to result from an increase in the number of ionized carboxylic binding sites. Other research groups [16, 17] have reported a similar phenomenon. By using the nonlinear regression on the binding isotherms (Eq. 5), the conditional interaction constants (β) of Pu_{total} with humic acid can be calculated (see Table 2). From Table 2 and Figure 3, it is apparent that the conditional interaction constants appear insensitive to pH.

Table 2*.Bmax and log β of Putotal with humic acid as a function of pH in 0.1 mol l^{-1} $NaClO_4$*

	pH		
	3.83	5.10	5.94
B_{max} (μmol g^{-1})	0.81 ± 0.39	1.15 ± 0.65	1.37 ± 0.47
Log β (l mol^{-1})	7.17 ± 0.18	7.81 ± 0.17	7.43 ± 0.28

Calculation of the conditional interaction constants of PuHA (log β_{PuHA})

The log β values for Pu_{total} with humic acid are presented in Table 2. From this table the conditional interaction constants of Pu^{4+} with humic acid (β_{PuHA}) can be calculated by using Eq. 10 and hydrolysis constants from Guillaumont et al. [14]. Fig. 4 shows the pH dependency of log β_{PuHA}. The β_{PuHA} varies linearly between $10^{15.17}$ at pH 3.83 to $10^{22.01}$ at pH 5.94. The regression line has the following equation:

$$\log \beta_{PuHA} = 3.26 \pm 0.15\ pH + 2.76\ (\pm 0.74) \text{ with } r^2 = 0.998.$$

The observation that the β value linearly increases with pH is expected since this behaviour is observed on complexation of metal ions by humic substances [18, 19].

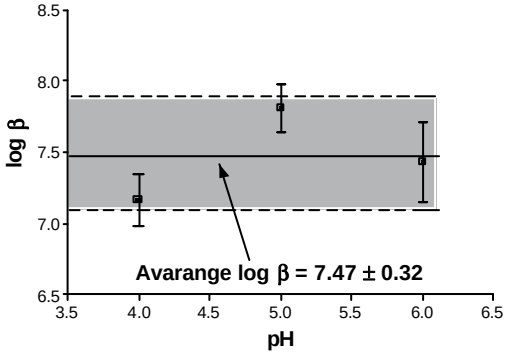

Figure. 3*. Dependence of the interaction constants log ß$_{Total}$ for Pu humic complexes as a function of pH.*

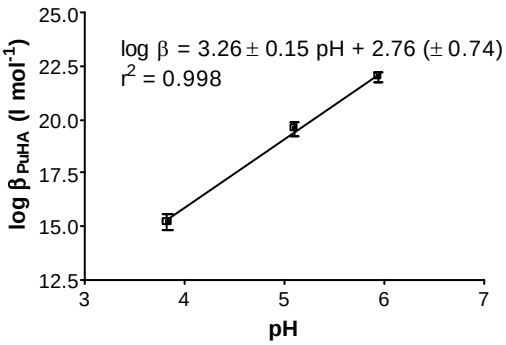

Figure. 4*. Variation of the stability constant log β_{PuHA} for Pu^{4+} humic complexes as a function of pH.*

Table 3. *Conditional interaction constants (log β) of Putotal, side reaction coefficient (log αPu) and log βPuHA, as a function of pH in 0.1 mol l-1 NaClO4, according to the hydrolysis constants from Guillaumont et al. [14].*

	pH		
	3.83	5.10	5.94
Log β_{total} (l mol^{-1})	7.17 ± 0.18	7.81 ± 0.17	7.43 ± 0.28
Log α_{Pu}	8.01	11.75	14.58
Log β_{PuHA} (l mol^{-1})	15.18 ± 0.35	19.56 ± 0.34	22.01 ± 0.23

Modelling

Derivation of complexation constants on the basis of the presented experimental data is only valid under the prerequisite that dissolved and SiO_2-HA sorbed Pu(IV) species exist exclusively in the studied system. Even though it was established that >92% of the Pu in the stock solution was tetravalent, we cannot exclude that in the sorption experiments significant Pu-amounts existed in higher oxidation states or as polynuclear species with sizes < 25 nm. In previous studies [20, 21] it was shown that various Pu species, PuO_{2+x} colloids and dissolved Pu(VI, V, IV, III) species can coexist in various ratios depending on the given redox conditions, Pu concentrations and reaction times.

Conclusions

The ready synthesis of SiO_2-HA has been established. The potential of such materials to complex cations such as Pu^{4+} has been demonstrated. From an examination of the sorption isotherms of Pu(IV) at different pHs it is apparent that conditional stability constants of Pu^{4+} (log β_{PuHA}) can be easily calculated. However, those β-values have to be considered with care as they are calculated under the prerequisite that only dissolved and SiO_2-HA sorbed Pu(IV) species exist under given experimental conditions. This might not be true and further studies are underway to study Pu speciation in those experiments in detail. This investigation indicates that humic acid materials such as SiO_2-HA are likely to be valuable for modelling the role of humates in interacting with complexes of transuranic entities, such as Pu(IV).

Acknowledgements

This work was partly supported by European Commission, EC Contract No. FP6-516514 (FUNMIG).

References

[1] Choppin, G.R., Allard, B.: Complexes of actinides with naturally occurring organic compounds. In: Handbook on the Physics and Chemistry of the Actinides (Freeman, A.J., Keller, C. Eds.) Amsterdam 1986, Chap 11.

[2] Choppin, G. R.: The role of natural organics in radionuclide migration in natural aquifer system. Radiochim. Acta, 58/59, 113 (1992).

[3] Moulin, V., Tits, J., Ouzounian, G.:Actinide speciation in the presence of humic substances in natural water conditions, *Radiochimica Acta*, 58/59 (1992) 179

[4] Livens, F.R., Singleton, D.L.: Plutonium and americium in soil organic matter, *J. Environ. Radioact.*, 13 (1991) 323

[5] Bulman, R. A., Szabó, Gy.: Investigations of the interactions of transuranic radionuclides with humic and fulvic acids immobilized on silica gel, *Lect. Notes Earth Sci*., 33 (1991) 329

[6] Moulin, V., Moulin, C.: Fate of actinides in the presence of humic substances under conditions relevant to nuclear waste disposal, *Appl. Geochem*. 10 (1992) 573

[7] Neck, V., Kim, J.I.: Solubility and hydrolysis of tetravalent actinides. *Radiochim. Acta*, 89, 1 (2001).

[8] Fanghanel, Th., Neck, V.: Aquatic chemistry and solubility phenomena of actinide oxides/hydroxides. Pure Appl. Chem., 74, 1895 (2002).

[9] Östhols, E.: Thorium sorption on amorphous silica. *Geochim. Cosmochim. Acta*, 59, 1249 (1995).

[10] Szabó, Gy., Guczi J., Koblinger-Bokori E., Bulman R.A.: An examination of the sorption characteristics of ^{241}Am(III) and Eu(III) bound by humic substances chemically immobilized on silica gel. *Radiochim. Acta*, 82, 355 (1998).

[11] Nitsche, H., Lee, S.C., Gatti, R.C.: Determination of plutonium oxidation states at trace levels pertinent to nuclear waste disposal. *J. Radioanal. Nucl. Chem*. 124 No. 1, 171 (1988)

[12] Schramke, J.A., Rai, D., Fulton, R.W., Choppin, G.R.: determination of aqueous plutonium oxidation states by solvent extraction. *J. Radioanal. Nucl. Chem*. 130 No. 2, 333 (1989)

[13] Neck, V., Kim, J.I.: Solubility and hydrolysis of tetravalent actinides. *Radiochim. Acta*, 89, 1 (2001).

[14] Guillaumont, R., Fanghänel, T., Fuger, J., Grenthe, I., Neck, V., Palmer, D.A. and Rand, M., 2003. Update on the chemical thermodynamics of uranium, neptunium, plutonium, americium and technetium. Elsevier.

[15] Ringböm A., Complexation in Analytical Chemistry, Interscience, New York, 1963.

[16] Kim, J.I., Rhee, D., Buckau, G.: Complexation of Am(III) with humic acids of different origin. *Radiochim. Acta*, 52/53, 49 (1991).

[17] Moulin, V., Tits, J., Moulin, C., Decambox, P., Mauchien, P., de Ruty, O.: Complexation behaviour of humic substances towards actinides and lanthanides studied by Time-Resolved Laser-Induced Spectrofluorometry. *Radiochimica Acta*, 58/59, 121 (1992).

[18] Hummel, W.: Binding Model for Humic Substances. In: Modelling in Aquatic Chemistry, Ed. Grenthe, I., Puigdomenech, I., NEA-OECD (1997).

[19] Reiller, P., Moulin, V., Casanova, F., Dautel, C.: On the study of Th(IV)-humic acid interactions by competition sorption studies with silica and determination of global interaction constants. *Radiochim. Acta,* 91, 513 (2003).

[20] Marquardt, C. M., Seibert, A., Artinger, R., Denecke, M. A., Kuczewski, B., Schild, D., Fanghänel, Th., The redox behaviour of plutonium in humic rich groundwater, *Radiochim. Acta* 92, 617–623 (2004).

[21]Neck, V., Altmaier, M., Fanghänel, Th., Solubility and Redox Reactions of Plutonium(IV) hydrous oxide in the presence of oxygen, in May, I., Alvares, R., Bryan, N. (eds.), Recent Advances in Actinide Science, RSC publishing Cambridge (2006)

EFFECT OF METAL ION COMPLEXATION ON HUMIC ACID CONFORMATION

K. Kolokassidou[1]; F. Luschtinetz[2]; S. Eidner[2]; I. Pashalidis[1] and M. U.Kumke[2,*]

[1] *University of Cyprus, Department of Chemistry, 1678 Nicosia, Cyprus*
[2] *University of Potsdam, Institute of Chemistry, Karl-Liebknecht-Str. 24-25, 14476 Potsdam-Golm, Germany*

*Corresponding author: Kumke@uni-potsdam.de

Abstract

The intrinsic fluorescence of Gohy573 humic acid (HA) was used to investigate the effect of metal ion complexation on the HA conformation. Results of steady-state and stopped-flow fluorescence quenching experiments indicated that due to the binding of metal ions, the molecular conformation of HA was altered. Upon metal binding the fluorescence spectrum showed a spectral shift of up to $\Delta\lambda$ = 43 nm depending on the concentration of metal ion. For fulvic acids (FA) no such effect could be observed. In addition, also the binding kinetics of metal ions pointed towards the involvement of conformational reorientation processes since in contrast to FA the binding process is a combination of a very fast first binding followed by a second slower process on the millisecond to second time scale. The slower process has been attributed to conformational alterations of HA, which might include aggregation of HA as well. The stopped-flow data were evaluated according to a Stern-Volmer analysis. The relative fluorescence quenching was dependent on the time after mixing, which also supports the conclusion that for HA additional processes like changes in conformation are induced by metal binding.

Time-resolved fluorescence anisotropy measurements were performed in order to further investigate possible alteration of the HA conformation in the presence of metal ions. The rotational correlation times indicated that the overall motion of the HA molecules became faster upon addition of metal ions. From the results it is attractive to assume that the metal ions lead to a contraction of the HA molecules and hence, a reduction of the rotational volume. The determined rotational correlation times were very fast which also indicated that the loss of anisotropy is not only caused by rotational motions but by e.g., energy processes as well.

Introduction

Humic substances (HS) are ubiquitous in the environment and play a key role in the transport of xenobiotics. Due to binding interaction the bioavailability

and subsequently the toxicity of xenobiotics is altered. HS are polyelectrolytes and can form complexes with metal ions, which show an altered mobility in soil and ground water. Hence, for a reliable modelling of such processes the underlying mechanisms of metal binding and parameters affecting them need to be understood as detailed as possible. Questions of interest are the complexation kinetics and the effect on the size of the HS due to complexation. The latter has wide influence on the mobility of the complexes formed in subsurface layers.

Objectives

In this study stopped-flow and time-resolved anisotropy measurements were performed in order to investigate the effect of metal ion binding on the conformation of HS. The conformation of macromolecules can be an important parameter for their transport behaviour, e.g., it is tempting to connect changes in size/volume of a molecule with alterations in its conformation.

Experimental

In the experiments a humic acid (HA) and a fulvic acid (FA) fraction isolated according to IHSS standard procedure from the Gorleben aquifer (Gohy573 HA and Gohy573 FA) was used. The ionic strength of the HS solutions was adjusted using $NaClO_4$ and was set to 0.1 mol/L in anisotropy measurements and to 0.01 mol/L in stopped-flow experiments, respectively. The final HS concentration in the solutions was 10 mg/L. Eu(III) was added as metal ion. A stopped-flow reaction analyzer SX.18MV-R (Applied Photophysics) was used for the measurement of the complexation kinetics (20 µL detection volume, 1.2 ms dead time). In these measurements the HS were excited at λ_{ex} = 325 nm and the intrinsic HS fluorescence intensity in the range from 360 nm to 440 nm was detected. In the fluorescence anisotropy experiments a Ti:Sapphire-Laser (Tsunami, Spectra Physics) was used (THG@266 nm). The fluorescence signal was detected by a multi channel plate (Europhoton) with a Glenn-Thomson polarizer in front of the emission monochromator. The fluorescence of the samples was measured with the polarizer oriented at 0°, 90° and at the magic angel. The fluorescence decay curves were recorded with a FL920 (Edinburgh Instruments) operated in single photon counting (SPC) mode. The fluorescence anisotropy was calculated from the experimental data according to:

$$r(t) = \frac{I(t)_V - I(t)_h}{I(t)_V + 2 \cdot I(t)_h} \qquad (1)$$

Results

The humic acid (HA) investigated in this study show the typical broad fluorescence in the spectral range of 350 nm < λ_{em} < 625 nm with a fluorescence maximum around λ_{em} = 460 nm. Upon addition of Ln(III) the intrinsic fluorescence of the HA is quenched. However, in contrast to fulvic acid (FA) fractions the shape

of the HA fluorescence spectrum is altered [1]. Due to the addition of Tb(III) the fluorescence spectrum showed a hypsochromic shift $\Delta\lambda$, which reached $\Delta\lambda_{max} = 43$ nm at the highest Tb(III) concentration investigated. Possible explanations could be a) the formation of new fluorescent entities in HA and/or b) the inhibition of deactivation processes due to a more rigid structure of HA in the presence of metal ions.

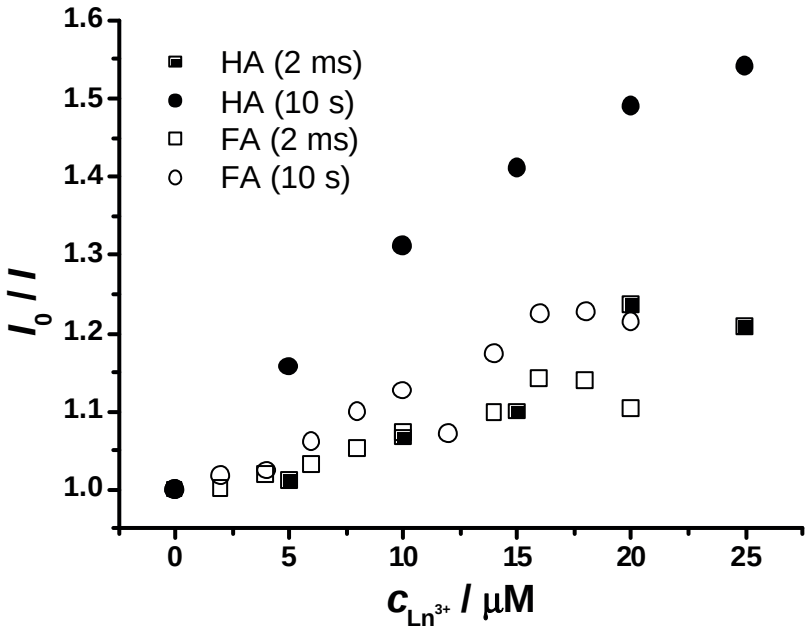

***Figure 1**: Fluorescence quenching of FA and HA after different times of mixing (Gohy573 FA and HA, c_{HS} = 10 mg/L, pH 5, λ_{ex} = 325 nm). The fluorescence quenching of the intrinsic FA fluorescence is independent on time after mixing which is in contrast to HA.*

The difference in the complexation behavior between FA and HA is also found in the kinetics of the metal binding. In stopped-flow experiments the quenching of the intrinsic HS fluorescence upon addition of Ln(III) was measured. In addition to a very fast quenching process, which was also found for FA, additional slower processes on a millisecond to second time scale were found for HA [2]. The intensity data extracted from stopped-flow time traces were evaluated according to a standard Stern-Volmer analysis at different time intervals: a) 2 ms after mixing (time interval A) and b) at 10-20 s after mixing (time interval B).

In contrast to FA the comparison of fluorescence quenching data of HA evaluated after 2 ms (time interval A) and after 10 s (time interval B) (or longer, e.g., standard steady state fluorescence quenching experiments) showed considerable differences. In metal competition experiments with Ca(II) and Al(III) slow exchange reactions of Tb(III) on a time scale of seconds to minutes were observed and attributed to different types of binding sites in HS [3]. Wu et al. observed two complexation processes with different reaction rate on a second time-scale and attributed those to different binding sites as well as to the possibility of

conformational changes of the HS due to the metal complexation [4]. In the experiments with divalent metal ions the complexation reaction was completed within 30 seconds after addition [4-6]. It is tempting to attribute the observed difference between FA and HA fraction to macromolecular effects such as conformational changes of HA that are induced upon metal ion binding (this might include aggregation processes). On the other hand, FA are less affected since they act more or less as a small ligand and do not show conformational reorientation upon metal ion complexation. The importance of conformational alterations of HS due to interactions with metal ions has been pointed out recently and has been considered in an advanced data analysis approach [7].

In order to further elucidate the contribution of conformational processes to the fluorescence properties of HA, time-resolved anisotropy measurements were carried out. The time-resolved anisotropy of HA in the presence and absence of Eu(III) was calculated according to equation (1). The anisotropy data were analyzed using a global fit approach and the characteristic rotational correlation time ϕ was determined as a function of temperature in the absence and presence of Eu(III). The anisotropy decays were found to be sufficiently represented by a monoexponential decay law, which is surprising considering the highly complex fluorescence decay behavior [8,9]. After approximately 2 ns the anisotropy decay was completed and decayed to zero. The rotational correlation times calculated were $\phi \sim 0.5$ ns. As a general tendency a decrease of ϕ was found upon increasing the temperature, which is most probably connected to the decrease of the solvent viscosity (see Figure 2). A lower viscosity will allow a faster rotational motion either of the whole molecule or of molecule segments containing fluorescent groups.

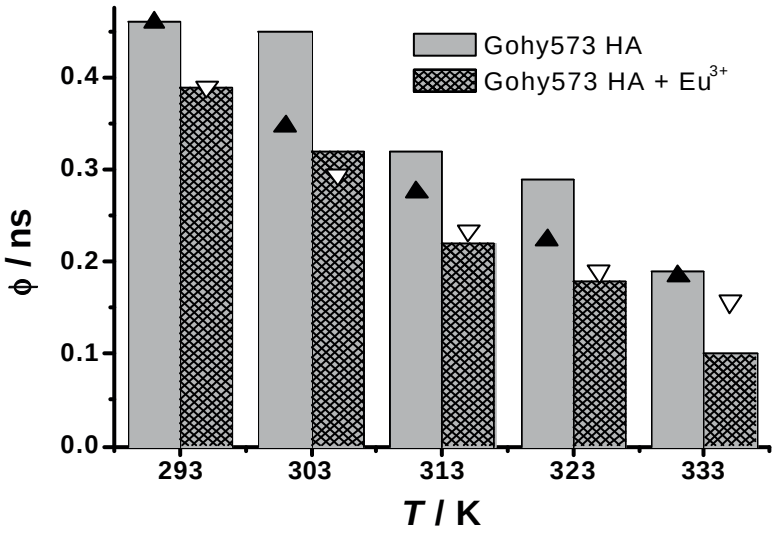

***Figure 2**: Rotational correlation times ϕ of Gohy573 HA (c_{HA} = 10 mg/L, pH 5, λ_{em} = 465 nm, $c_{Eu(III)} = 1.6\times10^{-5}$ mol/L). The triangles represent the theoretical expected trend according to the Perrin equation $\phi(T) = \eta V (RT)^{-1}$. Where η is the viscosity of the solvent, R the universal gas constant, T the temperature and V the volume of the rotator.*

Upon addition of Eu(III) a decrease of the rotational correlation times was observed. In Figure 2 the rotational correlation times ϕ for Gohy573 HA in the absence and presence of Eu(III) at different temperatures are compared. Independent on the temperature, the addition of Eu(III) always decreased ϕ, which points towards a faster rotational motion and subsequently to a decrease of the HA fluorescence connected to the molecular volume.

Conclusions

It is attractive to attribute the observed differences in the metal binding kinetics of FA and HA to a multiple step binding of the metal ions in case of HA. In a first, fast step the metal ion is nonspecifically bound to HA (e.g., via pure coulomb forces, or to easily accessible carboxylate groups) similar to the binding mechanisms in FA. In a second, slower process the more specific binding becomes effective, in which conformational reorientations of the HA molecule are necessary. These conformational changes require more time (on a second time scale). The assumption that in the first step the binding of metal ions to FA and HA is quite similar – at least when the induced fluorescence quenching due to metal binding is considered – is further supported by the identical fluorescence quenching of FA and HA calculated for time interval A. The view of FA as relatively small molecules that act as simpler ligands in metal complexes is supported by results obtained in ultra high-resolution mass spectrometry measurements, in which FA are identified as low molecular weight compounds with a high degree of similarities [10].

Compared to literature data the ϕ values reported in the present study are considerably shorter, which might be a) related to the HS used in this study or b) a result of a very fast segmental motion of fluorophores in HS or c) caused by energy transfer across the HA molecule (or HA aggregates). The latter has been reported for polymers as a main reason for the very fast loss of anisotropy. The dependence of the fluorescence decay of HS on the emission wavelength has been discussed recently [8,9]. It was suggested that the observed emission wavelength dependence is caused by effective intramolecular (or intermolecular, in case of the formation of weakly bound HS associates, e.g., via H-bonds) energy transfer between different chromophores inside HS. This would be supported by the short rotational correlation times ϕ found in this study. However, the rotational correlation times became shorter upon increasing temperature and upon addition of europium. It is tempting to attribute the latter effect to a decrease in the effective rotational volume due to a contraction of the HS caused by the metal binding. The good agreement of the experimentally found and theoretically predicted temperature dependence of the rotational correlation times ϕ points toward the contribution of rotational motion to the overall fluorescence depolarization process. For an anisotropy loss purely driven by energy transfer processes the observed temperature dependence would be unusual, unless also the increased (intra)molecular motion of the molecule would increase the energy transfer efficiency.

The results presented show that upon metal ion complexation the conformation of HA is altered. The conformational reorientation processes can be related to intra- or intermolecular interactions of the metal ion with binding sites.

This effect is only seen for HA, while FA show a much simpler complexation scheme probably pointing towards their lower mass, which make them act as "simple" ligands. Future work, in which the competition between metal ions for HS binding sites and pH changes are added to the investigated parameters will help to further elucidate the contribution from energy transfer processes and conformational alterations to the overall fluorescence properties of HS.

References

[1] Kumke, M.U.; Eidner, S.; Krüger T. (2005) Fluorescence Quenching and Luminescence Sensitization in Complexes of Tb^{3+} and Eu^{3+} with Humic Substances, Environmental Science & Technology, 39(24), 9528-9533

[2] Kumke, M.U.; Eidner, S.; Marmodée B.; Primus P. Complexation of lanthanide ions by humic substances: New aspects from luminescence sensitization and photodynamics of humic substances, Proceedings of 1st Annual Meeting FUNMIG, Saclay

[3] Bidoglio, G.; Omenetto, N.; Robouch, P. (1991) Kinetic studies of lanthanide interactions with humic substances by time resolved laser induced fluorescence, Radiochimica Acta, 52/53, 57-63.

[4] Wu, F.C.; Mills, R.B.; Evans, R.D.; Dillon P.J. (2004) Kinetics of metal-fulvic acid complexation using a stopped-flow technique and three-dimensional excitation emission fluorescence spectrophotometer, Analytical Chemistry, 76, 110-113.

[5] Saar, R.A.; Weber, J.H. (1980) Comparison of spectrofluorometry and ion-selective electrode potentiometry for determination of complexes between fulvic acid and heavy-metal ions, Analytical Chemistry, 52, 2095-2100.

[6] Cabaniss, S.E. (1992) Synchronous fluorescence spectra of metal-fulvic acid complexes, Environmental Science & Technology, 26, 1133-1139.

[7] Hays, M.D.; Ryan, D.K; Pennell, S. (2004) A modified multisite Stern-Volmer equation for the determination of conditional stability constants and ligand concentrations of soil fulvic acid with metal ions, Analytical Chemistry, 76, 848-854.

[8] Kumke, M.U.; Abbt-Braun, G.; Frimmel F.H. (1998) Time-Resolved Fluorescence Measurements of Aquatic Natural Organic Matter, Acta Hydrochimica et Hydrobiologica, 26, 73-81

[9] Kumke, M.U.; Tiseanu, C.; Abbt-Braun, G.; Frimmel, F.H. (1998) Fluorescence Decay of Natural Organic Matter (NOM) – Influence of Fractionation, Oxidation, and Metal Ion Complexation, Journal of Fluorescence, 8, 309-318

[10] Stenson, A. C.; Marshall, A. G.; Cooper, W. T. (2003) Exact masses and chemical formulas of individual Suwannee river fulvic acids from ultra high-resolution electrospray ionization Fourier transform ion cyclotron resonance mass spectra, Analytical Chemistry, 75, 1275-1284.

COLLOID DETECTION IN NATURAL GROUND WATER FROM RUPRECHTOV BY LASER-INDUCED BREAKDOWN DETECTION

W. Hauser [1,*], H. Geckeis [1], R. Götz [1], U. Noseck [2] and A. Laciok [3]

[1] Institut für Nukleare Entsorgung (INE), Forschungszentrum Karlsruhe GmbH
D-76021 Karlsruhe, Germany
[2] Gesellschaft für Anlagen- und Reaktorsicherheit (GRS) mbH, Abt. Geochemie,
Theodor-Heuss-Str. 4, D-38122 Braunschweig, Germany
[3] Nuclear Research Institute Res, Czech Republic

* Corresponding author: hauser@ine.fzk.de

Abstract

A borehole ground water sampling system and a mobile laser-induced breakdown detection (LIBD) equipment for colloid detection combined with a geo-monitoring unit have been applied to characterize the natural background colloid concentration in ground waters of the Ruprechtov natural analogue site (Czech Republic). Ground water has been sampled using steel cylinders. To minimize artifacts during ground water sampling the contact to atmospheric oxygen has been excluded. The ground water samples collected in this way are transported to the laboratory where they have been connected to a series of flow-through detection cells. Argon gas is used to press the ground water through these detection cells for colloid analysis (LIBD), pH, Eh, electrical conductivity and oxygen content. After the above mentioned analysis additional samples are taken for chemical analysis by ICP-AES, ICP-MS, IC- and DOC-detection.

Our data obtained by in-situ- and laboratory- measurements point out that the natural colloid concentration found at the Ruprechtov site is a strong function of the ground water ionic strength.

The LIBD determined natural background colloid concentrations found at Ruprechtov are compared with data of studies performed in Äspö (Sweden) and Grimsel (Switzerland).

Introduction

Colloid analysis has been performed in ground water samples collected at a site near Ruprechtov, Czech Republic. During a drilling programme clayey sediment layers with lignite intercalations and local uranium enrichment have been found.

The geological situation at the Ruprechtov site is at a first glance very similar to the overburden of the Gorleben salt dome system and can serve as a natural analogue to study processes relevant for radionuclide and notably uranium accumulation in such a far-field environment. The uranium is assumed to be released from weathered granite in the neighbourhood of the investigated area and subsequently enriched within the clay/lignite sediment layers.

The migration and enrichment processes are up to now not fully understood. Aquatic colloids are known to be one parameter controlling the radionuclide mobility in ground water systems. Therefore, sampling campaigns were accomplished to gain information on the current background colloid concentration in these ground waters. Samples are taken with a modified sampling system avoiding artifial oxidation of samples through atmospheric contact. Colloid analysis was subsequently performed by laser-induced breakdown detection (LIBD) in the laboratory using a closed flow-through detection cell under oxygen exclusion. Furthermore, a complete chemical analysis of the water samples was performed.

Experimental

The principle of LIBD as well as the instrumentation for the colloid detection are described in detail elsewhere [1]. A new flow-through detection cell has been developed for water pressures up to ~35 bar. This set-up is suitable to measure on-site in-line colloids under the natural water pressure found e.g. in the Äspö Hard Rock Laboratory (Sweden) [2] or at the Grimsel Test Site (Switzerland) [3]. This detection cell has also been applied in combination with a borehole sampling system for the detection of ground water colloids at the Ruprechtov site.

For the borehole sampling five steel cylinders with 3 litres internal volume were used. These cylinders have been intensively cleaned and checked in the laboratory. The tests included leak tests as well as the examination of the compatibility of the sampling cylinder coupling to the LIBD laboratory setup, e.g. with regard to a possible release of particles from the inner container surface (e.g. corrosion products). Prior to the sampling campaign the cylinders were flushed with Argon gas and successively evacuated (pressure ~10^{-2} bar) to avoid any oxygen introduction and artificial colloid generation in the borehole during the sampling procedure.

At the Ruprechtov site a complete sampling system with cable winch, three-leg crane and sampling cylinder was installed on top of each borehole. The system allows a remote ground water sampling in deep boreholes. The locations of the boreholes are displayed in Fig. 1. Besides the investigated boreholes with sampling horizons in granite (RP1, NA8), in kaolin (NA7) and in clay / lignite sediments (NA6, NA12, NA13, NA10, RP2), a private well was sampled at a depth of about 7 m to obtain reference colloid input data upstream of the investigation area. The sampling depths in the investigated boreholes varied from –15 m to –37 m below ground level with about 1 m water column between sampling container and borehole bottom.

Several days after field sampling, each cylinder was connected in the laboratory with the LIBD setup containing the high-pressure flow-through detection cell of the LIBD system and a geo-monitoring unit consisting of pH, Eh, electrical conductivity, oxygen probes. A scheme of the corresponding laboratory setup is plotted in Fig. 2.

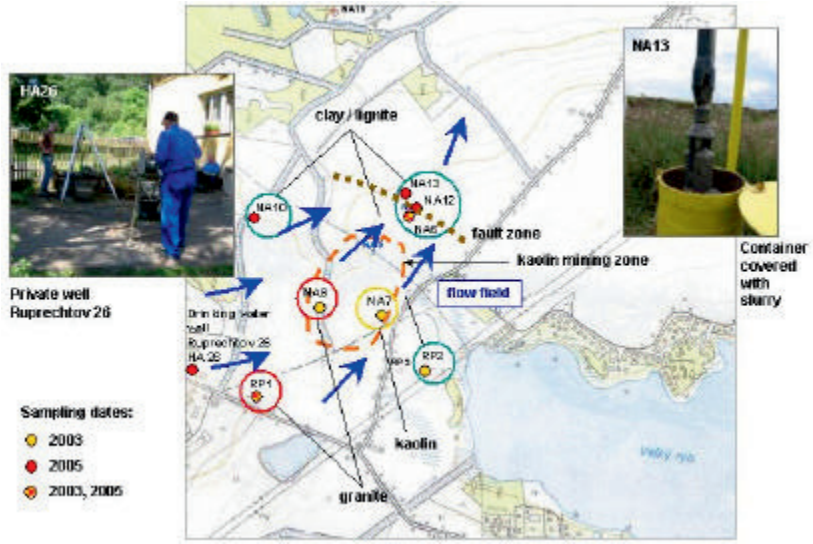

***Figure. 1**: Ruprechtov sampling positions*

Ground water samples were collected at the outlet of the pressure holder (PH) for subsequent chemical analysis with ICP-AES, ICP-MS and for the detection of inorganic carbon (IC) and dissolved organic carbon (DOC).

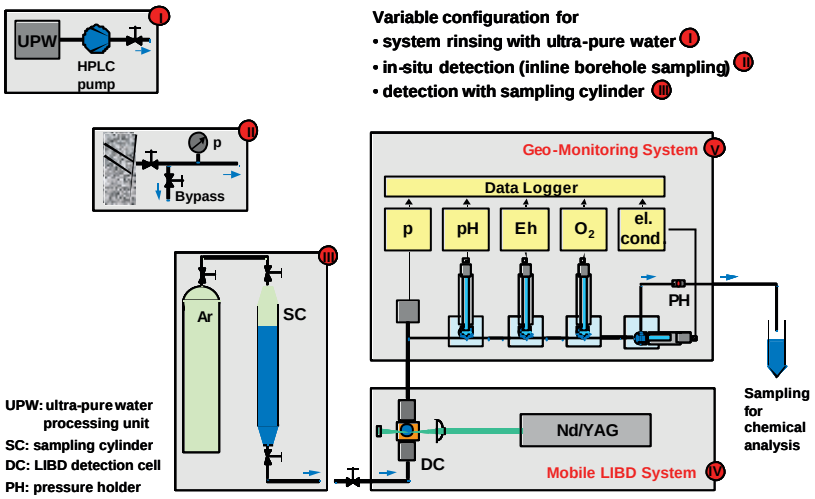

***Figure. 2:** Laboratory setup for in-line LIBD colloid analysis and ground water monitoring*

Results

In Table 1, the measured geochemical parameters Ruprechtov ground water characteristics and colloid concentrations are summarized. The data have been measured between May, 2003 and March, 2006.

One of the aims of the study was to verify that geochemical conditions (especially weakly reducing conditions) are maintained within the sampling container during transport and storage. A comparison of Eh and pH values (RP1, NA8, NA7, NA6) measured 14 days and 161 days after sampling show that with the exception of sample RP 2 no clear shift could be observed. We take that as an indication that the sample cylinders are gas tight and original geochemical conditions are maintained.

Eh and pH values detected in the laboratory were additionally measured with an in-situ borehole probe at Ruprechtov site (Table 1; GRS data given in brackets). In some cases, the data correspond closely with the laboratory determined data (RP1, NA8, NA7). In the case of significant deviations (NA6, NA12, NA13) it is not clear, whether hydrochemical conditions in the flow field have changed (contact with oxygen) or sampling cylinders were leaking. The fact that all Eh values measured in-situ in March 2006 were positive even though they have been negative in some boreholes (e.g. NA7 and NA6) during an earlier measuring campaign (Mai 2003), suggests a change in geochemistry with time.

***Table 1**: Ruprechtov ground water properties and colloid concentrations*

Ground water characterisation (geological horizon)	Borehole ID	Sampling depth m	Sampling date	Electrical conductivity mS/cm	Redox (AgCl) mV	Eh (SHE) mV	pH	Colloid diameter nm	Colloid conc. µg/l
Private well	**HA26**	- 7.4	27.7.05	**0.500**	**73**	**287**	**7.02**	**347**	**361**
Ground water from (altered?) granite	**RP 1**	- 15	21.5.03	0.320 **0.303**[a]	101 (49) **20**[a]	315 (246) **234**[a]	6.35 (6.81) **6.50**[a]	2170 **830**[a]	2306 **193**[a]
			27.7.05	**0.350**	**39**	**253**	**6.78**	**910**	**281**
			30.3.06		(- 25)	(172)	(6.45)		
	NA 8	- 18	21.5.03	0.216 **0.206**[a]	19 (48) **20**[a]	233 (245) **234**[a]	6.16 (6.2) **6.30**[a]	726 **422**[a]	1676 **170**[a]
Ground water from kaolin	**NA 7**	- 17.5	21.5.03	0.673 **0.640**[a]	- 178 (- 232) **- 190**[a]	34 (- 35) **24**[a]	7.77 (8.0) **7.85**[a]	169; 918 **228**[a]	3; 239 **239**[a]
			30.3.06		(- 180)	(17)	(7.47)		
Mixed ground water from clay/lignite	**NA 6**	- 35	21.5.03	0.530 **0.520**[a]	- 257 (- 360) **- 280**[a]	- 43 (- 163) **- 66**[a]	7.28 (8.0) **7.39**[a]	overflow **165; 1463**	overflow **18; 271**
			26.7.05	**0.590**	**- 111**	**103**	**7.53**	**232; 1167**	**10; 97**
			27.7.05	0.590	0	214	7.65	170; 1367	4; 463
	NA12	- 37	25.5.04 26.7.05	**0.480**	(- 275) **87**	(- 78) **301**	(6.5) **6.86**	**1177**	**744**
			30.3.06		(36)	(233)	(6.44)		
	NA13	- 36[b]	28.5.04 26.7.05	**0.620**[b]	(- 275) **39**[b]	(- 78) **253**[b]	(7.28) **7.57**[b]	**772**[b]	**688**[b]
	NA10	- 26	26.5.04 26.7.05	**0.430**	(43) **47**	(240) **261**	(7.43) **7.19**	**329; 1642**	**15; 359**
			30.3.06		(- 109)	(88)	(6.89)		
	RP 2	- 26	21.5.03	**1.050** 0.970[a]	**- 54** 105[a]	**160** 319[a]	**7.30** 7.40[a]	**84; 1589** 1519[a]	**1; 396** 448[a]

[a] : Detection 161 days after borehole sampling
( ): GRS data, in situ detected in borehole

[b] : After lifting, container was completely covered with slurry

The measured pH/Eh-data of different ground waters measured at the Ruprechtov site suggests that the system is anoxic and buffered by the Fe(II)/Fe(III) or Mn(II)/Mn(IV) redox pairs [4]. Similar data were determined in ground water samples taken along the access tunnel in the underground laboratory Äspö / Sweden, and in Forsmark / Sweden (Site investigation program).

Colloid concentrations vary between 170 and 740 µg/l with a number weighted mean diameter mostly larger 450 nm (Table 1). As such large colloids are

expected to settle in the absence of hydrodynamic forces as e.g. fast ground water flow velocities, it is presently not clear, whether those colloids are stable for long time periods. The concentrations may, however be considered as upper limit values. A clear correlation of colloid concentration with element concentrations could not be observed. Therefore, we cannot draw any conclusions towards the chemical nature of the colloids. Furthermore, a dependency of the detected colloid concentrations on the sampling site, i.e. the borehole geology, could not be drawn.

DOC (dissolved organic carbon) concentrations were rather low (1 – 4 mg/l) and did not show any correlation with LIBD determined colloid concentrations. This is a clear difference to the Gorleben system, where an increase of ground water DOC concentrations up to ~ 100 mg/l and the production of humic/fulvic acids due to the microbiological turn-over of lignite intercalations has been observed [5]. Such significant differences call for a closer inspection of the geochemical conditions and most notably the type of organic material and the microbiology in this system.

Earlier colloid studies claimed the existence of a significant correlation of colloid concentrations in ground water with the salinity (ionic strength) of the ground water [6,7] New LIBD results from in situ investigations at Äspö corroborate earlier studies and show colloid concentrations < 0.1 µg/l for ground waters with chloride concentrations ≥ 4 g/l. In two high saline ground waters with chloride concentrations > 10 g/l, the colloid concentrations were even close to the LIBD detection limit (~ 8 ng/l).

A comprehensive representation of colloid concentrations in different water samples as determined by LIBD as a function of the respective ionic strength is given in Fig. 3. Increasing ionic strength usually forces colloid aggregation which is reflected in lower colloid concentration in the respective groundwater

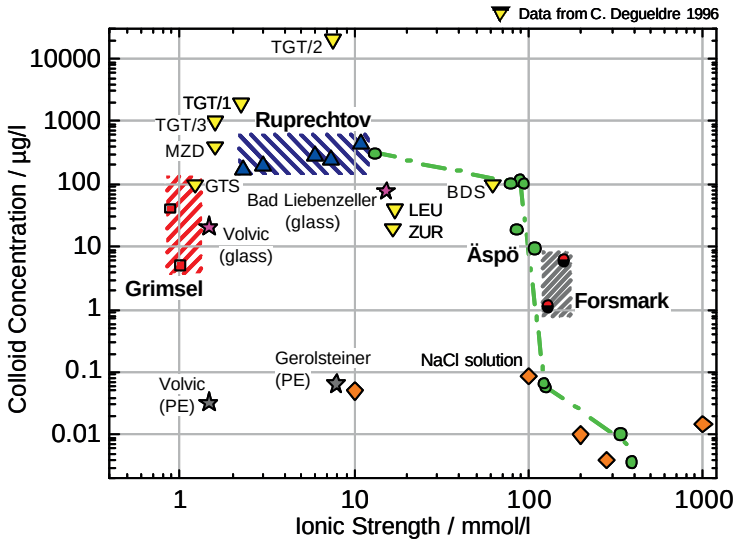

***Figure. 3**: Comparison of colloid concentration in different types of natural ground water, mineral water and synthetic NaCl-solution versus ionic strength (8 Ruprechtov; Grimsel CRR tunnel; O Äspö tunnel; ψ mineral water; M NaCl solution ; X Data from [8]: TGT: transit gas tunnel, MZD: Menzenschwand, GTS: Grimsel test site, BDS: Bad Säckingen, LEU: Leuggern, ZUR: Zurzach)*

In the Ruprechtov ground water samples the ionic strength varies in the range of 2 x 10^{-3} to 1.1 x 10^{-2} mol/l without any significant influence on the measured colloid concentration. The broad bandwidth of detected colloid concentrations in ground water of ionic strength < 100 mmol/l (Grimsel, Ruprechtov) suggests that different parameters besides ionic strength as e.g. pH and/or ground water velocity may control the actual colloid concentrations.

However, our studies suggest that an ionic strength of 100 mmol/l represents some kind of upper limit: colloids may persist in ground water with ionic strengths below this value for considerable time scales and variable colloid concentrations. At ionic strengths above 100 mmol/l natural aquatic colloid stability is effectively decreased. As a consequence, for ground water samples from Äspö and simulated NaCl solutions a clear dependency of the maximum colloid concentrations with the salinity of the solution is found.

Conclusions

The investigations demonstrate that the mobile LIBD with a geo-monitoring unit and a borehole sampling system allows the characterization of natural ground water and colloids under in-situ conditions. In cases where on-site analysis is not possible, a remote borehole sampling technique with steel cylinders and the subsequent sample characterization with in-line LIBD detection of colloids and measurement of electrical conductivity, pH, Eh is found to provide reasonable data. For this strategy it is shown that the genuine redox conditions of samples can be maintained in most cases with minimal access of atmosphere oxygen.

Our in-situ- and laboratory- obtained data point out that the relevant natural colloid concentration can be strongly limited by the ionic strength of the natural ground water. A critical value of 100 mmol/l for the ionic strength is suggested. Above this limit natural groundwater colloids appear to be rather unstable. The quantitative role of dissolved natural organic matter as a colloid stabilizing component is still unclear and requires further studies in this context. The measured ionic strengths of the sampled Ruprechtov ground waters are fairly below this limit (I < 100 mmol/l) so that the relatively high colloid concentrations found are coherent.

References

[1] W. Hauser, H. Geckeis, J.I. Kim, Th. Fierz, A mobile laser-induced breakdown detection system and its application for the in situ-monitoring of collod migration, Coll. Surf. 203, 2002, 37-45

[2] W. Hauser, H. Geckeis, R. Götz, In situ determination of natural ground water colloids in granite shear zones along the Äspö HRL Tunnel by LIBD, 27th Int. conf.on Scientific Basis for Nuclear Waste Management, Kalmar, S, June 15-18, 2003

[3] Geckeis, H., Schäfer, T., Rabung, T., Hauser, W., Möri, A., Missana, T., Eikenberg, J., Degueldre, C., Fierz, T., Alexander, W.R., Inorganic colloid borne actinide migration studied under in-situ conditions at the Grimsel test site, 9th Int. conf. on Chemistry and Migration Behavior of Actinides and Fission Products in the Geosphere, Migration '03, Gyeongju, Korea, Sept. 21- 26, 2003

[4] L. Sigg, W. Stumm, Aquatische Chemie, VDF, Zürich, Teubner, Stuttgart, 1989

[5] G. Buckau, R. Artinger, P. Fritz, S. Geyer, J.I. Kim, M. Wolf, Origin and mobility of humic colloids in the Gorleben aquifer system, Appl. Geochem., 15 (2000) 183-191

[6] Degueldre, C., Triay, I., Kim, J.I., Vilks, P., Laaksoharju, M., Miekeley, N., Ground water colloid properties: a global approach, Appl. Geochem. 15 (2000) 1043-1051

[7] Hauser, W., Geckeis, H., Götz, R., In situ determination of natural ground water colloids in granite shear zones along the Äspö HRL Tunnel by LIBD, 27th Int. Conf. on Scientific Basis for Nuclear Waste Management, Kalmar, S, June 15-18, 2003

[8] Degueldre, R. Grauer, A. Laube, A. Oess, H. Silby, Colloid properties in granitite ground water systems. II. Stability and transport study, Appl. Geochem. 11 (1996) 697-710

COMPARISON OF PALAEOHYDROLOGICAL DATA FROM CRYSTALLINE ROCKS IN GLACIATED AND NON-GLACIATED AREAS

K. Einsalo[1,*]; N. Marcos[1] and J. Gylling[1]

[1]Helsinki University of Technology, PO Box 6200, 02015 TKK, Finland

* Corresponding author; Klaus.Einsalo@tkk.fi

Abstract

This paper is a part of a publication in preparation which will be published as a research report of Geoenvironmental Technology, Helsinki University of Technology.

In the Fennoscandian region (Sweden and Finland) key palaeohydrologic questions relevant to site evaluation for nuclear waste disposal include the depth of penetration of glacial melt water, the long-term stability of the deep saline groundwater, and the extent of seawater penetration.

The geochemical cycling of natural radioactive elements in the Fennoscandian shield provides information concerning the palaeohydrological evolution of the region in the light of past climatic changes, in particular ice ages. U-series disequilibria can be used to derive a time-line for glaciation events in the geologically recent past.

Introduction

Palaeohydrological research has demonstrated a significant multidisciplinary impact and shown how palaeohydrology can provide an important contribution to the study of global change [8].

In palaeohydrological studies U-series disequilibria studies play a significant role in determining the occurrence and extent of past hydrogeological processes. In this study we examine and compare U-series disequilibria data from glaciated and non-glaciated areas to get knowledge of past hydrological events.

Palaeohydrological data from glaciated areas

Palaeohydrological data from glaciated areas has been collected from the Canadian Shield [6; 7], Finland [11; 12; 14] and Russia [4]. Saline groundwaters

and brines in crystalline basement rocks are encountered in all these places. The deep waters are typically reducing in character, and the long-term stability of these reducing conditions is important in the selection of materials for spent fuel containers (e.g. [2, 10].

Isotopic compositions of C ($d^{13}C$), O ($d^{18}O$) and Sr ($d^{87}Sr$) were determined for calcite fracture fillings in the crystalline rock at Laxemar near the Äspö Hard Rock Laboratory in southern Sweden. Calcite fracture fillings in the bedrock mark the pathways of past fluid movement. Up to 40 ka old fracture minerals may be dated by radiocarbon, older minerals (up to 500 ka) by U-series and even older deposits might be datable by the U-Pb method [17].

Calcite fracture fillings have been studied in Palmottu area [3]. The study shows that the calcites formed at high temperatures not consistent with temperatures of formation during glacial recharge. Therefore, it is likely that they have not been reactivated as transmissive fractures since that initial hydrothermal episode, even during the Quaternary history in which the formation was subjected to ice sheet loading and unloading [3].

Uranium minerals have been also used to date past events. Uranium has two valence states in natural conditions (IV and VI). U(VI) is the more mobile form of U and it occurs in oxidizing waters and in many U-secondary minerals (e.g. [9]).

In Southern Finland uranium minerals were collected from open fractures at Palmottu and Hyrkkölä. The activity ratios (AR) were measured and are presented in Table 1. These values show uranium accumulation. Some of these accumulations indicates maximum ages of formation ranging from 110 to 40 ka ago, which may correspond to past glacial events [16]

Table 1. *ARs from Uranium fracture minerals at the Palmottu and Hyrkkölä sites [16]*

Palmottu		Hyrkkölä	
depth (m)	$^{238}U/^{230}Th$	depth (m)	$^{238}U/^{230}Th$
7.03	1.23±0.02	49.32	1.48
	1.61±0.02		1.60
	1.71±0.03		1.64
	1.13±0.03		1.67
25.51	1.62±0.04		1.76
	1.88±0.03		1.74
	3.32±0.09	62.62	1.67
	3.35±0.08		1.58
	1.62±0.03		1.50
	3.88±0.09		1.55
	1.68±0.04		1.58
	1.96±0.04		1.70
	4.11±0.05		1.61
	3.62±0.05		
	1.63±0.03		
	3.23±0.07		

Comparison of past glacial events and mineral ages in the Fennoscandian shield: Finland (Palmottu and Hyrkkölä) and Sweden.

U-Th ages have been derived from secondary uranyl minerals, principally uranophane, that occur in relatively large fractures at various depths. They denote the time at which the crystals were precipitated from groundwater. This may or may not be contemporaneous with the oxidative dissolution of uraninite in the matrix [16].

There is a pronounced gap in reported ages between 40 and 70 ka BP. The gap suggests that the process responsible for uranyl silicate formation was temporarily halted, owing to a change in geochemical conditions, the hydrogeological regime or both. Secondary uranium minerals from Palmottu and Hyrkkölä display clusters of ages at 70 to 100 ka BP and around 20 to 30 ka BP. There is a correlation between the study sites both in Finland and in Sweden [13]. It is suggested that the reason behind this grouping is a major climatic event [16].

There are several possible causes for the change in geochemical conditions. Permafrost could have stopped groundwater flow into the rock matrix. This would have decreased recharge of deeper waters. Another cause could be the establishment of anoxic geochemical conditions where dissolution of the U source minerals would be prevented. It is likely that the effects of such a climatic event would be coupled [16].

It is suggested that the trigger for uranium release at significant depths in the bedrock is the intrusion of oxidising, glacial melt waters. It is also possible for uranium (VI) minerals to form during interglacial periods by sub-aerial weathering though this process is confined to the near surface [16].

Palaeohydrological data from non-glaciated areas

The El Berrocal fracture fillings have been studied to understand migration/retention processes of natural radionuclides in a granitic environment.

The El Berrocal site is located in a granitic pluton, which is in the central part of the Central Iberian Zone, close to the contact between the Tajo River tertiary basin and the Sierra de Gredos. The El Berrocal granite hosts U-sulphide-bearing quartz vein [15].

Bulk samples from different locations in the fracture system have been analyzed for U and Th-series disequilibrium (Table 2). The detailed study of the mineralogy of the fracture fillings shows that U is basically retained by precipitation, by co-precipitation or adsorption onto Fe-oxyhydroxides. The variability of U and Th series disequilibria indicate that the infill materials can be recently or currently releasing or gaining U to or from the groundwaters, consistent with the extremely open character of the system [15].

***Table 2**. ARs from the El Berrocal (after[15]) and Mina Fe [5] sites*

	$^{234}U/^{230}Th$	
Depth interval (m)	El Berrocal	Mina Fe
0-10	-	0.88-6.67
10-20	-	0.88-3.33
20-30	-	0.97
30-40	0.88-1.35	-
40-50	0.82-1.04	-
50-70	1.16-1.41	-
110-120	0.96-1	-
210-220	1.09-1.16	-

In Mina Fe U-series disequilibrium of bulk samples shows that about 50% of the samples are almost in secular equilibrium for the upper part of the U series, indicating that they have remained as closed systems in the last million years (Table 2).

In Mina Fe the distribution of the AR values, as a function of depth, indicates that neither the closed isotopic system nor the identified water/rock processes show any defined trend in relation to the location of fractures, even when considering samples from the redox transition zone of the system [5].

Conclusions

Large Activity Ratio values (AR > 1) in groundwater and rock samples may indicate redox front phenomena and past flow paths. In the deep bedrock where anoxic conditions and slow water movement should prevail high activity ratios in glaciated areas most probably reflect hydrological activity in the past [1].

In non-glaciated areas where glacial melt waters do not exist, high ARs are not encountered in the deep bedrock. Here hydrological phenomena are evident in the top parts of bedrock where weathering occurs. The fractures need to be open to allow U migration. In strongly weathered systems fractures tend to be filled and it keeps uranium from migrating to deeper parts of the bedrock.

In glaciated areas melt waters have reached deeper in the bedrock during past glacial events and this can be observed at a regional scale also in the formation of U-minerals associated to the last glaciation cycle.

Methodology for obtaining palaeohydrological data is somewhat different from each other. Some studies have been conducted by measuring ARs from bulk samples and leachates. Other studies measure ARs directly from secondary U minerals. Also ARs have been measured from groundwater. It is recommended to use only one method systematically to ensure that all the data is comparable.

References

[1] Blomqvist, R., Ruskeeniemi, T., Kaija, J., Ahonen, L., Paananen, M., Smellie, J., Grundfelt, B., Pedersen, K., Bruno, J., Pérez del Villar, L., Cera, E., Rasilainen, K., Pitkänen, P., Suksi, J., Casanova, J., Read, D., Frape, S. 2000. The Palmottu natural analogue project. Phase II: Transport of radionuclides in a

natural flow system at Palmottu. Final report. European Commission Nuclear Science and Technology Series EUR 19611 EN. Luxembourg: Office for Official Publications of the European Communities. 174 p.

[2] Blomqvist, R., 1999, Hydrogeochemistry of deep groundwaters in the central part of the Fennoscandian Shield, Doctoral Thesis, Geological Survey of Finland, Special Publication.

[3] Blyth, A., Frape, S., Ruskeeniemi, T., Blomqvist, R. 2004. Origins, closed system formation and preservation of calcites in glaciated crystalline bedrock: evidence from the Palmottu natural analogue site, Finland, Applied Geochemistry 19, pp. 675-686.

[4] Borevski, L.V., Vartanyan, G.S. and Kulikov, T.B. 1984. Hydrogeological essay. In: Kozlovky, Y.A. Editor, 1984. The superdeep well of the Kola Peninsula Springer-Verlag, New York.

[5] Crespo, M.T., Perez del Villar, L., Quejido, A.J., Sanchez, M., Cozar, J.S., Fernandez-Diaz, M., 2003, U-series in Fe-U-rich fracture fillings from the oxidised cap of the "Mina Fe" uranium deposit (Spain): implications for processes in a radwaste repository, Applied Geochemistry 18, pp.1251-1266.

[6] Fritz, P. and Frape, S.K., 1982. Saline groundwaters in the Canadian Shield—a first review. Chem. Geol. 36, pp. 179–190.

[7] Gascoyne, M., Davison, C.C., Ross, J.D. and Pearson, R., 1987. Saline groundwaters and brines in plutons in the Canadian Precambrian Shield. In: Fritz, P., Frape, S.K. (Eds.), Saline Water and Gases in Crystalline Rocks. Geol. Assoc. of Canada Spec. Paper 33, 53–68.

[8] Gregory, K.J., Starkel, L. and Baker, V.R. 1995. Global Continental Palaeohydrology, ISBN: 0-471-95420-9, 346 pp.

[9] Ivanovich, M., Latham, A.G., Longworth, G., Gascoyne, M., 1992. Applications to radioactive waste disposal studies. In Ivanovich, M., Harmon, R.S. (Eds.), Uranium Series Disequilibrium: Applications to Earth, Marine, and Environmental Sciences. Oxford Science Publications, pp. 583-630.

[10] Laaksoharju, M., Tullborg, E.-L., Wikberg, P., Wallin, B. and Smellie, J., 1999. Hydrogeochemical conditions and evolution at the Äspö HRL, Sweden. Appl. Geochem. 14, 835–859.

[11] Lahermo, P.W. and Lampén, P.H., 1987. Brackish and saline groundwaters in Finland. In: Fritz, P., Frape, S.K. (Eds.), Saline Water and Gases in Crystalline Rocks. Geol. Assoc. of Canada Spec. Paper 33, 103–109.

[12] Lahermo, P.W. and Kankainen, T., 1986. Elemental and isotopic geochemistry of brackish and saline groundwater in coastal areas of Finland. In: Fifth Int. Symp. on Water-Rock interaction. Extended abstracts, Raykjavik, Iceland. Geochim. Cosmochim. Acta 50, 341–344.

[13] Löfvendahl, R. and Holm, E., 1981. Radioactive disequilibria and apparent ages of secondary uranium minerals from Sweden. Lithos 14, 189-201.

[14] Nurmi, P.A., Kukkonen, I.T. and Lahermo, P.W., 1988. Geochemistry of saline groundwaters in the Fennoscandian Shield. Appl. Geochem. 3, 185–203.

[15] Perez del Villar, L., Pelayo, M., Cozar, J.S., Reyes, E., Caballero, E., Delgado, A., Nunez, R., Ivanovich, M., Hasler, S.E., 1997, Mineralogical and geochemical evidence of the migration/retention processes of U and Th in fracture fillings from the El Berrocal granitic site (Spain), Journal of Contaminant Hydrology 26, pp.45-60.

[16] Read, D., Black, S., Buckby, T., Proust, D., Marcos, N., Siitari-Kauppi, M, 2005: Secondary Uranium Mineralization in Southern Fennoscandia. Helsinki University of Technology, Geoenvironmental Technology, A Research Report 2, TKK-GT-A2.

[17] Wallin, B. and Peterman, Z. 1999. Calcite fracture fillings as indicators of palaeohydrology at Laxemar at the Äspö Hard Rock Laboratory, southern Sweden. Applied Geochemistry, 14, 953-962.

URANYL UPTAKE ON GRANITIC MINERALS IN PRESENCE OF CARBONATE

S. Regenspurg[1*]; T. Schäfer[2]; K. Dardenne[2];
D. Schild[2]; M. E. Malmstöm[1]

[1] Industrial Ecology, Royal Institute of Technology (KTH), Stockholm, Sweden

[2] Institute for Nuclear Waste Disposal, Forschungszentrum Karlsruhe, Germany

*Corresponding author: simona.regenspurg@epfl.ch

Abstract

The aim of this work was to study the uptake of U(VI) on some granitic minerals with special focus on possible reductive sorption. The interaction of aqueous U(VI) with the minerals biotite, phlogopite, magnetite, hematite, pyrite, and galena was investigated in bicarbonate solutions (1 mM). Surface area normalized U uptake on the Fe(II) mica (biotite) was clearly higher than on the Fe(II)-poor mica (phlogopite), indicating a possible reductive uptake process. The uptake to the oxide and sulphide minerals was higher for the Fe(II)-free minerals (hematite and galena) than for the Fe(II) containing minerals (magnetite and pyrite). Both XANES and XPS spectra gave no direct evidence for reduced U at the mineral surfaces. However, since Fe(III) was detected by XPS for biotite samples and connected to U uptake, we propose that U(VI) reduction may have taken place by Fe(II) oxidation during the batch experiments, and that the U later was reoxidized during sample handling and storage.

Introduction

Uranium(VI) mobility in groundwater is influenced by sorption of U(VI) (uranyl, UO_2^{2+}) to mineral surfaces and by reduction to U(IV), which in turn may be sorbed or form sparingly soluble phases (e.g. uraninite; UO_2). Since sorption is often a readily reversible process, reduction of uranyl and subsequent sorption/precipitation of less soluble U(IV) would be a more efficient sequence of processes for long-term immobilisation of uranium. Reduction of U(VI) is known to take place by structural ferrous iron in minerals [2]. In Sweden, radioactive waste is planned to be placed in the deep granitic environment, characterised by anoxic, pH neutral to alkaline, saline conditions, with high aqueous concentrations of NaCl and bicarbonate. The uranyl interaction with the minerals biotite (mica with ideal composition $K[Mg,Fe]_3AlSi_3O_{10}(OH,F)_2$), magnetite (oxide mineral; Fe_3O_4), and

pyrite (sulphide mineral; FeS_2) at these conditions is of special interest, as these minerals are the most frequently occurring Fe(II)-minerals in Swedish granite. The presence of high bicarbonate concentrations in aqueous solution results in uranyl-(bi)carbonate complex formation, which affects uranyl sorption and possibly reduction.

Objectives

The goal of this work was to study the sorption of uranyl on granitic minerals at near natural conditions with focus on the possible reduction of uranyl. For this purpose, we used batch experiments to quantify and compare the uptake of uranyl on natural Fe(II) containing minerals and similar Fe(II)-free minerals: phlogopite (mica with ideal composition $KMg_3AlSi_3O_{10}(OH,F)_2$), hematite (oxide mineral; Fe_2O_3), and galena (sulphide mineral; PbS). We used spectroscopic techniques (X-ray photoelectron spectroscopy (XPS) and X-ray absorption spectroscopy (XAS)) to provide information on redox state and surface coordination of mineral bound U.

Experimental

Mineral preparation and characterization

The minerals used in this study were obtained from the Swedish Museum of Natural History, Stockholm (Table 1). At the museum, the minerals had been stored over several years in contact with air at room temperature. We deem this exposure to molecular oxygen to be of minor importance to our experimental results, as most of the mineral surface was freshly prepared and stored at anoxic conditions prior to the experiment.

Biotite and phlogopite were peeled from a piece of specimen and cut to small particles by an electric mixer. Sieving separated the size fraction of 50-90 µm. Pieces of hematite, magnetite, pyrite, and galena were first smashed with a hammer, then ground with a mortar and sieved to a particle size of 20-50 µm. All size fractioned samples were ultrasonically washed three times in ethanol to remove ultra fine particles. In case of magnetite, galena, and pyrite, samples were prepared in nitrogen filled glove bag in order to prevent as far as possible surface oxidation. Samples were stored in HDPE tubes, flushed with Ar to dryness, sealed and placed into the refrigerator before characterization and experimental use. The mineral content of the fractioned mineral powders was determined by X-ray powder diffraction (XRD) and their element content by X-ray fluorescence spectroscopy (XRF). XRF indicated that U is contained in small amounts in biotite (2.45 mg/kg), phlogopite (0.27 mg/kg), hematite (0.07 mg/kg), and magnetite (0.45 mg/kg), whereas sulphide minerals were essentially free of U. The surface area was determined by the BET method using nitrogen gas adsorption (Table 1).

***Table 1**. Mineral origin and characteristics*

Sample*	Origin	Catalog-Nr¤	BET-area (m^2/g)
Phlogopite (Pp) $KMg_{3.2}Fe_{0.1}(Si_{2.9}Al_{0.5})O_{10}(F_{0.8},OH_{1.2})$	Petteby, (Fi)	24875	1.45
Biotite (Bt) $K_{1.08}Fe_{2.68}Mg_{0.27}Mn_{0.20}Ti_{0.33}(Si_{2.6}Al_{0.88})O_{10}(OH_2)$	Brevig, (No)	5213	1.58
Magnetite (Mt) Fe_3O_4	Bisperg, Dalarna (Se)	890280	0.71
Hematite (Ht) Fe_2O_3	Långbon, Värmland, (Se)	251856	0.09
Galena (Gl) PbS	Vegebock, Värmland, (Se)	19060083	0.21
Pyrite (Pt) FeS_2	Torsåker, Hofors (Se)	530060	0.98

Se-Sweden, No Norway, Fi-Finland * Preliminary results of chemical composition
* Provided by the Swedish Museum of Natural History, Stockholm, Sweden.

Batch experiments

200 mg of the minerals were added to 20 mL of degassed ionic medium (0.1 M NaCl, 0.001 M $NaHCO_3$) in separate PE bottles and the pH was adjusted with HCl and NaOH to 6. The suspensions were flushed with Ar, placed into a PE box, which was continuously shaken under Ar flow. After 10 days the pH was readjusted to 6 and a uranyl chloride solution was added to obtain final U concentration of 0, 0.9, 1.9, 8.7, 17.3, 86.7, 172.6, and 823.2 µM. All experiments were performed in two replicates. After 4 weeks, the bottles were opened in Ar filled glove bags and 0.2 µm membrane filtered. After pH measurements, the solution was acidified and uranyl was analyzed either by a photo spectrometric method with arsenazo(III) at 653 nm (Kressin, 1984) (detection limit 0.5 ppm) or by ICP-MS (detection limit 8 ppb). Final pH and U concentration were plotted in a predominance diagram, which indicates the dominance of different uranyl carbonate complexes in the aqueous solution (Figure 1). In case of pyrite, the pH decreased during the experiments to below 6, which prevented adsorption of cations on the mineral surface. Therefore, the experiment was repeated with 0.01 M $NaHCO_3$ as a stronger pH buffer. In these samples the final pH was between 7.4 and 7.6 and the predominant U species was $UO_2(CO_3)_3^{4-}$. The pH in the other mineral suspensions shifted to higher values. For some samples the aqueous solutions were oversaturated with respect to schoepite $UO_2(OH)_2*H_2O$ (Figure 1).

Solids were stored after the experiment in sealed, Ar flushed PE bottles in the refrigerator. As indicated by our experimental results, this procedure may have been insufficient to protect the samples from surface oxidation. We believe oxidation could have occurred as a consequence of the long storage time (several months), during which some oxygen may have entered the bottles.

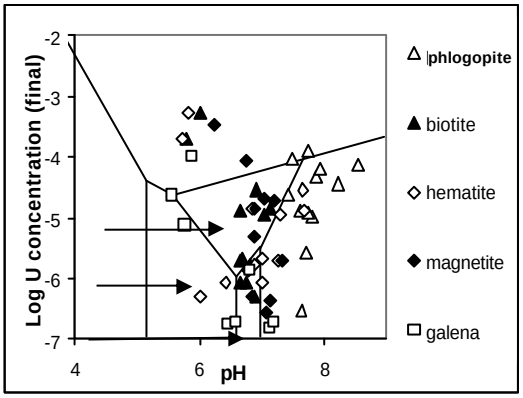

Figure 1. *Plot of final pH and aqueous uranyl concentration (M) in the batch experiments into predominance diagram (MEDUSA/ HYDRA, Puigdomenech, 2004).*
$[CO_3^{2-}]_{tot}$ = 0.001M; I = 0.1 M for phlogopite, biotite, magnetite, hematite and galena.

X-ray absorption spectroscopy (XAS)

Uranium L3-edge spectra were collected for several solid samples at room temperature in fluorescence mode at the INE beamline at the Ångströmquelle Karlsruhe (ANKA). The instrument is equipped with a Canberra LEGe 5-element solid-state detector. Ge<422> crystals were used in the monochromator, operating in fixed-exit mode, and incident intensity was held constant by means of a piezo-driven feedback system to the second crystal. The parallel alignment of the crystal faces was detuned to ~70% of the maximum beam intensity. Spectra were energy calibrated against the white line of the U L3 edge of schoepite set at 17.170 keV. For each sample, 8 to 16 scans were averaged. The spectra were energy-normalized and first preliminary fits to U(VI)- oxide and carbonate clusters with the WinXAS software have been obtained [4]

X-ray photoelectron absorption spectroscopy (XPS)

XPS was measured on powder samples, prepared onto In-foil under inert gas. The instrument was a Physical Electronics Inc. model PHI5600ci with Mg Kα, Al Kα, and Al Kα monochromator. A neutralizer, emitting slow electrons was used to compensate charging due to the emitting photo- and Auger electrons from the sample surface. Narrow scans of the elemental lines (U 4f and Fe 2p) were measured with pass energy of 23.5 eV of the hemispherical analyzer. Scans were charge referenced to the C 1s line of aliphatic hydrocarbons at 284.8 eV. The Ti $2p_{3/2}$ line is at 458.8 eV if present, which coincides with the reference value of TiO_2.

Results

Batch experiments

Surface area normalized U uptake by the different minerals as a function of U concentration in the aqueous solution at the end of the batch experiments (resembles equilibrium concentrations) at 5.8<pH<8.7 is shown in Figure 2. The uptake of U by the Fe(II)-poor mineral phlogopite was less compared to biotite, possibly indicating reductive sorption by biotite (see Figure 2). In the case of the

oxide and sulphide mineral couples, it turned out that the Fe(II)-free minerals took up more U per surface area.

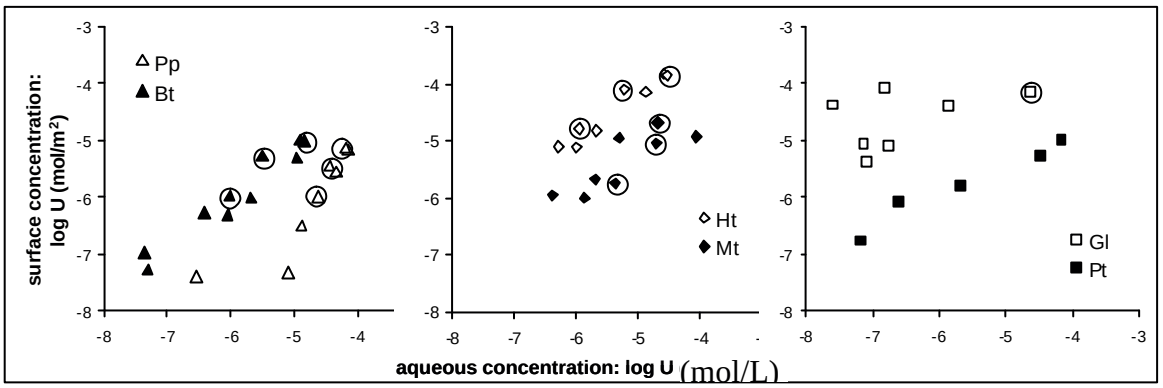

Figure 2. *Surface area normalized U uptake as function of aqueous concentration of U at the end of the experiments (after 4 weeks). Samples, where schoepite is expected to precipitate (Figure 1), have been excluded. The pH values are given in Figure 1. Samples marked with circles were used for XAS and XPS (see below). Mineral abbreviations according to Table 1.*

Spectroscopic analysis of solid phase

X-ray absorption spectroscopy (XAS)

Some of the minerals obtained from the batch experiments were examined with XANES (X-ray absorption near edge structure) and EXAFS (extended X-ray absorption fine structure) spectroscopy. XANES spectra of the U L3 absorption edge of the different samples (Figure 3) match with the position of U(VI) standard schoepite and thus it is likely, based on the quantitative relationship by Bertsch et al. [1], that >90 % of the U in these samples is in the +VI oxidation state. EXAFS results indicate that U(VI) is bound as a carbonate complex to the minerals. However, fitting and interpretation of EXAFS data is still underway.

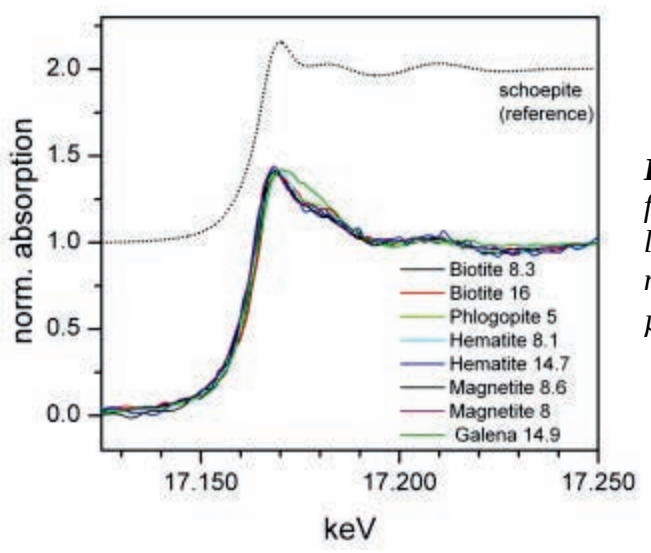

Figure 3. *Normalized U L3 XANES for investigated samples. In the legend, the number behind the mineral names indicate U uptake in µmol/g.*

X-ray photoelectron absorption spectroscopy (XPS)

Figure 4 (left) exemplifies a narrow scan XPS spectrum of U 4f obtained for a biotite sample with 16 µmol/g U. For all mineral samples, the XPS spectra indicated no presence of reduced U on the surface of the solids, since the U $4f_{7/2}$ peaks were located at 381.4 eV, which corresponds to U(VI). However, investigation of the Fe 2p peaks in the same sample indicated that, with increasing U content on the surface, the Fe 2p peaks shift to higher energies (Figure 4, right) indicating additional formation of Fe(III). The Fe 2p peak position of biotite with low U uptake (Figure 5, blue spectrum) corresponded to more Fe(II). Thus, we assume that oxidation of surface Fe(II) is connected to surface accumulation of U, possibly coupled to reduction of U(VI).

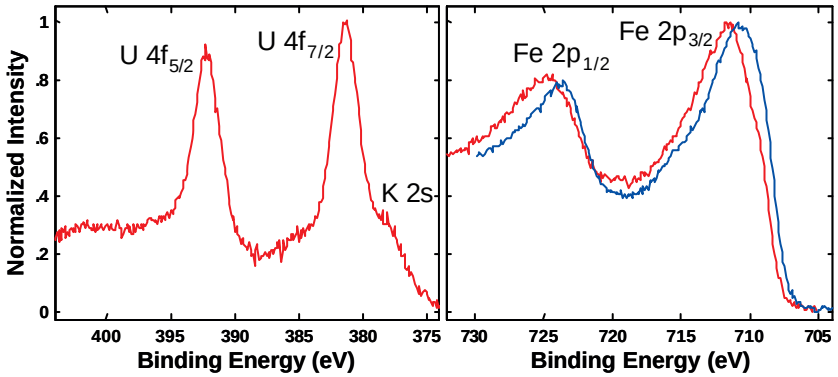

Figure 4. *Narrow scan XPS spectra of biotite surface.Left: U 4f spectrum of biotite with 16 µmol/g U; Binding energy of U4f 7/2 381.4 eV indicates U(VI).Right: Fe2p spectra of biotite with 16 µmol/g U (red) and 1.5 µmol/g U (blue).*

Conclusions

Our experiments showed that U was to different degree adsorbed to the surfaces of biotite, phlogopite, magnetite, hematite, pyrite, and galena at 5.8<pH<8.7 in presence of carbonate. For the experimental conditions used in our experiments, where U(VI) carbonate complexes dominate in the aqueous solution, our EXAFS results indicate that U is dominantly bound to the mineral surface through a U(VI)-carbonate complex. No direct evidence of reduced U at the mineral surface was found for any of the minerals with the techniques used in this study. However, the formation of oxidised iron in presence of U(VI) is an indication that U reduction occurs by Fe(II) oxidation. We propose that U was first reduced at the mineral surface during the batch experiment and later re-oxidised during sample handling and storage. Future experiments are planned where re-oxidation of U will be prevented as far as possible.

Acknowledgments

We gratefully acknowledge Boris Brendebach and Jörg Rothe for their assistance and ANKA for user beamtime allotment and the Swedish Museum of Natural History (Stockholm) for providing minerals. Travel expenses were funded by NoE ACTINET.

References

[1] Bertsch, P.M., Hunter, D.B., Sutton, S.R., Bajt, S., Rivers, M.L. (1994) In situ chemical speciation of uranium in soils and sediments by micro X-ray absorption spectroscopy, Environ. Sci. Technol, **28**, 980-984.

[2] Ilton, E.S., Haduic, A., Moses, C.O., Heald, S.M., Elbert, D.C., Veblen, D.R. (2004) Heterogeneous reduction of uranyl by micas: Crystal chemical and solution controls. Geochim. Cosmochim. Acta, **68(11),** 2417-2435.

[3] Puigdomenech, I. (2004) HYDRA and MEDUSA Chemical Equilibrium Software. Software and documentation available from http://web.telia.com/~u15651596/

[4] Ressler, T. (1997) WinXas: A new software package not only for the analysis of energy disperse XAS data. J. Phys. IV, **7**, C2, 269-270.

THE REDUCTION OF PLUTONIUM: COMPARISON BETWEEN HYDROQUINONE AND FULVIC ACID AS REDUCING COMPOUND

C.M. Marquardt[1*] and A. Seibert[2]

[1] Institut für Nukleare Entsorgung (INE, Forschungszentrum Karlsruhe, P.O. Box 3640, 76021 Karlsruhe, Germany
[2] European Commission, Joint Research Centre, Institute for Transuranium Elements, PO Box 2340, D-76125 Karlsruhe, Germany

*Corresponding author: Marquardt@ine.fzk.de

Abstract

In first experiments the reduction sequence of Pu starting with Pu(VI) was studied in presence of hydroquinone (HQ) and fulvic acid (FA) as reducing compounds at various pH values between pH 1 and 7. The Pu species were monitored by UV-Vis spectroscopy and liquid-liquid extraction. Pu(V) and (VI) are not stable in aqueous solutions containing hydroquinone and fulvic acid (FA) at pH 1 to 7. With 200 mg/L FA the reduction of Pu(VI) to Pu(V) is fast and complete after 30 minutes at pH 3. Compared to the reduction reaction at similar concentration of HQ, the FA reduction is slower. We also observed that Pu(VI) is unstable in solutions devoid of FA at pH values > 3, but that the rate is much slower than in presence of FA and HQ. Pu(V) in same solutions is converted to Pu(IV), the most stable oxidation state in aqueous solutions containing FA at pH 3 - 7 (relevant for natural aquifers). Reduction of Pu(IV) to Pu(III) was found only at pH values < 5 for HQ and < 3 for FA. The reactions were also monitored by Eh measurements. The present studies showed that a correlation between Eh values and thermodynamic calculations might be a capable tool for modelling redox reactions between Pu ions and hydroquinone or hydroquinone-like compounds like FA. It cannot be excluded that Pu(III) is more stable in solutions containing organic compounds with lower redox potential than the GoHy-573-FA batch used in the present studies.

Introduction

The interaction of humic substances with radionuclides in aqueous solutions are manifold, and include complexation of free metal ions, sorption of metal colloids and redox reactions. The redox reactions of plutonium ions in aqueous

solution in presence of humic substances is subject of the present work. Here, we focus on the interaction of Pu with fulvic acid (FA). The experiments have been performed between pH 1 and 7 and are compared to results obtained from earlier studies of the interaction between Pu and hydroquinone (HQ). HQ was used as a model compound for the HS with respect to their redox properties. We started the studies at more acidic conditions to minimise colloid formation of Pu(IV) and to ease the interpretation of the results. The results are modelled on basis of equilibrium thermodynamics by introducing the pe value. Here, theoretically calculated pe values are contrasted to experimentally measured pe (Eh) values and oxidation state speciation to test the modelling.

Objectives

Objective of these studies is to get insight into the redox interaction between humic substances and plutonium. The results obtained by using model compound hydroquinone are compared with results by using natural fulvic acid to elucidate the mechanism of reduction. Thermodynamic calculations are used for the description of the experimental results considering latest results of thermodynamic studies on plutonium redox chemistry including solid phases and colloids of tetravalent plutonium [3]. The output of the investigations will be thermodynamic parameters usable for PA.

Experimental

Hexavalent plutonium (PuO_2^{2+}) was added to fulvic acid (FA) solution at various pH values and 0.1 M $NaClO_4$ as background electrolyte. Pu(VI) was prepared by potentiostatic electrolysis of a stock solution of plutonium in perchloric acid. The fulvic acid was a natural fulvic acid isolated from a deep anaerobic groundwater (GoHy-573) at the Gorleben site in North Germany. The final Pu and FA concentration were typically $1\text{-}2\cdot10^{-4}$ M and 4 – 200 mg/L ($2.7\cdot10^{-5}$ – $1.7\cdot10^{-3}$ eq/L proton exchange capacity), respectively. The pH values varied between pH 1 and 7. The process of the reduction has been followed by absorption spectroscopy and solvent extraction with PMBP [4] as chelating agent.

Results and Discussion

Reduction of Pu(VI)

The kinetic of reduction of Pu(VI) to Pu(V) by hydroquinone is very fast and could not studied with the experimental set-up described in the former FUNMIG Workshop Proceeding. For the fulvic acid the reduction rate is slow enough to observe a dependence on the concentration of the fulvic acid (Figure 1). At excess concentrations of FA with respect to proton exchange capacity (PEC) the Pu(VI) is reduced fast and the reduction is completed after about 30 minutes. With decreasing concentration of FA the reaction rate decreases, too. It must be emphasized that the Pu(VI) is also reduced in a solution devoid of FA, but with a much slower kinetic.

At low FA concentrations, e.g. 4 mg/L FA, the reaction rate is governed first by the reduction of FA and changes than to the slow reduction kinetic observed for Pu(VI) in pure solution. For both reactions an equilibrium has not been reached after 2500 hours (104 d). At higher FA concentration the Pu(VI) is totally reduced rather fast to Pu(V) and the slow reduction kinetic cannot be observed.

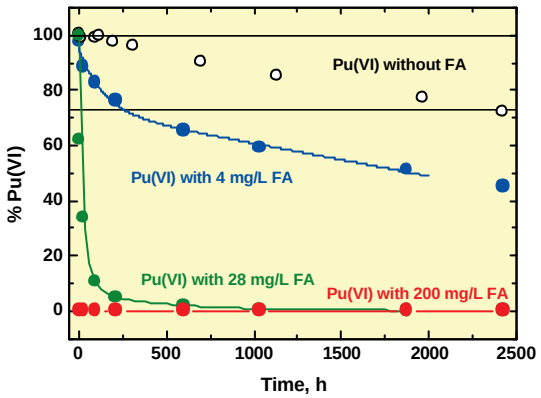

Figure 1: *Reduction of Pu(VI) by various concentration of fulvic acid and at pH 3.*
$[Pu]_{tot}$ = 1.8 - 2.0 x 10^{-4}M,
$[FA]_{tot}$ = 2.7 x10^{-5}- 1.4 x 10^{-3}eq/L proton exchange capacity.

Reduction of Pu(V)

The kinetic of the reduction of Pu(V) and Pu(IV) by hydroquinone is shown in Figure 2. The total plutonium concentration $[Pu]_{tot}$ and the total hydroquinone concentration [HQ] was $1.2 \cdot 10^{-4}$ mol/L and $2.8 \cdot 10^{-3}$ mol/L, respectively. In the time period up to 20 days, the kinetic of the reduction depends on the pH value. The reaction rate increases with increasing pH from 3 to 7. Pu(V) is fully reduced at pH 3 after about 20 days, whereas at pH 7 Pu(V) is already completely converted to Pu(IV) after about 2 days.

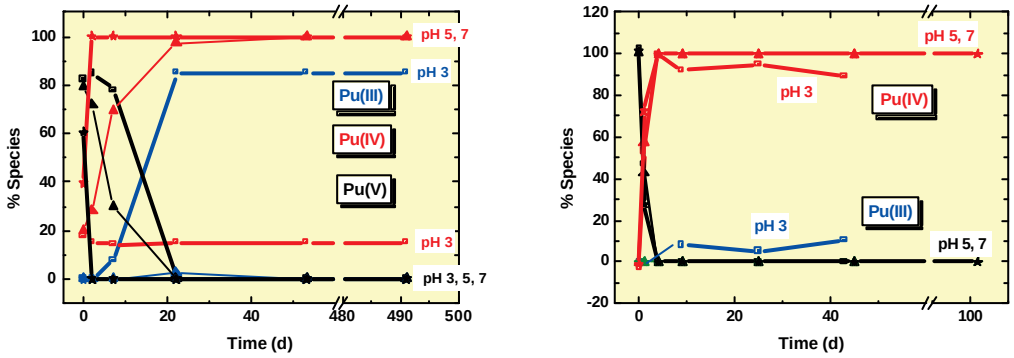

Figure 2: *Reduction of Pu(V) and Pu(IV) in hydroquinone solution (left, $[Pu]_{tot}$ = $1.2 \cdot 10^{-4}$ mol/L and $[HQ]_{tot}$ = $2.8 \cdot 10^{-3}$ mol/L) and fulvic acid solution (right, $[Pu]_{tot}$ = 1.8-2.0$\cdot 10^{-4}$ mol/L and $[FA]_{tot}$ = $1.4 \cdot 10^{-3}$ eq/L proton exchange capacity).*

The time changes of Pu(VI) in a fulvic acid solution at pH 3, 5, and 7 are also shown in Figure 2. The concentrations of Pu and FA are similar to the experiment with HQ: $[Pu]_{tot}$ = 1.8-2.0·10^{-4} mol/L and [FA] = 1.4·10^{-3} eq/L exchangeable protons. The reduction rate of Pu(V) is more or less independent on the pH value. Only at pH 7 a slightly higher rate is observed. All Pu(V) is reduced after 4 days, that is faster as it was found for HQ at pH 3 but similar to HQ reduction at pH 7. A reason for that observation cannot be given yet.

Reduction of Pu(IV)

In HQ solutions the Pu(IV) remains stable up to 500 days at pH values of 5 and 7. At pH 3 and lower, Pu(IV) was reduced to Pu(III) to reach a constant Pu(III)/Pu(IV) ratio after 20 days. In this solution 85% Pu(III) and 15% Pu(IV) was formed.

In FA solutions the Pu(IV) remains stable at pH 5 and 7over a time period of 100 days, which is similar by using HQ as reductive. At pH 3 also Pu(III) was formed by FA and the ratio Pu(III)/Pu(IV) remains constant after 10 days of reaction. In contrast to HQ, only 10% Pu(III) was formed and most part of the Pu stays in the tetravalent state (90%).

Figure 3 summarises the quasi-equilibrium percentage of Pu(III) and Pu(IV) in HQ and FA solutions at pH values 1 to 7 of all performed experiments. It is obvious that HQ and GoHy-573-FA behave very similar with respect to the reducing strength at pH 1 and pH values larger than 4. At pH 1 only Pu(III) is the stable oxidation state, at pH >4 only Pu(IV) occurs. Between pH 1 and 4 we found mixture of Pu(III) and Pu(IV) in various ratios and quite different for HQ and FA.

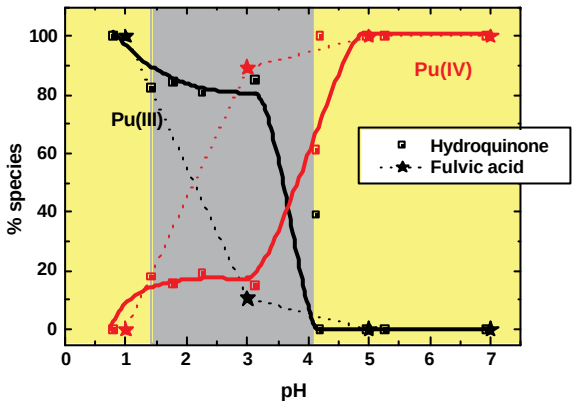

Figure 3: *Percentage of Pu species after reaching the quasi-equilibrium state in hydroquinone and fulvic acid solution as function of the pH value. The grey area denotes a pH zone of mixtures of Pu(III) and Pu(IV) in several ratios.*

In most of the solutions containing plutonium and HQ or FA the Eh value were measured. The data are plotted as pe, the negative logarithm of the electron activity, as a function of pH in Figure 4, with pe = Eh·16.9. The pe values of all solutions, irrespective HQ or FA, lie in a narrow band with a slope of –1. Also a solution of FA without plutonium was measured at various pH values. The values of

the pure FA lie at pe values much lower as it was observed for the solutions with plutonium. Explanation for that observation can not be given so far. In all experiments an excess of the reducing compound, HQ or FA(red), should be existent, and hence, the observed pe value should be governed by the redox properties of the reducing agent. Seemingly, that is not the case for Pu in FA solution.

Modelling

The description of the oxidation states distribution of plutonium as well as of measured pe values should be feasible on the basis of thermodynamics. By consideration of the contemplable redox reactions and the corresponding redox potential or equilibrium constant, the pe values can be theoretically calculated and compared with measured pe values. For comparison purpose a more reducing anthraquinone ((9,l0-anthraquinone-2,6-disulfonate, AH2DS) than the used hydroquinone was additionally considered. The results are plotted in Figure 4.

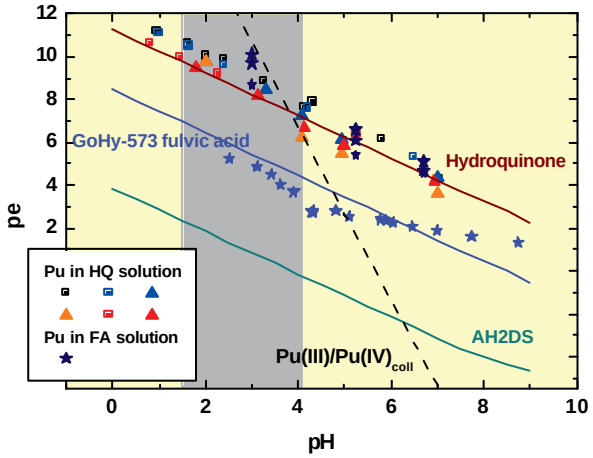

Figure 4: *Experimentally measured (points) and calculated (lines) pe values as a function of pH value. The purple stars are pe values from FA solutions without Pu.*

The corresponding plutonium reactions for the Pu(III) / Pu(IV) equilibrium are:

$Pu^{4+} + e^- \Leftrightarrow Pu^{3+}$	$\log K°_{III-IV}$	$= 17.69 \pm 0.04$[1]
$Pu(OH)_4(am) + 4H^+ \Leftrightarrow Pu^{4+} + 4H_2O$	$\log {}^*K°_{s,0}$	$= -2.33 \pm 0.52$[2]
$Pu(OH)_4(coll) \Leftrightarrow Pu(OH)_4(am)$	$\log K°$	$= 8.33 \pm 1.0$[3]
$Pu(OH)_4(coll) + 4H^+ + e^- \Leftrightarrow Pu^{3+} + 4H_2O$	$\log K°$	$= 23.7 \pm 1.1$

1 From Guillaumont et al.,2003

2 From Guillaumont et al.,2003

3 From Neck et al.,2006

The hydroquinone where modelled by the following redox reaction and deprotonation reaction [1]:
$Q + 2H^+ + 2e^- \Leftrightarrow H_2Q$; $H_2Q \Leftrightarrow HQ^- + H^+$; $HQ^- \Leftrightarrow Q^{2-} + H^+$
and the Eh values is calculated according to

$$Eh = E0 + RT/2F*\ln(Q/H_2Q) + RT/2F*\ln[(H^+)^2 + Ka_1 (H^+) + Ka_1 Ka_2]$$ with

	E^0	K_{a1}	K_{a2}
Fulvic acid	0.5	$1.22x10^{-10}$	$9.28x10^{-13}$
Hydroquinone	0.6992	$1.22x10^{-10}$	$9.28x10^{-13}$
AH2DS	0.228	$8.00x10^{-9}$	$3.00x10^{-11}$

Because the dissociation constants of the hydroquinone entities in fulvic acid are unknown, the constants of the hydroquinone were used. The E^0 for FA was picked from [5], all other values from [1]. For hydroquinone a good agreement between measured and calculated pe values are obtained. Also for the pure FA solution the calculated pe values coincides with experimentally measured ones. In contrast to that after adding Pu to FA solution the pe values becomes much higher and they are in the range of the hydroquinone solutions. From the theoretical line of the equilibrium between Pu(III) and $Pu(OH)_4$(coll) the following conclusions can be drawn. Above pH 4 only Pu(IV) should occur in agreement with the experiment. Between pH 3 and 4 the pe lie near the line and mixture of Pu(III) and Pu(IV) should occur. Below pH 2 mostly Pu(III) should be the stable oxidation state. Both conclusions coincide again with the experiment.

Conclusions

We can conclude from the present experiments that the distribution of Pu oxidation state species in the quasi-equilibrium state of Pu in hydroquinone and fulvic acid solutions might be correlated to the measured pe values and the redox reactions of plutonium. Further and more detailed modelling in the future should confirm these preliminary results. For the hydroquinone and the pure fulvic acid solution the measured pe value can be calculated rather well, whereas a discrepancy occurs between the calculated and the measured pe value for fulvic acid after adding Pu. An explanation for that observation cannot be given here.

References

[1] Clark, W. M. (1960), Oxidation-Reduction Potentials of Organic Systems (Williams & Wilkins, Baltimore, MD.

[2] Guillaumont, R., Fanghänel, Th., Fuger, J., Grenthe, I., Neck, V., Palmer, D.A., Rand, M.H. (2003), (OECD, NEA-TDB) Chemical Thermodynamics Vol. 5.

Update on the Chemical Thermodynamics of Uranium, Neptunium, Americium, and Technetium. Elsevier, North-Holland, Amsterdam.

[3] Neck, V., Altmaier, M., Fanghänel, Th. (2006), Solubility and Redox Reactions of PuO2 x H2O in the presence of oxygen, in:, Recent Advances in Actinide Science, R. Alvarez, N.D. Bryan, I. May (Eds.), The Royal Society of Chemistry, RSC Publishing, p. 479 (RSC).

[4] Nitsche, H., Roberts, K., Xi, R., Prussin, T., Becraft, K., Mahamid, I.A., Silber, H.B., Carpenter, S.A., Gatti, R.C. (1994), Long Term Plutonium Solubility and Speciation Studies in a Synthetic Brine, Radiochim. Acta, 66, 3.

[5] Skogerboe,R.K.; Wilson,S.A. (1981), Reduction of ionic species by fulvic acid, Anal.Chem., 53, 228.

FEBEX BENTONITE COLLOID STABILITY IN GROUND WATER

H. Seher[1,*]; T. Schäfer[1]; H. Geckeis[1] and T. Fanghänel[2,3]

[1] Forschungszentrum Karlsruhe GmbH, Institut für Nukleare Entsorgung, Postfach 3640, D-76021 Karlsruhe, Germany
[2] European Commission, Joint Research Centre, Institute for Transuranium Elements, P.O. Box 2340, D-76125 Karlsruhe, Germany
[3] Ruprecht-Karls-Universität Heidelberg, Physikalisch-Chemisches Institut, Im Neuenheimer Feld 253, D-69120 Heidelberg, Germany

*Corresponding author: holger.seher@ine.fzk.de

Abstract

Coagulation experiments are accomplished to identify the geochemical conditions for the stability of Febex bentonite colloids in granite ground water. The experiments are carried out by varying pH, ionic strength and type of electrolyte. The dynamic light scattering technique (photon correlation spectroscopy) is used to measure the size evolution of the colloids with time. Agglomeration rates are higher in $MgCl_2$ and $CaCl_2$ than in NaCl solution. Relative agglomeration rates follow approximately the Schulze-Hardy rule. Increasing agglomeration rates at pH>8 are observed in experiments with $MgCl_2$ and $CaCl_2$ which are, however, caused by coprecipitation phenomena. Bentonite colloid stability fields derived from the colloid agglomeration experiments predict low colloid stabilization in granite ground water taken from Äspö, Sweden, and relatively high colloid stability in Grimsel ground water (Switzerland).

Introduction

Colloids are known to be ubiquituous in natural ground water and have been frequently discussed as potential carriers for radionuclides. Concepts for high-level nuclear waste disposal in crystalline rock foresee bentonite as appropriate barrier material both to inhibit ground water access to the waste canister and to retard radionuclide transport away from the repository near field. Smectite colloids have been observed to detach from the bentonite barrier by erosion phenomena when contacted with ground water [5]. The relevance of colloids for radionuclide migration is strongly controlled by their agglomeration, sedimentation, surface attachment and filtration behavior in a given aquifer system. Only under conditions where colloids are sufficiently stable, they may be able to transport sorbed radionuclides [3,6,8].

The present work describes first experimental results on bentonite colloid stability over a wide pH and ionic strength range, relevant to natural ground water conditions. Colloids have been prepared from a natural bentonite (FEBEX bentonite, Spain). NaCl, $CaCl_2$ and $MgCl_2$ are taken as electrolytes in order to compare the influence of 1:1 and 2:1 electrolytes on bentonite colloid stability.

Experimental

For the experiments the Febex (full-scale engineered barrier experiment) bentonite from the deposit of Cabo de Gata, Almería (Spain) is used. It is described as a smectite-rich bentonite [2].

A size fraction < 63 µm of the Febex bentonite is separated for the preparation of colloids used in this study. The clay is either equilibrated with a 1M NaCl, a 1M $CaCl_2$ or 1M $MgCl_2$ to establish a mono-ionic exchangeable cation composition. After one week equilibration, the cation exchanged bentonite is washed to remove excess salts by Milli-Q water. The suspension is centrifuged at 4,000 rpm for 40 min, the supernatant is discarded and the centrifugate is re-suspended in Milli-Q water. This washing cycle is repeated three times and the final supernatant containing bentonite colloids is taken as a colloid stock dispersion and stored in a refrigerator until experiments were performed. The extracted colloidal fraction consists quantitatively of montmorillonite as proved by XRD analysis. The bentonite colloid concentration is determined via alumina ICP-MS measurements. Taking into account the structural formula of the Febex bentonite given in [2] the bentonite colloid concentration could be calculated.

The coagulation rate of the bentonite colloids is determined by photon correlation spectroscopy (PCS) using a ZetaPlus system (Brookhaven Inc.). Measurements were performed over an investigation period of 180 min collection each 10 sec an autocorrelation function (ACF) up to 10 min and combining 10 ACF's of 40 sec measurement time each at longer aggregation times. The data evaluation is made by the built-in software (Version 2.27). The time resolved increase of the average colloid size is measured under variation of the parameters pH (pH 6-10), ionic strength (I: 0.001M-0.5M) and electrolyte type (NaCl, $MgCl_2$, $CaCl_2$) using a colloid concentration of 3.7 mg/L.

The calculation of the stability ratio W from the coagulation rate is described in [4]. The stability ratio is calculated based on the following equation:

$$W = \frac{\left[\left(d r_h / dt\right)_{t\to 0} / C\right]^{(f)}}{\left[\left(d r_h / dt\right)_{t\to 0} / C\right]} \qquad (1)$$

whereas W is the stability ratio, r_h is the hydrodynamic radius, C the colloid concentration and the superscript (*f*) refers to measurements in the regime of fast (diffusion limited) coagulation. The advantage to determine colloid stability by means of W is the independency on the colloid concentration used throughout the experiments as shown in formula 1. Therefore, stability ratio determined in this study can directly be compared with data published in the literature.

Results and discussion

The PCS determined mean bentonite colloid size used throughout the stability investigations was 185 nm with a half width of 90 nm recalculated from the polydispersivity index of 0.24. The rather broad size distribution determined by PCS is in accordance with literature data [7]

Figure 1a shows the stability ratio (W) for different ionic strengths in the $MgCl_2$ system as a function of pH. Initially, W increases with increasing pH value starting from pH 6 until a maximum value of $W = 3.5 \cdot 10^2$ at pH 7.2 for an ionic strength of 0.001M is reached. At pH > 8 the stability ratio decreases again. Increasing the ionic strength from 1mM to 0.5M decreases the stability ratio to values around one showing diffusion controlled aggregation for the pH range investigated.

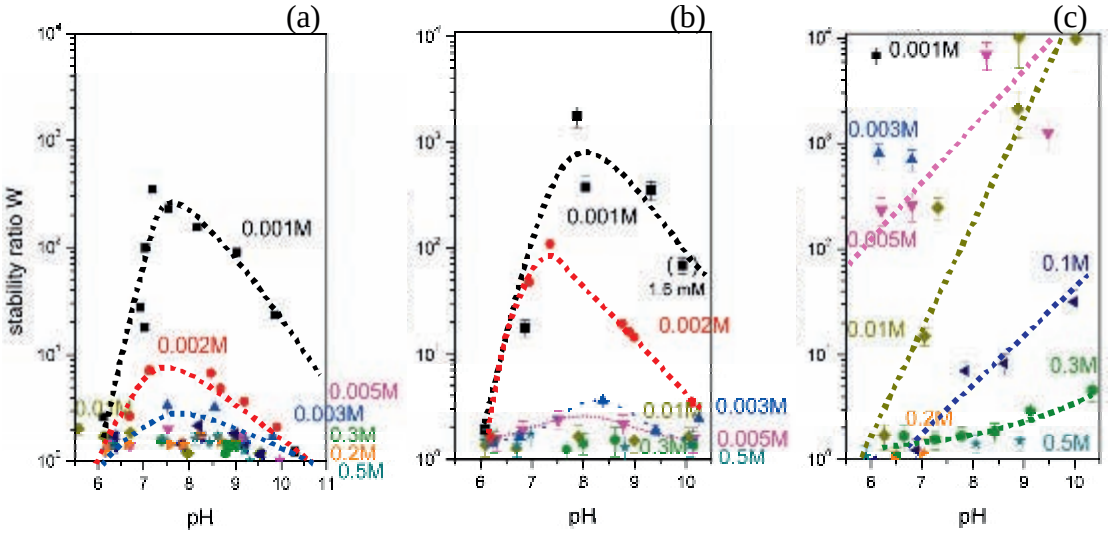

***Figure 1**: Measured stability ratios W as a function of ionic strength and pH for $MgCl_2$ (a), $CaCl_2$ (b) and NaCl (c) solutions; electrolyte concentrations are given in terms of ionic strength.*

Comparable results were obtained for the $CaCl_2$ system (Figure 1b). The highest stability ratio of $1.7 \cdot 10^3$ is found at pH 7.9 for an ionic strength of 0.001M and appears to be slightly higher than that found in the $MgCl_2$ system under similar conditions. The variations of W as a function of pH and ionic strength are comparable in the two bivalent systems investigated, namely $CaCl_2$ and $MgCl_2$.

The highest stability ratios have been measured in the NaCl system (Figure 1c). At all ionic strengths an increase of W with increasing pH is observed and no decrease under alkaline conditions could be detected. Stability ratios larger than $5 \cdot 10^2$ are detected for solution with ionic strengths < 0.003 M in the full pH range investigated. Under alkaline conditions (pH > 9) bentonite colloids are even stable within the observation period in 0.01 M solutions.

The low stability ratio at pH values = 6 in all systems investigated can be explained by edge-face interactions of the colloids leading to cart house type

structures. Taking into account the pH dependent edge charge with a point of zero charge (pH_{PZC}) around pH 6-7 neutral or positive charged clay edges due to protonation of Al-OH edge groups are expected [9]. Below the pH_{PZC} clay colloid edges are positively charged and thus interaction with permanently negative charged basal planes induced by isomorphous substitutions in the bentonite structure can be expected. At pH values above the pH_{PZC} both the edge and basal planes are negatively charged and therefore bentonite colloids are electrostatically stabilized due to repulsive forces. Higher ionic strengths decrease the electrical double layer thickness and coagulation is again initiated [9].

The observed decrease of the stability ratio in the $MgCl_2$ and $CaCl_2$ systems at pH > 8 cannot be explained taking simple electrostatic interactions into account. The observed destabilization has to be attributed to the precipitation of $MgCO_3$ and $CaCO_3$, thus scavenging the bentonite colloids. $MgCO_3$ and $CaCO_3$ precipitation due to oversaturation of electrolyte solutions under atmospheric pCO_2 cannot be ruled out and are focus of further investigations.

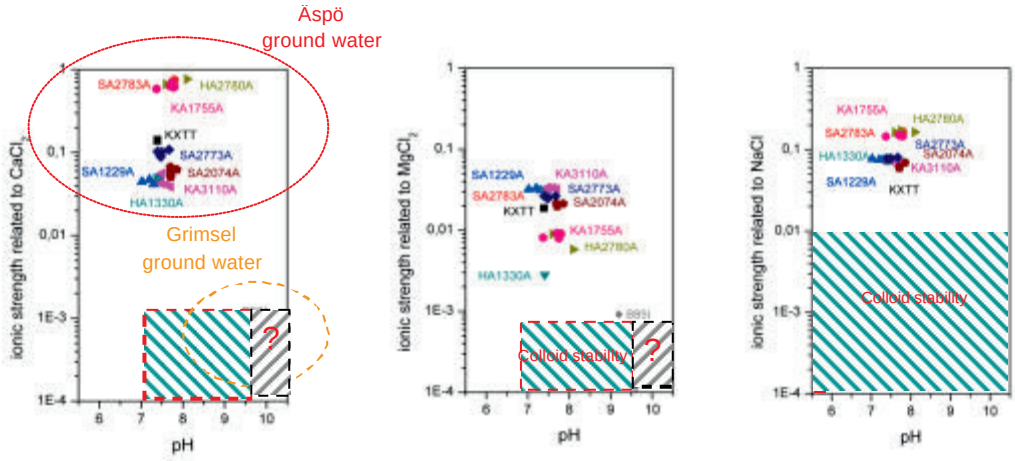

Figure 2: *Comparison between bentonite colloid stability fields as a function of ionic strength and pH value determined in this study and the ionic strength for the electrolyte composition found in the Äspö and Grimsel ground water systems. From left to right the results are shown for the $CaCl_2$, $MgCl_2$ and NaCl system. Concentrations given for the $MgCl_2$ ionic strength in the Grimsel system are multiplied by a factor of 100.*

For stability ratios > $5 \cdot 10^2$ or, in other words, coagulation rates < 10 nm/hour we operational defined colloidal stability. These regions are mapped as fields of stability in Figure 2. Comparing the actual ionic strengths found in Äspö ground water with these stability fields (Fig. 2) it can be clearly shown that bentonite colloids derived from backfill material are not expected to be stable and therefore mobile under the current geochemical situation. However, the comparison with the Grimsel ground water system shows that granite ground water chemistry can vary in such that colloid stability might be expected.

Conclusions

Bentonite colloid stability increases as expected with increasing pH due to increasing charge repulsion by deprotonated surfacial OH groups. Increase in ionic strength screens the surface charge and thus causes a clear stability decrease. Measurable coagulation is found for all electrolyte concentrations starting from 3.3 10^{-4} M for $MgCl_2$ and $CaCl_2$ (corresponding to an ionic strength of 1 10^{-3} M). For NaCl solutions W exceeds a value of 10^3 indicating high colloid stability at ionic strength <0.01 and pH>8. The faster colloid agglomeration rates observed in $MgCl_2$ and $CaCl_2$ solutions as compared to NaCl solutions of identical ionic strength follows the known Schulze-Hardy rule [1]. Edge-face interaction delimits colloid stability at low pH. Depending on the composition of a given natural ground water it is thus possible to predict bentonite colloid behavior. Further studies will focus on the influence of low DOC (i.e. fulvic acid) concentration in the range of 1-10 mg/L as usually found in fractured rock systems and their effect on bentonite stability.

References

[1] Bastos D. and de las Nieves F. J. (1994) Colloidal stability of sulfonated polystyrene model colloids. Correlation with electrokinetic data. *Colloid & Polymer Science* **272**, 592-597.

[2] Cama J., Ganor J., Ayora C., and Lasaga A. (2000) Smectite dissolution kinetics at 80°C and pH 8.8. *Geochimica Et Cosmochimica Acta* **64**, 2701-2717.

[3] Geckeis H., Schäfer T., Hauser W., Rabung T., Missana T., Degueldre C., Möri A., Eikenberg J., Fierz T., and Alexander W. R. (2004) Results of the Colloid and Radionuclide Retention experiment (CRR) at the Grimsel Test Site (GTS), Switzerland -Impact of reaction kinetics and speciation on radionuclide migration-. *Radiochimica Acta* **92**(9-11), 765-774.

[4] Kretzschmar R., Holthoff H., and Sticher H. (1998) Influence of pH and humic acid on coagulation kinetics of kaolinite: a dynamic light scattering study. *J. Colloid and Interface Science* **202**, 95-103.

[5] Missana T., Alonso T., and Turrero M. J. S. (2003) Generation and stability of bentonite colloids at the bentonite/granite interface of a deep geological radioactive waste repository. *Journal of Contaminant Hydrology* **61**(1-4), 17-31.

[6] Möri A., Alexander W. R., Geckeis H., Hauser W., Schäfer T., Eikenberg J., Fierz T., Degueldre C., and Missana T. (2003) The colloid and radionuclide retardation experiment at the Grimsel Test Site: influence of bentonite colloids on radionuclide migration in a fractured rock. *Colloids and Surfaces a-Physicochemical and Engineering Aspects* **217**(1-3), 33-47.

[7] Plaschke M., Schäfer T., Bundschuh T., Manh T. N., Knopp R., Geckeis H., and Kim J. I. (2001) Size characterization of bentonite colloids by different methods. *Analytical Chemistry* **73**(17), 4338-4347.

[8] Schäfer T., Geckeis H., Bouby M., and Fanghänel T. (2004) U, Th, Eu and colloid mobility in a granite fracture under near-natural flow conditions. *Radiochimica Acta* **92**, 731-737.

[9] Schäfer T., Geckeis H., Bouby M., Mihai S., Delos A., Alonso U., and Missana T. (2006) Bentonite colloid stability in natural and simulated granite groundwater. In *1st annual workshop proceedings of integrated project fundamental processes of radionuclide migration IP FUNMIG*, Vol. CEA-R-6122 (ed. P. Reiller, G. Buckau, B. Kienzler, L. Duro, and M. Martell), pp. 248. Commissariat à l'énergie atomique.

QUANTUM CHEMICAL PREDICTION OF PARAMAGNETIC NMR SPECTRA OF LANTHANIDE COMPLEXES WITH SALICYLIC ACID IN WATER SOLUTION.

P. Hrobárik[1], O. L. Malkina[1], V. G. Malkin[1,*]; B. Schimmelpfennig[2]; R. Reviakine[3] and M. Kaupp[3]

[1] Institute of Inorganic Chemistry, Slovak Academy of Sciences, Dúbravská cesta 9, SK-84536, Bratislava, Slovak Republic
[2] Forschungszentrum Karlsruhe GmbH, Institut für Nukleare Entsorgung(INE), Hermann-von-Helmholtz-Platz 1, D-76344 Eggestein-Leopoldshafen, Germany
[3] Institut für Anorganische Chemie, Universität Würzburg, Am Hubland, D-97074 Würzburg, Germany

* Corresponding author; Vladimir.Malkin@savba.sk

Abstract

^{17}O and ^{13}C paramagnetic NMR (PNMR) shifts have been calculated for Gd complexes with salicylic acid in water solution. These complexes served us as model compounds for simulation of more complicated lanthanide complexes with humic acids. The obtained data demonstrate that paramagnetic NMR spectra are very sensitive to the bonding details of the ligand. Our calculations suggest that formation of Gd(III) complex with salicylic acid in water solution via carboxyl group with uni-dentate coordination is preferable. New experimental studies with the enriched ^{17}O and ^{13}C nuclei of carboxylate groups of the salicylic and humic acids are extremely desirable.

Introduction and objectives

Paramagnetic NMR (PNMR) is potentially a powerful method for structure determination of lanthanide and actinide complexes in solution. In particular, this method can be helpful for determination of structures of actinide/lanthanide complexes with humic acids and other organic molecules in water solution. However, there is only a very limited amount of the experimental data related to the topic. Since such experimental NMR studies are very complicated and often expensive, theoretical predictions of the resulting spectra are very desirable. These theoretical studies require development of adequate quantum chemical programs, very careful benchmark calculations and pilot applications on model compounds.

Modelling

For calculation of paramagnetic NMR (PNMR) shifts on ligand nuclei of a lanthanide complex with salicylic acid in water solution we have applied a perturbational approach developed by us recently [1]. The investigated complexes served us as simplified models of lanthanide complexes with humic acids in natural environment. In particular, we choose a Gd complex with salicylic acid in water solution since Gd is less problematic from the computational point of view. We believe that the information obtained for Gd can be used directly or can be transferable for prediction of PNMR shifts for complexes with other lanthanides.

The calculations were performed on a complex of Gd with salicylic acid and 8 water molecules which were treated explicitly. The whole complex was placed inside a polarizable continuum to simulate liquid water environment. The optimization of the geometry of the complex was performed using Turbomole 5.7 program package [2] at B3LYP level of theory [3] using COSMO solvatation model [4] (dielectric constant of water 78.39 was assumed). All electron Ahlrichs TZVP basis set [5] on ligand atoms was employed and relativistic large core (53 core electrons) pseudopotential with the corresponding valence basis set was used on the central Gd atom. During the structure optimization a number of minima (which correspond to different isomers) were found. Six structures with the lowest energies are presented on the Fig. 1 (structures A – F) together with their energies with respect to the most stable structure A. The first 3 structures (A-C) are bounded to Gd via single Gd-O bond whereas structure D is double-bonded (via carboxylate oxygens). These two relatively equal Gd-O bonds form together with carboxylate C a 4-membered ring. Two remaining structures (E-F) also have two Gd-O bonds (one through carboxylate and one through phenol oxygens) but these bonds are part of the 6-membered rings.

The hyperfine structure required for calculation of paramagnetic NMR shifts was calculated with Gaussian03 [6] at B3PW91 level of theory using relativistic small core (28 core electrons) Stuttgart-1997 pseudopotential [7] with the corresponding valence basis set of (12s11p9d8f)/[5s5p4d3f] quality on Gd and IGLO-III basis set [8] on the light ligand atoms. Polarizable continuum model (PCM) was also applied to represent the effect of solvent (water). In Table 1, we show the calculated paramagnetic contact shifts (with respect to analogous diamagnetic complexes of salicylic acid with lanthanum or lutetium) for selected nuclei (i.e. the nuclei which are the most affected at least in one of the isomers).

The 3 groups of isomers mentioned above (A-C, D and E-F) are clearly distinguished by the data presented in Table 1. For single-bonded complexes A-C one of the carboxylate oxygens has a strong down-field shift (around -2300 ÷ -2600 ppm) whereas all other nuclei are less affected, but their shifts are still informative (particularly a carboxylate carbon and a carbon atom attached to the former). Going away from paramagnetic center, lanthanide induced shifts are getting smaller and their absolute values are becoming below the accuracy of DFT methods. The double-bounded (4-membered) complex D has two rather large shifts on carboxylate oxygens (-842 and -735 ppm) which reflect their similar bounding situation. Remarkably, the carboxylate carbon has also a significant shift (357 ppm) that provides a very firm indicator for the 4-membered ring bonding. Finally, the

structures of the third group (E-F) have a very strong shift on one of the carboxylate oxygens and the twice smaller shift on the phenol oxygen (-3290 and -1724 ppm for complex E and -3024 and -1314 ppm for structure F). Taken all together, our data show that these 3 groups of the possible complexes can be distinguished based on experimental paramagnetic NMR studies accompanied by theoretical quantum chemical calculations.

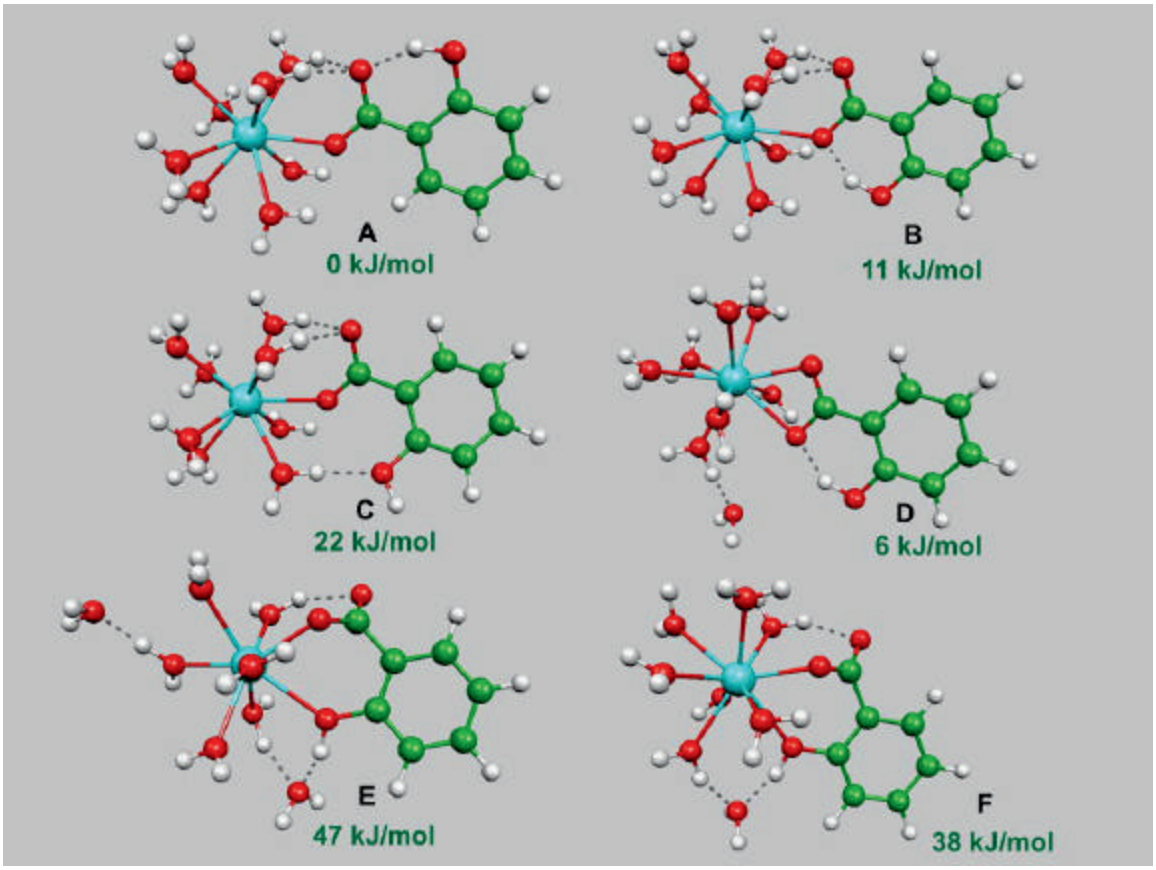

Figure. 1. *Structures of 6 most stable isomers of the Gd complex with salicylic acid and 8 water molecules (Gd shown in blue, O – red, C – green and H – white). The energy differences are given with respect to structure* ***A****.*

Table 1. *Lanthanide (Gd) induced paramagnetic contact shifts (with respect to free ligands; in ppm) on* ^{17}O *and* ^{13}C *nuclei in Gd complexes with salicylic acid and 8 water molecules.*

isomer	X	r(Gd-X) [Å]	A_{iso} [MHz]	d^{para} [ppm]
A	$O_{carboxylate}$	2.435	0.611	-2394
	$O_{carboxylate}$	3.693	-0.007	26
	O_{phenol}	6.172	-0.001	2
	$C_{carboxylate}$	3.439	0.037	79
	C-$C_{carboxylate}$	4.780	-0.070	-148

B	$O_{carboxylate}$	2.452	0.601	-2356
	$O_{carboxylate}$	3.678	-0.006	25
	O_{phenol}	4.667	-0.004	16
	$C_{carboxylate}$	3.450	0.043	91
	C-$C_{carboxylate}$	4.792	-0.058	-122
C	$O_{carboxylate}$	2.384	0.667	-2616
	$O_{carboxylate}$	3.729	-0.013	51
	O_{phenol}	4.507	-0.024	95
	$C_{carboxylate}$	3.409	0.039	83
	C-$C_{carboxylate}$	4.711	-0.071	-149
D	$O_{carboxylate}$	2.472	0.215	-842
	$O_{carboxylate}$	2.507	0.187	-735
	O_{phenol}	5.078	-0.005	20
	$C_{carboxylate}$	2.886	0.169	357
	C-$C_{carboxylate}$	4.358	-0.095	-200
E	$O_{carboxylate}$	2.273	0.839	-3290
	$O_{carboxylate}$	4.013	-0.021	84
	O_{phenol}	2.576	0.440	-1724
	$C_{carboxylate}$	3.240	-0.015	-31
	C-$C_{carboxylate}$	3.938	0.001	3
F	$O_{carboxylate}$	2.312	0.771	-3024
	$O_{carboxylate}$	4.037	-0.014	56
	O_{phenol}	2.655	0.335	-1314
	$C_{carboxylate}$	3.277	-0.004	-8
	C-$C_{carboxylate}$	3.997	0.003	7

The rationalization of the observed trends is rather straightforward: since in the case of isomers E and F a carboxylate group of salicylic acid is twisted away from the benzene ring plane (by about 40°), possibility of delocalization of the electron spin density is strongly reduced. It results in increasing relative energies of E and F in comparison with other isomers and decreasing the absolute values of spin densities on carboxylate carbon as well as on neighboring atoms.

While our data should be considered as preliminary, a few conclusions and outlooks for future work could be already drawn. First, the optimized structures represent reasonable but static models – dynamical effects should be taken into account. Then probably structures A-C would not be distinguished any more (complexes A and B have similar structures and most probably they would have fast exchange (in NMR time scale) with complex C). Complexes E and F are also basically equivalent. Thus one can expect that only averaging shifts for A, B and C structures would be accessible experimentally (the same is true for complexes E and F). Dynamical effects can be taken into account by applying Car-Parrinello quantum molecular dynamics approach [9] (that would be a computationally demanding study). Recently we performed a similar study for a simple system of Gd aqua complex [10]. Probably it is the best possible approach to simulate real

experimental conditions and we plan such study of the Gd-complexes in future. Second, only the contact shift calculated with the Breit-Pauli Hamiltonian was used in the present study. While the used approach should be adequate for the systems under consideration, we plan to use our recent theoretical developments to recalculate the shifts on a more rigorous theoretical background. Third, the major remaining question is whether experimental NMR studies on Gd complex with salicylic acid in water solution would provide information about ^{17}O and ^{13}C shifts on the particular atoms mentioned above. The use of enriched by those isotopes ligands is the must.

Though we chose Gd in our present study (to reduce computational problems) a certain transferability of the results on complexes with other lanthanides could be expected. However, since pseudo-contact shifts induced in the other lanthanide complexes are not negligible and in principle could be even larger than contact shifts, a special care has to be taken in such estimations. Pseudo-contact shifts can also be assessable by quantum-chemical calculations [1].

Application to PA

Knowledge of the structure of the humic/radionuclei complexes is of central importance for understanding and prediction of physicochemical behaviour of those complexes in water solution. We performed a quantum-chemical prediction of paramagnetic NMR spectra of Gd with salicylic acid in water solution. The results of these calculations demonstrate that complexes formed via carboxyl group with uni-dentate coordination are more stable. The analysis of our predicted NMR spectra and our previous experimental data supports this founding. We believe that our pilot study forms a firm basis for future joint theoretical/experimental investigations which would provide important structural information on the structure of humic/radionuclei complexes.

Conclusions

^{17}O and ^{13}C paramagnetic NMR (PNMR) shifts were calculated for Gd complexes with salicylic acid in water solution. These complexes served us as model compounds for simulation of more complicated lanthanide complexes with humic acids. The obtained data demonstrate that paramagnetic NMR spectra are very sensitive to the bonding details of the ligand. Our calculations suggest that formation of Gd(III) complex with salicylic acid in water solution via carboxyl group with uni-dentate coordination is preferable. New experimental studies with the enriched ^{17}O and ^{13}C nuclei of carboxylate groups of the salicylic and humic acids are extremely desirable. We believe, that such experimental studies combined with our quantum-chemical calculations would provide a conclusive information on structural aspects of lanthanide complexes with humic acids.

Acknowledgment.

The work in Bratislava has also been supported by the Slovak Grant Agency APVT (No. 51-045502).

References

[1] Hrobárik, P.; Reviakine, R.; Arbuznikov, A.V.; Malkina, O.L.; Malkin, V.G.; Köhler, F.H.; Kaupp M. (2006) Density Functional Calculations of NMR Shielding Tensors for Paramagnetic Systems with Arbitrary Spin Multiplicity. Validation on 3d-Metallocenes, *J. Chem. Phys*., in press.

[2] Ahlrichs, R.; Bär, M.; Baron, H.; et al., Turbomole, Version 5.7 (Quantum Chemistry Group, University of Karlsruhe, Karlsruhe, Germany, 2002).

[3] Lee, C.; Yang, W.; Parr, R.G., (1988) *Phys. Rev*. B 37, 785. Stephens, P.J.; Devlin, F.J.; Chabalowski, C.F.; Frisch, M.J.; (1994) *J. Phys. Chem*. 98, 11623.

[4] Schäfer, A.; Klamt, A.; Sattel, D.; Lohrenz, J.C.W.; Eckert, F. (2000) *Phys. Chem. Chem. Phys.* 2, 2187.

[5] Schäfer, A.; Huber, C.; Ahlrichs, R. (1994) *J. Chem. Phys*. 100, 5829.

[6] Frisch, M.J.; Trucks, G.W.; Schlegel, H.B.; et al., Gaussian 03, Revision C.02 (Gaussian, Inc., Wallingford, 2004).

[7] Cao X.; Dolg, M. (2001) *J. Chem. Phys*. 115, 7348.

[8] Kutzelnigg, W.; Fleischer, U.; Schindler, M. in *NMR Basic Principles and Progress*; edited by Diehl, P.; Fluck, E.; Günther, H.; Kosfeld, R.; Seelig, J. (Springer Verlag, Berlin/Heidelberg, 1991).

[9] Car R.; Parrinello, M. (1985) Unified Approach for Molecular Dynamics and Density-Functional Theory, *Phys. Rev. Lett*. 55, 2471-2474.

[10] Yazyev O.V.; Helm L.; Malkin V.G.; Malkina O.L. (2005) Quantum chemical investigation of hyperfine coupling constants on first coordination sphere water molecule of Gadolinium(III) aqua complexes, *J. Phys. Chem. A*, 109, 10997-11005.

DIFFUSION OF ANIONIC SPECIES IN BORECORE SAMPLES OF BODA CLAYSTONE FORMATION

K. Lázár[1,*]; J. Megyeri[1] and Z. Máthé[2]

1 Institute of Isotopes, Budapest, P.O.B. 77, H-1525, Hungary
[2] Mecsekérc Co., Esztergár L. 19., Pécs, H-7633, Hungary

*Corresponding author: lazar@iki.kfki.hu

Abstract

Diffusion of ^{99}Tc and ^{14}C radioisotopes in anionic forms of TcO_4^- and $H^{14}CO_3^-$ were studied in samples originated from Boda Claystone Formation by using break-through measurements. The ^{99}Tc solution was spiked (5×10^{-4} mol/l), whereas the HCO_3^- concentration was the same as in the respective ground water of the formation (1.2×10^{-2} mol/l). The apparent diffusivity constants were estimated from the slope of the increase of the activity concentrations observed within 230 day period. Similar values were obtained: 1.1×10^{-12} m^2 s^{-1} for technetate and 1.3×10^{-12} m^2 s^{-1} for hydrocarbonate. These results can be compared with previous studies carried out under similar conditions with ^{125}I, where practically the same value was obtained for the apparent diffusivity. Thus, it can be concluded that anionic species migrate with a similar rate in the studied Boda Claystone samples, and do not interact noticeably with the rock. In correlation with the diffusion of TcO_4^- the actual redox state of the rock sample was characterized by determining the Fe^{3+}/Fe^{2+} ratio with Mössbauer spectroscopy. In spite of the significant amount of ferrous iron present, the redox processes probably do not considerably influence the migration rate of the studied anions.

Introduction

The long-term and/or final disposal of nuclear waste is a matter of consideration in Hungary, too. Results of preliminary explorations suggested that the Boda Claystone Formation (BCF) may provide a prospective host media. To collect data in sufficient amount an underground research laboratory (URL) was established in a depth of 1050 m in 1994, and had been kept in operation till 1999. Wide scale characterisations were performed, the results were compiled into a nine-volume report. A shorter Digest had also been prepared [3]. The obtained detailed results are promising, although the mission of the URL is ceased. For further studies the Boda Claystone is still preferred, the target of the recent studies is the exploration in modest depths (300 – 400 m) by drilling, since the BCF is tilted and reaches the surface (Fig. 1. [Kovács]). Important results of these studies have also

been published in the more open literature. For instance, an overview on the genesis, mineral composition, geochemistry etc. is provided in [1].

Isotope migration studies have also been performed among the wide scale characterisations. As a hardly sorbing anionic component, iodine was selected and the diffusion rate was measured with various techniques under static conditions without any transport (filtration, etc.) of the ground water The results showed a certain scatter depending on the method, as an average 10^{-12} m^2 s^{-1} is proposed for the apparent diffusivity constant [4].

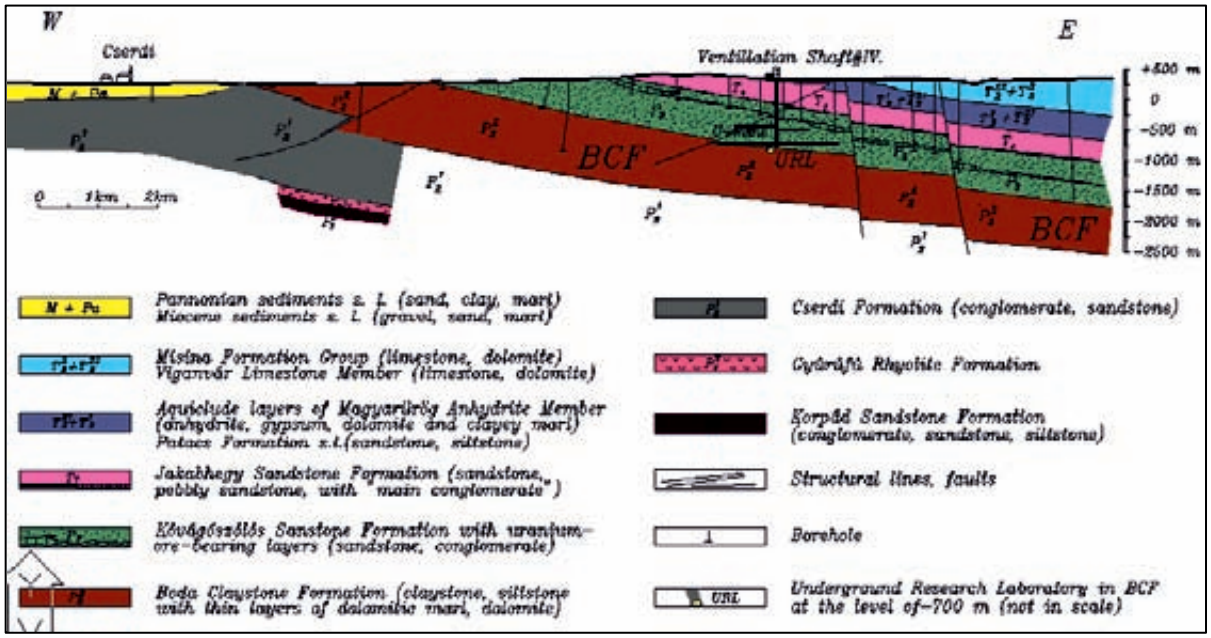

Figure. 1. *Geological cross section of the Eastern-Western direction in the Western-Mecsek Anticline*

Objectives

The primary aim of the present study was to expand the examinations with other anions on Boda Claystone samples. These studies may contribute to answering the question, whether the high migration rate is observable with other anions as well. In the first stage ^{99}Tc (half life $\tau_{1/2}$ = 2 x 10^5 y) and ^{14}C ($\tau_{1/2}$ = 5700 y) were selected. Both elements may occur in anionic form at the slightly basic conditions characteristic in the formation (pH = 8), namely in form of TcO_4^- and HCO_3^-, respectively [Brookins]. Prior to the break-through measurements the redox property of the Boda Claystone sample was also characterized by determining the Fe^{2+}/Fe^{3+} ratio with Mössbauer spectroscopy. Namely, the apparent redox conditions may occasionally change the charge and the valence state of the diffusing species, via redox processes. In consequence, the rate of diffusion may change accordingly.

Experimental

The studied samples were obtained from drills driven from the URL in the Boda Claystone Formation. Their dominant mineral components (~ 40 % each) are albite and illite/muscovite, the minor components (< 10 % each) are hematite, dolomite, calcite, quartz and chlorite [1.]. The porosity of samples is c.a. 0.5 – 2.3 %, with pore diameters in the range of 0.01 – 1 micron (data are obtained with mercury porosimetry) [3]. For Mössbauer measurements c.a. 300 mg grained stone, whereas for break-through measurements c.a. 10 mm thick discs were cut from the borecores (Fig. 2.).

Figure. 2. *Photograph of the bore core sample for testing in break through experiment*

A Mössbauer spectrum was recorded at room temperature in constant acceleration mode. The spectrum (Fig 3.) reveals the presence of two iron-bearing components. The first component exhibits a magnetic sextet (51 Tesla) with a quadrupole splitting of 0.22 mm/s. These values are typical for ferric oxide, hematite. The second iron-bearing component is chlorite, (isomer shift 1.14, quadrupole splitting 2.64 mm/s), containing iron in ferrous state [5]. The contribution of the ferric component (Fe_2O_3) is dominant (78 %), the remainder 22 % belongs to the ferrous state in chlorite.

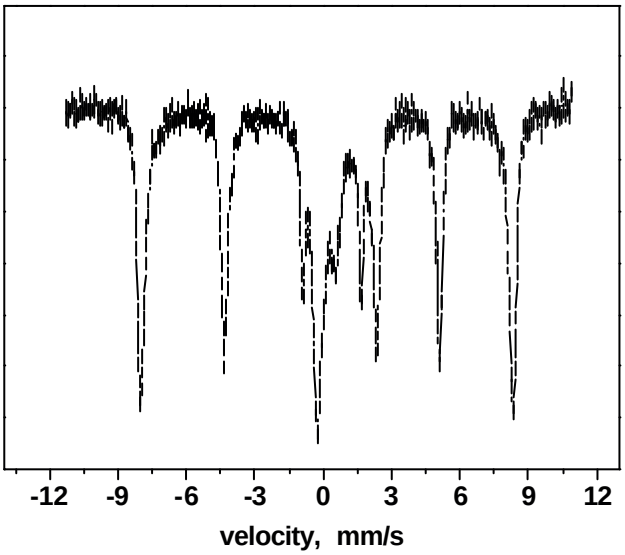

Figure. 3. *The Mössbauer spectrum of the Boda Claystone sample*

Conventional break-through measurements were carried out, in two-compartment cells where the two compartments are separated by the studied rock sample. At the beginning of the experiment one of the compartments is filled up with the solution containing the radiotracer, whereas inactive solution, suitably groundwater is filled into the other compartment. As time passes, the radioisotope diffuses through the sample and its concentration increases in the originally inactive solution. By following the increase of its amount the diffusion constant can be calculated (see below in the Modelling section).

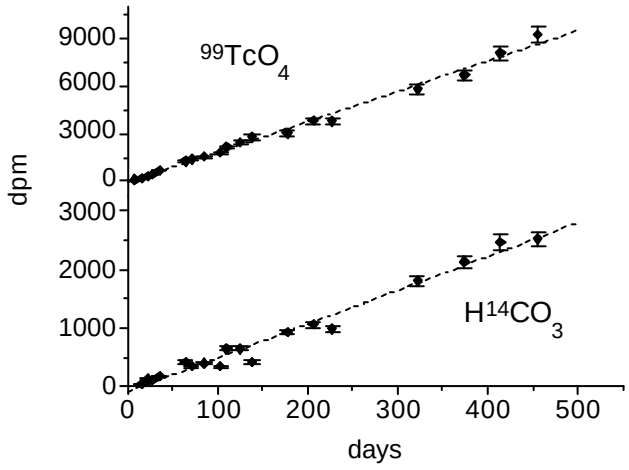

Figure. 4*. Increase of the activity concentrations using* $^{99}TcO_4^-$ *(top) and* $H^{14}CO_3^-$ *(bottom) tracer in break-through experiment with Boda Claystone sample*

In our experiments synthetic ground water was used. In the case of Tc, the active solution contained 5 x 10^{-4} mol/l $^{99}TcO_4^-$. As for the other series with ^{14}C, the ground water contains HCO_3^- present already in a concentration of 1.2 x 10^{-2} mol/l. This amount was spiked with 3.7 MBq $H^{14}CO_3^-$, which results only in a negligible increase of the concentration of hydrocarbonate anion. The pH of solutions was adjusted to 8.

The increase of activity concentrations had been followed for c.a. 230 days, 50 – 50 µl samples were taken regularly from the solutions and measured by the sensitive liquid scintillation detection. Typical results are presented in Fig. 4.

Modelling

The conventional equation is used for evaluation [4]:

$$\frac{C'(t)}{C_0} = \frac{AD_e}{V'L}t - \frac{\alpha AL}{6V'} \qquad \text{(Eq. 1)}$$

where *C*-s are the activity concentrations, *A* is the cross section of the sample, *V* is the volume of solutions, *L* is the thickness of the sample, *t* is the time elapsed, α is the rock capacity factor. By fitting a straight line to the measured points in Figs 2 and 3, the apparent diffusivity constants D_e can be estimated.

By using this approach 1.1 x 10^{-12} m^2 s^{-1} is obtained for the apparent diffusivity of TcO_4^- and 1.3 x 10^{-12} m^2 s^{-1} is obtained for HCO_3^-.

Conclusions

The Mössbauer analysis attests for a value of c.a. 3 as for the Fe^{3+}/Fe^{2+} ratio. In a first approach, the exclusive presence of ferric component might be expected by considering the strongly oxidizing conditions experienced during the diagenesis of the formation [Árkay]. The appearance of the ferrous component and its inclusion into chlorite can be attributed to later post-diagenetic hydrothermal processes. The presence of Fe^{2+} may give a concern whether the reduction of Tc(VII) to a lower valence state may proceed. It can be suggested however, that the Tc(VII) state remains preserved, regarding the high rate of break-through found experimentally and the broad stability field reported for technetate anion in the E_h - pH dependence [2].

The studied two anionic species exhibited similar migration rate in the break-through experiments. Furthermore, this value is practically the same as obtained in similar experiments for iodine. Thus, it can be suggested that in the studied samples the anionic species exhibit similar migration rate regardless on their identity, whether iodine, technetate or hydrocarbonate anions are considered.

Considering the order of magnitude, 10^{-12} m^2 s^{-1}, the value is less with c.a. two orders of magnitute than the self diffusion constant in strong aqueous electrolytes. Taking into account the small porosity (0.5 – 2.3 %), a similar 10^{-12}

order of magnitute could be estimated for the strong electrolytes as well. Thus, this approach attest also for the negligible interaction between the anions and the rock.

The values obtained can be used as input data for PA evaluation. In correspondence, a simplified rough approximation can also be performed. Assuming that the studied geological formation is in equilibrium, i.e. there is no pressure-, concentration-, temperature-, etc. gradient in it (there is no flow of any sort), as a very first approach, the general formula for the distance covered by diffusion ($x \sim (D_e\, t)^{1/2}$) can be used. (It was mentioned that concentrations of the spiking isotopes are negligible, so their addition practically do not raise any concentration gradient.). Considering the magnitude of the long half life of certain isotopes present in the high-level waste (~ 10^6 year) a characteristic distance of c.a. 30 m covered by the migrating anionic species can be estimated within this time span.

References

[1] Árkai, P., Balogh, K., Demény, A., Fórizs, I., Nagy, G., Máthé, Z., (2000) Composition, diagenetic and post-diagenetic alterations of a possible radioactive waste repository site: the Boda Albitic Claystone Formation, southern Hungary, *Acta Geologica Hungarica,* **43**, 351-360.

[2] Brookins, D.G. (1988) Eh-pH Diagrams for Geochemistry, Springer-Verlag, pp.177.

[3] Kovács, L. (Ed.) (1999) Digest on the results of the short-term characterisation programme of the Boda Claystone Formation, *Mecsekérc-PURAM report* pp. 65.

[4] Mell, P., Megyeri, J., Riess, L.,. Máthé, Z., Hámos, G., Lázár, K., (2006) Diffusion of Sr, Cs, Co and I in argillaceous rock as studied by radiotracers, *Journal of Radioanalytical and Nuclear Chemistry,* **268,** 411-417.

[5] Stevens, J.G., Khasanov, A.M., Miller, J.W., Pollak, H., Li, Z., (Eds.), (1998) Mössbauer Mineral Handbook, *MössbauerEffect Data Center.*

ADDITIONAL CONTRIBUTION

OVERVIEW OF THE ACTIVITIES CARRIED OUT AT THE FEBEX SITE

T. Missana[1], A. Pérez-Estaún[2], R. Carbonell[2], J. Suso[3], G. Carretero[3], J. Bueno[3], L. Martínez[3], B. Buil[1], A. Garralón[1], P. Gómez[1*] and P. Hernán[5].

[1] CIEMAT, Spain
[2] Instituto Jaume Almera, CSIC, Spain
[3] AITEMIN, Spain
[4] Universidad Politécnica Cataluña, Spain
[5] ENRESA, Spain

* Corresponding author: paloma.gomez@ciemat.es

Abstract

One of the main aim of WP 4.1 and 4.2 is to study solute migration mechanisms in crystalline host-rock in realistic conditions. Many organisations are participating in a joint study that is being performed in the FEBEX gallery (NAGRA's Grimsel Test Site, GTS, Switzerland). The FEBEX experiment reproduces at a real scale a high-level waste repository in granite and was installed more than 9 years ago. At moment, it represents the most realistic environment where the processes affecting radionuclide migration from the bentonite to granite can be studied.

This paper summarises the main activities carried out at the FEBEX site during the second year of the project.

Introduction

Studies conducted during the last years in the URL located in the granitic test site of Grimsel (Switzerland) can provide relevant insights on the major processes affecting radionuclide migration in crystalline rock and, in the case of the FEBEX site, on the solute migration mechanisms in granitic host-rock, influenced by the presence of the bentonite buffer. Bentonite clay is an element present in most of the concepts of radioactive waste disposal in crystalline rocks and therefore it is of interest to analyse the consequences of possible geochemical gradients generated.

The FEBEX experiment represents a unique opportunity to study in "realistic" condition the migration of solutes from a repository into the crystalline host rock. In particular, the migration through granite of conservative ions like I^- and ReO_4^- can be studied because appropriated sources of these elements were placed at the bentonite surface, in the FEBEX experiment, more than eight years ago.

The generation of colloids from the bentonite backfill surface and their mobility are, at present, issues of interest that can be also analysed *in-situ* at the FEBEX site.

In order to carry out *in-situ* studies of the geochemical processes related with the migration of solutes in crystalline rocks, two hydro-geochemical investigation boreholes (FUN-05.001 and FUN-05.002) were drilled at the end of 2005 in the FEBEX gallery at the Grimsel Test Site (GTS). In addition, 3 short (3 m) boreholes FUN-05.003, FUN-05.004 and FUN-05.005, were drilled, perpendicular to the gallery and with different inclinations, to support the geophysical survey campaign. All the boreholes had a diameter of 86 mm.

FUN-05.001 is parallel to the FEBEX gallery axis and has 17.81 m of length. FUN-05.002 has a length of 17.67 m and it presents a vertical deviation (2 º) in relation to the axis of the gallery and 1º in direction with the parallel to the gallery.

The location of these boreholes was selected after a thorough revision of water chemistry, geological, hydrogeological and geochemical previous data of the FEBEX site, in a close collaboration between several organisations involved in WP 4.1 and WP 4.2 by interdisciplinary studies.

From the chemistry point of view, the boreholes location had to be as near as possible to the bentonite surface, for evaluating the existence of chemical gradients and mass transfer from the bentonite to granite, in particular of the tracers located at the bentonite surface, as well as the existence of bentonite colloids. The chemical requirements were also strictly constrained by the geological and hydrogeological characteristics of the FEBEX tunnel. It was considered of interest, for example, to drill the boreholes so that different type of discontinuities (fracture families) geometric elements and different infills, could be analysed, maintaining the connection between WP 4.1 and WP 4.2.

At least four main different fracture groups (Pérez-Estaún et al, 2006) were considered of importance: 1) Open fractures (tardimagmatics) with quartz and biotite as infills; 2) Lamprophyre; 3) Vertical fractures present in the final part of the tunnel; 4) "Riedel" fracturing. Even these last fractures are not particularly large they may be of importance allowing the connectivity between all the other fracture systems.

On the other hand, hydrogeological models suggested the existence of high trasmissivity zone in the lower part (related to fractures of groups 3 and 4). This section is close to the bentonite and therefore of interest.

Apart from the drilling of new boreholes, to support the hydrogeochemical work, it was considered necessary to locate a new instrumentation in the old FBX2 borehole, which is parallel to the FEBEX gallery.

This paper summarises the main activities carried out at the FEBEX site during the second year of the project, during and after the new boreholes drilling. Supporting laboratory studies to those field studies will be carried out by most of the organizations involved in RTDC 4.

Objectives

The main aim of WP 4.1 and 4.2 is the study of solute migration mechanisms in crystalline host-rock in realistic conditions. Geological, hydrogeological, geophysical and hydro-geochemical studies are combined.

Experimental activities

Drilling of new boreholes and monitoring of piezometric level (AITEMIN)

The drilling of the boreholes was monitored by the piezometric level in all the sections of the already existing boreholes of the FEBEX and NF-PRO experiments in order to detect the possible hydraulic connections between them. The main variations (general pressure drop) were registered when FUN-05.001 and FUN-05.003 cut the lamprophyre dyke. Piezometric data, monitored and collected in continuous are available from AITEMIN.

Geophysical campaign and preliminary analysis of the core samples (CSIC)

A previous characterization of the fractures from borehole logging was carried out which was fundamental for the decision on the type and length of the intervals to be instrumented. The main objective of the geophysical campaign was: to obtain knowledge on the geometry of the fracture network; obtain GPS images using the new boreholes; obtain seismic images using the newly drilled boreholes and the old FBX2.

The structural study of boreholes FUN-05.001 and FUN-05.002 allowed identifying the existing fractures and those regions of major interest for studying migration processes.

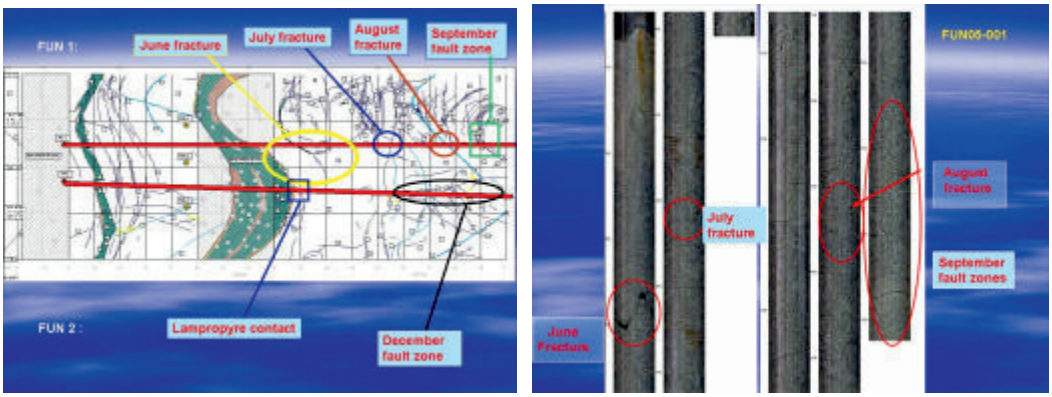

***Figure 1**: (Left) Different regions identified as interesting for future studies. (Right) (Right) Images from BTW of the cores.*

Figure 1 (left) shows the most important fractures cut by the new boreholes, Figure 1 (right) shows the images of the most interesting cores of FUN05.001. This borehole is parallel to the gallery and relatively near to the bentonite surface (20 cm) and intersected several interesting regions. The *June* fracture (8.57m) which

corresponds to a small lamprophyre band; the *July* fracture (11.8m), with presence of quartz which is a nearly closed fracture; the *August* fracture (14.8m) which lies approximately 22 cm near to the bentonite surface and presents certain water conductivity. Finally the *September* fault zone, starting from 15 to 17.8m. These small fractures can play a role in communicating other regions.

FUN05.002 presents a vertical deviation (2 º) in relation to the axis of the gallery and 1º in direction with the parallel to the gallery. It lies approximately 60 cm far from the bentonite surface. As also indicated in Figure 1, two regions were considered of interest here: the lamprophyre reactivated contact (9.20 m.) and the *December* shear zone.

The lamprophyre contact can be of interest for geochemical studies due to the contact with the concrete plug. The study of the Riedel fracturing in the December fault zone (along to the analysis of SF13-SF23) may be very useful for improving the hydrogeological model and also important for analyzing the chemical data.

Geophysical experiments included Natural Gamma, Borehole Ground Penetrating Radar (GPR) and Cross-hole Ultrasonic Tomography. The preliminary processing and integration of these different data sets indicated that the GPR record is adequate to provide images of the fractures, especially if they are fluid filled. The anomalies measured by the natural gamma can be correlated with the "diffractions" in the GPR and the fractures imaged by the borehole televiewer. More details on the geophysical campaign can be found in Carbonell et al. (2006, this volume).

Instrumentation of FUN-05.001, FUN-05.002 and FUN-05.003 (AITEMIN)

According to the previously mentioned analysis, the sampling intervals were selected in Figure 2. In the borehole FUN 05.001 the volume inside the most interesting intervals has been reduced below 5 litres to assure that the water samples to be taken are from the fracture of interest without any others influences. Pressure transducers and water sampling ports have been installed in all the intervals to control the hydraulic heads evolution and take water samples.

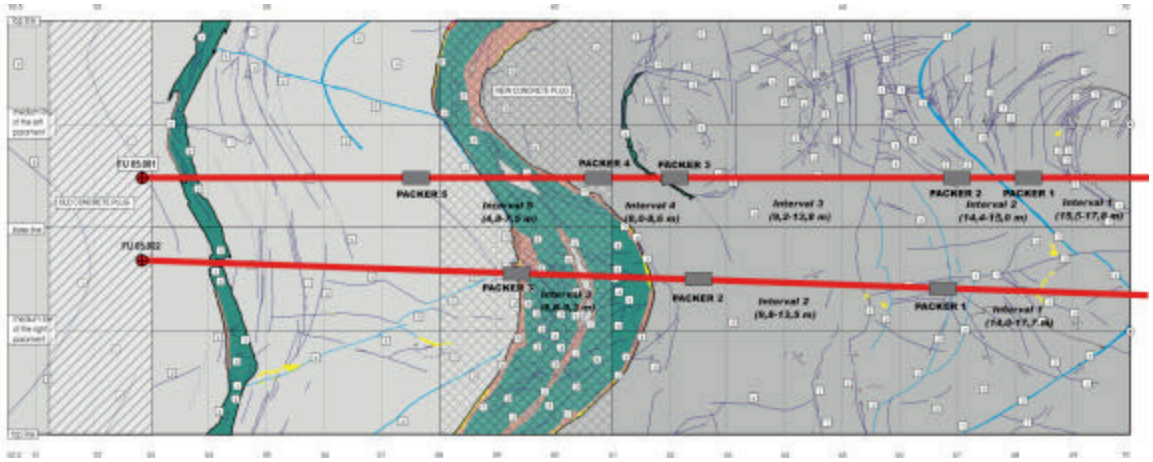

***Figure 2**: Schematic of the borehole instrumentation*

In the FUN.05-001, the target objectives for the sampling intervals are described below.

- Interval 1 (I1, 2.3 m length, from 15.5 to 17.8 m, 17 l volume): isolation the *September* fault region at the end of the borehole; Interval 2 (I2, 0.88 m length, from 14.1 to 15 m, 2.1 l volume): isolation of the quartz dyke at 14.9 m (*August* fracture). Due to the vicinity to the bentonite surface this interval is very interesting from the chemistry point of view and also for the analysis of bentonite colloid presence; Interval 3 (I3, 4.88 m length, from 8.7 to 13.6 m, 13.7 l volume): isolation of a transition zone and other potentially interesting fracture (*July*, 11.8 m); Interval 4 (I4, 0.87 m length, from 7.4 to 8.6 m, 2 l volume): isolation of the small lamprophyre at 8.5 m; Interval 5: (I5, 2.8 m length, from 4. to 6.9 m, 7.9 l volume): characterisation of the lamprophyre dyke region.

In the FUN.05-002, the target objectives for the sampling intervals are described below.

- Interval 1: (I1, 3.7 m length, from 14.0 to 17.7 m, 20 l volume): isolation of the fractures at the end of the borehole (*December* fault zone); Interval 2: (I2, 3.8 m length, from 9.6 to 13.5 m, 10 l volume): isolation of a transient region; Interval 3: (I3, 2.8 m length, from 6.3 to 9.1 m, 8 l volume): characterisation of the lamprophyre dyke region.

Due to the strong affection caused in the piezometric distribution during the drilling of the FUN.05-003, this borehole was also packed and the piezometric levels controlled.

Instrumentation of FBX2 (AITEMIN)

The hydraulic instrumentation of borehole FBX 95.002 was changed (January, 2006) in order to shorten the length of sections controlling fractures near the heater. Five control intervals have been instrumented with different lengths from 62 m to 1,57 m: interval 1: 61 m; interval 2: 4,0 m; interval 3: 5,5; interval 4: 3,5; and interval 5: 14 m length. All intervals have been instrumented with pressure transducer to control the piezometric evolution and water sampling lines.

Preliminary hydraulic tests (AITEMIN, UPC)

The hydraulic testing of the boreholes for the characterization of the flow around the gallery was initiated. Pulse tests have been carried out in order to characterize the hydraulic properties of FUN-05.001, FUN-05.002 and FBX2. The preliminary results are shown in Table 1.

Table 1: *Preliminary results of hydraulic tests*

INTERVAL	T (m^2/s)	L (m)	K (m/s)	S (-)	Sw (m^2)	Structures
FBX2-1	9,1E-10	60,00	1,5E-11	1,9E-05	2,1E-06	Fractures and quartz dykes
FBX2-2	3,8E-12	2,00	1,9E-12	2,1E-06	2.6E-07	Quartz veins
FBX2-3	6,4E-10	2,50	2,6E-10	2.1E-05	6,5E-08	Fracture at 68 m
FBX2-4	4,2E-09	1.50	2.8E-09	5,7E-08	7,9E-07	Fracture at 64 m
FBX2-5	1,6E-08	11,92	-	4,7E-07	2,5E-07	Thick Lamprophyre Dyke
FU1-1	5,6E-10	2,29	2,4E-10	4,1E-8	2,8E-6	Small fractures at total depth
FU1-2	1,0E-11	0,88	1,1E-11	5,1E-07	1,0E-07	Quartz dyke at 15 m
FU1-3	4,2E-12	4,88	8,6E-13	7,1E-08	4.1E-08	Granite (matrix)
FU1-4	3,9E-11	0,87	4,5E-11	5,3E-04	1,1E-05	Lamprophyre at 12 m
FU2-1	1.6E-11	3,67	4,3E-12	1.2E-05	1,2E-07	Fractures at total depth

INTERVAL	T (m^2/s)	L (m)	K (m/s)	S (-)	Sw (m^2)	Structures
FU2-2	6,2E-11	3,84	1,6E-11	9,6E-07	3,6E-07	Quartz dykes

T= Transmissivity L= Length of interval
K= Hydraulic conductivity S= Storage coefficient
S_w= Well storage

Water sampling and analysis (CIEMAT)

In September 06, a new sampling campaign was carried out. The water was sampled from all the old radial boreholes, the new instrumented FBX2 and the new drilled boreholes. Analyses of mayor, minor and trace elements are ongoing.

A preliminary analysis of water samples from the new boreholes to determine the presence of colloids has been carried out. The "as-received" samples presented a non negligible disturbance due to particle of large size, most probably resulted from the recent excavation. However, the first results indicate in the interval 2 of the FUN05.001, i.e. in the region nearest to the bentonite surface, the colloid concentration is at least one order of magnitude higher than the concentration in the groundwater (GW). Colloid size in this interval was around 100 nm with a low poly-dispersivity. The samples from FUN05.002 did not present colloid concentration significantly higher than the GW background. It is interesting noticing that colloids of similar size where observed in FUN 3 and SJ5-3, FBX2-4 (I4, 63-64.5, 1.5 m).

Conclusions

In order to provide the basis for understanding the major geochemical conditions prevailing in crystalline rock and in bentonite/crystalline rock interface of a high level waste repository, in situ studies are being carried out at the Grimsel Test Site at the FEBEX gallery. Two boreholes have been drilled cutting the target fractures identified along the whole gallery. One of the two new drilled boreholes is located very near to the bentonite surface in an optimum position for studying the mass transfer from the bentonite to granite and the migration of the tracers emplaced 8 years ago in the bentonite. Instrumentation of these boreholes allows the measurements of piezometric levels and provides data to implement the actual flow model.

Water samples from these fractures were obtained. The chemical analysis of these samples will provide new data for improving the bentonite to granite mass transfer modelling. Preliminary analysis for the presence of colloids has been carried out. The concentration of colloids in some intervals of the FUN.05.001 borehole is more than one order of magnitude higher than in the Grimsel water. More studies are needed for a deeper characterisation of these particles.

References

[1] Carbonell, R., Pérez-Estaún, A., Missana, T., Suso, J., Carretero, G., Bueno, J., Martínez, L., Buil, B., Garralón, A., Gómez, P., Hernán, P. Geology and Geophysics of new boreholes at the FEBEX site (2006), 2nd FUNMIG Annual Workshop Proceedings (Stockholm, Nov. 2006).

[2] Pérez-Estaún, A. Carbonell, R. Martínez, L, Dentz, M. Suso, J. Carretero, G. Bueno, J. Buil, B. Garralón, A. Gómez, P, Arcos, D. Hernán, P. (2006) New boreholes to investigate the bentonite/crystalline rock interface in the FEBEX tunnel (Grimsel, Switzerland), 1st. Annual Workshop Proceedings 6TH EC FP - FUNMIG IP.